Seismic assessment of reinforced concrete buildings in Australia including the response of gravity frames

Anita Amirsardari

A thesis submitted in total fulfilment of the requirements
for the degree of Doctor of Philosophy

April 2018

Department of Infrastructure Engineering
The University of Melbourne

ABSTRACT

Over recent years there has been a growing need to assess the seismic performance of potentially vulnerable buildings in Australia in order to make informed risk mitigation decisions. The aim of this study has been to assess the seismic performance of in-situ reinforced concrete (RC) buildings under 10-storeys high and constructed prior to 1995. This class of buildings has been identified to be particularly vulnerable to earthquakes due to the relatively low natural periods of buildings in this height range, and lack of consideration given to seismic design and detailing. The buildings assessed have core walls as the lateral load resisting system, also referred to as the primary system, and perimeter moment resisting frames together with band-beam or flat-slab floor systems as the gravity load resisting system, also referred to as the secondary system. There have been concerns about the displacement compatibility between the primary and secondary system and the loss of axial load carrying capacity of the gravity system (resulting in the total collapse of the building) prior to or immediately after the primary system loses its lateral load carrying capacity. Therefore, the assessment of the buildings conducted in this study has involved the seismic performance of both the lateral load resisting system and the gravity load resisting system.

The assessment procedure adopted in this study has been in line with the performance-based earthquake engineering (PBEE) assessment framework. The main outcome of the study has been the development of fragility curves, thus the three key stages of the PBEE assessment process have been undertaken, including: hazard analysis, structural analysis, and damage analysis.

The hazard analysis stage involved conducting a review of the seismic hazard models developed for Australia. The most recent models which have been proposed for the Australian earthquake loading standard, AS 1170.4, have resulted in significant reductions in hazard values in comparison to the current hazard model in AS 1170.4:2007. However, there has been a lack of consensus amongst researchers about the changes and hence the proposed models are still under development. Therefore, in this study the evaluation of the seismic performance of the buildings has been based on the current hazard model in AS 1170.4:2007.

Furthermore, a detailed study was conducted to investigate the validity of the method used in AS 1170.4:2007 for incorporating local site effects. The study demonstrated the

importance of considering site period, rather than the average shear wave velocity up to a depth of 30 m, in understanding the seismic site response. Based on the findings, re-classification of the site classes in AS 1170.4:2007 were recommended, with an emphasis on site period as a key criteria in classifying soil/soft rock classes. A new systematic method was also proposed for obtaining the displacement response spectra. This method helps to significantly improve the prediction of displacement response in the short period range up to the second corner period at which maximum spectral displacement response occurs.

The structural analysis phase was conducted by developing archetypal buildings for assessment. An investigation was conducted to obtain the history of the design of RC buildings in Australia to provide an understanding of the existing building stock, including typical building configurations and design detailing. This was achieved by speaking to and corresponding with experienced practicing structural engineers and from reviewing older editions of the Australian concrete structures and loading standards. Based on the findings six archetypal buildings were designed. Three buildings heights were investigated; 2-, 5-, and 9-storeys, and for each building height two plan configurations were analysed; one with plan symmetry and the other with plan asymmetry.

The expected governing failure mechanisms of the building components were identified, including the core walls, beam-column joints, columns and beams. This was achieved by reviewing reconnaissance reports and experimental studies for buildings and building components with similar detailing to the archetypal buildings. In general, it was identified that the building components were vulnerable to brittle failures and experiencing significant strength and stiffness degradation after the peak capacity was reached. This is because the buildings which have been assessed have a poor quality of detailing; typically referred to as non-ductile or seismically non-conforming detailing in the literature.

In order to develop the 3-dimensional nonlinear models of the archetypal buildings a critical review of the existing state-of-the-art approach for modelling non-ductile RC building components in a macro-finite element modelling space was conducted. The modelling methods investigated included the incorporation of the inelastic response of beam-column joints, flexural response of members, bar-slip of longitudinal reinforcement bars, flexure-shear behaviour of members, and methods for modelling non-planar walls. The review revealed that there was a lack of consensus amongst researchers about the best method to model the various building components for the purpose of global analysis. Therefore, various modelling approaches were evaluated by examining their performance

against three key criteria: accuracy, computational efficiency, and numerical stability and reliability. The accuracy of the various models was predominantly examined at a component level by comparing simulated results with experimental results. The computational efficiency, and the numerical stability and reliability of the various modelling approaches were examined based on running simulations at a component level and then at a system level where the approach was utilised in 2D and 3D nonlinear models. In general, it was evident that the two competing modelling approaches suitable for global analysis could be broadly characterised as the distributed plasticity and the lumped plasticity approaches. Based on the three key criteria, the lumped plasticity approach was selected to be the most suitable and reliable approach for global analysis of non-ductile buildings analysed up to the point of axial load failure of the building components.

Nonlinear dynamic time history analyses were conducted to obtain the seismic performance of the archetypal buildings. The ground motion records were selected such that they were characteristic of Australian earthquakes, they include a combination of: stochastically generated rock records, historical records, and simulated records on various site conditions. Damage analysis of the buildings was achieved by using the cloud analysis method to develop the probabilistic seismic demand model of the buildings at various performance levels. Careful consideration was given to selecting suitable intensity measure and accounting for various uncertainties to develop the fragility curves. Finally, the seismic performance of the buildings was evaluated by comparing the response obtained from fragility curves with respect to performance objectives. The results illustrated that the plan-asymmetric buildings and the 2-storey plan symmetric buildings were particularly vulnerable to exceeding the *Life Safety* limit state under a 500 year return period event and the *Collapse Prevention* limit state under a 2500 year return period event if located on soft sites.

DECLARATION

This is to certify that:

i. The thesis comprises only my original work
ii. Due acknowledgement has been made in the text to all material used
iii. The thesis is less than 100,000 words in length exclusive of tables, maps, references, and appendices

Anita Amirsardari
April 2018

ACKNOWLEDGMENTS

First and foremost, I would like to express my sincere gratitude to my principal supervisor, A/Prof. Helen Goldsworthy, for her continuous support and encouragement, and the careful and thorough revisions of my work. She has provided invaluable advising throughout the years and she has truly been an inspirational teacher and mentor.

I would also like to express my sincere gratitude to my co-supervisor, Dr. Elisa Lumantarna, for her continuous guidance and assistance, and for having confidence in my work and for encouraging me to explore different avenues.

I would like to express my deepest gratitude to Dr. Pathmanathan Rajeev, who has played a very important role in assisting with this research. I would like to sincerely thank him for sharing his invaluable knowledge and time.

I am also grateful to all of the professors and staff who have helped me over the years, with special thanks to Prof. Nelson Lam, Dr. Massoud Sofi, and Dr. Hing-Ho Tsang.

I wish to also express my gratitude to the practicing engineers for their significant contributions to this research, including: Peter McBean, Graeme Rowe, John Woodside, David Law, Shan Kumar, and Scott Munter.

I would also like to acknowledge the Department of Infrastructure Engineering at the University of Melbourne and the Bushfire and Natural Hazards Cooperative Research Centre which have supported the research conducted in this study.

I would like to thank all of my friends and colleagues who have made this experience enjoyable. I have appreciated all of our discussions, and I thank you for your support, kind words of encouragement, and friendship.

Finally, I would like to thank my family. I will forever be grateful to my mother, my father, and my sister for their continuous support, encouragement, patience, and countless sacrifices.

LIST OF PUBLICATIONS

Research outcomes from this PhD study have been published in one journal and six peer reviewed conference papers. A complete list of the publications is provided as follows:

Journal publications

Amirsardari, A., Goldsworthy, H. M., & Lumantarna, E. (2017). Seismic site response analysis leading to revised design response spectra for Australia. Journal of Earthquake Engineering, 21(6), 861-890. doi: 10.1080/13632469.2016.1210058

Conference publications

Amirsardari, A., Goldsworthy, H. M., Lumantarna, E., & Rajeev, P. (2017). Seismic fragility curves for limited ductile RC buildings including the response of gravity frames. Paper presented at the Australian Earthquake Engineering Society 2016 Conference, Canberra, ACT.

Amirsardari, A., Rajeev, P., Goldsworthy, H. M., & Lumantarna, E. (2016). The effect of modelling inelastic beam-column joints on the displacement capacity of reinforced concrete gravity moment resisting frames. Paper presented at the Australasian Structural Engineering 2016 Conference, Brisbane, Queensland.

Amirsardari, A., Rajeev, P., Goldsworthy, H. M., & Lumantarna, E. (2016). Modelling non-ductile reinforced concrete columns. Paper presented at the Australian Earthquake Engineering Society 2016 Conference, Melbourne, Victoria.

Amirsardari, A., Goldsworthy, H. M., & Lumantarna, E. (2015). Modelling non-ductile reinforced concrete beam-column joints. Paper presented at the Proceedings of the Tenth Pacific Conference on Earthquake Engineering, Sydney, Australia.

Amirsardari, A., Lumantarna, E., & Goldsworthy, H. M. (2014). Seismic site response analysis for Australia. Paper presented at the Australian Earthquake Engineering Society 2014 Conference, Lorne, Victoria.

Hoult, R. D., Amirsardari, A., Sandiford, D., Lumantarna, E., Goldsworthy, H. M., Gibson, G., & Asten, M. (2014). The 2012 Moe Earthquake and earthquake attenuation in south eastern Australia. Paper presented at the Australian Earthquake Engineering Society 2014 Conference, Lorne, Victoria.

TABLE OF CONTENTS

LIST OF TABLES

LIST OF FIGURES

LIST OF NOTATIONS

A_{cc}	is the confined area of a column cross-section
A_{cv}	is the shear area of a section
A_{fl}	is a factor which accounts for the depth of the component when computing the mean f_{ct} in accordance with *fib* (2010)
A_g	is the gross cross-sectional area of a member
A_j	is the joint cross-sectional area
A_s	is the total cross-sectional area of longitudinal reinforcement
A_{str}	is the strut area
A_{sv}	is the cross-sectional area of transverse reinforcement (ties)
a	is the shear span of a member
$a \ and \ b$	are the parameters obtained from regression analysis (for a power-law demand model)
b_b	is the width of a beam cross-section in the plane of bending
b_c	is the width of a column cross-section in the plane of bending
b_{ef}	is the effective width of a beam cross-section
b_j	is the effective width of a joint
b_w	is the width of the web of a member
c	is the collapse situation
$\bar{c}$	is the non-collapse situation
D_s	is the diagonal strut capacity
d	is the depth from the ground surface to bedrock; or is the effective depth of a cross-section in the plane of bending
d_b	is the diameter of a bar
$d_{b,b}$	is the beam longitudinal reinforcement bar diameter
$d_{b,c}$	is the column longitudinal reinforcement bar diameter
d_{bt}	is the transverse reinforcement (ties) bar diameter
d_i	is the thickness of the soil layer i
E	is the elastic modulus of concrete
F_E	is the site amplification factor applied at the natural period of 5 seconds
F_a	is the site amplification factor in the acceleration controlled region of the response spectra
F_{site}	is the maximum amplification factor of a site
F_u	is the lateral strength at ultimate capacity
F_v	is the site amplification factor in the velocity controlled region of the response spectra
F_y	is the lateral strength at yield capacity
f_h	is a factor which represents the horizontal confinement effects due to the transverse reinforcement in the joint
f_c	is the compressive strength of concrete in a finished structure
f_c'	is the compressive strength of concrete

f'_{cc}	is the compressive strength of confined concrete
f_{cmi}	is the mean compressive strength of concrete
f_{ct}	is the uniaxial tensile strength of concrete
$f_{ct.f}$	is the flexural tensile strength of concrete
f_{cu}	is the effective strut compressive strength
f'_{cyl}	is the measured compressive strength of concrete at 28 days
f_s	is the stress in the reinforcement
$f_{s.max}$	is the maximum reinforcement stress
f_u	is the ultimate strength of reinforcement
f_v	is the axial load stress on the joint
f_y	is the yield strength of reinforcement
f_{yt}	is the yield strength of transverse reinforcement (ties)
G	is the shear modulus of concrete
G_{eff}	is the effective shear modulus of concrete
H	is the element height
H_e	is the effective wall height
H_n	is the shear span of a wall
h	is the depth of a cross-section in the plane of bending
h_b	is the depth of a beam cross-section in the plane of bending
h_c	is the depth of a column cross-section in the plane of bending
h_{sp}	is the link spacing (used in wide column model)
IM	is the intensity measure
I_g	is the gross second moment of area of a section
K_c	is a factor to account for the curing procedure (when computing f_c)
K_{deg}	is the degrading shear slope
K^t_{deg}	is the total degrading stiffness
K^t_{deg,θ_back}	is the degrading slope for the backbone definition of a moment-rotation spring
$K^{t\ *}_{deg,\theta}$	is the global degrading slope for half the double curvature column (or beam) moment-rotation response
K_s	is the shear form factor which is taken as $5/6$ for rectangular walls
$K_{torsion}$	is the torsional stiffness of horizontal links (used in wide column model)
K_{unload}	is the flexural degrading stiffness
K_w	is a factor to account for workmanship (when computing f_c)
k	is a factor which accounts for joint position and detailing
k_p	is the probability factor for the annual probability of exceedance for the limit state under consideration in accordance with AS 3600:2009
L	is the member clear height
L_c	is the column height
L_p	is the equivalent plastic hinge length for a member
L_{sp}	is the strain penetration length
L_w	is the wall length

l_b	is the provided reinforcement embedment length
l_d	is the required reinforcement development length
M_N	is the nominal yield moment capacity of a section
M_{bl} & M_{br}	are the expected moment capacities of the adjacent beams (left and right) at the centroid of the joint
M_{ca} & M_{cb}	are the expected moment capacities of the adjacent columns (above and below) at the centroid of the joint
M_{cr}	is the cracking moment capacity of a section
M_{max}	is the maximum moment capacity of a section
M_u	is the ultimate moment capacity of a section
M_y	is the yield moment capacity of a section
n_t	is the number of grids of transverse reinforcement (for walls)
P	is the axial load on the member
P^*	is the axial load on the member due to gravity and seismic loading
PGA	is the peak ground acceleration
PGD	is the peak ground displacement
PGV	is the peak ground velocity
RSA	is the acceleration response spectra
RSA_{max}	is the maximum spectral acceleration response
RSD	is the displacement response spectra
RSD_{max}	is the maximum spectral displacement response
$RSD_{rock\ at\ T_{sf}}$	is the rock displacement response at the site's degraded period (T_{sf})
RSV_{max}	is the maximum spectral velocity response
S_C	is the median value of the structural limit state (capacity)
S_D	is the median value of the demand as a function of IM
S_i	is the sway potential index
S_s	is the longitudinal reinforcement slip
s	is the spacing of transverse reinforcement (ties)
T	is the natural period
T_1	is the first corner period; or is the fundamental building period
T_2	is the second corner period; or is the second fundamental building period
T_{2ampl} $(T_{2amplification})$	is the period at which the hard rock displacement response is amplified by F_{site} to calculate the magnitude of RSD_{max}
T_{2spec} $(T_{2spectra})$	is the second corner period used to construct the response spectra, it represents the period at which RSD_{max} initiates
T_3	is the period for which the maximum displacement response ends
T_4	is the period for which a constant value of spectral displacement response is reached in the long period range
T_s	is the fundamental natural site period
T_{sf}	is the degraded (or final) site period
T_{si}	is the initial site period

t_w	is the wall thickness
u_e	is the elastic bond stress
u_p	is the plastic bond stress
V	is the shear force
V_{jh}	is the horizontal joint shear force
$V_{jh.cap}$	is the horizontal joint shear strength
V_s	is the weighted average shear wave velocity over the full depth of the profile until rock conditions are reached
V_{s10}	is the weighted average shear wave velocity at a depth of 10 m
V_{s30}	is the weighted average shear wave velocity at a depth of 30 m
V_{s5-20}	is the weighted average shear wave velocity at a depth of 5 to 20 m
V_u	is the ultimate shear capacity
V_{uc}	is the concrete contribution to shear strength
V_{us}	is the transverse reinforcement contribution to shear strength
v	is the average normalised shear stress (for walls)
v_{si}	is the shear wave velocity of layer i
$Y, \frac{\theta_D}{\theta_C}$	is the critical demand-to-capacity ratio
$Y_{x,y.SRSS}$	is the square-root-of-the-sum-of-squares of the critical demand-to-capacity ratio in the x- and y-direction
$Y_{x,y.max}$	is the greater of Y_x and Y_y
Y_x	is the critical demand-to-capacity ratio in the x-direction
Y_y	is the critical demand-to-capacity ratio in the y-direction
Z	is the hazard earthquake factor
α	is the reduction factor to account for bond-slip of beam longitudinal reinforcement bars
β	is the logarithmic standard deviation of the demand as a function of IM
β_C	is the capacity uncertainty
β_M	is the modelling uncertainty
$\beta_{Y\|IM}$	is the dispersion (logarithmic standard deviation) of the critical demand-to-capacity ratio as a function of IM
$\beta_{Y\|IM,\bar{c}}$	is the dispersion of the critical demand-to-capacity ratio as a function of IM for non-collapse situations
β_s	is the concrete softening coefficient
γ	is the shear strain
γ_1	is the shear strain corresponding to the first point of the joint shear stress-strain curve
γ_2	is the shear strain corresponding to the second point of the joint shear stress-strain curve
γ_3	is the shear strain corresponding to the third point of the joint shear stress-strain curve
γ_4	is the shear strain corresponding to the fourth point of the joint shear stress-strain curve
Δ_a	is the lateral displacement at axial load failure

Δ_{flex}	is the flexural displacement
Δ_s	is the lateral displacement at shear failure
Δ_{shear}	is the shear displacement
Δ_{slip}	is the lateral displacement due to bar-slip
Δ_u	is the lateral displacement at ultimate capacity
Δ_y	is the lateral displacement at yield capacity
δ_a	is the drift at axial load failure
δ_s	is the drift at shear failure
δ_u	is the drift at ultimate capacity
δ_y	is the drift at yield capacity
ε_m	is the axial strain at the centroid of the wall
ε_s	is the strain in the reinforcement
ε_{su}	is the strain of the reinforcement at ultimate tensile strength
$\eta_{Y\|IM,\bar{c}}$	is the median critical demand-to-capacity ratio as a function IM for non-collapse situations
$\eta_{Y\|IM}$	is the median critical demand-to-capacity ratio as a function IM
θ_a	is the rotation at axial load failure for the total response of a member
θ_{a_back}	is the rotation at axial load failure for the backbone definition of a moment-rotation spring
θ_{ny}	is the rotation at nominal yield for the total response of a member
θ_{ny_back}	is the rotation at nominal yield for the backbone definition of a moment-rotation spring
θ_s	is the strut angle; or is the rotation at shear failure for the total response of a member
θ_{s_back}	is the rotation at shear failure for the backbone definition of the moment-rotation spring
λ	is a factor to account for the weight of concrete aggregate when calculating nominal joint shear capacity in accordance with ASCE 41 (ASCE/SEI, 2013)
μ	is the structural ductility factor
ρ_l	is the longitudinal reinforcement ratio of a section
ρ_t	is the area ratio of transverse reinforcement of a section
ρ_{tv}	is the volumetric ratio of transverse reinforcement
$\rho_{wl.min}$	is the minimum longitudinal reinforcement ratio required to form secondary cracking for walls
Υ_n	is a factor to account for joint type when calculating nominal joint shear capacity in accordance with ASCE 41 (ASCE/SEI, 2013)
τ_{jh}	is the horizontal joint shear stress
$\tau_{jh.1}$	is the horizontal shear stress corresponding to the first point of the joint shear stress-strain backbone
$\tau_{jh.2}$	is the horizontal shear stress corresponding to the second point of the joint shear stress-strain backbone
$\tau_{jh.3}$	is the horizontal shear stress corresponding to the third point of the joint shear stress-strain backbone
$\tau_{jh.4}$	is the horizontal shear stress corresponding to the fourth point of the joint shear stress-strain backbone

$\tau_{jh.cap}$	is the horizontal shear stress corresponding to the joint shear strength
$\tau_{jh.cr}$	is the horizontal joint shear cracking stress
$\tau_{jh.max}$	is the maximum horizontal joint shear stress
$\tau_{jh.res}$	is the horizontal joint shear residual stress
$\tau_{jh.u}$	is the horizontal shear stress corresponding to the stress induced in the joint due to the adjacent beam/s or column/s reaching ultimate capacity
$\tau_{jh.y}$	is the horizontal shear stress corresponding to the stress induced in the joint due to the adjacent beam/s or column/s reaching yield capacity
ϕ	is the curvature of a section; or is the strength reduction factor; or is the standard normal cumulative distribution function
ϕ_{ny}	is the curvature at nominal yield
ϕ_u	is the curvature at ultimate capacity
ϕ_y	is the curvature at initial yield

CHAPTER 1: INTRODUCTION

1.1 BACKGROUND

The standard of earthquake-resistant design and detailing in Australia has generally been low, especially for those buildings designed prior to the gazetting of the earthquake loading standard, AS 1170.4 in 1995. This is mainly due to the low-to-moderate seismicity in Australia (which means that, at a given site, significant earthquakes occur infrequently), the generally poor understanding in the engineering structural design community of the response of buildings to large seismic excitations, and the lack of enforcement of appropriate practice for seismic design and detailing. Therefore, it is generally accepted that many buildings in Australia are not likely to perform well in the event of a large earthquake. However, over recent years there has been an increasing interest in assessing the seismic resilience of potentially vulnerable buildings in Australia and to improve design standards and codes. This is primarily due to greater global awareness of the catastrophic losses caused by earthquakes. In particular, the Christchurch earthquake which occurred on 22nd February 2011 (Canterbury Earthquakes Royal Commission, 2012b) was influential in encouraging a movement towards better design and detailing in the Australian structural design community. This was because the Christchurch earthquake occurred on an unknown fault in a moderate seismic region, with a faulting mechanism very similar to that exhibited by the type of earthquakes which occur in Australia: shallow, reverse faulting with high stress drop (Brown & Gibson, 2004; Goldsworthy, 2013). In addition, the Christchurch earthquake highlighted the poor performance of non-conforming or poorly detailed RC buildings and unreinforced masonry structures for which the design practice resembles that used in Australia. This raised alarm bells in Australia because of the great uncertainty regarding the economic and social impact on one of the capital cities if a large earthquake occurred, even though the likelihood of such an event is very rare.

In order to make informed decisions regarding the vulnerability of buildings to earthquakes, including the need for seismic retrofitting, changes to design standards and codes, and the development of insurance policies, it is necessary to conduct assessment of vulnerable buildings. To assist with risk mitigation decisions in Australia, the *Cost-Effective Mitigation Strategy Development for Building Related Earthquake Risk* project was established under the Bushfire and Natural Hazards Cooperative Research Centre

(BNHCRC). This study forms part of the BNHCRC project with the aim of assessing the vulnerability of older existing RC buildings.

The seismic vulnerability of buildings, usually categorised based on height range, construction material, and structural system, is typically assessed by developing fragility curves. Fragility functions define the building's probability of exceeding a damage limit state as a function of a ground motion intensity measure. There are three main approaches used to develop fragility curves; observation from previous earthquakes, expert opinion, and structural analysis and simulations (Baker, 2015; Jeon, 2013; Porter et al., 2007). Observation based procedures have the benefit of using historical events, however, they have significant limitations due to lack of sufficient damage data (especially in regions of low and moderate seismicity) and variation in seismic intensity. Fragility functions developed from expert opinion are also highly subjective and the quantification of unknowns and uncertainties is not possible. The most objective and reliable approach for developing fragility curves is via structural analysis and simulations. However, knowledge from previous earthquakes and knowledge gained from expert opinions can be used to help improve the results obtained from structural simulations.

The development of fragility curves from structural analysis forms a critical component of the performance-based earthquake engineering (PBEE) framework for risk assessment. PBEE was initially developed by the Pacific Earthquake Engineering Research Center (PEER) and aims to improve the design and assessment methods used to determine the behaviour of buildings under seismic loading in order to improve seismic risk mitigation decisions (Deierlein et al., 2003). Performance-based seismic assessment specifically aims to quantify the likely response of buildings to different intensities of seismic excitation via a probabilistic approach. The PBEE framework for the purpose of conducting assessment is summarised into four stages (Calvi et al., 2014; Moehle & Deierlein, 2004): (i) hazard analysis; the site hazard is defined usually by conducting a probabilistic seismic hazard analysis (PSHA) study which allows the site hazard to be related to a suitable intensity measure and appropriate ground motion records are selected for conducting structural analysis, (ii) structural analysis; nonlinear model of the building is created and time history analyses are conducted to obtain the building response which may be defined by various engineering demand parameters, including interstorey drift, component chord rotations, and floor accelerations (iii) damage analysis; engineering demand parameters are related to damage measures or performance levels and based on the probabilistic seismic demand model, fragility curves are computed, and (iv) loss analysis; the probabilistic description of the damage obtained in the previous step is related to loss

quantities associated with risk management decisions, including cost for down-time, repair, and fatalities. An overview of the four stages is provided in Figure 1-1.

The current platform established in Australia for modelling earthquake hazard and estimating losses is EQRM (Robinson et al., 2005). It is maintained by Geoscience Australia and it incorporates the methodology adopted by HAZUS developed by the Federal Emergency Management Agency (FEMA, 2010). However, the fragility curves which are currently utilised by Geoscience Australia are primarily based on expert opinion (Maqsood et al., 2014) and are therefore highly subjective.

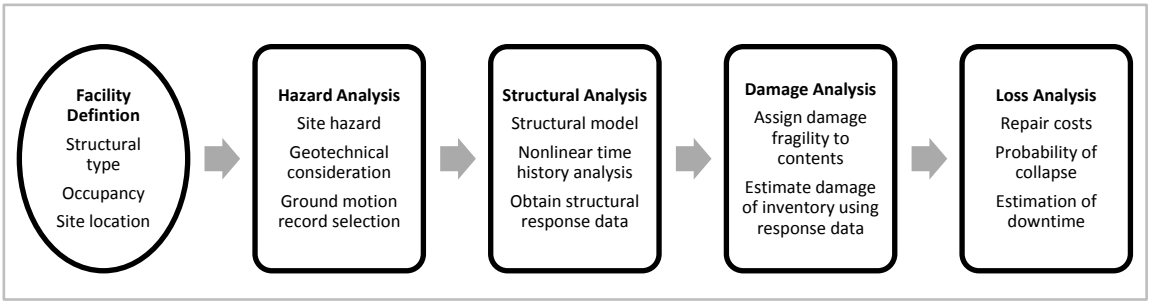

Figure 1-1: Overview of the four stages of the PEER PBEE framework, adapted from Calvi et al. (2014)

1.2 PROBLEM STATEMENT

The aim of this study is to assess the seismic performance of in-situ reinforced concrete buildings by developing fragility curves and evaluating their response with respect to performance objectives. The buildings assessed are under 10-storeys high and constructed prior to 1995. This class of buildings has been identified to be particularly vulnerable to earthquakes due to the relatively low natural periods of buildings in this height range, and lack of consideration given to seismic design and detailing. These buildings typically have core walls as the lateral load resisting system, also referred to as the primary system, and perimeter moment resisting frames (MRFs) together with band-beam or flat-slab floor systems as the gravity load resisting system, also referred to as the secondary system. This form of construction, where the walls are designed to carry all of the lateral loading, has been very popular in Australia. The usual approach has been to design the primary system and secondary system separately, and, in retrospect, this has led to concerns about the displacement compatibility between the two systems. This is particularly a concern for buildings with plan asymmetry due to eccentrically placed core walls which has been a popular form of construction in the past from an architectural perspective. Furthermore, earthquake reconnaissance studies have highlighted that the collapse of buildings may occur due to failure of the gravity load resisting systems (Goldsworthy & Gibson, 2012;

Kam et al., 2011; Norton et al., 1994), therefore it is important that a holistic approach is taken to assess the seismic performance of existing RC buildings. Hence, in this study, the seismic performance of the buildings is assessed by considering both the lateral load resisting system and the gravity load resisting system.

The fragility curves are developed in line with the first three steps involved in the PBEE assessment procedure. The issues and challenges involved in conducting hazard analysis, structural analysis, and damage analysis in relation to this study are discussed in the following subsections.

1.2.1 Hazard analysis

For regions of low-to-moderate seismicity the quantification of seismic hazard is particularly challenging and debatable in comparison to regions with high seismicity predominantly due to the paucity of historical events in the former case. A review of existing hazard models is needed to select an appropriate model to represent the seismic demand for Australia. Furthermore, the paucity of historical records in regions of low-to-moderate seismicity produces a challenge in conducting dynamic time history analyses. Hence, careful consideration needs to be given to selecting suitable ground motion records to conduct analyses.

Local site conditions can also significantly influence the intensity of the shaking that can take place at a site. The effect of these conditions is taken into account in the Australian earthquake loading standard, AS 1170.4:2007, however the current approach needs to be improved. In the current procedure within AS 1170.4:2007, the response spectrum for various site conditions is obtained by modifying the rock response spectra by the use of amplification factors. These amplification factors are based on studies which obtain the response spectra for the various classes by taking the average site response from various historical records or alternatively from numerical analyses representative of a particular class. This approach was adopted within the study conducted by Crouse and McGuire (1996) and has formed the basis of the International Building Code and AS 1170.4 (Wilson & Lam, 2007). However, recent studies have highlighted that the current codified approaches have significant limitations, especially when used to determine the seismic demand on non-ductile buildings (Lam & Wilson, 2004; Tsang et al., 2013).

1.2.2 Structural analysis

A thorough understanding of the construction and design of older buildings is needed in order to characterise the vulnerable buildings to be assessed. This includes determining

typical building configurations and the detailing that was used for the various components, and determining suitable material properties to be adopted for assessment. Furthermore, the likely failure mechanism of building components and global building response needs to be determined. Based on this information archetypal buildings can be developed for which nonlinear structural models are created and analysed.

In general, the buildings which are being assessed in this study have seismically non-conforming detailing when compared with what is considered best practice in high seismic regions including the United States and New Zealand. The building components have been designed with *ordinary* or *limited ductile* reinforcement detailing in accordance with the terminology adopted in the concrete structures standards, AS 3600:2009 (Standards Australia, 2009). This form of detailing is commonly referred to as *non-ductile* detailing and it will be the terminology used in this study. It is also sometimes interchangeably used with *non-conforming* detailing. The typical detailing deficiencies which are characteristic of non-ductile RC frame components include: inadequate ties in beams and columns (for shear strength and confinement), insufficient ties in beam-column joints, poor anchorage and splices of longitudinal bars in beams and columns, splices of longitudinal bars located in potential hinge regions, and columns having bending moment capacities which are approximately the same or less than the adjoining beams thus making the frame vulnerable to the undesirable weak-column strong-beam scenario under lateral loading. The typical detailing deficiencies common to non-ductile RC walls include: low percentage of longitudinal reinforcement ratio, insufficient or no confinement in the boundary regions, and insufficient and poorly anchored transverse reinforcement for shear strength.

The modelling and prediction of the response for non-conforming RC buildings is much more challenging when compared with seismically well designed buildings. The detailing deficiencies common to non-ductile building components make them susceptible to undesirable and brittle failure mechanisms which are not necessarily accounted for using regular macro-finite element modelling techniques. Therefore special modelling techniques need to be utilised to capture the true response of the non-ductile buildings up to the point of collapse. For non-ductile buildings this usually corresponds to loss of axial load carrying capacity of the building components rather than instability or sideway collapse which is typical of ductile buildings. A detailed evaluation of the current state-of-the-art modelling approaches is needed in order to determine the most suitable method for the type of buildings which are being assessed. Furthermore, since the assessment of the buildings includes plan-asymmetric buildings, 3-dimensional (3D) nonlinear models

will need to be developed to obtain the torsional response of the buildings. Dynamic time history analysis (instead of static pushover analysis) will need to be conducted since higher mode effects may be significant for plan-asymmetric buildings. Furthermore, the displaced shape of the building is also likely to change during the analysis depending on whether the response of the building is governed by the primary lateral load resisting system or the gravity load resisting system (once the primary system loses its stiffness and strength). Hence, a predefined force distribution cannot be imposed on the building as done in pushover analysis to obtain the building response up to collapse. Therefore, the modelling methods adopted will need to be suitable for 3D nonlinear time history analysis. In addition, to ensure the approach is effective it needs to achieve three key criteria, including; accuracy, computational efficiency, and numerical stability and reliability.

1.2.3 Damage Analysis

A critical component of damage analysis is to develop suitable structural damage limits and non-structural drift limits to define performance levels. These damage limits will need to be selected such that they are appropriate for the type of buildings assessed in this study. Furthermore, a suitable method to develop the probabilistic seismic demand model needs to be determined in order to develop fragility curves. Careful consideration also needs to be given to the selection of a suitable intensity measure as it can significantly affect the conclusions derived from fragility curves. Finally, appropriate performance objectives need to be defined in order to evaluate the seismic performance of the archetypal buildings.

1.3 RESEARCH OBJECTIVES

The following objectives are required in order to successfully achieve the overall aim of this study:

i. Characterise the seismic demand and determine a suitable hazard model to be adopted for Australia.
ii. Select suitable ground motions for site response analyses and nonlinear time history analyses of RC buildings.
iii. Evaluate and improve the methods currently used to incorporate the influence of local site conditions on seismic site response.
iv. Review the history of building design and construction in Australia and develop archetypal building designs representative of older existing buildings.

v. Identify the governing failure mechanisms of the building components belonging to the lateral load and gravity load resisting systems; that is, the core walls and the moment resisting frames.
vi. Determine appropriate material properties to be adopted for the assessment of the archetypal buildings.
vii. Evaluate various macro-finite element nonlinear modelling methods and determine a suitable approach to model the archetypal buildings. The models need to be capable of simulating damage progression up to the point of (near) collapse defined as loss of axial load carrying capacity of the building components.
viii. Determine an appropriate framework for conducting seismic fragility assessment of the buildings.
ix. Conduct the analyses and develop fragility curves for the archetypal buildings.
x. Evaluate the seismic performance of the archetypal buildings.

1.4 THESIS OUTLINE

This thesis is presented in eight chapters. The chapters have been organised such that they follow the seismic fragility assessment procedure. Therefore, for clarity and coherence, the literature review related to each phase of the assessment procedure has been provided in separate chapters, namely the literature review related to: (i) Hazard Analysis is provided in Chapter 2, (ii) Structural Analysis is provided in Chapters 3 and 4, and (iii) Damage Analysis is provided in Chapter 6. A brief description of each chapter is provided below.

CHAPTER 1 is an introductory chapter providing a brief background and motivation for the initiation of the work conducted in this thesis. It highlights the issues and challenges associated with assessing the seismic performance of RC buildings in Australia and the objectives of this study.

CHAPTER 2 focuses on the seismic demand and characterisation of earthquake hazard. A review of the seismicity of Australia is provided as well as the current challenges associated with quantifying hazard levels. A critical review of existing approaches for incorporating seismic site effects is also provided. This is followed by a detailed study investigating the effects of various site conditions on seismic site response and the proposal of a new systematic approach to be used to incorporate site effects when developing response spectra in codes and standards.

CHAPTER 3 provides a brief history of Australian building design and construction. The typical characteristics of the RC buildings to be assessed in this study are presented. This

includes the detailing deficiencies of non-ductile RC walls and moment resisting frames and the likely failure mechanisms of the various building components. The importance of considering the response of both the primary and secondary structural systems is also discussed. Furthermore, reasons are given for the choice of material properties that are to be adopted for conducting assessments of the archetypal buildings.

CHAPTER 4 presents a critical review of the state-of-the-art nonlinear macro-finite element modelling methods with a focus on the modelling of non-ductile RC components. The review includes the macro-modelling of: beam-column joints, flexural response of members, bar-slip, flexure-shear response of columns, and the planar and non-planar RC walls.

CHAPTER 5 evaluates the suitability of the macro-finite element modelling methods (discussed in Chapter 4) in the specific application considered here, that is, for simulating the response of non-ductile RC moment resisting frame components and walls. Comparisons are made between simulated and experimental results available in the literature for non-ductile RC components to examine the validity of the various approaches. Limitations of some of the state-of-the-art modelling approaches are discussed in relation to their use in performing global analyses. The modelling methods selected to create the 3-dimensional nonlinear models of the archetypal buildings are determined based on the evaluation of their response using three key criteria: accuracy, computational efficiency, and numerical stability and reliability.

CHAPTER 6 provides a review of the seismic fragility assessment framework. The selection and justification for the various aspects of the assessment procedure adopted in this study are discussed, including: the probabilistic seismic demand models, the performance levels, and performance objectives. The advantages and disadvantages of various intensity measures, as well as the different methods used to calculate the intensity measure for developing fragility curves, are also provided.

CHAPTER 7 presents the results for the seismic fragility assessment of six archetypal buildings. The importance of carefully selecting a suitable intensity measure is discussed as it can significantly affect the interpretation of fragility curves and the conclusions derived about the seismic performance of the buildings. Lastly, the seismic performance of the buildings is evaluated by examining their response, as obtained from the fragility assessment, with respect to the key performance objectives.

CHAPTER 8 summarises the key findings of this study and provides recommendations for future work in this area of research.

CHAPTER 2: CHARACTERISATION OF EARTHQUAKE HAZARD

2.1 INTRODUCTION

A critical part of assessing the seismic performance of a structure is determining the expected level of shaking at the site. The seismic ground motions that occur at a site are highly dependent on: (i) the source characteristics of the earthquake (including faulting mechanisms and magnitude of energy released), (ii) the attenuation characteristics of the path that the seismic waves travel from the source to the location of the site, and (iii) the characteristics of the local ground conditions as the seismic waves propagate to the surface (see Figure 2-1). The quantification of the first two characteristics defines the seismicity of a region and the level of shaking expected on rock conditions. It is usually determined by seismologists. The quantification of the third component; seismic site effects, is a highly localised effect and requires expertise within the field of seismology, geotechnical engineering, and structural engineering. For the purpose of assessment of structures, the quantification of the level of shaking experienced by a structure on a site may be determined via static analysis or modal dynamic analysis using response spectra or via dynamic analysis using ground motion time histories; all of these require knowledge of the ground motions experienced at the foundation level of the structure.

This chapter begins by providing an overview of the seismicity of Australia and the existing models which aim to define the level of shaking on rock conditions. It is then followed by a critical review of existing codified approaches for incorporating local site effects to develop response spectra. Significant limitations of the existing methods are highlighted, especially for regions of low-to-moderate seismicity. Thus a detailed study investigating the effect of local site conditions on seismic site response is presented and a new systematic method is proposed for obtaining response spectra. It is noted that this study has been published in the Journal of Earthquake Engineering by Amirsardari et al. (2017).

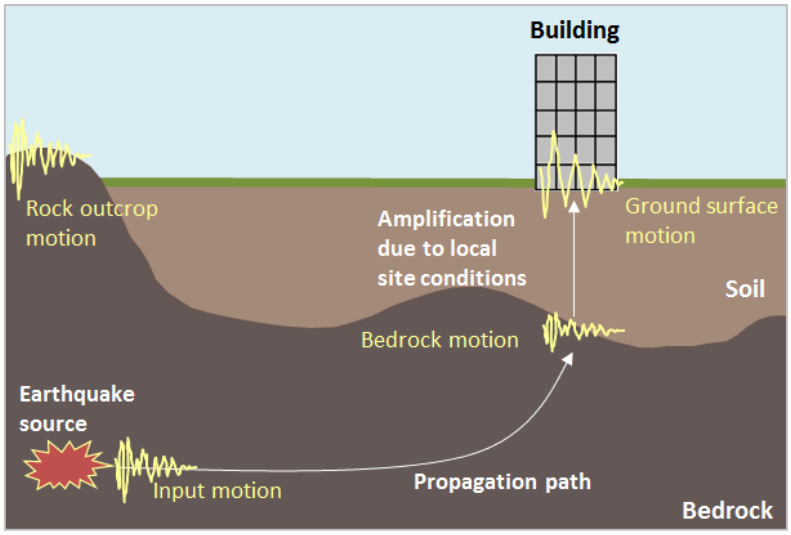

Figure 2-1: Propagation path of seismic waves from source to building site

2.2 SEISMICITY OF AUSTRALIA

Australia is considered to be a low-to-moderate seismic country; however it is also one of the most active intraplate regions in the world which is under compression due to the Indo-Australian plate moving towards the Eurasian and Pacific plates (Goldsworthy, 2013). The most damaging and costly earthquake that Australia has experienced thus far has been the magnitude 5.6, 1989 Newcastle (New South Wales) earthquake, causing a total of 13 fatalities, 160 injuries requiring hospital treatment, and a total of loss of greater than $1 billion which would be an equivalent of $2-3 billion if it were to recur today (Walker, 2011). Larger magnitude earthquakes have also occurred in Australia but due to their remote locations the damage caused by these earthquakes has not been as great as that in the Newcastle earthquake. In fact, it has been observed that the average frequency of magnitude 6 or greater earthquake over the last 110 years has been around 1 in 5 years (Wilson & Lam, 2007). Australian earthquakes are typically shallow, and have a reverse faulting mechanism with a high stress drop and have aftershocks which last for prolonged periods. These characteristics are very similar to the 2011 Christchurch earthquake (Brown & Gibson, 2004; Goldsworthy, 2013). While the characteristics of the Australian earthquakes are well understood, the quantification of the level of hazard is very debatable and prone to change due to the paucity of historical records.

The seismic hazard of the various regions in a country is typically displayed in the form of a hazard map based on probabilistic seismic hazard assessment/analysis (PSHA). These studies are usually conducted for rock ground conditions and from these studies generalised response spectra, commonly in the form of uniform hazard spectra (UHS), are produced for various return period events. The current Australian earthquake hazard map

in the Australian earthquake loading standard, AS 1170.4:2007 (Standards Australia, 2007) is based on the map produced by McCue and colleagues in 1993 which has been developed from the work conducted by Gaull and colleagues in 1990 (Burbidge, 2012). The hazard map shows 10 % probability of exceedance in 50 years of ground motions on rock. This equates to a return period of 475 years which is commonly rounded to 500 years. Thus the hazard factor (Z) provided in AS 1170.4 (Standards Australia, 2007) approximates the peak ground acceleration (PGA) on site class B for a 500 year return period event. The current hazard map of Australia is provided in Figure 2-2.

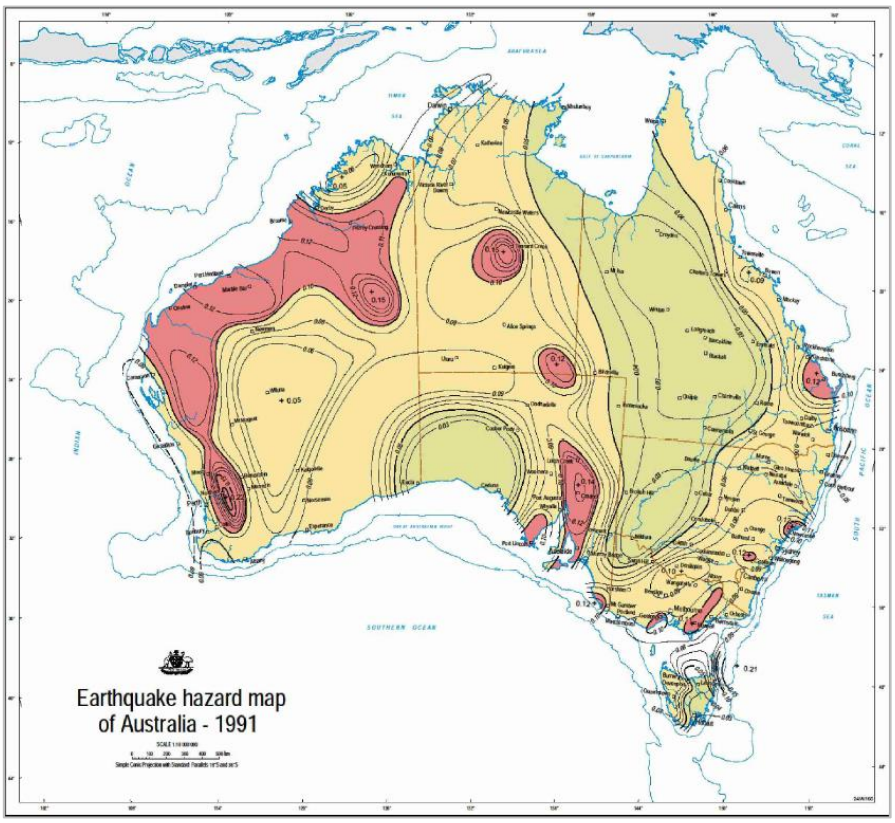

Figure 2-2: Current hazard map in AS 1170.4:2007 (Burbidge, 2012)

In 2009 Geoscience Australia (GA) decided to update the hazard map by using the latest available methods and data. Initial results were released in 2012 (Burbidge, 2012) and in 2013 (Leonard et al., 2013) and they are currently still being updated as part of the National Seismic Hazard Assessment (NSHA) poject (Geoscience Australia, 2017). The 2013 hazard map for a return period of 500 years at zero period which is equivalent to PGA is provided in Figure 2-3. Furthermore, in 2013 GA extended the study for longer return periods as it was identified as being necessary by the Australian Earthquake Engineering Society (AEES) and by various technical experts (Leonard et al., 2013).

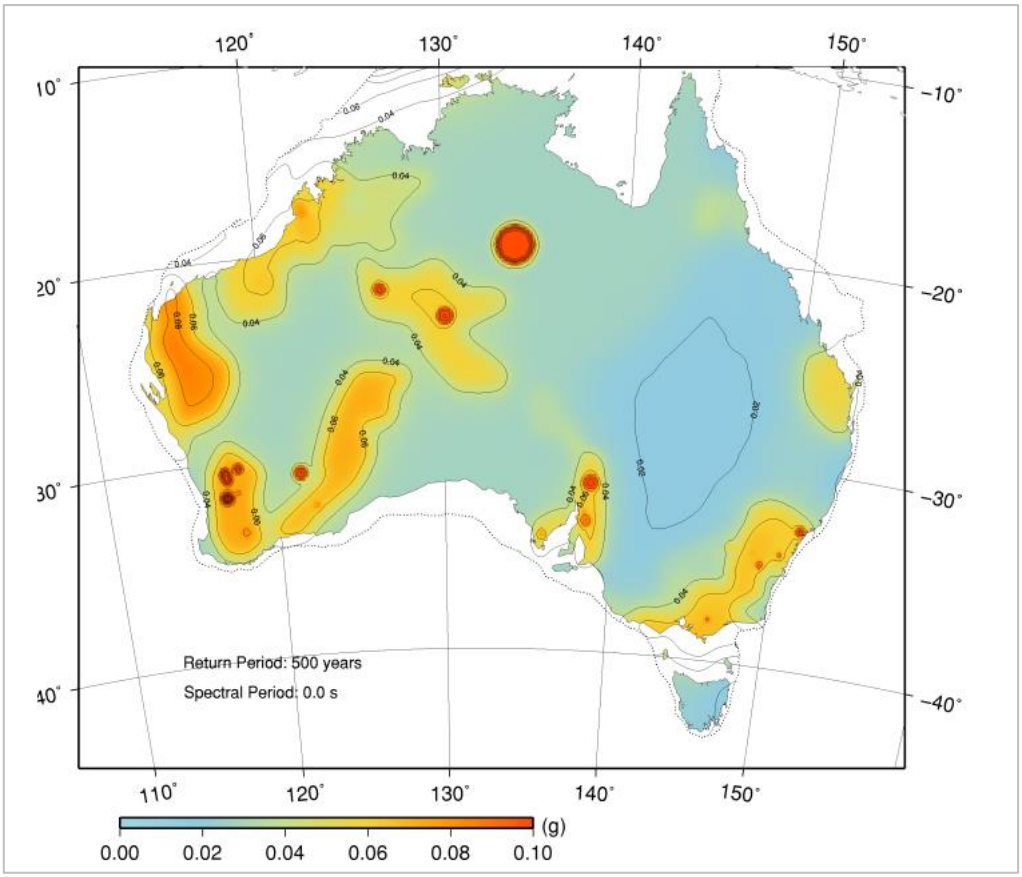

Figure 2-3: 2013 GA hazard map at zero period for return period of 500 years (i.e. equivalent to PGA) (Leonard et al., 2013)

Interestingly, the recent studies conducted by GA have resulted in a significant decrease in hazard for a return period of 500 years as shown in Figure 2-4 and Figure 2-5. The hazard in most capital cities is approximately three quarters of the current hazard levels specified in AS 1170.4 (Leonard et al., 2013). Furthermore, as illustrated in Figure 2-5, the proposed acceleration response spectra by GA for a 2500 year return period event is approximately equal to the acceleration response spectra for a 500 year return period event in AS 1170.4:2007. The lower hazard levels are believed to be due to higher attenuation within the ground motion prediction equations (GMPEs) used in the recent studies and the improved calibration of local magnitude scales (M_L) which have resulted in reduction of some of the recorded magnitudes (Leonard et al., 2013). In contrast, the ratio of a 2500 year return period event normalised with respect to a 500 year return period event, which is represented by the probability factor, k_p, has increased relative to that in AS 1170.4: 2007. However this is expected since currently the k_p factor in AS 1170.4:2007 is based on values that are appropriate for high seismic areas. For low-to-moderate seismic regions a significantly higher level of energy is released relative to that released for low return periods (Nordenson & Bell, 2000); this is illustrated in Figure 2-6.

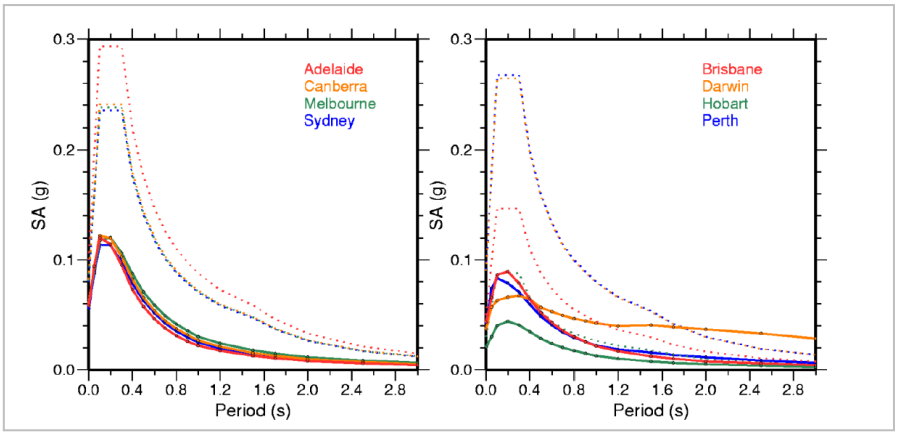

Figure 2-4: 500 year return period acceleration response spectra for the capital cities proposed by GA (solid lines) and in AS 1170.4:2007 (dotted lines) (Leonard et al., 2013)

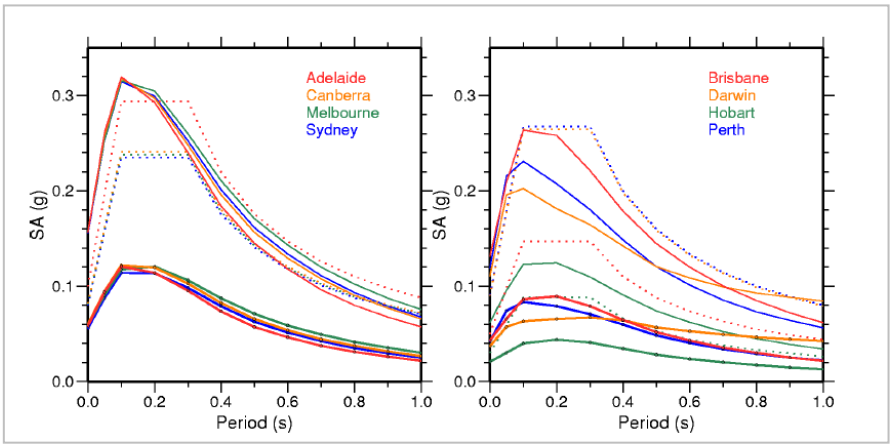

Figure 2-5: 500 year (thick solid lines) and 2500 year (thin solid lines) return period acceleration response spectra proposed by GA, and 500 return period acceleration response spectra in AS 1170.4:2007 (dotted lines) (Leonard et al., 2013)

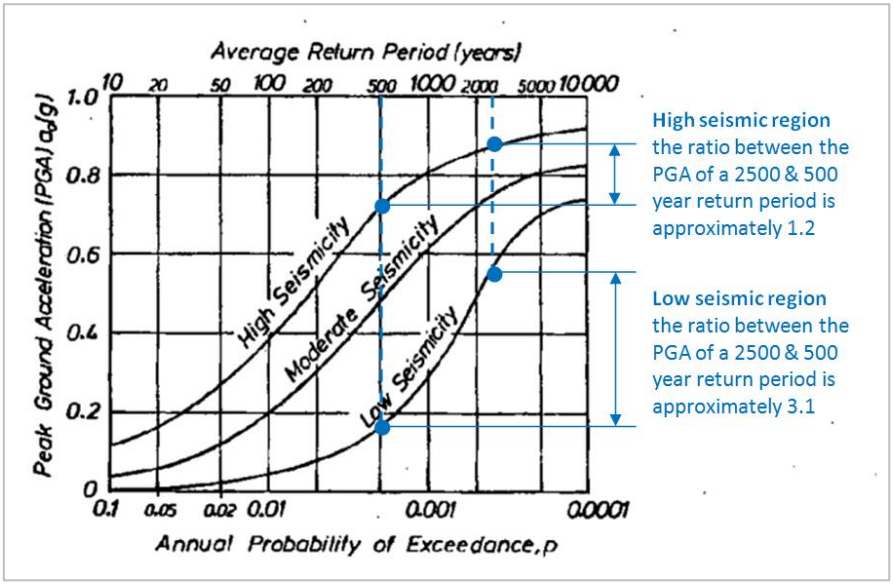

Figure 2-6: Relationship between peak ground acceleration and annual probability of exceedance for different seismic regions (adapted from Paulay & Priestley, 1992)

The recent results published by GA have caused great controversy amongst seismologists and earthquake engineer which have questioned some of the methods utilised in the hazard study. For example McCue (2013) discusses the reduction in hazard for Tasmania presented by GA to be due to the assessment only considering records post 1965 and ignoring paleo-seismological records on the basis of incomplete samples. A potential solution to the lack of agreement amongst experts about the seismicity of Australia for the purpose of the design of new buildings is to provide a minimal threshold hazard level as proposed by some AEES members. Currently the proposed threshold is 0.08 g for a 500 year return period event which represents the current hazard for some of the capital cities of Australia, including Melbourne and Sydney. At present there is still no consensus about the most appropriate hazard map and generalised response spectra for Australia, thus making the task of assessing structures very challenging. For the purpose of assessment in this study, the hazard values in AS 1170.4:2007 will be used as a guide to represent the seismicity of Australia since it is the current well established model which is available. In addition, it provides conservative approximations in comparison to the new models proposed by GA.

2.3 SEISMIC SITE RESPONSE AND REVIEW OF EXISTING APPROACHES

Modification of the seismic shear waves takes place as they travel through the soil or rock overlying the bedrock. Thus, local site conditions have a significant effect on the ground's response to seismic excitation. However, there are significant limitations to the approach adopted by many codes to classify sites and incorporate site effects to obtain the response spectra corresponding to various site conditions. In particular, most of the adopted methods are unable to represent the true ground response behaviour of soil sites since site resonance effects are not fully incorporated due to the averaging process involved in obtaining amplification factors and the lack of consideration of the depth of soil to bedrock. Recent studies have highlighted that such methods are particularly unsuitable for regions of low-to-moderate seismicity where buildings typically have low ductility and hence are incapable of damping soil-structure resonance effects (Lam & Wilson, 2004; Tsang et al., 2013). The following subsections describe codified and well established methods that are currently used to define site classification systems and to incorporate site effects when developing suitable response spectra for design.

2.3.1 Site classification system

Many site classification systems define sites based on qualitative descriptions and quantitative measurements to represent the stiffness of the sites. The National Earthquake

Hazards Reduction Program, NEHRP (Federal Emergency Management Agency, 2003), the International Building Code (International Code Council, 2012) and the European Code, EN 1998-1 (European Standard, 2004b), define sites according to the weighted average shear wave velocity over a depth of 30 m (V_{s30}):

$$V_{s30} = \frac{30}{\sum_{i=1}^{n}\left(\frac{d_i}{v_{si}}\right)} \quad \text{Eq. 2-1}$$

Where d_i is the thickness of the soil layer i (within a depth of 30 m from the ground surface)

v_{si} is the shear wave velocity of layer i

The use of V_{s30} to categorise sites is based on numerous empirical studies, initially conducted by Borcherdt in 1993 (cited in Dobry et al., 2000) which showed a correlation between amplification factors and sites defined according to V_{s30}. In addition, such a method is preferred in practice because it provides a simple and consistent manner to categorise sites. However, studies have shown that the combination of both depth to bedrock (d) and the weighted average shear wave velocity (V_s), which define the fundamental natural site period (T_s), is required to accurately categorise sites (Pitilakis et al., 2013; Rodríguez-Marek et al., 1999; Rodríguez-Marek et al., 2001). This is because T_s, which may be calculated by using Eq. 2-2, provides a better indication of the site's response to seismic excitation. Furthermore, recent studies focusing on site response of shallow bedrock regions have also highlighted the limitation of V_{s30} since the stiffness of sites is over-predicted for sites with a depth to bedrock that is less than 30 m deep (Anbazhagan et al., 2013; Lee et al., 2012) and this may lead to an under-prediction of the site response. Therefore, instead of V_{s30} it is suggested that V_s is calculated over a depth of soil from the surface to the depth at which rock conditions (typically defined as having shear wave velocities greater than 760 m/s) or a significant impedance contrast is reached.

$$T_s = \frac{4\sum_{i=1}^{n}(d_i)}{V_s} \quad \text{Eq. 2-2}$$

Where V_s is the weighted average shear wave velocity over the full depth of the profile until rock conditions are reached and defined as:

$$V_s = \frac{\sum_{i=1}^{n}(d_i)}{\sum_{i=1}^{n}\left(\frac{d_i}{v_{si}}\right)}$$

d_i is the thickness of the soil layer i (over the full depth of the profile until rock conditions are reached)

The Australian and New Zealand earthquake loading standards, AS 1170.4:2007 and NZS 1170.5:2004 incorporate T_s to define some of the non-rock classes. It should be noted, however, that in AS 1170.4:2007 and NZS 1170.5:2004 the site class B which refers to rock site conditions, is based on V_{s30} within the range of 360-1500 m/s. This range is much greater than the other codes, which usually restrict the rock class to a minimum V_{s30} of 760 m/s or 800 m/s to exclude weathered rock conditions which can, in fact, behave significantly differently to competent rock (Rodríguez-Marek et al., 1999; Rodríguez-Marek et al., 2001). Comparisons of site classification from various guidelines and standards are provided in Table 2-1.

Table 2-1: Site classifications of various codes

Class & description according to AS 1170.4 (2007)		AS 1170.4 (2007) & NZS 1170.5 (2004)	NEHRP (2003)	EN 1998-1 (2004)
A	Hard rock	$V_{s30} > 1500$	$V_{s30} > 1500$	$V_{s30} > 800$
B	Rock	$360 \le V_{s30} \le 1500$	$760 < V_{s30} \le 1500$	
C	Shallow soil sites	$T_s \le 0.6$	$360 < V_{s30} \le 760$	$360 < V_{s30} < 800$
D	Deep or soft soil	$T_s > 0.6$	$180 < V_{s30} \le 360$	$180 < V_{s30} < 360$
E	Very soft soil	$V_{s10} \le 150$	$V_{s30} < 180$	$V_{s30} < 180$
NA*	Shallow soft sites			$180 < V_{s5\text{-}20} < 360$
NA*	Sites requiring special evaluation	Not provided	Generally high plasticity clays, weak, vulnerable and liquefiable soils	

*Category not available in AS 1170.4:2007

2.3.2 Incorporation of site effects

Based on the site classifications, response spectra for the various classes are usually obtained by modifying the rock response spectra by the use of amplification factors. These amplification factors are based on studies which obtain the response spectra of the various classes by taking the average site response from various historical records or alternatively from numerical analyses representative of a particular class. The amplification factors are then calculated at specific periods corresponding to acceleration

and velocity controlled regions, F_a and F_v respectively, as shown in Figure 2-7. This approach was adopted by the study conducted by Crouse and McGuire (1996) which has formed the basis of the International Building Code and AS 1170.4 (Wilson & Lam, 2007).

There are two key limitations to this approach. Firstly, the response spectrum obtained is highly dependent on the range of site profiles considered in the analysis. Thus the spectra proposed by these studies are highly dependent on the particular profiles or records included in the database. Secondly, the averaging process utilised to obtain amplification factors results in the loss of the true ground response behaviour; this is particularly evident with respect to the maximum displacement response associated with resonance effects. The response experienced at the surface of a site is due to modifications of the seismic shear waves by the soil/rock overlying the bedrock which are strongly influenced by the impedance contrast between the rock and soil layers and the thickness of the soil layers (Lam et al., 2001). Studies conducted for low-to-moderate seismic regions have highlighted that the maximum displacement response of soil sites is predominantly due to resonance effects of the reflected wave components of the propogating seismic wave with period similar to the period of the site during seismic excitation. Therefore, these studies have suggested that the period at which maximum displacement response occurs, may be approximated by the period of the site during an earthquake (Chandler et al., 2001; Lam et al., 2001; Tsang et al., 2006a, 2006b). This period, at which resonance effects are observed, is longer than the initial site period due to stiffness degradation experienced by the soil during the earthquake, and therefore it referred to as the degraded (or final) site period in this study. However, it is noted that, this phenomenon (i.e. maximum displacement response occuring at approximately the site period) is mainly observed for low-to-moderate levels of seismic excitation since the strains induced in the soil are minimal, and therefore the softening of the initial site period is minimal during the excitation. For a higher level of seismic excitation, the contribution of nonlinear effects of the soil becomes more predominant and the final degraded period of the site may be significantly longer than the period at which resonance effects take place during seismic excitation.

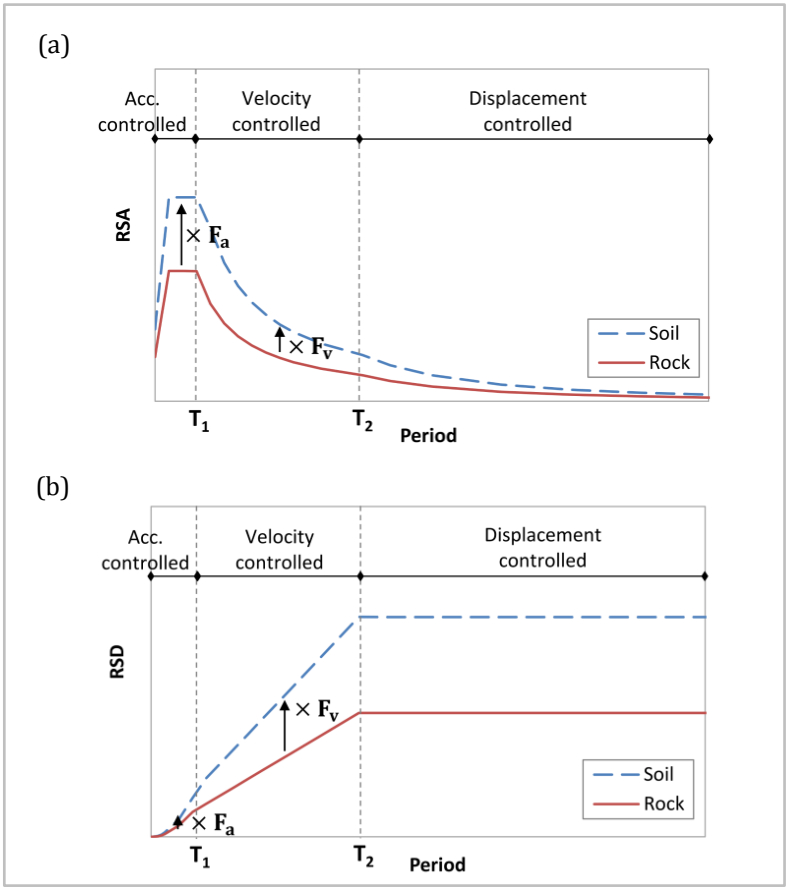

Figure 2-7: Response spectra showing acceleration, velocity, and displacement controlled regions: (a) acceleration response spectra, (b) displacement response spectra

Based on the mechanisms discussed, it is clear that both V_s and depth to bedrock are important parameters contributing to seismic site response. Therefore, studies which calculate the average response of a site, especially when sites have been categorised according to V_{s30}, are incapable of capturing the true site response since site resonance effects are smeared. This problem associated with the averaging process is well known and it is accepted in regions of high seismicity on the basis that site-structure resonance effects can be suppressed by the damping of structures; however, this is not the case for non-ductile buildings which are common in low-to-moderate seismic regions (Lam & Wilson, 2004; Tsang et al., 2013). Therefore it is not appropriate for the response spectra in codes to implicitly assume a certain level of energy dissipation capability of the building in regions of low-to-moderate seismicity where limited consideration is given to seismic resistant design.

The code approach to obtain the displacement response spectra (RSD) is to calculate it from the acceleration response spectra (RSA) using the relationship; $RSD = \left(\frac{T}{2\pi}\right)^2 RSA$. A critical parameter for defining the RSD is the second corner period (T_2), shown in Figure

2-7(b). The averaging process discussed previously has also resulted in a poor estimation of T_2 (Lumantarna et al., 2012). For rock conditions, T_2 is currently based on the maximum considered earthquake magnitude and has been determined as 1.5 seconds for Australia based on extensive studies conducted by Lam et al. (2000a, 2000b). Interestingly, the use of the same value of T_2 has also been extended to all other site classes in AS 1170.4:2007 and other codes such as EN 1998-1:2004, even though it is well recognised that there is a significant difference between the seismic response of rock and soil sites. Instead of using this simplified approach it would be preferable to define T_2 correctly for the various site classes, as the accuracy of the resulting RSD is strongly influenced by this variable. It is also noted that an improved idealisation of the RSD in the longer period range is preferred to account for the significant reduction in response after the maximum displacement response for some soil sites. The European code (European Standard, 2004b) accounts for this behaviour in the Annex, by providing an alternative RSD for regions of high seismicity in which the displacement gradually reduces to the peak ground displacement at a period of ten seconds.

2.3.3 Effect of ground stiffness on acceleration response spectra

The stiffness of the ground above the bedrock has the greatest influence on the seismic response of sites. It is generally accepted that the acceleration response of sites increases as the site becomes softer, which is consistent with wave theories on impedance discontinuity. This is illustrated in Figure 2-8, where the spectral ordinates provided in AS 1170.4:2007 are plotted for the various site classes. Conversely, some studies (Dhakal et al., 2013; Seed et al., 1976) have shown that in the acceleration controlled region, the acceleration response of stiffer sites is higher in comparison to softer sites. This observation is in agreement with basic structural dynamic theory, that is, stiffer systems experience higher acceleration response (Dhakal et al., 2013). This is illustrated by the response spectra of three different site conditions from the 2011 Christchurch earthquake, recorded at stations LPCC, LPOC and HVSC which are all within approximately 1 km from each other, shown in Figure 2-9. For periods greater than approximately 1.3 seconds, it is observed that for the soft site the response is greater than the other two stiffer sites (V_{s30} of 650 m/s and 422 m/s). However, for the lower period range (i.e. periods less than 1.3 seconds), the response of the stiffer sites is significantly greater than for the soft sites.

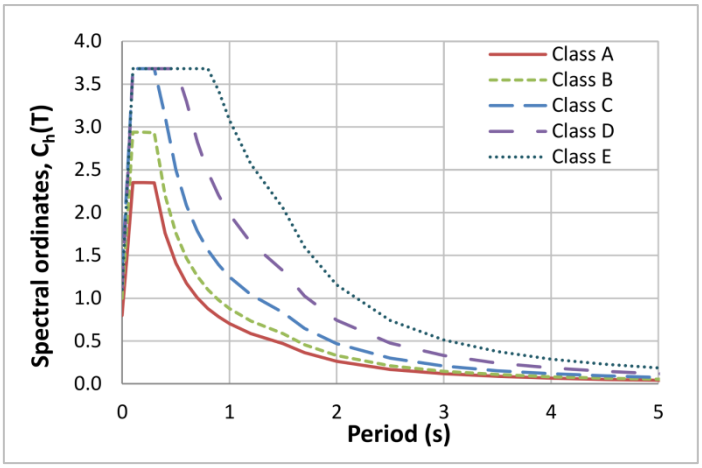

Figure 2-8: Spectral shape factors in AS 1170.4:2007

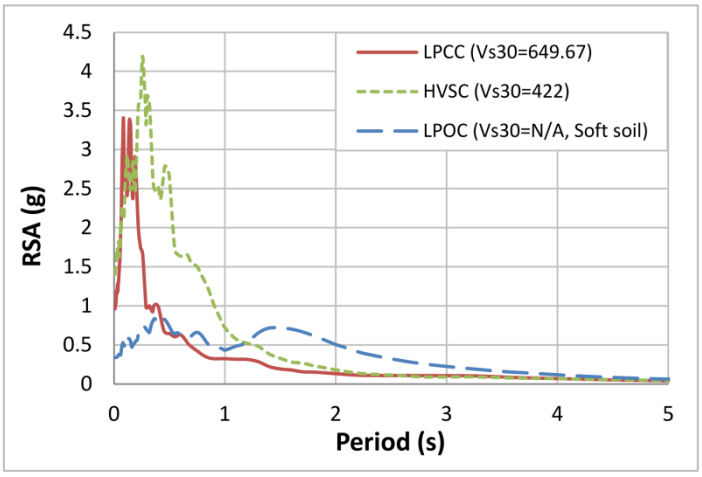

Figure 2-9: Three recordings of the 2011 Christchurch earthquake from stations located at close proximity to each other

2.3.4 Effect of bedrock motion intensity

Higher intensity ground motions induce lower amplification of seismic waves relative to that induced by lower intensity motions since, in the case of higher intensities, the site experiences greater nonlinear behaviour due to high levels of strain degradation. Hence the rock/soil overlying the bedrock has a lower ability to transfer the higher intensity seismic waves to the surface. The effects of bedrock motion intensity have been incorporated in some codes and guidelines including NEHRP. However, some codes, including AS 1170.4:2007 do not currently account for these effects. The incorporation of lower amplification factors for higher intensities is becoming more important with the introduction of performance objectives in the design of buildings which require collapse prevention under higher return period events.

2.4 SEISMIC SITE RESPONSE ANALYSIS LEADING TO REVISED DESIGN RESPONSE SPECTRA FOR AUSTRALIA

Section 2.3 identified key limitations of current approaches used to incorporate site effects when developing response spectra which are used for design and assessment of buildings. Therefore a detailed study has been undertaken to explore the effects of local site conditions on seismic site response. In particular, the study examines the validity of the approach adopted in AS 1170.4:2007. This is achieved by conducting an extensive numerical analysis to examine the effects of weighted average site shear wave velocity (V_s), depth to bedrock (d), and intensity of earthquakes on the site response for rock, sand and clay sites. The primary focus of this study is improving the method used to obtain the displacement response spectra since an accurate representation of this is needed in the displacement-based seismic design and assessment of buildings. Thus the key contribution from this study is the proposal for a new systematic method to obtain the RSD for various site classes (for 5 % damping) directly from a hard rock response spectrum. This spectrum is assumed to be known and would ideally be produced using probabilistic seismic hazard analysis (PSHA) studies. The principle behind the approach used to find the RSD is similar to that used in the theoretical models proposed by Lam et al. (2001) and Tsang et al. (2006a, 2006b). It is based on the correlations that exist between initial site properties of individual rock/soil profiles and site response parameters. These site response parameters include: (i) amplification factors, defined as the ratio between the response spectrum at the ground surface and at the outcrop rock, and (ii) the degraded fundamental natural site period, which is the period of the site after seismic excitation. A method is also suggested for obtaining the acceleration response spectra for the various site classes and this is calculated from the proposed RSD. Furthermore, modifications to the site classification systems incorporated in AS 1170.4:2007 are recommended.

It is emphasised that the proposed method is developed in such a way as to be suitable for standards and codes and hence it provides response spectra that are characteristic of a general class of site conditions. Therefore, the method presented is not intended to replace site specific studies where the site response is obtained via 1-, 2-, and 3-dimensional equivalent linear or nonlinear analyses. These studies are typically conducted for larger scale projects for which detailed ground conditions are known. For smaller scale projects, especially in regions of low-to-moderate seismicity, site investigations are often limited in scope and the shear wave velocity of the rock/soil, which is a critical parameter required to categorise sites, is estimated simply from empirical correlations with other ground investigation parameters such as Standard Penetration Test (SPT) N-values. There will

usually be considerable inaccuracy in these estimates. Therefore, it is important for the response spectra in standards and codes to account for uncertainties associated with determining site properties, as well as the inherent variability of soils and rocks, by providing response spectra which are representative of a class of site conditions and providing the maximum response over a range of possible sites within that class.

2.4.1 Methodology and numerical analysis procedure

Numerical analyses of various site conditions have been conducted to obtain a better understanding of the effect of the weighted average site shear wave velocity, depth of rock/soil to bedrock, soil type and intensity of earthquake. Equivalent-linear programs are commonly used for seismic site response analysis especially when it is expected that the site will experience relatively small strain levels, which is commonly the case for low-to-moderate seismic regions. Papaspiliou et al. (2012) suggest that the difference between equivalent-linear and nonlinear programs is minimal for clay sites with strain limits less than 1 %, and 0.5 % for sandy sites. Since almost all of the sites for this study experienced strains less than these values, the analysis has been conducted with the well-established equivalent-linear, one-dimensional site-specific response program, SHAKE2000 (Ordonez, 2014).

The following subsections describe the three key steps involved in the numerical analysis; that is, the selection of input ground motions, the selection of site properties, and the analysis of site response.

2.4.1.1 Selection of input ground motions

Ground motions were selected such that their median response spectra match the RSA and RSD corresponding to Class A in AS 1170.4:2007 for k_pZ factors of 0.1 g and 0.3 g. The k_pZ factors in AS 1170.4:2007 have been established for Class B rock conditions and correspond to the peak ground acceleration (PGA), where k_p is the probability factor for the annual probability of exceedance for the limit state under consideration, and Z is the hazard earthquake factor which is equivalent to the PGA on a Class B site for a 500 year return period (YRP) event. Since the Class A spectra is lower than the Class B by a factor of 0.8 in AS 1170.4:2007, the PGAs of 0.1 g and 0.3 g for Class B correspond to PGAs of 0.08 g and 0.24 g respectively for Class A hard rock conditions. The k_pZ factors of 0.1 g and 0.3 g approximately correspond to 500 and 2500 YRP events, respectively for most of the major cities of Australia. This covers the range of return periods for which buildings must be designed in accordance with the current National Construction Code (NCC) (Australian Building Code Board, 2016). It is noted that a k_p value of 3 instead of 1.8 as suggested in

AS 1170.4:2007 was selected to represent the probability factor for a 2500 year return period event. This is because, as discussed Section 2.2, it is believed that the current k_p values in AS 1170.4:2007 underestimate the increase in the level of shaking between low and high return period events. While there are no stringent rules, ground motions have been selected following Kramer (1996) using (i) historical records which are representative of earthquakes within the region of interest, supplemented by (ii) generated or artificial earthquakes, since sufficient suitable historical records are not available.

Historical records have been obtained from the Pacific Earthquake Engineering Research Center (PEER, 2014) and the Internet Site for European Strong-Motion Database (ISESD, 2014), as they contain high quality processed ground motions. Accelerograms on rock were selected based on characteristics typical of Australian earthquakes: shallow earthquakes with reverse fault mechanisms (Brown & Gibson, 2004), and realistic magnitude and distance (M-R) combinations based on the attenuation models from Gaull et al. (1990) and Lam et al. (2000a).

Furthermore, to avoid problems associated with simple amplitude scaling, stochastically generated earthquakes were obtained using the program GENQKE (Lam, 1999) which is capable of producing ground motions that are representative of Australian earthquakes. This was to ensure that sufficient records can be used in order to obtain statistical stability. In total, 45 and 42 horizontal ground motions were obtained for k_pZ factors of 0.1 g and 0.3 g, respectively. Approximately 40 % of these records were historical and the remaining were generated ground motions. Details of the selected historical and stochastically generated earthquakes are provided in Appendix A.

Figure 2-10 and Figure 2-11 show the RSA and RSD of the selected ground motions and their median compared with the target spectra for k_pZ factors of 0.1 g and 0.3 g, respectively. It is noted that the RSA and RSD provided in AS 1170.4:2007 and the generated ground motions are valid up to a period of five seconds, therefore the results in this study are presented for natural periods of up to five seconds.

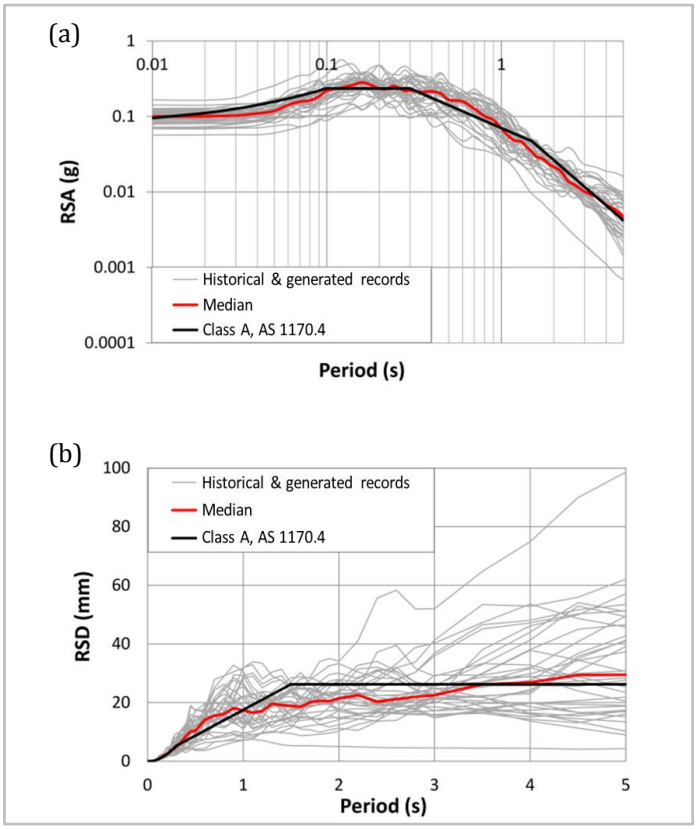

Figure 2-10: Input ground motions and target spectra for k_pZ factor of 0.1 g: (a) RSA, (b) RSD

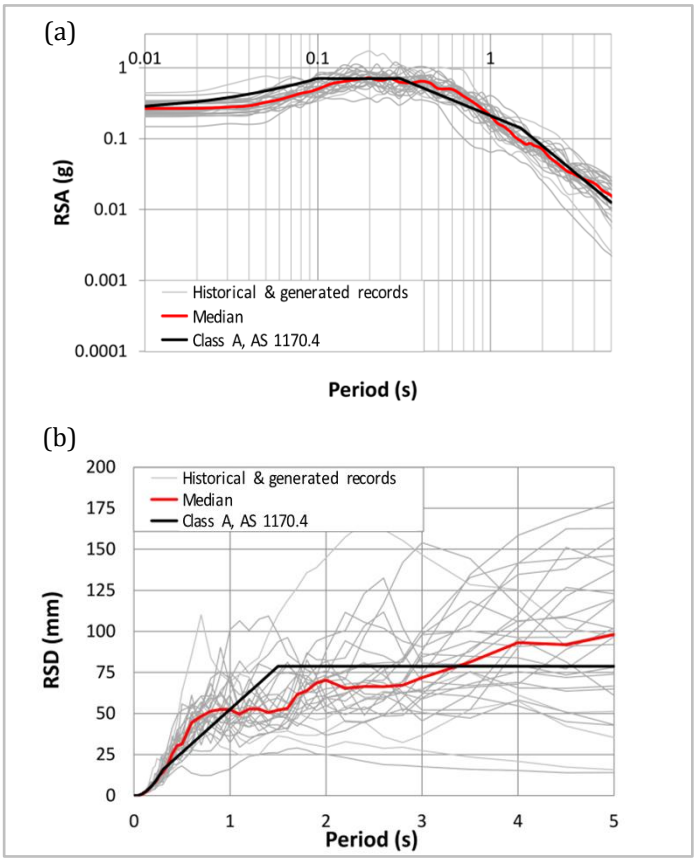

Figure 2-11: Input ground motions and target spectra for k_pZ factor of 0.3 g: (a) RSA, (b) RSD

2.4.1.2 Selection of site properties

The most important site properties in seismic site response analysis are the shear wave velocity profiles of the soil layers down to the bedrock, the shear wave velocity of the bedrock and the nonlinear properties including shear modulus reduction and damping curves which are defined according to the selected type of rock and soil. The selection of these properties is discussed in the following subsections.

2.4.1.2.1 Shear wave velocity profiles and depth to bedrock

The relationship between the shear wave velocity and depth is highly variable as illustrated in Figure 2-12 which shows the rock/soil profiles of 50 sites across Australia. These profiles were obtained by Kayen et al. (2015) using spectral analysis of surface waves methods, however, it is noted that such methods are not conducted in regular site investigations in Australia to determine the site conditions for the construction of structures. Instead, the shear wave velocity profile of sites is based on other ground investigation parameters such as SPT N-values. Since the aim of this study was to establish a systematic approach to obtain the response spectra for a range of site conditions possible within a site category, the analysis has been conducted for rock and soil profiles which have weighted average shear wave velocities and site periods ranging from the minimum and maximum possible values allowed within each category, for depths to bedrock of 30 to 150 m. The combination of V_S and depth to bedrock of the profiles considered are selected such that their site period values are within those calculated from the 50 Australian shear wave velocity profiles provided in Figure 2-12. This ensures that the sites considered are representative of real sites. It is noted that some studies have highlighted that the seismic site response can vary depending on the variability of the shear wave velocity of the different layers within a profile (Lam & Wilson, 2004). However other studies have stated that the difference in response between a site in which the properties of the given layers have been considered explicitly and that in which the same site has been modelled with a weighted average shear wave velocity over the depth to bedrock is insignificant (Dhakal et al., 2013). The effect of layering of soil deposits on seismic response varies from one case to another, and consideration of the many possible combinations of soil layering is beyond the scope of this study. Nevertheless, analysis of existing shear wave velocity profiles with varying shear wave velocity are also presented in the results (Section 2.4.4.4) to illustrate that the proposed response spectra are capable of capturing the response of sites with realistic shear wave velocity profiles. It is also noted that the effect of layering of a site may be particularly important for sites which have very low shear wave velocity at shallow depths and abrupt transitions to much

higher shear wave velocities; these sites are typically classified as Class E in AS 1170.4:2007 which is not examined in this study.

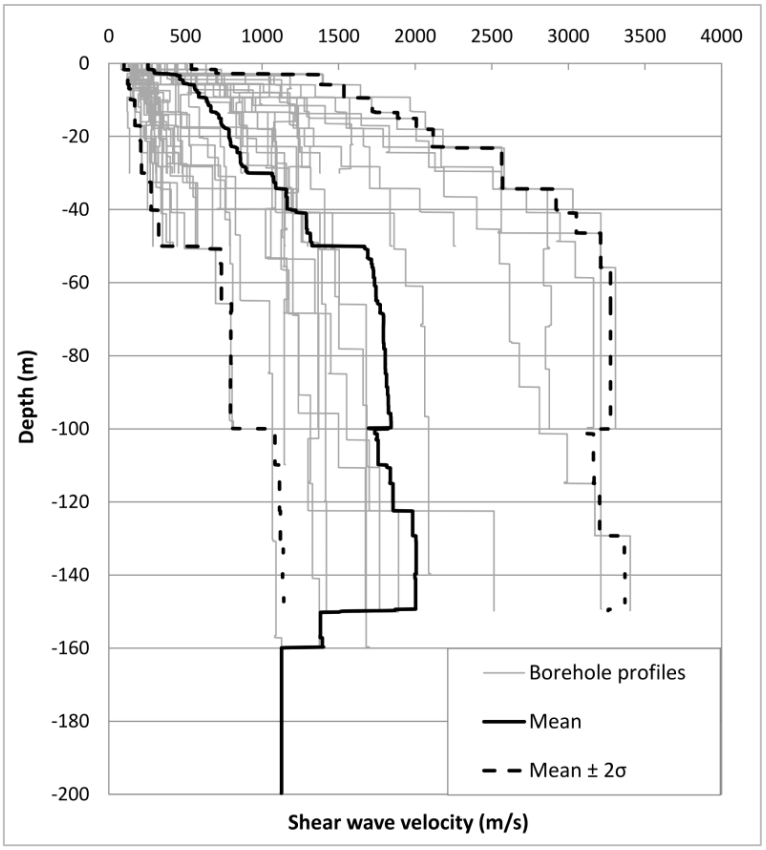

Figure 2-12: Shear wave velocity profiles of 50 sites around Australia from Kayen et al. (2015)

The appropriate selection of the shear wave velocity of the bedrock is also important and challenging since it varies from site to site and with depth. Sensitivity studies investigating the effect of bedrock shear wave velocity on amplification factors have shown that the amplification factors can increase between 20-30 % when the bedrock shear wave velocities are increased from 1000 m/s to 3000 m/s (Lam et al., 2001; Venkatesan et al., 2006). Various bedrock shear wave velocities have been reported in the literature for Australia, ranging from 900 m/s to approximately 3500 m/s (Kayen et al., 2015; McPherson & Hall, 2013). Based on the shear wave velocity profiles provided by Kayen et al. (2015) (shown in Figure 2-12) it can be seen that the higher bedrock shear wave velocities are achieved with a gradual increase in shear wave velocity of the rock. Since this is not explicitly modelled in the analysis conducted it would be over-conservative to adopt very high bedrock shear wave velocities because there would be an unrealistic change in the impedance between the bedrock and soil/rock profile. In addition, for this study it was desired to normalise the amplification factors with respect to Class A (hard rock) in order to obtain the amplification factors between Class A and Class B (discussed

in Section 2.4.1.3), therefore it was necessary to adopt a bedrock shear wave velocity greater than 1500 m/s. Thus, based on these factors the bedrock shear wave velocity of 1800 m/s was selected to be suitable for this study.

2.4.1.2.2 Soil type - nonlinear properties

Currently standards and codes do not explicitly distinguish the response between sand (cohesionless soils) and clay (cohesive soils) sites, even though their seismic response is significantly different (Papaspiliou et al., 2012). The difference in response of various types of soils is predominantly due to their nonlinear properties such as shear modulus reduction and damping curves, which are dependent on the plasticity index (PI) (Dobry et al., 2000; Tsang et al., 2006a, 2006b). Soils with higher PI display higher amplification of seismic waves because they exhibit less nonlinear behaviour with lower shear modulus degradation and lower damping at high strain levels. The analysis for this study has been conducted for rock, sand and clay sites. The following rock and soil models were selected in SHAKE2000 (Ordonez, 2014):

- Rock: Schnabel 1973
- Sand: average, Seed and Idriss 1970
- Clay: PI=30, OCR1-15, Vucetic and Dobry 1991

It is noted that a plasticity index of 30 % that was selected to represent clay sites is typically considered as moderate to high. The high plasticity was selected to provide response that is conservative for most clay sites. Sand sites were also analysed to obtain results for sites with zero plasticity.

2.4.1.3 Analysis of site response

In total more than 50 rock/soil profiles were analysed for each of the two earthquake intensities considered; k_pZ factors of 0.1 g and 0.3 g. The surface acceleration and displacement response spectra for each individual rock or soil profile were obtained by calculating the median of the responses obtained from SHAKE2000 (Ordonez, 2014). It is noted that the geometric mean of each pair of historical responses was calculated first before the median was calculated. In addition, the amplification spectra were calculated for each rock or soil profile as they provide important insights about the effects of various ground conditions and this process minimises the effect of input ground motion variability. The amplification spectra were calculated by dividing the acceleration response spectra for each individual record by the acceleration response spectra for the outcrop bedrock motion corresponding to that record at each period. The median amplification spectra for each rock/soil profile were then calculated in a similar manner to the RSA and RSD. It is highlighted that in this study amplification spectra and therefore

amplification factors have been calculated relative to Class A response spectra rather than Class B.

2.4.2 Results: observed correlations and trends

In order to establish a systematic method to obtain the response spectra for the various site conditions, it is important to first identify the correlations that exist between initial site properties and site response parameters. The following section presents the key correlations and trends which were observed.

2.4.2.1 Site amplification factor

The strongest correlation which exists between amplification factors and site properties is between the magnitude of the maximum amplification factor of a site, referred to as site amplification factor (F_{site}) and the site's average shear wave velocity. Furthermore, as expected, the period at which F_{site} occurs is associated with the site period and it approximately corresponds to the degraded site (or final) period (T_{sf}) which accounts for the stiffness degradation experienced by the site during seismic excitation. This signifies the importance of considering both the average shear wave velocity and the depth of rock/soil to bedrock when evaluating the seismic response for different site conditions. While the magnitude of F_{site} can be similar for sites with the same V_s with various depths to bedrock, the actual response, such as the displacement response, can vary significantly. This is illustrated in Figure 2-13 where the amplification and displacement response spectra are provided for three sites with different depths to bedrock but with the same V_s of 360 m/s. It is observed that the value of the F_{site} factor obtained for all three sites is similar, however, the maximum displacement response of the sites varies significantly. This is because the rock response is significantly higher at longer periods, consequently resulting, for the same amplification factor, in a higher displacement response for a deeper site (which has a longer site period).

In Figure 2-14 the F_{site} factor is plotted against V_s for the various site conditions. It is noted that since the results for soft/weathered rock with V_s less than 760 m/s were similar to clay sites, the response parameters for rock sites with V_s between 360 m/s and 760 m/s are plotted with the clay site response parameters. As expected, it is shown that the amplification factors are generally lower for higher intensity ground motions. The difference in response is more apparent at sites with lower V_s as their response is governed more strongly by nonlinear behaviour. More interestingly, it is observed that there is also a significant difference between sand and clay sites. This illustrates the dependency of seismic site response on the level of shear modulus degradation and

damping and hence the importance of considering the soil type when evaluating the response of various site conditions.

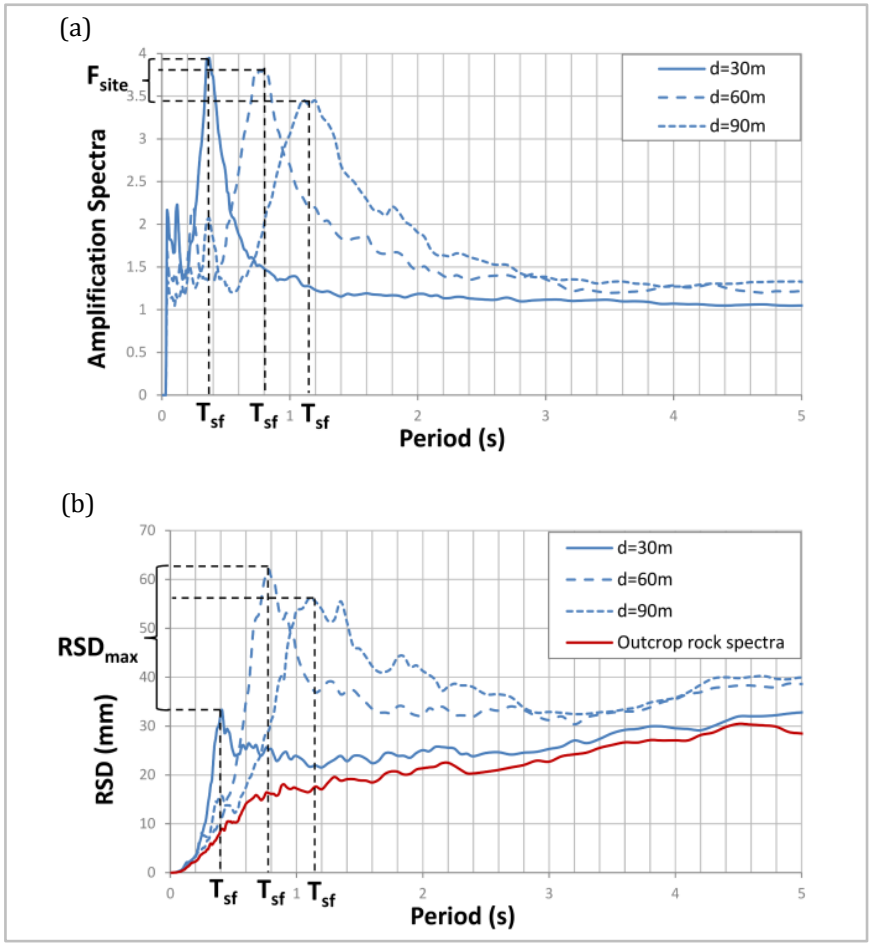

Figure 2-13: Response spectra of three soil profiles with constant shear wave velocity of 360 m/s with varying depths: (a) amplification spectra, (b) displacement response spectra

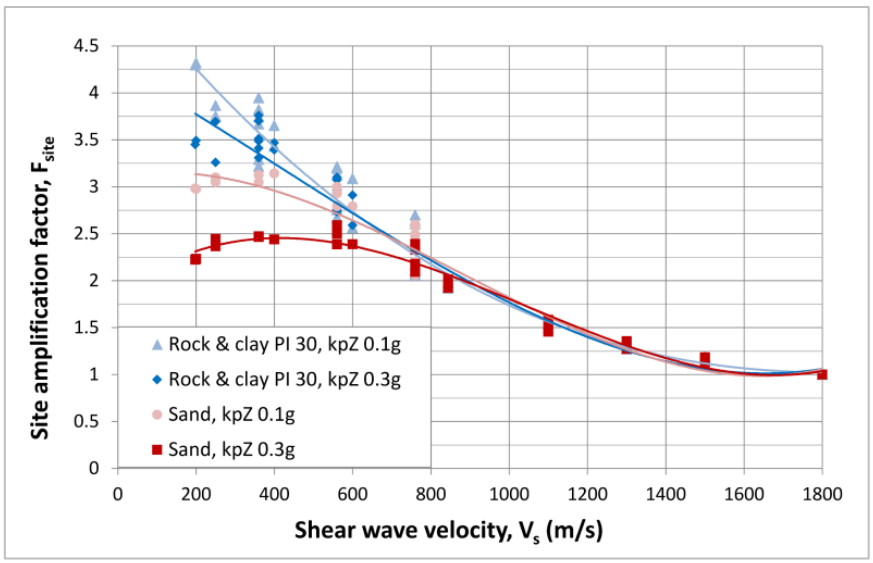

Figure 2-14: Site amplification factors versus average shear wave velocity for various site conditions

2.4.2.2 Ratio of final to initial site period and V_s

It is also observed that there is a correlation between the ratio of the degraded site period to initial site period (T_{sf}/T_{si}) and the weighted average shear wave velocity of the site, as illustrated in Figure 2-15. As the intensity of the earthquake increases, the T_{sf}/T_{si} increases since the site experiences greater shear strain and hence greater degradation (softening). Furthermore, the results show that, in general, sand sites experience higher degradation than rock and clay sites since it is observed that the T_{sf}/T_{si} is significantly larger for sand sites.

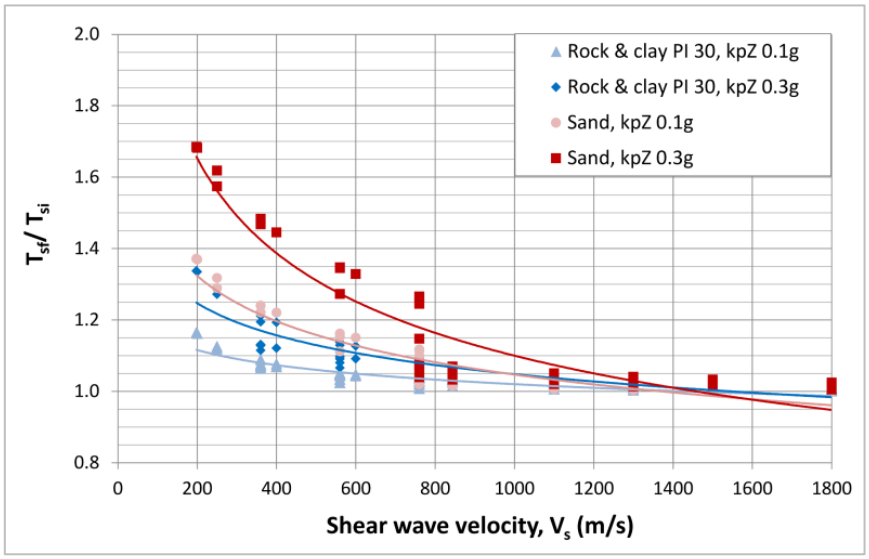

Figure 2-15: T_{sf}/T_{si} versus average shear wave velocity for various site conditions

Based on the correlations observed in Figure 2-14 and Figure 2-15 it is possible to estimate the maximum displacement response (RSD_{max}) of soft rock/soil sites:

$$RSD_{max} = RSD_{rock\ at\ T_{sf}} \times F_{site} \qquad \text{Eq. 2-3}$$

Where RSD_{max} is the maximum site displacement response

$RSD_{rock\ at\ T_{sf}}$ is the rock displacement response at the site's degraded period (T_{sf})

Eq. 2-3 is commonly used by theoretical models to create a bi-linear RSD for soil and soft rock sites, as illustrated in Figure 2-16.

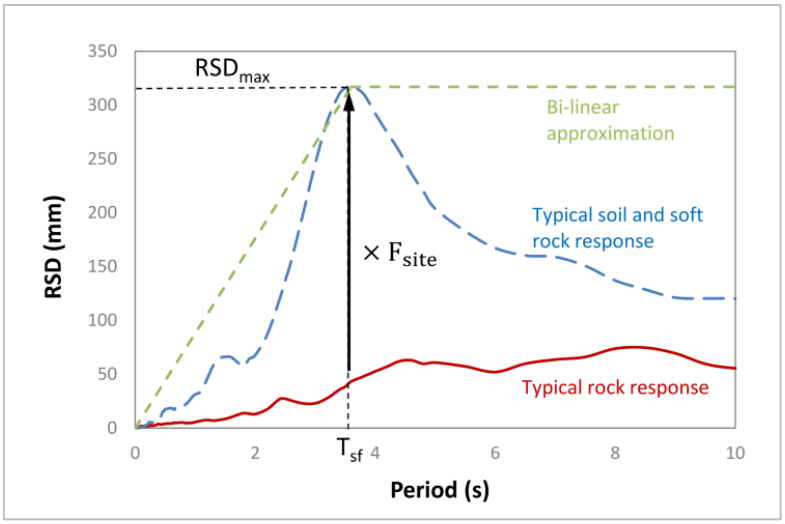

Figure 2-16: Typical rock and soil RSD

2.4.2.3 Acceleration response of various site conditions

The correlations discussed thus far provide a systematic method to obtain the RSD for the various site conditions. In order to be able to calculate a representative RSA from the RSD it is necessary to understand the behaviour of the various sites in the acceleration controlled region. The first corner period (T_1), which defines the period at which the acceleration response starts to decrease, is a critical parameter used to define the RSA. T_1 is particularly important when the RSA is derived from the RSD as it directly controls the magnitude of the maximum acceleration response (RSA_{max}). It is not possible to establish a direct correlation between T_1 and site properties, since T_1 is also related to the input ground motions. As discussed by Chandler et al. (2001), the period at which the maximum acceleration response occurs is influenced by the dominant period of the bedrock motion. Therefore, in this study T_1 will be based on the observed acceleration response to the considered ground motions.

To illustrate the trend in behaviour for various site conditions, amplification factors in the acceleration controlled region (F_a) have been calculated at the period at which RSA_{max} of the site occurs for the k_pZ factor of 0.1 g (shown in Figure 2-17). In Figure 2-17(a) it is evident that when the sites are categorised according to the fundamental initial site period, stiffer sites (low T_{si}) tend to experience higher acceleration response in comparison to softer sites (high T_{si}). However, when F_a is plotted against the average shear wave velocity, as shown in Figure 2-17(b), the trend in the behaviour of the sites is less conclusive and highly dependent on the depth to bedrock. This highlights the importance of the method used to categorise sites, in particular the effect of ground stiffness on seismic site response.

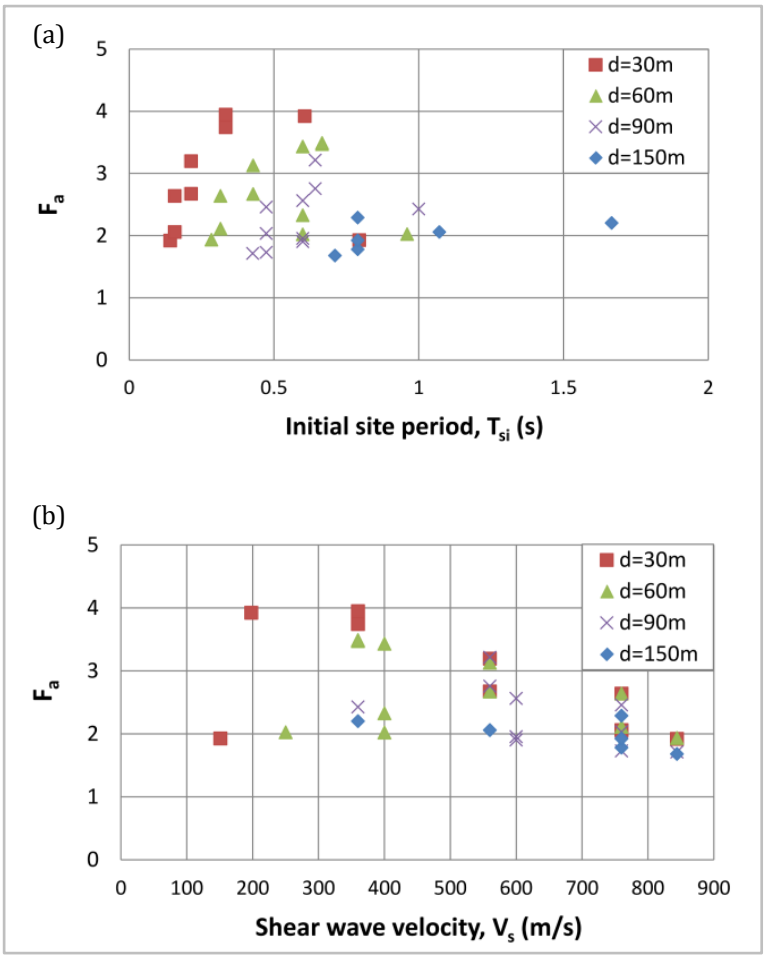

Figure 2-17: Amplification factors within the acceleration controlled region for rock and clay sites for k_pZ factor of 0.1 g: (a) sites categorised according to T_{si}, (b) sites categorised according to V_s

2.4.3 Comparison between numerical analyses and historical records

This section provides a comparison between the correlations and trends observed from the numerical analyses with those from historical records. In order to accurately determine site effects observed from past earthquake events it is necessary to obtain records at the surface of the ground and at the bedrock level. However, the availability (and quality) of such records are limited, therefore for this study historical records on competent rock and soil (and softer rock) sites at close proximity to each other for a single event have been selected. The selection process involved carefully examining the records to ensure other factors influencing the observed response were minimal. This included selecting soil (and soft rock) records which were within 500 m of the competent rock record and positioned on the same side of the fault. In addition, records were selected with competent rock records with PGAs up to 0.2 g such that the results are comparable with those obtained from the numerical analysis for k_pZ factor of 0.1 g. In total, 14 soil (and soft rock) records were obtained from the PEER (2014) database.

The estimated F_{site} of the historical records (obtained from the amplification spectra), the line of best fit obtained from this study (for both rock and clay, and for sand), and the line of best fit obtained from the theoretical model developed by Tsang et al. (2006b) for a k_pZ factor of 0.1 g are plotted in Figure 2-18. It can be seen that majority of the historical F_{site} values are lower than the average response obtained from this study. This is expected since in this study the amplification factors are normalised with respect to Class A hard rock conditions (with V_s greater than 1500 m/s), whereas the historical records have been normalised with respect to rock conditions with average shear wave velocities varying from 790 to 1430 m/s, therefore resulting in lower amplifications. Furthermore, it can be seen that a good match is obtained between this study and the theoretical model by Tsang et al. (2006b) for clay and rock sites.

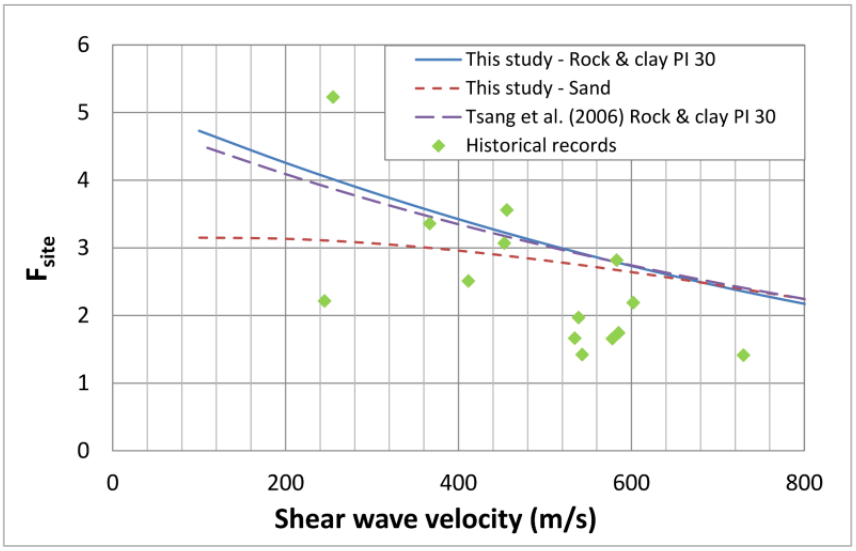

Figure 2-18: Site amplification factors obtained from this study, historical records and, Tsang et al. (2006b) theoretical model

In the numerical analyses presented in Section 2.4.2.3 it was observed that stiffer soil sites generally experienced a higher acceleration response in the short period range in comparison to softer sites (Figure 2-17(a)). This trend is also observed with the historical data (Figure 2-19(a)). In Figure 2-19(a) the F_a values are plotted against the degraded site period (T_{sf}) as opposed to the initial site period (T_{si}). This is because for the historical records it is only possible to approximate the degraded site period from the amplification spectra since insufficient information is provided about the depth to bedrock, and hence it is not possible to determine the initial site period. Nevertheless, it is generally shown that when sites are categorised according to the degraded site period, higher amplification factors occur for stiffer sites (sites with lower T_{sf}). However, when F_a is plotted against the average shear wave velocity of the site, the trend in behaviour of the various site

conditions is less conclusive. It is also noted that F_a for the numerical analyses and historical records are significantly higher than those suggested in AS 1170.4:2007 (normalised with respect to Class A) for the various classes. This is mainly due to the fact that the F_a plotted for this study and the historical records are representative of the amplification which occurs at RSA_{max} of the site, rather than the average amplification at a specific period in the acceleration controlled region. This also illustrates the limitation of the averaging procedure that is currently used to obtain the site spectra, as it may significantly under-estimate a response based on the range of profiles considered in the analysis.

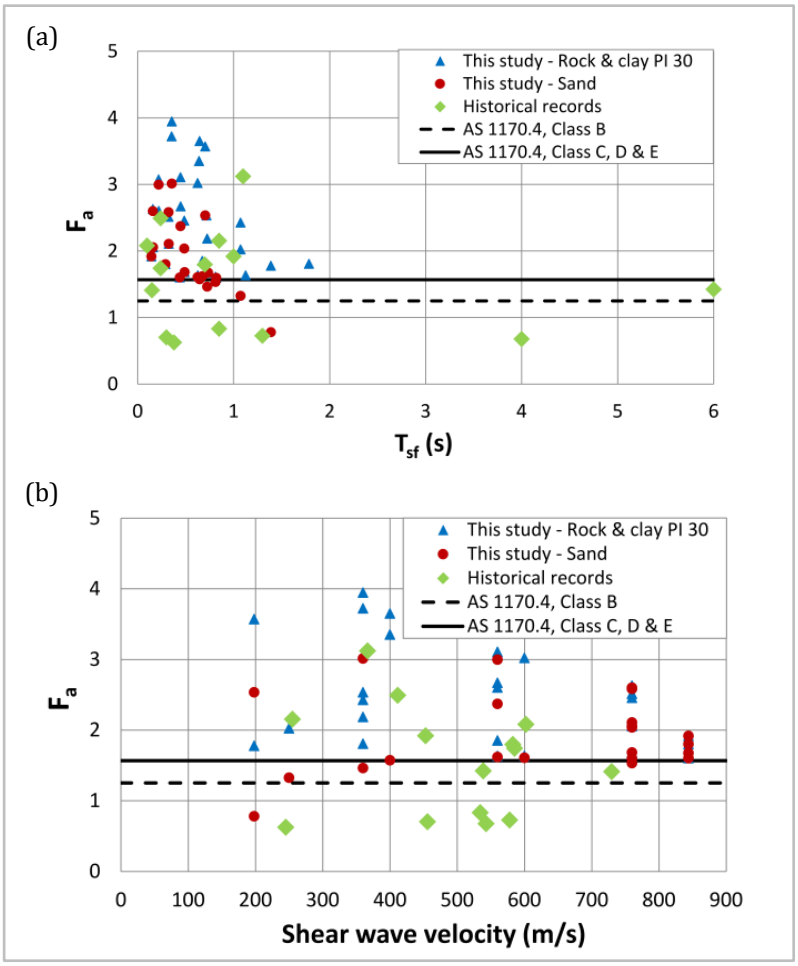

Figure 2-19: Amplification factors within the acceleration controlled region obtained from numerical analyses, historical records, and AS 1170.4: (a) sites categorised according to T_{sf}, (b) sites categorised according to V_s

2.4.4 Proposed model

2.4.4.1 Site classification system

Based on the observed behaviour of the various site conditions, amendments to the current site classification system in AS 1170.4:2007 are recommended as shown in Table

2-2. As it has been demonstrated, the site response of various site conditions is highly dependent on the average shear wave velocity of sites and depth to bedrock or when a significant impedance contrast is reached (especially for the displacement response), therefore the suggested classification system has a greater emphasis on the use of initial site period to categorise sites. The Class B rock condition is restricted to a minimum weighted average shear wave velocity of 760 m/s, since it was observed that soft/weathered rock behaved in a similar manner to the stiff clay condition and, as such, they are grouped together in Class C. It is noted that both Class A and B are classified according to V_S, rather than T_S, since it was observed that the effect of depth to bedrock is not very significant for rock sites with V_S greater than 760 m/s. Furthermore, Class C is restricted to a maximum site period of 0.6 seconds, similar to the classification system currently in AS 1170.4:2007. Class D is also restricted to a maximum site period of 1.6 seconds. This is because sites with site periods greater than 1.6 seconds correspond to very deep sites which may experience significant degradation and nonlinear effects and thus require a higher level of analysis to determine their response. Class E was not investigated in this study, however, it is suggested that it should be classified as sites requiring special evaluation since very soft and deep sites should be examined on a case by case basis. In addition, sites with very high plasticity, defined as a PI of 40 % or greater as recommended in EN 1998-1:2004 require special consideration and therefore they are also included in the definition of Class E sites. This is because high plasticity soils can experience significantly higher acceleration and displacement response. Furthermore, it is recommended that the type of soil should also be considered when determining the response spectra (especially for softer soils) as discussed in Section 2.4.4.2

Table 2-2: Recommended site classification

Site Class	**Description**	**Suggested site classification**	**AS 1170.4:2007 site classification**
A	Hard rock	$V_s > 1500$ m/s	$V_{s30} > 1500$ m/s
B	Rock	760 m/s ≤ V_s ≤ 1500 m/s	360 m/s ≤ V_{s30} ≤ 1500 m/s
C	Stiff shallow sites	$T_s \leq 0.6$ s	$T_s \leq 0.6$ s
D	Soft shallow sites or stiff deep sites	0.6 s < $T_s \leq 1.6$ s	$T_s > 0.6$ s
E	Very soft and deep sites requiring special evaluation	$T_s > 1.6$ s Or $V_{s10} \leq 150$ m/s Or high plasticity soils; PI > 40 %	$V_{s10} \leq 150$ m/s

2.4.4.2 Incorporation of site effects

Based on the observed correlations a systematic method is proposed to obtain the response spectra corresponding to the various site conditions. It differs from the approach typically adopted by the codes in that it does not use an averaging process to define the response of a particular class; instead, it is based on correlations that were observed for individual rock/soil profiles. The proposed method incorporates both the average shear wave velocity and depth to bedrock (which defines T_s) in the construction of the response spectra. Furthermore, it is conservatively recommended that the general design spectra for each site class should accommodate the worst case scenario which occurs within that class. Therefore corner periods and F_{site} have been defined such that the envelope of the median responses of the displacement response within each site class is obtained.

The graphical representation of the key parameters for the RSD is shown in Figure 2-20. The proposed model requires a hard rock displacement response spectrum which may be obtained from PSHA studies.

The critical parameters and the method required to construct the RSA and RSD are described in the next subsections. The suggested values for the parameters are provided in Table 2-3 and Table 2-4, which are in accordance with the site classification system suggested in Table 2-2. Two sets of F_{site} factors are recommended for k_pZ factor that is less than 0.3 g and k_pZ factor that is greater than or equal to 0.3 g. This is because it was clearly observed that the amplification factors varied according to the level of the ground motion intensity. The amplification factors are higher for lower intensity levels, and therefore the F_{site} factors from the analysis with intensity of k_pZ factor of 0.1 g are conservatively adopted for intensity levels of k_pZ factors less than 0.3 g. For intensities greater than or equal to k_pZ of 0.3 g, the F_{site} factors from k_pZ factor of 0.3 g are adopted. Further reduction in amplification factors would be possible at higher intensities but these were not investigated in this study. For the softer site classes, different response parameters are suggested for the clay (including soft rock) and sand sites, since it was observed that the difference in response is highly dependent on the plasticity of the soils.

2.4.4.2.1 First corner period, T_1

As discussed previously in Section 2.4.2.3 the definition of T_1 cannot be directly determined from correlations between site properties and site response parameters. Therefore T_1 values have been selected based on the observed RSA for each site class.

2.4.4.2.2 Second corner period, T_{2ampl} and T_{2spec}

Two definitions of second corner period have been introduced to ensure that the RSD obtained is representative of all site conditions within a class:

T_{2ampl} ($T_{2amplification}$):

The period at which the hard rock displacement response is amplified by F_{site} to calculate the magnitude of RSD_{max}. The suggested value is determined from the longest degraded site period possible for a particular class based on the correlation between T_{sf}/T_{si} and V_s (shown in Figure 2-15).

T_{2spec} ($T_{2spectra}$):

The second corner period used to construct the response spectra, it represents the period at which RSD_{max} initiates. The suggested value is based on the period at which the stiffest ground condition within each class experiences maximum displacement response.

2.4.4.2.3 Longer period limits, T_3 and T_4 - only for Class C and Class D

For an improved idealisation of RSD for Classes C and D two more period limits are conservatively defined based on observed RSD for each class:

T_3:

The period for which the maximum displacement response ends.

$$T_3 = 1.5 \times T_{2ampl} \quad \text{Eq. 2-4}$$

T_4:

The period for which a constant value of RSD is reached in the long period range.

$$T_4 = 2.5 \times T_{2ampl} \quad \text{Eq. 2-5}$$

2.4.4.2.4 Site amplification factor, F_{site}

The F_{site} factor within each class is selected based on the observed correlation in Figure 2-14 in order to obtain the maximum displacement response within a site class.

2.4.4.2.5 Amplification factor at 5 seconds, F_E - only for Class C and Class D

Amplification factors at five seconds are suggested to account for the significant reduction in displacement response observed for Classes C and D.

2.4.4.2.6 Formulae required to construct RSA and RSD

The formulae required to obtain the RSA and RSD are provided below.

Displacement response spectra for Class B:

$$RSD_{max} = RSD_{hard\ rock\ at\ T_{2ampl}} \times F_{site} \qquad for: T \geq T_{2spec} \qquad \text{Eq. 2-6}$$

$$RSD = RSD_{max} \times \left(\frac{T^2}{T_{2spec} T_1}\right) \qquad for: 0 \leq T \leq T_1 \qquad \text{Eq. 2-7}$$

$$RSD = \frac{RSD_{max}}{T_{2spec}} \times T \qquad for: T_1 < T < T_{2spec} \qquad \text{Eq. 2-8}$$

Displacement response spectra for Classes C and D:

Eq. 2-7and Eq. 2-8 applies for $0 \leq T \leq T_1$ and $T_1 < T < T_{2spec}$

$$RSD_{max} = RSD_{hard\ rock\ at\ T_{2ampl}} \times F_{site} \qquad for: T_{2spec} \leq T \leq T_3 \qquad \text{Eq. 2-9}$$

$$RSD = \left(\frac{F_E \times RSD_{hard\ rock\ at\ 5sec} - RSD_{max}}{T_4 - T_3}\right) \times (T - T_3) + RSD_{max} \qquad for: T_3 < T \leq T_4 \qquad \text{Eq. 2-10}$$

$$RSD = F_E \times RSD_{hard\ rock\ at\ 5sec} \qquad for: T > T_4 \qquad \text{Eq. 2-11}$$

Acceleration response spectra (for all classes):

$$RSA = RSD \times \left(\frac{2\pi}{T}\right)^2 \qquad for: 0 \leq T \leq 5 \qquad \text{Eq. 2-12}$$

Note:

$$RSA_{max} = RSV_{max} \times \left(\frac{2\pi}{T_1}\right) \qquad \text{Eq. 2-13}$$

$$RSV_{max} = RSD_{max} \times \left(\frac{2\pi}{T_{2spec}}\right) \qquad \text{Eq. 2-14}$$

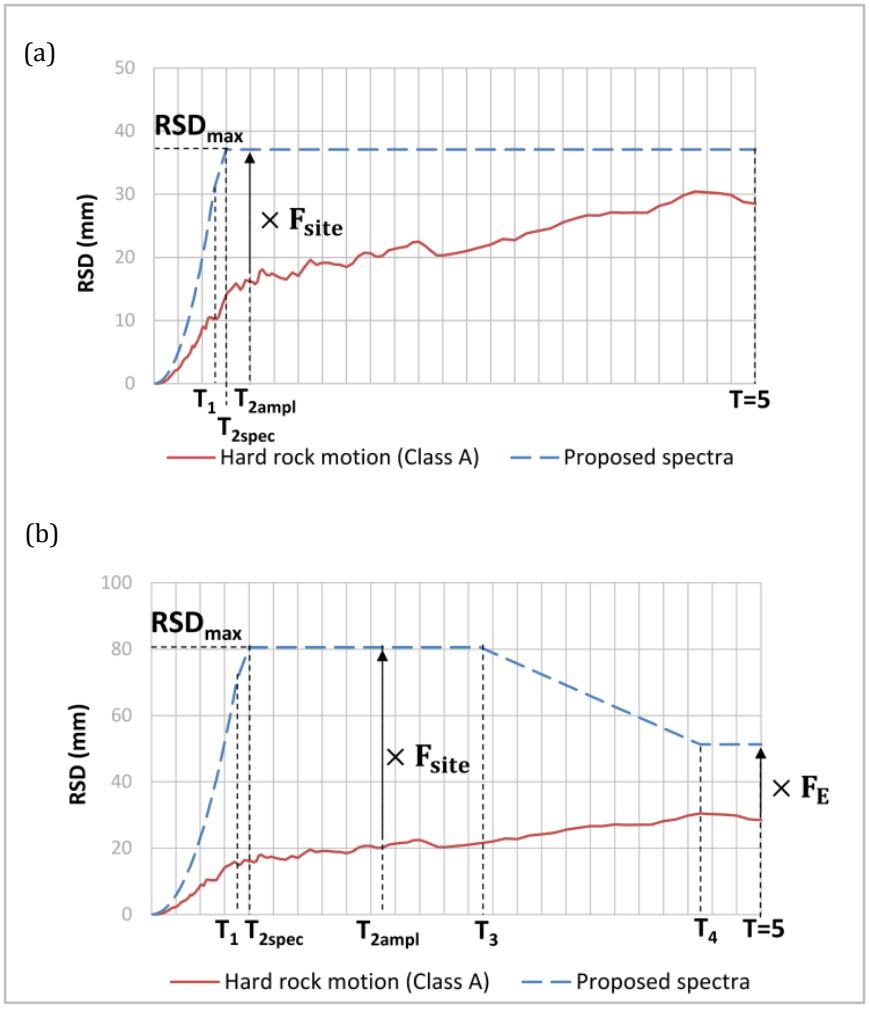

Figure 2-20: Graphical representation of proposed method for obtaining RSD: (a) Model 1 for Class B (b) Model 2 for Classes C and D

Table 2-3: Suggested amplification factors and corner periods for $k_pZ < 0.3$ g

	Class B	**Class C**	**Class D**	
		Rock, clay & sand	Rock & clay	Sand
Corner periods				
T_1	0.5	0.5	0.7	0.7
T_{2spec}	0.6	0.6	0.8	1.0
T_{2ampl}	0.8	0.8	1.8	2.0
Amplification factors				
F_{site}	2.3	3.4	3.6	2.6
F_E	-	1.4	1.8	1.8

Table 2-4: Suggested amplification factors and corner periods for $k_pZ \geq 0.3$ g

	Class B	**Class C**		**Class D**	
		Rock & clay	Sand	Rock & clay	Sand
Corner periods					
T_1	0.5	0.5	0.5	0.7	0.8
T_{2spec}	0.7	0.7	0.7	0.9	1.2
T_{2ampl}	0.9	0.9	0.9	1.9	3.2
Amplification factors					
F_{site}	2.2	3.3	2.4	3.3	2.2
F_E	-	1.2	1.2	1.7	1.7

2.4.4.3 Response spectra obtained using proposed model

Figure 2-21 and Figure 2-22 show the RSA and RSD spectra obtained using the proposed method for k_pZ factors of 0.1 g and 0.3 g respectively. The results are compared with the current response spectra in AS 1170.4:2007 and the envelope of the median responses of the site conditions obtained from the numerical analyses within each class. It is observed that the proposed acceleration response in the short period region is significantly higher than the current acceleration response suggested in AS 1170.4:2007. This is due to the fact that the proposed spectra are based on the envelope of median site response within a class rather than the average response. It is also noted that the significantly higher amplifications within the acceleration controlled region were also observed with historical records as illustrated in Figure 2-19(a). In addition, it is evident that there is a significant difference in site response between cohesive and cohesionless soils, which again would be masked in studies which simply take the average site responses categorised according to V_{s30}. The difference in response due to soil type is greater for softer soil sites as the nonlinear property of the site becomes more significant in this case.

Significant improvement of the RSD in the short period range is observed with the proposed model since it is capable of capturing the high displacement response in the short period range. This improvement is due to the consideration of the relationship between the site period and the second corner period for each site class, since maximum displacement response occurs approximately at the degraded site period for a low-to-moderate level of seismic excitation. Furthermore, it is observed that the proposed spectra over-estimate the displacement response in the long period range. This is, however, a significant improvement when compared with the RSD currently obtained using AS 1170.4:2007. Conservative parameters have currently been suggested for the long

period range due to: (i) uncertainty in the displacement response at long periods, and (ii) uncertainty in determining the effective fundamental period of structures from which the displacement demand imposed on the structure is approximated. It is recommended that to further improve the representation of the displacement response spectra in the long period range (and thus reduce inherent conservatism) further research is required.

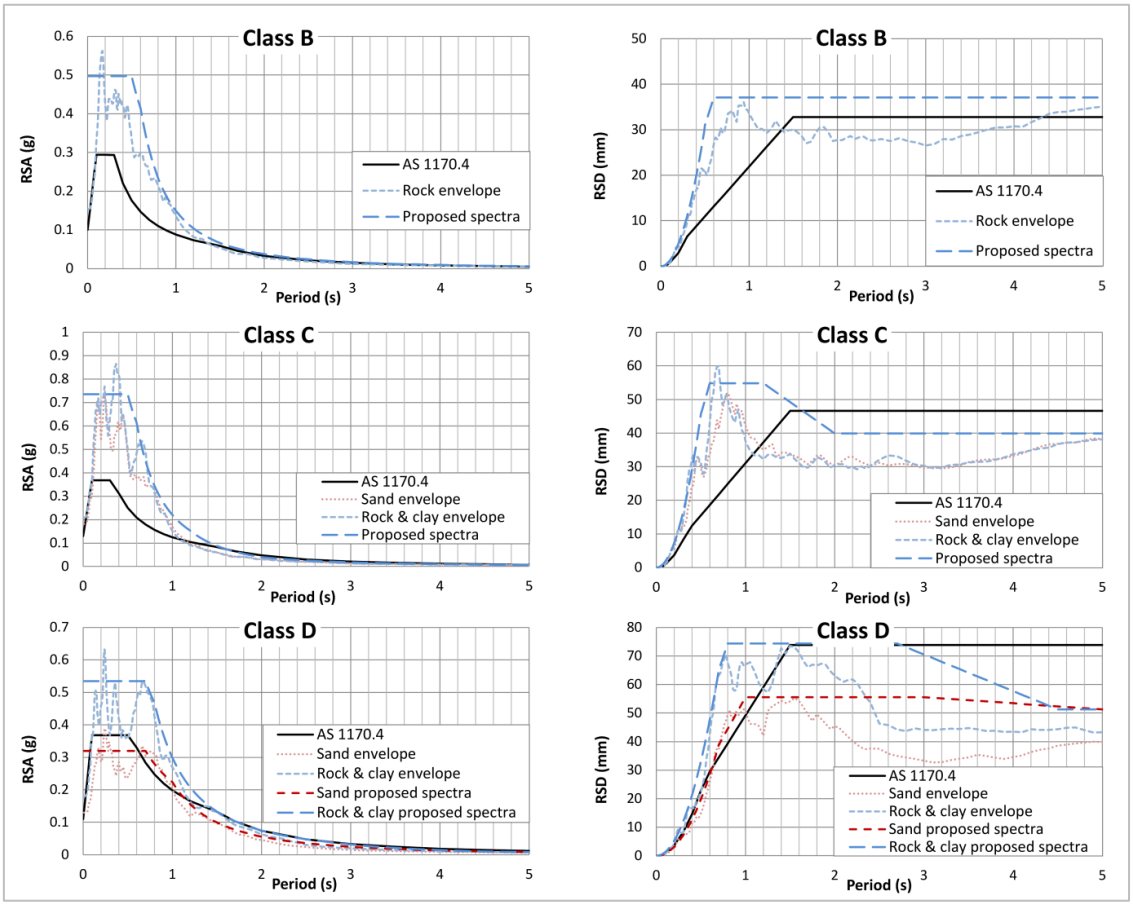

Figure 2-21: RSA and RSD of proposed method, envelope results from numerical analysis, and AS 1170.4 spectra for k_pZ factor of 0.1 g

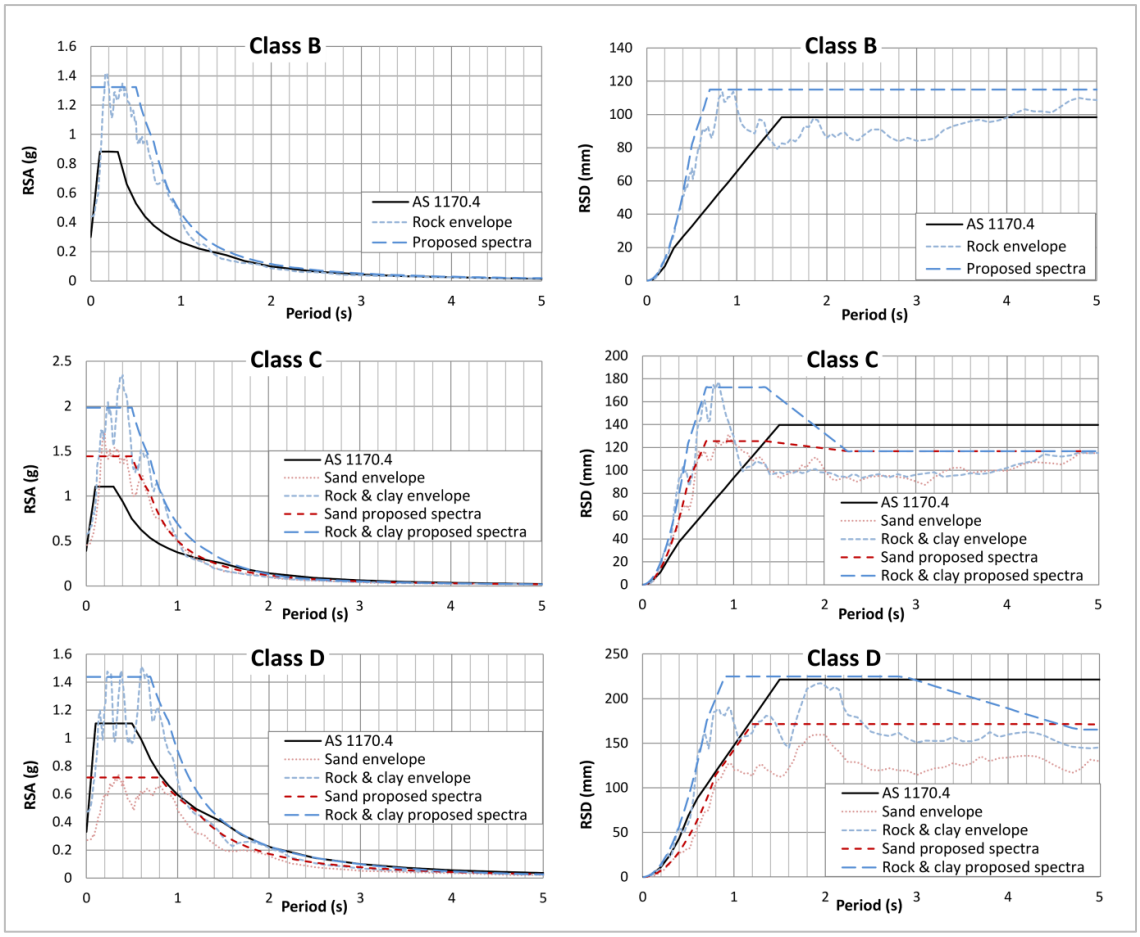

Figure 2-22: RSA and RSD of proposed method, envelope results from numerical analysis, and AS 1170.4 spectra for k_pZ factor of 0.3 g

2.4.4.4 Proposed response spectra and response of existing shear wave velocity profiles

To illustrate the validity of the proposed spectra, eight of the shear wave velocity profiles provided in Kayen et al. (2015) are modelled in SHAKE2000 (Ordonez, 2014) to obtain the acceleration and displacement response spectra. They have been classified as Class C or Class D sites according to the classification system proposed in Section 2.4.4.1 and they have been modelled as clay sites. It is noted that for some sites the shear wave velocity profile at deeper depths had to be artificially generated (based on other existing profiles) such that the profile reached bedrock with a shear wave velocity of at least 1800 m/s. The response spectra of these sites are provided in Figure 2-23 and Figure 2-24 and are compared with the proposed response spectra. The shear wave velocity profiles of the sites are also provided in Appendix B. It is observed that the proposed displacement response spectra are generally capable of enveloping the response of the eight sites. Furthermore, it is clearly seen that the gradient of the displacement spectra up to the second corner period matches very well with the response spectra of the various soil

profiles. This is because the second corner period in the proposed response spectra is associated with the site period. Interestingly, it is also observed that the acceleration response of the shear wave velocity profiles analysed can actually exceed the proposed spectra in the short period range even though these proposed spectral values are already significantly higher than those in AS 1170.4:2007. This is because the acceleration response in the short period range is governed by the frequency content of the input ground motion as well as the stiffness of the ground at shallower depths. That is, RSA_{max} for soil sites does not occur at the fundamental period of the site (unlike RSD_{max}) but rather at shorter periods. Hence, the prediction of the acceleration response in the short period range is much more complicated and variable. The research carried out here suggests that the RSA is underestimated by current codes and standards in the low period range. Further research in this area is required since it would signify a significant change if it were required to be used in force-based design.

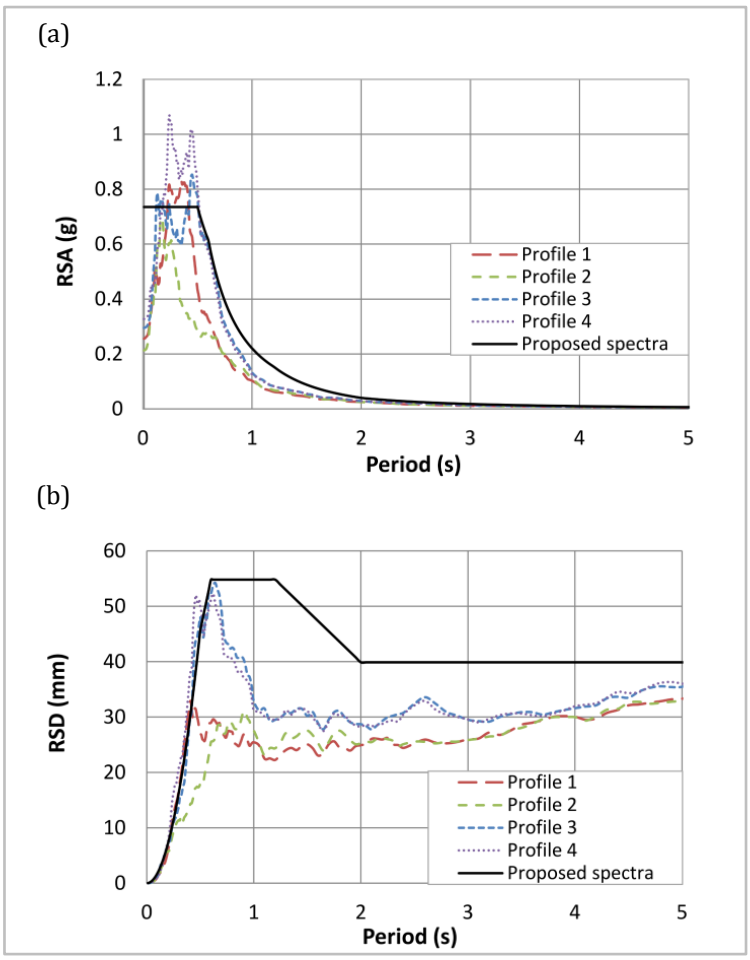

Figure 2-23: Response spectra of shear wave velocity profiles and proposed response spectra for Class C: (a) RSA, (b) RSD

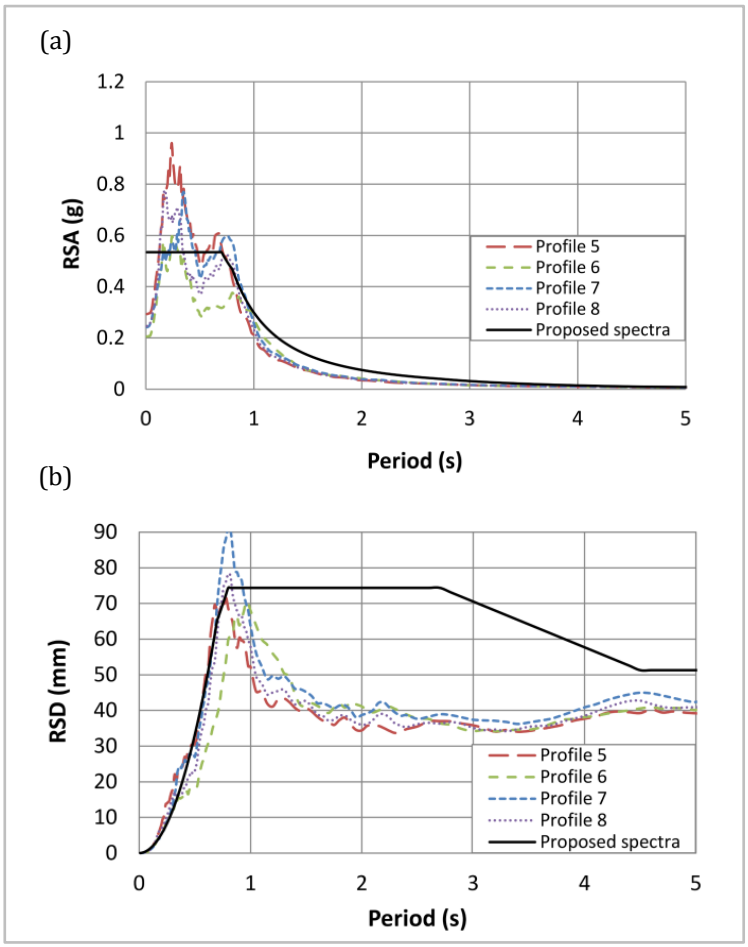

Figure 2-24: Response spectra of shear wave velocity profiles and proposed response spectra for Class D: (a) RSA, (b) RSD

2.4.5 Conclusions from seismic site response study

This study has investigated the effects of local site conditions, namely the weighted average shear wave velocity, depth to bedrock, and intensity of ground motions, on the seismic response of typical rock, clay and sand sites. In doing so, the study has examined the validity of the current method used to incorporate site effects in codes, in particular that used in AS 1170.4:2007. The effects of local site conditions have been obtained from correlations and observation of trends between site properties representative of individual rock/soil profiles and seismic site response parameters. The results illustrate the importance of considering the fundamental site period, which is a function of V_s and depth to bedrock, rather than V_{s30} alone, in understanding the seismic site response. Furthermore, it is demonstrated that the method of analysis adopted in this study allows the true site behaviour to be captured and for this reason it preferable to methods which calculate amplification factors based on the average response of sites. The consideration of true site behaviour is particularly important for low-to-moderate seismic regions since the

buildings are typically non-ductile and therefore have very limited ability to damp the site-structure resonance effects.

Based on the findings, re-classification of the site classes in AS 1170.4:2007 is recommended, with emphasis on site period as a key criteria in classifying soil/soft rock classes. A new systematic method is then proposed for obtaining the displacement response spectra and this significantly improves the prediction of displacement response in the short period range up to the second corner period at which maximum displacement response occurs. This improvement of the representation of the displacement response in the short period range comes about because the second corner period for the various site classes is associated with the site period. Furthermore, the amplification factors represent the maximum amplification possible within a site category rather than an average amplification, thus ensuring that the maximum response within a site category is captured by the displacement response spectra. In the long period range, the suggested displacement response spectrum for the softer soil classes is an improvement on the code representation. Currently these suggested improved spectra still appear to over-predict the response and this is because of the deliberate choice of conservative factors that reflect the uncertainty in this range. It is recommended that further research needs to be conducted to improve the representation of displacement response spectra in the longer period range.

The acceleration response spectra resulting from this study are significantly higher than those in AS 1170.4:2007. Further research in this area is required since the change would cause a significant increase in the design actions for earthquake resistant design of structures if force-based methods are used.

Furthermore, the results of this study have indicated that the response of softer sites is highly dependent on the PI of the soil. This study has investigated the response of sand sites and clay with PI of 30 %. Future studies should further investigate the effects of various PI values on site response and the effect of selecting different shear modulus reduction and damping curves. Currently none of the standards and codes account for soil type even though it has a significant effect on site response.

2.5 SUMMARY

In this chapter background information has been provided about the seismicity of Australia and the current models used to define the level of hazard and response spectra for rock conditions. Significant research is currently being undertaken to improve the

seismic hazard map of Australia. However, a consensus has not been reached amongst the experts. A key challenge for regions of low-to-moderate seismicity, such as Australia, is the paucity of historical records which makes the selection of ground motion prediction equations difficult and inconsistent. In this study, to evaluate the seismic performance of the archetypal buildings, the hazard values in AS 1170.4:2007 will be used as a guide to represent the seismicity of Australia since it is the current well established model which is available.

Furthermore, in this chapter an overview of the effect of local site conditions on response spectra have been presented with a particular focus on the limitations of codified approaches to incorporate site effects. The limitations of the approaches are particularly important for regions of low-to-moderate seismicity which typically have non-ductile buildings. A detailed study has been conducted to explore the effects of local site conditions and to examine the validity of the method provided in AS 1170.4:2007. The results indicated that the true site response behaviour is not accurately captured in codified approaches for all site types. Based on the findings, re-classification of the site classes in AS 1170.4:2007 has been recommended, and a new systematic method has been proposed for obtaining the displacement response spectra and the acceleration response spectra. However, it is concluded that further research in this field is necessary.

CHAPTER 3: CHARACTERISATION OF VULNERABLE RC BUILDINGS

3.1 INTRODUCTION

The aim of this chapter is to characterise the vulnerable RC buildings to be assessed in this study. This is achieved by first reviewing the history of the design of RC buildings in Australia to provide an understanding of the existing building stock, including typical building configurations and design detailing. The seismic detailing deficiencies of the buildings in Australia are then presented followed by the likely component response and failure mechanism of the frame and wall components. The importance of considering the response of the lateral load resisting system and the gravity load resisting system is examined with a particular focus on the deformation compatibility between the two systems. Finally, the selection of suitable material properties for the purpose of assessment of the buildings is discussed.

3.2 HISTORY OF RC BUILDING DESIGN IN AUSTRALIA

To define the characteristics of existing buildings for assessment it is necessary to determine how buildings have been designed and constructed over the years. Unlike some countries such as New Zealand and the United States, Australia does not have a publicly available comprehensive inventory on the structural information of existing buildings. Therefore, most of the information relating to the design of the buildings for this study has been obtained by speaking to and corresponding with experienced practicing structural engineers and from reviewing older editions of the Australian loading and concrete structures standards. The discussions with structural engineers have helped to establish typical building configurations and design details, including: member spans, floor-to-floor heights, material properties, reinforcement detailing and typical axial load ratios of members. This information will be used to develop the archetypal buildings for assessment in Chapter 7. The following subsections provide background information relating to the design of buildings to resist gravity and lateral loads, the development of design and loading standards, and the design material properties which have been used in Australia.

3.2.1 Design of RC buildings in Australia

Many existing buildings in Australia which are mid-rise in height typically employ lateral load resisting systems and gravity load resisting systems that have been designed independently of each other. The lateral load resisting system usually consists of planar

and/or non-planar (core) walls which are designed to carry 100 % of the lateral load. However, prior to the 1980-1990s the magnitude of the lateral load was often underestimated or not considered at all and therefore the layout of the core walls in buildings has often been governed by access and ingress requirements (such as for fire); including lift cores and stair cores. As a result, most of the buildings constructed in this period have eccentrically placed cores since it was preferred from an architectural standpoint. Some of the guidelines for distances to exits as specified in the Building Code of Australia (BCA) (ABCB, 2015) are provided in Figure 3-1 for office and commercial buildings. This provides an indication of the maximum allowable distances between core walls.

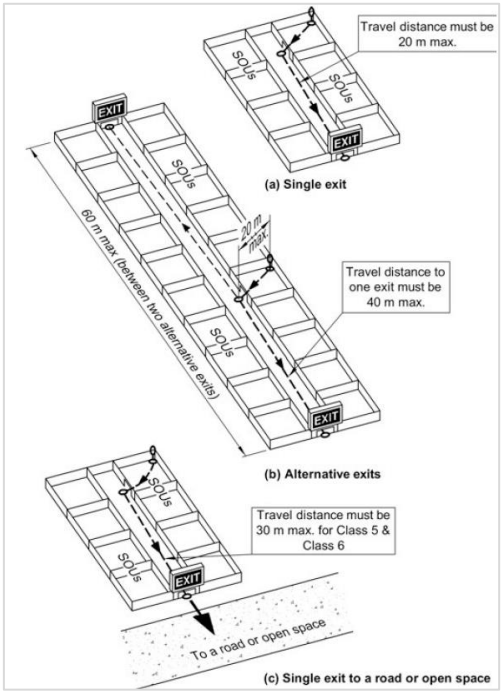

Figure 3-1: Distances to exits for office and commercial buildings (ABCB, 2015)

The design of the gravity load resisting system has changed over the decades. The gravity system of buildings constructed prior to and during the 1960s typically includes ordinary beam and slab construction for the floor system. This is because there were fewer restrictions to the floor-to-floor heights and minimal service requirements had to be met. Furthermore, during this period beam spans were significantly shorter than current construction, ranging from six to seven metres. In the 1970s and 1980s, flat-slab and band-beam construction became more popular. The floor-to-floor heights were usually limited to 3.3 to 3.6 m which allowed approximately 900 mm space for structural and mechanical services, including air-conditioning services. Deep edge beams were always provided around the outer perimeter of the building, typically 600 to 900 mm for fire

requirements. During this period column spacing was typically 7.4 to 8.4 m. In the late 1980s and early 1990s prestressing was introduced and prestressed construction slowly became the norm, especially for gravity load resisting systems since much longer spans became achievable which is desired from an architectural perspective.

The methods used to analyse buildings under gravity and lateral loads has also changed with time. Prior to the 1980s, buildings were analysed using hand calculations and moment distributions. During the 1980s the initiation of the use of technology to analyse buildings developed with 2D computer analysis packages. Therefore buildings constructed prior to and during the 1980s are usually considered to be unsophisticated and are sometimes perceived to be robust and over-designed. However, it is important to note that the perceived over-design of these buildings does not necessarily translate to a better performance or robustness under seismic loading. This is because the detailing of older buildings is poor due to lack of consideration and understanding of the building's response to seismic loading.

By the 1990s computer technology became readily available in design offices and significant improvements were made to structural analysis programs leading up to the programs with the design capabilities available today. This allowed the design of buildings to become more sophisticated as they could be engineered to provide a range of feasible solutions. However, associated with the use of these programs, there are also concerns about the possibility of modern buildings pushing the boundaries and losing their inherent robustness. As reliance on computer programs for the analysis of buildings increases there are also concerns about the ability of structural engineers to ensure a safe design by following a thought process that shows a deep understanding of the overall design issues. Nevertheless, the advancement in technology has helped the development of structural engineering and design and if it used with care it allows for improved and innovative solutions.

3.2.2 Development of design and lateral loading standards

Over the past few decades significant changes have been made to standards and codes which have directly impacted on the way buildings have been designed and constructed. The first significant change to the concrete design standard was in the mid-1970s as the design of structures changed from working stress to ultimate strength design methods with the introduction of the concrete standard, AS 1480:1974. The second significant change was in 1988, with the establishment of the concrete structures standard, AS 3600 (Standards Australia, 1988), which was the first limit state design standard in Australia.

Significant improvements were also made to durability and fire resistant provisions. Since the introduction of AS 3600:1988 other minor changes have been made to the concrete structures standard; these have been predominantly related to detailing and RC material property changes. The current concrete structures standard is AS 3600:2009 (Standards Australia, 2009).

With respect to wind load and lateral stability, it is generally accepted that they were poorly considered in Australia until the late 1980s. Although the first wind loading standard known as Australian Standard CA34, Part II, was published in Australia in 1971 (Australasian Wind Engineering Society, 2012), the wind load considered prior to the late 1980s was much lower than what is considered currently in accordance with AS/NZS 1170.2 (Standards Australia and Standards New Zealand, 2011).

The first earthquake loading and design standard, known as the SAA Earthquake code, AS 2121, was published in Australia in 1979. This was a result of the 1968 Meckering earthquake in Western Australia, which was one of the most damaging earthquakes that Australia had experienced at the time. AS 2121:1979 was based on the 1977 edition of the Structural Engineers Association of California (SEAOC) code however it was altered for Australian earthquake conditions. In 1993, a new earthquake loading standard was published as AS 1170.4 and this replaced AS 2121:1979. The introduction of AS 1170.4 led to the need for extra detailing requirements which were provided in AS 3600, the concrete structures standard, and not in the earthquake code. In 2007, AS 1170.4 was revised and it is the current version of the earthquake loading standard, however, a new version is due to be published soon. Revision of the seismic detailing requirements in AS 3600 has also been undertaken by a subcommittee of the Standards Australia BD-002 Concrete Structures Committee.

It is important to note that even though the first earthquake loading and design standard was published in 1979, it was not adopted by all states until a later period. South Australia was the first state to adopt seismic design, and in particular the city of Adelaide; where it is believed that seismic design was adopted since 1982. This is probably because historically Adelaide has had the highest seismicity in comparison to the other capital cities of Australia and therefore the designers have been more cautious. Nationally, seismic design was not considered until 1995 when the requirement for earthquake loading and design was referred to in the BCA and had to be adopted by all states and territories. This was influenced by the occurrence of the 1989 Newcastle earthquake in New South Wales, which caused 13 fatalities and high economic loss (Walker, 2011).

3.2.3 RC material properties used in Australia

In addition to changes made to design standards and analyses methods, there have also been significant changes to the properties of the materials used to make reinforced concrete. For example, the concrete compressive strength has increased significantly over the last few decades. A summary of the typical minimum characteristic concrete compressive strengths used in design during various periods is provided in Table 3-1. It is noted that the (lower/minimum) characteristic material properties stated in the Australian standards correspond to the value of the material property, as assessed by standard test, which is exceeded by 95 % of the material.

The steel reinforcement properties have also changed over the past decades. A summary of the lower characteristic steel reinforcement properties over the past seven decades is provided in Table 3-2. Initially plain round bars were used for longitudinal and transverse reinforcement, however, during later periods plain bars were limited to ties and fitments. In the late 1970s hot-rolled, Grade 410Y (later revised to 400) reinforcement bars were introduced which overtook cold work Grade 410C deformed bars. During the period between 1991 and 2001, it can be seen that a significantly higher ductility was required, with a minimum characteristic uniform elongation strain (i.e. ultimate strain) of 0.16. Interestingly, in 2001, Grade 500N bars were introduced with significantly lower ductility, requiring a minimum characteristic uniform elongation strain (also referred to as ultimate strain) of just 0.05.

Table 3-1: Typical lower characteristic concrete strengths (in MPa) for building components for various periods in Australia

	Pre 1960s	**1960 to mid-1980s**	**mid-1980s to 2001**	**2001 to current**
Slab	15-25	25	25	32
Beam	15-25	25	25	32
Column and walls	25-35	30-40	40	40-50+

Table 3-2: Summary of the lower characteristic properties of reinforcement bars used in Australia (Concrete Institute of Australia, 2007; Liberty OneSteel)

	Deformed Bars						**Plain bars**	
Production method	Cold-twisted	Hot-rolled	Hot-rolled	Hot-rolled	Hot-rolled	Hot-rolled	Hot-rolled	Hot-rolled
Bar	410C (CW60)	230S	250S	410Y	500N	500L [(1)]	230R	250R
Period	1958 - 1983	1973 - 1991	1991 - 2001	1977 - 2001	2001 - current	2001 - current	1973 - 2001	1991-2001
Standard	AS A83	AS 1302	AS 1302	AS 1302	AS/NZS 4671	AS/NZS 4671	AS 1302	AS 1302
Yield stress (MPa)	> 410 Max limit not specified	> 230 Max limit not specified	> 250 Max limit not specified	> 410 (1977 -1991) > 400 (1991-2001) Max limit not specified	> 500 ≤ 650	> 500 ≤ 750	>230 Max limit not specified	250 Max limit not specified
Tensile (ultimate) to yield stress ratio	1.17 (1958-1977) 1.08 (1977-1982) 1.05 (1982-1983)	1.87 (1973-1977) 1.15 (1977-1991)	1.10 (1991-2001)	1.15 (1977-1982) [(2)] 1.05 (1982-1991) 1.10 (1991-2001)	1.08	1.03	1.87 (1973-1977) 1.15 (1977-1991) 1.10 (1991-2001)	1.10
Uniform elongation (ε_{su})	0.14 (1958-1977) 0.12 (1977-1983)	0.22	0.22	0.12 (1977-1991) 0.16 (1991-2001)	0.05	0.015	0.22	0.22

ε_{su}: is the strain at ultimate tensile strength | [(1)] AS 3600:2001 sets restrictions to the use of 500L and generally not commonly used | [(2)] Y-bars were not very common during 1977-1982 period

3.3 DEFICIENCIES OF NON-DUCTILE RC FRAME COMPONENTS AND WALLS

Many of the existing RC buildings in Australia have building components that have been designed with *ordinary* and *limited ductile* reinforcement detailing, namely; ordinary moment resisting frames (OMRFs) and limited ductile shear walls. This level of reinforcement detailing has been consistent with the requirements of the main body of the concrete structures standards over the years and it allows the designers to adopt a ductility factor (μ) of 2 when calculating the earthquake actions induced on the building in accordance with the current earthquake loading standard, AS 1170.4:2007 (Standards Australia, 2007). More stringent detailing requirements may be adopted, for example the design of intermediate and special moment resisting frames and ductile shear walls, which allow the designer to adopt higher ductility factors to reduce earthquake actions. However, this has not been common practice in Australia due to it being in a region of low-to-moderate seismicity. The detailing requirements for *ordinary* and *limited ductile* building components in Australia are, in general, consistent with the detailing of the RC buildings constructed in high seismic regions prior to the mid-1970s; that is, prior to the introduction of seismic detailing and capacity design principles. This level of detailing is generally categorised in the literature as *non-ductile* detailing and therefore this term is adopted from this point onwards in the thesis. It is also sometimes interchangeably used with *non-conforming* detailing.

Extensive research has been conducted in high seismic regions aimed at understanding the behaviour of non-ductile RC buildings in order to improve design provisions and to assess the vulnerability of existing buildings. In addition, reconnaissance from previous earthquakes has also provided very useful information in understanding the deficiencies of non-ductile buildings which contribute to local failure mechanisms and ultimately the global collapse of buildings. The typical detailing deficiencies which have been reported in the literature for non-ductile RC frames (Celik, 2007; Hakuto et al., 2000) and walls (Henry, 2013; Hoult et al., 2017) are listed below and illustrated in Figure 3-2 and Figure 3-3. These deficiencies are directly applicable to the detailing of RC frames and walls in older buildings as well as the requirements for current buildings in accordance with AS 3600:2009.

The typical deficiencies of non-ductile RC frames include:

- Inadequate transverse reinforcement (also referred to as ties or stirrups) in beams and columns for shear strength and confinement

- Poor anchorage and splices of longitudinal bars in beams and columns, in particular bottom beam bars are terminated within the beam-column joint region with a short embedment length.
- Splices of longitudinal bars located in potential hinge regions
- Columns having bending moment capacities which are approximately the same or less than the adjoining beams thus making the frame vulnerable to the undesirable weak column-strong beam scenario under lateral loading.
- Insufficient transverse reinforcement in beam-column joint regions

The typical deficiencies of non-ductile RC walls include:

- Low percentage of longitudinal reinforcement
- Inadequate transverse reinforcement for confinement of concrete and to provide lateral support of longitudinal bars to prevent buckling
- Insufficient transverse reinforcement for shear strength
- Poor anchorage and splices of longitudinal bars (with splices located in potential hinge region)

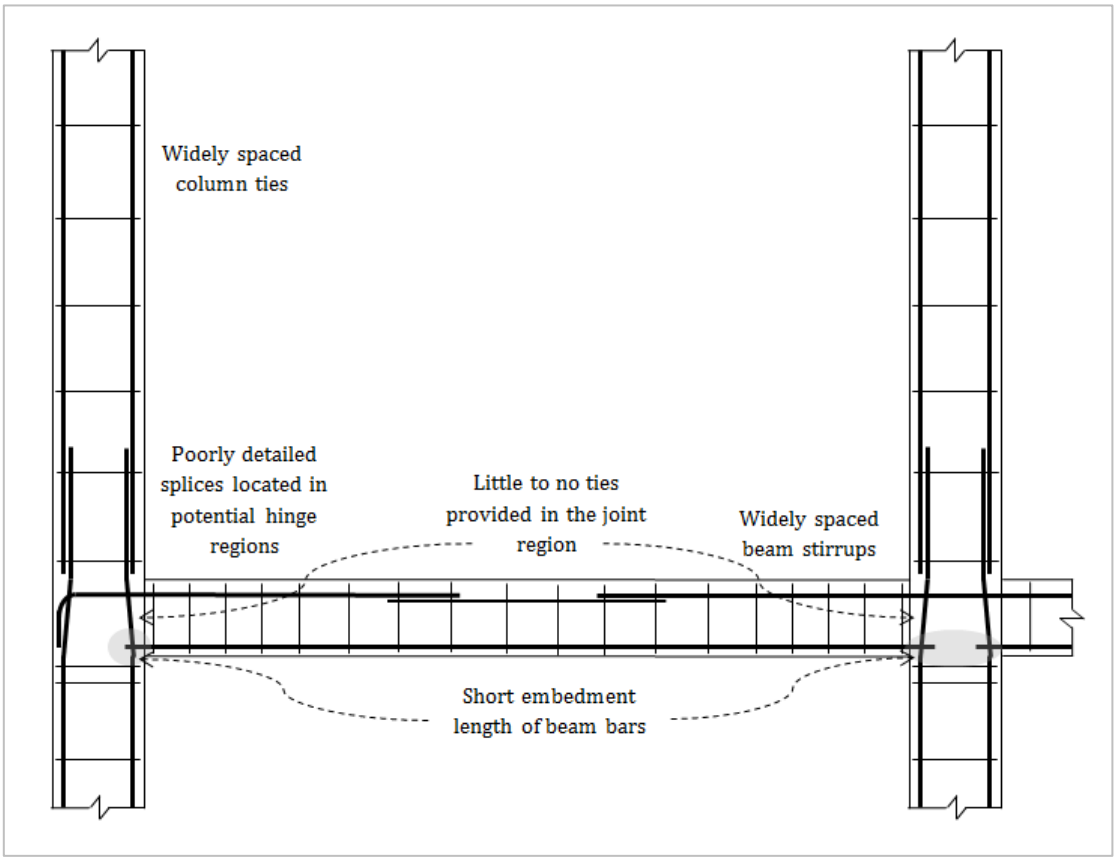

Figure 3-2: Schematic of detailing deficiencies of non-ductile RC MRFs

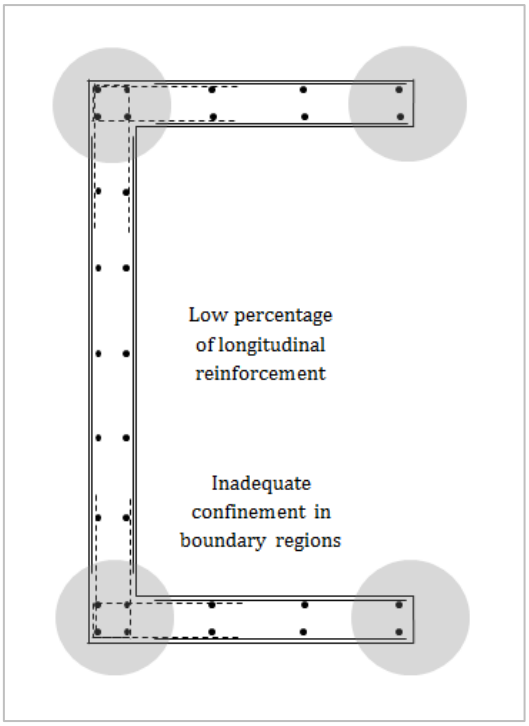

Figure 3-3: Schematic of some of the detailing deficiencies of non-ductile walls

3.4 RESPONSE AND FAILURE MECHANISMS OF NON-DUCTILE RC FRAME COMPONENTS AND WALLS

The following subsections discuss failure mechanisms of non-ductile RC building components observed during past earthquakes and in experimental testing presented in the literature. For RC frames, particular focus is provided on the shear response of columns and beam-column joints as they have been identified as the most vulnerable and likely failure mechanisms which take place in non-ductile RC frames and may lead to the collapse of buildings (Ghannoum & Moehle, 2012; Park & Mosalam, 2013b).

3.4.1 Beam-column joints

The greatest uncertainty when evaluating the performance of frames is associated with the performance of beam-column joints which have little to no transverse reinforcement (Hakuto et al., 2000; Park, 2002). The primary function of joints is to transfer forces between beams and columns. However, lack of transverse reinforcement and slip of longitudinal bars can lead to premature failure of the joints before the full capacity of the frame members has developed. Joint failure mechanisms can be categorised as (Jeon et al., 2015):

i. Joint shear failure after yielding of beams which results in gradual strength degradation

ii. Joint shear failure before yielding of beams and columns which results in rapid strength and stiffness degradation

iii. Bond failure, predominantly due to slip of beam reinforcement bars

The last two failure mechanisms are very brittle failures which are common to non-ductile joints and can lead to joint failure at relatively low displacement demands (Calvi et al., 2002) and may be followed by eventual global collapse of the frame. Figure 3-4 and Figure 3-5 clearly illustrate beam-column joint failures observed during past earthquakes where the beams and columns have remained undamaged while the joint failure has led to global failure of the frames. The two key factors that need to be considered when assessing the performance of the joints are the strength of the joint and the large deformations which can take place in the joint. Large deformations in the joint may significantly increase the interstorey drift (Park and Mosalam, 2013b).

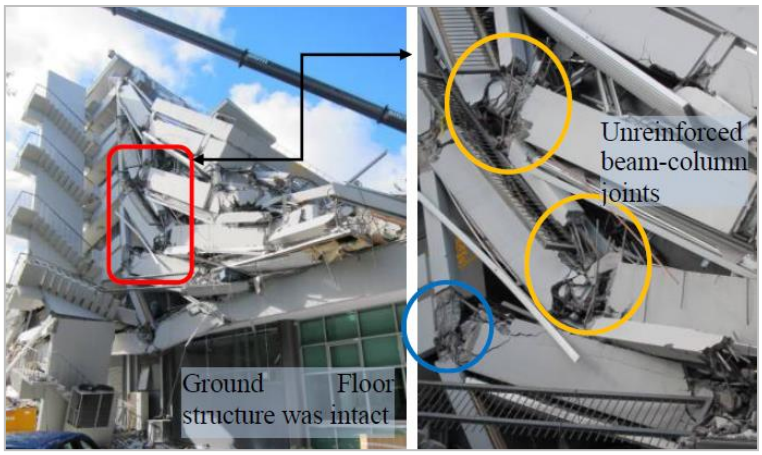

Figure 3-4: Beam-column joint failure experienced in PGC building during the Christchurch earthquake in 2011 (Kam et al., 2011)

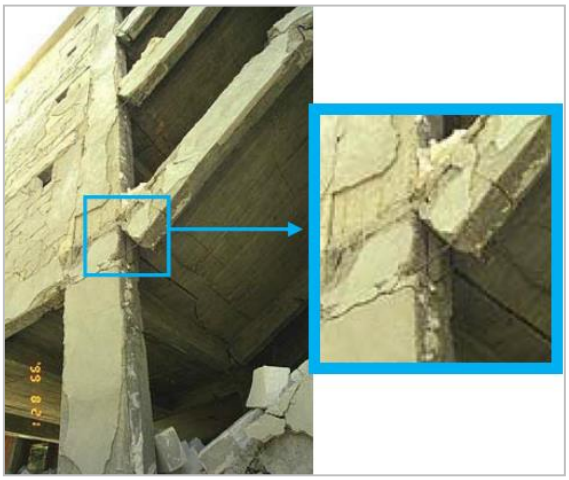

Figure 3-5: Slip of bottom beam bars due to poor embedment of bars in the joint region (Sezen et al., 2000)

Joint shear behaviour is commonly explained via strut and tie models as shown in Figure 3-6 and Figure 3-7 for exterior and interior joints, respectively. The concrete strut mechanism provides shear resistance from force transfer to the joint panel via the compression zones of the adjacent beam/s and column/s. The truss mechanism provides shear resistance from force transfer to the joint panel through the bond between the reinforcement and the surrounding concrete (Kim & LaFave, 2009; Paulay et al., 1978). It is discussed in Hakuto et al. (2000) that shear failure of joints without ties initiates due to diagonal tension cracking which eventually leads to diagonal compression (strut) failure. This is why a strong relationship is observed in experimental results between maximum nominal horizontal joint shear stress ($\tau_{jh.max}$) and concrete compressive strength (f_c').

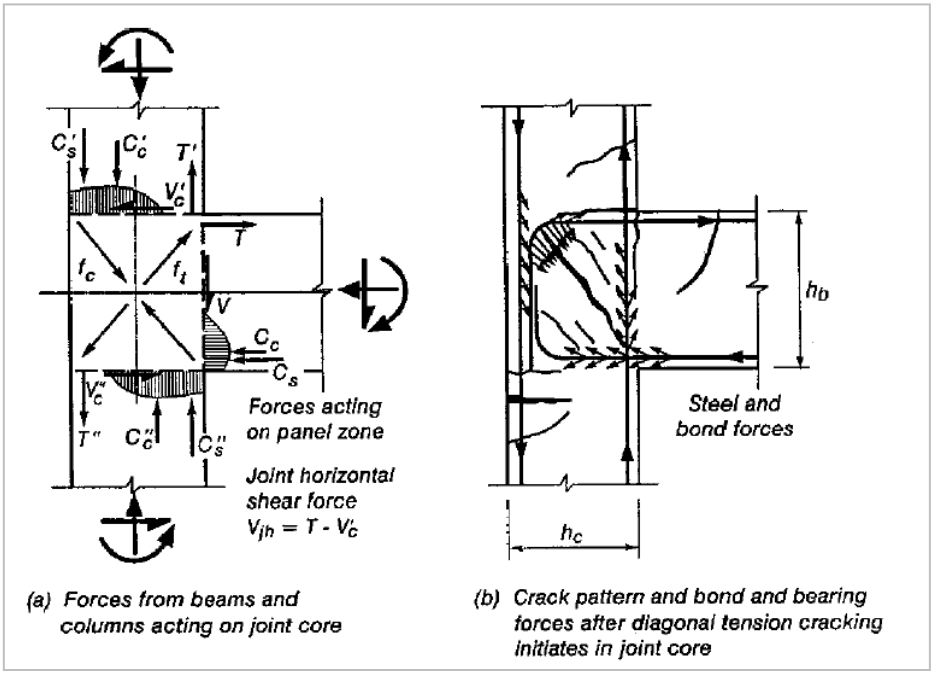

Figure 3-6: Exterior joint behaviour subjected to lateral loading (Hakuto et al., 2000)

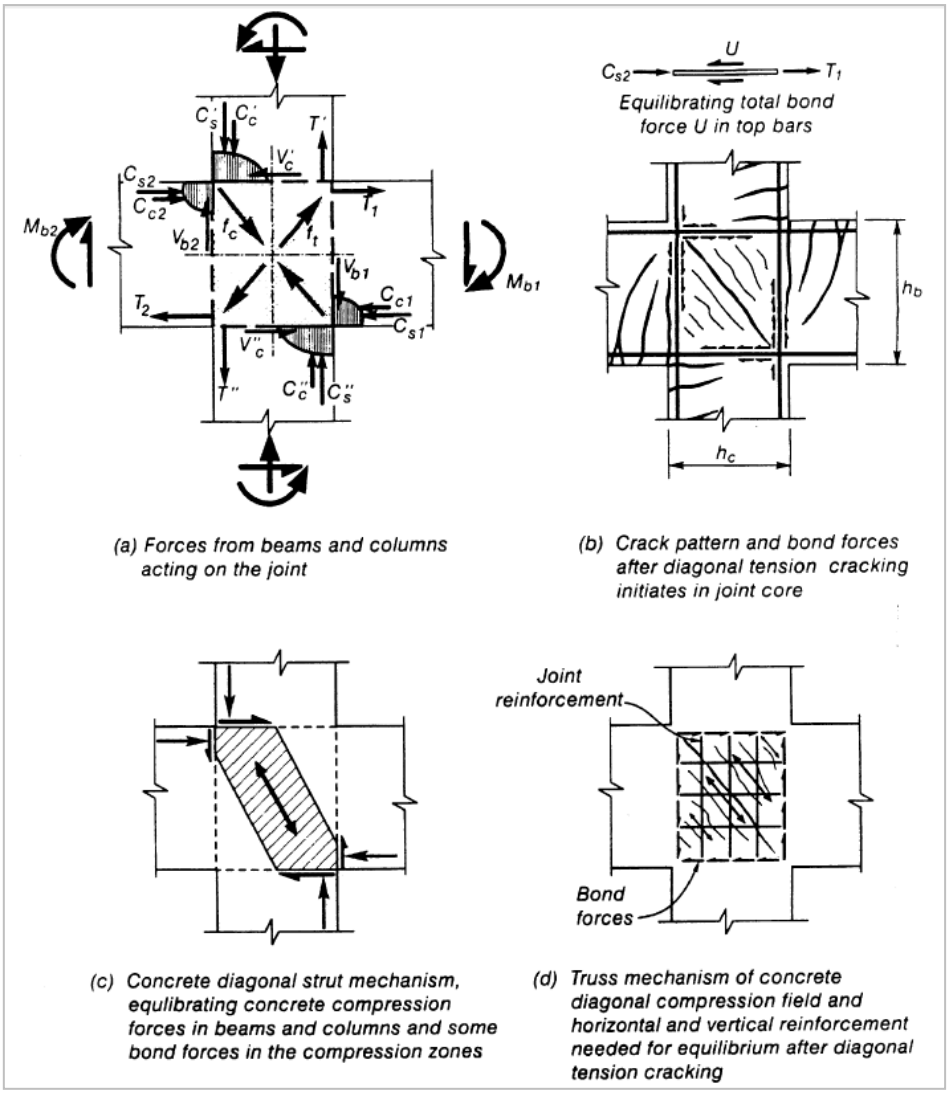

Figure 3-7: Interior joint behaviour subjected to lateral loading (Hakuto et al., 2000)

The response of beam-column joints is dependent on various parameters. Some of the key considerations include:

- Transverse reinforcement in the joint region
- Discontinuous bottom longitudinal beam bars
- Longitudinal bar properties
- Joint aspect ratio (h_b/h_c)
- Column bar splices near the joint region
- Transverse beams
- Slab
- Axial load
- Speed of lateral load (pseudo-static versus dynamic cyclic loading)

The research findings associated with these parameters are discussed in the following subsections.

3.4.1.1 Transverse reinforcement in the joint region

Numerous tests have shown that the joint shear capacity increases as more transverse reinforcement is placed in the joint region, especially for joints which are not confined by transverse beams (Ehsani & Wight, 1985; Kurose et al., 1988; Paulay et al., 1978). This is because the ties in the joint region are able to resist shear stresses in addition to the shear resisted by the concrete. Furthermore, ties provide confinement to the joint region and thus reduce the size of shear cracks which in turn reduces or delays bar pull-out, hence improving the joint's strength and deformation capacity (Ehsani & Wight, 1985).

3.4.1.2 Discontinuous bottom longitudinal beam bars

Discontinuous bottom longitudinal beam bars which are poorly anchored cause a reduction in the positive bending capacity of the beams. Full-scale tests on beam-column joints have indicated that for interior joints (with strong column-weak beam subassemblages), where the embedment lengths of the bottom bars were 150 mm (6 inches), the pull-out of beam bottom beam bars reduced the positive bending capacity of beams by up to 30-50 % (Beres et al., 1992; Pessiki et al., 1990). Similarly reductions in positive bending capacity of beams have been observed for exterior joints, with the reduction being reported as greater than 50 % (Pantelides et al., 2002). To account for bond-slip and the decrease in the bending capacity of the beam FEMA 356 (2000) suggests limiting the stress in the steel according to Eq. 3-1.

$$f_{s.max} = f_y \times \frac{l_b}{l_d} \qquad \text{Eq. 3-1}$$

Where
- $f_{s.max}$ is the maximum reinforcement stress
- f_y is the yield strength of reinforcement
- l_b is the provided embedment length of reinforcement
- l_d is the reinforcement development length required by ACI 318-08

It is interesting to note that studies which have investigated the effect of providing continuous bottom or sufficiently anchored bottom beam bars have reported that the failure mechanism may shift to column-sway rather than beam-sway (Kunnath et al., 1995). This has a negative impact on the global response of the frame as higher drifts and soft-storey effects are observed. This highlights the importance of capacity design principles, and that what may seem as an improvement in the detailing may actually have detrimental effects if the global response of the frame is not considered.

3.4.1.3 Longitudinal bar properties

Force is transferred between reinforcing bars and the surrounding concrete via three mechanisms: chemical adhesion, frictional resistance, and mechanical interlock (Lutz & Gergely, 1967, cited in Pessiki et al., 1990). The principal mechanisms for force transfer are mechanical interlock and friction for deformed bars, and only friction for smooth bars (Calvi et al., 2002). Hence, in general, plain round longitudinal reinforcement bars have poor bond in comparison to deformed bars. This results in lower bending capacity of adjoining members due to bar-slip; this may be particularly important when considering the moment capacity of columns, as neglecting the effect may result in falsely predicting strong column-weak beam mechanisms (Calvi et al., 2002). However, there are very few experimental results for weak column-strong beam subassemblages with plain bars, and further testing is needed to give conclusive results.

Furthermore, the ratio of the column depth to the diameter of the beam longitudinal reinforcement ($h_c/d_{b,b}$), and the ratio of the beam depth to the diameter of the column longitudinal reinforcement ($h_b/d_{b,c}$) may have an effect on the joint response due to bond deterioration if they are too low. Hence, some codes provide minimal depth requirements based on longitudinal bar diameters. ACI 318R (2008) recommends $h_c/d_{b,b}$ to be equal or greater than 20 for interior joints belonging to special moment resisting frames. This is to reduce the extent of slip when beam hinging takes place during a series of large moment reversals. Studies have suggested that for limited ductile columns restriction of $h_c/d_{b,b}$ is not necessary (Ruitong & Park, 1987) and that the loss in moment capacity of adjoining beams to slip is insignificant (Hakuto et al., 1999 cited in NZSEE, 2016). In addition, since the concrete strut is the key mechanism developed to resist joint shear, it is concluded that for the purpose of assessment of non-ductile joints the effect of bond deterioration on joint shear strength may be ignored.

3.4.1.4 Joint aspect ratio (h_b/h_c)

The joint aspect ratio, that is, the beam-to-column depth ratio (h_b/h_c), has a significant effect on the joint shear strength. The joint shear capacity decreases with an increase in beam-to-column depth ratio (Kurose et al., 1988; Park & Mosalam, 2013a; Pessiki et al., 1990). This is because the diagonal compressive strut formed in the joint region becomes steeper and hence its effectiveness in resisting horizontal joint shear stress is reduced. In addition, researchers have reported that joint aspect ratio has an effect on the joint deformation capacity, the larger the ratio the less flexible the joint behaviour (Park & Mosalam, 2013b).

3.4.1.5 Column bar splices near the joint region

Experimental tests have also been conducted to investigate the effect of column longitudinal bar splices near the joint region where the subassemblages have been designed to have a weak column-strong beam strength hierarchy with continuous beam bottom bars. The results indicate that if the joints are vulnerable to shear failure then the presence of lapped splices does not significantly contribute to the failure mechanism of the subassemblage and that the lapped splices perform adequately (Pessiki et al., 1990). However, once sufficient ties are provided within the joint region the failure mechanism changes to column bar buckling due to the poor confinement of the lapped splices located in the potential hinge regions. However, this type of failure occurs at much larger drifts since the joint is able to sustain larger deformations.

3.4.1.6 Transverse beams

The presence of transverse beams in general is believed to improve the performance of beam-column joints. This is due to the passive confinement provided by the longitudinal reinforcement of the transverse beam/s which can resist the joint panel's expansion in the out-of-plane direction (Kim & LaFave, 2009). However, observations from experimental results provide inconsistent results about the amount of improvement transverse beam/s provide. Based on the database of 84 interior joints, for which 27 joints had one or two transverse beams, Kurose et al. (1988) concluded that the presence of one transverse beam had an insignificant effect on the joints' performance in comparison to when no transverse beams were provided, while the inclusion of two transverse beams resulted in an approximately 30 % increase in the joint shear strength. Kim and LaFave (2009) examined 341 joint subassemblages from which 36 had transverse beam/s. They concluded that the presence of two transverse beams resulted in slightly higher joint shear stresses being achieved in experimental tests in comparison to subassemblages with one or no transverse beam. Similarly, Pessiki et al. (1990) reported only a small increase in the peak pull-out resistance of interior joints due to inclusion of two transverse beams. Therefore, it is likely that improvement on joint shear strength is only observed if the joint has two transverse beams, although the improvement is likely to be marginal.

3.4.1.7 Slab

Tests conducted on ductile joints with and without slabs have shown that the incorporation of slabs usually enhances the subassemblage behaviour due to the increase in flexural resistance of the beam (Ahmed & Gunasekaran, 2014). However, this also results in higher induced joint shear stresses and column shear demand which can change the failure mode from beam-sway to shear failure of the joint and/or column-sway.

Therefore, it is important to consider the increase in the flexural strength of beams due to the contribution of the slab since it may have a negative impact on the expected failure mechanism of the frame. Kurose et al. (1988) recommend including slab reinforcement within one-third of the slab on each side of the beams when calculating the negative moment capacity of beams. In comparison, recent code provisions and guidelines, such as ASCE 41 (ASCE/SEI, 2006) and the New Zealand Society for Earthquake Engineering (NZSEE, 2006), recommend that the effective width of the slab be equal to one-fifth and one-fourth of the span of the transverse beam, respectively. Recent testing conducted by Park and Mosalam (2013a) of corner joints with slab and transverse beam indicated that the contribution of the slab to the beam moment capacity is dependent on the strain level of the beam longitudinal bars. Hence, the contribution of the slab is actually dependent on the type of joint failure expected, for example joint failure prior to beam yielding versus joint failure after beam yielding. Furthermore, Park and Mosalam (2013a) recommend that the contribution of the bottom slab reinforcement bars may be ignored if they are poorly anchored into the beam.

3.4.1.8 Axial load

In general, an increase in axial load leads to an increase in joint shear capacity since the growth of cracks is restrained by compression in the surrounding concrete (Pessiki et al., 1990). Interestingly some studies have also reported that axial load has an insignificant effect on the joint shear capacity (Kurose et al., 1988). This is likely to be due to the type of failure mode experienced by the joints. Experimental testing of corner joints by Hassan (2011) indicated that high axial loads did not have an effect on joint strength if significant beam yielding occurred prior to joint failure. However, the test results showed that high axial loads increase the joint shear strength if shear failure of the joint occurs prior to beam yielding. Interestingly, it was also observed that the deformation capacity of the joint reduces with increasing axial load. This can be explained by the axial load failure mechanism experienced by joints as discussed in Hassan (2011). Once the joints experience shear failure the axial load is resisted by the shear friction on the diagonal shear failure plane and via the column bars. As sliding occurs along the shear crack, the full axial load is then resisted by the column bars which eventually buckle or sway as they reach their axial load capacity. Hence, joints with higher axial load are likely to have lower deformation capacity since the column bars are more vulnerable to reaching their axial capacity.

3.4.1.9 Speed of lateral load (pseudo-static versus dynamic cyclic loading)

Most studies which have looked at the performance of non-ductile joints have conducted slow quasi-static loading for the experimental tests. Dhakal et al. (2005) conducted cyclic loading of six full-scale non-ductile RC beam-column joints for which displacement cycles were applied at different speeds to the specimens. The loading speed varied from slow pseudo loading to up to 20 Hz which corresponds to explosion-induced ground shock frequencies. In general, it was observed that the shear strength increased with loading speed, however, based on the results presented this trend did not seem to be consistent or significant and hence it may be disregarded for the purpose of design or assessment. Furthermore, the 20 % drop of storey shear force which is commonly defined as shear failure in pseudo testing did not show consistent damage conditions when observed during high speed testing. However, consistent damage conditions were observed between pseudo and high speed loading at 80 % loss of shear stiffness. This indicates that residual shear stiffness may be a better parameter to be used for indicating the level of damage due to loading at various speeds. Nevertheless, the results indicate that testing conducted using pseudo loading may be conservatively used to assess the seismic performance of joints.

3.4.2 Columns and beams

Non-seismically designed RC frames are particularly vulnerable to column failures rather beam failures. This is because non-ductile RC frames do not follow capacity design principles and therefore hinges usually form in the columns rather than the beams due to their lower moment capacities. Furthermore, column failures can have more detrimental effects on the global response of frames and their failure may lead to the global collapse of buildings. Therefore, this section primarily focuses on the response of columns; however most of the discussion is also relevant to beams.

In general, RC column and beam failures may be categorised as flexural (F), flexure-shear (FS), shear (S) and bond failures. A brief description of the various failure mechanisms is provided below:

i. *Flexure dominated members* are described as members which reach their ultimate bending capacity, and failure is initiated due to spalling of concrete cover followed by buckling or by fracture of longitudinal bars.
ii. *Flexure-shear dominated members* are characterised as members which initially experience flexural yielding, but with deterioration of the plastic hinge region, critical shear cracks are formed. The loss of axial load capacity of the column is due

to sliding of the column along the critical shear crack as the frictional resistance reduces.

iii. *Shear governed members* are described as members which experience lateral strength degradation prior to yielding of longitudinal bars. Failure occurs due to sudden propagation of one or more critical cracks.

iv. *Bond failure* is associated with bar-slip of the longitudinal bars at the ends of the member resulting in rigid body rotations which can significantly increase the member flexibility; however ultimate failure of the member is often associated with another mechanism: flexure, flexure-shear, or shear failure.

Current methods of assessment involve determining the expected failure mechanisms which are likely to govern the response in order to determine the drift capacity of the member. In reality, column and beam failures are often due to a combination of failure mechanisms. For the purpose of assessment, if multiple failure mechanisms are expected, the drift capacity of the lower one should be taken. It has been identified that non-ductile RC columns are particularly vulnerable to flexure-shear and sometimes shear failure modes (Elwood & Moehle, 2003; Park & Mosalam, 2013b). Therefore, previous studies focusing on the macro-modelling of non-seismically designed columns assume the critical failure mode to be flexure-shear, and hence ignore flexural failure modes since the degradation of shear strength occurs before flexural deformation capacity is reached (Elwood & Moehle, 2003, 2005; Jeon et al., 2015; LeBorgne & Ghannoum, 2014a). Figure 3-8 and Figure 3-9 show non-ductile RC column failures during earthquakes predominantly due to lack of shear reinforcement and confinement.

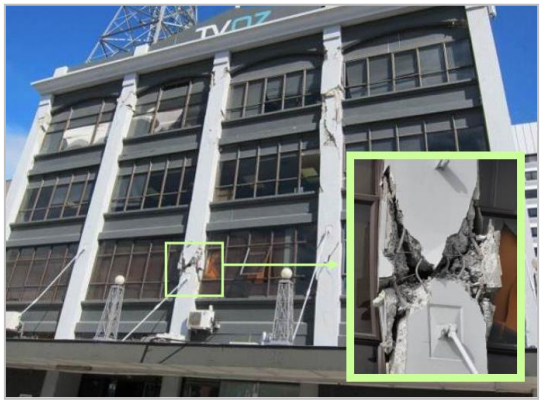

Figure 3-8: Column shear failure of a 4-storey RC frame-wall building during Christchurch earthquake in 2011 (Kam et al., 2011)

Figure 3-9: Damage experienced at the end of columns during the Kocaeli (Turkey) earthquake in 1999 (Sezen et al., 2000)

The lateral displacement response of members is predominantly due to flexural, shear, and slip deformations. The idealisation of these mechanisms is illustrated for a column under monotonic lateral loading in Figure 3-10. Some of the key parameters which have been identified as ones that affect the response of non-ductile RC columns (some of which also apply to beams) are:

- Lap-splice in potential hinge regions
- Transverse reinforcement detailing
- Axial load
- Longitudinal reinforcement ratio
- Aspect ratio
- Direction of loading

A brief description of the effect of these parameters is discussed in the following subsections.

3.4.2.1 Lap-splices in potential hinge regions

In non-seismically designed RC frames, lap-splices in the columns are often located just above the floor level. This is a high stress region (and hence a potential plastic hinge region) under lateral loading. If the region is poorly confined and the longitudinal bars have insufficient length, the yield capacity of the column may not be achieved or sustained under lateral loading. Full-scale experimental tests were conducted by Lynn et al. (1996) to investigate the effect of splices on non-seismically designed columns. The splices were $20d_b$ to $25d_b$ in length (where d_b is the diameter of the longitudinal bar). It was observed that while significant cracks formed just above the lap splice, the global response of the columns was similar to those with continuous longitudinal bars. Therefore it was

concluded that the lap-splices were sufficient in length to achieve the yield capacity, however, due to poor confinement the bending capacity was not sustained during cyclic loading and significant lateral strength degradation was observed. It should be noted, however, that this occurred in a similar manner to those columns with continuous bars. The requirement for lap-splice lengths has varied in the Australian concrete structures standard over the years. In general, the lap-splice length required for longitudinal bars in beams and columns has been $25d_b$ to $29d_b$ for bars under tension (AS 3600:1988 and AS 3600:2009, respectively) and $30d_b$ to $40d_b$ for bars under compression (AS 3600:1988 and AS 3600:2009, respectively) with larger lengths required for plain bars. Thus, it is likely that the columns in existing buildings in Australia will develop their bending capacity, however lateral strength degradation is likely to follow.

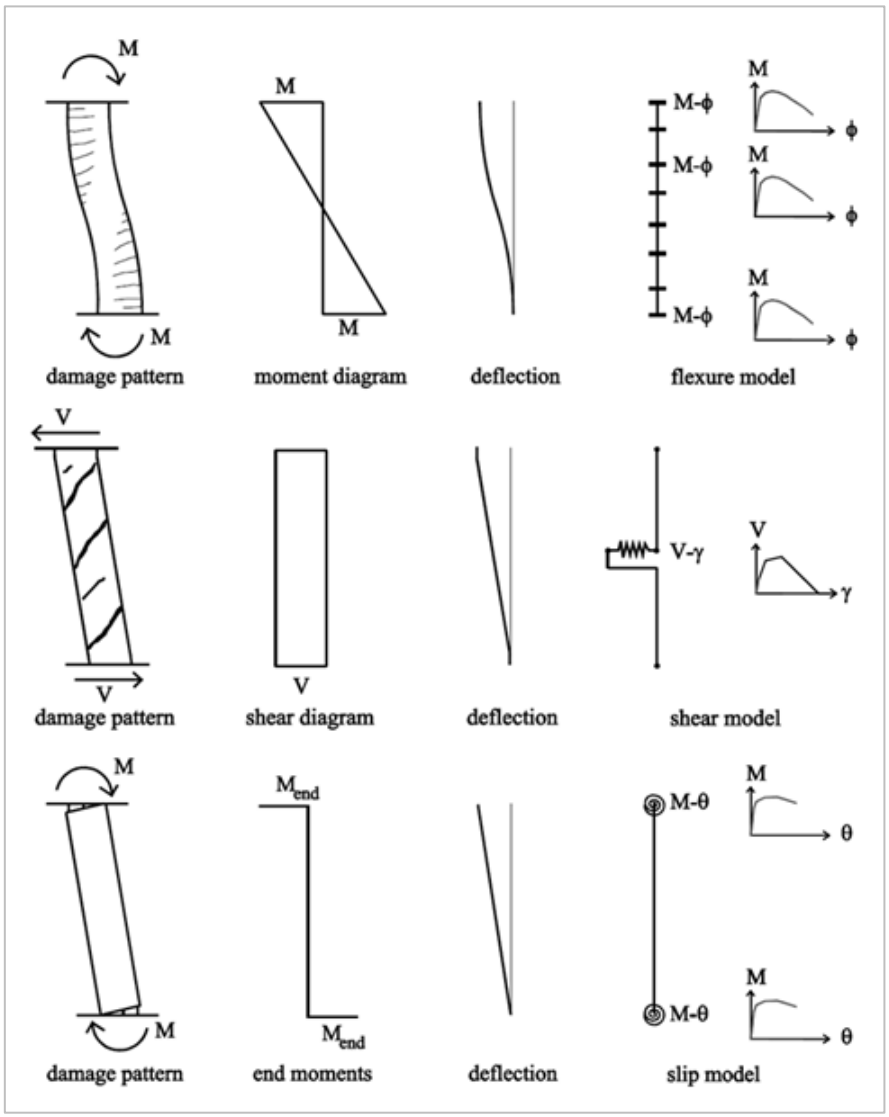

Figure 3-10: Idealised lateral response of RC columns under monotonic lateral loading (Sezen, 2002)

3.4.2.2 Transverse reinforcement detailing

Non-seismically designed columns or beams typically have widely spaced transverse reinforcement with a poor configuration that, in general, does not give sufficient lateral restraint to the longitudinal bars. This results in poor confinement of the concrete core since the transverse concrete strains resulting from axial compressive stresses are not adequately restrained by the concrete arching between the longitudinal bars which, ideally, would act as abutments for the arches. The lack of proper restraint being applied to the longitudinal bars makes them vulnerable to buckling subsequent to the spalling of the outer concrete. Furthermore, poor detailing of the ties reduces the shear capacity of the members thus making them vulnerable to shear and flexure-shear failures. Experiments consistently show that as the detailing of ties is improved the column response improves in terms of ductility and stability of hysteresis loops (Lynn et al., 1996; Saatcioglu & Ozcebe, 1989). In order to provide an indication of what is considered to be poor detailing of ties a quick summary of the criteria used to define unconfined or non-ductile beams and columns in the NZSEE (2016) guide for seismic assessment of buildings, and also in ASCE 41 (ASCE/SEI, 2013), is provided in Table 3-3. It is noted that ASCE 41 (ASCE/SEI, 2013) provides an extensive list of criteria used to define the backbone response of beams and columns based on the detailing provided; Table 3-3 only provides the worst case transverse reinforcement detailing definitions considered in ASCE 41. Furthermore, for comparison the minimum transverse reinforcement spacing requirements required in the main section of AS 3600:2009 (same requirements are required in AS 3600:1988) are also provided in Table 3-3. The comparison shows that the detailing requirements in AS 3600 for beams and columns would in general be classified as unconfined or non-ductile in accordance with the criteria in the NZSEE guide and ASCE 41. The most stringent requirement for tie spacing is that stated in ASCE 41 for beams which are considered to be controlled by flexure; requiring a minimum tie spacing of one third of the effective depth of the section. The minimum tie spacing for beams recommended in AS 3600 and NZSEE guide would be considered as beams controlled by shear in accordance with ASCE 41. Furthermore, the minimum tie spacing requirement for columns based on the gross or effective section depth is the least stringent in AS 3600, which requires the minimum spacing to be equal to the gross section depth, whereas the NZSEE guide and ASCE 41 require the spacing to be at least half the effective depth of the section.

Table 3-3: Definition of unconfined or non-ductile columns and beams in accordance with NZSEE Guide and ASCE 41, and detailing requirements in accordance with AS 3600

	NZSEE Guide (2016)	**ASCE 41 (ASCE/SEI, 2013)**	**AS 3600**
Transverse reinforcement configuration	Ties are only provided around corner bars, and/or ties are not bent back into the core, i.e. ties which have 90° hooks	Ties with 90° hooks or lap-spliced ties	Ties may be provided only around the corner bars depending on the spacing between longitudinal bars, and if internal one leg ties are required they may have 90° hook on one end and 135° hook on the other end
Transverse reinforcement spacing	Spacing of ties in the plastic hinge regions for beams and columns are: $s \geq \frac{d}{2}$, or $s \geq 16d_b$	Spacing of ties for beams are: $s \geq \frac{d}{3}$ for beams controlled by flexure $s \geq \frac{d}{2}$ for beams controlled by shear or inadequate development lengths or splicing along the span Spacing of ties for columns are: $s \geq \frac{d}{2}$, or $\frac{A_{sv}}{b_w s} \leq 0.002$	Spacing of ties for beams is the smaller of: $s \leq 0.5h_b$, or 300 mm If the shear demand is less than 70 % of the shear strength provided with minimum reinforcement then the spacing of ties for beams is the smaller of: $s \leq 0.75h_b$, or 500 mm Spacing of ties for columns is the smaller of $s \leq D_c$, or $15d_b$

s: is the tie spacing | d: is the effective depth of the beam/column section in the plane of bending | d_b: is the diameter of the longitudinal reinforcement | A_{sv}: is the cross-sectional area of transverse reinforcement | b_w: is the width of the web

3.4.2.3 Axial load

In general, an increase in axial load results in higher flexural strength (and shear strength); however, it also significantly reduces the deformation capacity of columns. Numerous experiments have demonstrated that as the applied axial load increases, the strength and stiffness degradation accelerates during cyclic loading and loss of axial-load carrying capacity of the column occurs at much lower drifts (Fardipour, 2012; Lynn et al., 1996; Saatcioglu & Ozcebe, 1989; Sezen, 2002). Thus, the response of columns is highly

dependent on the amount of axial load applied, which is often expressed as the axial load ratio (ALR) and is calculated using Eq. 3-2.

$$ALR = \frac{P}{f_c' A_g} \quad \text{Eq. 3-2}$$

Where P is the axial load on the member

A_g is the gross cross-sectional area of the member

Furthermore, under earthquake loading columns in the perimeter frame are likely to experience changes in axial load, especially if the frame forms part of the primary lateral load resisting system. In an experimental test Sezen (2002) compared the response of a column subjected to a constant axial load of 2670 kN corresponding to an axial load ratio of 0.6 to that of a column subject to a varying axial load ranging from 2670 kN to -250 kN with an initial gravity axial load ratio of 0.25. It was observed that the column subjected to varying axial load lost its axial load capacity at a higher drift of approximately 2.9 % in comparison to the column subjected to a constant axial load, which collapsed at a drift of 1.9 %. This indicates that the increase in compressive axial load during lateral loading has a less detrimental effect than the initial gravity loading.

3.4.2.4 Longitudinal reinforcement ratio

An increase in longitudinal reinforcement ratio leads to an increase in flexural strength, however, it has been observed in experiments that it may decrease the drift capacity of members. The decrease in the drift capacity of the member is predominantly due to the change of failure mechanism of the member. Fardipour (2012) tested two non-seismically detailed columns under an axial load ratio of 0.2 with longitudinal reinforcement ratios of 0.56 % and 1.0 %. It was observed that the column with the higher reinforcement ratio experienced a loss of axial load carrying capacity at half the drift achieved by the column with the lower longitudinal reinforcement ratio. The column with the lower reinforcement ratio displayed a flexural failure mechanism (experiencing axial load failure at 5.0 % drift) whereas the column with the higher longitudinal reinforcement ratio displayed a flexure-shear failure mechanism (failing at 2.5 % drift). The experiment was repeated for a higher axial load ratio of 0.4, but similar trends were not observed. Despite both columns having different longitudinal reinforcement ratios, they failed at approximately the same drift (at 1.5 %) and both displayed a flexure-shear failure mechanism.

3.4.2.5 Aspect ratio

The aspect ratio of columns and beams, which is defined as the ratio of the shear span to the depth of the cross-section, affects the type of failure mode expected. As the aspect ratio increases the failure mode changes from flexural to shear. Interestingly though, results from experimental tests have shown that the aspect ratio has an insignificant effect on the ultimate drift capacity of columns, especially for columns with aspect ratios greater than 2.5 (Fardipour, 2012; Rodsin, 2007). Other parameters, including the detailing of the reinforcement and axial load on the columns have a more significant effect on the drift capacity achieved by columns.

3.4.2.6 Direction of loading

The strength and displacement capacity of columns is significantly influenced by the loading path, in particular loading which causes biaxial bending. However, detailed experimental results are still limited for columns tested under biaxial lateral cyclic bending (with axial load), especially for flexure-shear critical columns. This is reflected in the absence of recommendations and guidelines for calculating the capacity of columns, in particular deformation capacity of columns, under biaxial bending.

One of the early experimental studies which investigated the effect of deformation path applied to RC columns was conducted by Saatcioglu and Ozcebe (1989). They investigated the response of shear-flexure critical square RC columns by conducting 14 full-scale tests. Three types of loading protocols were investigated: (i) unidirectional cyclic deformations applied to a principal axis, (ii) diagonal cyclic loading which produced equal components of bending and shear in the two principal directions, and (iii) elliptical bidirectional cyclic deformations (this was conducted for only two of the 14 columns tested). It was reported that the overall hysteretic response, including strength and stiffness degradation, was not affected by biaxial bending if the load followed a straight line path; that is, the diagonal loading protocol. However, the columns subjected to simultaneously varying bidirectional load reversals displayed a significantly different response in comparison to the columns subjected to unidirectional loading. The level of damage in one direction significantly affected the column response in the other direction once yield deformation was reached in one direction. Once yield deformations were reached in both directions, significant strength and stiffness degradation occurred. Based on the reported values, the reduction in ultimate moment capacity of the columns under bidirectional loading were approximately 70 % of those obtained under unidirectional loading. For two different column types (B1 and B2), the response of the columns tested under two different types of

bidirectional loading, and of a column with similar detailing tested under unidirectional loading (U4 or U3), are presented in Figure 3-11 and Figure 3-12.

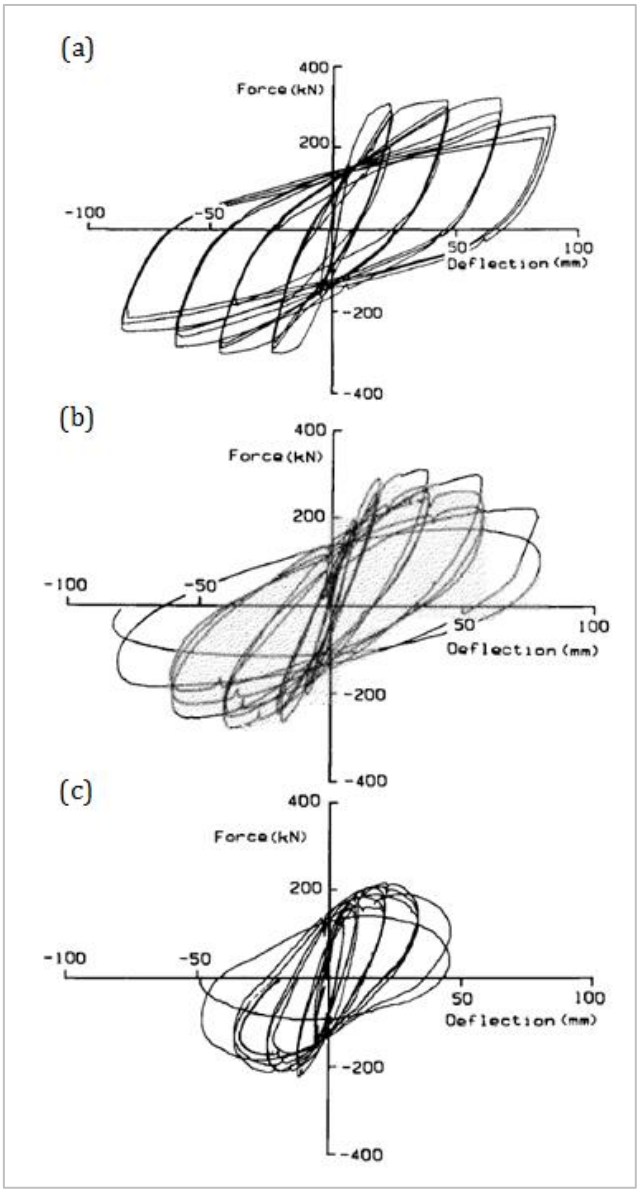

Figure 3-11: Columns tested by Saatcioglu and Ozcebe (1989): (a) response under unidirectional (specimen U4), (b) North-South response under bidirectional loading (specimen B1), (c) East-West response under bidirectional loading (specimen B1),

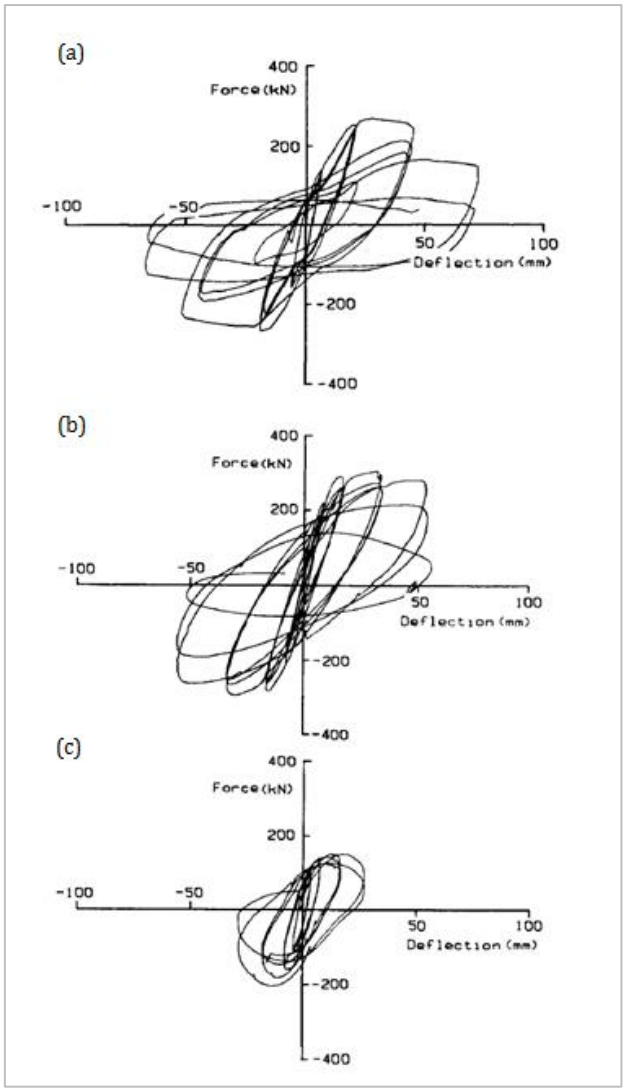

Figure 3-12: Columns tested by Saatcioglu and Ozcebe (1989): (a) response under unidirectional (specimen U3), (b) North-South response under bidirectional loading (specimen B2), (c) East-West response under bidirectional loading (specimen B2),

More recently, detailed experimental results were presented by Rodrigues et al. (2013) who tested 24 RC columns under uniaxial and biaxial loading. It was reported that the columns tested under biaxial loading experienced a 20-30 % reduction in maximum strength in their weak direction and 8-15 % reduction in the strong direction when compared with those tested under uniaxial loading. The drift demands at cracking were reported to be the same for the columns tested under biaxial and uniaxial loading. At spalling, the drifts of the columns tested under biaxial loading were 50-75 % of those observed under uniaxial loading, and at bar buckling, the drifts for the biaxial tests were 65-75 % of those observed in the uniaxial tests. It is noted that the columns tested by Rodrigues et al. (2013) were flexure governed columns, and interestingly it was observed

that the plastic hinge length was approximately the same for columns tested under uniaxial and biaxial loading.

Based on numerical modelling Zoppo et al., (2016) investigated the deformation capacity of non-conforming, flexure governed RC columns under biaxial bending. While the results were not validated with experimental tests, they provide an insight and a better understanding of column response under biaxial bending. In total, Zoppo et al., (2016) obtained numerical results for 780 square and rectangular columns and used these to investigate the influence of axial load, geometry, amount of longitudinal reinforcement and mechanical properties on the ultimate chord rotation of the columns. It is reported that the maximum chord rotation capacity under biaxial bending reaches only approximately 40-50 % of the uniaxial chord rotation for axial load ratios of less than 20 %, for both square and rectangular cross-sections. Interestingly, in the case of higher axial load ratios, the effect of biaxial bending was reported to be less dramatic, with the deformation capacity reduced to approximately 80 % (for axial load ratio of 60 %) of the uniaxial case. It is demonstrated that the amount of reduction of the deformation capacity of biaxially loaded columns is highly dependent on angle of incidence of the imposed displacements. For square columns with symmetrical reinforcement detailing, the minimum deformation capacity occurs when the angle of incidence is 45 degrees, for rectangular columns, the minimum deformation capacity is dependent on geometry and axial load ratio as well as the angle of incidence. Furthermore, Zoppo et al., (2016) also concluded that the reduction of deformation capacity due to the simultaneous presence of the two components of bending is higher than the reduction of strength, which is evident in the experimental results discussed earlier.

3.4.3 Walls

Similar to columns and beams, the failure mechanism of walls can be predominantly categorised as flexural, flexure-shear, and shear. Bond failure and splice failure may also take place, however, the ultimate failure mechanisms of walls is associated with one of the three predominant failure mechanisms. The predominant failure mechanism of the walls is highly dependent on the aspect ratio, that is, the ratio of wall height to wall length. Flexure controlled behaviour is typically expected for slender walls, defined as having aspect ratios greater than or equal to 2.0 (Pugh et al., 2015). In addition, Wibowo et al. (2013) explain that moderate walls, defined as having aspect ratios between 1.0 and 2.0, are also likely to develop a flexural failure mechanism. This is explained to be particularly the case for lightly reinforced walls due to the inherent shear strength of the concrete compared to the lateral force that can be developed by the wall under flexure. The flexural

response of the walls with low aspect ratios was observed for the six walls tested by Kuang and Ho (2007) where cyclic testing of walls with aspect ratios of 1.0 and 1.5 with longitudinal and transverse reinforcement ratio of approximately 1 % were conducted. Since the walls in this study are lightly reinforced and mostly have aspect ratios greater than 2.0, the flexural failure mechanisms of the walls will be examined. It should be noted that the only walls with aspect ratios less than 2.0 are a couple of the two-storey walls; they have aspect ratios between 1.0 and 2.0 which are considered acceptable for the reasons given above. The loss of lateral load carrying capacity of walls due to the flexure controlled mechanism can occur in the following ways (Pugh et al., 2015):

i. Compression failure: crushing of concrete core and buckling of longitudinal reinforcement
ii. Low-cycle fatigue of the reinforcement: buckling of bars followed by fracture of longitudinal reinforcement
iii. Tension failure: rupture of longitudinal reinforcement

As part of an on-going research at the University of Melbourne and Swinburne University of Technology to assess the seismic performance of RC buildings, significant research has been conducted to investigate the seismic performance of walls with detailing typical of Australian buildings (Goldsworthy & Gibson, 2012; Hoult et al., 2017; Hoult, 2017; Hoult et al., 2014; Wibowo et al., 2013; J. L. Wilson et al., 2015). Consistently, the key parameters which have been identified as ones that influence the capacity and response of the flexure governed walls include the longitudinal reinforcement ratio, confining reinforcement, and axial load ratio. These parameters as well as the effect of bidirectional loading on the response of walls are discussed in the following subsections.

3.4.3.1 Longitudinal reinforcement ratio

Experimental and numerical studies have highlighted that RC walls with low longitudinal reinforcement ratios, which is common design practice in regions of low-to-moderate seismicity (Wibowo et al., 2013), are particularly vulnerable to brittle tension failure due to an insufficient number of cracks forming in the plastic hinge region (Henry, 2013; Hoult et al., 2017; Lu et al., 2016). Walls with a single crack formation have been reported in reconnaissance reports, including the 1985 Chile earthquake (Wood et al., 1991) and the 2011 Christchurch earthquake (Buchanan et al., 2011; Kam et al., 2011; Sritharan et al., 2014). An example which clearly demonstrates the formation of concentrated cracking at the base of the wall and fracture of longitudinal bars after an earthquake is shown in Figure 3-13. The wall belongs to the Gallery Apartments building which survived the

Christchurch earthquake without collapsing but had to be demolished due to extensive damage.

The response of walls due to various degrees of crack formation is illustrated in Figure 3-14. Once the wall cracks close to the base, the tension forces developed in the lightly reinforced wall are insufficient to develop secondary cracking in the surrounding concrete, and hence high strains are developed in the longitudinal steel over a concentrated length of the wall, leading to fracture of the bars at low displacement demands. The formation of a single crack or minimal cracking is always expected for a member if the cracking moment capacity is higher than the yield (or ultimate) moment capacity of the wall (Goldsworthy & Gibson, 2012; Henry, 2013; Wibowo et al., 2013). Figure 3-15 illustrates the moment-curvature analysis conducted by (Henry, 2013) to explain why one of the walls (with a longitudinal reinforcement ratio of 0.16 %), belonging to the Gallery Apartments building, failed during the Christchurch earthquake due to fracture of longitudinal bars while displaying only minimal cracks at the base. To prevent this type of failure for flexural members, standards and codes have minimum tensile reinforcement area requirements. The recommendations are based on requiring the cracking moment of the section to be lower than the nominal bending capacity to ensure that a ductile response may be achieved. AS 3600:2009 requires the ultimate capacity of a flexural member to be 1.2 times the cracking moment capacity. However, some studies recommend greater precaution and suggest that the moment capacity should be at least 1.5 to 2.0 times the cracking moment capacity (Morris et al., 2015; Paulay & Priestley, 1992). Based on finite element analyses of lightly reinforced rectangular walls, Hoult et al. (2017) demonstrated that a minimum moment capacity of 2.0 times the cracking moment is required for a good distribution of inelastic behaviour.

In AS 3600:2009, all walls do not need to be designed as flexural members. If the calculated design actions indicate that the critical wall section is only subjected to compression, then in-plane bending may be neglected and a simplified design method may be adopted for the design of vertical compressive forces. Therefore, in terms of the minimum longitudinal reinforcement ratio, the only requirement which needs to be met is a minimum of 0.15 % which has been established to control shrinkage and thermal effects as discussed in the commentary of AS 3600 (Standards Australia, 2014). Hence, many older buildings and new low- to mid-rise buildings constructed in Australia tend to have very low longitudinal reinforcement ratios.

Figure 3-13: Fracturing of wall reinforcement in the Gallery Apartments building during the Canterbury earthquakes: (a) small crack at the base of the wall, (b) fracture of longitudinal bars is revealed after concrete removal (Sritharan et al., 2014)

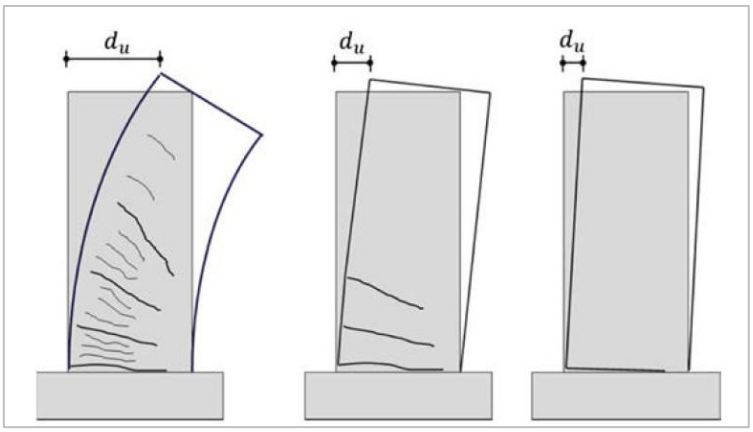

Figure 3-14: Wall response due various crack formation: (a) distributed cracks, (b) limited cracks, and (c) single crack (Lu et al., 2016)

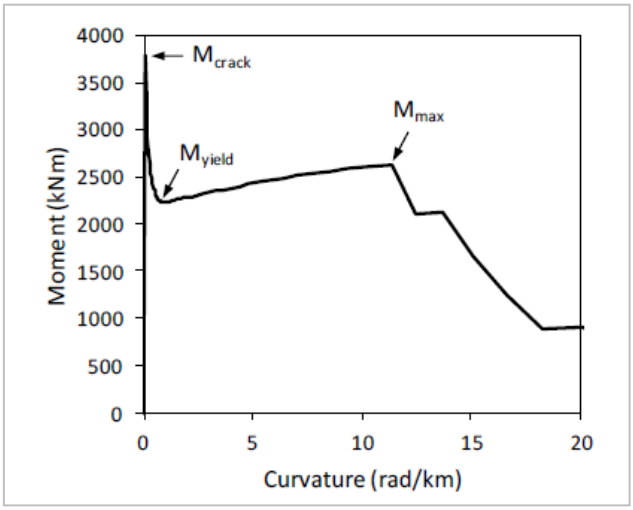

Figure 3-15: Moment-curvature analysis conducted for one of the walls belonging to the Gallery Apartments building (Henry, 2013)

3.4.3.2 Confining reinforcement

Experimental studies have illustrated that the displacement capacity of the walls controlled by compression failure is improved with confining reinforcement in boundary regions (Thomsen & Wallace, 2004; Wibowo et al., 2013). This is because the concrete core is capable of reaching higher strains and thus delaying crushing of the core concrete. The concrete outside of the core will spall off if the strain reaches about 0.003 and the longitudinal bars are then vulnerable to buckling outward, especially if they have yielded previously in tension. The transverse reinforcement, if closely spaced, also tends to delay the onset of buckling of the reinforcement bars. As discussed in Hoult (2017), it is typical for walls constructed in Australia, especially in older buildings and current buildings which are in general mid-rise in height, to have no confinement. Therefore, it is likely that the walls assessed in this study will be vulnerable to brittle compression failures.

3.4.3.3 Axial load ratio

Similar to columns, the displacement capacity and hence ductility of walls is highly dependent on the axial load ratio (Dazio et al., 2009; Wibowo et al., 2013). Experimental results demonstrate that walls with low axial load ratios display higher displacement capacities when compared with walls with high axial load ratios since those with the higher ratios tend to undergo brittle compression failures at lower displacement levels. However, the walls assessed in this study are likely to have low axial load ratios (less than 10 %) due to the height of buildings assessed and the separate design of the gravity load and lateral load resisting systems.

3.4.3.4 Bidirectional loading

During an earthquake it is likely that the walls forming part of the lateral load resisting system will experience bidirectional loading. This is particularly the case for non-planar walls which are designed to resist lateral loads along both principal axes. However, in most of the wall component experimental tests that have been conducted, the walls have been subjected to unidirectional loading and thus there is great uncertainty about the response of walls under bidirectional loading. Recent studies in Europe and America have tried to bridge this gap by conducting experimental studies on non-planar walls subjected to bidirectional loading (Behrouzi et al., 2010; Beyer et al., 2008b; Beyer et al., 2017; Constantin & Beyer, 2016).

Beyer et al. (2017) have provided a review of existing experimental results for planar and non-planar walls subjected to unidirectional and bidirectional quasi-static cyclic loading. The results of three independent studies on planar walls (Almeida et al., 2017;

Kabeyasawa et al., 2014; Tatsuya, 1996) demonstrated that the ultimate strength of the walls was not impacted by bidirectional loading. However, the displacement capacity of the walls subjected to bidirectional loading was, on average, 75-85 % of the displacement capacity of the walls subjected to unidirectional loading. In contrast, the review of the response obtained for non-planar walls, namely U-shaped walls tested by Ile and Reynouard (2005), revealed that bi-directional loading may reduce the ultimate strength of the walls; in particular it reduces the ultimate strength of these walls about the axis for which pre-existing displacements in the orthogonal direction had been induced due to the loading protocol. The results obtained by Ile and Reynouard (2005) are provided in Figure 3-16. It can be seen that the ultimate strength from the bidirectional results is similar to that from the results obtained under unidirectional loading for the positive y-direction and negative x-direction, and for bending about the weak and strong axis respectively. However, the ultimate strength and stiffness from the bidirectional results are significantly lower than those from the results obtained from the unidirectional loading for the negative y-direction and positive x-direction. The difference in the response is explained to be due to the loading sequence and pre-existing deformations in the orthogonal direction. Based on the results presented, the reduction in ultimate strength obtained under bidirectional loading is approximately 80-90 % about the direction for which strength reduction is observed. The results also illustrate displacement capacity reductions in the principal directions. The displacement capacity for bi-directional loading was observed to be 67 % of that obtained during unidirectional loading (Beyer et al., 2017). Interestingly, Beyer et al. (2017) notes that the displacement capacity along the diagonal direction for the wall tested under bidirectional loading is approximately equal to the displacement capacity along the principal directions of the wall tested under unidirectional loading.

Similar results were also observed from the experimental results presented by Behrouzi et al. (2010). Three U-shaped walls were tested; one under unidirectional loading (along the main axis of the wall) and two under different bidirectional loading protocols. It was observed that the drift capacity of the walls under bidirectional loading reduced to approximately 67-90 % of the drift capacity obtained under unidirectional loading. In addition, the moment capacities obtained from the test were compared to the nominal flexural strengths calculated according to ACI 318. It was observed that the maximum base moment about the weak axis of both walls tested under bidirectional loading ranged from 79 to 100 % of the ACI 318 nominal flexural strength and it was concluded that the reduction is likely to be due to the imposed displacement history during the loading

protocol. The experimental results obtained for the wall tested under unidirectional loading, and for one of the walls tested under bidirectional loading, are presented in Figure 3-17 and Figure 3-18, respectively.

It is noted that the experimental tests conducted in the studies discussed above involve non-planar walls with reinforcement detailing much superior than the detailing of the walls to be assessed in this study. Nevertheless, these studies provide an insight into the response of walls when subjected to bidirectional loading. To the knowledge of the author, no Australian based studies have been conducted to investigate the response of lightly reinforced walls to bidirectional loading.

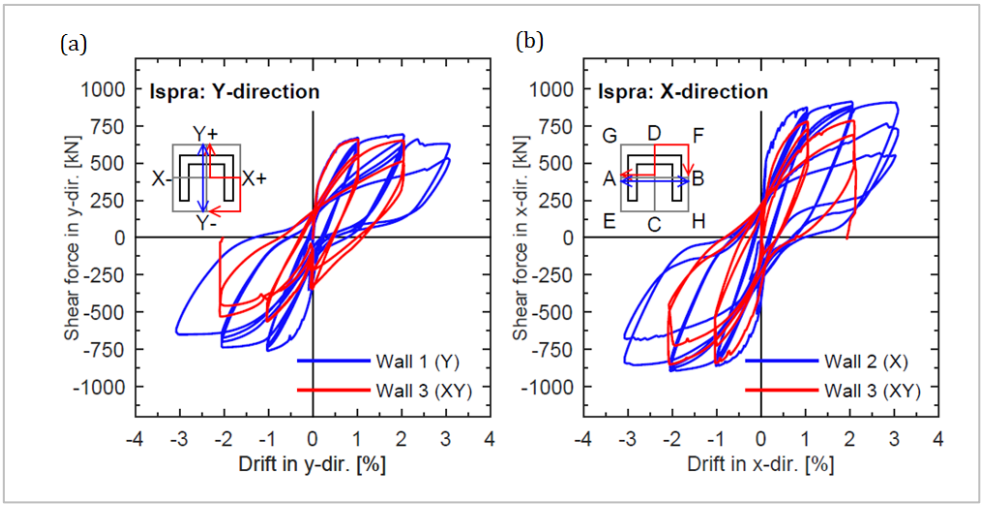

Figure 3-16: Force-displacement response of U-shaped walls tested by Ile and Reynouard (2005) under unidirectional loading (in blue) and bidirectional loading (in red): (a) parallel to flanges, (b) parallel to web, from Beyer et al. (2017)

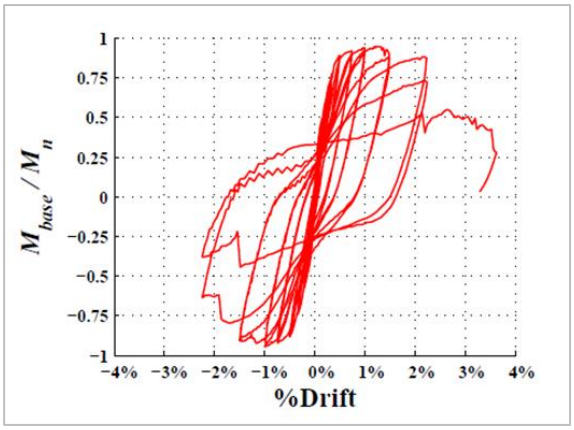

Figure 3-17: Normalised moment-drift response of U-shaped wall tested under unidirectional loading by Behrouzi et al. (2010)

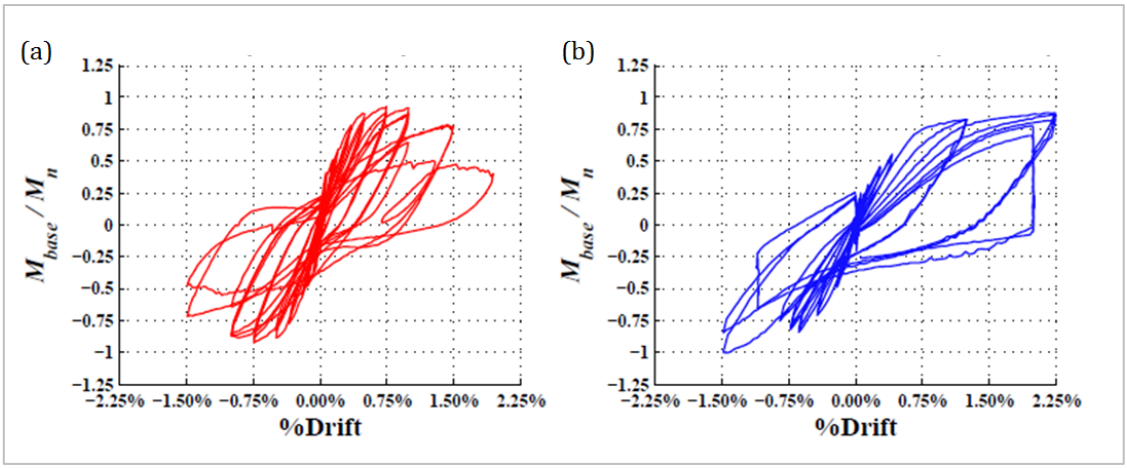

Figure 3-18: Normalised moment-drift response of U-shaped wall tested under bidirectional loading by Behrouzi et al. (2010): (a) strong axis, (b) weak axis

3.5 CONSIDERATION OF LATERAL LOAD AND GRAVITY LOAD RESISTING SYSTEMS

Researchers have highlighted that it is critical to consider the response of both the lateral load resisting system, typically referred to as the primary structural system, and the gravity load resisting system, typically referred to as the secondary structural system, when assessing the seismic performance of buildings. The main reason for the need to incorporate the response of the secondary system, as well as the primary system, is to assess if the gravity load resisting system is able to sustain the deformations imposed by the primary system. Some studies argue that it is possible for the gravity system to fail prior to the loss of lateral load carrying capacity of the primary system due to applied deformations exceeding the displacement capacity of the gravity system (Goldsworthy & Gibson, 2012; Kam & Jury, 2017; Kim et al., 2004). This is primarily a concern for buildings with non-ductile gravity systems since they are vulnerable to sudden brittle failures, especially if the primary system does not provide adequate protection to load paths thus leading to diaphragm detachments, punching shear and slab-to-column connection failures. The vulnerability of the gravity system is exacerbated for buildings with plan asymmetry as the torsion induced during seismic excitation can significantly increase the displacement demand imposed on the gravity system. Furthermore, studies have highlighted that when assessing the performance of the buildings up to the collapse limit state, to avoid over-conservatism, it is necessary to define the structural damage limit as when loss of axial load carrying capacity rather than loss of lateral load carrying capacity is reached (Baradaran Shoraka et al., 2013; Elwood & Moehle, 2003). Since loss of axial load failure may initiate in the gravity system prior to or immediately after the loss of

lateral load carrying capacity of the primary system, it is necessary to assess the performance of both the primary and secondary systems.

Interestingly, most studies which have been conducted in the literature to assess the seismic performance of buildings primarily focus on modelling and analysing the primary lateral load resisting system (Baradaran Shoraka et al., 2013; Jeon et al., 2015). This is because most studies have assessed the performance of buildings for which the gravity and lateral load resistance is provided by the same system (most of the collapse studies conducted thus far have focused on moment resisting frames) or there is an assumption that the gravity load resisting system is more flexible than the primary lateral load resisting system, and hence the gravity load resisting system will have sufficient displacement capacity to move with the primary lateral load resisting system during an earthquake.

A well-known example which illustrated the importance of considering displacement compatibility between the primary and the secondary system is the collapse of the carpark at the California State University Northridge Campus during the 1994 Northridge earthquake (Norton et al., 1994). The carpark had ductile perimeter moment frames and non-ductile interior gravity frames which collapsed as they were not detailed to sustain the large displacements imposed on them. Figure 3-19 shows a photograph of the carpark taken after the earthquake which clearly illustrates the flexibility of the perimeter frame which is intact after the earthquake; however it has fallen into the interior gravity system which was incapable of resisting the large imposed deformations.

Figure 3-19: Photograph of the carpark at the California State University Northridge Campus taken after the 1994 Northridge (The Atlantic Monthly Group, 2014)

The importance of the interaction between the primary and secondary structural systems is now well understood in regions of high seismicity. The current standard and codes in these regions require that displacement compatibility between the two structural systems is checked during the seismic design and assessment of buildings (American Society of Civil Engineers (ASCE/SEI), 2013; NZSEE, 2016). The Australian earthquake loading standard, AS 1170.4:2007, also requires that displacement compatibility is maintained between the primary and lateral loading resisting system. However, in Australia, often the lateral load resisting system and the gravity resisting system are designed separately and it not clear to what extend displacement compatibility is checked in practice. In addition, most older existing buildings (buildings built prior to 1995) were not designed for seismic loads and therefore displacement compatibility may be a concern for these buildings. Although, it is noted that the assumption of displacement compatibility between the primary and secondary system may be valid in Australia if brittle and sudden failure mechanisms do not take place. This is because the gravity load resisting system (normally consisting of moment resisting frames and/or band-beam and flat slab floor systems) is usually more flexible than the lateral load resisting system (normally consisting of core or shear walls).

Furthermore, for the inherent robustness of buildings it is also desirable that the gravity load resisting system has the capacity to deform (without collapse) in excess of the drifts calculated for the lateral load resisting system using the code-specified design event (typically just a 500 year return period for most buildings). This is because it is the failure of the gravity load resisting system that leads to catastrophic failures of buildings in cases where the primary lateral resisting system reaches its capacity or does not perform as expected. This was illustrated with the collapse of both CTV and Pyne Gould Corporation (PGC) buildings in Christchurch.

The CTV building was constructed in 1986 and it was designed such that the lateral load resistance was provided only by the shear walls, and gravity load was resisted by the frames. The building plan drawing for level two is provided in Figure 3-20. The extensive details of the reasons for the collapse of the building are discussed in the Canterbury Earthquakes Royal Commission (CERC) (2012a) report. The primary structural cause of the collapse of the building was due to the loss of slab connection between the walls and the columns and the large displacement demands imposed (partly due to plan irregularity of the building) on the poorly detailed beam-column joints and columns. The columns had insufficient displacement capacity due to inadequate transverse reinforcement, lower concrete strength than expected, and also higher axial load than intended most likely due

to the vertical accelerations induced by the earthquake. The joints also responded in a brittle manner due to lack of transverse reinforcement and discontinuous reinforcement in the joint panel. In summary, the main cause of the rapid collapse of the building may be concluded to be due to "limited robustness (tying together of the building) and redundancy (alternative load path)" (CERC, 2012a).

The PGC building also collapsed after the Christchurch earthquake. It was constructed in 1966, thus before ductile and capacity design standards were introduced in New Zealand. A typical upper floor level plan drawing is provided in Figure 3-21. The building collapse was due to initially the RC walls and cores reaching their ultimate capacity, and hence afterwards large displacement demands were imposed on the gravity system which eventually exceeded its capacity and resulted in the pancake collapse of the floors. The progressive collapse of the building based on analysis conducted by Beca is illustrated in Figure 3-22.

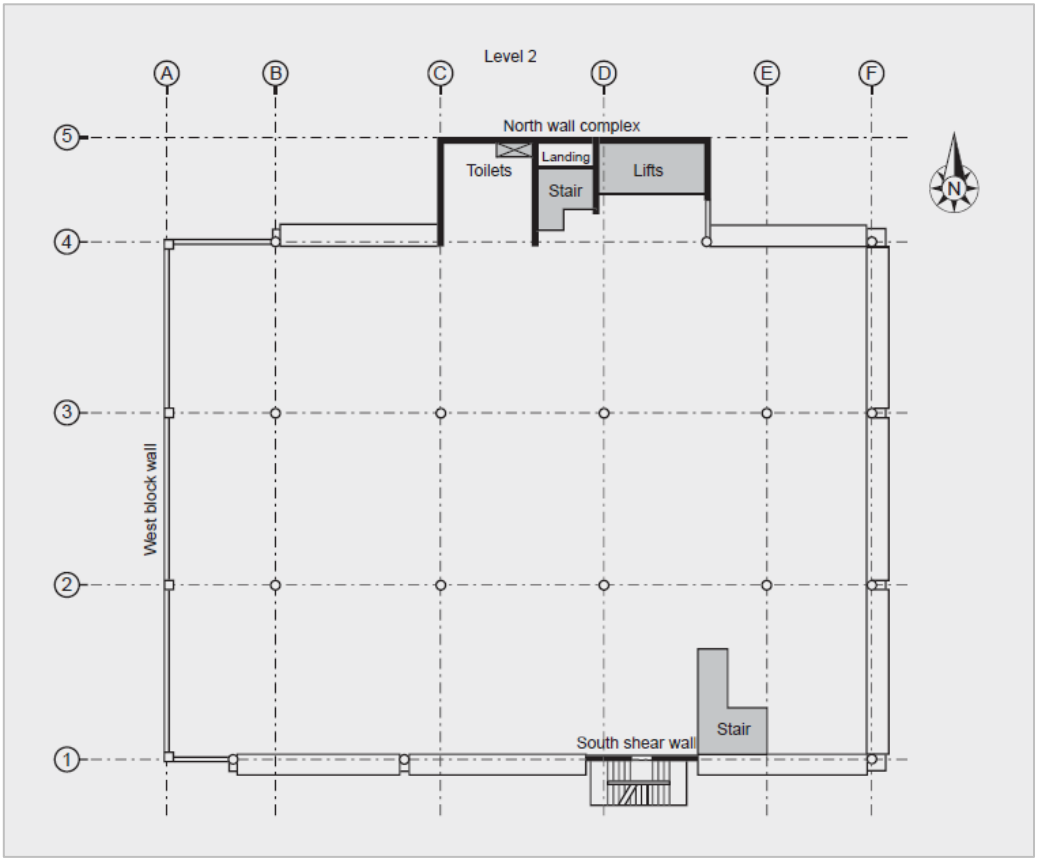

Figure 3-20: CTV building plan for level 2, (CERC, 2012b)

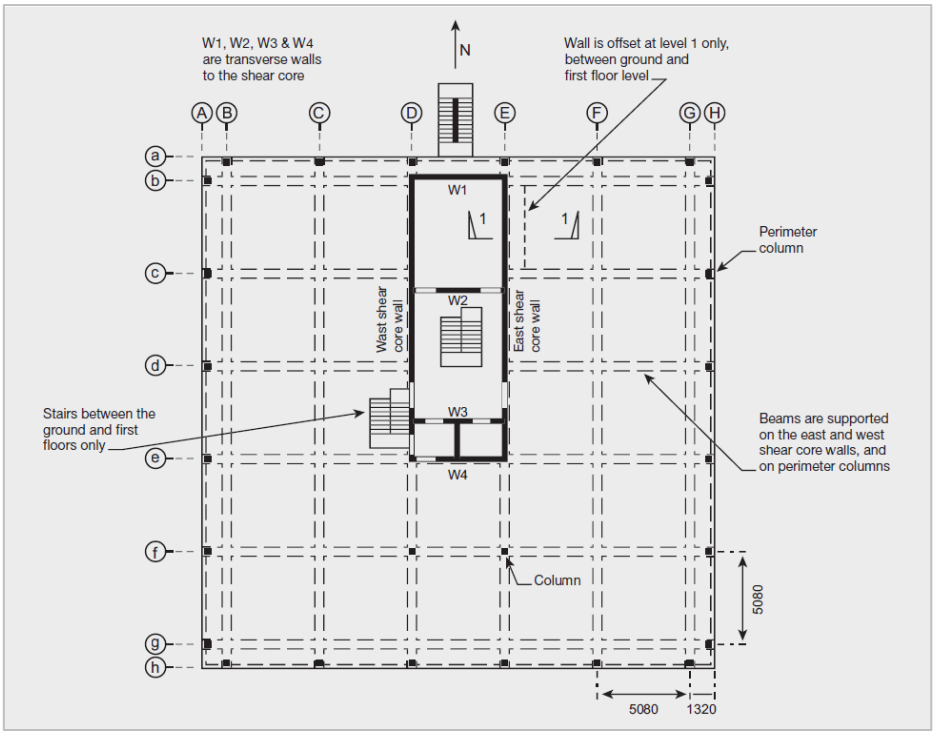

Figure 3-21: PGC typical upper level building plan, (CERC, 2012b)

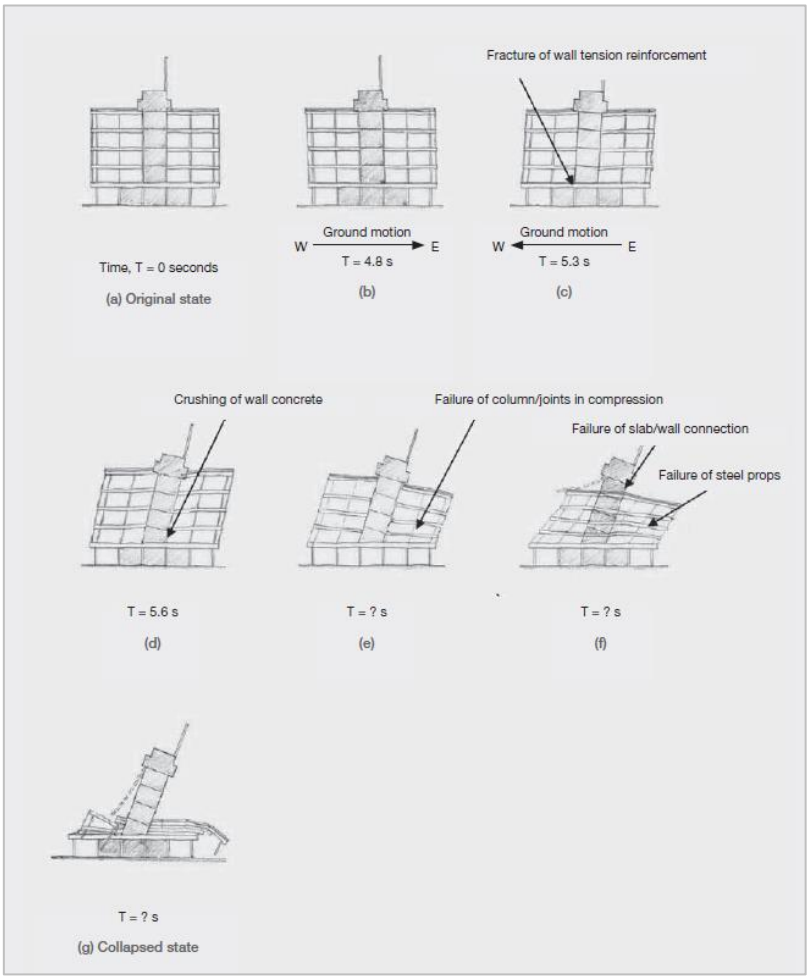

Figure 3-22: Progressive collapse scenario based on analysis conducted by Beca (CERC, 2012b)

3.6 MATERIAL PROPERTIES FOR ASSESSMENT

When assessing the performance of existing structures it is ideal to use material properties obtained from these structures. This is because there are many different factors that can cause a difference in material properties (especially strength) from the specified design values. However, when assessing the performance of a class of buildings using the approach of developing archetypal buildings, as done in this study, it is necessary to use probable or expected material properties. These values are usually based on testing conducted on a large number of samples taken from existing structures or from products produced by manufacturers. Furthermore, it will often suffice to adopt the median or mean values, since studies which have investigated the effect of using a random combination of material strengths using sampling methods (such as Latin Hypercube Sampling) have concluded that the effect is negligible when comparisons are made with the behaviour obtained using mean/median material properties (Jeon et al., 2015; Kwon & Elnashai, 2006). These studies have predominantly investigated the effect of adopting different concrete compressive strengths and steel yield strengths for which the material strengths were varied with coefficient of variance of up to approximately 30 %. Thus, the following subsections discuss the probable material properties to be adopted in this study to assess the performance of the archetypal buildings in Chapter 7.

3.6.1 Steel reinforcement

The buildings assessed in this study are representative of buildings constructed prior to 1995 and as it will be discussed in Chapter 7, the archetypal buildings will be designed in accordance with AS 3600:1988. Therefore, the buildings are likely to have 410Y or 400Y bars as the main reinforcement. There were two types of Y-bars which were available in Australia: *Tempcore*, supplied by BHP, and *Welbend*, supplied by Smorgon Steel. The tensile steel properties provided in the *Tempcore* and *Welbend* specifications document are summarised in Table 3-4. In addition, the nominal properties specified by AS 1302 (Standards Australia, 1991) are also provided in Table 3-4 for comparison. It is noted that both suppliers report the total elongation strain rather than the uniform elongation strain (i.e. the strain at the ultimate tensile strength) and thus the uniform elongation strain values provided in Table 3-4 are obtained from the typical stress-strain curves provided in the specifications handbook (provided in Figure 3-23) for the purpose of comparison. The total and uniform elongation values are defined as shown in Figure 3-23(b).

Based on the material properties presented in Table 3-4, it can be seen that the *Welbend* Y-bars tend to have better tensile properties than the *Tempcore* Y-bars. Hence the mean

material properties of *Tempcore* Y-bars are to be adopted in this study to provide conservatism in the prediction of the reinforcement properties.

Table 3-4: Summary of tensile properties of Y-bars

	Yield strength (MPa)	Tensile to yield strength ratio	Uniform elongation	Total elongation
AS 1302: nominal values	400-410	1.05-1.1	0.12-0.16	NA
Tempcore: mean properties	460	1.21	0.12*	0.25
Tempcore: standard deviation	17	0.03	NA	0.02
Welbend: mean properties	495	1.26	0.21*	0.268
Welbend: standard deviation	20.6	0.035	NA	0.017

* Uniform elongation values based on testing have not been reported, the values presented in this table are obtained from typical stress-strain curves provided in the specifications by the suppliers | NA: not available

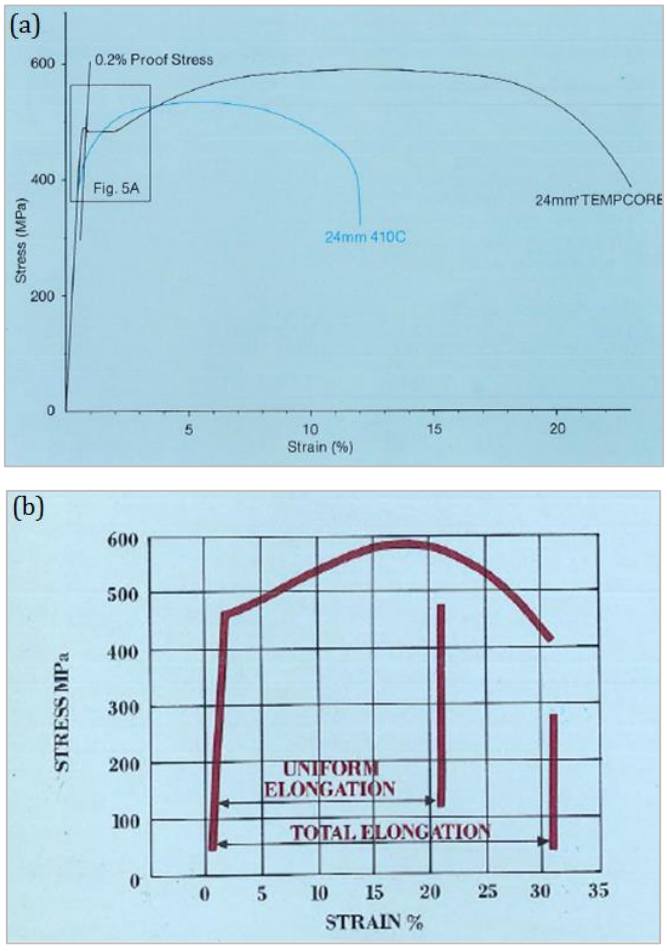

Figure 3-23: Typical stress-strain curves for Y-bars provided by: (a) Tempcore, (b) Welbend

3.6.2 Concrete

The average concrete compressive strength can vary significantly from the specified characteristic design strength for numerous reasons, including: the target strength (average value) will necessarily be higher than the characteristic value used in design which is a 5 percentile value (if a large number of specimens were tested 95 % should lie above this value at 28 days), quality of construction (noting that quality control may have been less stringent with older buildings), and concrete aging. Therefore, it is difficult to predict the probable strength of concrete without in-situ testing from the structures to be assessed.

Cook et al. (2014) discuss proposed changes to the New Zealand Concrete Structures Standard, NZS 3101, which includes an equation to determine the minimum reinforcement requirement for walls. This requirement is dependent on the expected material properties of concrete and steel. It is suggested that the concrete compressive strength be multiplied by a factor of 1.2 to convert from the lower characteristic concrete compressive strength (f_c') to the average target compressive strength, and by 1.1 to increase the concrete compressive strength due to age. The technical guideline for seismic assessment of existing buildings provided by NZSEE (2016) recommend taking the probable compressive strength of concrete as 1.5 times the characteristic concrete compressive strength. This factor specifically accounts for the increase in compressive strength of concrete due to age and the ratio between probable and lower characteristic strength (i.e. fifth-percentile) values. The factor for aging is predominantly based on the recommended equation by Eurocode 2 Part 1 (European Standard, 2004a) where the aging factor asymptotes after 10-20 years to approximately 1.2 to 1.4 depending on the cement class.

Recently, a study was conducted by Foster et al. (2016) which focused on the statistical analysis of material properties in an Australian context. It is discussed that the compressive strength of concrete in a finished structure (f_c) can be taken as:

$$f_c = K_c K_w f'_{cyl} \qquad \text{Eq. 3-3}$$

Where
- K_c is a factor to account for the curing procedure
- K_w is a factor to account for workmanship
- f'_{cyl} is the measured compressive strength of concrete at 28 days

Foster et al. (2016) suggest using the statistical data provided by Pham (1985), which is also an Australian based study, to calculate the compressive strength of concrete in a finished structure. Based on more than 200 tests collected between 1962 and 1981, Pham (1985, cited in Foster et al., 2016), reported the mean ratio of the 28 day concrete cylinder strength (f'_{cyl}) to the specified concrete compressive strength (i.e. the characteristic concrete compressive strength, f'_c) to be 1.18, and the mean factor accounting for curing process and workmanship to be 0.88. Therefore, the mean ratio of the compressive strength of concrete in a finished structure to the specified concrete compressive strength is 1.03 (i.e. $mean\ (f_c/f'_c) = 1.03$).

Due to the uncertainty of predicting the probable compressive strength of concrete, a lower bound estimate is usually preferred. However, this may not always result in conservative estimates, especially when determining the failure mechanism of lightly reinforced walls. This is because a lower estimate of the compressive concrete strength may lead to a lower estimate of the tensile strength of concrete. Furthermore, it is also critical to account for the fact that the compressive strength of concrete in structures is highly dependent on the curing process and workmanship as considered in Pham (1985) and Foster et al. (2016). Therefore, in this study the probable concrete compressive strength is taken as 1.2 times the characteristic concrete compressive strength (f'_c). This accounts for the mean relationship between that the compressive strength of concrete in a finished structure and the specified concrete compressive strength, as suggested by Pham (1985) (i.e. $mean\ (f_c/f'_c) = 1.03$) and an aging factor of approximately 1.2.

The tensile strength of concrete is usually conservatively ignored in the design and assessment of RC beams and columns. However, it is necessary to consider the tensile strength of concrete when assessing the performance of RC walls as, if it is neglected it may lead to non-conservative or overly conservative results depending on the failure mechanism of the wall. If the tensile strength of concrete is not considered or it is under-estimated then the mechanism which leads to single crack or minimal cracking of lightly reinforced walls may not be detected. Hence, care should be taken when determining the failure mechanisms of components and the effect of the assumption of material properties.

The tensile strength of concrete is often represented in two forms: (i) uniaxial tensile strength of concrete (f_{ct}), and (ii) flexural tensile strength ($f_{ct.f}$). The Australian Standard, AS 3600:2009, recommends in the absence of accurate data that the mean uniaxial tensile strength of concrete and the mean flexural strength of concrete be calculated in accordance with Eq. 3-4 and Eq. 3-5, respectively.

$$mean(f_{ct}) = 1.4 \times 0.36\sqrt{f_c'} = 0.50\sqrt{f_c'} \quad \text{Eq. 3-4}$$

$$mean\left(f_{ct.f}\right) = 1.4 \times 0.6\sqrt{f_c'} = 0.84\sqrt{f_c'} \quad \text{Eq. 3-5}$$

For the purpose of assessment, Cook et al. (2014) propose calculating the tensile strength of concrete using Eq. 3-6 for flexural cracking. The 1.2 factor is included to account for the gain in tensile strength due to age. Furthermore, Cook et al. (2014) propose Eq. 3-7 to determine the minimal reinforcement requirement for the design of walls, which is based on the ratio of expected tensile strength of concrete and yield strength of the reinforcement. It can be seen that the expected tensile strength of concrete obtained from these equations is approximately the same.

$$assessment\left(f_{ct.f}\right) = 0.55\sqrt{1.2f_c'} \approx 0.60\sqrt{f_c'} \quad \text{Eq. 3-6}$$

$$A_{s,min} = \frac{1.2 \times 0.85 \times 0.52 \times \sqrt{1.2 \times 1.1 \times f_c'}}{1.1 \times 1.08 \times f_y} \approx \frac{0.6\sqrt{f_c'}}{1.1 \times 1.08 \times f_y} \quad \text{Eq. 3-7}$$

Where

1.2	factor (outside the square root) accounts for the tensile strength increase of concrete due to dynamic loading
0.85	factor relates to the drying shrinkage of concrete imposing tensile strains into the concrete
0.52	factor relates the mean tensile strength to the upper characteristic (95 percentile) tensile strength of concrete
1.2	factor (inside the square root) relates the average target compressive strength to the lower characteristic strength (5 percentile)
1.1	factor relates to the increase in concrete compressive strength due to age

The model code proposed by the International Federation for Structural Concrete (*fib*, 2010), assumes that the flexural tensile strength of concrete is a function of the uniaxial strength of the concrete and the depth of the RC member. It is suggested that the mean flexural tensile strength of concrete be calculated in accordance with Eq. 3-8 (*fib*, 2010). The equation accounts for the fact that the flexural tensile strength is approximately equal to the axial tensile strength of concrete for members with deep sections.

$$mean(f_{ct.f}) = \frac{mean(f_{ct})}{A_{fl}} \quad \text{Eq. 3-8}$$

Where $mean(f_{ct})$ is the mean uniaxial tensile strength of concrete

A_{fl} is a factor which accounts for the depth of the component:

$$A_{fl} = \frac{0.06h^{0.7}}{1 + 0.06h^{0.7}}$$

where h is the depth of the member cross-section in the plane of bending (i.e. wall length for walls and cores)

Figure 3-24 plots the prediction of the flexural tensile strength using the three different equations that have been proposed in AS 3600:2009 (Eq. 3-5), Cook et al. (2014) (Eq. 3-6), and *fib* (2010) (Eq. 3-8). It can be seen that the Cook et al. (2014) and *fib* (2010) equations tend to predict similar values for the mean flexural tensile strength of concrete, whereas the AS 3600:2009 prediction is approximately 50 % higher. In this study, the equation proposed by Cook et al., (2014) is to be adopted since it has been specifically derived for the purpose of assessment.

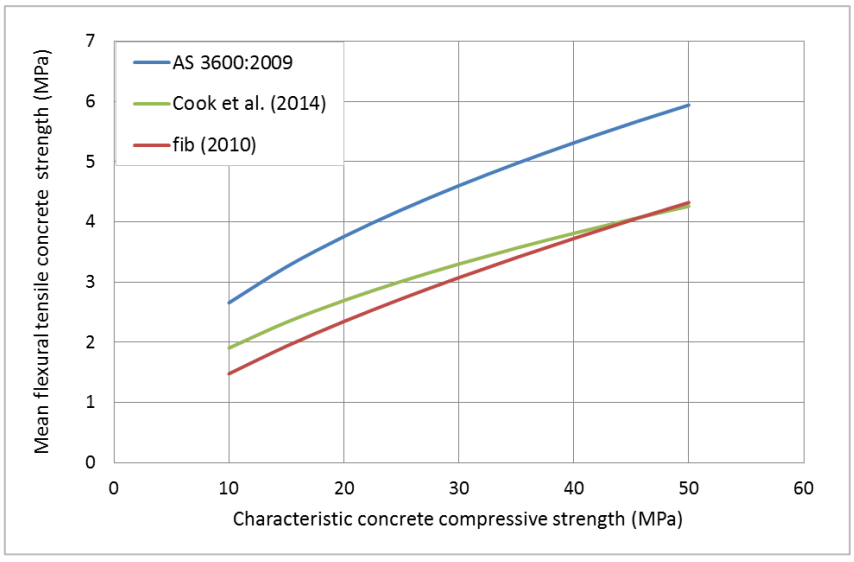

Figure 3-24: Predicted mean flexural tensile strength from characteristic concrete compressive strength (fib (2010) values are based on wall length of 3000 mm)

3.7 SUMMARY

This chapter has briefly highlighted the history of RC design in Australia, including the typical building configurations, development of concrete structures and lateral loading

standards, and RC material properties used in construction of the buildings. The late implementation of the earthquake loading standard, and the current limited consideration of seismic design in Australia due to it being in a region of low-to-moderate seismicity, have resulted in most of the buildings being designed using non-ductile detailing. The buildings which are particularly vulnerable are those constructed prior to 1995, which corresponds to a period where seismic design was rarely considered and lateral loads due to wind were also poorly understood. As a result, the buildings constructed in this period have non-ductile detailing and asymmetric building plans with large eccentricities since torsional effects due to lateral loading were practically neglected. The review of the detailing deficiencies of non-ductile buildings which have characteristics similar to the building stock in Australia has highlighted the likely failure mechanisms of the building components. For RC frames, the behaviour of beam-column joints and columns has been identified as critical, since poor behaviour of these is often the cause of the global collapse of buildings. For RC walls, flexural failure is likely to occur in a sudden brittle manner due to the low longitudinal reinforcement ratio and lack of confinement. Furthermore, the importance of considering both the lateral load resisting system and the gravity load resisting system has been discussed. This is especially the case when assessing the performance of the buildings up to complete damage and collapse since the ultimate cause of collapse may be due to the failure of the gravity load resisting system as demonstrated in reconnaissance reports of past earthquakes. The selection of suitable material properties for the purpose of assessment of the archetypal buildings has also presented. The findings of this chapter will assist with the review and selection of suitable nonlinear modelling methods for non-ductile RC buildings; discussed in Chapters 4 and 5, and the development of the archetypal buildings which will be assessed in Chapter 7.

CHAPTER 4: CRITICAL REVIEW OF NONLINEAR MACRO-MODELLING METHODS

4.1 INTRODUCTION

This chapter provides a critical review of existing state-of-the-art approaches for modelling RC building components in a macro-finite element modelling space. In particular, modelling approaches are investigated which are capable of capturing the detailing deficiencies and the likely response mechanisms of non-ductile RC frame components and walls as identified in Chapter 3. The chapter begins by reviewing the modelling methods to incorporate the inelastic response of beam-column joints. Then, the various macro-modelling techniques for capturing flexural response of members and bar-slip of longitudinal reinforcement are presented. This is followed by a detailed discussion on the current modelling approaches for simulating flexure-shear behaviour which is critical for accurately modelling the response of non-ductile RC columns. Lastly, the current modelling approaches in the literature for the macro-modelling of RC planar and non-planar walls are presented.

4.2 BEAM-COLUMN JOINTS

In the design of RC frames it is common practice to assume rigid joints irrespective of the type of detailing provided. This assumption is not necessarily correct, especially when assessing the seismic performance of non-ductile RC frames due to the detailing deficiencies discussed in Section 3.3 which may cause a significant reduction in joint rigidity. In addition, joint failure may occur prior to the adjoining beams and columns reaching their ultimate capacity. Hence, when assessing the seismic performance of non-ductile RC frames, it is critical that joint inelastic behaviour is modelled correctly, which involves the consideration of two key mechanisms (discussed in Section 3.4.1): (i) the shear response of the joint core; and (ii) bond-slip of longitudinal beam bars. The following sections review the various methods for modelling joint flexibility and defining the load-deformation response of beam-column joints.

4.2.1 Beam-column joint models

Various macro-models have been established to incorporate joint behaviour in the global modelling of frames. Some of these models, including two types of rigid joint models, are illustrated in Figure 4-1**.** The centre-line model and the rigid joint model (Figure 4-1(a) and Figure 4-1(b)) ignore effects of joint flexibility, which is the common practice for the

design of RC frames. In these models it is implicitly assumed that the response of the frame under lateral loading will be governed only by the bending and shear capacity of the beams and the columns. The explicit modelling of joint response has become possible with the introduction of zero-length rotational spring elements, which also allow the decoupling of the inelastic response of beams and columns. One of the first models to incorporate zero-length rotational spring elements was developed by El-Metwally and Chen (1988, cited Celik & Ellingwood, 2008) where the spring is located at the intersection of the beam and column members (Figure 4-1 (c)). The inelastic behaviour of the joint is defined through the spring via a load-deformation response. This model is sometimes referred to as the scissors model without rigid joints, and was later improved by Alath and Kunnath (1995) and is known as the scissors model (Figure 4-1(d)). The shear deformation of the joint core (panel) is simulated via the zero-length rotational spring element; however, the beams and the columns are connected via rigid links in this model and are capable of rotating independently.

More recently a continuum type of element has been introduced, combined with transition interface elements to allow for compatibility with beam-column line elements. An example of this is the model introduced by Lowes and Altoontash (2003) (Figure 4-1(e)). The model explicitly simulates three inelastic mechanisms of a joint consisting of: (i) one rotational spring to model the shear response of the joint core, (ii) eight bar-slip springs to represent the bond failure of the longitudinal bars within the beams and the columns, and (iii) four interface-shear springs to model the loss of shear load transfer at the beam-joint and column-joint interfaces due to crushing of the concrete. While the model provides high control over the various inputs its disadvantage is the increased computational effort. Also there is a lack of availability of models of the detailed response of various components (such as bond-slip). Therefore the model by Lowes and Altoontash (2003) was simplified by Altoontash (2004) and the simplified model is commonly referred to as Joint2D (Figure 4-1(f)). Joint2D has a rotational spring to model the shear deformations within the joint core, and it has four zero-length rotational springs at the beam-joint and column-joint interfaces to model bond-slip behaviour of the longitudinal beam and column bars. Both the Lowes and Altoontash (2003) model and Joint2D model have been implemented in OpenSEES (McKenna et al., 2000).

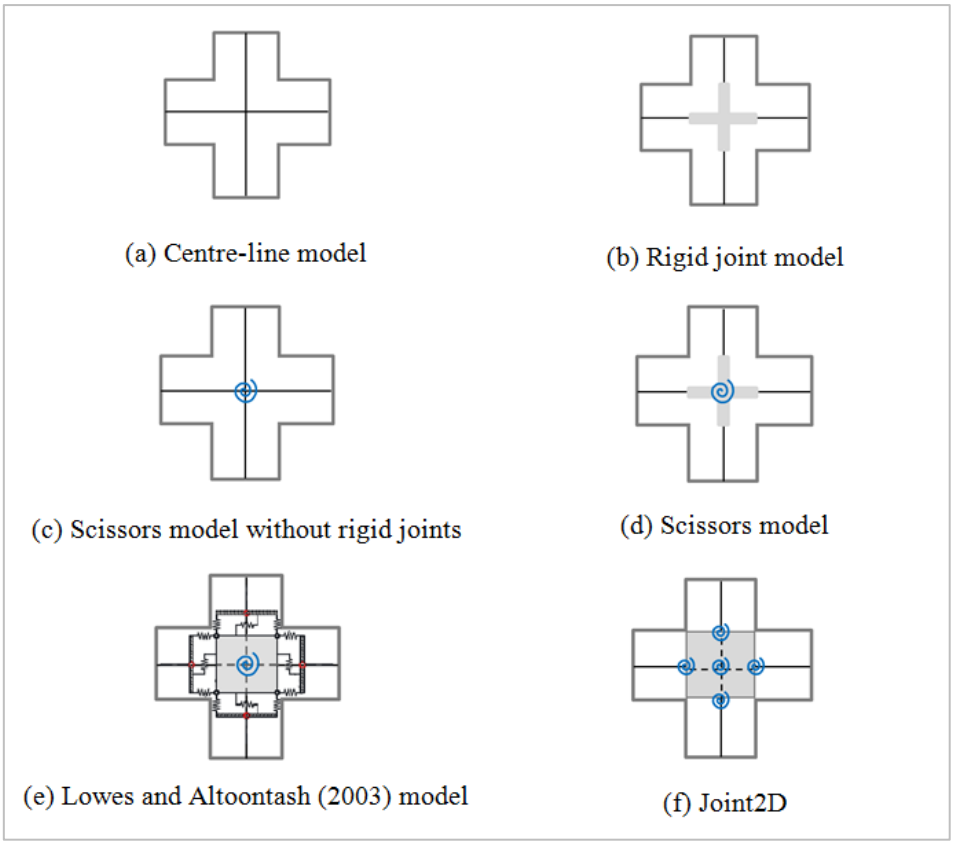

Figure 4-1: Summary of various beam-column joint models

4.2.2 Joint load-deformation response

The most important part of any of the macro-models which attempt to simulate beam-column joint response is the load-deformation hysteretic model used to define the behaviour of the zero-length springs. This is usually achieved by one-dimensional hysteresis material models. The most accurate method to obtain the load-deformation response is from experimental testing in order to capture the complex behaviour of joints. Since this is neither a feasible nor an efficient method for conducting assessment of numerous frames; empirical or semi-empirical based methods are usually adopted to approximate the load-deformation response of joints. The following subsections discuss the key components required to accurately model the load-deformation response of joints.

4.2.2.1 Backbone curve

A critical part of defining the load-deformation response of the joints is defining the envelope stress-strain relationship of the response of the joints to lateral loading, commonly referred to as the backbone curve. The curve is typically defined by four critical points as illustrated in Figure 4-2. A well-established method for determining the critical points of the backbone is that described by Celik and Ellingwood (2008), where τ_1 is the shear cracking stress, τ_2 and τ_3 is the shear induced in the joint due to the beams or

columns reaching their yield and ultimate capacity and both values are limited by the shear strength of the joint, τ_4 is the residual strength, and the γ values are the corresponding values of shear strain. A summary of the approach for defining the shear stress values of the four critical points is provided in Table 4-1. The effects of shear response of the joint panel and bar-slip of bottom longitudinal beam bars are combined in a single stress-strain curve. Bar-slip is taken into account by reducing the yield and ultimate moment capacity of the beam under positive bending based on a reduction factor obtained from numerous experiments. In order to determine the stress values for points two and three, it is necessary to determine the type of joint failure; that is whether hinges form in the beams or the column (referred to as BJ or CJ failure, respectively), or if the joint shear strength is reached prior to the adjoining members reaching their yield and ultimate capacity (referred to as J failure).

The sway potential index (S_i) is used to determine whether column-sway or beam-sway mechanism is expected. It may be calculated using Eq. 4-1 which suggests that plastic hinges form in columns if S_i > 1.0. However, Priestley (1995) recommends to assume plastic hinges form in the columns if $S_i > 0.85$ to account for higher modes of vibration and potential overestimation of column flexural strength. A similar recommendation is also adopted by recent studies and guidelines for assessment of moment resisting frames (ASCE/SEI 41, 2013; NZSEE, 2006, 2016; Priestley et al., 2007; Sullivan et al., 2014). It is noted that for the purpose of design, especially design of special moment resisting frames, more stringent factors are suggested to ensure that hinges are not formed in columns (Priestley et al., 2007; Standards New Zealand, 2006).

$$S_i = \frac{\sum(M_{bl} + M_{br})}{\sum(M_{ca} + M_{cb})} \qquad \text{Eq. 4-1}$$

Where M_{bl} & M_{br} are the expected moment capacities of the adjacent beams (left and right) at the centroid of the joint

M_{ca} & M_{cb} are the expected moment capacities of the adjacent columns (above and below) at the centroid of the joint

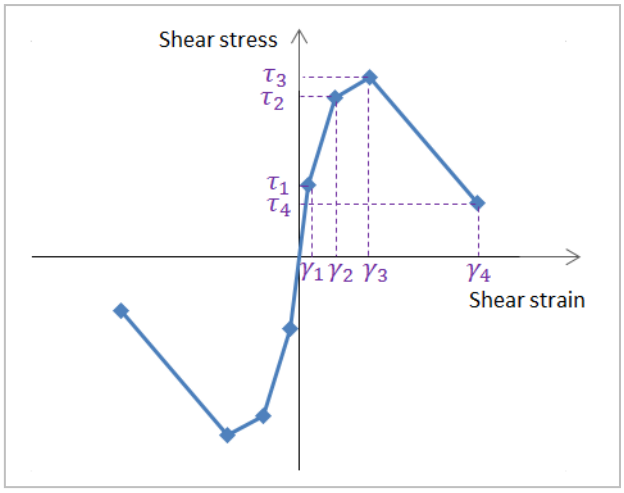

Figure 4-2: Backbone curve for beam-column joint response

Table 4-1: Celik and Ellingwood (2008) approach for calculating critical joint shear stress values

Critical point	Positive envelope	Negative envelope
1. Shear cracking strength, $\tau_{jh.cr}$	$\tau_{jh.cr} = 24\sqrt{\left(\frac{1}{145}\right)\left(1 + 0.002\left(\frac{P}{A_g}\right)\right)}$ Where P/A_g is in MPa	$\tau_{jh.cr} = 24\sqrt{\left(\frac{1}{145}\right)\left(1 + 0.002\left(\frac{P}{A_g}\right)\right)}$ Where P/A_g is in MPa
2. Reinforcement yielding, $\tau_{jh.y}$	$\tau_{jh.y} \leq \tau_{jh.cap}$ Where: $\tau_{jh.y}$ is the shear stress corresponding to the stress induced in the joint due to the adjacent beam/s or column/s reaching yield capacity, reduced by α to account for bond-slip of longitudinal bars. $(0.4 \leq \alpha \leq 0.7)$ $\tau_{jh.cap}$ is the joint shear strength obtained from a strut and tie model.	$\tau_{jh.y} \leq \tau_{jh.cap}$ Where: $\tau_{jh.y}$ is the shear stress corresponding to the stress induced in the joint due to the adjacent beam/s or column/s reaching yield capacity.
3. Ultimate capacity, $\tau_{jh.u}$	$\tau_{jh.u} \leq \tau_{jh.cap}$ Where: $\tau_{jh.u}$ is the shear stress corresponding to the stress induced in the joint due to the adjacent beam/s or column/s reaching ultimate capacity, reduced by α to account for bond-slip of bars.	$\tau_{jh.u} \leq \tau_{jh.cap}$ Where: $\tau_{jh.u}$ is the shear stress corresponding to the stress induced in the joint due to the adjacent beam/s or column/s reaching ultimate capacity.
4. Residual strength, $\tau_{jh.res}$	$\tau_{jh.res} = \tau_{jh.cr}$	$\tau_{jh.res} = \tau_{jh.cr}$

To establish the backbone curve it is necessary to define the angular shear strain values corresponding to the four key shear stress values and hence the deformation response of the joint. Most of the literature focuses on accurately defining the joint shear stress capacity rather than the deformation capacity of the joint; especially the shear strain at which the joint loses its axial load carrying capacity. It should be noted that for the assessment of joints forming part of the primary lateral load resisting system, a reduction of 20 % in peak strength is the criterion typically used to define the joint failure. This criterion corresponds to a loss of lateral load carrying capacity and it is therefore too conservative to adopt it for frames forming part of the secondary (gravity) structural system for the definition of the collapse prevention or near collapse limit state. Since most frames assessed in the literature form part of the primary structural system, the experimental testing conducted on non-ductile joints has been terminated when significant joint damage and loss of lateral load carrying capacity is observed. At these lower strain limits, especially at the initiation of joint failure (i.e. the strain at which peak joint shear stress capacity is reached), the joint strain is somewhat constant for various joints, indicating that the shear strain values are less affected by the detailing of the joint (Park & Mosalam, 2013a). A summary of the recommended shear stress and shear strain values from recent studies for interior and exterior joints is provided in Table 4-2 and Table 4-3, respectively. Based on the recommendations it can be seen that Park and Mosalam (2013b) have identified that the joint aspect ratio has an influence on the joint shear strain response, and the recommendation by Jeon et al. (2015) clearly indicates that exterior joints have lower joint deformation capacity in comparison to interior joints as expected. Furthermore, Jeon et al. (2015) account for the effect of bar-slip on the deformation response of exterior joints. The recommendations by Celik and Ellingwood (2008) are provided only as a guide and are based on experimental results; hence a range of values are given for each critical point.

A recent study which looked at the response of joints without transverse reinforcement up until axial load failure was reported in Hassan (2011) and Hassan and Moehle (2012). The study was limited to exterior joints only. However, it was reported that the residual capacity of the joint at which significant damage was observed should be taken as 70-80 % of the peak capacity of the joint. The maximum recommended shear strain for the positive envelope (i.e. when the bottom beam bars are under tension) is 0.03. Furthermore, it was stated that if axial load failure was of particular interest, the final point on the backbone curve may be extended to the shear strain that corresponds to 50 % of the peak capacity of the joint.

Once the stress-strain backbone is obtained then the moment-rotation backbone may be obtained. The corresponding moment values may be calculated based on the geometry and dimensions of the joint, beam, and column as described in Celik and Ellingwood (2008). Furthermore, the joint rotation may be taken to be equal to the angular joint shear strain (Celik & Ellingwood, 2008).

Table 4-2: Recommended stress-strain values for exterior joints by various studies

Celik and Ellingwood (2008)	**Park and Mosalam (2013)**	**Jeon et al. (2015)**
$\tau_{jh.1} = \tau_{jh.cr}$ $0.0001 \leq \gamma_1 \leq 0.0013$	$\tau_{jh.1} = 0.65\tau_{jh.max}$ $\gamma_1 = 0.0025$	$\tau_{jh.1} = 0.48\sqrt{f_c'}$ $\gamma_1 = 0.00043$
$\tau_{jh.2} = \tau_{jh.y}\ (\leq \tau_{jh.cap})$ $0.002 \leq \gamma_2 \leq 0.01$	$\tau_{jh.2} = 0.9\tau_{jh.max}$ $\gamma_2 = 0.005$	$\tau_{jh.2} = 0.95\tau_{jh.max}$ $\gamma_2 = 0.006$
$\tau_{jh.3} = \tau_{jh.u}\ (\leq \tau_{jh.cap})$ $0.01 \leq \gamma_3 \leq 0.03$	$\tau_{jh.3} = \tau_{jh.max}$ $\gamma_3 = 0.0325 - 0.0125\frac{h_b}{h_c}$	$\tau_{jh.3} = \tau_{jh.max}$ $\gamma_3 = 0.015$ [C] or $\gamma_3 = 0.010$ [D]
$\tau_{jh.4} = \tau_{jh.cr}$ $0.03 \leq \gamma_4 \leq 0.1$	$\tau_{jh.4} = 0.5\tau_{jh.max}$ $\gamma_4 = \gamma_3 + 0.03$	$\tau_{jh.4} = 0.2\tau_{jh.max}$ $\gamma_4 = \gamma_3 + \frac{\tau_{jh.3} - \tau_{jh.4}}{75}$

$\tau_{jh.max}$: is the maximum joint shear stress | C: for continuous longitudinal beam bars | D: for discontinuous or poorly anchored longitudinal beam bars

Table 4-3: Recommended stress-strain values for interior joints by various studies

Celik and Ellingwood (2008)	**Park and Mosalam (2013b)**	**Jeon et al. (2015)**
$\tau_{jh.1} = \tau_{jh.cr}$ $0.0001 \leq \gamma_1 \leq 0.0013$	$\tau_{jh.1} = 0.65\tau_{jh.max}$ $\gamma_1 = 0.0050$	$\tau_{jh.1} = 0.48\sqrt{f_c'}$ $\gamma_1 = 0.00043$
$\tau_{jh.2} = \tau_{jh.y}$ $0.002 \leq \gamma_2 \leq 0.01$	$\tau_{jh.2} = 0.9\tau_{jh.max}$ $\gamma_2 = 0.010$	$\tau_{jh.2} = 0.95\tau_{jh.max}$ $\gamma_2 = 0.006$
$\tau_{jh.3} = \tau_{jh.u}$ $0.01 \leq \gamma_3 \leq 0.03$	$\tau_{jh.3} = \tau_{jh.max}$ $\gamma_3 = 0.0325 - 0.0125\frac{h_b}{h_c}$	$\tau_{jh.3} = \tau_{jh.max}$ $\gamma_3 = 0.02$
$\tau_{jh.4} = \tau_{jh.cr}$ $0.03 \leq \gamma_4 \leq 0.1$	$\tau_{jh.4} = 0.5\tau_{jh.max}$ $\gamma_4 = \gamma_3 + 0.03$	$\tau_{jh.4} = 0.2\tau_{jh.max}$ $\gamma_4 = \gamma_3 + \frac{\tau_{jh.3} - \tau_{jh.4}}{80}$

4.2.2.2 Joint shear capacity

Currently there is no consensus on one suitable empirical or numerical model that is capable of estimating the beam-column joint shear strength of joints with different detailing. It is generally accepted that for seismically detailed beam-column joints, modified compression field theory (MCFT) may be used to provide a good approximation

of the expected backbone curve (Altoontash, 2004); although this approach is generally not suitable for non-ductile joints (Celik & Ellingwood, 2008). Instead, for non-ductile joints, strut and tie models are preferred to obtain the joint shear strength since the primary mechanism through which forces are transferred is a single compression strut formed between the compression zones of the adjacent beam/s and column/s as discussed in Section 3.4.1. However, due to the complexity of the strut and tie modelling approach, codified provisions and recent studies have adopted other approaches to estimate the joint shear strength.

As discussed in Section 3.4.1, a strong correlation exists between the compressive concrete strength and the shear capacity of non-ductile joints, and therefore many studies predict the joint shear capacity as a function of $\sqrt{f_c'}$ for non-seismically designed joints. The factors obtained by these studies are highly empirical and are dependent on the database of joints considered in the regression analysis and hence care should be taken if such models are adopted for assessment of buildings. This approach is also adopted by code provisions such as ASCE 41 (ASCE/SEI, 2013) which is based on the following pre-standards: FEMA 356 (2000) and FEMA 273 (1997). ASCE 41 (ASCE/SEI, 2013), in which the nominal joint shear strength is given by Eq. 4-2, also includes factors to account for the location of the joint and the presence of transverse beams. The factor Υ_n takes into account whether the joint provided has conforming or non-conforming transverse reinforcement, where the joint transverse reinforcement is defined as conforming if the spacing of the ties is less than or equal to $h_c/2$ within the joint.

$$V_{jh.cap} = 0.083\lambda\Upsilon_n\sqrt{f_c'}b_j h_c \qquad \text{(MPa units)} \qquad \text{Eq. 4-2}$$

Where
- λ is 0.75 for lightweight aggregate concrete, and 1.0 for normal-weight aggregate concrete
- Υ_n is a factor which accounts for joint type (see Figure 4-3), when multiplied by $\sqrt{f_c'}$, is the joint shear strength.
- b_j is the effective joint width, $b_j = \frac{b_b + b_c}{2}$, where b_b & b_c are the width of the beam and the column cross-sections, respectively

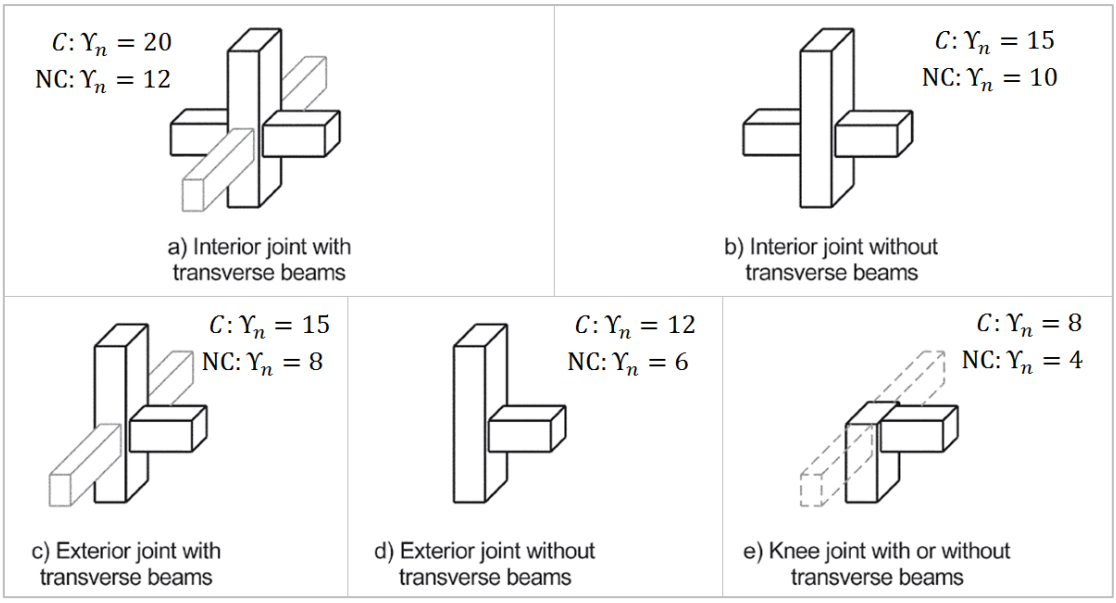

C: joints with conforming transverse reinforcement | NC: joints with non-conforming transverse reinforcement

Figure 4-3: Joint classification and Υ_n values in ASCE/SEI 41 (adopted from ASCE/SEI 2013)

The recommendation by the New Zealand Society for Earthquake Engineering (NZSEE, 2006) for calculating the maximum horizontal shear strength for joints with no or an insufficient number of ties is provided in Eq. 4-3. The effect of axial load has been included by using the Mohr's circle technique; the horizontal shear stress is calculated based on the assumption that the diagonal tensile shear stress of concrete is $k\sqrt{f_c'}$ and the vertical compressive stress is $\frac{P^*}{A_g}$. A similar approach was suggested by Priestley (1997). The factor k suggested in NZSEE (2006) is predominantly based on the work conducted by Hakuto et al. (2000) with an additional strength reduction factor of 0.85 to calculate $V_{jh.cap}$.

$$V_{jh.cap} = 0.85\tau_{jh} b_j h_c \qquad \text{Eq. 4-3(a)}$$

$$V_{jh.cap} = 0.85\sqrt{f_c'}\sqrt{1 + \frac{P^*}{A_g k\sqrt{f_c'}}}\, b_j h_c \le 1.92\sqrt{f_c'} b_j h_c \qquad \text{Eq. 4-3(b)}$$

Where

τ_{jh}	is the nominal horizontal shear stress (carried by a diagonal compressive strut mechanism crossing the joint)
P^*	is the axial load due to gravity and seismic loading
A_g	is the gross sectional area of the column

k is a factor which accounts for joint position and detailing;
$k = 1.0$ for interior joints
$k = 0.4$ for exterior joints with bars bent towards the joint region
$k = 0.25$ for exterior joints with bars bent away from the joint region

The more recent recommendations by NZSEE (2016) have suggested that the contribution of ties within the joint region (if they are provided) may be incorporated in calculating the joint shear strength based on the Eurocode 8 expression for determining the amount of ties required for design. Hence, the joint shear stress may be calculated according to Eq. 4-4 and Eq. 4-5 for exterior and interior joints, respectively.

$$\tau_{jh} = 0.85k\sqrt{f_c'}\sqrt{1 + k\sqrt{f_c'}(f_v + f_h) + f_v f_h} \quad \text{for exterior joints} \qquad \text{Eq. 4-4}$$

$$\tau_{jh} = 0.85f_c'\sqrt{1 + kf_c'(f_v + f_h) + f_v f_h} \quad \text{for interior joints} \qquad \text{Eq. 4-5}$$

Where
f_v is the axial load stress on the joint, $f_v = \frac{P}{A_g}$
f_h is a factor which represents the horizontal confinement effects due to the transverse reinforcement in the joint and is calculated as the maximum tension stress that the ties develop at yield, $f_h = \frac{A_{sv}f_{y.f}}{b_j h_b}$, where
A_{sv} is the cross-sectional area of ties, and
f_{yt} is the yield strength of the ties

The current and older versions of the Australian concrete structures standards (1988-2009) have required ties be provided within the joint region if the joint is not restrained on all sides. However, the minimum cross-sectional area of ties or lateral reinforcement (A_{sv}) required within the joint (provided in Eq. 4-6) is very small, often resulting in only one or two ties within the joint. Hence, for the purpose of assessment it may be assumed that no ties are provided within the joint region.

$$A_{sv} \geq \frac{0.35 b_b s}{f_{yt}} \quad \text{Eq. 4-6}$$

Where b_b is the beam width

s is the spacing of ties within the joint

The approach taken in more recent studies to predict the joint strength has been to identify the most influential factors and to then obtain an equation for the strength based on regression analysis and/or simplifications made to the strut and tie modelling approach (Jeon et al., 2015; Park & Mosalam, 2012, 2013a). While these studies have been able to show good predictions of the joint strength with experimental testing, the adopted approach is inherently highly empirical and dependent on the joint types and detailing considered in the database. Furthermore, care should be taken when these approaches are adopted for assessment of RC frames since the material properties may be different to those considered in the database. In addition, some of these studies adopt empirically based equations for the prediction of joint strength without consideration of the type of joint failure; that is, examining whether the joint shear strength is lower or greater than the shear induced in the joint due to column or beam yielding.

4.2.2.3 Hysteretic response

Once the backbone response is determined, the next step is to define the hysteretic behaviour of the joint. Parameters that are used in defining the type of hysteresis that occurs are as follows: (i) stiffness degradation (during unloading and reloading), (ii) pinching behaviour, (iii) and strength degradation (in-cyclic and cyclic degradation). Examples are given in Figure 4-4. These parameters are dependent on material properties, geometry, reinforcement detailing, and loading protocol (intensity and number of cycles, and sequence of loading) (FEMA P440A, 2009).

It is noted that the envelope or backbone curve (discussed in Section 4.2.2.1) should ideally be developed and calibrated with monotonic testing. Then, the hysteresis rules which are calibrated for different cyclic loading protocols (FEMA P440A, 2009), should incorporate cyclic degradation. However, the availability of experimental results to enable the determination of the necessary parameters to define the hysteresis rules is scarce and often the response of components is validated with experimental results obtained under one type of cyclic loading protocol. Therefore, often the envelope is calibrated and validated with component response obtained under cyclic loading. FEMA P440A (2009) explains that this method is conservative if the cyclic loading protocol does not push the structure to its maximum limit at each cycle. Other studies take the approach of predicting

the monotonic response from the cyclic loading response in order to then calibrate the cyclic degradation parameters (Haselton et al., 2008). This approach is questionable and is highly dependent on how the monotonic response of the component is predicted. Hence, due to the scarcity of experimental results for a single component subassemblage under monotonic and various cyclic loading protocols the method of calibrating the envelope response with cyclic testing is considered to be a valid approach.

Many relationships that determine the type of hysteresis being experienced have been created over the years, including the *Takeda* model (Takeda et al., 1970), the *Ibarra-Medina-Krawinkler Deterioration* model (Ibarra et al., 2005), and the *Pinching4* model (Lowes & Altoontash, 2003; Lowes et al., 2004) (see Figure 4-5). The most widely used hysteretic model in recent years has been the *Pinching4* model (available in OpenSEES as a uniaxial material model) due to its versatility. However, recent studies have criticised the practical use of the *Pinching4* model as it requires a total of 39 parameters to define the behaviour of the hysteretic model and have therefore suggested the use of other hysteretic models which require the definition of fewer parameters (Ning et al., 2016). However, the key advantage of the *Pinching4* model is that the input parameters include the definition of four critical points to directly define the positive and negative backbone, and hence the envelope response can be easily calibrated for joints as discussed in Section 4.2.2.1. All of the other hysteretic models that are available in various programs, including OpenSEES, only allow the direct definition of a maximum of three critical points when defining the positive and negative envelope (e.g. *Modified Ibarra-Medina-Krawinkler Deterioration Model, Hysteretic Material Model*); this usually results in a poor estimation of the initial stiffness due to the simplification of using three points rather than four points to define the backbone. Hence, the selection of a suitable hysteretic model often requires a compromise between the practicality of defining the hysteretic behaviour and the accuracy of the envelope response.

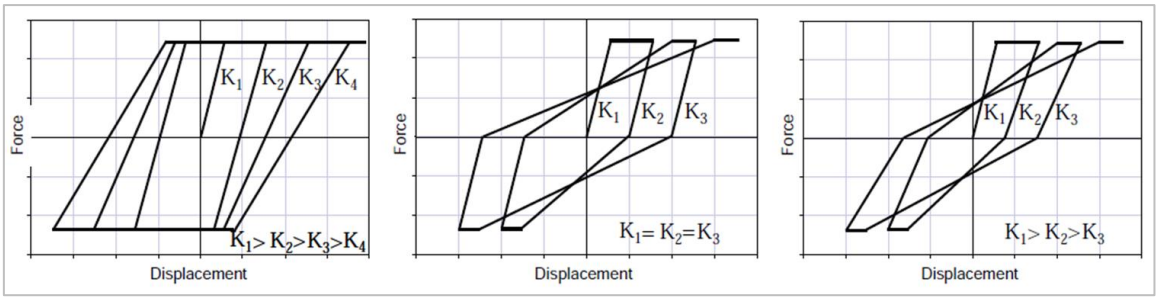

(a) Examples of hysteretic models with various stiffness degradation behaviours

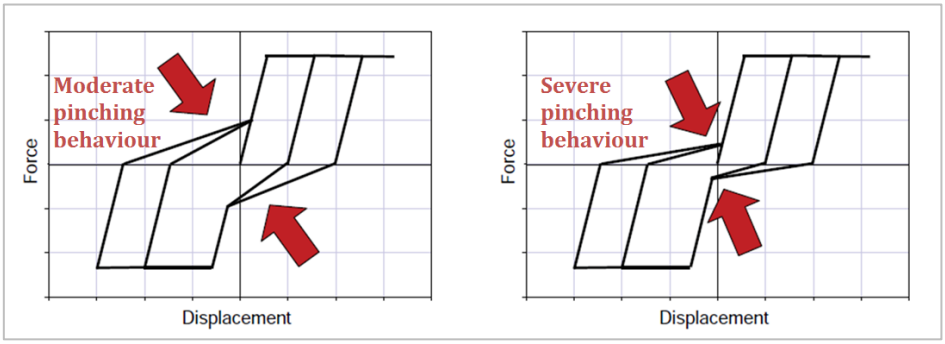

(b) Examples of hysteretic models with various levels of pinching

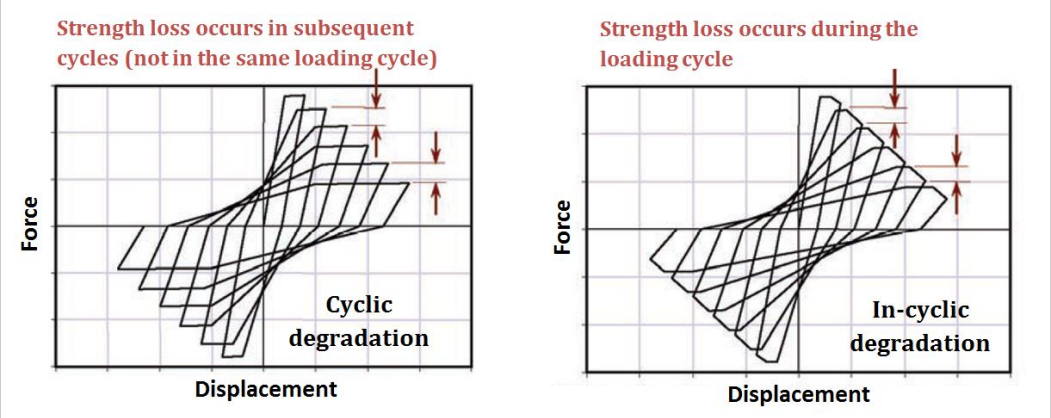

(c) Examples of hysteretic models with various strength degradation behaviours

Figure 4-4: Various hysteretic responses, adopted from FEMA P44A (2009)

A summary of the parameters recommended in various studies for use in the *Pinching4* hysteretic model for non-ductile joints is provided in Table 4-4. It can be seen that there is no real trend in the recommended values, especially for those which control strength and stiffness degradation. Some studies have argued that the definition of strength and stiffness degradation may be ignored on the basis of simplicity and due to the insignificant effect they have on modelling of structural collapse (Park & Mosalam, 2013b). FEMA P440A (2009) reported a detailed summary of existing research on the impact of utilising strength and stiffness degradation on the global response of structures during incremental dynamic analysis (IDA). It is noted that these studies looked at sideways

collapse, which is suitable for ductile structures, rather than vertical collapse, which is typical of non-ductile structures and may occur at much lower drift limits than sideways collapse. Nevertheless, it was reported that, in general, hysteretic response parameters tend to have an insignificant effect on the peak displacements experienced by long-period structures (structures with fundamental periods longer than 1.0 second). However, the parameters did have a greater significance for shorter-period structures or for structures located on soft soils; that is, when the period of the structure was shorter than the predominant period of the ground motion. The peak displacement demand is under-estimated if hysteretic behaviour is not considered for the short-period structures.

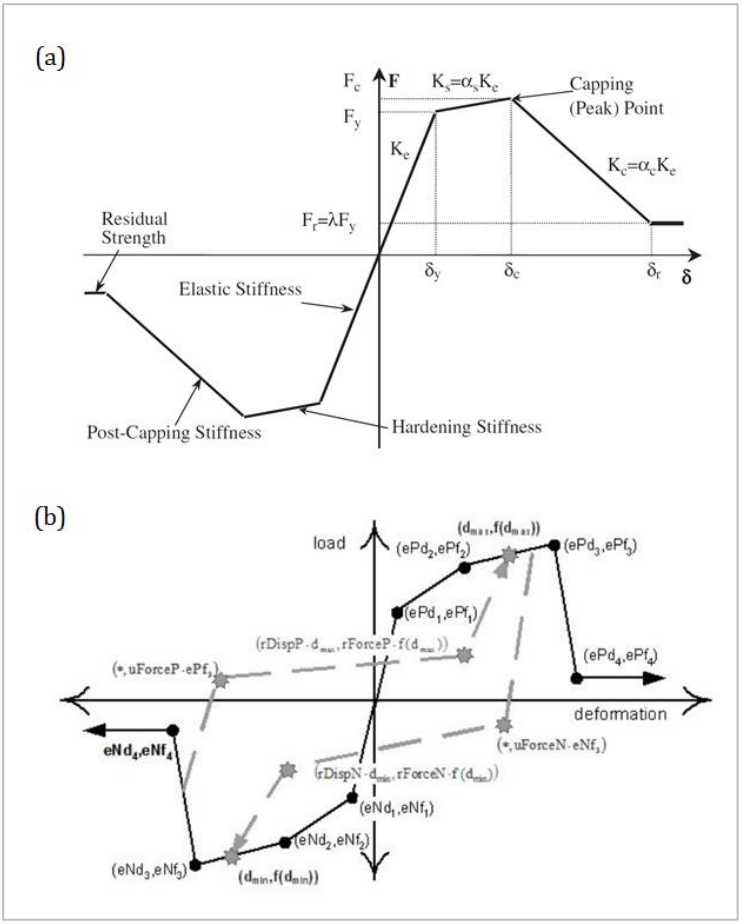

Figure 4-5: Hysteretic models: (a) Ibarra-Medina-Krawinkler Deterioration Model (Ibarra et al., 2005) model (b) Pinching4 model (Lowes & Altoontash; Lowes et al., 2004)

Table 4-4: Recommended Pinching4 parameters by various studies

Parameter type	Parameter name	Celik & Ellingwood (2008)	Hassan (2011)	Park & Mosalam (2013b)	Jeon et al. (2015)	
					Exterior joints	Interior joints
Pinching	rDispP	0.15	0.15	0.5	0.20	0.20
	rForceP	0.15	0.35	0.25	0.20	0.20
	uForceP	-0.10	-0.10	0.05	0.0	0.0
	rDispN	0.15	0.15	0.5	0.20	0.20
	rForceN	0.15	0.15	0.25	0.20	0.20
	uForceN	-0.10	-0.40	0.05	0.0	0.0
Cyclic unloading stiffness degradation	gK1	NU	0.50	NU	0.95	1.0
	gK2	NU	0.20	NU	0.0	0.0
	gK3	NU	0.10	NU	0.10	0.10
	gK4	NU	-0.40	NU	0.0	0.0
	gKlim	NU	0.99	NU	0.95	0.95
Cyclic reloading stiffness degradation	gD1	NU	0.10	NU	0.35	0.30
	gD2	NU	0.40	NU	0.0	0.0
	gD3	NU	1.00	NU	0.15	0.15
	gD4	NU	0.50	NU	0.0	0.0
	gDlim	NU	0.99	NU	0.95	0.95
Cyclic strength degradation	gF1	NU	0.05	NU	0.05	0.15
	gF2	NU	0.02	NU	0.0	0.0
	gF3	NU	1.00	NU	0.32	0.32
	gF4	NU	0.05	NU	0.0	0.0
	gFLim	NU	0.99	NU	0.25	0.25
Maximum energy dissipation under cyclic loading	gE	NA	10.0	NA	NA	NA
Damage type (cyclic or energy)	dmgType	NA	energy	NA	NA	NA

NA: not available | NU: not utilised

4.3 FLEXURAL RESPONSE OF MEMBERS

The two common approaches for simulating the flexural response of members are based on the use of lumped plasticity elements and distributed plasticity elements. The schematic of the two approaches is provided in Figure 4-6. Each approach has its own set of advantages and disadvantages which needs to be considered for the type and purpose of the analysis being conducted. A review of each approach is provided in the following subsections.

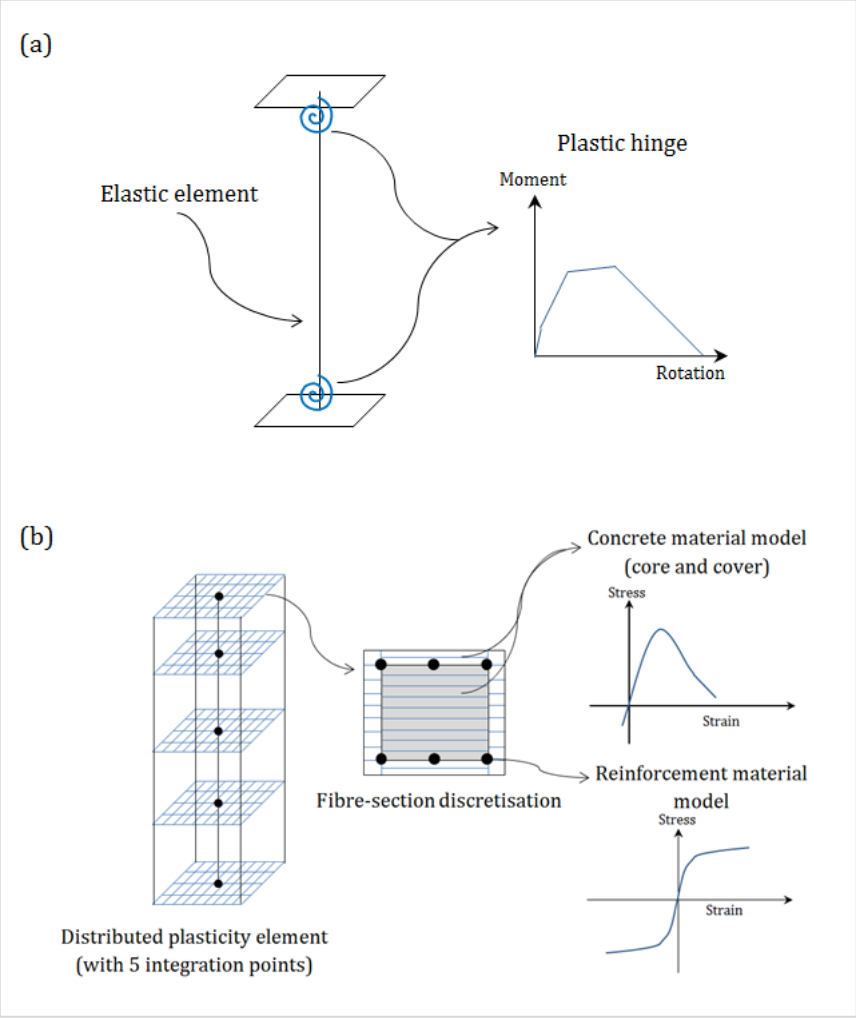

Figure 4-6: Flexural response modelling approaches: (a) lumped plasticity element, (b) distributed plasticity element

4.3.1 Lumped plasticity elements

The lumped plasticity approach, also sometimes referred to as the concentrated plasticity approach, involves modelling the member with elastic elements which have plastic hinges at each end. The inelastic behaviour of the member is simulated through the plastic hinges which are modelled typically with zero-length springs and moment-rotation laws which

do not account for the simulation of axial-flexural interactions. However, it is also possible to simulate the response of the hinges by using more complex moment-rotation laws or fibre-sections which account for axial-flexural interactions. The definition of the inelastic moment-rotation response is usually highly dependent on empirically based equations and hence suitable approaches need to be selected based on the detailing of the member. The values suggested by the standards and codes for frame components have been criticised as being too conservative and hence not suitable for assessment purposes (Haselton et al., 2008). Furthermore, codified approaches do not provide any guidance for determining the hysteretic behaviour of the components.

Researchers have tried to improve the accuracy of the lumped plasticity approach (which use moment-rotation laws to define the inelastic response of elements), predominantly for frame components, by adopting the plastic hinge analysis approach to determine the backbone response of components. The moment values used to define the critical points on the backbone response of the members are usually obtained from sectional analyses, including: yield or nominal yield, and ultimate bending capacities. The corresponding deformation capacities are computed using analytical models which commonly use the curvatures obtained from sectional analyses. A critical part of the approach involves defining the plastic hinge length to determine the plastic deformation capacity of the member. It is noted that the plastic hinge length is not the real plastic hinge length observed in experiments in which the length over which the actual plasticity spread is determined. Instead it is the equivalent plastic hinge length along which the curvature is assumed to be constant and from which a reasonably accurate prediction can be made of the plastic rotation capacity of the member as illustrated in Figure 4-7. This approximation helps to account for the increase in displacement resulting from other mechanisms including tension shift and to some extent shear deformations (Priestley et al., 2007). Numerous equations have been proposed by past researchers (Berry & Eberhard, 2008; Kazaz, 2013; Köroglu et al., 2014; Priestley et al., 2007; Zhao et al., 2011). However, most of these studies have focused on simulating the flexural response of ductile or seismically detailed RC frame components and hence their suitability for determining the response of non-ductile members should be examined. Furthermore, for collapse analysis it is necessary to determine the response of members up to axial load failure, however, only a few studies propose deformation capacities at this limit (Elwood & Moehle, 2003; Wibowo et al., 2014; J. L. Wilson et al., 2015). In addition to the backbone response the hysteretic behaviour of the moment-rotation spring also needs to be determined. This is achieved by calibrating the simulated response with experimental results. This approach has similar

challenges and issues to those discussed in Section 4.2.2.3 with respect to defining the hysteretic response for the modelling of beam-column joints.

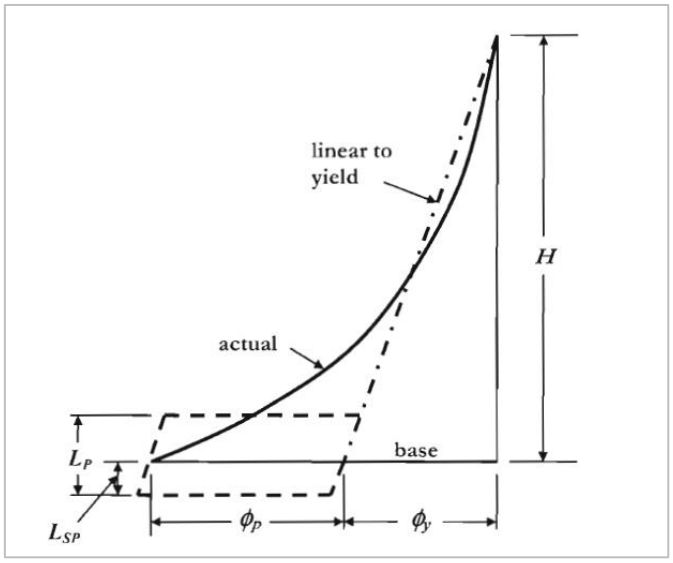

Figure 4-7: Idealisation of linear curvature distribution for the purpose of plastic hinge analysis, from (Priestley et al., 2007) where L_P is equivalent plastic hinge length and L_{SP} is the strain penetration length

Even though it is challenging to determine a general approach for defining the inelastic response of members at an element level, the ability to directly calibrate the response of elements with experimental results and to include phenomenological mechanisms is one of the main advantages of the lumped plasticity approach. These phenomenological mechanisms may be associated with flexural response of members such as strain-softening related to reinforcement buckling and low-cycle fatigue, something that is still not well incorporated in material models used in fibre-sections and distributed plasticity elements (Haselton et al., 2008). Other mechanisms may also be indirectly simulated such as the shear response of members (ASCE, 2013; FEMA, 2000).

The other key advantages of the lumped plasticity approach include computational efficiency and reliability. These attributes are particularly crucial for 3-dimensional nonlinear building models for which the performance of the building up to the collapse limit state is of interest. Thus, many studies which conduct collapse modelling of buildings have adopted the lumped plasticity approach to develop the nonlinear building models (Badri et al., 2015; Haselton et al., 2011; Karimiyan et al., 2014; Liel et al., 2011; Manie et al., 2015; Stathopoulos & Anagnostopoulos, 2005).

4.3.2 Distributed plasticity elements

The distributed plasticity approach involves defining the cross-section of the element with fibre-sections. The element response is determined by a weighted integration of the fibre-section response at each integration point, therefore allowing nonlinear behaviour to be modelled along the length of the member. Generally, the distributed plasticity approach is considered to be advantageous over the lumped plasticity approach because it does not involve determining a predefined length of the member where inelastic behaviour is assumed to take place. However, as discussed in the following section, the modelling of elements which involve a softening (rather than a hardening) flexural response is dependent on the location of integration points and therefore a distributed plasticity approach in which the length of the plastic hinge is defined is required to obtain accurate simulation of flexural response of members. Furthermore, the disadvantage of the distributed plasticity approach includes increase in computational effort and numerical instabilities. The following subsections discuss some of the key inputs that need to be considered for the distributed plasticity approach, namely: selection of uniaxial material models, force-based and displacement-based elements, number of integration points, and number of fibres.

4.3.2.1 Uniaxial material models for the distributed plasticity approach

The fibre-sections are modelled with nonlinear uniaxial material models which define the longitudinal reinforcement and concrete material properties. Often the core and cover concrete are modelled separately to account for the confinement effect, although for non-ductile columns the effect of confinement is very small. Furthermore, for global analysis of RC structures it is often assumed that the behaviour of the reinforcement is the same in tension and compression. In reality the stress-strain relationship of the reinforcement is different in tension and compression due to the Bauschinger effect and buckling. However, there is still insufficient understanding about buckling of bars and a consensus does not exist about the most suitable method to model the behaviour. Nevertheless, numerous studies exist in which analytical models have been proposed based on experimental testing (e.g. Dhakal & Maekawa, 2002; Gomes & Appleton, 1997).

4.3.2.2 Force-based and displacement-based elements for the distributed plasticity approach

Distributed plasticity elements may be force-based or displacement-based elements. Displacement-based elements follow the assumption of linear curvature and constant axial deformation along the length of the element, whereas force-based elements follow the assumption of linear moment and constant axial force distribution along the length of the

member (Pugh et al., 2015). Both displacement-based and force-based elements provide similar solutions if modelled correctly. Displacement-based elements require multiple elements to accurately model a single member whereas a single force-based element will often suffice for a single member (Almeida et al., 2016; *fib*, 2008; Scott & Fenves, 2006). However, force-based elements may encounter more numerical convergence issues especially when strength degradation occurs. This is because the finite element space is displacement-based and nodal displacements are determined such that nodal equilibrium is satisfied. Hence, force-based elements require intra-element solutions to determine the force distributions which create nodal displacements that satisfy nodal equilibrium and compatibility between elements (Pugh et al., 2015).

4.3.2.3 Number of integration points for the distributed plasticity approach

When modelling the response of a member for which a hardening response is expected, that is the failure mechanism is governed by longitudinal reinforcement yielding prior to concrete crushing, the selection of the number of integration points (IP) is often based on a compromise between accuracy and computational efficiency. The response of the element converges to a single solution as the number of integration points increases and usually four IPs suffice to obtain accurate results (*fib*, 2008). However, when the member experiences a softening response, the failure mechanism is governed by concrete crushing or longitudinal bars buckling, the conventional distributed plasticity approach of modelling members is not accurate and the solution is highly dependent on the number of integration points. This is due to deformation localisation problems within the first integration point; this is illustrated in Figure 4-8 for a force-based cantilever element. For a softening section response a single solution does not exist and therefore the response obtained is dependent on the characteristic length of the first integration point (i.e. the section undergoing strain softening) which is equal to the integration weight (Scott & Fenves, 2006). Hence, if the same integration rule is used, the more integration points used the shorter the length becomes to the first integration point, thus requiring higher curvatures to achieve the same displacement at the tip of the cantilever. The compressive strain in the concrete fibres increases rapidly resulting in significant material stiffness degradation. Therefore for members with degrading flexural response, the selection of a higher number of IPs does not necessarily result in a more accurate response of the member and it may in fact over-predict the brittleness of a member (*fib*, 2008).

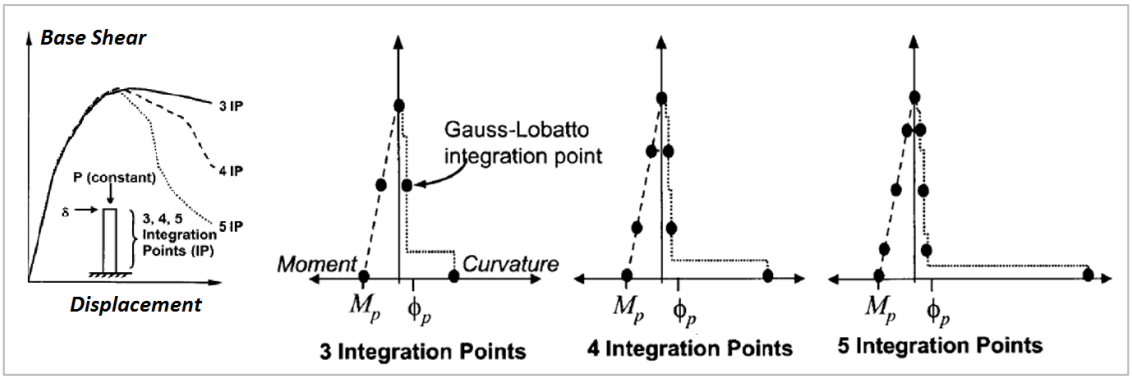

Figure 4-8: Simulated response of an elastic-perfectly plastic cantilever RC column with degrading strength for various number of integration points, adapted from Coleman and Spacone (2001)

Material regularisation is an approach which has been suggested in the past to overcome the sensitivity of the member response to the mesh size, or in this case the number of integration points (Coleman & Spacone, 2001; *fib*, 2008), although, this is not common practice for line elements (Pugh et al., 2015). The method involves regularising the post-peak material stress-strain response based on the fracture energy (tensile response), or the unconfined and confined concrete crushing energy (compressive response), and the length of the integration point. While material regularisation in theory is quite robust, it is not common practice to calculate crushing energy during testing of specimens and therefore there are only few studies which recommend models for calculating the crushing energy.

Another approach which has been suggested to overcome the dependence of the response on the number of IPs is the use of plastic hinge length in the distributed plasticity approach (Scott & Fenves, 2006). This element is implemented in OpenSEES (McKenna et al., 2000) as *forceBeamColumn* element and it essentially determines the weight of the first integration point based on the plastic hinge length, which is an input parameter. The key advantage of this approach is that the only additional input which is required is the plastic hinge length which has a direct structural response meaning and many studies provide recommendations for calculating this length based on geometric and/or detailing properties. Figure 4-9 shows the results of a comparative study conducted by Scott and Fenves (2006) for a bridge pier to illustrate the difference in monotonic response obtained using: (i) a force-based distributed plasticity element with various number of integration points (referred to as N_p in the legend), (ii) the linear regularisation method for various integration points, and (iii) *forceBeamColumn* element with different plastic hinge lengths (L_p) based on various recommendations. The results show significant improvements in

the predicted response when using the new element (*forceBeamColumn* element) in comparison to the response predicted using conventional force-based elements which significantly underestimate the displacement capacity of the bridge pier. It is also evident that the approach of using material regularisation produces a good match with the experimental results.

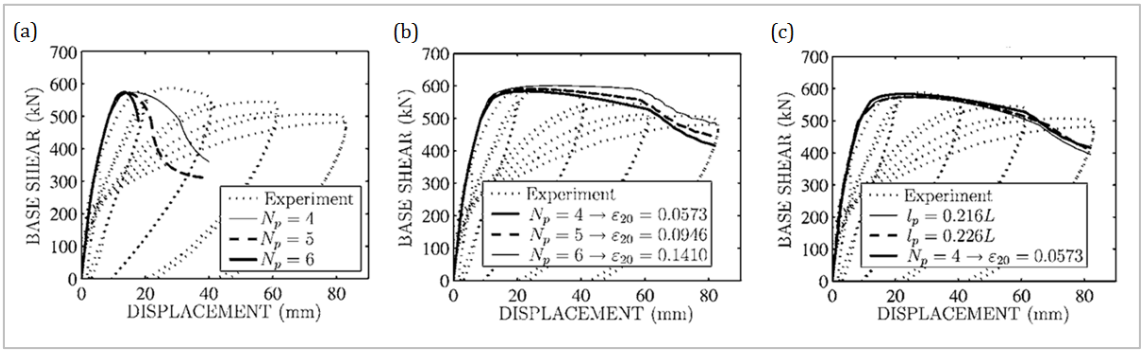

Figure 4-9: Simulated force-displacement response of a bridge pier investigated by Scott and Fenves (2006) using: (a) Force-based element, (b) Forced-based element with material regularisation, and (c) forceBeamColumn element

4.3.2.4 Number of fibres for the distributed plasticity approach

The distributed plasticity approach also requires the appropriate selection of the number of fibres used to model a cross-section. *fib* (2008) suggest 15 layers for rectangular sections, however, it also recommends conducting sensitivity studies on a simple structure (such as a beam or column) to determine a suitable fibre size.

4.4 BAR-SLIP

Bar-slip causes rigid body rotations which can significantly increase the member flexibility. It can be incorporated in a finite-element model via a zero-length spring for which the behaviour is defined with a moment-rotation hysteretic model. As explained in Ghannoum and Moehle (2012) the amount of slip (S_s) experienced by longitudinal bars in the anchorage (or joint) region of a column, illustrated in Figure 4-10, can be calculated by integrating the strain profile within the anchorage (or joint) region under the assumption of bi-uniform bond stress (Lehman & Moehle, 2000):

$$S_s = \frac{\varepsilon_s f_s d_b}{8u_e}, for\ \varepsilon_s \leq \varepsilon_y \qquad \text{Eq. 4-7}$$

$$S_s = \frac{\varepsilon_y f_y d_b}{8u_e} + \frac{(\varepsilon_s + \varepsilon_y)(f_s - f_y)d_b}{8u_p}, for\ \varepsilon_s > \varepsilon_y$$

Where f_s is the bar stress at the interface

ε_s is the bar strain at the interface

ε_y is the bar yield strain

u_e is a the elastic bond stress

u_p is the plastic bond stress

Thus at yield, the total lateral displacement due to bar-slip can be obtained via Eq. 4-8 from Elwood and Moehle (2003):

$$\Delta_{slip} = \frac{L_c f_y d_b \phi_{ny}}{8u_e}, for\ \varepsilon_s = \varepsilon_y \quad \text{Eq. 4-8}$$

Where ϕ_{ny} is the curvature at nominal yield

L_c is the column height

Another approach for incorporating bar-slip is with zero-length fibre-sections (Berry, 2006; Ghannoum & Moehle, 2012; Zhao & Sritharan, 2007). The section has the same geometry as the actual member section, but the material properties for the concrete and steel fibres are altered, as shown in Figure 4-11. The critical strain values which define the concrete and steel model are amplified by a factor which is dependent on the amount of slip expected. The main advantage of using the zero-length fiber-section to model bond-slip over the zero-length spring is that it allows the adjustment of the neutral axis location based on the applied axial load and loading direction (Ghannoum & Moehle, 2012); however, it does reduce computational efficiency.

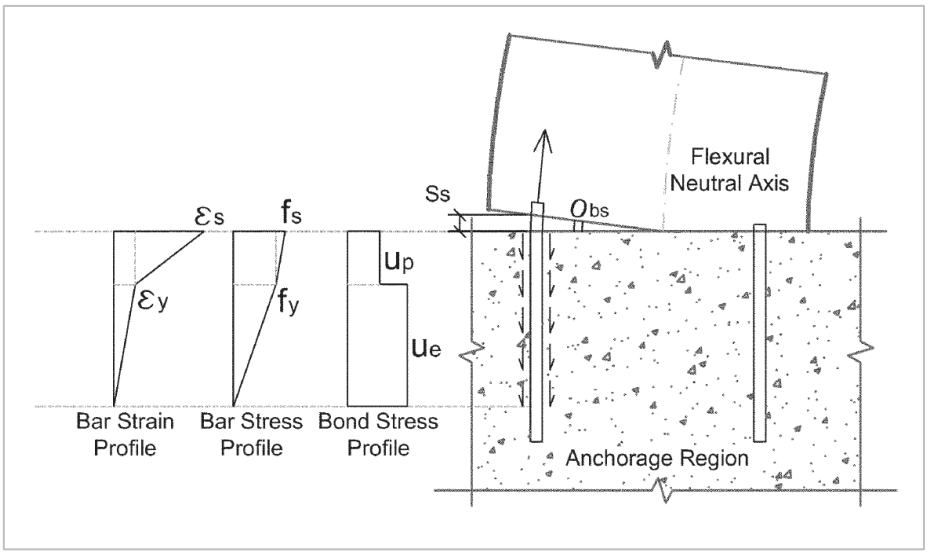

Figure 4-10: Longitudinal bar anchorage stresses and strains (Ghannoum & Moehle, 2012)

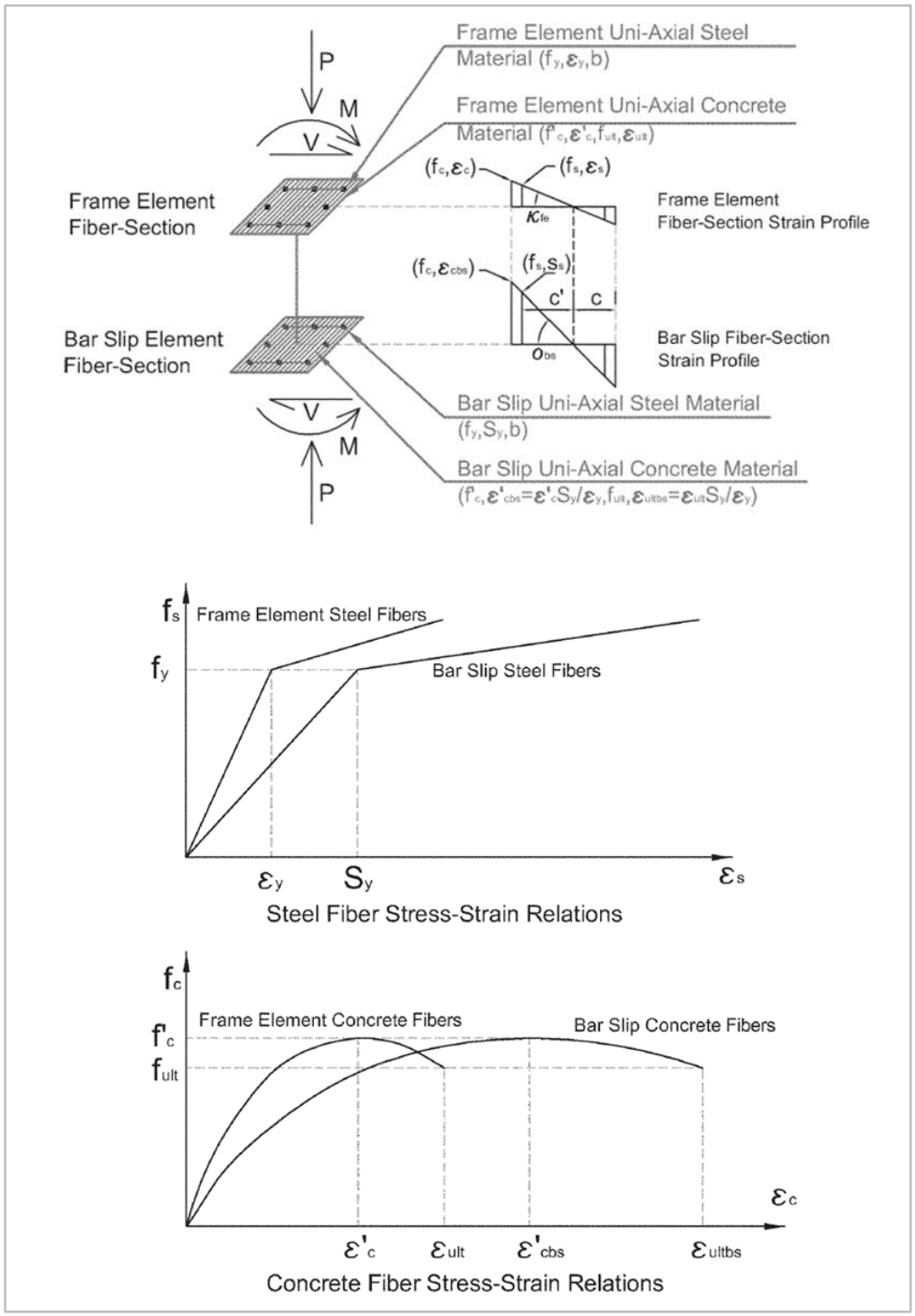

Figure 4-11: Altered material properties for zero-length fibre-section to simulate bar-slip (Ghannoum & Moehle, 2012)

4.5 FLEXURE-SHEAR RESPONSE OF NON-DUCTILE COLUMNS

As discussed in Section 3.4.2, the response of non-ductile columns is likely to be flexure-shear; with significant strength and stiffness degradation taking place after the ultimate bending capacity of the column is reached due to loss of shear capacity. Currently the parameters required to model the shear response of columns are approximated by

empirically based equations and at this stage there is no consensus on the best available model. Two critical deformation limits must be determined in order to define the degrading response of the column after ultimate capacity (F_u) up to the point of axial load failure: (i) deformation at shear failure (Δ_s), and (ii) deformation at axial load failure (Δ_a). Figure 4-12 illustrates the envelope response of columns to lateral loading and the critical points which are usually defined in the literature by various studies.

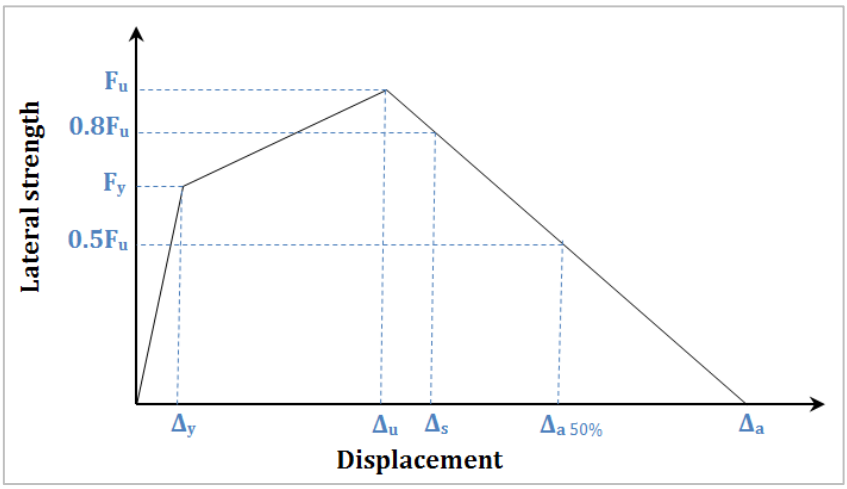

Figure 4-12: Definition of critical points for the lateral strength-displacement response of non-ductile columns

Extensive research has been done by previous researchers to develop models to predict the response of non-ductile columns. These models are usually to some extent empirical in nature. Three well established models available in the literature for non-ductile columns are reviewed:

- Model 1: Elwood and Moehle (2003)
- Model 2: LeBorgne (2012), LeBorgne and Ghannoum (2014b)
- Model 3: Wibowo et al. (2014), J L Wilson et al. (2015)

A summary of the database for the three models is provided in Table 4-5. The proposed equations for the various deformation limits are primarily based on conducting regression analysis on a database of experimental results obtained from the literature for columns with non-ductile or non-seismically conforming detailing. However, it is noted that the proposed deformation limit for axial load failure by Elwood and Moehle (2003) is based on the classical-shear friction mechanism and the effective coefficient of friction is based on experimental tests. A summary of the equations proposed for use in each model are provided in Table 4-6.

The definition of the critical points associated with the column response varies from one model to the next. Deformation at shear failure (Δ_s) in Models 1 and 3 is defined as the displacement at which the shear resistance drops below 80 % of the maximum shear recorded; this is the conventional method of defining lateral strength failure. In Model 2, the deformation limit at shear failure is determined based on the total rotation limit (θ_f) allowed in the plastic hinge region, and it corresponds to the deformation at which the maximum (peak) shear force was recorded (referred to as the ultimate displacement in this study, Δ_u). The deformation limit at axial load failure (Δ_a) in Model 1 is defined as the displacement at which axial load failure was observed in the experiment, that is the point at which the column is no longer capable of resisting the axial load; this approximately corresponds to the displacement at which the shear resistance dropped to zero. The deformation limit at axial failure in Model 2 is not directly provided; rather the shear displacement, corresponding to the difference between the displacement at which ultimate shear force and residual lateral strength were observed in the experiment (Δ_r) (shown in Figure 4-13), is provided. The deformation limit at axial failure in Model 3 refers to the displacement at which the shear resistance drops below 50 % of the maximum applied shear force ($\Delta_{a\ 50\%}$).

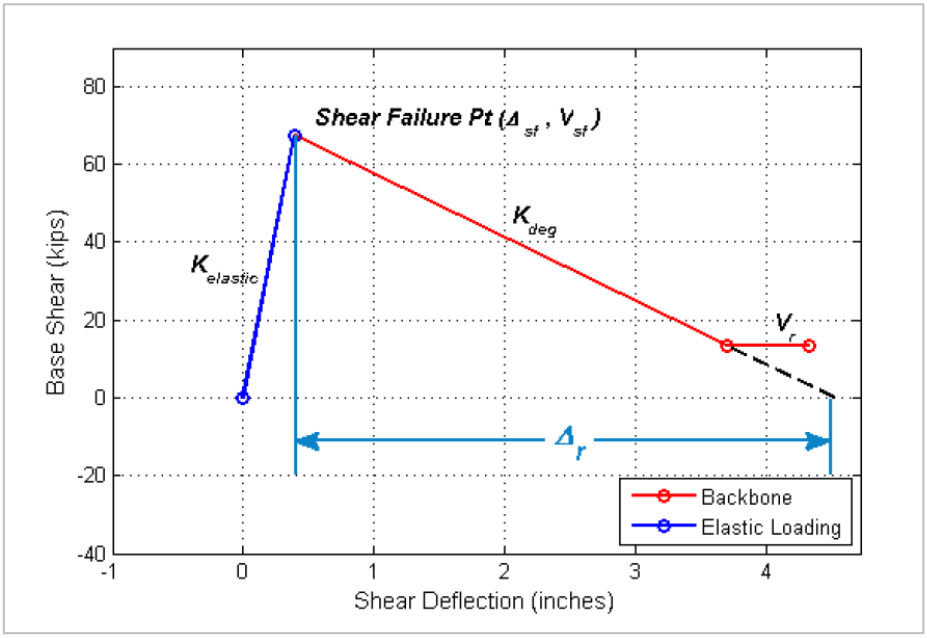

Figure 4-13: Shear force-deflection backbone defined by LeBorgne (2012)

Table 4-5: Summary of the three empirical based models defining column deformation limits

Database and Model Detail	**Model 1**	**Model 2**	**Model 3**
Number of specimens	50 columns for determining Δ_s, and 12 columns for determining Δ_a	32 columns	46 columns
Method used to determine proposed equations	Δ_s is based on curve fitting with experimental data. Δ_a is based on the classical shear-friction mechanism and the effective coefficient of friction is based on experimental tests.	Proposed equations are based on regression analysis.	Δ_u determined based on yield and plastic curvatures. Δ_a is determined based on curve fitting with experimental data. Δ_s is determined by linear interpolation between Δ_u and Δ_a.
Range of parameters in database			
Concrete compressive strength	$13.1 \leq f_c' \leq 44.8$ *MPa*	$19.3 \leq f_c' \leq 46.9$ *MPa*	*NA*
Longitudinal reinforcement yield stress	$324.1 \leq f_{yl} \leq 542.0$ *MPa*	$330.7 \leq f_{yl} \leq 523.6$ *MPa*	*NA*
Longitudinal reinforcement ratio	$0.01 \leq \rho_l \leq 0.04$	$0.01 \lesssim \rho_l \lesssim 0.04$	$\rho_l \leq 0.02$
Shear span to depth ratio	$2.0 \leq \frac{a}{h} \leq 4.0$	$1.5 \lesssim \frac{a}{h} \lesssim 4.0$	$1.0 \leq \frac{a}{h} \leq 5.5$
Transverse reinforcement spacing to depth ratio	$0.2 \leq s/h \leq 1.2$	$0.1 \lesssim s/h \lesssim 1.2$	*NA*
Transverse reinforcement yield stress	$317.2 \leq f_{yt} \leq$*648.1 MPa*	$316.9 \leq f_{yt} \leq$*565.0 MPa*	*NA*
Transverse reinforcement ratio	$0.0010 \leq \rho_t \leq 0.0065$	$0.0010 \lesssim \rho_t \lesssim 0.014$	$\rho_t \leq 0.004$
Maximum shear stress	$0.23 \leq \frac{v}{\sqrt{f_c'\,(MPa)}} \leq 0.71$	*NA*	*NA*
Axial load ratio	$0.0 \leq \frac{P}{A_g f_c'} \leq 0.6$	$0.0 \leq \frac{P}{A_g f_c'} \leq 0.6$	$0.0 \leq \frac{P}{A_g f_c'} \leq 0.65$

h: is the depth of the cross-section in the plane of bending | a: is the shear span of a member| NA: not available

Table 4-6: Summary of empirical equations defining deformation limits for the three models

	Critical parameter	Equation
Model 1	Drift at shear failure	$\delta_s = \frac{\Delta_s}{L} = \frac{3}{100} + 4\rho_t - \frac{1}{40}\frac{v}{\sqrt{f_c'}} - \frac{1}{40}\frac{P}{A_g f_c'} \geq \frac{1}{100}$ Where: L is the clear column height ρ_t is the transverse reinforcement ratio v is the nominal shear stress (in MPa) P is the axial load on the column A_g is the column cross-sectional area
	Drift at axial load failure	$\delta_a = \frac{\Delta_a}{L} = \frac{4}{100}\frac{1 + (\tan\theta_{cr})^2}{\tan\theta + P\left(\frac{s}{A_{sv} f_{yt} d_{ct} \tan\theta_{cr}}\right)}$ Where: A_{sv} is the area of the transverse reinforcement f_{yt} is the yield strength of the transverse reinforcement θ_{cr} is the critical crack angle from the horizontal, assumed to be 65°
Model 2	Total rotation limit of hinge region	$\theta_f = 0.027 - 0.033\frac{P}{A_g f_c'} - \frac{0.01s}{d} \geq 0.006$ Where: d is the effective depth of the column
	Residual drift ratio of the shear spring	$\delta_r = \frac{\Delta_r}{L} = 0.16 - 15.4\rho_t - 0.009\frac{l_d}{d_b} + \frac{0.7A_{cc}}{A_g} + 0.58\frac{f_y A_s}{f_c' A_g} \geq 0.02$ Where: l_d is the development length of the longitudinal bars as given by ACI A_{cc} is the confined area of the column cross-section A_s is the total area of the longitudinal bars
Model 3	Drift at ultimate shear force	$\delta_u = \frac{\Delta_u}{L} = \frac{\Delta_y}{L} + \frac{\Delta_p}{L}$ Where: $\Delta_y = \frac{\phi_y L^2}{3}$ for cantilever columns, where ϕ_y is the curvature from sectional analysis $\frac{\Delta_p}{L} = (\phi_u - \phi_y)L_p$, where: L_p is equivalent plastic hinge length $L_p = 0.5h_c$ ϕ_u is the ultimate curvature from sectional analysis
	Drift at axial load failure (when shear resistance drops below 50% of the peak strength)	$\delta_{a\,50\%} = \frac{\Delta_{a\,50\%}}{L} = 5(1 + \rho_l)^{-\frac{1}{1-\beta}} + 7\rho_t + \frac{1}{5n}$ Where: ρ_l is the longitudinal reinforcement ratio $\beta = \frac{n}{n_b}$, where n is the axial load ratio, and n_b is the axial load ratio at the balance point on the interaction diagram
	Drift at shear failure	Calculated using linear interpolation between $\frac{\Delta_u}{L}$ and $\frac{\Delta_a}{L}$

To simulate the flexure-shear response of columns the shear behaviour of columns needs to be added to the elements used to simulate flexural behaviour. For the lumped plasticity approach, the flexure-shear response of columns can be directly included in the uniaxial hysteretic model used to define the moment-rotation response of the zero-length springs. For the distributed plasticity approach, shear response may be added to columns via zero length shear spring elements where the shear response of the columns is explicitly defined by the uniaxial hysteretic model. Traditionally, the use of shear springs to capture shear response of members has only been capable of simulating shear failure (i.e. degradation in strength of the member) if the shear strength was less than the flexural strength of the member. This is illustrated in Figure 4-14. This modelling approach does not allow the simulation of flexure-shear critical columns where the shear capacity of columns decreases due to increased inelastic deformations. To overcome this problem, Elwood (2004) developed a new uniaxial material model known as the *Limit State Material* model which is implemented in OpenSEES (McKenna et al., 2000). The *Limit State Material* model is capable of detecting shear failure due to exceedance of shear force capacity, or exceedance of shear drift capacity, as shown in Figure 4-15. It achieves this by not only monitoring the shear forces in the member but also the drift experienced by the member. Once the shear strength or drift capacity is exceeded (which is defined using empirically based equations), the shear spring backbone is redefined to include the user-defined degrading shear slope, K_{deg}, and residual force, F_{res}. Due to the series nature of the elements K_{deg} may be calculated using Eq. 4-9.

$$K_{deg} = \left(\frac{1}{K_{deg}^{t}} - \frac{1}{K_{unload}}\right)^{-1} \quad \text{Eq. 4-9}$$

Where K_{deg}^{t} is the total degrading stiffness, $K_{deg}^{t} = \frac{V_u}{(\Delta_a - \Delta_s)}$, where V_u is the peak shear strength, Δ_s and Δ_a are the displacements at shear and axial load failure, respectively

K_{unload} is the flexural degrading stiffness

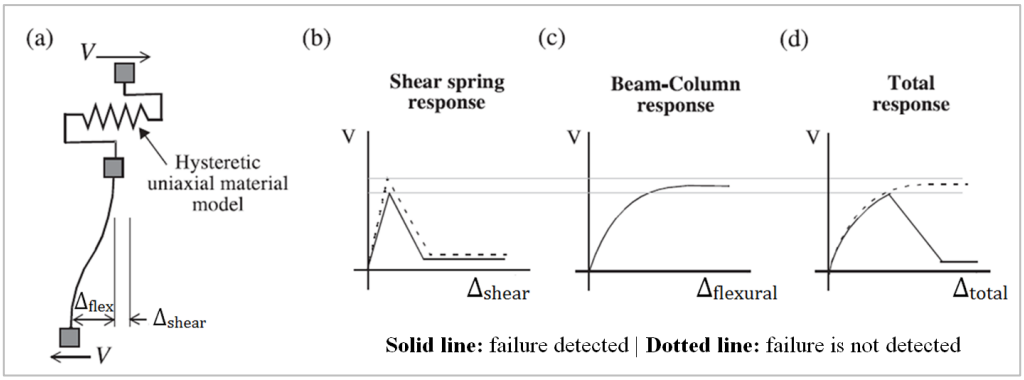

Figure 4-14: Material model capturing shear failure for columns with shear strength less than the flexural strength, adapted from Elwood (2004).

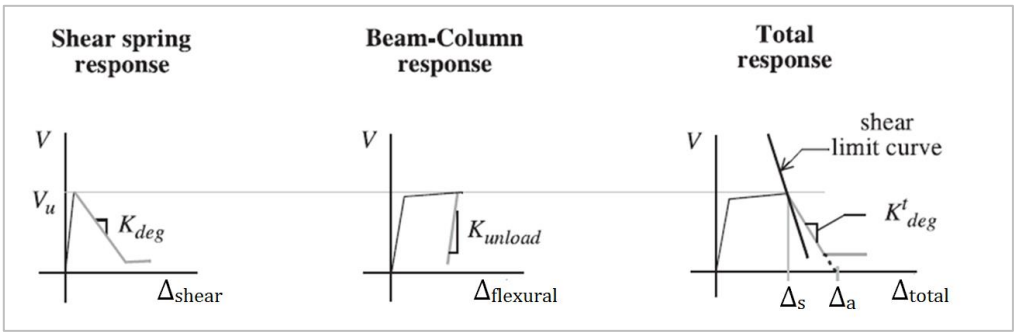

Figure 4-15: Material model capturing shear failure due to exceedance of shear displacement capacity, adapted from Elwood, (2004)

While the limit state material model is a significant advancement in capturing shear failure after flexural yielding, Elwood (2004) explains that convergence issues may occur if the beam-column experiences a negative loading slope (that is a softening flexural response) prior to shear failure since multiple solutions are possible, this is illustrated in Figure 4-16. Therefore, it is suggested that the material properties of the beam-column element should be altered such that a positive slope is maintained prior to shear failure. Furthermore, it is explained that due to the nature of the series modelling approach, there is an offset of *e* in the flexural displacement once shear strength initiates after reloading, as illustrated in Figure 4-17**.** However, Elwood (2004) concludes that the offset *e* does not significantly reduce the effectiveness of the model.

LeBorgne (2012) and LeBorgne and Ghannoum (2014a) built on the work conducted by Elwood (2004) and introduced a new uniaxial material called the *Pinching Limit State Material*, which is also implemented in OpenSEES. The *Pinching Limit State Material* has overcome some of the limitations of the *Limit State Material,* namely the offset flexural displacement due to the series modelling approach. Furthermore, the *Pinching Limit State Material* model monitors rotation within in the plastic hinge region rather than interstorey

drift as the deformation limit to initiate shear degradation. However, LeBorgne (2012) and LeBorgne and Ghannoum (2014a) do not discuss if the numerical convergence issues related to softening flexural response have been addressed. Flexural degradation is typical of non-ductile columns (due to poor confinement) and columns with high axial loads, and as such numerical instability issues related to softening response of columns may be a key limitation of both limit state material models.

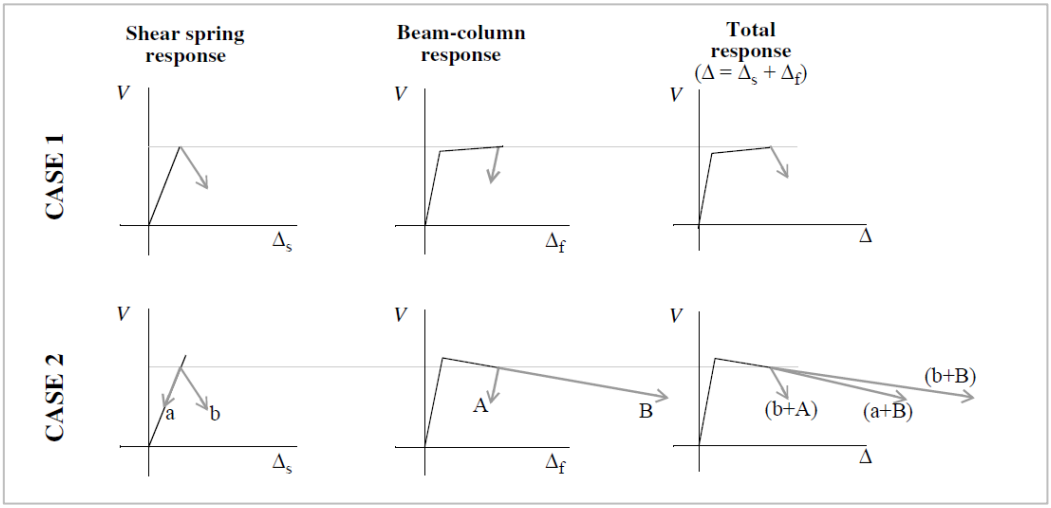

Figure 4-16: Numerical solutions possible for: (a) hardening flexural response, and (b) softening flexural response, from Elwood (2004)

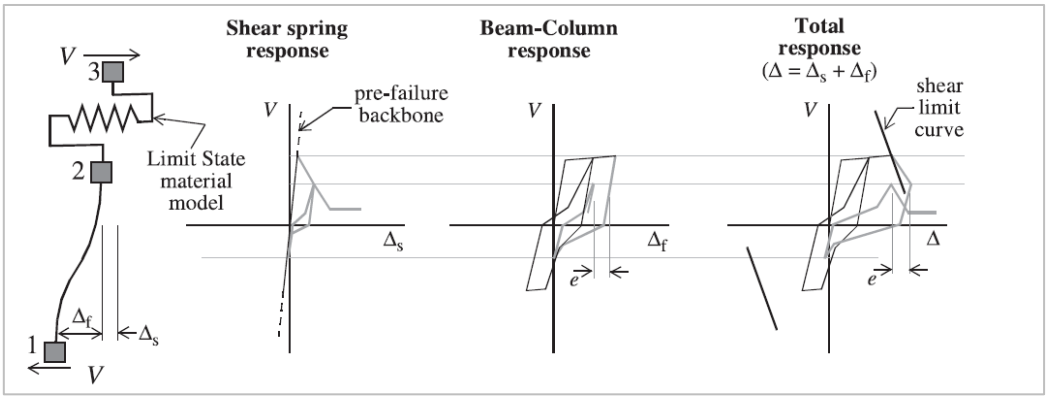

Figure 4-17: Limitation of series modelling approach resulting in an offset of e *in the flexural displacement, from Elwood (2004)*

4.6 MODELLING OF PLANAR AND NON-PLANAR WALLS

The most accurate method available to model planar and non-planar walls is with continuum elements such as shell and solid elements. This is because continuum elements are capable of simulating the interaction between the axial-flexural and shear response of the walls since they are not based on the assumption that plane sections remain plane. Therefore accurate simulation of vertical strain distribution along the wall length may be

obtained. However, similar to distributed plasticity elements, calibration of element/mesh size is necessary to ensure objective response is obtained when a softening response is simulated (Scott & Fenves, 2006). The accurate simulation of strain distributions is particularly important for walls because the damage limits for assessment of walls are usually determined by strain limits of the concrete and reinforcing bars rather than rotation and drift limits. However, for the purpose of global analysis; continuum elements are computational inefficient and most importantly they are not numerically robust and reliable. Due to these limitations continuum elements are usually not utilised for macro-modelling of buildings and other modelling methods need to be adopted.

Researchers have shown that, if implemented carefully, distributed plasticity elements can accurately simulate the response of RC planar and non-planar walls displaying predominantly flexure controlled behaviour (Beyer et al., 2008a; Pugh et al., 2015). However, it is noted that the use of fibre-sections for walls which demonstrate a single crack or minimal cracking is unknown. To the knowledge of the author, no attempt has been made to develop nonlinear macro-models of buildings which contain non-ductile or lightly reinforced walls discussed in Section 3.4.3; especially those displaying a cracking moment that is higher than the yield moment capacity.

The following subsections describe some of the important aspects discussed in the literature related to the modelling of walls, including: the incorporation of plastic hinge length to accurately simulate flexural behaviour, incorporation of shear deformations, modelling of non-planar walls, and the sensitivity of the simulated response of interconnected walls to modelling assumptions.

4.6.1 Plastic hinge length for flexural response

Studies have highlighted that the use of strain limits for conducting assessment of the walls should be used with caution since the strain distribution of distributed plasticity elements is not reliable unless some form of calibration has been conducted (Beyer et al., 2008a; Pugh et al., 2015). In Section 4.3.2.3 it was discussed that explicit modelling of the plastic hinge region can help to solve strain localisation issues. The same approach also helps to improve the prediction of strain since the principle of the approach is based on improving the accuracy of the distribution of plasticity along the member. Therefore to accurately simulate the response of the walls using the distributed plasticity approach it is necessary to determine the plastic hinge length (L_p) of the walls.

Over the years, many different plastic hinge equations have been proposed by various studies for the prediction of the plastic hinge length of walls including Bohl and Adebar

(2011), Kazaz (2013), and Priestley et al. (2007). Most of these studies have been developed for seismically designed walls or walls displaying a ductile response. Therefore they are unlikely to be suitable for the walls to be assessed in this study since they have non-ductile detailing. In addition, most of the plastic hinge equations have been developed based on numerical or experimental results for rectangular walls only. As part of the on-going research at the University of Melbourne to assess the seismic performance of buildings in Australia, detailed finite element analyses have been conducted by Hoult (2017) and Hoult et al. (2017; in press) (2017, 2018) to assess the lateral response of both rectangular and C-shaped walls. The walls analysed were in 3- to 12-storey buildings and had detailing following the Australian Standards; therefore they were often lightly reinforced walls with little to no confinement. The results illustrated that the existing plastic hinge equations are unsuitable for walls with detailing representative of Australian construction as they over-estimate the plastic hinge length and hence the deformation capacity of the walls. This was particularly the case for walls with very low longitudinal reinforcement ratios which developed only a single crack at the base of the wall. Hoult (2017) proposes new plastic hinge length equations suitable for rectangular and C-shaped walls with non-ductile detailing. Separate plastic hinge lengths are proposed based on the likelihood of secondary cracking developing within the hinge region; this is checked by comparing the longitudinal reinforcement ratio (ρ_l) (within the boundary element if provided) with the minimum longitudinal reinforcement ratio ($\rho_{wl.min}$) required to form secondary cracking, where $\rho_{wl.min}$ is calculated in accordance with Eq. 4-10 (Hoult, 2017).

$$\rho_{wl.min} = \frac{(t_w - n_t d_{bt}) f_{ct.f}}{f_u t} \quad \text{Eq. 4-10}$$

Where
- t_w is the wall thickness
- n_t is the number of grids of transverse reinforcement
- d_{bt} is the diameter of the transverse reinforcement

If it is predicted that secondary cracking will form (i.e. $\rho_l > \rho_{wl.min}$) then the plastic hinge length for rectangular walls is determined in accordance with Eq. 4-11. This equation is recommended for assessment purposes.

$$L_p = (0.1L_w + 0.075H_e)\left(1 - 6.0\left(\frac{P}{A_g f_{cmi}}\right)\right) \leq 0.5L_w \quad \text{Eq. 4-11}$$

Where L_w is the wall length
H_e is the effective wall height
A_g is the cross-sectional area of the wall
f_{cmi} is the (mean) concrete strength

If secondary cracking is predicted for C-shaped walls, Hoult (2017) recommends Eq. 4-12(a), (b), and (c) for calculating the plastic hinge lengths. Three different equations are proposed by Hoult (2017) since the numerical analyses suggested different plastic hinge lengths depending on the direction of bending.

Bending about the major axis:

$$L_p = (0.1L_w + 0.013H_e)(1 - 13ALR)(7.0e^{-0.5v}) \leq 0.5L_w \quad \text{Eq. 4-12(a)}$$

Bending about the minor axis with web in compression:

$$L_p = (0.5L_w + 0.015H_e)(1 - 13ALR)(1.6e^{-0.1v}) \leq 0.5L_w \quad \text{Eq. 4-12(b)}$$

Bending about the minor axis with web in tension:

$$L_p = (1.3L_w + 0.082H_e)(1 - 11ALR)(1.0e^{-1.1v}) \leq 0.5L_w \quad \text{Eq. 4-12(c)}$$

Where ALR is the axial load ratio on the wall
v is the average normalised shear stress

If it is predicted that only a single crack will form (i.e. $\rho_l < \rho_{wl.min}$), Hoult (2017) conservatively recommends adopting a plastic hinge length of 150 mm for the assessment of lightly reinforced rectangular and C-shaped walls.

4.6.2 Shear deformations for walls

Simple linear elastic shear hysteretic models are usually adopted to incorporate shear deformations for the global analysis of walls. The shear response may be added to line elements at an element or section level depending on the type of elements used (Pugh et al., 2015). For force-based elements the shear response may be incorporated at a section level. The shear behaviour is defined via a shear force-shear strain ($V - \gamma$) relationship and is added to each integration point. For displacement-based elements or lumped plasticity elements, the response is incorporated with a single shear spring positioned at the bottom of the wall element or multiple springs may be used and distributed along the wall height at each storey. The response of the spring is defined with a shear force-shear displacement ($V - \Delta_{shear}$) relationship, where the shear displacement is obtained by multiplying the shear strain with the element height (H), (i.e. $\Delta_{shear} = \gamma H$).

Typically the shear stiffness is calculated using a portion of the gross section and elastic properties. For example, (Pugh et al., 2015) recommend calculating the shear stiffness using Eq. 4-13 for their proposed modelling technique for flexural RC walls using line-elements.

$$k_{shear} = \frac{V}{\gamma} = G_{eff} K_s A_{cv} \quad \text{Eq. 4-13}$$

Where
- G_{eff} is the effective shear modulus of concrete, $G_{eff} = 0.1G_c = 0.04E_c$, where E_c is the elastic modulus of concrete
- K_s is the shear form factor which is taken as 5/6 for rectangular walls
- A_{cv} is the shear area of the section

Other studies have highlighted that it is more accurate to calculate shear deformations (and hence shear stiffness) based on the amount of flexural deformation experienced at a certain ductility level. This is because experimental results from numerous studies have demonstrated that the ratio of shear deformations to flexural deformations is constant during inelastic response of flexural walls, including rectangular walls (Dazio et al., 2009) and non-rectangular walls if the direction of loading is considered (Beyer et al., 2008b). This suggests that the shear deformations induced in the wall are dependent on the level of shear force and inelastic flexural deformations (Beyer et al., 2011). Based on these observations and building on previous work conducted by Hines et al. (2004) and Priestley et al. (2007), Beyer et al. (2011) suggests a new equation for estimating the ratio of shear deformations to flexural deformations $\left(\frac{\Delta_{shear}}{\Delta_{flex}}\right)$, and this is shown in Eq. 4-14.

$$\frac{\Delta_{shear}}{\Delta_{flex}} = 1.5 \frac{\varepsilon_m}{\phi \tan(\beta) H_n} \quad \text{Eq. 4-14}$$

Where
- ε_m is the axial strain at the centroid of the wall (at nominal yield)
- ϕ is the curvature of the wall section (at nominal yield)
- β is the cracking angle
- H_n Shear span of the wall

Eq. 4-14 is based on the assumption that for flexure governed walls, that is for walls that do not display a significant degradation in shear-transfer mechanism, the shear

deformations are primarily dependent on the mean axial strain. In addition, it is based on the plastic hinge model which assumes the curvature and hence the mean axial strain is constant along the length of the plastic hinge length. Therefore, for a given cracking angle, shear strain is also constant and hence the shear deformations may be approximated using Eq. 4-15 assuming that shear deformations outside the plastic hinge length are insignificant.

$$\Delta_{shear} \approx \gamma L_p = \frac{\varepsilon_m}{\tan(\beta)} L_p \qquad \text{Eq. 4-15}$$

It is also assumed that the total inelastic flexural deformations are confined to the plastic hinge region, and hence flexural deformations may be approximated as:

$$\Delta_{flex} \approx \gamma L_p = \phi L_p H_n \qquad \text{Eq. 4-16}$$

Using Eq. 4-15 and Eq. 4-16, the ratio of shear-to-flexural deformation is obtained in Eq. 4-14 with a correction factor 1.5 which was added by Beyer et al. (2011) to match experimental results. The use of this factor is justified on the basis of overcoming some of the limitations of the model (such as under prediction of shear deformations for not accounting for the strain in the horizontal reinforcement and the strain in the compression strut). Furthermore, when modelling the shear spring with a linear elastic hysteretic model it is necessary to determine the ratio of shear-to-flexural deformations at a particular displacement demand. Beyer et al. (2014) suggest determining the ratio at nominal yield (i.e. corresponding to a displacement ductility of one, $\mu_\Delta = 1$) since the compatibility forces between the walls with different stiffness are the largest at the onset of the yielding of walls.

4.6.3 Non-planar walls

The conventional method of modelling non-planar walls using distributed plasticity elements involves assigning a single fibre-section to the line element. This approach is capable of accurately simulating the flexural response of an individual wall. However, the approach has some limitations when examining the wall behaviour in a building. To help improve the simulation of non-planar walls using distributed plasticity elements, especially for the purpose of design, Beyer et al. (2008a) suggests using the wide-column model (WCM). Details of the approach are provided for simulating the inelastic response of C-shaped walls, however, the approach may be adopted for other non-planar wall shapes. The model is based on the wide column analogy, also known as the equivalent frame method, which has been utilised within elastic systems for the modelling of planar

walls with openings, walls coupled with beams and slabs, and for non-planar walls. The wide-column model involves modelling each planar component of the wall with an individual line element which is assigned to a rectangular fibre-section, for example a C-shaped wall is modelled with three members as illustrated in Figure 4-18. The components of the wall section are connected to each other using horizontal link elements. The vertical elements may be modelled as force-based or displacement-based distributed plasticity elements. If displacement-based elements are used, then multiple elements need to be used between link elements to ensure accurate response of the wall is simulated. The main advantage of the wide-column model is that it allows non-planar walls to be modelled in three-dimensions unlike one-dimensional stick models, and hence it provides the following benefits (Beyer et al., 2008a):

- It models the distribution of the shear force between the web and the flanges of the C-shaped cross-section.
- It inherently models the torsional stiffness of C-shaped walls as there is a lever arm between the two flanges.
- It allows the monitoring of the sectional forces acting on the individual components of the C-shaped wall and hence assesses the likelihood of shear strength failure.

Beyer et al. (2008a) also discuss some of the disadvantages associated with the wide-column model, namely the parasitic bending moments due to shear stresses along the wall edges. However, it is explained that the effect of the parasitic bending moments can minimised by reducing the length at which the link elements are positioned to connect the various components of the wall section. Based on parametric studies and previous recommendations by Stafford Smith and Girgis (in 1986), Beyer et al. (2008a) suggest limiting the space between the links to the smaller of one-fifth of the effective wall height or half of the wall length (where the wall length was taken as the larger of the flange or web length), whichever is smaller.

The horizontal link elements require the definition of flexural, shear, and torsional stiffness. Usually they are modelled as rigid except for the torsional stiffness which allows warping of the wall components, that is; it is no longer assumed that the total wall section remains plane. Based on the elastic analysis Reynouard and Fardis (2001, cited in Beyer et al., 2008a) recommend setting the torsional flexibility for both the web and flange link elements to:

$$\mathrm{K}_{\mathrm{torsion}} = G\frac{h_{sp}t_w^3}{3} \qquad \text{Eq. 4-17}$$

Where G is the shear modulus of concrete

h_{sp} is the link spacing

Beyer et al. (2008a) suggest using a reduction factor of 0.25 to the torsional flexibility calculated in Eq. 4-17 to account for the inelastic behaviour, however, it is mentioned that this parameter does not significantly affect the wall response.

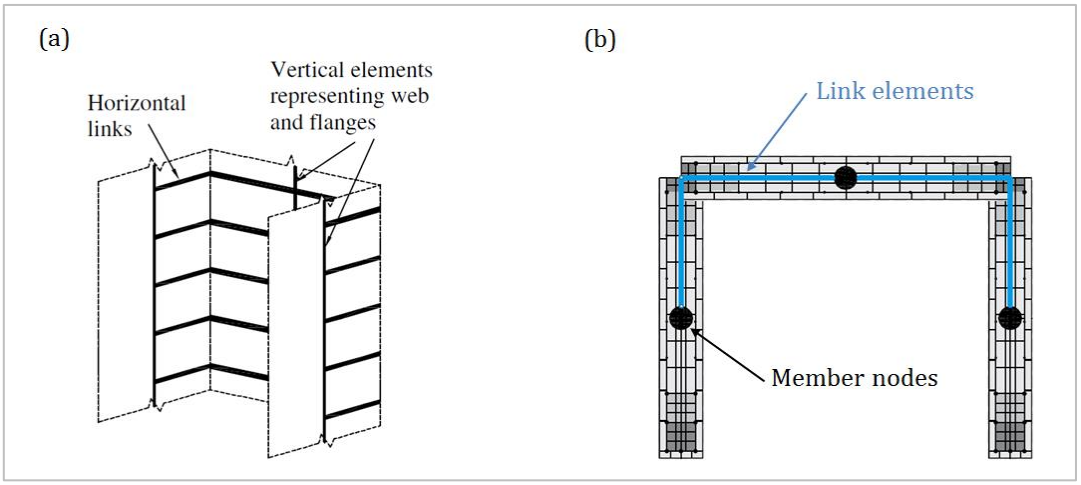

Figure 4-18: Wide-column model: (a) C-shaped wall member positioning, (b) C-shaped wall cross-section idealisation; two flange members and one web member, adapted from Beyer et al. (2008a)

4.6.4 Interconnected wall response

When conducting global analysis of RC buildings it is necessary to consider the behaviour of individual components in a system response. One particular issue that has been reported is the distribution of shear forces between interconnected walls, that is, walls that are connected to each other with a diaphragm (usually assumed to be rigid for modelling purposes). Studies have illustrated that the shear force distribution between interconnected walls, particularly with different yield deformation capacities, can vary significantly due to modelling assumptions.

Multiple studies have highlighted, with respect to ductile walls, that the distribution of the base shear amongst interconnected cantilever walls with different lengths varies during nonlinear pushover analysis (Beyer, 2005; Rutenberg, 2004; Simonini et al., 2012). Initially, when all of the walls are responding in the elastic range, the distribution of lateral force between the walls is proportional to their lateral stiffness. When all of the walls yield, the distribution of base shear is proportional to the moment capacity at the wall

base. Between the two stages, that is when some walls are elastic and while others yield, the base shear distribution is not proportional to the elastic stiffness or the wall strength. During this middle stage, the lateral deformations of walls at the floor levels would have been different if they were not interconnected due to their different deflection profiles (i.e. yield and plastic deflection profiles). However, if a rigid diaphragm is imposed, then the displacement at each storey must be the same, thus the floor diaphragm must transfer in-plane forces to achieve this. These compatibility forces alter the distribution of base shear between the walls; the wall that yields first experiences a decrease in shear force while the walls which have not yielded yet experience an increase in shear force. It is noted that the total base shear of the system is not affected by these internal forces.

Beyer et al. (2014) show the difference in shear distribution obtained using different modelling assumptions by looking at the response of an 8-storey cantilever wall system consisting of two walls with different lengths. The walls are modelled using: (i) shell element model (SEM); which is taken as the benchmark, (ii) distributed plasticity beam element (DPBE), and (iii) lumped plasticity beam element (LPBE). Firstly, it is illustrated that the response obtained using all three models match well if the individual pushover curves of the walls are compared (the results are provided in Figure 4-19). However, the results obtained for the interconnected walls (connected using a rigid diaphragm assumption) show that the shear distribution in each wall is dependent on the modelling approach, shown in Figure 4-20(a). The lumped plasticity approach overestimates the shear developed in the short (i.e. flexible) wall. In addition, it can be seen that the total response of the system is not affected by the different modelling approaches. One approach which Beyer et al. (2014) suggest to improve the accuracy of the results obtained using DPBE and LPBE is to add shear flexibility to the model by incorporating shear springs at mid-height of each storey. The improved results obtained for the distributed and lumped plasticity approach are provided in Figure 4-20(b) and Figure 4-20(c), respectively. Clearly, the degree of improvement is dependent on the calibration of the shear flexibility.

The findings discussed here indicate the importance of examining the system response of components and the dependability and sensitivity of the results obtained to modelling assumptions. In addition, it highlights the importance of selecting suitable parameters to determine the response of components. For example, the results from the lumped plasticity approach suggest that the induced shear force may not be a reliable parameter for determining loss of lateral load carrying capacity of the walls.

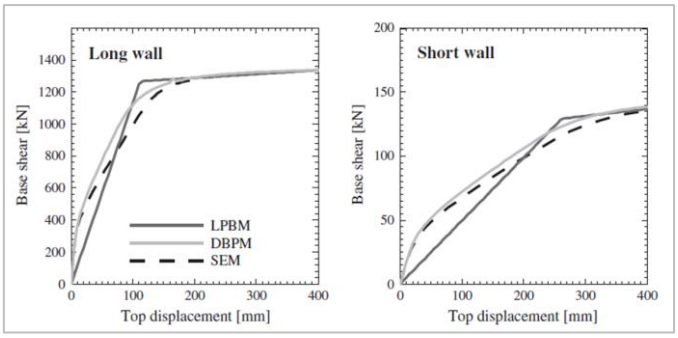

Figure 4-19: Results presented in Beyer et al. (2014) comparing force-deformation response of individual for various modelling approaches

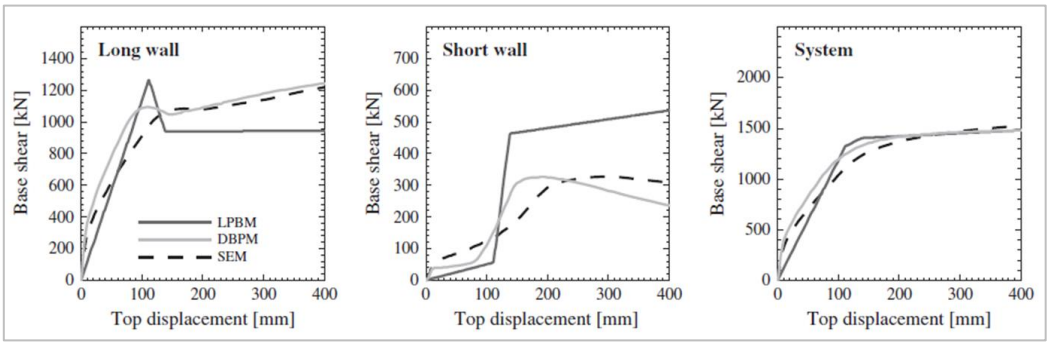

(a) Comparison of the response obtained using SEM, DPBE and LPBE

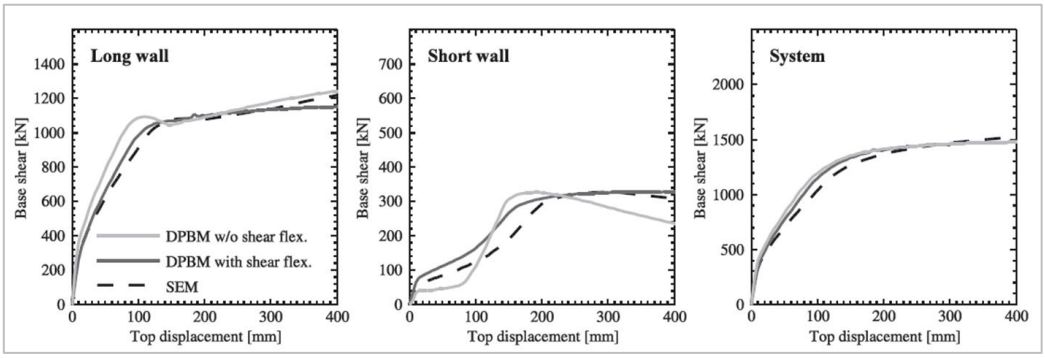

(b) Comparison of the response obtained using DPBE with and without shear flexibility

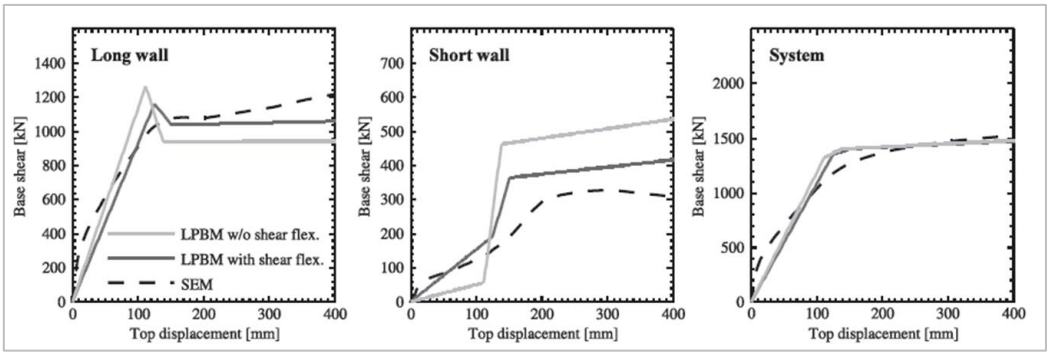

(c) Comparison of the response obtained using LPBE with and without shear flexibility

Figure 4-20: Results presented in Beyer et al. (2014) comparing force-deformation response of interconnected walls and the total system for various modelling approaches

4.7 SUMMARY

This chapter has provided a critical review of the current macro-finite element modelling techniques and challenges for simulating the response of RC buildings. In particular, modelling techniques have been examined which attempt to simulate the response of non-ductile RC building components, including: beam-column joints, columns and beams, and walls. In general, there appears to be a lack of consensus amongst researchers about which method to adopt when modelling the various components of buildings for the purpose of global analysis. Furthermore, most of the approaches require the incorporation of empirically based numerical models to capture the true response of the members. It is also evident that the various modelling techniques which are currently available require a compromise between: (i) the capability to accurately model the expected governing failure mechanisms and to capture axial, flexure, and shear interactions, (ii) numerical efficiency, and (iii) numerical stability and reliability. In order to select the most suitable approach to conduct global analysis of non-ductile RC buildings, the various modelling approaches are evaluated in Chapter 5 and the selected approach is adopted to conduct the assessment of the archetypal buildings in Chapter 7.

CHAPTER 5: EVALUATION OF NONLINEAR MACRO-MODELLING METHODS FOR NON-DUCTILE RC BUILDINGS

5.1 INTRODUCTION

This chapter describes the approach adopted for modelling non-ductile building components for the purpose of conducting global analysis in a macro-finite element modelling space. Specifically, the modelling techniques described are to be implemented in OpenSEES (McKenna et al., 2000), however, they may be adopted and modified as necessary for other programs. The basis of any of the modelling methods involves defining the cross-section of the components with fibre-sections to conduct sectional analysis or using distributed plasticity elements. Therefore, this chapter begins by outlining the material models adopted for defining fibre-sections and obtaining the critical points from sectional analysis. Then, the specific modelling approaches used to simulate the response of beam-column joints, columns and beams, and walls are evaluated and the approach to be adopted for global analysis of the archetypal buildings in Chapter 7 is described.

5.2 DEFINING FIBRE-SECTIONS AND CONDUCTING SECTIONAL ANALYSIS

To define the response of fibre-sections, uniaxial material models need to be assigned to describe the load-deformation response of the concrete and steel fibres. In this study the concrete fibres are modelled using the Popovics (1973) uniaxial concrete stress-strain material model which is available in OpenSEES as *Concrete04* and the reinforcement bars are modelled using the Giuffré-Menegotto-Pinto uniaxial material model (Menegotto & Pinto, 1973) which is available as *Steel02* model in OpenSEES. The hysteretic behaviour of the material models is illustrated in Figure 5-1 and Figure 5-2. Both of these material models are well established ones; they have been selected because of their versatility and also because they generally provide better numerical stability in comparison to some of the other material models available in OpenSEES.

When the simulated results for the overall behaviour of a specimen are compared with the experimental results for that specimen, the material properties are based on the reported values from the experiments (if these are available). The input parameters required for the *Concrete04* material model are given in Table 5-1. These parameters are either found directly from material tests, or are determined using the equations given in Table 5-1. The effect of confinement provided by the transverse reinforcement is accounted for by using the Mander et al. (1988) model, although it is noted that the effect of confinement is

minimal for non-ductile RC components and may be ignored, especially for assessment purposes. In addition, unless stated otherwise, the criteria presented in Table 5-2 are used to define the key points obtained from sectional analyses; these points are used in this Chapter when comparing simulated results with experimental responses.

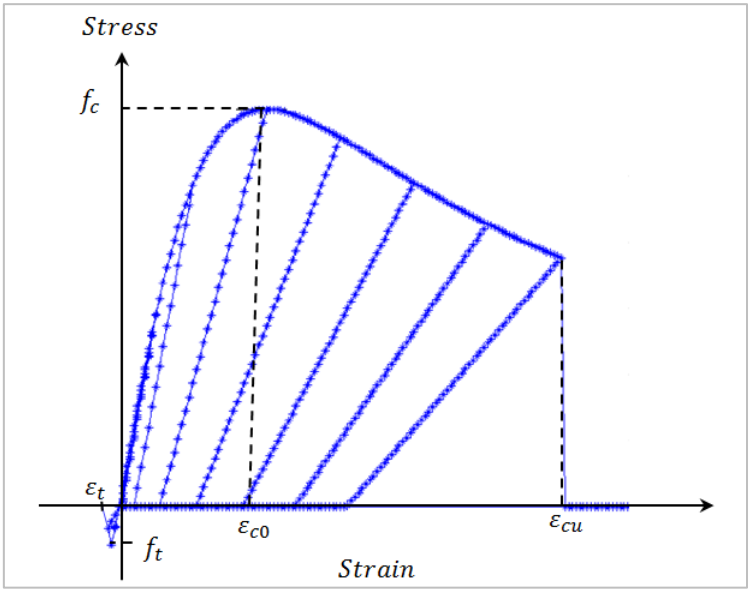

Figure 5-1: Concrete04 material model, adapted from McKenna et al. (2000)

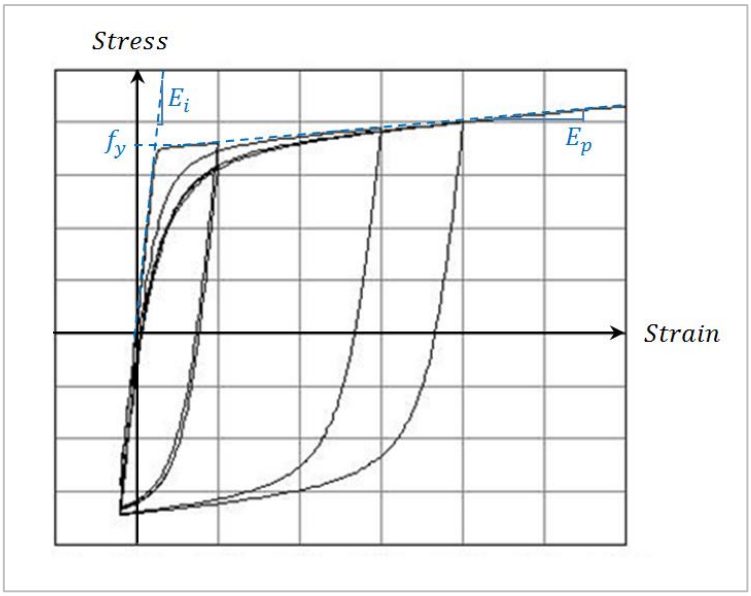

Figure 5-2: Steel02 material model without isotropic hardening, adapted from McKenna et al. (2000) (where E_i is initial stiffness and E_p is post yield stiffness)

Table 5-1: Input parameters adopted for Concrete04 material model for evaluating different modelling approaches

Input parameter	Unconfined concrete	Confined concrete
Concrete compressive strength	f_c'	Confined concrete compressive strength: $f_{cc}' = Kf_c'$ where K is the confinement factor according to Mander et al., (1988)
Strain at maximum strength	$\varepsilon_{c0} = 0.002$	$\varepsilon_{cc0} = \varepsilon_{c0}(1 + 5(K - 1))$ (Mander et al, 1988)
Strain at crushing strain	$\varepsilon_{cu} = 0.012 - 0.0001f_c'$ (Reddiar, 2009)	$\varepsilon_{ccu} = 5\varepsilon_{cc0} + 0.004$ (Reddiar, 2009)
Elastic modulus	$E = 5000\sqrt{f_c'}$	$E = 5000\sqrt{f_c'}$
Maximum tensile strength	$f_{ct} = 0.6\sqrt{f_c'}$ (As 3600: 2009)	$f_{ct} = 0.6\sqrt{f_c'}$ (As 3600: 2009)
Ultimate tensile strain	$\varepsilon_t = 0.1\varepsilon_{cu}$	$\varepsilon_t = 0.1\varepsilon_{cu}$

Table 5-2: Criteria used to define critical moment-curvature points for evaluating different modelling approaches

Critical point	Criteria
Cracking Moment	Extreme tensile concrete fibre stress equals the flexural tensile strength of concrete (f_{ct}); $f_{ct} = 0.6\sqrt{f_c'}$ in accordance with AS 3600:2009.
Yield Moment	Extreme tensile steel fibre stress equals to the yield strength (f_y), or when the extreme compressive concrete fibre strain is equal to 0.002, depending on whichever occurs first as suggested by Priestley et al. (2007).
Nominal Yield Moment	Extreme tensile steel fibre strain equals to 0.015, or when the extreme compressive concrete fibre strain equals to 0.004, depending on whichever occurs first as suggested by Priestley et al. (2007). The curvature at nominal yield is then calculated; $\phi_{ny} = \frac{M_N}{M_y}\phi_y$
Ultimate Moment	Is the point at which maximum moment is observed but it is also limited to the following conditions, depending on whichever occurs first; when the extreme tensile steel fibre strain equals to 0.1 (an approximation of the ultimate tensile strain), or when the extreme compressive concrete fibre strain equals to 0.006.

5.3 MODELLING NON-DUCTILE BEAM-COLUMN JOINTS

The following subsection describes and evaluates the modelling approach for incorporating the inelastic response of non-ductile beam-column joints. The approach is similar to that suggested by Celik and Ellingwood (2008) which involves determining the type of failure expected (BJ, CJ, or J) to define the backbone response (discussed in Section 4.2.2.1). A single load-deformation relationship is used to define the shear panel response and the bar-slip of bottom longitudinal beam bars. Hence, the approach is suitable for the scissors model, although it can also be adopted for the continuum type elements to define the response of the central spring and setting all other springs to behave as rigid links. The definition of the load-deformation response and the comparison of the adopted approach with experimental results are provided in the following subsections.

5.3.1 Load-deformation response

The following sections provide the methods used to determine the four critical points to define the envelope response, as well as the hysteretic parameters required for the *Pinching4* uniaxial hysteretic model available in OpenSEES.

5.3.1.1 Point 1: shear cracking

The first point of the backbone is defined as the point at which shear cracking of the joint initiates. The shear stress at this point can be calculated using Eq. 5-1 (Celik & Ellingwood, 2008).

$$\tau_{jh.cr} = 24\sqrt{\left(\frac{1}{145}\right)\left(1 + 0.002\left(\frac{P}{A_g}\right)\right)} \qquad \text{Eq. 5-1}$$

Where P is the axial load on the joint

A_g is the cross-sectional area of the column

(Note P/A_g is in MPa)

5.3.1.2 Points 2 and 3: yield, ultimate or joint shear capacity

The definitions of the second and third points depend on the type of joint failure expected; that is if yielding and ultimate capacity of the beams and the columns occurs prior to or after joint shear strength is reached. This involves first determining if a column-sway or beam-sway mechanism is expected via the sway potential index (S_i). As discussed in Section 4.2.2.1, $S_i > 0.85$ is adopted to determine when the column-sway mechanism is likely to occur.

Once the sway mechanism is determined it is possible to calculate the corresponding shear induced in the joint based on joint equilibrium. It is noted that for joints which have poorly anchored bottom longitudinal beam bars, the positive yield and ultimate bending capacity of the beam is reduced by multiplying the capacities by α, where α is 0.40 and 0.55 for exterior and interior joints, respectively. The reduction factor is used to account for bar-slip as described in Celik and Ellingwood (2008). A summary of the procedure for obtaining the shear stress induced in the joint due to beams reaching their yield and ultimate capacities is provided in Table 5-3 and Table 5-4 for exterior and interior joints, respectively. Some of the terms used to calculate the shear stresses are shown in Figure 5-3 which illustrates the internal and external forces acting on exterior and interior joints due to beam yielding. A similar procedure is also followed if column-sway is expected, however, the moment induced in the beams is calculated based on the yield and ultimate bending capacity of the columns while ensuring that the moment induced in the beam under positive bending is limited by the reduced capacity due to bar-slip.

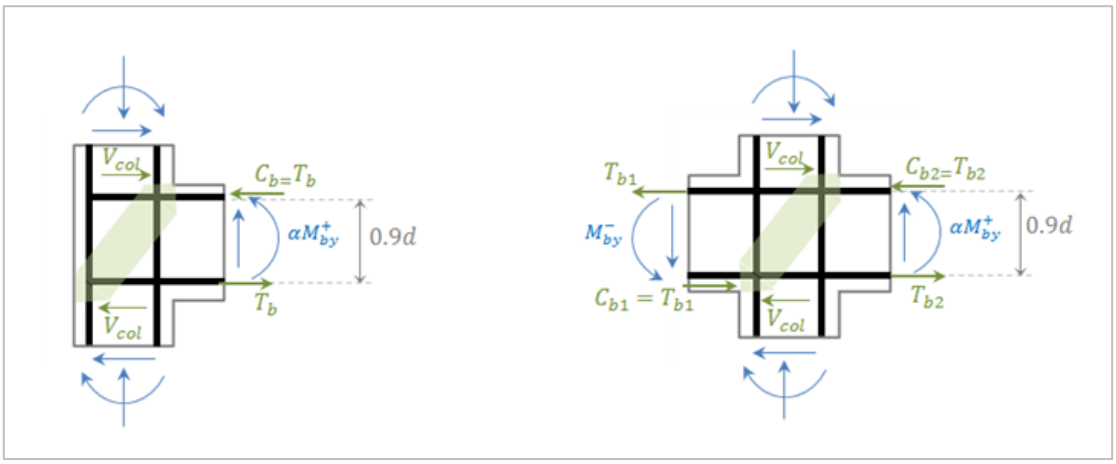

Figure 5-3: Moment, shear and axial forces (in blue), and internal forces (in green) acting on an exterior and interior joint

Table 5-3: Procedure for calculating shear stress induced in exterior joints due to beam yielding

	Positive envelope (beam under sagging moment)	**Negative envelope (beam under hogging moment)**
STEP 1	The positive and negative bending yield moments (M_{by}^{+} and M_{by}^{-}) are obtained from sectional analysis conducted in OpenSEES. For joint subassemblages which include a slab, the effective beam width (b_{ef}) is calculated according to AS 3600:2009 and the top slab bars within the effective width are included.	
STEP 2	Reduce the positive bending capacity of poorly anchored bars to account for bar-slip: αM_{by}^{+}	
STEP 3	Calculate the tensile force corresponding to the beam moment (T_b): (Assume a constant level arm of $0.9d$) $T_b = \frac{\alpha M_{by}^{+}}{0.9d}$	$T_b = \frac{M_{by}^{-}}{0.9d}$
STEP 4	Calculate the shear induced in the columns (V_{col}): $V_{col} = \frac{\alpha M_{by}^{+}}{n_{col}} \times \frac{2}{L_c}$ Where n_{col} is the number of columns adjacent to the joint (i.e. 2 for floor joints and 1 for roof level joints), and L_c is the column height.	$V_{col} = \frac{M_{by}^{-}}{n_{col}} \times \frac{2}{L_c}$
STEP 5	Calculate the shear force acting on the joint core (V_{jh}): $V_{jh} = T_b - V_{col}$	$V_{jh} = T_b - V_{col}$
STEP 6	Calculate the corresponding joint shear stress (τ_{jh}): $\tau_{jh}^{+} = \frac{V_{jh}}{A_j}$ Where A_j is the joint cross-sectional area calculated in accordance with ACI 318 (2011)	$\tau_{jh}^{-} = \frac{V_{jh}}{A_j}$

Table 5-4: Procedure for calculating shear stress induced in interior joints due to beam yielding

	Positive and negative envelope
STEP 1	Obtain the yield and ultimate positive and negative bending capacity (M_{by}^{+} and M_{by}^{-}) from sectional analysis similar to exterior joints.
STEP 2	Reduce the positive bending capacity of poorly anchored bars to account for bar-slip: αM_{by}^{+}
STEP 3	Calculate the compressive and tensile force corresponding to the beam moments (C_b and T_b): $C_b = \frac{\alpha M_{by}^{+}}{0.9 d_b}$ $T_b = \frac{M_{by}^{-}}{0.9 d_b}$
STEP 4	Calculate the shear induced in the columns (V_{col}): $V_{col} = \frac{\alpha M_{by}^{+} + M_{by}^{-}}{n_{col}} \times \frac{2}{L_c}$
STEP 5	Calculate the shear force acting on the joint core (V_{jh}): $V_{jh} = C_b + T_b - V_{col}$
STEP 6	Calculate the corresponding joint shear stress (τ_{jh}): $\tau_{jh}^{+/-} = \frac{V_{jh}}{A_j}$

The shear stress induced due to the beams or columns reaching their yield and ultimate capacities is then compared to the joint shear stress capacity ($\tau_{jh,cap}$). If $\tau_{jh,cap}$ is lower than the induced shear stress due to beam or column yielding then shear failure of the joint is expected and hence the second and third point on the backbone curve are limited to $\tau_{jh,cap}$. As discussed in Section 4.2.2.2 there are many different empirically based equations which approximate joint shear capacity. The more accurate approach of obtaining the shear capacity directly from the strut and tie modelling approach is adopted to reduce the dependency of the predicted strength on the database of joints considered to develop the empirical based equations. The strut and tie modelling approach is similar to that suggested in Hassan (2011) for exterior joints which can also be extended to interior and roof level joints. A summary of the approach to compute $\tau_{jh,cap}$ is provided in Table 5-5. It is assumed that the contribution of ties to joint shear strength is zero since non-ductile joints have no or few ties provided in the joint region.

Table 5-5: Summary of adopted approach to calculate $\tau_{jh.cap}$

Effective strut compressive strength: $\boldsymbol{f_{cu} = \emptyset \beta_s . f'_c}$	Where: $\emptyset = 0.85$ β_s is the concrete softening coefficient, $\beta_s = \frac{1}{1+0.66cot^2\theta_s}$ in accordance with AS 3600:2009 for bottle-shaped strut θ_s is the strut angle (defined later)
Diagonal strut capacity: $\boldsymbol{D_s = f_{cu} A_{str}}$	A_{str} is the concrete strut area, $A_{str} = a_s . b_j$ b_j is the effective joint width according to ACI 318 (2011) a_s is the strut depth, $a_s = \beta_1 \sqrt{a_{b,c}^2 + a_{c,c}^2}$ for exterior and interior joints, $a_s = \beta_1 \sqrt{a_{b,c}^2 - \frac{\sqrt{a_{b,c}^2 + a_{c,c}^2}}{2}}$ for exterior roof joints $a_{b,c}$ is the compression zone depth of the beam, $a_b = k . d_{b,st}$ $k = \left((\rho_{st} + \rho_{sc})^2 n^2 + 2(\rho_{st} + \frac{\rho_{sc} d_{b,sc}}{d_{b,st}}) n \right)^{0.5} - (\rho_{st} + \rho_{sc}) n$ n is the modular ratio ($n = \frac{E_s}{E_c}$, where E_s is the elastic modulus of steel, and E_c is the elastic modulus of concrete) ρ_{st} is the ratio of the area of the longitudinal beam bars in tension to the beam cross-sectional area ρ_{sc} is the ratio of the area of the longitudinal beam bars in compression to the beam cross-sectional area $d_{b,st}$ is the distance to the centroid of the tensile longitudinal beam bars from the extreme compressive fibre $d_{b,sc}$ is the distance to the centroid of the compressive longitudinal beam bars from the extreme compressive fibre $\beta_1 = 1 - 0.05 \times 0.145(f'_c - 27.6) \leq 1.0$ $a_{c,c}$ is the compressive zone depth of the columns (approximated using the equation proposed by Paulay and Priestley) $a_{c,c} = \left(0.25 + 0.85 \left(\frac{P}{f'_c A_g} \right) \right) h_c \leq 0.4 h_c$ A_g is the cross-sectional area of the columns
Joint shear strength: $\boldsymbol{V_{jh.cap} = D_s . \cos(\theta)}$	$\theta_s = tan^{-1} \left(\frac{d_{b,st} - d_{b,sc}}{d_{c,st} - d_{c,sc}} \right)$ $d_{c,st}$ is the distance to the centroid of the tensile longitudinal column bars from the extreme compressive fibre $d_{c,sc}$ is the distance to the centroid of the compressive longitudinal column bar from the extreme compressive fibre
Joint shear stress: $\boldsymbol{\tau_{jh.cap} = \frac{V_{jh.cap}}{A_j}}$	$A_j = b_j h_c$

5.3.1.3 Point 4: residual capacity

The fourth point on the backbone corresponds to the residual capacity which is taken as 20 % of the maximum joint shear stress ($\tau_{jh.max}$) induced in the joint as suggested by Jeon et al. (2015).

5.3.1.4 Summary of stress-strain backbone response

As discussed in Section 4.2.2.1, the selection of strain values proposed by researchers for defining the backbone response is less dependent on joint design and detailing. Most studies recommend average values based on experimental results, therefore the recommendations are highly empirical and a variety of values are suggested by different studies. If upper-bound strain values are utilised, the frame response is more flexible and hence higher drifts demands are approximated. Thus this approach is suitable for assessing frames forming part of the primary system since their performance is usually determined by drift limits, that is, the drift is limited to prevent damage to non-structural components. If lower-bound strain limits are utilised, the response is more rigid, and a lower drift capacity of the frame is predicted. Since the aim of this study is to assess the performance of frames forming part of the secondary structural system in which the drift demands are dictated by the primary lateral force-resisting system, lower-bound shear strain values are selected to give a conservative estimate of the deformation capacity of the frames. Therefore, the strain values corresponding to the critical four points are based on the recommendations provided in Jeon et al. (2015) which generally provide lower-bound predictions in comparison to the other studies discussed in Section 4.2.2.1. A summary of the critical stress-strain values adopted in this study is provided in Table 5-6.

5.3.1.5 Hysteretic response

The recommended values by Jeon et al. (2015) for exterior joints, provided in Section 4.2.2.3, are adopted for defining the pinching, stiffness, and strength degradation behaviour for the *Pinching4* hysteretic model for both exterior and interior joints. Note that the suggested values for interior joints were not adopted as they tend to over-predict the strength degradation.

Table 5-6: Definition of critical backbone points adopted in this study

Exterior joints	**Interior joints**
$\tau_{jh.1} = \tau_{jh.cr}$	$\tau_{jh.1} = \tau_{jh.cr}$
$\gamma_1 = 0.00043$	$\gamma_1 = 0.00043$
$\tau_{jh.2} = the\ smaller\ of\ \tau_{jh.y}\ and\ \tau_{jh.cap}$	$\tau_{jh.2} = the\ smaller\ of\ \tau_{jh.y}\ and\ \tau_{jh.cap}$
$\gamma_2 = 0.006$	$\gamma_2 = 0.006$
$\tau_{jh.3} = the\ smaller\ of\ \tau_{jh.u}\ and\ \tau_{jh.cap}$	$\tau_{jh.3} = the\ smaller\ of\ \tau_{jh.u}\ and\ \tau_{jh.cap}$
$\gamma_3 = 0.015$ [C] or	$\gamma_3 = 0.020$ [C] or
$\gamma_3 = 0.010$ [D*]	$\gamma_3 = 0.015$ [D*]
$\tau_{jh.4} = 0.2\tau_{jh.max}$	$\tau_{jh.4} = 0.2\tau_{jh.max}$
$\gamma_4 = \gamma_3 + \frac{\tau_{jh.3} - \tau_{jh.4}}{75}$	$\gamma_4 = \gamma_3 + \frac{\tau_{jh.3} - \tau_{jh.4}}{80}$

$\tau_{jh.max}$: is the smaller of $\tau_{jh.u}$ and $\tau_{jh.cap}$ | C: for continuous longitudinal beam bars | D: for discontinuous or poorly anchored longitudinal beam bars | * adopted in this study

5.3.2 Comparison between simulated and experimental results

To evaluate the validity of the proposed approach, the simulated and experimental response of 12 non-ductile joints tested under quasi-static cyclic loading are compared. The material, dimensional and loading properties of these joints are given in Table 5-7. The joints selected in the literature have detailing that is consistent with how buildings have been constructed in Australia. Furthermore, joints are selected which include various factors that have been identified as ones that effect the joint response (discussed in Section 3.4.1) in order to examine the suitability of the proposed approach. Namely, in addition to variation in material properties, longitudinal reinforcement ratios, and axial load ratio (ALR) under gravity loading, the following factors which affect the joint response are included in some of the subassemblages considered:

- Poorly anchored bottom beam bars (for exterior and interior joints)
- Inclusion of slabs
- Inclusion of transverse beams
- Variation in axial load during lateral loading
- Roof level joints

Table 5-8 provides a summary of the predicted and experimental joint shear stress values as well as the reported and predicted joint failure mechanisms. It can be seen that there is a good agreement between the maximum shear stress experienced during the analysis and those predicted by the proposed method. Furthermore, the prediction of the failure mode corresponds very well with the reported failure mechanism for most of the joints investigated.

In Figure 5-4 the experimental and simulated shear force versus drift response of the 12 non-ductile beam-column joints is presented. In addition, a brief description of the observed failure mechanism is provided with a photograph of the joint at final stage of loading. In general, it is observed that the simulated results provide a very good approximation to the results obtained during the experiment. The worst prediction of maximum strength is for the Shafaei et al. (2014) specimen 3 when the beam is under positive bending; that is, the bottom poorly anchored beam bars are under tension. The prediction is approximately 80 % of the observed strength due to under prediction of the ultimate positive capacity. This level of inaccuracy is acceptable for the purpose of global analysis of RC buildings.

The joints tested by Hassan (2011) give a good representation of exterior corner joints in buildings since the subassemblage includes the slab as well as beams in both directions. Furthermore, the axial load ratio on the joints was varied during the application of the lateral load in the experiment (reaching a maximum of approximately 45 % at shear failure) to simulate the change in axial load ratio experienced by corner joints belonging to the primary lateral load resisting system. It can be seen that while the proposed model does not directly account for transverse beams and change in axial load (constant gravity axial load was used for the simulated results) the prediction of the simulated response matches well with the experimental results.

A limitation of the proposed model is that it does not directly predict the strain limits at which axial load failure occurs. In most cases it can be seen that the joint is able to reduce its lateral strength capacity by approximately 80 % without losing axial load carrying capacity (i.e. reaching residual capacity as defined in the proposed approach). However, there are exceptions, such as the Hassan (2011) UJ2 specimen which experiences axial load failure at approximately 3.0 % drift; this corresponds to a strength reduction of only 43 % of the peak strength obtained during negative loading. The photographs provided by Hassan (2011) of specimen UJ2 immediately before and after axial load failure illustrate the sudden change in damage level experienced by the joint with a minor increase in drift. This highlights the importance of being conservative in the prediction of axial load failure especially for non-ductile beam-column joints as they are vulnerable to sudden failures.

Table 5-7: Properties of non-ductile exterior and interior beam-column joints

No.	Specimen	Joint type	f_c' (MPa)	Beam		Column		Joint aspect ratio (h_b/h_c)	Bottom beam bar	Slab included	Trans. beam included	Gravity ALR	Axial load protocol	Axial load failure reported
				ρ_l	f_y	ρ_l	f_y							
1	Shafaei et al., (2014) Spec 2	Exterior	23.3	0.020	460	0.020	460	1	C	N	N	0.16	Constant	N
2	Shafaei et al., (2014) Spec 3	Exterior	24.7	0.020	460	0.020	460	1	D	N	N	0.16	Constant	N
3	Pantelides et al., (2002) Unit 1	Exterior	33.1	0.032	468	0.024	468	1	D	N	N	0.10	Constant	N
4	Pantelides et al., (2002) Unit 2	Exterior	30.2	0.032	468	0.024	468	1	D	N	N	0.25	Constant	N
5	Pantelides et al., (2002) Unit 3	Exterior	34.0	0.032	468	0.024	468	1	D	N	N	0.10	Constant	Y
6	Pantelides et al., (2002) Unit 4	Exterior	31.6	0.032	468	0.024	468	1	D	N	N	0.25	Constant	Y
7	Hassan (2011) UJ1 (EW beam)	Exterior (corner)	30.0	0.032	523	0.013	470	1	C	Y	Y	0.21	Varying	Y
8	Hassan (2011) UJ2 (EW beam)	Exterior (corner)	30.5	0.015	503/ 436	0.013	535	1.67	C	Y	Y	0.21	Varying	Y
9	Megget (2003) Spec 5	Exterior (roof level)	33.6	0.02	355	0.019	355	1	D*	N	N	not applied	-	N
10	Megget (2003) Spec 8	Exterior (roof level)	40.4	0.02	340	0.019	340	1	D*	N	N	not applied	-	N
11	Pessiki et al., (1990) Spec 7	Interior	32.5	0.02	480	0.013	461	1.5	D	N	N	0.36	Constant	N
12	Pessiki et al., (1990) Spec 9	Interior	34.6	0.02	420	0.013	461	1.5	D	N	N	0.10	Constant	N

C: continuous | D: discontinuous | * bottom beam bars bent away from the joint core | N: no | Y: yes

Table 5-8: Experimental and predicted joint shear stress and failure mechanism

No	Specimen	Experiment			Prediction					
		$\tau_{jh.max}^{+}$	$\tau_{jh.max}^{-}$	Failure type	$\tau_{jh.cap}$	$\tau_{jh.y}^{+}$	$\tau_{jh.y}^{-}$	$\tau_{jh.u}^{+}$	$\tau_{jh.u}^{-}$	Failure type
1	Shafaei et al., (2014) Spec 2	3.38	3.77	Slip & J	3.93	3	3.48	3.91	4.45	Slip and BJ/J
2	Shafaei et al., (2014) Spec 3	1.99	3.98	J	4.11	1.35	1.57	3.92	4.46	Slip and BJ/J
3	Pentalides et al., (2002) Unit 1	2.48	5.2	Slip	5.09	2.58	2.85	6.46	7.13	Slip and J
4	Pentalides et al., (2002) Unit 2	3.34	5.06	Slip	5.35	2.57	2.84	6.42	7.1	Slip and J
5	Pentalides et al., (2002) Unit 3	5.04	4.94	J (leads to axial load failure)	5.2	6.47	7.13	6.47	7.13	J
6	Pentalides et al., (2002) Unit 4	4.99	5.18	J (leads to axial load failure)	5.52	6.44	7.11	6.44	7.11	J
7	Hassan (2011) UJ1 (EW beam)	4.96	6.50	J (leads to axial load failure)	5.27	5.94	6.7	5.99	6.15	J
8	Hassan (2011) UJ2 (EW beam)	3.22	4.60	J (leads to axial load failure)	5.64	3.93	4.49	4.75	5.4	BJ
9	Megget (2003) Spec 5	1.33	2.43	J	2.45	1.26	2.82	1.45	3.19	Slip and J
10	Megget (2003) Spec 8	1.53	2.54	J	2.68	1.27	2.87	1.49	3.26	Slip and J
11	Pessiki et al., (1990) Spec 7	4.70	4.70	Slip & J (& damage to top & bottom columns)	4.75	6.43	6.88	6.43	6.88	J
12	Pessiki et al., (1990) Spec 9	4.69	4.69	Slip & J (& damage to top & bottom columns)	4.83	6.57	6.69	6.57	6.69	J

J: joint shear failure prior to yielding of beams/columns| BJ: yielding of beams prior to joint shear failure

Shafaei et al., (2014) Spec 2

Joint shear failure observed prior to the beams and the columns reaching their ultimate capacity. Analysis is terminated prior to loss of axial load carrying capacity of the joint.

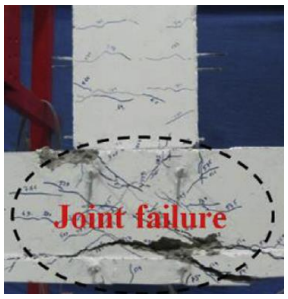

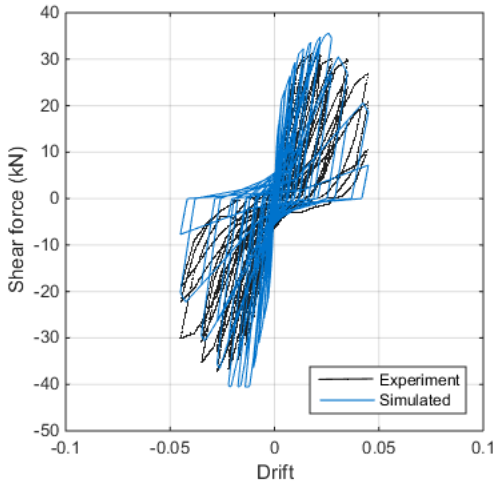

Shafaei et al., (2014) Spec 3

Joint shear failure and anchorage failure of poorly anchored bottom beam bar is observed. Analysis is terminated prior to loss of axial load carrying capacity of the joint.

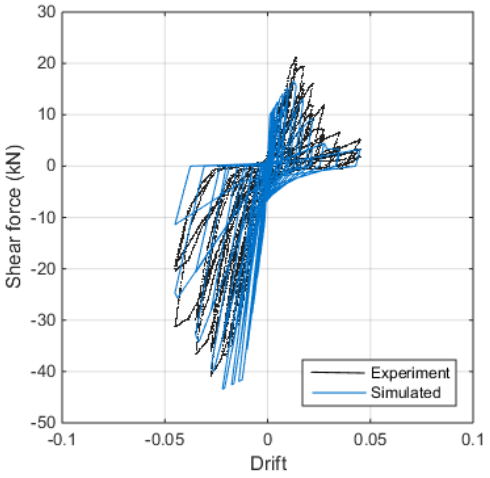

Pentalides et al., (2002) Unit 1

Joint shear failure and anchorage failure of poorly anchored bottom beam bar is observed. Loss of axial load carrying capacity of the joint is not reported.

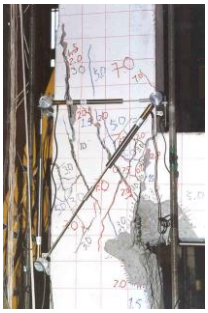

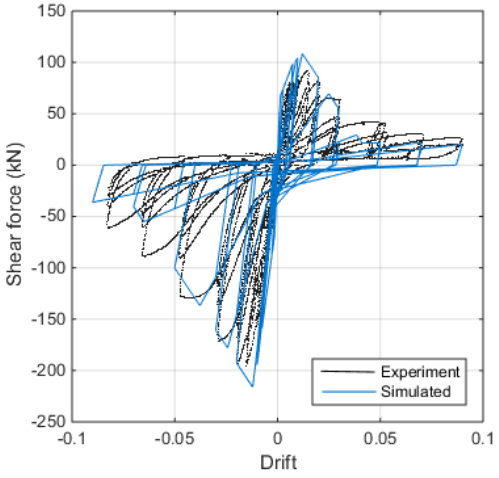

Figure 5-4 continued on next page

Pentalides et al., (2002) Unit 2

Joint shear failure and anchorage failure of poorly anchored bottom beam bars is observed. Loss of axial load carrying capacity of the joint is not reported.

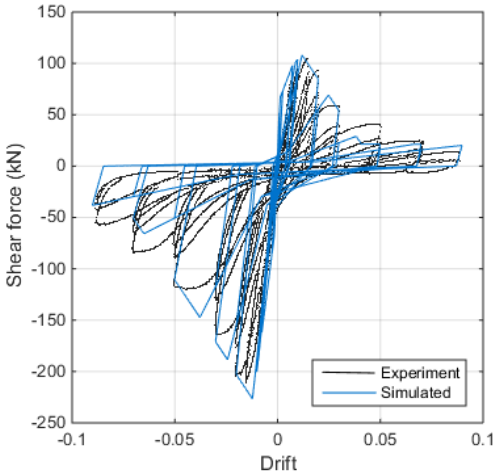

Pentalides et al., (2002) Unit 3

Joint shear failure is observed which eventually leads to axial load failure of the joint.

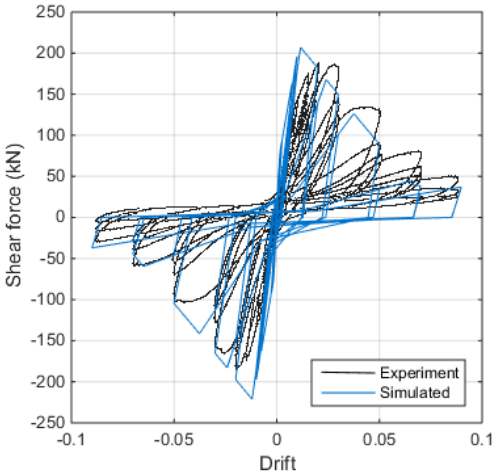

Pentalides et al., (2002) Unit 4

Joint shear failure is observed which eventually leads to axial load failure of the joint.

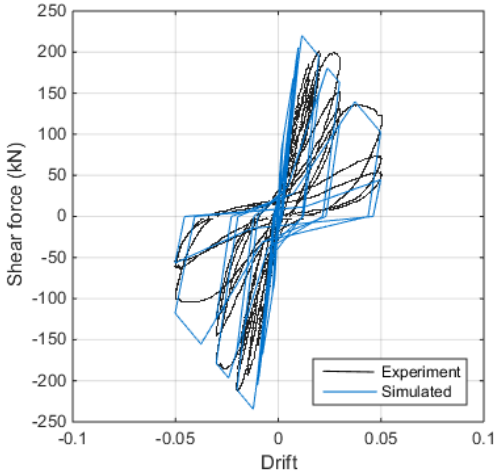

Figure 5-4 continued on next page

Megget (2003) Spec 5

Joint shear failure occurs prior to the beam reaching its yield capacity. Sudden strength degradation (approximately 50 % of peak strength) is observed under closing moment (i.e. when the adjacent top longitudinal beam bars are under tension). Axial load failure of the joint is not reported.

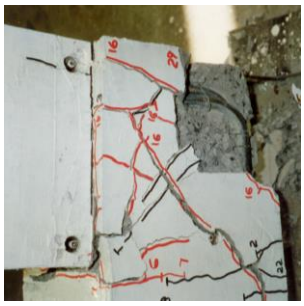

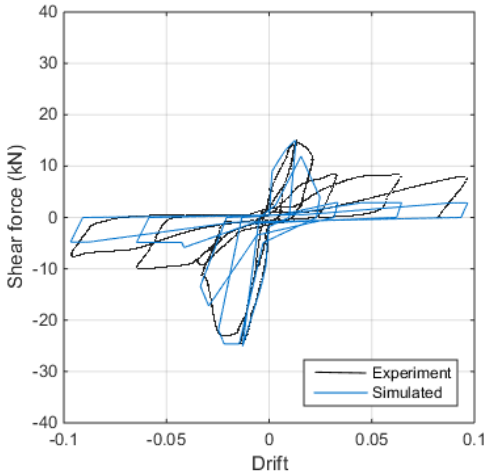

Megget (2003) Spec 8

Joint shear failure occurs prior to the beam reaching its yield capacity. Sudden strength degradation (approximately 50 % of peak strength) is observed under closing moment (i.e. when the adjacent top longitudinal beam bars are under tension). Axial load failure of the joint is not reported. A photograph of the joint damage is not provided, although, it is noted that the behaviour is very similar to Megget (2003) Spec 5 which have very similar detailing. Specimen 8 has deformed longitudinal bars whereas specimen 5 has plain longitudinal bars.

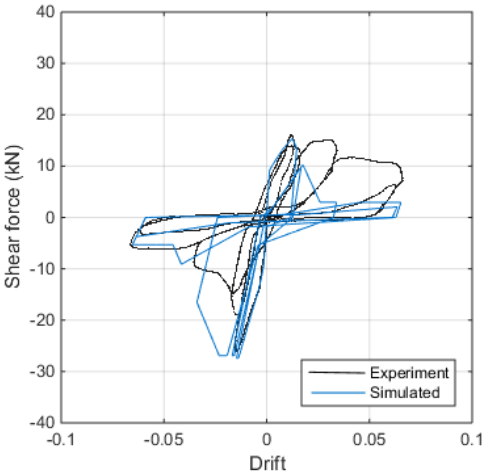

Hassan (2011) UJ1 (EW)

Joint shear failure is observed which eventually leads to axial load failure of the joint at high drift levels (around 9.7 %).

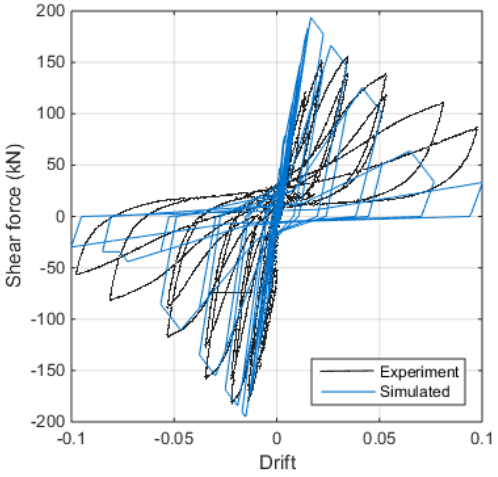

Figure 5-4 continued on next page

Hassan (2011) UJ2 (EW)

Joint shear failure is observed which eventually leads to sudden axial load failure of the joint at relatively low drift levels (around 3.0 %).

Instantly before axial failure

At axial failure

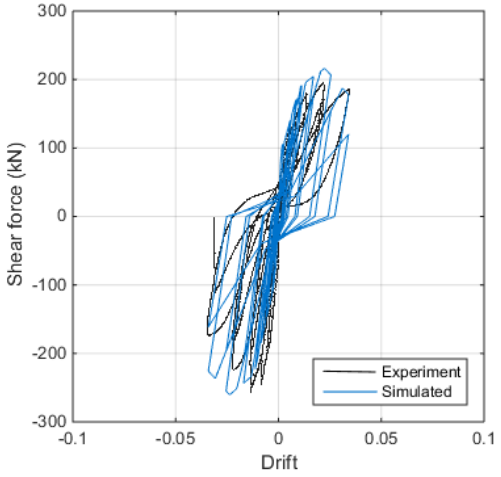

Pessiki et al., (1990) Spec 7

Predominant failure mode is due to bar pull-out of poorly anchored bottom longitudinal bars, and significant shear cracking in the joint region. Furthermore, significant damage to the columns is also reported.

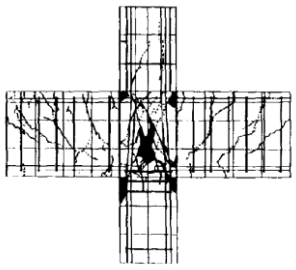

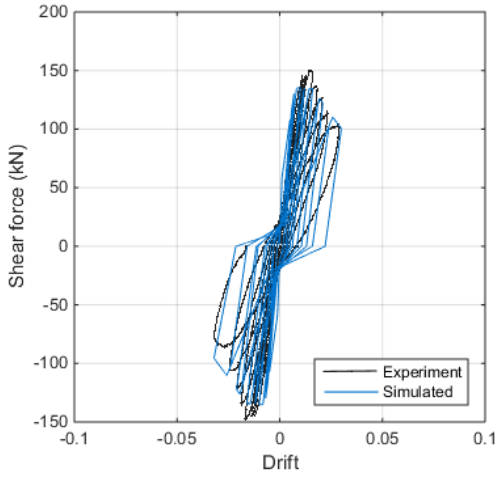

Pessiki et al., (1990) Spec 9

Significant shear cracking in the joint region occurred first followed by bar pull-out of poorly anchored bottom longitudinal bars. Furthermore, significant damage to the columns is also reported.

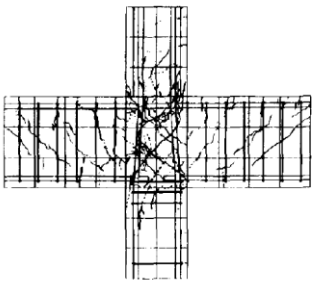

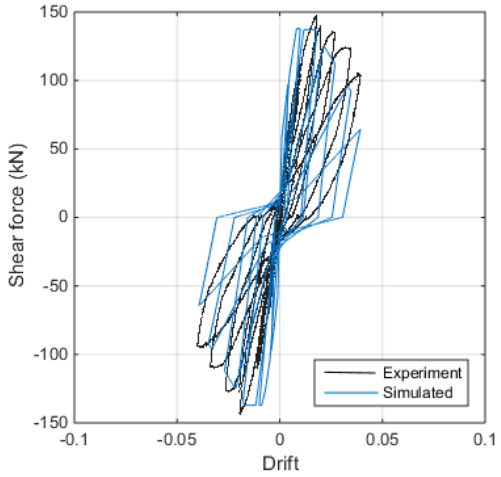

Figure 5-4: Comparison of simulated and experimental response of non-ductile joints with a brief description of the observed failure mechanism

5.4 MODELLING OF NON-DUCTILE COLUMNS AND BEAMS

The following subsection describes and evaluates the various macro-modelling approaches for simulating the response of non-ductile columns and beams. The focus is primarily on accurately simulating the response of columns since they are particularly vulnerable components in non-ductile frames and their failure can lead to global collapse of buildings. However, the same modelling approach for columns can be adopted for the modelling of the beams.

5.4.1 Selection of deformation limits

As discussed in Section 4.5, the response of non-ductile columns requires the definition of deformation limits which are usually predicted by empirically based equations to determine the degrading response of columns after ultimate bending capacity is reached. The validity of the three models presented in Section 4.5 is examined in this section to determine whether they are suitable for use in this study. The three models include:

- Model 1: Elwood and Moehle (2003)
- Model 2: LeBorgne (2012), LeBorgne and Ghannoum (2014)
- Model 3: Wibowo, Wilson, Lam, and Gad (2014), Wilson, Lam, and Gad (2015)

A database of 20 columns (details provided in Table 5-9), for which experimental results are available in the literature, was compiled in order to compare the critical experimental parameters with parameters calculated using the empirically based models. The columns included in the database are representative of existing RC columns in Australia. The purpose of comparing the models with a database compiled by the author was to reduce bias and to examine the applicability of the three models for columns with various detailing and loading conditions. Furthermore, it is noted that the failure mechanism of some of the columns included in the database is governed by the flexural mechanism in order to examine the applicability of the deformation limits not only for flexure-shear (FS) governed columns but also flexure (F) governed columns. As noted previously, the critical parameters in each model are in various forms and not directly comparable. Hence, suitable calculations are performed to change the parameters so that they are directly comparable, the following changes were made:

- The limit on rotation across the plastic hinge region (θ_f) in Model 2 was changed to interstorey drift limit by adding the yield deformation component (where the yield curvature was calculated using sectional analysis) to the plastic deformation.

- The axial drift limit in Model 3 ($\delta_{a\,50\%}$) was extended using linear interpolation to the point at which the shear capacity had dropped to zero (i.e. δ_a) so that it was easily comparable with Model 1 and experimental data.
- It was not possible to change δ_r of Model 2 to δ_a, thus the drift at axial failure of Model 2 cannot be directly compared with the other models.

A summary of the predicted and experimental drift ratios is provided in Table 5-10. The drift at shear failure for Model 1 and 3, and the ultimate drift for Model 2, are compared with experimental drift at ultimate strength in Figure 5-5. The experimental drift at 80 % of the peak strength was not compared since this was not provided in all of the studies. Note that it is expected that Model 1 and Model 3 will overestimate the drift in comparison with the experimental result, since the predicted drift at shear failure for these models is at 80 % of peak strength rather than at ultimate drift. However, this is not observed for Model 3 which actually tends to under-estimate the drift.

The calculated drifts at axial load failure (δ_a), for Models 1 and 3, are compared with experimental drifts at axial load failure in Figure 5-6. It is observed that Model 1 provides a very good match with experimental results, whereas Model 3 tends to overestimate the drift. It is important to note that the overestimation observed when using Model 3 may be due to the adoption in this study of δ_a as the drift at axial load failure rather than $\delta_{a\,50\%}$ which was used by Wibowo et al. (2014) when comparing their model to experimental results. Also it is observed that Model 3 does not match well with the experimental results at very low axial loads; see Table 5-10 for drift predictions for specimen U1 from Saatcioglu and Ozcebe (1989) which was not included in Figure 5-5 and Figure 5-6. It is not possible to directly compare Model 2 with experimental results in Figure 5-6**;** however, based on the results shown in Table 5-10, it can be seen that the prediction for δ_r tends to be significantly higher than δ_a for some columns, suggesting that the model significantly over-predicts the drifts at axial load failure. Based on the comparison made with the experimental results compiled in this study, Model 1 tends to provide the best estimate of the critical parameters. Therefore Model 1 is adopted in this study to define the deformation limits corresponding to shear failure and axial load failure.

Table 5-9: Detail of columns included in the database for this study

No.	Specimen	Failure type	ALR	h_c (mm)	b_c (mm)	L (mm)	a	f_c' (MPa)	Longitudinal reinforcement				Transverse reinforcement		
									ρ_l	f_y (MPa)	f_u (MPa)	Type	ρ_t	f_{yt} (MPa)	s (mm)
1	Sezen (2002) Spec 1	FS	0.15	457.2	457.2	2946.4	3.2	21.1	0.0250	434	645	C	0.0020	434	305
2	Sezen (2002) Spec 2	FS	0.60	457.2	457.2	2946.4	3.2	21.1	0.0250	434	645	C	0.0020	434	305
3	Sezen (2002) Spec 3	FS	0.25*	457.2	457.2	2946.4	3.2	20.9	0.0250	434	645	C	0.0020	434	305
4	Sezen (2002) Spec 4	FS	0.15	457.2	457.2	2946.4	3.2	21.8	0.0250	434	645	C	0.0020	434	305
5	Lynn et al. (1996) 3CLH18	FS/S	0.09	457.2	457.2	2946.4	3.2	25.6	0.0304	331	496	C	0.0007	400	457
6	Lynn et al. (1996) 2CLH18	FS/ F	0.07	457.2	457.2	2946.4	3.2	33.1	0.0194	331	496	C	0.0007	400	457
7	Lynn et al. (1996) 3SLH18	FS	0.09	457.2	457.2	2946.4	3.2	25.6	0.0194	331	496	S	0.0007	400	457
8	Lynn et al. (1996) 2SLH18	FS/F	0.07	457.2	457.2	2946.4	3.2	33.1	0.0194	331	496	S	0.0007	400	457
9	Lynn et al. (1996) 2CMH18	FS	0.28	457.2	457.2	2946.4	3.2	25.5	0.0194	331	496	C	0.0007	400	457
10	Lynn et al. (1996) 3CMH18	FS/S	0.26	457.2	457.2	2946.4	3.2	27.6	0.0304	331	496	C	0.0007	400	457
11	Lynn et al. (1996) 3CMD12	FS	0.26	457.2	457.2	2946.4	3.2	27.6	0.0304	331	496	C	0.0017	400	304
12	Lynn et al. (1996) 3SMD12	FS	0.28	457.2	457.2	2946.4	3.2	25.5	0.0304	331	496	S	0.0017	400	304
13	Ho and Pam (2004) 1A	F	0.13	325	325	3155.0	4.7	70.0	0.0086	531	648	C	0.0018	357	175
14	Ho and Pam (2004) 2A	F	0.33	325	325	3155.0	4.7	80.0	0.0238	522	663	C	0.0031	357	100
15	Fardipour (2012) Spec 1	F	0.20	300	270	2400.0	4.0	20.3	0.0056	527	NA	C	0.0007	365	300
16	Fardipour (2012) Spec 2	FS	0.20	300	270	2400.0	4.0	21.0	0.0100	515	NA	C	0.0007	365	300
17	Fardipour (2012) Spec 3	FS	0.40	300	270	2400.0	4.0	18.4	0.0100	515	NA	C	0.0007	365	300
18	Fardipour (2012) Spec 4	FS	0.40	300	270	2400.0	4.0	24.2	0.0056	527	NA	C	0.0007	365	300
19	Saatcioglu and Ozcebe (1989) U1	FS/F	0.0	350	350	2000.0	2.9	43.6	0.0320	430	NA	C	0.0030	470	150
20	Saatcioglu and Ozcebe (1989) U2	FS	0.16	350	350	2000.0	2.9	30.2	0.0320	453	NA	C	0.0030	470	150

L: double curvature column height | a: shear span to column depth ratio | * initial ALR, axial load varied during lateral loading | C: continuous bars | S: spliced bars

Table 5-10: Experimental and calculated drift ratios using the three models

Specimen	Experiment		Model 1		Model 2			Model 3		
	δ_u	δ_a	δ_s	δ_a	δ_s	$\delta_{a\ 50\%}$	δ_a	θ_f	δ_u	δ_r
Sezen (2002) Spec 1	0.019	0.050	0.025	0.055	0.016	0.034	0.060	0.014	0.015	0.237
Sezen (2002) Spec 2	0.009	0.019	0.013	0.022	0.011	0.018	0.032	0.006	0.006	0.237
Sezen (2002) Spec 3	0.009	0.029	0.022	0.042	0.011	0.018	0.032	0.006	0.006	0.237
Sezen (2002) Spec 4	0.021	0.055	0.025	0.055	0.016	0.034	0.060	0.014	0.015	0.237
Lynn et al. (1996) 3CLH18	0.010	0.021	0.025	0.035	0.018	0.034	0.064	0.012	0.013	0.270
Lynn et al. (1996) 2CLH18	0.026	0.031	0.025	0.035	0.018	0.046	0.088	0.013	0.014	0.224
Lynn et al. (1996) 3SLH18	0.010	0.036	0.025	0.035	0.018	0.034	0.064	0.012	0.013	0.270
Lynn et al. (1996) 2SLH18	0.021	0.036	0.025	0.035	0.018	0.046	0.088	0.013	0.014	0.224
Lynn et al. (1996) 2CMH18	0.010	0.010	0.018	0.014	0.009	0.013	0.019	0.006	0.006	0.230
Lynn et al. (1996) 3CMH18	0.010	0.021	0.019	0.015	0.009	0.013	0.021	0.007	0.007	0.268
Lynn et al. (1996) 3CMD12	0.016	0.023	0.021	0.029	0.013	0.023	0.040	0.010	0.011	0.247
Lynn et al. (1996) 3SMD12	0.016	0.021	0.020	0.029	0.012	0.021	0.037	0.010	0.010	0.255
Ho and Pam (2004) 1A	0.018	0.050	0.030	0.023	0.023	0.047	0.086	0.017	0.020	0.215
Ho and Pam (2004) 2A	0.014	0.025	0.027	0.015	0.016	0.028	0.047	0.013	0.016	0.174
Fardipour (2012) Spec 1	0.017	0.050	0.024	0.021	0.020	0.035	0.062	0.009	0.011	0.046
Fardipour (2012) Spec 2	0.017	0.025	0.022	0.021	0.017	0.027	0.045	0.009	0.011	0.021
Fardipour (2012) Spec 3	0.011	0.015	0.016	0.013	0.007	0.010	0.015	0.006	0.008	0.005
Fardipour (2012) Spec 4	0.010	0.015	0.017	0.010	0.006	0.010	0.016	0.006	0.008	0.069
Saatcioglu and Ozcebe (1989) U1	0.046	0.085	0.033	0.104	4.29	10.71	21.42	0.022	0.0219	0.217
Saatcioglu and Ozcebe (1989) U2	0.032	0.057	0.026	0.055	0.020	0.038	0.068	0.017	0.017	0.235

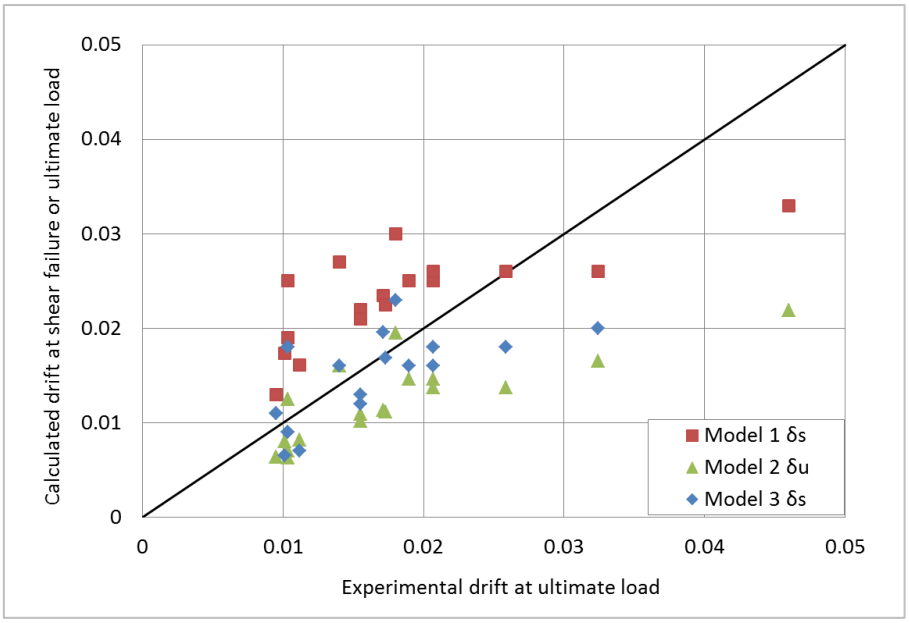

Figure 5-5: Comparison of drift at ultimate strength or at shear failure

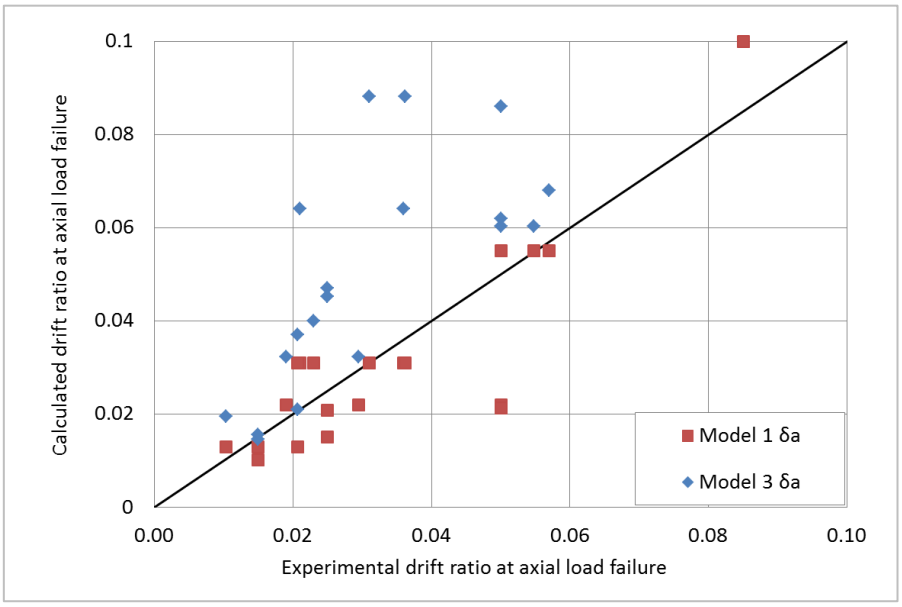

Figure 5-6: Comparison of drift at axial load failure

5.4.2 Distributed plasticity approach

Initially the state-of-the-art approach of using distributed plasticity elements in conjunction with limit state materials for modelling the shear degradation of columns is examined to model the response of non-ductile columns. The element configuration recommended in LeBorgne (2012) is adopted, which includes explicit modelling of the flexural, bar-slip and shear response as presented in Figure 5-7. The plastic hinge region is modelled with a force-based distributed plasticity element with a length equal to the depth of the column (h_c) and with two integration points. This is done to restrict the

plastic rotations to the end of the columns and to allow the monitoring of the rotation within the hinge region. The remaining portion of the column (i.e. $L - 2h_c$) is modelled with a single force-based distributed plasticity element with four integration points. It is noted that the fibre-sections are defined using material models discussed in Section 5.2. The shear response is modelled with a single shear spring at each end of the column and the behaviour is defined using the *Pinching Limit State Material* model. The deformation limit states are calculated using Model 1 (Elwood and Moehle, 2003) with suitable calculations to convert the interstorey drift limits to rotational limits within the plastic hinge region. Furthermore, bar-slip is modelled by using a zero-length fibre-section at each end of the column.

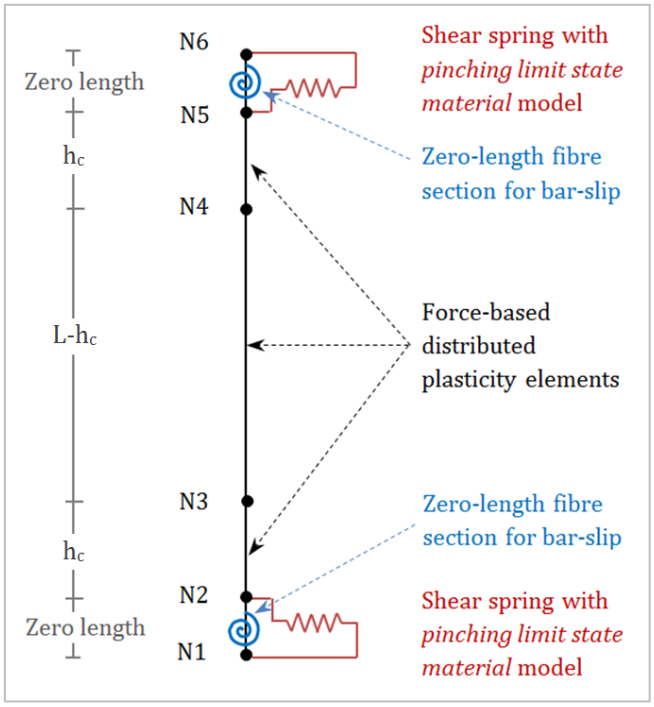

Figure 5-7: State-of-the-art column element modelling technique for distributed plasticity approach

To examine the validity of the state-of-the-art modelling approach, simulated results are compared with experimental results for four full-scale columns for which testing were conducted until axial load failure. All of the four columns were reported to exhibit a flexure-shear failure mechanism. A comparison of the experimental results and the simulated results is shown in Figure 5-8. The blue broken line illustrates the response obtained using the state-of-the-art modelling technique. The red line represents the monotonic response obtained if only the flexural behaviour of the column is considered. In addition, critical flexural response points have also been indicated on the simulated results in Figure 5-8, including:

i. Initial yielding of longitudinal reinforcement bars
ii. Initiation of spalling (i.e. when the extreme compressive concrete fibre strain reaches 0.003)
iii. Buckling of longitudinal bars, approximated by the buckling strain suggested by Moyer and Kowalsky (2003):

$$\varepsilon_{sb} = 3\left(\frac{Ks}{d_b}\right)^{-2.5} \quad \text{Eq. 5-2}$$

Where K is the effective length factor which may be taken as 1.0

It is observed that the simulated results match well with experimental results. The importance of incorporating the shear spring is evident for columns with lower axial loads such as Sezen (2002) Spec 1 and Lynn et al. (1996) 2CLH18, since the sudden strength and stiffness degradation would have not been simulated with the distributed plasticity elements. For columns with higher axial loads such as Sezen (2002) Spec 2 and Lynn et al. (1996) 2CMH18, it can be seen that the drift at which buckling of bars is expected according to Eq. 5-2 approximately corresponds to when instability in the model is observed, as illustrated by the sudden drop in the shear force. The instability in the model is due to the fact that when the deformation limit is reached, the degrading slope of the shear spring is very steep since the drift at shear and axial load failure are similar. In fact for Lynn et al. (1996) 2CMH18 the predicted drift at axial failure is lower than the drift at shear failure, and thus the column suddenly loses its ability to resist lateral and gravity loading (as observed during the experiment as well).

Even though it was possible to simulate the experimental results well for the four columns shown in Figure 5-8, just a slight change in a parameter, for example a material property, for the same columns often led to numerical instability issues. One potential reason for this may be due to the multiple solutions which are possible for the limit state material model when flexural degradation occurs prior to the deformation limit at which shear strength degradation initiates (described in Section 4.5). Due to the computational and numerical issues associated with the distributed plasticity approach the lumped plasticity approach is investigated; the findings are presented in the next section.

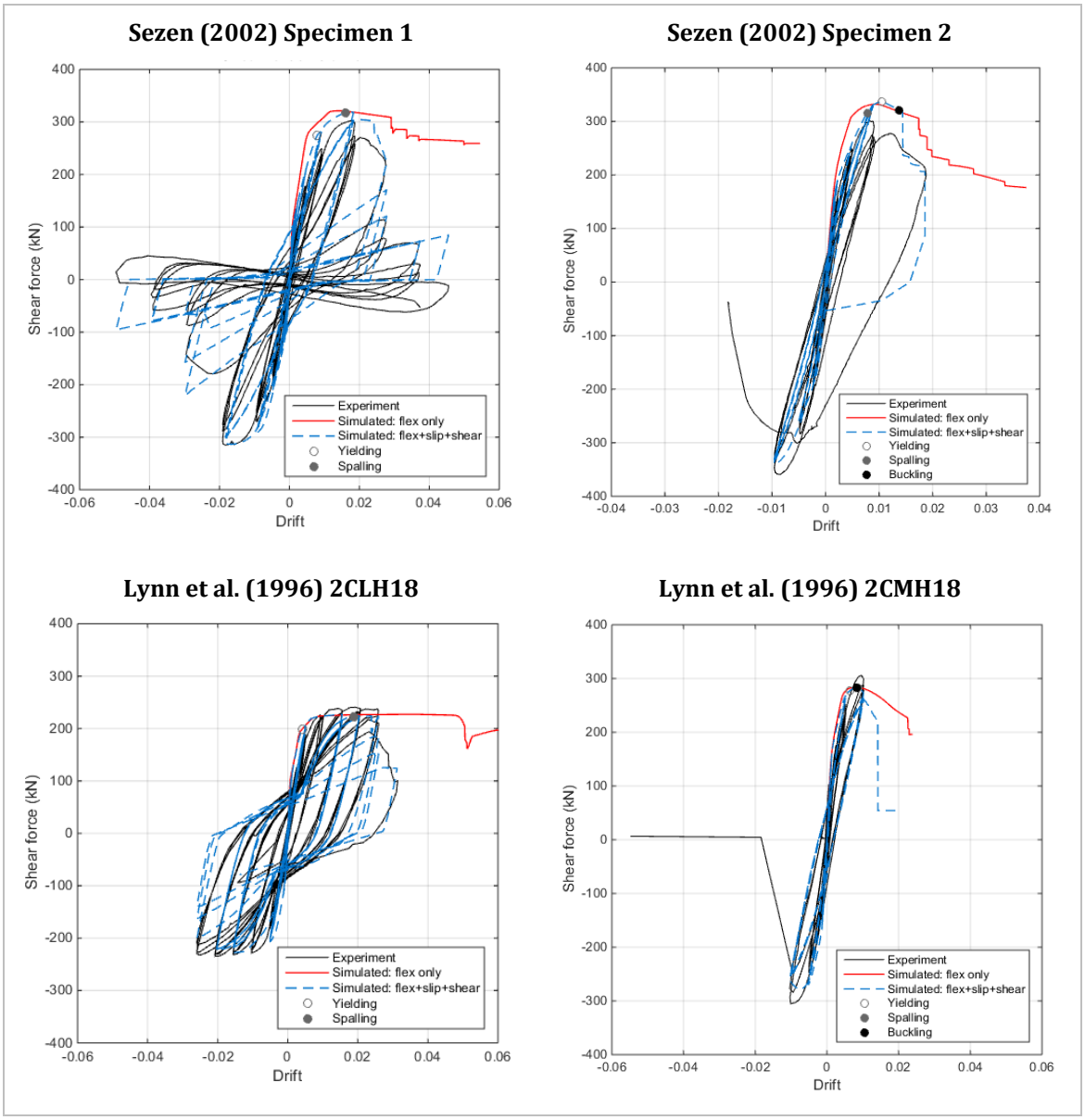

Figure 5-8: Comparison between simulated and experimental shear force versus drift response of columns

5.4.3 Lumped plasticity approach

The following section describes the lumped plasticity approach used to model the response of flexure-shear critical members. The suggested element configuration is provided in Figure 5-9. The method involves incorporating the inelastic flexural response, bar-slip, and shear response into a zero length moment-rotation spring located at each end of the column. The following subsection describes the key steps required in defining the envelope load-deformation response and hysteretic behaviour of the spring. The discussion is mainly with respect to columns; however, the same modelling approach is also appropriate for beams.

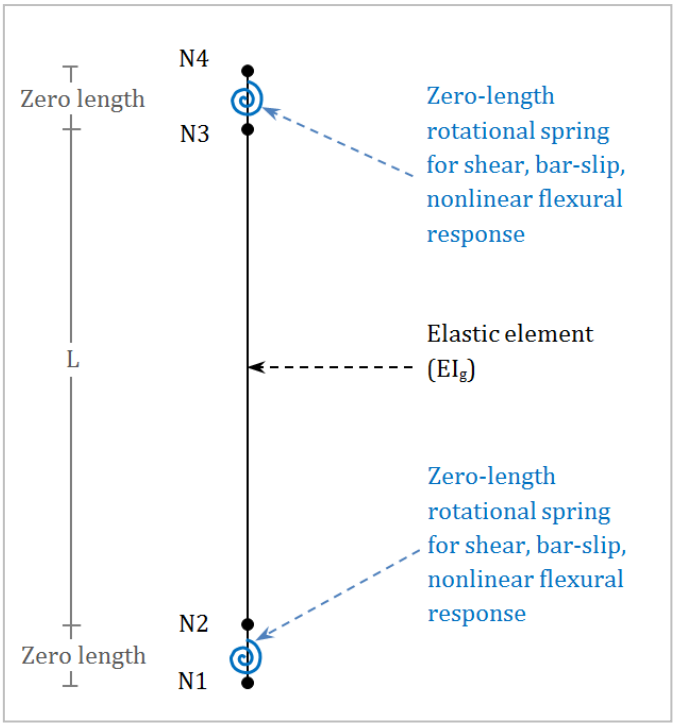

Figure 5-9: Proposed column element configuration for lumped plasticity approach

5.4.3.1 Load deformation response

Hysteretic models available in OpenSEES have a maximum of four critical points which can define the envelope response. Therefore the envelope response of columns and beams is to be idealised by using four critical points: (i) initiation of cracking, (ii) nominal yield, (iii) ultimate capacity and initiation of lateral strength degradation, and (iv) axial load failure. This is illustrated in Figure 5-10, where Figure 5-10(a) represents the global response of a column, and Figure 5-10(b) illustrates the backbone definition required for each of the zero length springs in Figure 5-9. It is noted that since a single rotational spring is located at each end of the column, the definition of the backbone for each spring is obtained by considering half the column height of the double curvature column (i.e. the shear span, a). The definition of the critical points and the hysteretic behaviour is discussed in the following subsections.

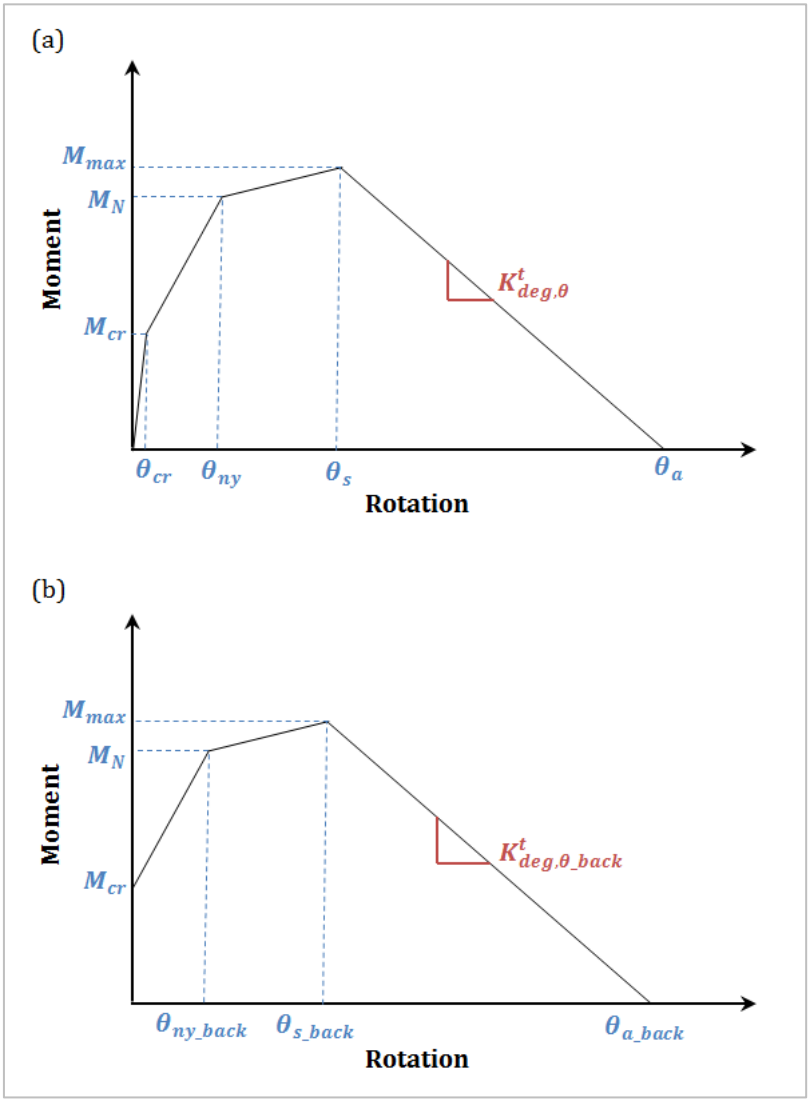

Figure 5-10: Idealised moment-rotation response of columns: (a) Global response, (b) Proposed backbone response for zero length springs

5.4.3.1.1 Cracking

The cracking moment (M_{cr}) is obtained from sectional analysis as described previously in Section 5.2. The rotation for the backbone response of the spring is set to zero since the rotation will be achieved by the elastic beam-column element since the springs and the elastic beam-column element are positioned in series.

5.4.3.1.2 Nominal yield

The nominal yield bending capacity (M_N) and curvature (ϕ_{ny}) are obtained from sectional analysis as described previously in Section 5.2.

The flexural displacement corresponding to the nominal yield may be calculated according to Eq. 5-3, which corresponds to the first moment of area of the curvature profile assuming a linear profile.

$$\Delta_{flex} = \frac{a^2}{3}\phi_{ny} \quad \text{Eq. 5-3}$$

To improve the prediction of the flexural displacement at yield, the first moment of area of the curvature profile is calculated by accounting for the change in the linear profile from cracking curvature to nominal yield curvature and the fixed end of the column.

The slip displacement is calculated according to Elwood and Moehle (2003) discussed in Section 4.4 and is provided again in Eq. 5-4.

$$\Delta_{slip} = \frac{a f_y d_b \phi_{ny}}{8 u_e} \quad \text{Eq. 5-4}$$

The shear displacement is calculated using Eq. 5-5.

$$\Delta_{shear} = \frac{M_N}{\frac{5}{6} G A_g} \quad \text{Eq. 5-5}$$

Hence, the rotation at nominal yield required to define the moment-rotation backbone is given by Eq. 5-6.

$$\theta_{ny\_back} = \left(\frac{\Delta_{flex} + \Delta_{slip} + \Delta_{shear}}{a}\right) - \left(\frac{M_N}{E I_g} \times \frac{a}{3}\right) \quad \text{Eq. 5-6}$$

Where E is the elastic modulus of concrete

I_g is the gross second moment of area of the column (or beam)

5.4.3.1.3 Ultimate capacity and drift at shear failure

The ultimate bending capacity (M_u) is obtained from sectional analysis as described previously in Section 5.2. In addition, the moment corresponding to the ultimate shear capacity (V_u) of the column is also calculated. The maximum moment for the backbone (M_{max}) is defined as the smaller of M_u or $V_u \times a$. The ultimate shear capacity is calculated according to Sezen and Moehle (2004):

$$V_u = V_{uc} + V_{us} \quad \text{Eq. 5-7}$$

Where V_{uc} is the concrete contribution to shear strength calculated according to Eq. 5-8

V_{us} is the transverse reinforcement contribution to shear strength calculated according to Eq. 5-9

$$V_{uc} = \frac{0.5\sqrt{f_c'}}{a/d}\sqrt{1+\frac{P}{0.5\sqrt{f_c'}A_g}}0.8A_g \quad \text{Eq. 5-8}$$

$$V_{uc} = \frac{A_{sv}f_{yt}d}{s} \quad \text{Eq. 5-9}$$

The corresponding drift at which M_{max} occurs is defined as the drift at which shear failure occurs since the hysteretic model in OpenSEES is limited to a maximum of four critical points. The drift at shear failure is defined according to Model 1, Elwood and Moehle (2003) provided in Section 4.5 and is provided again for convenience in Eq. 5-10.

$$\delta_s = \frac{3}{100} + 4\rho_t - \frac{1}{40}\frac{v}{\sqrt{f_c'}} - \frac{1}{40}\frac{P}{A_g f_c'} \geq \frac{1}{100} \quad \text{Eq. 5-10}$$

Hence, the rotation at shear failure required to define the moment-rotation backbone for the spring is given by Eq. 5-11.

$$\theta_{s\_back} = \delta_s - \left(\frac{M_{max}}{EI_g} \times \frac{a}{3}\right) \quad \text{Eq. 5-11}$$

5.4.3.1.4 Drift at axial load failure

The bending capacity at axial load failure is set to zero.

The drift at axial load failure is calculated according to Model 1, Elwood and Moehle (2003) provided in Section 4.5 and is provided again in Eq. 5-12.

$$\delta_a = \frac{4}{100}\frac{1+(\tan\theta_{cr})^2}{\tan\theta + P\left(\frac{s}{A_{sv}f_{yt}d_{ct}\tan\theta_{cr}}\right)} \quad \text{Eq. 5-12}$$

The global degrading slope for half the double curvature column ($K^t_{deg,\theta}{}^*$) is then calculated:

$$K_{deg,\theta}^{t\ *} = \frac{V_{max}}{\delta_a a - \delta_s a} \quad \text{Eq. 5-13}$$

Where V_{max} is the smaller of $\frac{M_u}{a}$ and V_u

Then, the degrading slope for the rotation spring (K_{tdeg,θ_back}) may be calculated:

$$K_{deg,\theta\_back}^{t} = \left(\frac{1}{K_{deg,\theta}^{t\ *}} + \frac{1}{K_{el}}\right)^{-1} \quad \text{Eq. 5-14}$$

Where $K_{el} = \frac{3EI_g}{a^3}$

Hence, the displacement at axial load failure at mid-height of the double curvature column ($\Delta_a{}^*$) excluding the elastic deformation experienced by the beam-column element is:

$$\Delta_a{}^* = \frac{V_{max}}{K_{deg,\theta\_back}^{t}} + \theta_{s\_back} \times a \quad \text{Eq. 5-15}$$

Finally, the rotation at axial load failure for the rotational backbone for the spring may be calculated:

$$\theta_{a\_back} = \frac{\Delta_a{}^*}{a} \quad \text{Eq. 5-16}$$

It is noted that if the drift at shear failure is predicted to be higher than the drift at axial load failure (i.e. $\delta_s > \delta_a$) then the drift at shear failure is set to the drift at axial load failure.

5.4.3.1.5 Hysteretic behaviour

The main challenge of using a four point rather than a three point backbone envelope is the definition of the hysteretic parameters required for the *Pinching4* model in comparison to other hysteretic models which require significantly fewer parameters to define the hysteretic response. The parameters adopted to define the hysteretic behaviour of the columns and beams are based on the parameters used for the beam-column joints with minor changes to improve the match with experimental results. A summary of the parameters is provided in Table 5-11. The pinching parameters rForce and rDisp have been calibrated based on the database of columns considered in this study since it was observed that the values were dependent on the axial load ratio (ALR). Hence, Eq. 5-17 is suggested to calculate rForce and rDisp:

$$rForce = rDisp = 0.33378e^{-3.776ALR} \quad for\ ALR < 0.4 \qquad \text{Eq. 5-17}$$

$$rForce = rDisp = 0.1 \quad for\ ALR \geq 0.4$$

Table 5-11: Recommended Pinching4 parameters for the modelling of column and beam response

Pinching parameters	**rDispP**	**rForceP**	**uForceP**	**rDispN**	**rForceN**	**uForceN**
	Eq. 5-17	Eq. 5-17	0.0	Eq. 5-17	Eq. 5-17	0.0
Cyclic unloading stiffness degradation parameters	**gK1**	**gK2**	**gK3**	**gk5**	**gKlim**	
	0.95	1.0	0.1	0.0	0.95	
Cyclic reloading stiffness degradation parameters	**gD1**	**gD2**	**gD4**	**gD4**	**gDlim**	
	0.35	0.0	0.15	0.0	0.95	
Cyclic strength degradation parameters	**gF1**	**gF2**	**gF3**	**gF4**	**gFlim**	
	0.05	0.0	0.32	0.0	0.25	

5.4.3.2 Comparison between experimental and simulated results

Figure 5-11 compares the experimental and simulated column shear force versus drift response for 10 of the columns included in Table 5-9 with a brief description of the failure mechanism and a photograph of the specimen at the final stage of lateral loading. The simulated results are obtained using the proposed lumped plasticity modelling approach, and both the cyclic and monotonic envelope response is provided. The columns have been selected such that a wide range of axial load ratios are considered (varying from 7 to 60 %), since axial load ratio has been identified to be a critical parameter in determining the drift capacity of the columns, especially for calculating the drift at axial load failure. Furthermore, one of the columns included had varying axial load applied during the experiment (specimen 3 tested by Sezen (2002)). In general, the simulated results illustrate a good match with experimental testing. The first four columns provided in Figure 5-11 correspond to the same columns simulated in Section 5.4.2 using the distributed plasticity approach. It can be seen that the accuracy achieved (at a component level) using the lumped plasticity approach is acceptable and comparable with that achieved using the distributed plasticity approach. A good match is also observed between the simulated and experimental results for specimen 3 tested by Sezen (2002) for which the applied axial load to the column was varied between -250 kN and 2670 kN. The adopted lumped plasticity approach does not account for the change in axial load applied

and thus the simulated results for specimen 3 (Sezen, 2002) were obtained by applying the initial axial load of 1112 kN (corresponding to an axial load ratio of 0.25). Although there is a good match in this particular test, the inability of the lumped plasticity model adopted in this study to account for a variation in the axial force, may lead to inaccuracies when trying to model other test results in which the axial force varies. The remaining 10 columns in Table 5-9 have also been modelled using the lumped plasticity modelling approach and the results are given in Appendix C. For most of these columns a conservative response is simulated in comparison to the experimental results. The conservatism predominantly stems from the equations used to define the deformation limit at shear and axial load failure (discussed in Section 5.4.1) and therefore it is not dependent on the modelling approach (i.e. lumped plasticity or distributed plasticity approach).

In addition, as discussed in Section 4.3.1, the lumped plasticity approach ensures computational efficiency and, more importantly, numerical stability when compared with the distributed plasticity approach. In simulations carried out here using both approaches to model the response of the columns at a component level, and also to model the response at a system level when these approaches were adopted to create 2-dimensional building models (discussed further in Section 5.4.3.3), the same general trend was observed, that is, the lumped plasticity approach proved to be robust and reliable relative to the distributed plasticity approach. In particular, when using the distributed plasticity approach, it was not possible to obtain numerical stability for the system response after the shear deformation limit of the columns was reached. Numerical efficiency, reliability and stability are particularly important for the development of nonlinear building models for which analysis needs to be conducted up to the collapse limit state. Therefore, the lumped plasticity approach is adopted for the assessment of the archetypal buildings in Chapter 7.

Sezen (2002) Spec 1

The column was loaded with a medium axial load ratio of 15 %. The column failed in a flexure-shear manner. Initially flexural cracks were formed in the hinge regions, but with increased lateral deformation an inclined crack was formed at mid-height of the column. The opening of this crack led to the failure of the column. No buckling or fracturing bars was observed.

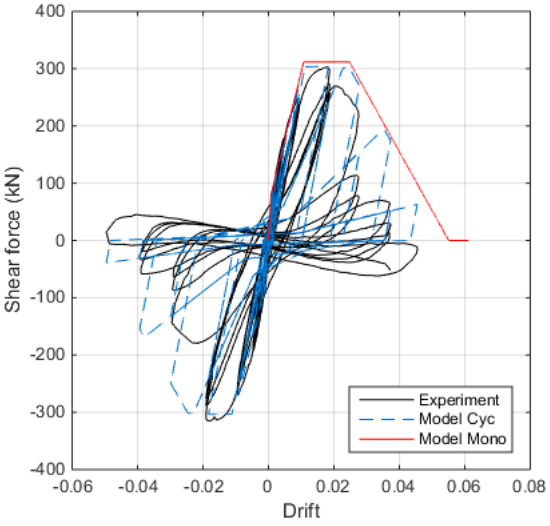

Sezen (2002) Spec 2

The column was loaded with a very high axial load ratio of 60 %. Initially flexural cracks formed in the hinge regions. Increase in lateral deformation caused a steep inclined crack to form within the upper part of the column which led to the opening of column ties and buckling of longitudinal bars, resulting in a sudden loss of lateral and axial load carrying capacity.

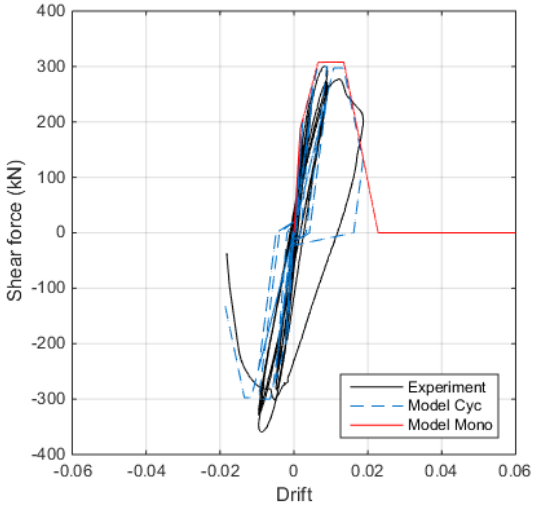

Lynn et al. (1996) 2CLH18

The column was load with relatively low axial load (ALR of 7 %). Significant flexural response was observed at the initial part of the lateral loading, however, based on the crack pattern towards the end of the loading the dominant failure mode reported was shear.

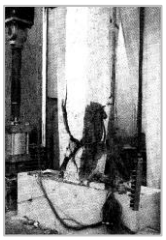

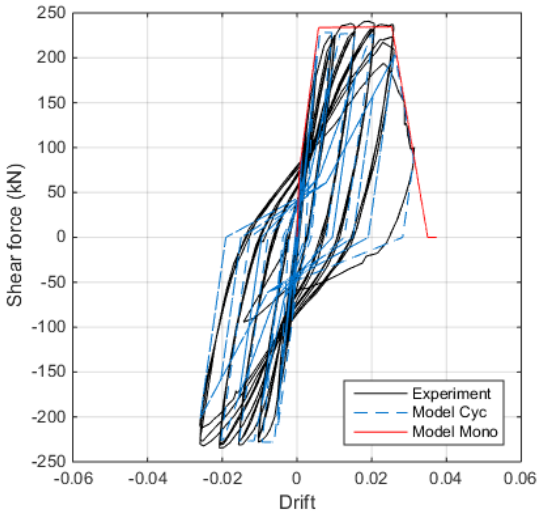

Figure 5-11 continued on next page

Lynn et al. (1996) 2CMH18

The column was loaded with a very high axial load ratio of approximately 30 %. Sudden loss of both lateral and axial load carrying capacity was observed after the yielding of longitudinal reinforcement bars.

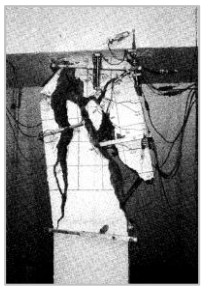

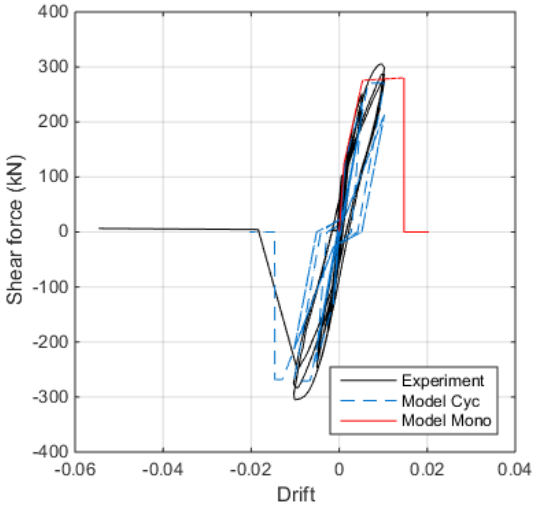

Lynn et al. (1996) 2SLH18

The column was loaded with a relatively low axial load ratio of 7 % with splices located at the bottom end of the column. Initially significant flexural response was observed, but with increasing lateral load, shear cracks formed just above splice region which eventually led to the failure of the column.

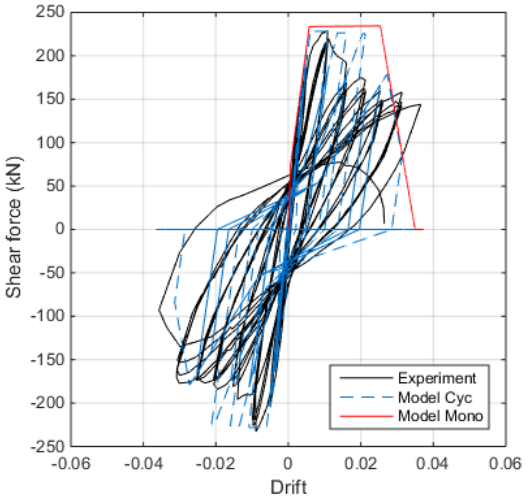

Sezen (2002) Spec 3

The column was initially loaded with an axial load ratio of 25 %, however the axial load applied varied during lateral loading. Crack formation was mainly near the top and bottom of the column. Inclined cracks formed with increasing lateral load and eventually the column failed due to buckling of bars and spalling of the concrete core.

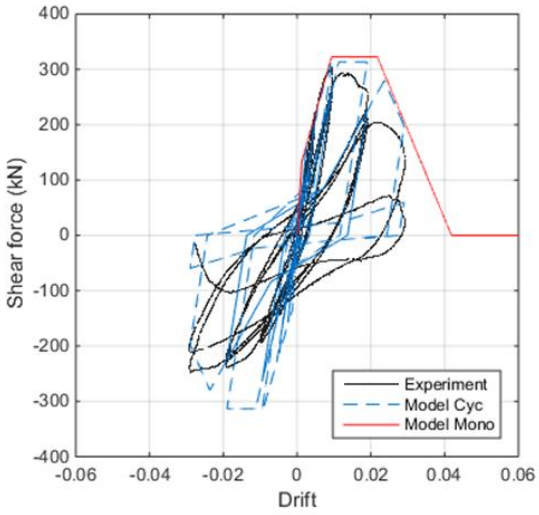

Figure 5-11 continued on next page

Sezen (2002) Spec 4

The column was loaded with a medium axial load ratio of 15 %. Cyclic loading was applied until yielding of longitudinal bars and then monotonic loading was applied until failure. Inclined cracks were observed near the top and bottom of the column during cyclic loading. Under monotonic loading, an inclined crack formed at the bottom and led to failure of the column including buckling of longitudinal bars and column tie failure.

Before axial load failure

After axial load failure

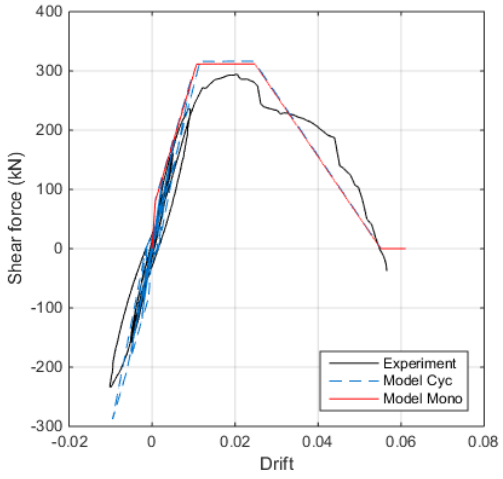

Lynn et al. (1996) 3CMD12

The column was loaded with an axial load ratio of 26 %. The longitudinal reinforcement ratio was relatively high at 3 % and improved column tie detailing was provided with a transverse reinforcement ratio of 0.17 %. Vertical cracks were observed during the loading indicating debonding of longitudinal bars. Ultimate failure of the column was due to an inclined crack which formed at the top of the column.

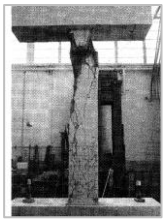

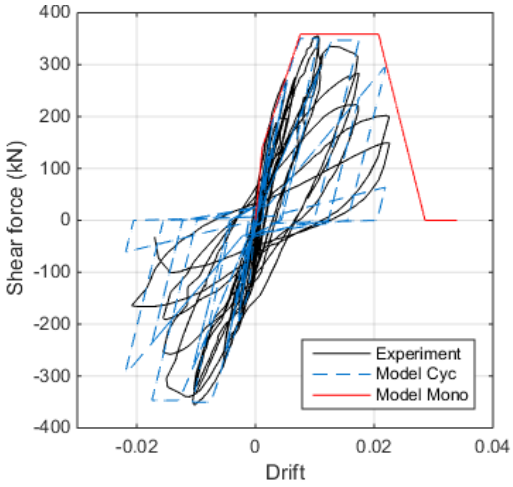

Saatcioglu and Ozcebe (1989) U1

No axial load was applied to the column, thus the behaviour of the column may be considered to be representative of beams. Both flexural and shear cracks were observed, and ultimate failure of the column was due to crushing of the concrete core. However loading was not applied up until axial load failure.

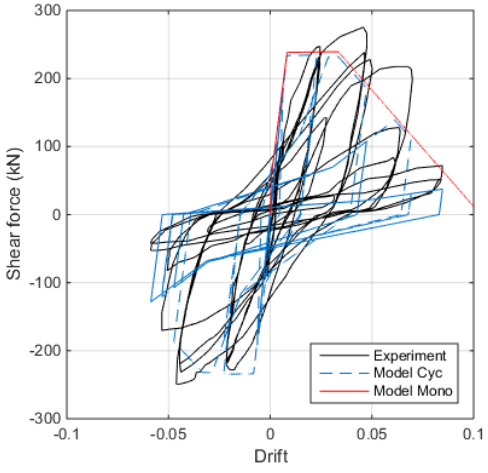

Figure 5-11 continued on next page

Saatcioglu and Ozcebe (1989) U1

The column was loaded with a medium axial load ratio of 16 %. Both flexural and shear cracks were observed, and ultimate failure of the column was due to disintegration of the concrete core. Loading was not applied up until axial load failure; however it was observed that the lateral load resistance approximately approached zero.

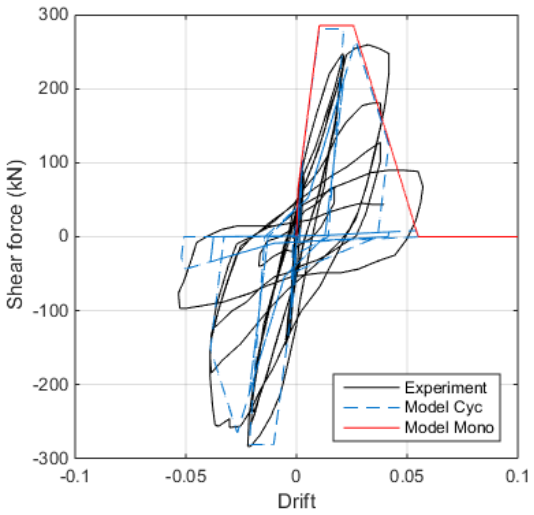

Figure 5-11: Comparison of simulated and experimental response of non-ductile columns with a brief description of the observed failure mechanism

5.4.3.3 Comparison between distributed and lumped plasticity approach

To provide a comparison of the effect on the global frame response of using the distributed and plasticity approaches for modelling column and beam members, a five storey RC frame is modelled using these approaches. The pushover analysis results are presented in Figure 5-12. The results for the distributed plasticity model have been obtained using the state-of-the-art approach described in Section 5.4.2, and it is assumed here that this approach provides a benchmark against which other results can be compared. Two modelling methods are adopted for the lumped plasticity approach. The first approach uses four points to define the moment-rotation backbone as described in Section 5.4.3.1. The second approach uses three points to define the moment-rotation backbone. The results from the approach of using three points to define the moment-rotation response are presented here since it is the usual approach adopted in other studies and codes that use the lumped plasticity approach to model frame components (ASCE/SEI, 2013; Haselton et al., 2016). The first point of the backbone is defined as the yield or nominal yield rather than cracking and therefore it results in a poor estimation of the initial stiffness of the frame. This is clearly seen in the results presented in Figure 5-12. The initial stiffness of the frame using the lumped plasticity approach matches much better to the distributed plasticity approach when four points rather than three are used to define the backbone response of the rotation spring elements. Furthermore, it is evident that the ultimate shear capacity of the frame is approximately the same using all three modelling approaches. However, the response varies between the lumped plasticity and distributed plasticity approaches in terms of the drift limits reached. The analysis conducted using the

distributed plasticity approach stops at approximately 2.5 % roof drift which corresponds to the point in the analysis for which the first column reaches the shear deformation limit. The model does not continue due to numerical convergence issues and this illustrates the limitations of using the distributed plasticity approach for the purpose of global collapse analysis of buildings. The comparison between the different modelling approaches confirms the suitability of using the lumped plasticity approach as defined in Section 5.4.3.1; hence this approach is to be adopted in this study for the assessment of the non-ductile frames.

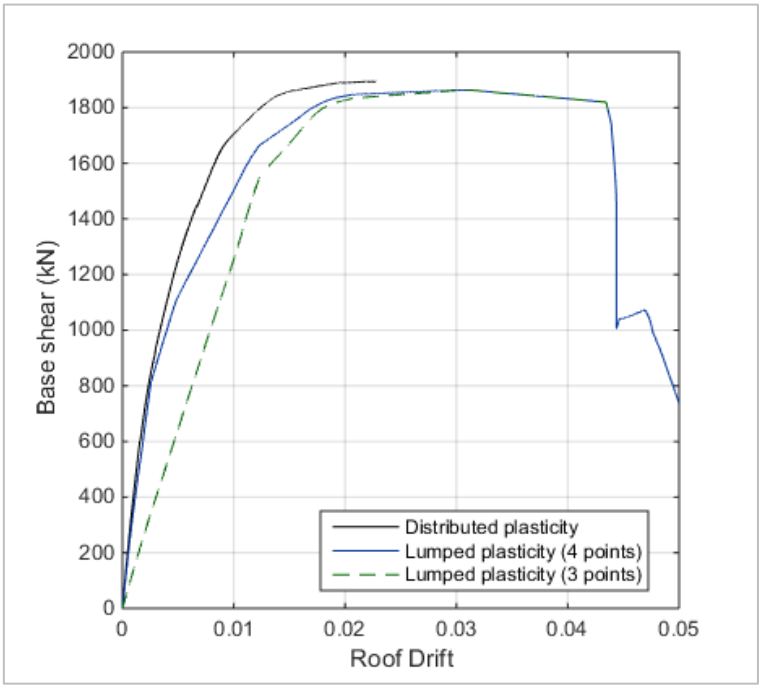

Figure 5-12: Pushover analysis of a 5-storey RC frame using different column modelling approaches

5.5 MODELLING OF NON-DUCTILE WALLS

The global analysis of RC walls which has been conducted in the literature has included walls with sufficient longitudinal reinforcement to cause distributed cracks to form in the plastic hinge region, and walls which typically have had a hardening response. Therefore, the failure of the walls has usually been determined during the post-processing phase of the analysis based on drift limits. This approach is suitable for walls (and in general buildings) which have ductile detailing because side-sway collapse is expected to occur prior to significant loss of lateral and axial load carrying capacity of the walls and the other building components. Hence, there are three key issues, which are predominantly associated with the response of non-ductile walls that have not been thoroughly addressed in the literature. Firstly, there are very few studies (Pugh et al., 2015; Scott &

Fenves, 2006) which have addressed the issue of localisation associated with distributed plasticity elements when a softening response is simulated. Secondly, there are minimal references which use strain limits (or curvatures) during the analysis to determine various performance limits (Fox et al., 2015), and these have not been explicitly validated with experimental results. The accurate simulation of strains is particularly important for the collapse modelling of buildings to ensure that the loss of lateral load carrying capacity (which may eventually lead to the loss of axial load carrying capacity) of the building is simulated at accurate deformations. Thirdly, there are no studies (to the knowledge of the author) in which global analysis has been conducted on structural systems that include lightly reinforced walls which form a single crack at the base with little secondary cracking when subjected to lateral loading.

To address the issues discussed above, the state-of-the-art modelling approaches using distributed plasticity elements are examined in the following subsections. Furthermore, due to the numerical instability issues related to distributed plasticity elements, in particular for modelling lightly reinforced non-ductile walls, the lumped plasticity approach is also investigated. Finally, the system response of interconnected walls is examined for the type of walls to be assessed in this study to determine which of the modelling methods is most suitable.

5.5.1 Distributed plasticity approach

5.5.1.1 Modelling of rectangular walls

To demonstrate the issues related to strain localisation and the dependency of the strains developed at the critical section on the number of integration points, simulated results are compared with experimental results for specimen WSH4 tested by Dazio et al. (2009) and specimen R1 tested by Oesterle et al. (1976), shown in Figure 5-13 and Figure 5-14, respectively. The response of each rectangular wall is modelled with a single force-based distributed plasticity element, using 3, 4, 5 and 7 integration points (IPs). The fibre-sections are defined using the approach discussed in Section 5.2. To illustrate the magnitude of the strains developed at the critical section, the following steel strain limits have also been plotted on the monotonic response of the walls:

- The compressive strain of the most extreme reinforcement reaching a value of 0.004, which, assuming perfect bond, coincides approximately with spalling of the cover concrete.
- The tensile strain of the most extreme reinforcement reaching 60 % of the reported ultimate tensile strain ($0.6\varepsilon_{su}$). The tensile strain limit is set to $0.6\varepsilon_{su}$ to

account for the reduction in ultimate strain capacity due to the effects of cyclic loading, including low-cycle fatigue (since buckling is not modelled), and tension shift effects as suggested by Priestley et al. (2007).

These strain limits provide an indication of when the ultimate capacity of the critical section has been reached, that is, the point prior to significant lateral strength degradation.

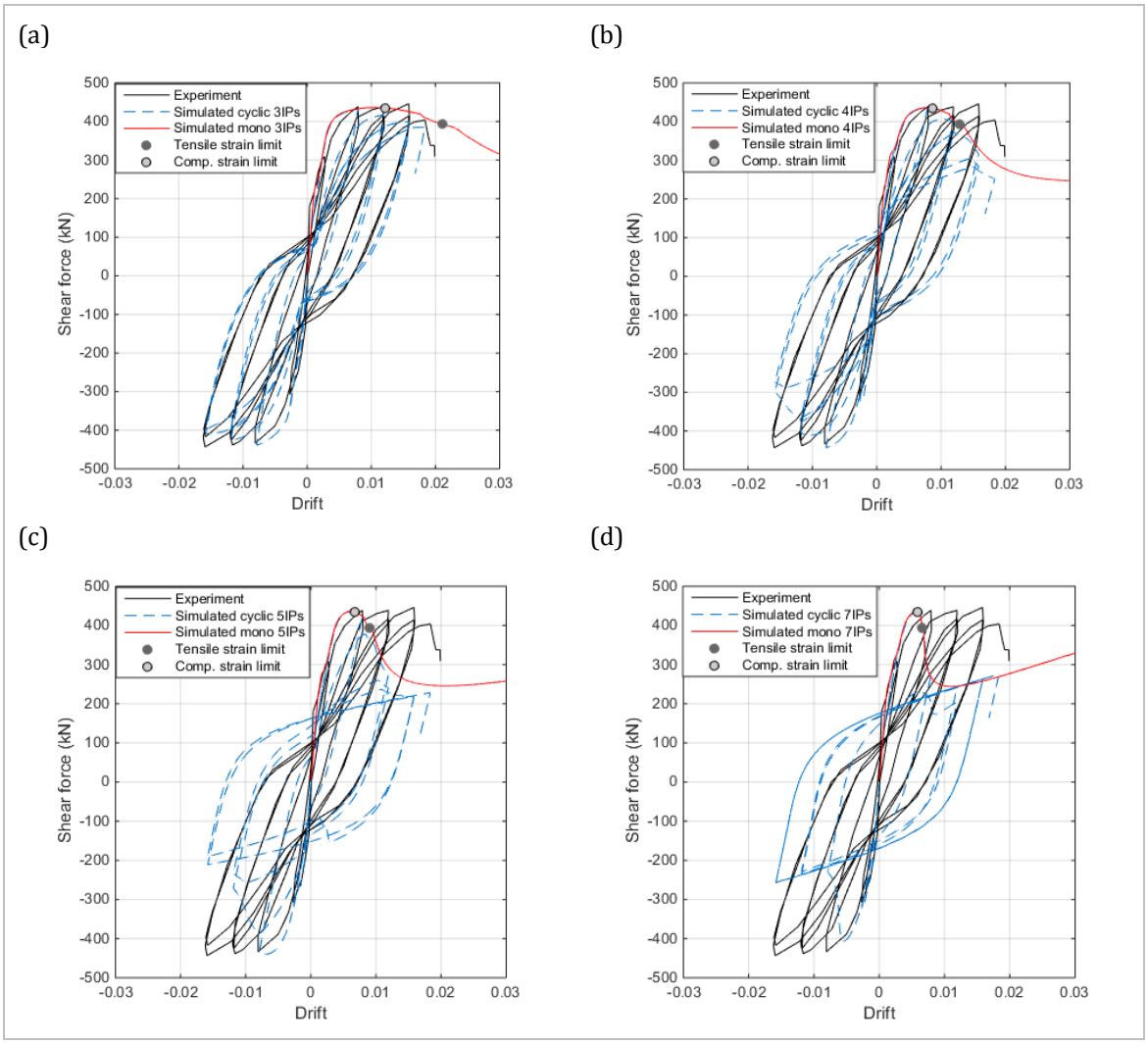

Figure 5-13: Simulation of softening wall response with different number of IPs: (a) 3 IPs, (b) 4 IPs, (c) 5 IPs, and (d) 7 IPs

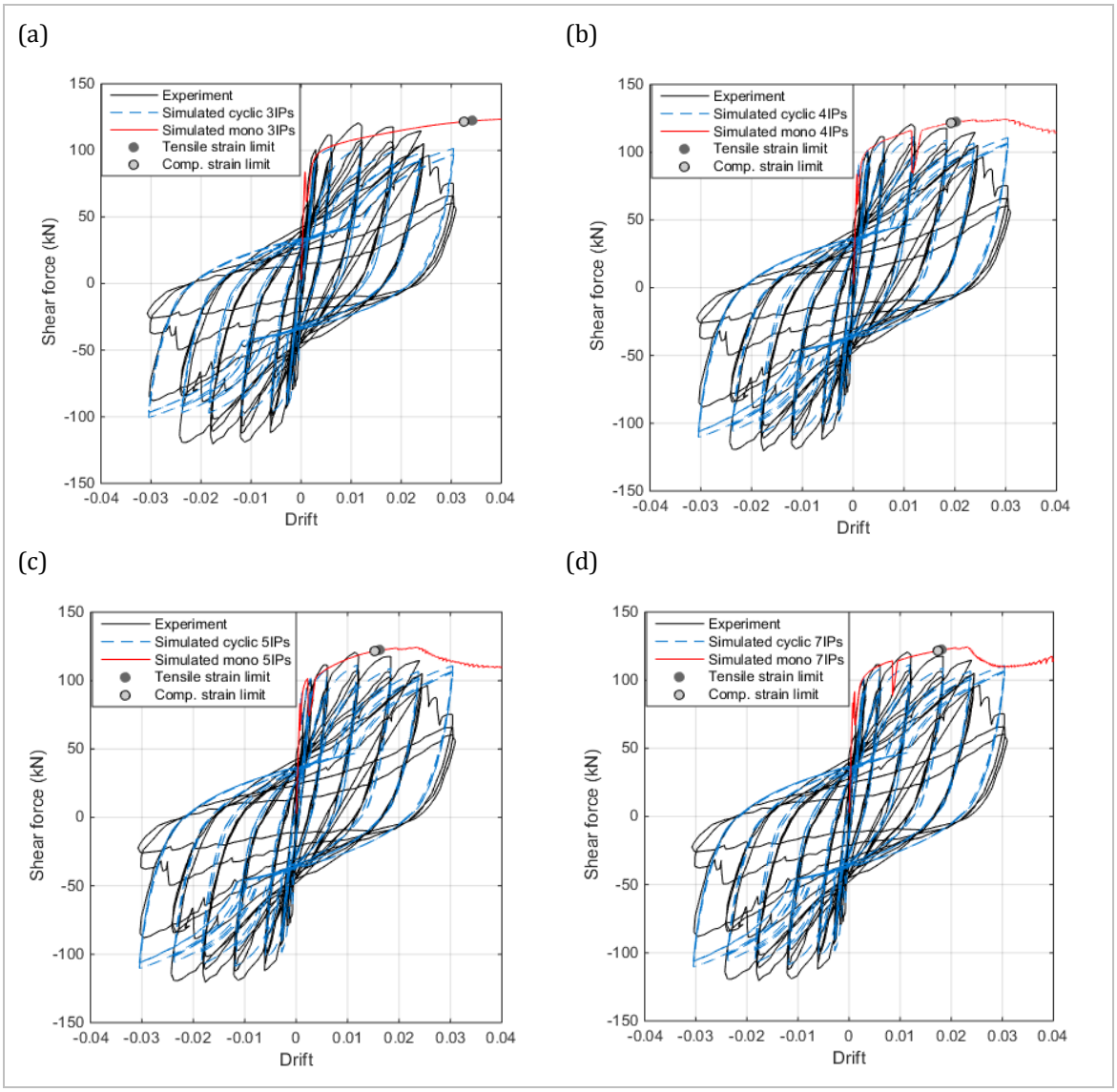

Figure 5-14: Simulation of hardening wall response with different number of IPs: (a) 3 IPs, (b) 4 IPs, (c) 5 IPs, and (d) 7 IPs

It can be seen in Figure 5-13 that a softening response is simulated for specimen WSH4, and hence the shear force-drift response is highly dependent on the number of integration points selected. Higher strains are developed at the critical section when a higher number of integration points are used, thus reducing the estimated displacement capacity of the walls. In this case the lowest number of integration points (IP = 3) provides the most accurate response because it is likely that the weight of the first integration point corresponds to the plastic hinge length of the wall (as discussed in Section 4.3.2.3). Figure 5-14 illustrates that a hardening response is simulated for specimen R1 (it is noted that minor softening is observed for 4IPs, 5IPs and 7IPs), and therefore it can be seen that the global response (i.e. shear force versus drift) is not sensitive to the number of integration points selected. It is important to note that the strains at the critical section are also to

some extent dependent on the number integration points, however, the sensitivity of the strains developed decreases as the number of integration points increases.

In order to overcome the issues related to strain localisation and the dependence of the strains developed on the number of integration points, it has been suggested that the response of walls be modelled such that the element length and weight of the IPs account for the expected length of the plastic hinge. This is the basis of the force-based distributed element with hinges developed by Scott and Fenves (2006). This element is particularly useful for modelling columns and beams since hinges are placed at both ends of the element. However, the inelastic behaviour of the walls is likely to be concentrated at the base of the walls, therefore explicit modelling of the plastic hinge region is predominately required for the base of the wall. Therefore, two methods are suggested for the explicit modelling of the hinge region:

i. *Method 1:* A single force-based element with two integration points to be placed at the bottom of the wall with a length equal to twice the expected plastic hinge length. When two integration points are specified, the default weight of the first integration (using the *Gauss-Lobatto Integration* method) point is half the element length and hence a constant curvature distribution of the critical section (i.e. at the bottom of the wall) will be integrated over the plastic hinge region of the wall.
ii. *Method 2:* A single force-based element with two integration points to be placed at the bottom of the wall where the weight of the integration point can be controlled by the user and it is set such that it equals to the equivalent plastic hinge region. This option is available in OpenSEES by using the *Low Order Integration* method.

Schematics of the proposed modelling techniques are given in Figure 5-15. The two approaches provide very similar responses, since the response is controlled by the integration of curvature at the critical section which is the same length using both methods, that is, the equivalent plastic hinge length. The second approach is recommended here for cases when the length of the plastic hinge is greater than half the storey height of the building. It is noted that a similar approach of specifying the bottom element length such that it is related to the expected plastic hinge length has also been suggested by Fox et al. (2015) for displacement-based distributed plasticity elements. However, the use of force-based distributed elements is suggested here due to the advantages discussed in Section 4.3.2.2.

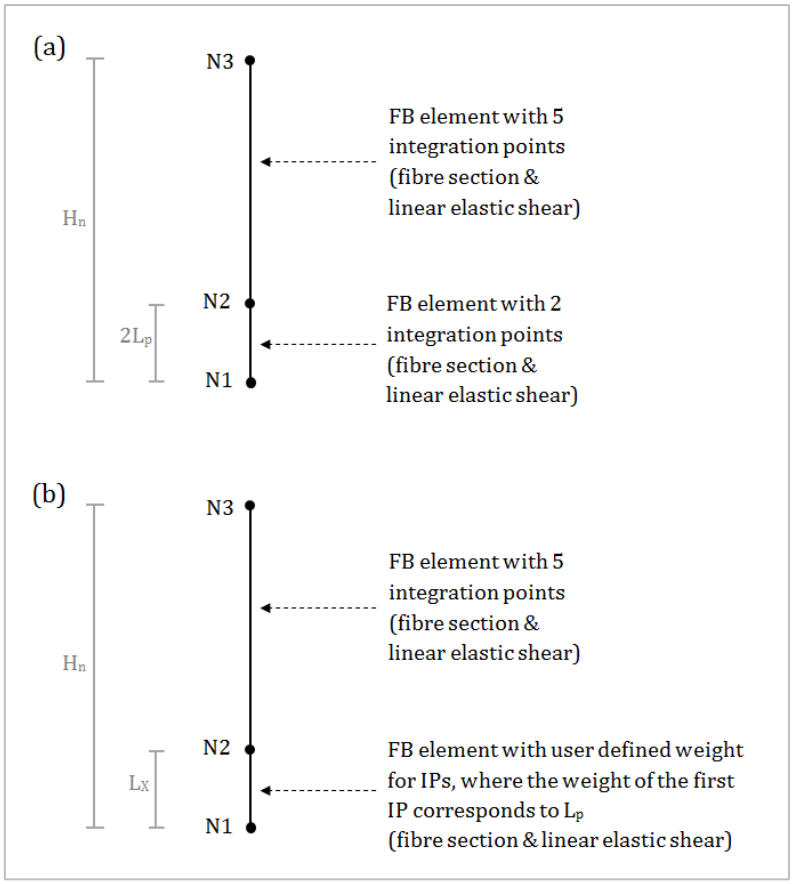

Figure 5-15: Modelling techniques for accurately simulating the flexural response of rectangular walls: (a) Method 1, (b) Method 2

The explicit modelling of the plastic hinge region also allows an increased accuracy to be achieved when modelling lightly reinforced RC walls. The reduced displacement capacity of lightly reinforced RC walls due to single crack formation or minimal secondary cracking can be simulated by using smaller equivalent plastic hinge lengths to model the plastic hinge region.

Furthermore, as discussed earlier, it is also important to ensure that the loss of lateral strength of the walls is modelled such that the redistribution of loads to the gravity frames is captured during the analysis of buildings. When the concrete compressive strains govern the response of the wall, this is usually automatically achieved since a softening response is simulated through the concrete material model (*Concrete04*) used to define the behaviour of the concrete fibres which incorporates the strength degradation of the concrete. However, when tensile strains govern and a hardening response is simulated, flexural degradation is not modelled. This is because steel material models are usually incapable of accurately simulating the softening response of steel. This is the case with the steel material model (*Steel02*) used in this study which is incapable of incorporating any form of strength degradation. Therefore, it is suggested here that the *MinMax* material

model available in OpenSEES be used in conjunction with *Steel02*. The *MinMax* material model is capable of tracking the strains developed in the fibres of distributed plasticity elements during the analysis in which their response has been defined by a particular material model (in this case *Steel02*) and to remove the fibre when it reaches a particular strain limit (by setting the strength and stiffness of the original material to zero). Hence, this allows the simulation of the gradual loss of lateral load carrying capacity of distributed plasticity elements and is especially useful for those which have a hardening response.

In order to examine the validity of the suggested modelling technique for the non-ductile walls to be assessed in this study, simulated results are compared with those recorded experimentally for six lightly reinforced rectangular walls which demonstrate secondary cracking or a dominant single crack failure. The details of the six walls are presented in Table 5-12. The equivalent plastic hinge lengths have been determined based on the recommendations provided by Hoult (2017) presented in Section 4.6.1. Firstly, the likelihood of developing secondary cracking or a single crack is determine by comparing the longitudinal reinforcement ratio (ρ_l) with the minimum reinforcement ratio required for secondary cracking form ($\rho_{wl.min}$). For walls for which secondary cracking is predicted the plastic hinge length is calculated using Eq. 5-18. The equation consists of the recommended plastic hinge equation (Eq. 4-11) by Hoult (2017) for the purpose of assessment and the strain penetration length (L_{sp}) recommended by Priestley et al. (2007). It is noted that the L_{sp} was added to the plastic hinge equation suggested by Hoult (2017) since it was not a parameter that was included in the analyses conducted by Hoult (2017) and also because it was observed that it provided more accurate results when used for the distributed plasticity approach of modelling the walls. For walls for which a single crack is predicted a slightly higher plastic length of 200 mm is adopted than the conservative recommendation of 150 mm by Hoult (2017). In addition, shear deformations are added to the wall response at each integration point using the effective shear stiffness suggest by Pugh et al. (2015) provided in Section 4.6.2. The *MinMax* material model is used to simulate the loss of strength in steel fibres when the steel strain exceeds 60 % of the reported ultimate tensile strain ($0.6\varepsilon_{su}$).

$$L_{p,rect} = (0.1L_w + 0.075H_e)\left(1 - 6.0\left(\frac{P}{A_g f_{cmi}}\right)\right) + L_{sp} \leq 0.5L_w \quad \text{Eq. 5-18}$$

Where L_{sp} is the strain penetration length,

$$L_{sp} = 0.022 f_y d_b$$

Figure 5-16 illustrates the response of three of the six walls; in all of these cases secondary cracking is predicted and hence the plastic hinge length was calculated in accordance with Eq. 5-18. The first two walls are the same walls which were used to highlight the limitations of using force-based elements with no consideration of plastic hinge length as shown previously in Figure 5-13 and Figure 5-14. Figure 5-16 also provides a brief description of the failure mechanism of the wall and a photo of the damaged wall at the end of the lateral loading. It can be seen that all three walls experienced secondary cracking as predicted by the equation. The simulated response includes both cyclic and monotonic response. Furthermore, to provide an indication of the magnitude of the simulated strains, the points at which the outermost reinforcement reaches a tensile strain limit of $0.6\varepsilon_{su}$, and a compressive strain of 0.004, are also provided on the monotonic response. Overall, it can be seen that the simulated shear force-drift responses matches very well to the experimental results. In addition, the results show that the development of strains is realistic. For all three specimens it is predicted that the ultimate capacity of the walls is governed by compression strain limits and this also corresponds to the reported failure mechanism.

Furthermore, the importance of imposing tensile strain limits is also illustrated. This is clearly apparent for specimen R1 Oesterle et al. (1976) which displays a hardening response and for which flexural degradation is simulated in the model due to the steel strain reaching the tensile limit of $0.6\varepsilon_{su}$. However, it is noted that the use of the *MinMax* material model increases the difficult of achieving numerical stability.

Figure 5-17 provides the response and failure mechanism of the remaining three rectangular walls. In these cases a single crack formation is predicted; hence the plastic hinge length is set to 200 mm. As expected the observed crack pattern indicates that all of these walls developed only one primary flexural crack. The simulated shear force-drift response of the walls provides a reasonably good match with the experimental results considering the difficulty in predicting the response of walls forming a single crack, especially via means of macro modelling techniques. The poorest match obtained is for specimen 1, Lu et al. (2016), for which the ductile behaviour of the wall is underestimated. Specimen 1 and 4 tested by Lu et al. (2016) had the same detailing and the only parameter which varied was the axial load ratio. Specimen 1 had an axial load ratio of 3.3 % and specimen 4 had no axial load applied during the analysis. Hence, the improved response of specimen 1 was due to the increase in the applied axial load. However, the ratio of the maximum moment capacity to the cracking moment capacity calculated from the experimental results was lower for specimen 1 than specimen 4. Therefore it is uncertain

why specimen 1 displayed a higher displacement capacity than specimen 4. Nevertheless, considering the unpredictable behaviour of walls that develop a predominant single crack, a conservative prediction of response is acceptable. Hence, the suggested modelling approach for lightly reinforced non-ductile walls is considered to provide an adequate degree of accuracy.

Table 5-12: Details of lightly reinforced rectangular walls

No.	Specimen	Failure type	ALR	L_w (mm)	t_w (mm)	H_e (mm)	H_e/L_w	f_c' (MPa)	f_y (MPa)	f_u (MPa)	$\rho_{l,b}$	ρ_l	ρ_t	$\rho_{wl,min}$	L_p (mm)	Predicted crack formation
1	Dazio et al. (2009) WSH4	CB	0.0566	2000	150	4560	2.3	40.9	576	675	0.0155	0.0082	0.0025	0.0052	510	Secondary cracks
2	Oesterle et al. (1976) R1	BR	0.0043	1905	101.6	4572	2.4	44.8	512	765	0.0103	0.0047	0.0027	0.0043	628	Secondary cracks
3	Altheeb (2016) Specimen 2	CB	0.0508	900	120	2650	2.9	34.7	500	720	0.0073	0.0073	0.0033	0.0045	311	Secondary cracks
4	Altheeb (2016) Specimen 1	BR	0.0500	900	120	2650	2.9	35.2	500	720	0.0036	0.0036	0.0033	0.0045	200	Single crack
5	Lu et al., (2016) Specimen 1	BR	0.0359	1400	150	2800	2.0	38.5	300	400	0.0052	0.0052	0.0025	0.0062	200	Single crack
6	Lu et al., (2016) Specimen 4	BR	0.0	1400	150	2800	2.0	34.7	300	400	0.0052	0.0052	0.0025	0.0057	200	Single crack

$\rho_{l,b}$: longitudinal reinforcement ratio within boundary region | CB: concrete crushing and buckling of bars | BR: buckling and fracture of bars

Dazio et al. (2009) specimen WSH4

Distributed flexural and flexure-shear cracks were observed along the length of the wall. The ultimate failure mechanism of the wall was due to crushing of the concrete and buckling of longitudinal bars.

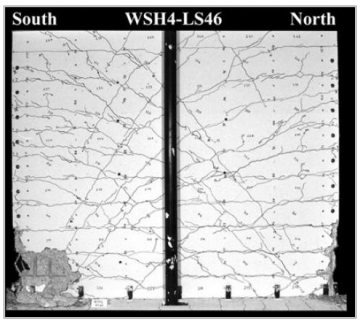

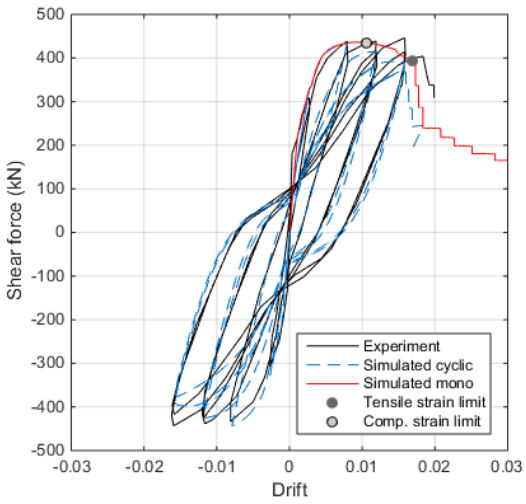

Oesterle et al. (1976) specimen R1

Observed cracks were limited within the plastic hinge region of the wall. Failure of the wall initiated with spalling of the cover concrete and buckling of longitudinal bars which was eventually followed by fracture of the bars.

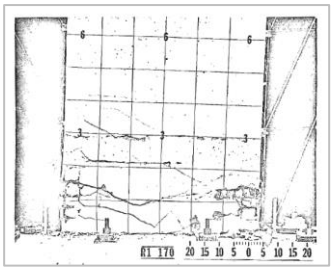

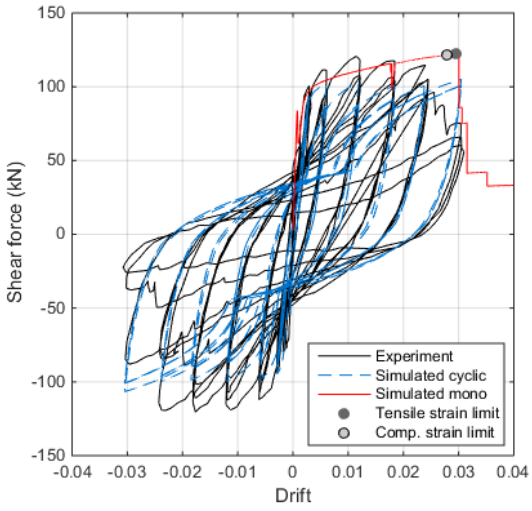

Altheeb (2016) specimen 2

Flexural cracks were observed along the height of the wall but they were mainly concentrated within the hinge region. Spalling initiated at approximately 2.0 % drift and buckling was observed from 2.7 %. Ultimate failure was due to crushing of concrete and buckling of bars. It is noted that the lateral load was applied for this test up until axial load failure.

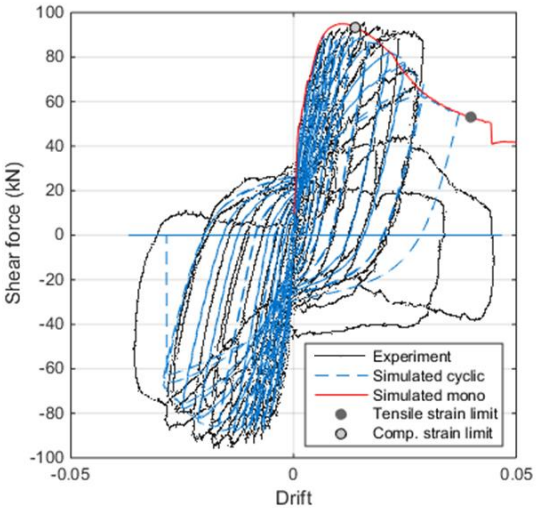

Figure 5-16: Comparison of simulated and experimental response of lightly reinforced walls for which secondary cracking is predicted, and a brief description of the observed failure mechanism

Altheeb (2016) specimen 1

One main flexural crack was observed at the base of the wall. Initiation of spalling occurred at 2.2 % followed by bar buckling, and eventually bar fracture was observed at 2.6 % drift. Lateral load was applied to the wall up until axial load failure. During the later staged of the loading the wall response was mainly governed by strain penetration.

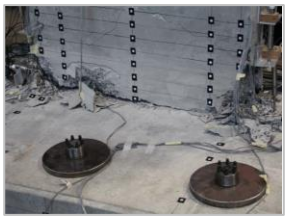

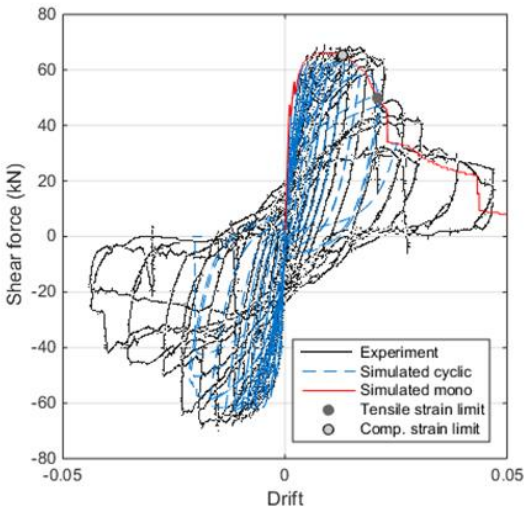

Lu et al. (2016) specimen 1

Three to four flexural cracks were observed within the lower one-fourth of the wall height, but the wall deformation was mainly concentrated at one large flexural crack at the wall base. Spalling of concrete initiated in the corners of the wall at 1 % drift, buckling of longitudinal reinforcement commenced at 1.5 % drift, core crushing occurred at 2.0 % drift, fracturing of corner bars occurred at 2.5 %.

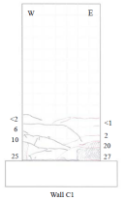

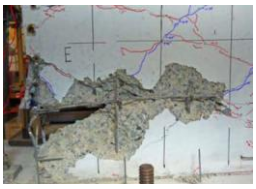

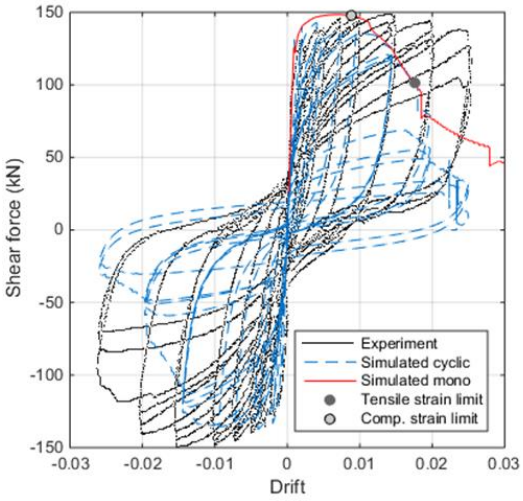

Lu et al. (2016) specimen 4

Three main flexural cracks were observed in the bottom one-fourth of the wall height; however the wall deformation was mainly concentrated at only one of the cracks. Spalling occurred at 0.75 %, followed by buckling of the bars. Crushing of core concrete occurred at around 1.0 % drift, and eventually fracture of the bars occurred at 1.5 % drift.

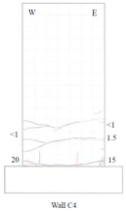

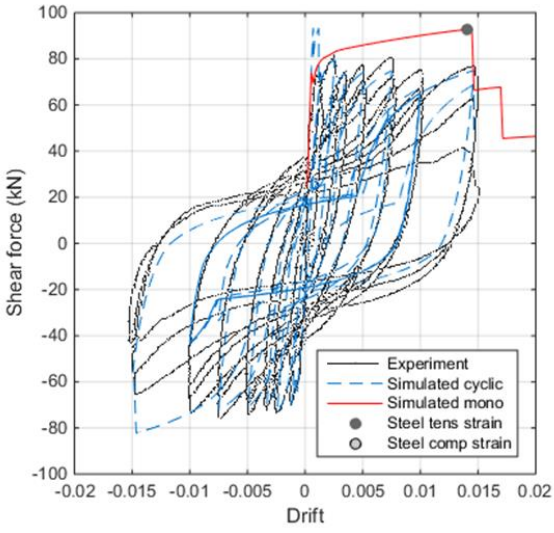

Figure 5-17: Comparison of simulated and experimental response of lightly reinforced walls for which a single crack is predicted, and a brief description of the observed failure mechanism

5.5.1.2 Modelling of non-planar walls

The buildings to be assessed in this study (in Chapter 7) have core walls and hence a modelling approach needs to be adopted which is most suitable for non-planar walls. Initially, the various distributed plasticity modelling approaches described in Section 4.6.3 are investigated. The first approach evaluated is the conventional one-dimensional stick model where a single fibre-section is assigned to the vertical line element, illustrated in Figure 5-18. The plastic hinge region is modelled in a similar manner to the rectangular walls, where the length of the first force-based (FB) element (with two integration points) corresponds to twice the plastic hinge length ($2L_p$) and the weight of the first integration point corresponds to the plastic hinge length. The second and third approaches use the wide-column model (WCM) as suggested by Beyer et al. (2008a). In these approaches the plastic hinge region is modelled explicitly using the same approach as the conventional one-dimensional stick models. Above the plastic hinge region, horizontal links are spaced at a distance corresponding to one-fifth of the effective wall height or half the wall length, whichever is smaller, as recommended by Beyer et al. (2008a). A single FB element is placed in between the horizontal links with 4-5 integration points. Two modelling methods are considered with respect to shear deformations and the stiffness properties of the horizontal links:

i. *Method 1:* Shear deformations are not included, and the horizontal links are modelled with an elastic element with rigid flexural, shear, and torsional stiffness.
ii. *Method 2:* Shear deformations are added at a section level similar to the method used for the modelling of rectangular walls, and the horizontal links are modelled with an elastic element with rigid flexural and shear stiffness, and the torsional stiffness is defined based on the recommendation from Beyer et al. (2008a) provided in Eq. 5-19.

$$\mathrm{K}_{\mathrm{torsion}} = 0.25G\,\frac{h_{sp}t_w^3}{3} \qquad \text{Eq. 5-19}$$

The two suggested modelling approaches are illustrated in Figure 5-19 for a C-shaped wall.

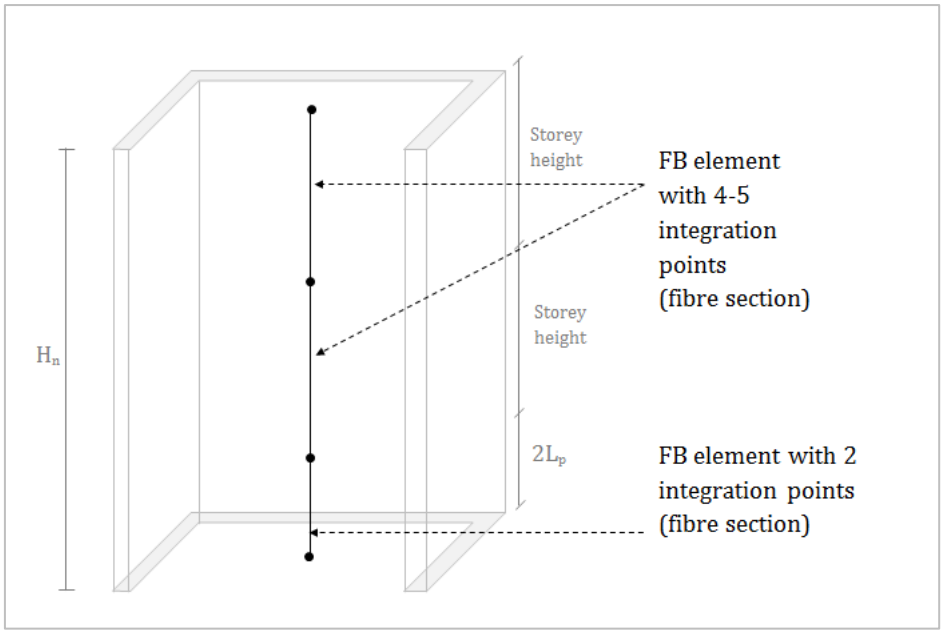

Figure 5-18: Conventional distributed plasticity approach (stick model) for modelling non-planar walls

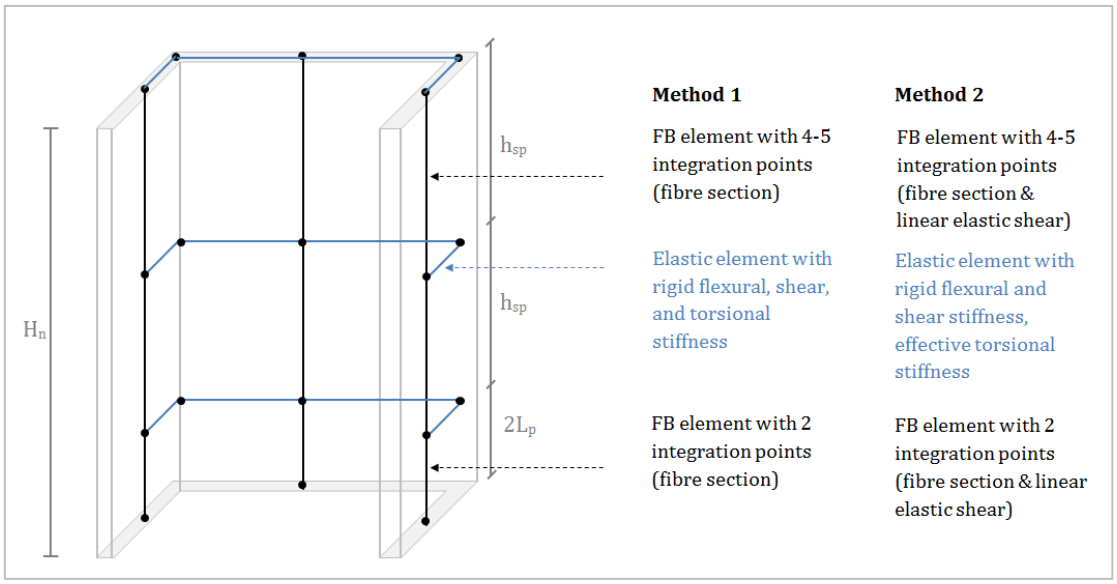

Figure 5-19: Wide column modelling technique for simulating the response of non-planar walls

Since there are currently no experimental results available in the literature for lightly reinforced non-planar walls, the suggested modelling technique is compared with experimental results for two C-shaped walls which have reasonably good reinforcement detailing. The details of the two walls are provided in Table 5-13 and the cross-sections of the two walls are provided in Figure 5-20. Specimen TUA tested by Beyer et al. (2008b) has longitudinal reinforcement ratio in the boundary region exceeding 1 %, and the axial load ratio of the specimen tested by Ile and Reynouard (2005) is 12 %; both of these parameters exceed the limits for which the plastic hinge equations suggested by Hoult

(2017) are valid. In addition, both walls have significant confinement within the boundary regions. Hence, for both of the walls the equations provided by Hoult (2017) are not applicable. Instead, the plastic hinge length of the walls is determined using Eq. 5-20 recommended by Paulay and Priestley (1992) which is suitable for well detailed walls. This equation was also used by Beyer et al. (2008b) to design specimen TUA.

$$L_p = the\ larger\ of \begin{Bmatrix} 0.08H_e + 0.022d_b f_y \\ 0.2L_w + 0.044H_e \end{Bmatrix} \quad \text{Eq. 5-20}$$

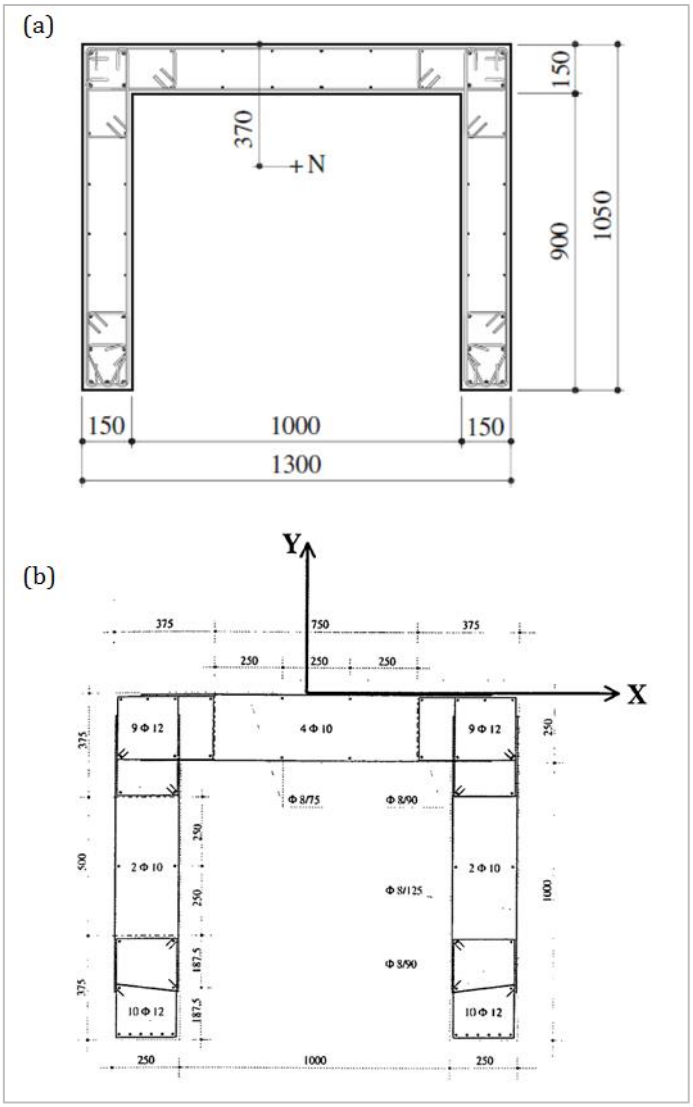

Figure 5-20: Cross-section of wall specimen tested by: (a) Beyer et al., (2008b) specimen TUA, (b) Ile and Reynouard (2005)

Table 5-13: Details of RC C-shaped walls

Specimen	**ALR**	**L_f & L_{wb} (mm)**	**t (mm)**	**H_e (mm)**	**H_e/L_f & H_e/L_w**	**f_c' (MPa)**	**f_y (MPa)**	**f_u (MPa)**	**$\rho_{wl,b}$**	**$\rho_{fl,b}$**	**ρ_l**	**ρ_t**
Beyer et al., (2008) TUA	0.02	1050 / 1300	150	2950[1]/ 3350[2]	2.81[1]/ 2.58[2]	77.90	488-518	595-681	0.0108	0.0184	0.0071	0.003[5 & 6]
Ile & Reynouard (2005)	0.10-0.12	1250 / 1500	250	3900	3.12[3]/ 2.60[4]	23.73	516-525	615-617	0.0081	0.0072	0.0056	0.0054[5]/ 0.0032[6]

L_f: is the length of the flanges of the C-shaped wall | L_w: is the length of the web of the C-shaped wall | $\rho_{wl,b}$: longitudinal reinforcement ratio within web-flange boundary region | $\rho_{wl,f}$: longitudinal reinforcement ratio within flange boundary region

Notes: [1] loading in NS direction | [2] loading in EW direction | [3] loading in Y-direction | [4] loading in X-direction | [5] web region | [6] flange region

During the experimental testing conducted by Beyer et al. (2008b), specimen TUA was subjected to North-South (NS), East-West (EW) and diagonal quasi-static cyclic loading. It is reported that the ultimate failure mechanism of the specimen was due to bar-fracture which was observed at a displacement ductility of 8.0 (that is, at the end of the testing). Bar-buckling was also reported, with the first bar buckling at a displacement ductility of 6.0. Furthermore, spalling of concrete was reported to initiate at a displacement ductility of 3.0; however, failure of the concrete due to crushing was not observed until the end of testing. It is also noted that the sliding shear experienced by the specimen was negligible. The crack pattern of the specimen at a displacement ductility of 6.0 is provided in Figure 5-21 and the crack pattern at the base of the wall and the rupturing of longitudinal reinforcement at a displacement ductility of 8.0 is illustrated in Figure 5-22.

The comparison between simulated results using the three methods discussed above and the experimental results under NS and EW loading for specimen TUA is provided in Figure 5-23. As previously done for the rectangular walls, the points at which the outermost reinforcement reaches a tensile strain limit of $0.6\varepsilon_{su}$, and a compressive strain of 0.004, are provided on the monotonic curve. These strain values give an indication of the drift level at which the ultimate capacity of the critical section has been reached. The results show that the simulated lateral force versus drift, for all three methods, matches very well with the experimental results. The hysteretic behaviour under the NS direction seems to be best represented by the wide column model (WCM) using Method 1. However, for the EW direction, there is no significant difference between the results obtained using the different approaches, although the conventional stick model provides a slightly better prediction of the unloading behaviour. In terms of strain limits, all three approaches tend to provide similar predictions which match well with what was reported in the experiment; all of the models predict longitudinal bar fracture towards the end of the analysis. The prediction of the drift at which the compressive strain limit is reached under EW loading with the web in tension (WiT) for the WCM is lower (approximately at 1.5 %) when compared with the conventional stick model for which the limit is predicted to be reached at the same drift as bar fracture (2.5 %). It is also noted that for the results presented for non-planar walls, the *MinMax* material model was not used to simulate loss of strength and stiffness of the steel fibres due to numerical instabilities.

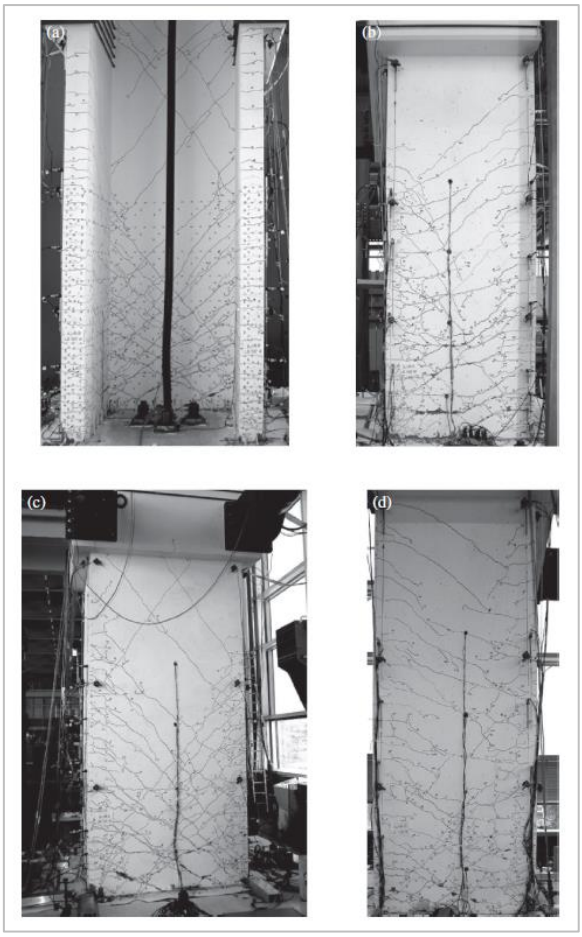

Figure 5-21: Specimen TUA crack pattern at displacement ductility of 6.0: (a) South face, (b) West face, (b) North face, (d) East face

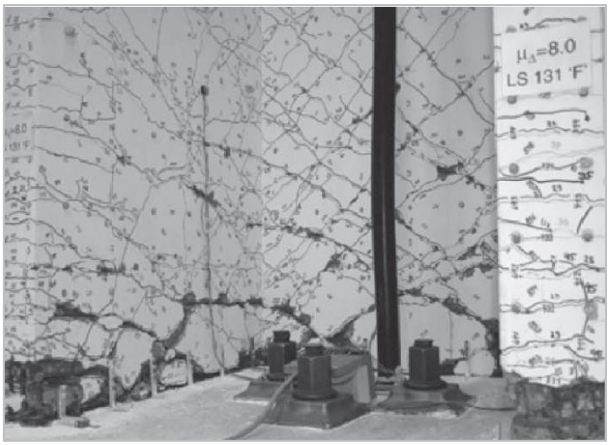

Figure 5-22: Specimen TUA crack pattern at a displacement ductility of 8.0 at the base of the wall and rupture of longitudinal bars in flange region

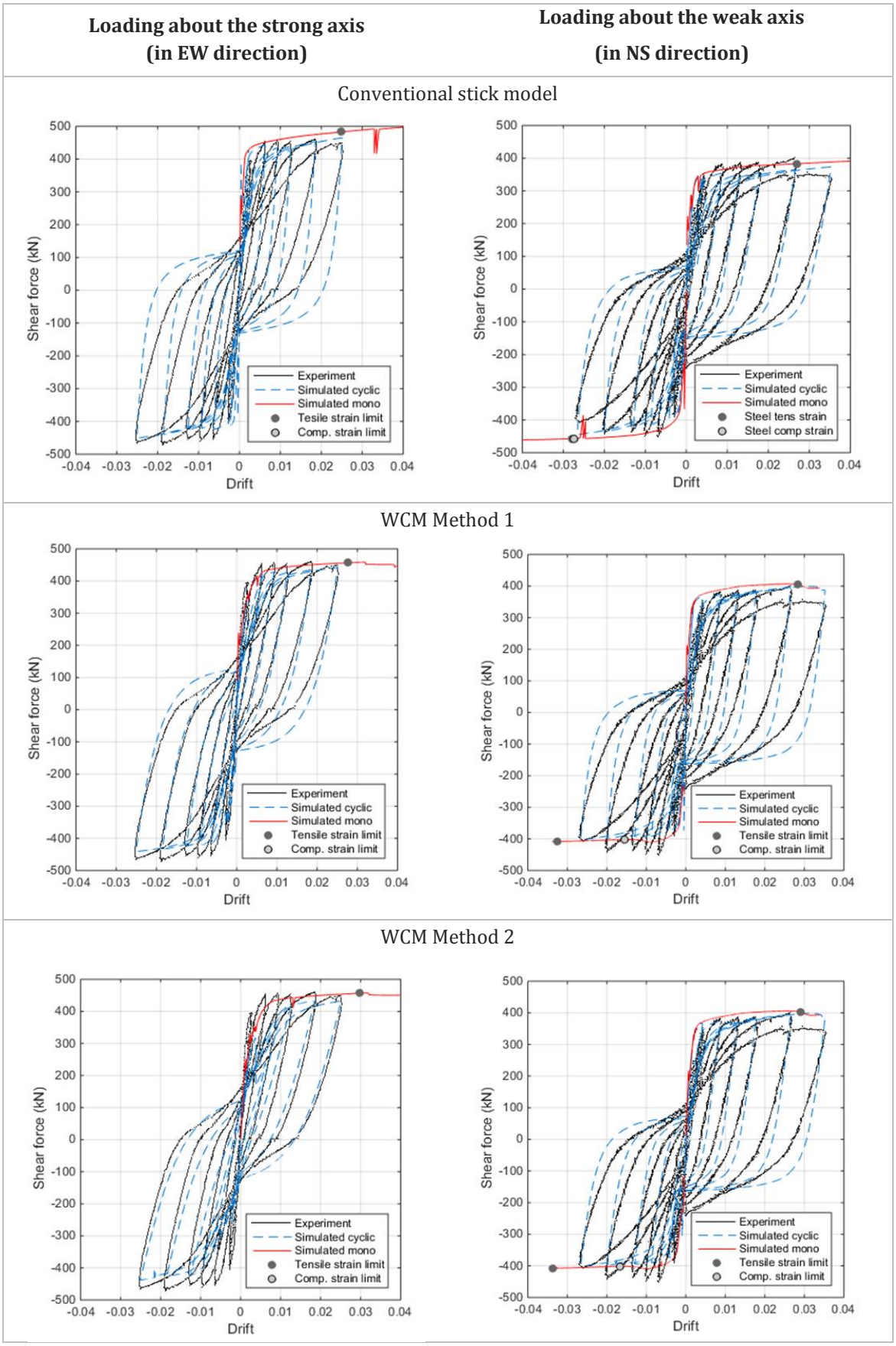

Figure 5-23: Comparison between simulated and experimental results for specimen TUA tested by Beyer et al., (2008) TUA

The experimental testing conducted by Ile and Reynouard (2005) included two specimens with identical detailing, one tested about the strong axis (i.e. loading applied along the X-direction) and the other about the weak axis (i.e. loading applied along the Y-direction). For the X-direction loading, initially flexure-shear cracks were observed in the flanges and the web. As the applied lateral load increased, severe buckling and rupture of the longitudinal bars (as well as some stirrups) occurred at the base of the flanges and at the web ends. For the Y-direction loading, the failure mechanism was primarily due to bars buckling in one of the flanges since a stirrup was missing at the base of the flange (it was not included during construction). The crack pattern of the specimens under X-direction and Y-direction loading is illustrated in Figure 5-24 and Figure 5-25, respectively.

The comparison between the simulated results and the experimental lateral force versus drift results are presented in Figure 5-26. The global response predicted by all three models is similar. The hysteretic behaviour, especially the unloading stiffness is best predicted by the WCM using Method 2 for the specimen loaded in the X-direction. For the specimen tested under Y-direction loading, there is no significant difference between the cyclic responses simulated by all three models. Furthermore, in terms of local response, that is the prediction of strain limits, all three models provide very similar results. All simulated results show that only the compressive strain limit is reached for the specimens tested under X- and Y-directional loading. This is consistent with the observed behaviour of the walls since bar buckling was the primary cause of the ultimate failure of the walls. For the specimen tested under X-direction loading, fracture of longitudinal bars was also observed, however this is not reflected in the simulated responses.

In summary, the comparisons between the simulated and experimental results indicate that all three models are capable of accurately representing the global response of the C-shaped walls. The accuracy achieved when modelling the hysteretic response of the walls is sometimes better using a particular approach; however the model that gives the best results is not consistent from one situation to the next, so this is not conclusive. It should be noted that the prediction of the cyclic response is likely to be improved by changing the parameters controlling the hysteretic behaviour of the steel material (i.e. *Steel02*), however a significantly larger database of experimental results would be needed if this were to be done. In terms of local response, it has been shown that the use of explicit modelling of the plastic hinge length helps to improve the prediction of strain limits. However, care must be taken if strain limits are used to assess the performance of building components, and not just interstorey drift limits. The strains developed in distributed plasticity elements are highly dependent on the equivalent plastic hinge length that is

chosen. Furthermore, it is noted that the *MinMax* material model used in OpenSEES to simulate loss of strength and stiffness of the steel fibres is likely to cause numerical instability when applied to the non-planar walls. For these reasons the distributed plasticity approach described in this section is limited in its ability to accurately simulate the loss of lateral strength of walls during global collapse analysis of buildings; this is even more limited for walls which initially experience a hardening response,.

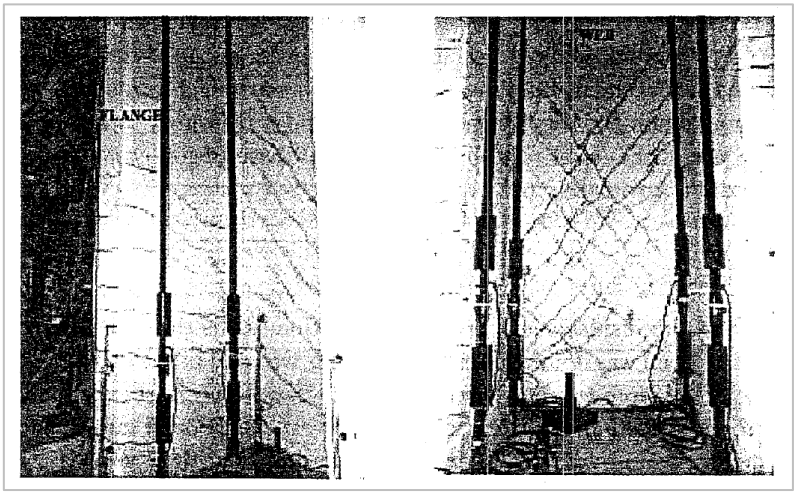

Figure 5-24: Crack pattern of wall during X-direction testing for specimen tested by Ile and Reynouard (2005)

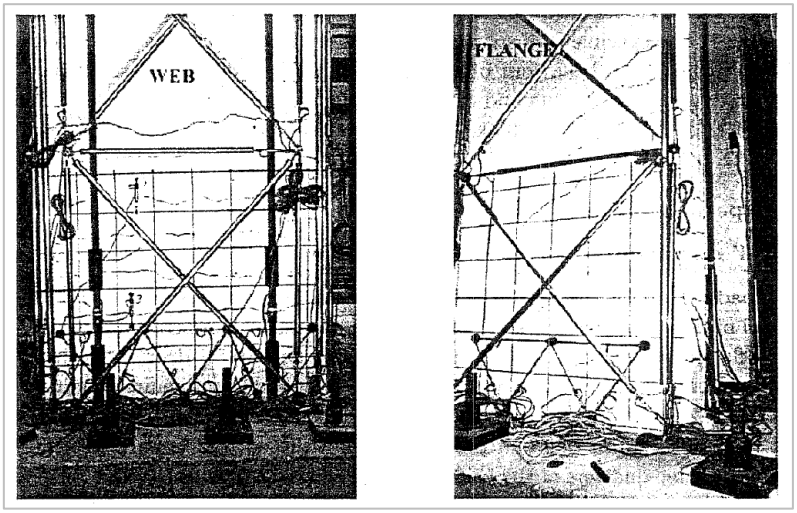

Figure 5-25: Crack pattern of wall during Y-direction testing for specimen tested by Ile and Reynouard (2005)

Loading about the strong axis (in X-direction)	Loading about the weak axis (in Y-direction)
Conventional stick model	
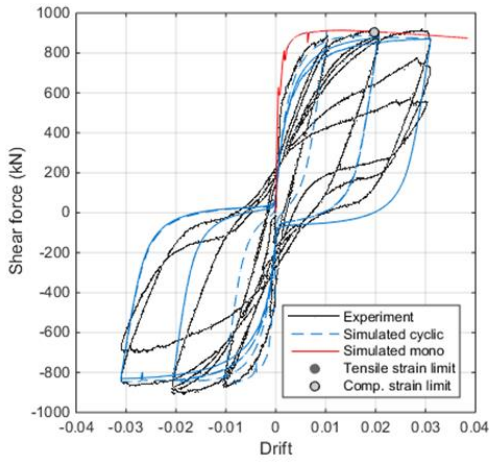	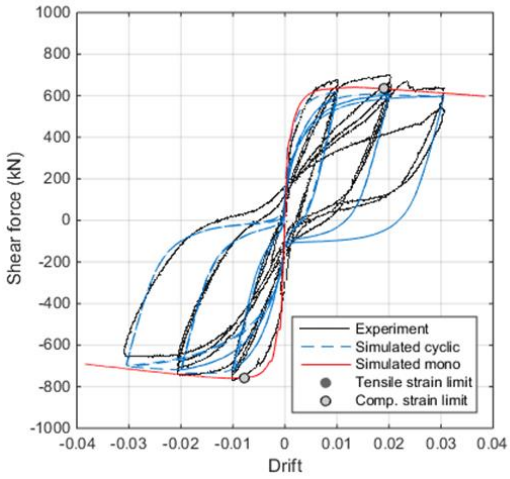
WCM Method 1	
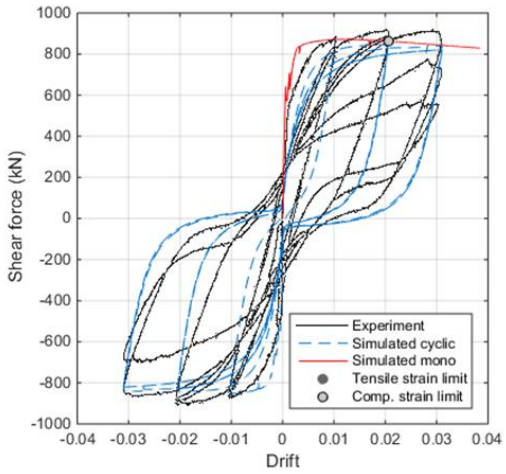	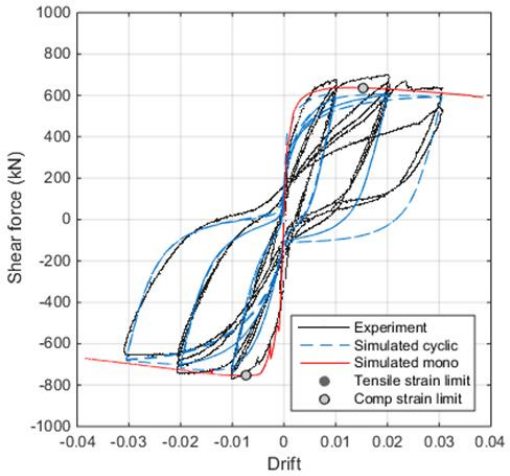
WCM Method 2	
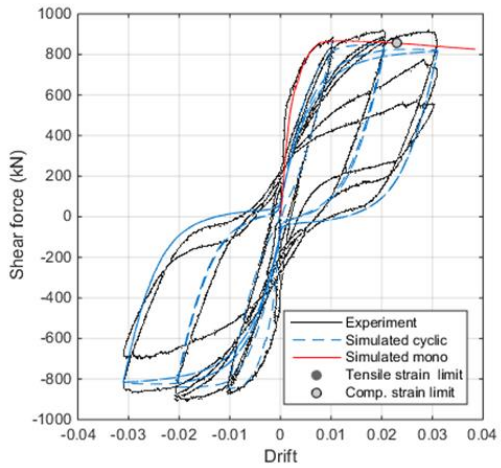	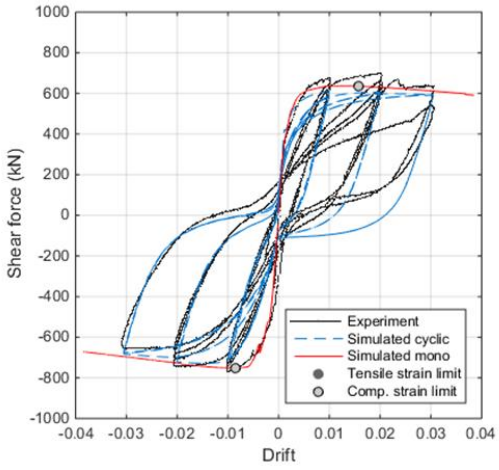

Figure 5-26: Comparison between simulated and experimental results for specimen tested by Ile and Reynouard (2005)

5.5.2 Lumped plasticity approach

In the previous section it was illustrated that the distributed plasticity approach is capable of simulating the global response of lightly reinforced rectangular walls and well detailed C-shaped core walls with a reasonable degree of accuracy. However, it was also identified that there are potential numerical instability issues, especially for simulating the post-peak behaviour of the walls. The reliable modelling of the post-peak behaviour of the walls is critical in this study, since the global analysis of the buildings is to be conducted up to the point of collapse, which is defined as loss of capacity of the gravity system to resist axial loads. Therefore the lumped plasticity approach is investigated in this section to examine its validity for the purpose of conducting global analysis. Furthermore, the buildings to be assessed in this study consist of lightly reinforced core walls with non-ductile detailing. Therefore, the simulated response of these core walls is investigated by comparing the results with numerical models proposed in the literature.

5.5.2.1 Modelling of lightly reinforced planar walls

As it has been highlighted previously for the modelling of beam-column joints, beams, and columns, using the lumped plasticity approach, the key aspect of accurately simulating the response of the components is the definition of the backbone curve. Since it has been demonstrated that the monotonic response of the walls obtained from pushover analysis using the distributed plasticity approach is capable of accurately simulating the observed response of walls, it is suggested here that the backbone curve for the lumped plasticity approach be constructed by using the critical points obtained from pushover analysis. Furthermore, since the walls to be assessed are likely to develop concentrated cracking at the base of the wall, it is suggested that the inelastic behaviour of the walls is simulated with a single moment-rotation spring at the base of the wall. The *Pinching4* hysteretic model available in OpenSEES is adopted to define the inelastic moment-rotation response of the walls. The four critical points are obtained from the pushover analysis of the wall using the distributed plasticity approach where the moment and deformation capacity are defined as:

- *Point 1 – Cracking:* when the extreme tensile concrete fibre reaches tensile strength of concrete
- *Point 2 – Yield:* when the extreme tensile steel fibre reaches yield strain or the extreme compressive concrete fibre reaches a strain of 0.002, whichever occurs first
- *Point 3 – Ultimate capacity:* when the extreme tensile steel fibre reaches $0.6\varepsilon_{su}$ or the extreme concrete compressive fibre reaches a strain of 0.004, whichever occurs first

- *Point 4 – Residual strength:* when the moment capacity reduces to 20 % of the ultimate capacity

The hysteretic parameters of the *Pinching4* model are defined using the same parameters discussed for the columns and beams. To examine the validity of the approach for lightly reinforced walls, simulated results are compared with the experimental results of the three rectangular walls presented in Section 5.5.1.1 for which a single crack was predicted by Hoult (2017). The results are presented in Figure 5-27. Furthermore, for direct comparison between the results obtained using the lumped plasticity and the distributed plasticity approach, the simulated results obtained using the distributed plasticity elements are also provided in the same figure. The accuracy of the simulated results is highly dependent on the backbone definition obtained from the monotonic response of the distributed plasticity approach and therefore similar simulated responses are obtained with both methods. Furthermore, the hysteretic behaviour predicted using the lumped plasticity approach compares well with the distributed plasticity approach. It is observed that a good prediction of the ultimate strength and deformation capacity is predicted using the lumped plasticity approach for specimen 1 tested by Altheeb (2016) and specimen 4 tested by Lu et al. (2016). In fact, the lumped plasticity approach is better able to simulate the last few cycles for specimen 1 tested by Altheeb (2016) and specimen 4 tested Lu et al. (2016) in comparison to the distributed plasticity approach which encounters numerical instability. The ductile behaviour of specimen 1 tested by Lu et al. (2016) is underestimated using the lumped plasticity approach in a similar manner to the simulated results obtained using the distributed plasticity approach.

In general, it is shown that the lumped plasticity approach is capable of predicting a good match with experimental results for the purpose of global analysis. It is noted that the approach is highly dependent on the assumption that the response of the walls may be obtained based on a pushover analysis following the first mode shape of the walls. This particularly affects the deformation capacities which are computed from the pushover analysis response obtained from the distributed plasticity approach. However, the assumption that the wall response will be governed by the first mode response is considered to be valid for the walls being assessed here since it is expected that higher mode effects will be negligible for the height of buildings considered (less than 10-storeys). In addition, concentrated inelastic behaviour is expected at the base of the walls due to the low longitudinal reinforcement ratio which limits the formation of secondary cracking, therefore validating the use of a single moment-rotation spring at the base of the wall.

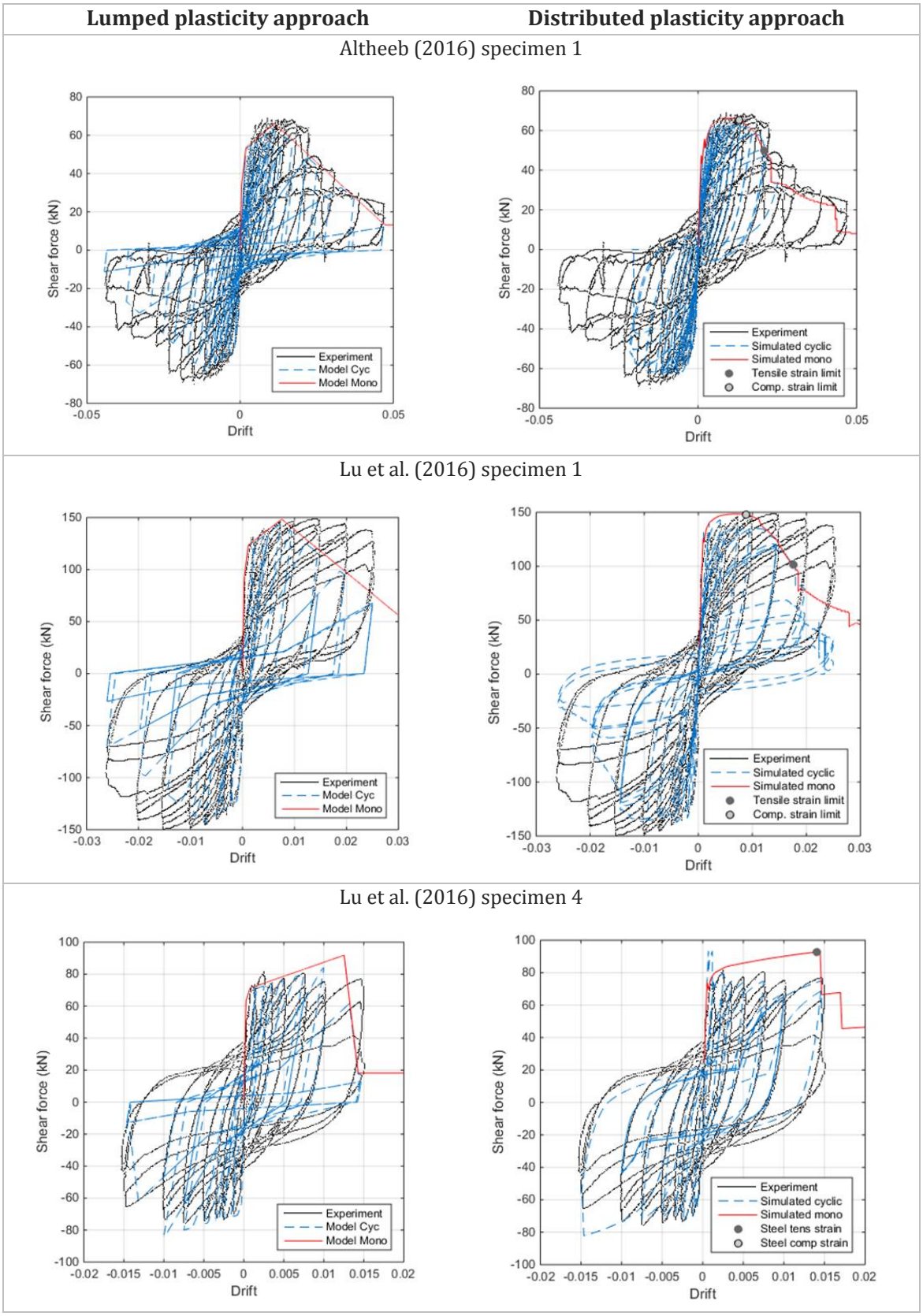

Figure 5-27: Comparison of simulated and experimental response of lightly reinforced rectangular walls for which a single crack is predicted, using lumped and distributed plasticity approach

5.5.2.2 Modelling of lightly reinforced non-planar walls

As mentioned earlier, there are currently no experimental results available for lightly reinforced non-planar walls which have non-ductile detailing. These are the type of core walls which exist in the buildings that are assessed in this study. Therefore to examine the validity of the modelling approach, the simulated monotonic response of lightly reinforced non-ductile non-planar walls are compared with the load-deformation response proposed by Hoult (2017) for C-shaped walls which is based on equivalent hinge analysis. As discussed in Section 4.6.1, Hoult (2017) conducted detailed micro finite element modelling of C-shaped walls which have detailing representative of core walls constructed in Australia.

In order to compare the simulated results with the load-deformation behaviour proposed by Hoult (2017), box-shaped and C-shaped core walls within a 5-storey building are examined. The core wall design is representative of construction in the 1980s period; the details of the walls are provided in Figure 5-28. The box-shaped wall is representative of stair cores (SC) and the C-shaped wall is representative of lift cores (LC) in the buildings being assessed here. The longitudinal reinforcement ratio is approximately 0.24 % for both the box-shaped and C-shaped core walls. Using the equation proposed by Hoult (2017) (Eq. 4-10), it is predicted that a single crack will form. Furthermore, sectional analysis of the walls also shows that the cracking moment of the walls is greater that the yield moment capacity. Thus the bilinear load-deformation equations proposed by Hoult (2017) are adapted to a trilinear backbone to predict the response of walls for which the cracking moment is greater than the yield moment. In addition, it is noted that Hoult (2017) did not assess the performance of box-shaped core walls, thus the equations for the C-shaped walls have been applied to provide an indication only of the predicted response for box-shaped walls.

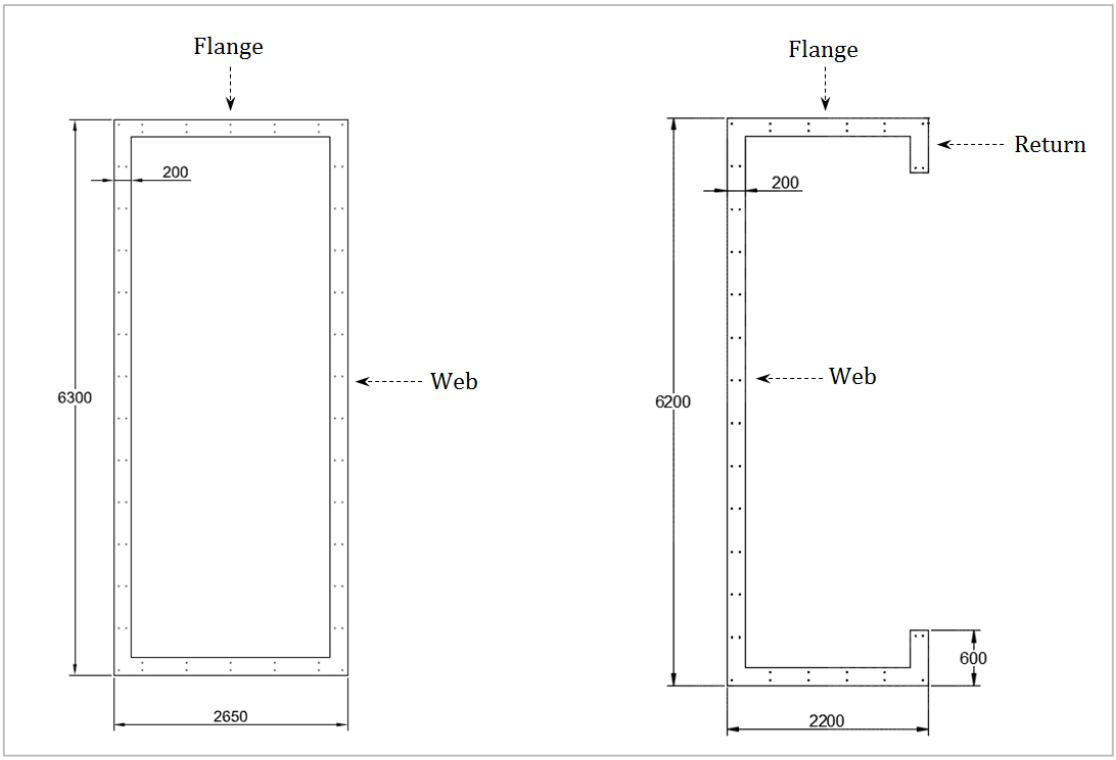

Figure 5-28: Box-shaped and C-shaped core wall detailing for a 5-storey building

The core walls have been modelled in OpenSEES using the conventional one-dimensional distributed plasticity approach discussed in Section 5.5.1, for which the plastic hinge length is assumed to be 200 mm given that a single crack is expected. From the pushover analysis, the backbone response is obtained, where the critical points are defined in a similar manner to those obtained for rectangular walls as discussed in 5.5.2.1. However, it is noted that the last point is not defined as residual capacity, since the walls assessed by Hoult (2017) were assessed only up to the point of ultimate capacity. This is because a sudden loss of lateral load carrying capacity is expected due to the detailing of the walls.

The results for the C-shaped core wall are presented in Figure 5-29 for bending about the minor axis with the web in compression (WiC) and the web in tension (WiT), and for bending about the major axis. It can be seen that the simulated load-deformation response using the distributed plasticity approach compares well with the load-deformation behaviour predicted using the adapted numerical model proposed by Hoult (2017). The ultimate deformation capacities predicted for the C-shaped wall about the major axis and minor axis with WiC very closely match the deformation capacity predicted by Hoult (2017). This is because for both of these cases the response of the core walls is governed by tensile strain limits. Due to the low longitudinal reinforcement ratio, relatively high tensile strains need to be developed to ensure that the tensile force is equal to the compressive force. A schematic of the strain distribution of the core walls is provided in

Figure 5-30 and Figure 5-31 for bending about the minor and major axes, respectively. Furthermore, the load-deformation responses in Figure 5-29 show that the deformation capacity predicted using the distributed plasticity approach for bending about the minor axis with WiT is slightly lower than that predicted by Hoult (2017). This is because for C-shaped walls bending about the minor axis with WiT, the response of the walls may be governed by either the compressive strain limits or tensile strain limits depending on the detailing of the wall. For walls which have sufficient longitudinal reinforcement, the response of the C-shaped core walls with WiT are typically governed by compressive strains, since large compressive strains need to be developed in the boundary of the flange region such that the compressive force is equal to the tensile force developed in the web of the C-shaped core wall. However, for lightly reinforced C-shaped core walls the tensile forces developed in the web region may be relatively low due to the low longitudinal reinforcement ratio and therefore high tensile strains may need to be developed to generate the tensile forces required for equilibrium. Therefore, a higher variability in response is expected between models for predicting the response of C-shaped walls bending about the minor axis with WiT since the results are also highly dependent on the behaviour of concrete for which the response is more variable due to modelling assumptions.

The load-deformation response of the box-shaped core walls are presented in Figure 5-32 for bending about the minor axis and major axis. For bending about the minor axis, two separate load-deformation responses are calculated using Hoult (2017) since the equations are developed for C-shaped walls with either WiC or WiT. The equation used to predict the response of C-shaped walls with WiC provides a similar match to the simulated response for the box-shaped wall. This is expected since the equation developed for WiC is governed by tensile strain limits developed in the boundary regions of the flanges. For lightly reinforced box-shaped core walls bending about the minor axis, compressive strains are not likely to govern due to the large area provided by the web of the box-core which allows large compressive forces to be developed even though the compressive strains remain reasonably low. Therefore, the behaviour of the walls is likely to be controlled by the tensile strain limits of the longitudinal reinforcement in the web-region. A very good match is also observed for the simulated load-deformation response for the box-shape core wall bending about the major axis and the response predicted using the Hoult (2017) numerical model for C-shaped walls. This is because the response of the box-core walls is governed by the tensile strain limits developed in the flanges of the box-shaped core in a similar manner to the C-shaped core walls.

In summary, the results suggest that that the distributed plasticity approach of explicitly modelling the plastic hinge region is able to accurately predict the response of lightly reinforced non-ductile RC core walls since a good match is obtained with the Hoult (2017) numerical model which is based on extensive micro finite element analyses of C-shaped core walls. In addition, it appears that the method of obtaining the backbone response for the lumped plasticity approach from the pushover analysis of the distributed plasticity element is a viable approach for conducting global analysis of buildings, at least in the limited cases considered here.

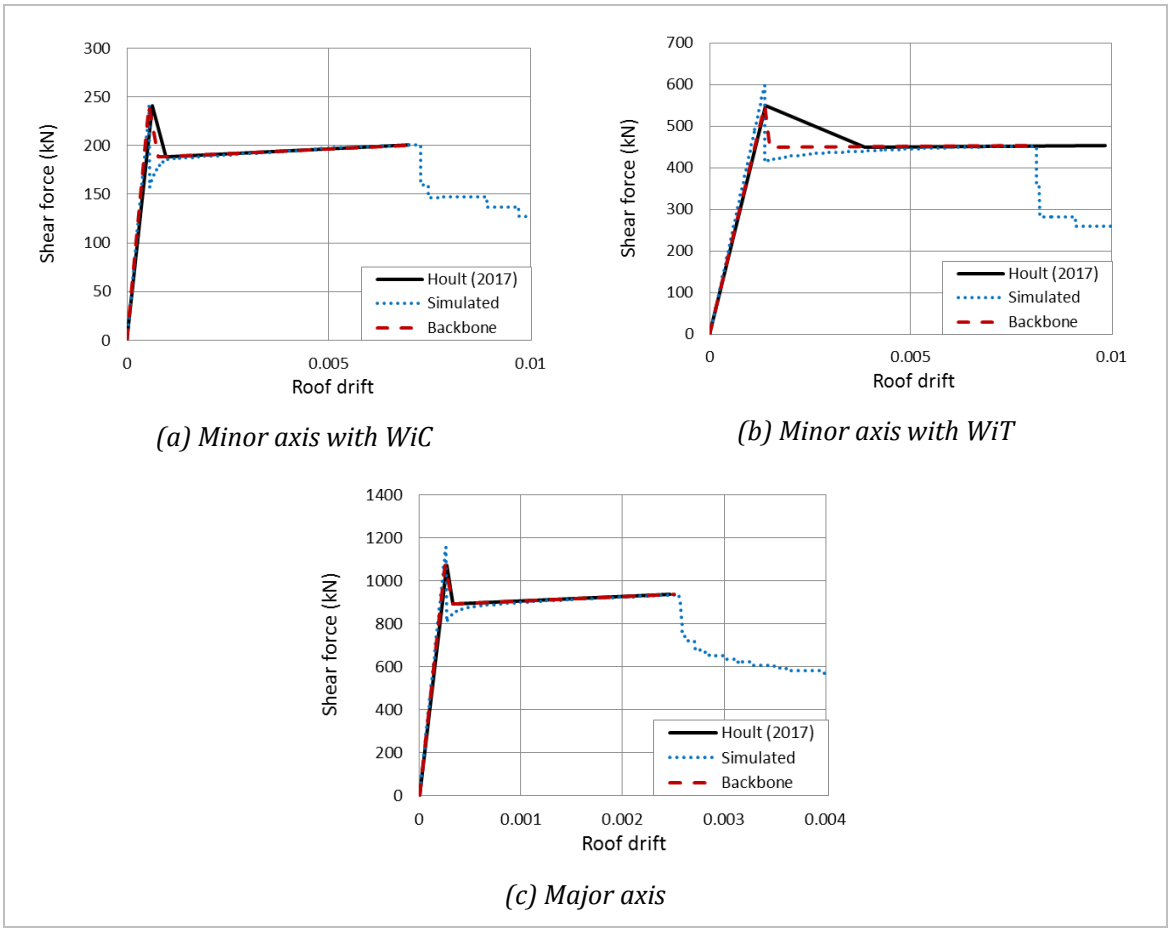

Figure 5-29: Force-deformation response of C-shaped core walls; comparison between Hoult (2017) analytical model, simulated response using distributed plasticity approach, and backbone for lumped plasticity approach

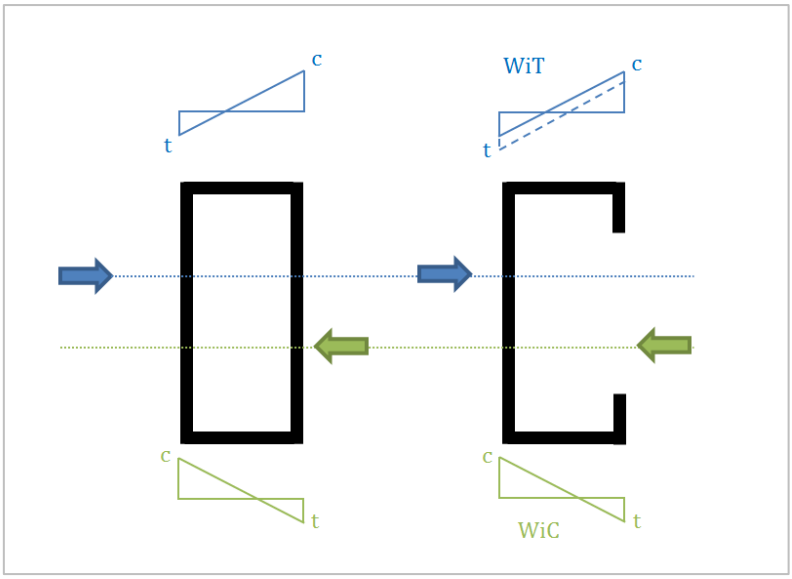

Figure 5-30: Strain distribution of lightly reinforces box-shaped and C-shaped core walls for bending about the minor axis (t: tensile strain, c: compressive strain)

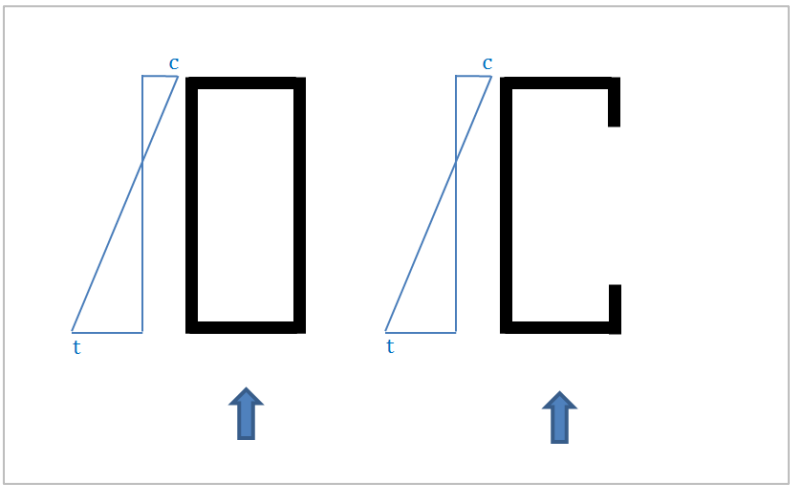

Figure 5-31: Strain distribution of lightly reinforces box-shaped and C-shaped core walls for bending about the major axis (t: tensile strain, c: compressive strain)

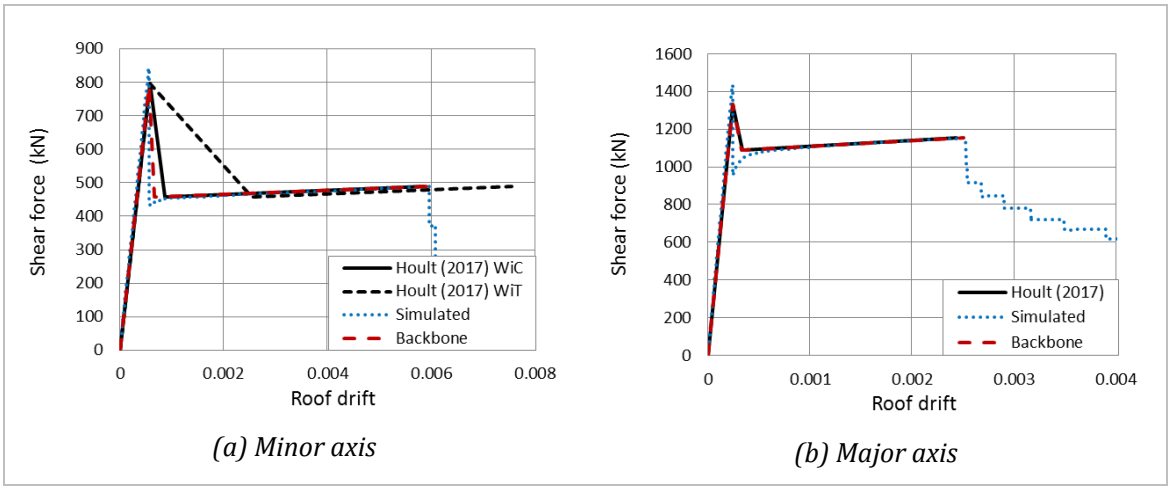

(a) Minor axis *(b) Major axis*

Figure 5-32: Force-deformation response of box-shaped core walls; comparison between Hoult (2017) analytical model, simulated response using distributed plasticity approach, and backbone for lumped plasticity approach

5.5.3 Interconnected wall response

To further investigate the suitable method for modelling the walls for global analysis of the non-ductile buildings, the wall response for three core walls belonging to a 5-storey building is investigated. The configuration of the 3 core walls are provided in Figure 5-33 and the detailing of the walls are the same as in Figure 5-28. Initially the walls are modelled considering only the flexural response of the walls. Two models are created: (i) force-based distributed plasticity elements are used to model the core walls using the conventional stick model and the plastic hinge region is explicitly modelled as described in Section 5.5.1 based on the equivalent plastic hinge length, (ii) lumped plasticity approach is used to model the inelastic response of the walls with a moment-rotation spring at the base of the wall. The three core walls are connected via a rigid diaphragm, schematic of both approaches is illustrated in Figure 5-34.

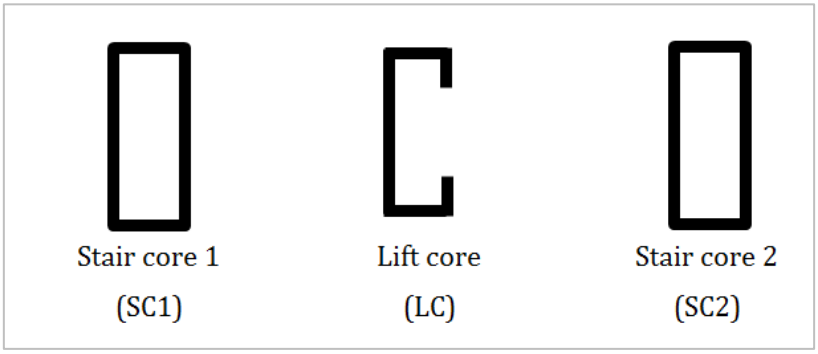

Figure 5-33: Schematic showing plan congfiguration of interconnected core walls

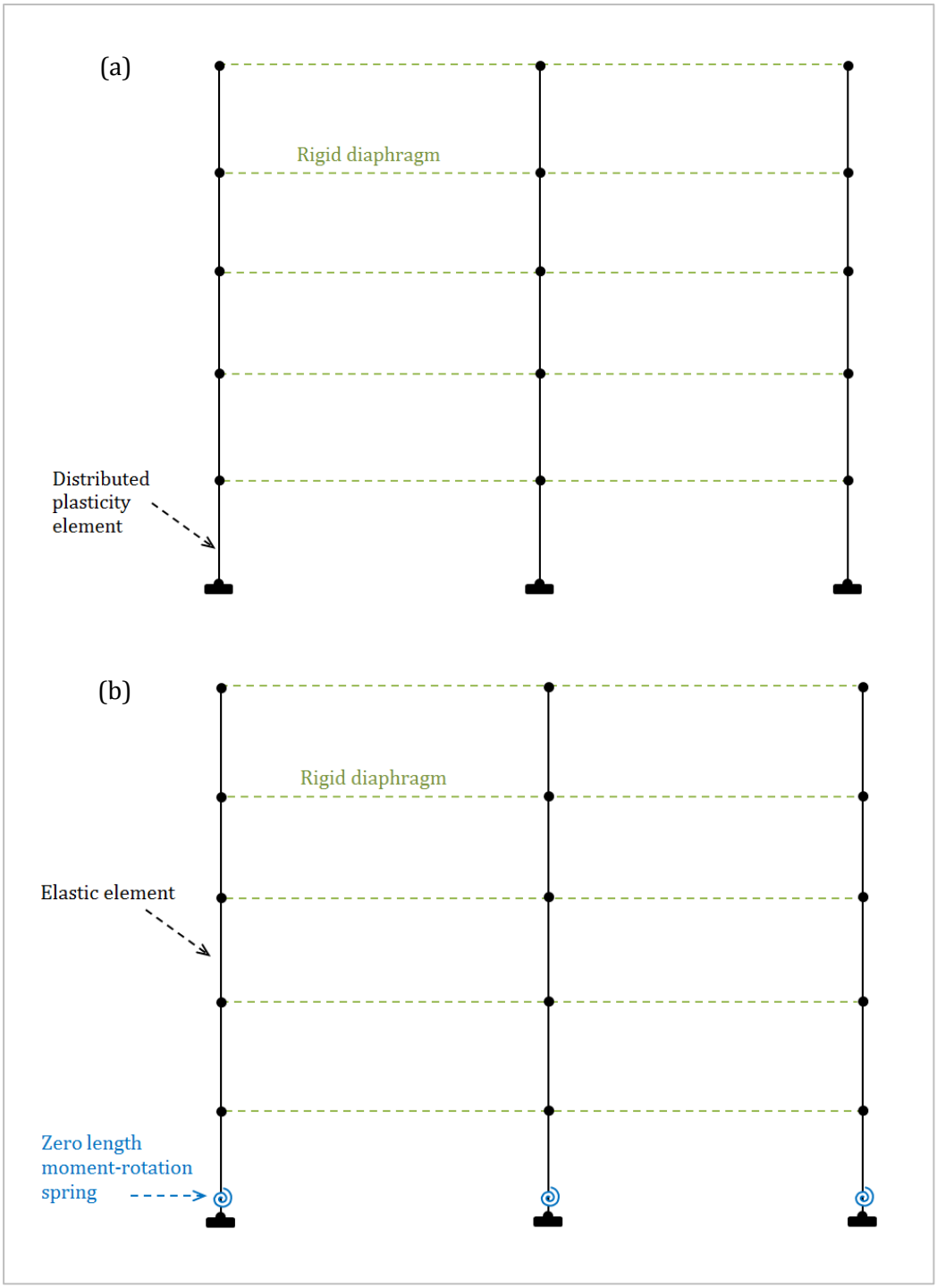

Figure 5-34: Schematic showing the elevation configuration of interconnected core walls: (a) distributed plasticity approach, (b) lumped plasticity approach

Pushover analysis is conducted on the interconnected core walls with an applied force distribution that follows the first mode of the walls. A displacement controlled integrator is used to conduct the pushover analysis to allow the simulation of the reduction in the applied forces due to the change in the stiffness of the system (i.e. after the peak capacity of the system is reached). The base moment and base shear response versus the roof

displacement for the two approaches are provided in Figure 5-35. It is noted that it was very difficult to achieve numerical stability for the distributed plasticity approach. Therefore, other methods of modelling and simplifications were also considered, including only modelling the plastic hinge region with either a force-based or displacement-based distributed plasticity element and the remaining portion of the wall with elastic elements. However, none of the approaches helped to improve numerical stability. This is due to the nature of the walls being assessed, with low longitudinal reinforcement ratio and non-ductile detailing which results in sudden lateral strength degradation. This effect is exacerbated when the walls have a higher cracking moment than the yield moment capacity. Once the cracking moment is reached, which occurs at a very low displacement, abrupt degradation in the lateral strength occurs as the strength reduces to the yield moment capacity and hence the forces applied to the system need to be redistributed to the adjoining components.

The plot of base-shear versus roof displacement in Figure 5-35 indicate that once the two stair cores reach the cracking moment (this occurs simultaneously for the two box-shaped core walls since they have identical detailing), very high shear forces are developed in the lift core, that is, the C-shaped wall which is more flexible than the stair cores. This occurs due to the internal forces which are developed to maintain the same displacement at each storey (due to the rigid diaphragm assumption), since the displacement profile of the stair cores changes from an elastic response to a plastic response after cracking. Furthermore, an increase in shear force is also induced in the lift core once the stair cores reach their ultimate bending capacity since their bending capacity decreases after that. This same behaviour was described in Section 4.6.4 with respect to yielding of two walls with different wall lengths; however, for the interconnected wall response considered here the phenomenon occurs after the cracking moment, and subsequently the ultimate moment, of the stiffer walls are reached. The results show that the shear induced in the lift core is higher for the model which used the distributed plasticity approach than for the model which used the lumped plasticity approach, especially after the cracking moment of the stiffer walls is reached. This is in contrast to the behaviour described in Beyer et al. (2014), where it was shown that the shear force induced in the flexible wall was higher for the lumped plasticity approach in comparison to the distributed plasticity approach. The conflicting results are purely numerical, and the peak shear forces developed are not reliable. As expected, it can be seen that the total response of the system is approximately the same for the distributed and lumped plasticity approach. Furthermore, the base-moment versus roof displacement response is also approximately the same for the

distributed and lumped plasticity approach for both the total system response and the individual core wall responses.

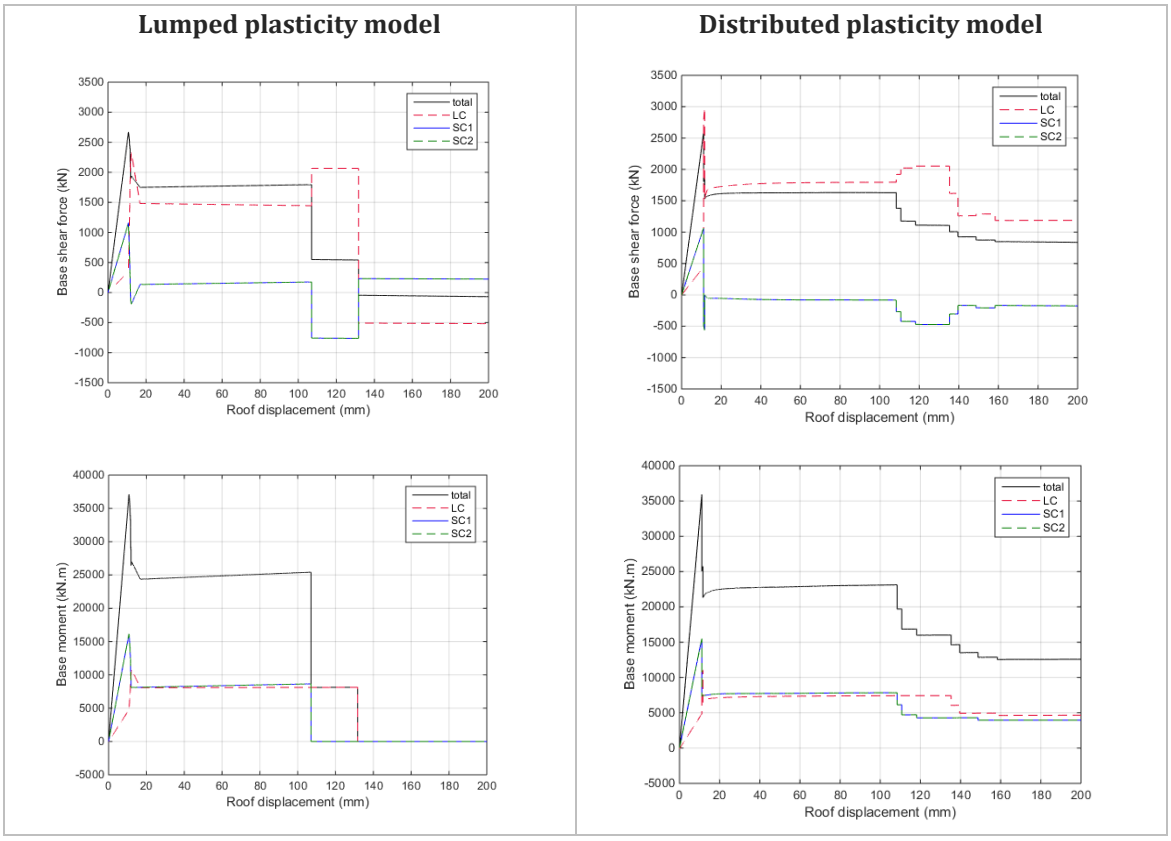

Figure 5-35: Response of interconnected core walls under pushover analyses for walls modelled using lumped plasticity and distributed plasticity approach

Due to the computational inefficiency and unreliability of the distributed plasticity approach for simulating the interconnected wall response for the type of walls to be assessed in this study, the lumped plasticity approach is adopted to conduct the assessment of the buildings in Chapter 7. As discussed in Section 3.4.3, it is expected that the walls will predominantly fail in a flexural manner due to the aspect ratio of the walls assessed and also due to the limited cracking forming at the base of the walls. However, since the interconnected wall response indicated that high shear forces may be developed, the sensitivity of the shear forces induced in the core walls due to modelling assumptions is further investigated to ensure that the walls are not vulnerable to shear failure due to high shear force demands. Shear springs are added at the base of the wall (illustrated in Figure 5-36) to include shear flexibility of the walls as suggested by Beyer et al. (2014) to improve the shear distribution between interconnected walls. The approach suggested by Beyer et al. (2011) (discussed in Section 4.6.2), which involves computing shear deformations based on the ratio of shear deformation to flexural deformation $\left(\frac{\Delta_{shear}}{\Delta_{flex}}\right)$, is

used to quantify the stiffness of the linear elastic shear spring. Three different shear deformation to flexural deformation ratios are investigated, which are calculated at nominal yield:

i. $\frac{\Delta_{shear}}{\Delta_{flex}} = 1\%$

ii. $\frac{\Delta_{shear}}{\Delta_{flex}}$ is calculated according to the method proposed by Beyer et al. (2011), for which the shear deformations to flexural deformations is approximated 4 to 10 %

iii. $\frac{\Delta_{shear}}{\Delta_{flex}} = 10\ \%$

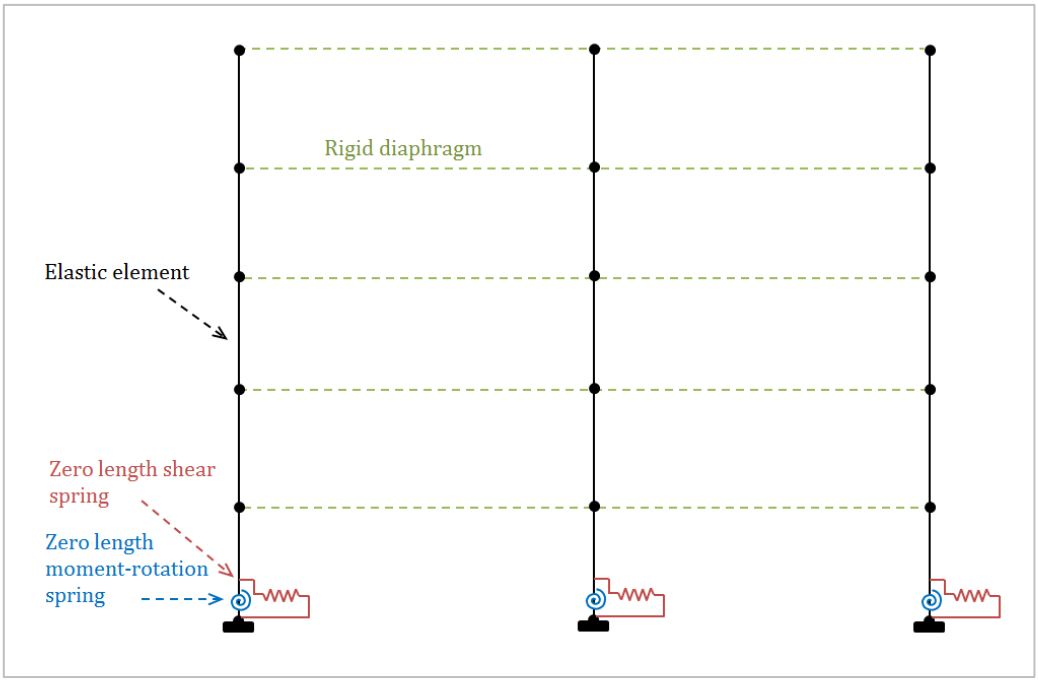

Figure 5-36: Schematic showing the elevation configuration of interconnected core walls with moment rotation spring and shear spring

The base-shear versus roof displacement and base-moment versus roof displacement for the different shear deformation to flexural deformation ratios are presented in Figure 5-38 and Figure 5-37 for pushover analyses about the minor axis of the interconnected core walls with WiT and WiC for the lift core, respectively. The results show up to more than 50 % reduction in the peak shear force developed in the lift core (the more flexible wall) once shear flexibility is incorporated and using the assumption that the shear deformation to flexural deformation ratio is only 1 %. Further reductions in the peak shear force are observed when the shear deformation to flexural deformation ratio is calculated in accordance with the method proposed in Beyer et al. (2011), and when the shear deformation to flexural deformation ratio is set to 10 %. The significant reduction in shear force indicates that shear failure of the walls is unlikely to occur prior to the flexural

failure of the walls, since the peak shear forces observed during the analysis are predominantly numerical. Furthermore, in addition to the shear flexibility of the core walls, there are also other factors that may affect the redistribution of shear forces which are not explicitly modelled, including slab flexibility and foundation flexibility, which may result in lower shear forces induced in the core walls. For the example interconnected wall system considered here, the shear capacity of the core walls along the weak direction (calculated in accordance with AS 3600:2009) is approximately more than twice the induced shear force obtained from the pushover analysis when the shear flexibility of the walls is calculated using the method proposed in Beyer et al. (2011). Since the simulation of the distribution of shear forces is not highly reliable (due to modelling limitations) and the likelihood of shear failure for the walls assessed is low, shear failure of the walls is not considered for the assessment of the archetypal buildings in Chapter 7.

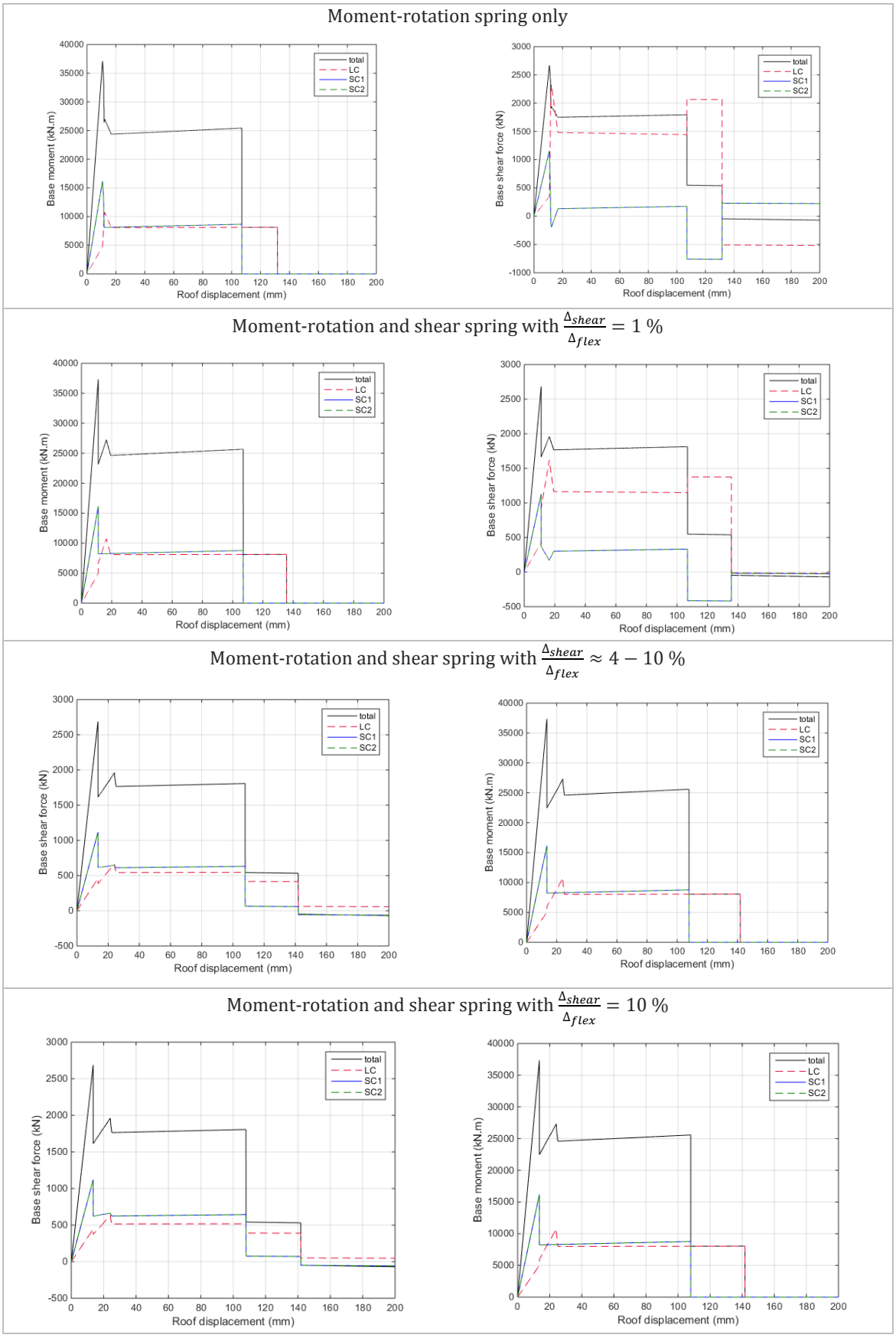

Figure 5-37: Response of interconnected core walls under pushover analyses with lift core WiT for different levels of shear flexibilities

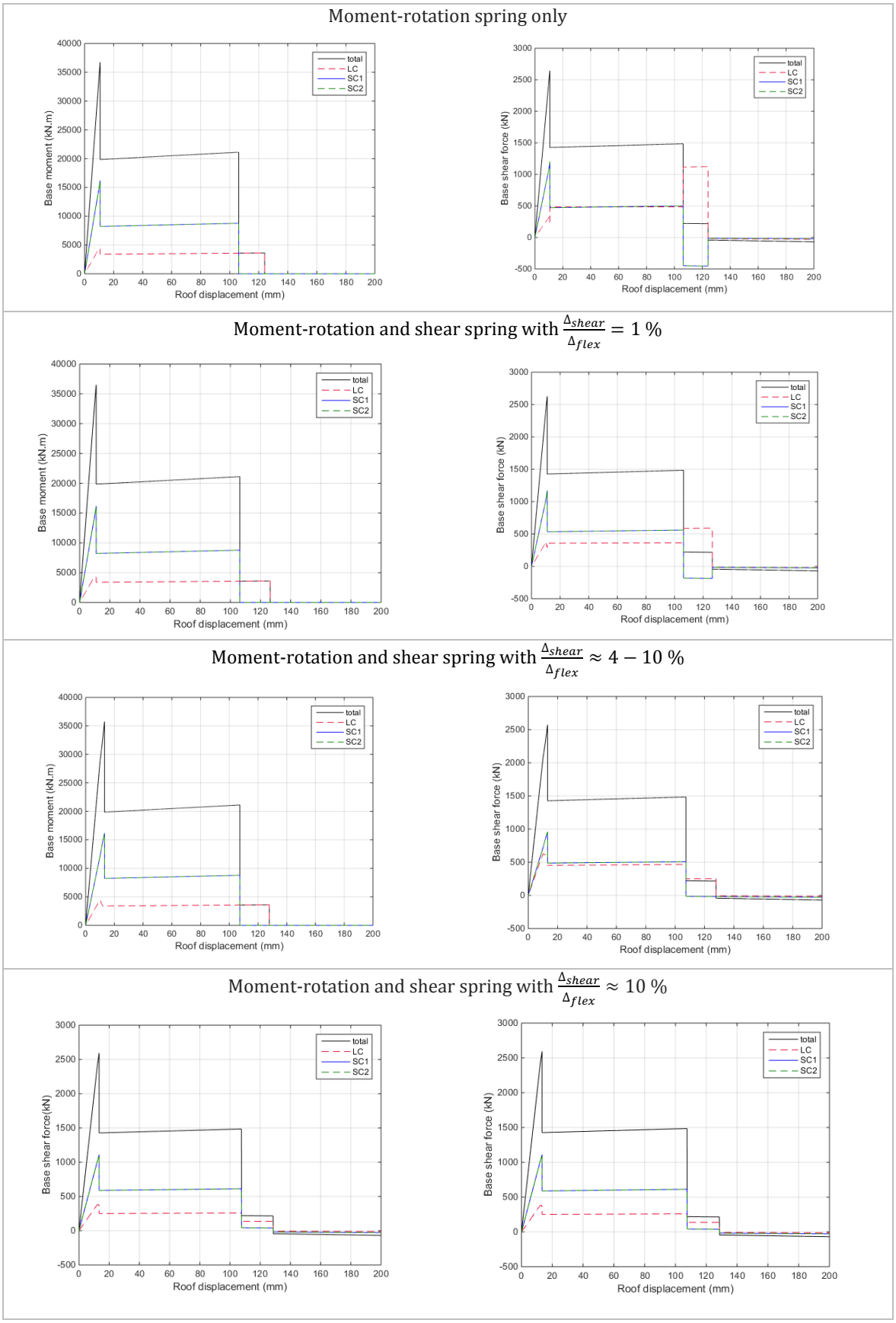

Figure 5-38: Response of interconnected core walls under pushover analyses with lift core WiC for different levels of shear flexibilities

5.6 SUMMARY

This chapter has provided a detailed evaluation of macro-modelling approaches for simulating the response and failure mechanisms of various building components including: beam-column joints, columns and beams, and walls. Specifically, the modelling approaches have been evaluated for the type of detailing that the building components are likely to have for the archetypal buildings to be assessed in Chapter 7. In general, the non-ductile detailing of the building components significantly increases the difficulty of simulating their response under seismic loading since sudden lateral strength and stiffness degradation are likely to occur after the peak capacity of the components is reached. The sudden degradation of lateral strength and stiffness typically causes numerical instabilities and convergence issues, especially when considering the system response of the building. Furthermore, some response mechanisms, namely shear and bar-slip, are not directly modelled using conventional macro-modelling approaches and must be included indirectly; this is especially true if the response is likely to govern the failure mechanism of the component. Additionally, these mechanisms are usually computed using empirically based equations and thus suitable equations need to be selected for the components being assessed. The component modelling approaches which are to be adopted for conducting the assessment of the archetypal buildings have been validated by comparing the simulated response of the components with experimental results or numerical models established from micro-finite element modelling analyses. Furthermore, a range of modelling approaches has been evaluated and the ones chosen for each component have required a compromise between accuracy, computational efficiency and reliability. This has resulted in the selection of the lumped plasticity approach rather than the distributed plasticity approach for modelling the various building components.

CHAPTER 6: FRAMEWORK FOR SEISMIC FRAGILITY ASSESSMENT

6.1 INTRODUCTION

In this chapter a review of the seismic fragility assessment framework is provided as well as the approach to be adopted to assess the seismic performance of the archetypal buildings presented in Chapter 7. The formulation for fragility curves, including the incorporation of aleatoric and epistemic uncertainties, is described. The selection and justification of the various aspects of the assessment framework are provided, including: the probabilistic seismic demand models, performance levels, and performance objectives. Furthermore, the advantages and disadvantages of the various ground motion intensity measures and the different methods to compute the intensity measure are presented.

6.2 SEISMIC FRAGILITY FUNCTIONS

Seismic fragility functions define the building's probability of exceeding a damage limit state as a function of ground motion intensity measure (IM). In its most common form it is defined by the lognormal cumulative distribution function (Porter, 2016) given in Eq. 6-1. Hence, it is assumed that the relationship between the seismic demand (D) and the structural capacity (C) is normally distributed. This has been proven to be a reasonable assumption by numerous studies as discussed in Baker (2015), although, different distributions may be adopted to produce fragility curves.

$$P[D > C|IM] = \phi \frac{\ln(S_D/S_C)}{\beta} \quad \text{Eq. 6-1}$$

Where ϕ is the standard normal cumulative distribution function

S_C is the median value of the structural limit state (i.e. the capacity of the structural limit state)

S_D is the median value of the demand as a function of IM

β is the logarithmic standard deviation of the demand as a function of IM

The fragility function expressed in Eq. 6-1 is suitable when the engineering demand parameter (EDP) used to assess the performance of the buildings is not dependent on individual component capacities. In this study, the performance levels for the buildings are based on when the first component in a building reaches a structural damage limit or when the interstorey drift demand exceeds the interstorey drift limits; this is discussed in detail in Section 6.4. Therefore, the EDP adopted in this study is the critical demand-to-

capacity ratio (Y) which corresponds to the component response or interstorey drift that will first cause the building to reach the performance level (Jalayer et al., 2007). The fragility function for which the engineering demand parameter is the critical demand-to-capacity ratio is provided in Eq. 6-2. Furthermore, Eq. 6-2 also incorporates aleatoric and epistemic uncertainties within the fragility function.

$$P[\mathrm{Y} > 1|IM] = \phi \frac{\ln(\eta_{\mathrm{Y}|IM})}{\sqrt{\beta^2_{\mathrm{Y}|IM} + \beta_C^2 + \beta_M^2}} \quad \text{Eq. 6-2}$$

Where $\eta_{\mathrm{Y}|IM}$ is the median critical demand-to-capacity ratio as a function IM

$\beta_{\mathrm{Y}|IM}$ is the dispersion (logarithmic standard deviation) of the critical demand-to-capacity ratio as a function of IM

β_C is the capacity uncertainty

β_M is the modelling uncertainty

Aleatoric uncertainties are caused by factors that are inherently random in nature, whereas epistemic uncertainties are knowledge-based due to assumptions and modelling limitations and hence may be reduced with improved knowledge and modelling methods (Celik, 2007). The aleatoric uncertainty related to the critical demand-to-capacity ratio (as a function of IM), $\beta_{Y|IM}$ is calculated based on the time history analysis results. The dispersion related to the uncertainty of determining the capacity of structural components, β_C (aleatoric uncertainty) and the dispersion due to modelling uncertainties, β_M (epistemic uncertainty) are usually computed based on recommendations provided by other studies and guidelines (Jeon et al., 2015; Nazari, 2017; Seo et al., 2015). Wen et al. (2004) investigated the effect of developing fragility curves for older RC frames using three different levels of modelling uncertainty: 0.2, 0.3, and 0.4. The results demonstrated relatively insignificant differences between the fragility curves obtained and therefore suggest using 0.3. FEMA-P695 (Applied Technology Council, 2012) provides recommendations for modelling uncertainty depending on how well the index archetype building models represent the various range of structural collapse characteristics, and the accuracy and robustness of the model for capturing the various structural collapse mechanisms. The recommended values are provided in Table 6-1. With respect to predicting the capacity of components FEMA-P58 (Applied Technology Council, 2012) discusses that the uncertainty depends on the type of failure mode. It suggests that for brittle failure modes higher uncertainty factors should be adopted due to the greater difficulty in predicting the capacity. It is suggested that a default value of 0.25 can be adopted for brittle failure modes.

In this study the dispersion associated with modelling uncertainty (β_M) is set to 0.2 since according to the FEMA-P695 (Applied Technology Council, 2009) classification a Good representation of structural collapse is provided by the archetypal building models. The dispersion related to uncertainty in predicting the capacity of components (β_C) is conservatively set to 0.3 (slightly greater than the FEMA-P58 suggestion) since the buildings assessed have non-ductile detailing and are vulnerable to brittle and sudden failures.

Table 6-1: FEMA-P695 recommended quality rating for index archetype models (Applied Technology Council, 2009) discusses

Representation of Collapse Characteristics	Accuracy and Robustness of Models		
	High	Medium	Low
High. Index models capture the full range of the archetype design space and structural behavioral effects that contribute to collapse.	(A) Superior $\beta_{MDL} = 0.10$	(B) Good $\beta_{MDL} = 0.20$	(C) Fair $\beta_{MDL} = 0.35$
Medium. Index models are generally comprehensive and representative of the design space and behavioral effects that contribute to collapse.	(B) Good $\beta_{MDL} = 0.20$	(C) Fair $\beta_{MDL} = 0.35$	(D) Poor $\beta_{MDL} = 0.50$
Low. Significant aspects of the design space and/or collapse behavior are not captured in the index models.	(C) Fair $\beta_{MDL} = 0.35$	(D) Poor $\beta_{MDL} = 0.50$	--

6.3 PROBABILISTIC SEISMIC DEMAND MODEL

To compute the fragility function, it is first necessary to develop a probabilistic seismic demand model (PSDM) which relates the engineering demand parameter (in this study, the critical demand-to-capacity ratio) to the intensity measure. There are various procedures used to obtain the PSDM; the well-established methods which are obtained through conducting dynamic nonlinear time history analysis (THA) are incremental dynamic analysis, multiple stripe analysis, and cloud analysis.

Incremental dynamic analysis (IDA) involves scaling a suite of ground motions until the required structural damage limit is reached (Vamvatsikos & Cornell, 2002). The advantage of this approach is that the ground motion variability is eliminated at various ground motion intensities. However, there are many issues and limitations to using scaled records, including the loss of true earthquake characteristics in the scaling process, especially when large scaling factors are used. Despite the limitation of using scaled records, IDA is considered to produce the most complete PSDM due to the numerous time

history analyses conducted at a particular ground motion intensity. The probability of exceeding a damage limit state for each intensity measure is estimated by the fraction of records which cause the damage limit state to be exceeded. Based on this information the empirical cumulative distribution can be plotted for each IM and from which the fragility function parameters; S_D and $\beta_{D|IM}$ (or in this study $\eta_{Y|IM}$ and $\beta_{Y|IM}$) may be approximated as shown in Eq. 6-3 and Eq. 6-4 (Baker, 2015). The procedure is highly computationally expensive since significant number of time history analyses need to be conducted to obtain the fragility function parameters. It is noted that the analyses must be conducted up to an IM for which the building response reaches the damage limit state for all of the records considered in the selected suite of ground motions. Therefore in practice, it is usually only feasible for studies that simplify the building response (i.e. multi-degree-of-freedom system) to a single-degree-of-freedom system.

$$\ln(S_D) = \frac{1}{n}\sum_{i=1}^{n} \ln(IM_i) \qquad \text{Eq. 6-3}$$

$$\beta_{D|IM} = \sqrt{\frac{1}{n-1}\sum_{i=1}^{n}\left(ln\left(\frac{IM_i}{S_D}\right)\right)^2} \qquad \text{Eq. 6-4}$$

Where n is the number ground motions considered

IM_i is the IM value associated with the onset of collapse (or exceedance of damage limit sate) for the i^{th} ground motion

The multiple stripe analysis (MSA) involves conducting multiple time history analyses for a discrete set of IM and for each IM a different suite of ground motion records is selected (Jalayer & Cornell, 2009). The records may still be scaled to the required intensity measure. The method is commonly used when the ground motion properties change for each IM, for example when the conditional spectrum method is used to select ground motions (Baker, 2015). Hence, the method has the potential to provide the most accurate results especially if unscaled records are used for each intensity measure, however, this is rarely done in practice and scaled records are commonly used. Due to the inherent variability of the records used at different intensities, the response obtained from the time history analyses may not necessarily result in an increase of the fraction of responses exceeding the damage limit state with increasing level of IM. Furthermore, unlike IDA, MSA does not require the analyses to be conducted up to an IM for which all of the records cause the building response to exceed the damage limit state. Therefore, the same

procedure used for IDA cannot be adopted to calculate the fragility function parameters. Baker (2015) discusses using the maximum likelihood procedure and binomial distribution to approximate the best fit for the fragility function (i.e. estimates of S_D and $\beta_{D|IM}$) to the data obtained from MSA. Similar to IDA, MSA is computationally expensive if conducted in a manner to meet its full potential.

The most efficient method for obtaining the PSDM is by conducting cloud analysis. It involves using unscaled records to obtain a *cloud* of intensity-response data points. Regression analysis is conducted for the cloud of data to approximate the fragility function parameters. The method requires significantly less THA since multiple analyses at a certain IM is not necessary. However, record selection plays a key role on the accuracy of the method and it is recommended that the suite of records selected cover a wide range of IM and that a significant portion of the records provide data points near the damage limit state (i.e. for this study when Y=1) (Jalayer et al., 2017; Rajeev et al., 2014). Furthermore, unscaled records must be used which eliminates the issues related to using scaled records. Another key advantage of the cloud analysis method is that for the same set of analyses different IMs may be selected to obtain different PSDM and from the regression analyses it is possible to select the best IM to represent the demand quantity (Rajeev et al., 2014). A disadvantage of cloud analysis is that it assumes a constant conditional standard deviation for the probability distribution of the engineering demand parameter given IM (Jalayer et al., 2014). The method was in fact initially utilised by Cornell et al. (2002) to support a power-law demand model with a constant standard deviation of the natural logarithm, provided in Eq. 6-5. More complex demand models have been proposed by other researchers (Aslani & Miranda, 2005), however, studies have illustrated that Eq. 6-5 is capable of providing accurate results and it is preferred due to its simplicity and because it ensures closed-form solutions (Rajeev et al., 2014).

$$\eta_{\mathrm{Y}|IM} = a.IM^{b} \qquad \text{Eq. 6-5}$$

Where $a\ and\ b$ are the parameters obtained from regression analysis

Furthermore, since the parameters $\eta_{\mathrm{Y}|IM}$ and $\beta_{\mathrm{Y}|IM}$ obtained using the cloud analysis method are based on the correlation of the structural response to a given intensity measure, it may be necessary to separate the results obtained from the analyses which have encountered numerical instabilities. This is particularly important when evaluating the response of nonlinear building models up to the point of collapse since it is likely that numerical instabilities will occur for stronger ground motion records. Therefore

researchers have suggested calculating the fragility function according to Eq. 6-6, where the collapse (c) and non-collapse ($\bar{c}$) cases are separated (Rajeev et al., 2008; Shome & Cornell, 2000). It is noted that collapse cases do not refer to all cases for which the performance level has been exceeded (i.e. in this study when Y > 1.0); instead, it refers to cases for which the results are considered to be unreliable due to numerical instabilities (which occur after the building exceeds the Collapse Prevention or Near Collapse performance levels) or the performance level has been exceeded by a significant amount. In this study four different performance levels are investigated, therefore it is expected that Y will be significantly greater than 1.0 for performance levels corresponding to lower levels of damage. Thus, limits defining *collapse* cases should be carefully defined for each performance level.

$$P(\mathrm{Y} > 1|IM) = P(\mathrm{Y} > 1|IM, \bar{c}).[1 - P(c|IM)] + P(c|IM) \quad \text{Eq. 6-6}$$

Where $\bar{c}$ is the non-collapse situation

c is the collapse situation

$P(\mathrm{Y} > 1|IM, \bar{c})$ is provided in Eq. 6-7

$P(c|IM)$ is provided in Eq. 6-8

$$P(\mathrm{Y} > 1|IM, \bar{c}) = \frac{\ln(\eta_{Y|IM,\bar{c}})}{\sqrt{\beta^2_{Y|IM,\bar{c}} + \beta^2_C + \beta^2_M}} \quad \text{Eq. 6-7}$$

$$P(c|IM) = \frac{no.of\ records\ causing\ collapse}{total\ no.of\ records} \quad \text{Eq. 6-8}$$

In this study the cloud analysis method is adopted to obtain the PSDM due to the advantages discussed above. It is the most suitable method for conducting 3D global analysis of buildings for which limit states are determined based on component responses. The fragility function is computed using Eq. 6-6 and Eq. 6-5 is adopted to approximate the fragility function parameters.

6.4 PERFORMANCE LEVELS

There are many different performance levels which are defined in the literature and codes, each with different acceptance criteria. In general, the acceptance criteria in codes are considered to be conservative, and often researchers try to change the definition of the performance levels using the improved accuracy from numerical models and modelling methods to incorporate various failure mechanisms. The following section provides a

review of the performance levels defined in the literature and codes, and the proposed levels for this study are presented. Since there are numerous terminologies used to define various performance levels, the section below provides a review for four general damage states: (i) slight damage, (ii) moderate damage, (iii) extensive damage, and (iv) complete damage. Furthermore, in this study both primary (RC walls) and secondary (gravity RC frames) structural systems are modelled, therefore, the performance levels are defined separately for the different systems. A similar approach is recommended by ASCE 41 (ASCE/SEI, 2013). Interstorey drift limits are also provided to control the damage caused to non-structural components and to alleviate the danger of a side-sway collapse mechanism forming. It is noted that in this study, interstorey drift is expressed as a ratio of the interstorey relative lateral displacement to the storey height.

6.4.1 Slight damage

Performance limits that typically fall within the *Slight Damage* criteria are: *Operational*, *Serviceability*, and *Immediate Occupancy*.

The *Operational* or *Serviceability* limit state essentially refers to a limit state for which the structure remains operational after an earthquake, and hence the damage (if any) is very minor. This damage state corresponds to the building elements remaining elastic or close to elastic.

Priestley et al. (2007) define the *Serviceability* limit state by proposing strain limits. They state that the compression strain limit at this limit state should be a "conservative estimate of the strain at which spalling initiates." They suggest a compression strain limit of 0.004 for concrete and 0.002 for masonry. For the tensile limit, Priestley et al. (2007) argue that an 'elastic' or 'near elastic' limit which is the traditional approach, is too conservative since strains of several times the yield strain can be sustained by the reinforcement without requiring repair. Instead, they state that the tensile limit should be based on limiting crack widths to approximately 1.0 mm. Based on experimental findings; they recommend tensile strain limits of 0.015 for members carrying axial compression, and 0.01 for members without axial compression. Hoult (2017) assessed the performance of RC walls in Australia and adopted more conservative strain limits than Priestley et al. (2007) for the *Serviceability* limit state due to the non-ductile detailing of the walls that were assessed. Hoult (2017) suggested adopting a compression strain limit of 0.001 to ensure a close to elastic response for the concrete, and a tensile strain limit of 0.005 to ensure small residual crack widths.

The *Immediate Occupancy* structural performance level is defined in ASCE 41 (2013) as "… postearthquake damage state in which only very limited structural damage has occurred" and that the "… basic vertical- and lateral-force-resisting systems of the building retain almost all of their preearthquake strength and stiffness." A similar definition was adopted by Celik and Ellingwood (2010) who assessed the performance of limited ductile RC frames.

It is also necessary to adopt non-structural performance limits to account for the damage that may occur to non-structural components. Sullivan et al. (2012) suggest limiting the maximum interstorey drift to 0.4 % for buildings with brittle non-structural elements and 0.7 % for buildings with ductile structural elements. These drift limits correspond to a performance limit state defined as *No Damage*.

The *Serviceability* performance level is selected here to correspond to *Slight Damage* limit state. Since the walls in this study are likely to experience a single crack and to have cracking moment capacities which exceed the yield moment capacity, it is suggested that the *Serviceability* limit state is defined as when the walls reach initial yield. This is because a significant increase in strains, especially in the longitudinal reinforcement bars, is likely to follow shortly after initial yield is reached. For the sake of completeness, nominal yield is taken as determining when the *Serviceability* limit state for the secondary structure is reached, although this is unlikely to govern. For non-structural damage, a maximum interstorey drift of 0.4 % is suggested as older buildings (and current buildings) are likely to have brittle non-structural components.

6.4.2 Moderate damage

The *Moderate Damage* state corresponds to damage levels which are repairable and therefore it has been identified here to correspond to *Damage Control* and *Repairable Damage* performance levels described in the literature.

Priestley et al. (2007) define the compressive strain limit at the *Damage Control* limit state to correspond to when the transverse reinforcement confining the core fractures. The compressive strain limit at this limit state is obtained by adding the strain-energy capacity of the confining steel to the unconfined strain energy of the concrete. Hence, the compressive strain at damage control ($\varepsilon_{c.dc}$) is defined as:

$$\varepsilon_{c.dc} = 0.004 + 1.4\frac{\rho_{tv} f_{yt} \varepsilon_{su}}{f'_{cc}} \quad \text{Eq. 6-9}$$

Where ρ_{tv} is the volumetric ratio of transverse reinforcement

f'_{cc} is the compression strength of confined concrete

For the tensile limit at the *Damage Control* limit state, Priestley et al. (2007) recommend adopting 0.6 times the ultimate tensile strain of steel obtained from monotonic tensile tests. The reduced ultimate tensile strain is said to account for the decrease of steel tensile strain capacity due to: cyclic loading, vulnerability of reinforcement to buckling after it has experienced tensile strains, low-cycle fatigue, slip between reinforcing steel and concrete at critical section, and tension shift effects which result in higher strains being developed in the steel than those obtained from sectional analyses which assume plane-sections. However, Priestley et al. (2007) state that to ensure this level of strain is attainable without the buckling of longitudinal bars, the spacing of transverse reinforcement hoops and ties (s) should not exceed the value calculated in accordance with Eq. 6-10.

$$s = 3 + 6\left(\frac{f_u}{f_y} - 1\right) d_b \qquad \text{Eq. 6-10}$$

Hoult (2017) suggests adopting a compression strain limit of 0.002 to reduce the likelihood of spalling and a tensile strain limit of 0.01 to reduce the likelihood of low-cycle fatigue and out of plane buckling of the reinforcement during load reversals.

Sullivan et al. (2012) suggest limiting the maximum interstorey drift to 2.5 % for buildings with both brittle and ductile non-structural elements, for performance limit state corresponding to *Repairable Damage*. The New Zealand Standard, NZS 1170.5 (Standards New Zealand, 2004) requires the interstorey drift limit to also be limited to 2.5 % for the performance limit state corresponding to *Damage Control*. The Australian Standard, AS 1170.4 (Standards Australia, 2007) requires a more conservative interstorey drift limit of 1.5 % for the *Ultimate* limit state. In the commentary for AS 1170.4 (Standards Australia, 1993) it is explained that this drift limit is intended to "… restrict damage to partitions, shaft and stair enclosures and glazing…" as well as indirectly providing an upper bound for P-delta effects. Thus the limit set by AS 1170.4:2007 may be interpreted as either the *Damage Control* or *Life Safety* performance limit state. However, it is important to note that in Australia little consideration is given to the seismic drift capacity of non-structural components. McBean (2008) highlighted, based on limited available data from manufacturers, that non-structural components (curtain walls) may reach ultimate conditions at interstorey relative displacements of 30-50 mm or less.

It is noted that the strain limits provided by Priestley et al. (2007) are predominantly based on the response of ductile components, and therefore they are considered to be un-conservative for non-ductile components. Non-ductile buildings display an "on-off" behaviour as described by Pampanin et al. (2011) where the building essentially responds in either an elastic manner or a brittle failure is experienced. This behaviour was observed for some of the non-ductile RC buildings in the Canterbury Earthquake sequence, namely the Pyne Gould and the CTV building. Both of these buildings displayed minor damage after the Darfield earthquake (which corresponded to approximately a 500 year return event for Christchurch), however, after the Christchurch earthquake (an approximately 2500 year return period event for Christchurch) both of the buildings failed catastrophically (Goldsworthy, 2012; Goldsworthy & Gibson, 2012). Therefore, conservative strain limits are suggested here to define the *Damage Control* limit state to alleviate the danger of sudden brittle failure mechanisms forming.

In non-ductile RC components ultimate flexural capacity is reached at when the cover concrete reaches compressive strains of 0.003 to 0.004 based on the assumption that the concrete in compression at these strain limits will crush. At slightly greater compressive strain limits significant spalling of the cover may lead to the buckling of longitudinal bars and crushing of the inner (core) concrete due to the lack of confinement provided. Therefore, the damage caused would lead to significant repair costs thus exceeding the *Damage Control* limit state. In addition, lower tensile strain limits than those suggested by Priestley et al. (2007) are likely to be suitable for walls with low longitudinal reinforcement ratios and with longitudinal bars that are not well restrained. This is because the walls are vulnerable to having a single crack form at the base leading to strain localisation, and to buckling after high strains have been reached in tension. Therefore, it is suggested for the primary structures (walls) assessed in this study that the *Damage Control* structural limit state should correspond to a concrete compressive strain limit of 0.002, and a tensile strain limit of 0.015, whichever one occurs first. A higher tensile strain limit than that adopted by Hoult (2017) is thought to be suitable in this study since the walls assessed have Y-bars and hence a design ultimate strain of 0.12, in comparison to the walls assessed by Hoult (2017) which had N-bars and hence a design ultimate strain of 0.05. For the purpose of this study the *Damage Control* limit state for the secondary structure (frame components) is defined as the component rotation corresponding to the point midway between the nominal yield rotation and the shear failure rotation. For the non-structural damage limit, a maximum interstorey drift of 0.8 % is suggested, although

it is acknowledged that further research is required for determining non-structural drift limits in Australia.

6.4.3 Extensive damage

The *Extensive Damage* limit state described here corresponds to the *Life Safety* performance level, which is defined in ASCE 41 (ASCE/SEI, 2013) as the post-earthquake damage state "… in which significant damage to the structure has occurred but some margin against either partial or total structural collapse remains." ASCE 41 (ASCE/SEI, 2013) describes the extent of this damage limit state for walls as one in which some spalling and crushing, and limited buckling of bars, are allowed. For secondary non-ductile frame elements, this corresponds to limited cracking and splice failure of some columns.

In this study the *Life Safety* limit state essentially describes the initiation of loss of the lateral load resisting system. It corresponds to the ultimate drift capacity for the RC walls. Therefore, it is suggested that the compressive strain limit in the primary structural system (walls) be limited to 0.004, which corresponds to the compressive strain used in this study to determine the ultimate moment capacity of wall sections. The tensile strain is limited to 0.6 times the uniform tensile strain for the reasons suggested by Priestley et al. (2007) for the *Damage Control* limit state, but due to the dangers associated with strain localisation, and hence the potential rupture of the longitudinal bars characteristic of the walls assessed in this study, these strain limits are more applicable at the *Life Safety* limit state. For the secondary system, it is suggested that the rotation of the elements be limited to the rotation which defines shear failure, since this corresponds to the point at which the lateral load resistance decreases. For the non-structural *Life Safety* limit state, a maximum interstorey drift of 1.5 % is suggested in accordance with AS 1170.4:2007 for the *Ultimate* limit state.

6.4.4 Complete damage

The *Complete Damage* limit state is defined here to refer to the *Collapse Prevention* or *Near Collapse* performance level. In more recent studies, the point at which a building may be defined as collapsed (or near collapse) has evolved and may be determined via various mechanisms as discussed in Baradaran Shoraka et al. (2013). These mechanisms can be categorised in to three groups:

i. Side-sway collapse

This mechanism may be obtained from incremental dynamic analysis (IDA) and it corresponds to the system experiencing large increase of lateral deformations with small increase in seismic intensity. This mechanism is usually observed with

ductile-structures that consist of components which are capable of experiencing large deformations prior to axial load failure.

ii. *First component failure*

Collapse of a building is determined based on the first component within the building to reach the collapse limit state. This is the approach which is usually adopted by codes, including ASCE/SEI 41 (2013).

iii. *Gravity-load collapse (system collapse)*

Collapse of a building is dependent on multiple components reaching the collapse limit state which will cause a global or system collapse of the building. Baradaran Shoraka et al. (2013) define gravity collapse as when the gravity load demand exceeds the gravity load capacity for a particular storey for the assessment of RC frames. It is noted this mechanism of collapse limit state can only be conducted if the nonlinear model has the ability to accurately simulate shear strength and axial load capacity degradation.

In the past, interstorey drift limits have also been provided as a guide to ensure that realistic building response is obtained (ASCE/SEI, 2006; FEMA, 2000). In FEMA 356 (2000) it is explained that the interstorey drift limits recommended for the structural response of the buildings is "… to illustrate the overall structural response associated with various Structural Performance Levels." The structural interstorey drift limit is particularly important at performance levels corresponding to high levels of damage since numerical models become less reliable. In addition, at the *Collapse Prevention* limit state, interstorey drift limits alleviate the danger of a side-sway collapse mechanism forming. For the *Collapse Prevention* limit state, FEMA 356 (2000) and ASCE 41 (2006) suggest limiting the maximum interstorey drift limit to 2 % and 4 % for buildings with concrete walls and concrete frames forming part of the lateral load resisting system, respectively. Interestingly, the recommendations for the structural interstorey drift limits are not provided in ASCE 41 (2013). Furthermore, it is noted that interstorey drift limits are not required for limiting damage to non-structural components at the *Collapse Prevention* limit state since it is likely that they would have completely failed at the *Extensive Damage* limit state.

In this study, the *Collapse Prevention* limit state is defined as when the first component reaches axial load failure. Hence the first component failure mechanism for defining a performance limit state is adopted which is consistent with the approach adopted for all the other performance limit states. The system collapse mechanism is not adopted because: (i) the degradation of axial load capacity is not modelled due computational

efficiency and numerical stability, (ii) accurate models (which are usually empirically based) for simulating axial load failure are limited and further research is required in this area, and (iii) the loss of axial load failure in one component is likely to be followed immediately by other components.

In this study significant effort has been made to define the axial load failure of frame elements, since the frames being assessed are part of the gravity load resisting system and hence they are responsible for carrying most of the axial load in the building, the walls generally have significantly lower levels of axial stress due to gravity loads in them. It is noted that the interior gravity load resisting system is not modelled in this study due to the significantly higher stiffness of the perimeter frames because of the nature of the buildings being assessed, discussed in Section 7.2.1. Therefore, the perimeter frames are likely to be subjected to greater seismic forces in comparison to the interior gravity system and hence are likely to fail first. Furthermore, for the asymmetric buildings being assessed, the perimeter frames are subjected to greater displacement demands as well. However, it is likely that the failure of the perimeter frame components will be followed immediately by the failure of the internal gravity system components (especially for the bottom storey columns which have very high axial loads). Therefore, the *Collapse Prevention* performance limit state is based on the axial failure limit reached by the perimeter frame components. This is defined as the rotation corresponding to a 50 % reduction of the ultimate moment capacity (illustrated in Figure 6-1). This limit has been defined (instead of the calculated rotation at axial load failure for columns/beams, and the rotation corresponding to residual strength for joints) to provide some conservatism in defining the axial load failure due to the limitations of the model. This includes the limited availability of experimental results to define and to validate axial load failure deformation limits for components. Furthermore, the change in axial load is not captured during seismic loading due to the nature of the lumped plasticity elements which are adopted (as discussed in Section 4.3). It is also noted that in this study it is assumed that the frame elements will undergo axial load failure prior to the primary lateral load resisting system. This is because the walls have relatively low axial loads acting on them and it is expected that they will successfully carry the axial load after their ultimate lateral strength capacity is reached. However, since the response of the walls is not modelled up to axial load failure, the interstorey drifts are limited to 2.0 % based on guidelines for structural interstorey drift limits.

6.4.5 Summary of performance levels

A summary of the adopted performance levels is provided in Table 6-2. Furthermore, the structural damage limits defining performance levels based on component responses are illustrated graphically in Figure 6-1.

Table 6-2: Summary of the adopted performance levels

Performance level	Damage state	Primary structure	Secondary structure	Interstorey drift limit
Serviceability (S)	Slight	Wall reaching initial yield rotational limit	Frame component reaching nominal yield rotational limit	0.004
Damage Control (DC)	Moderate	Wall reaching a rotational limit corresponding to a compressive strain of 0.002, or tensile strain of 0.015, whichever occurs first	Frame component reaching rotation which is at mid-point between nominal yield and shear failure rotational limits	0.008
Life Safety (LS)	Extensive	Wall reaching ultimate rotational limit, corresponding to a compressive strain of 0.004, or tensile strain of $0.6\varepsilon_{su}$, whichever occurs first	Frame component reaches the rotation corresponding to shear failure	0.015
Collapse Prevention (CP)	Complete	NA	Frame component reaches the rotation corresponding to 50 % reduction in ultimate lateral strength	0.020

NA: Not applicable

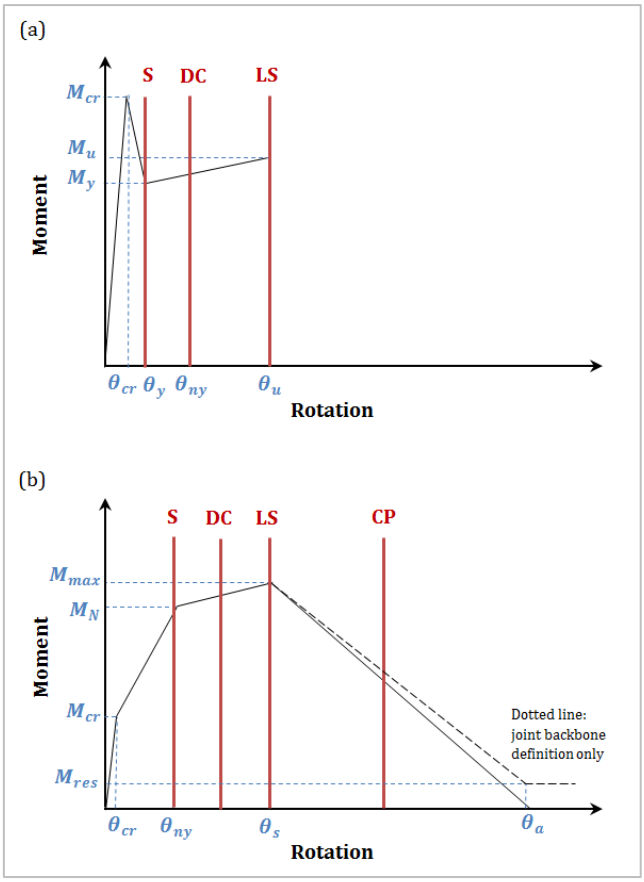

Figure 6-1: Graphical representation of performance levels: (a) walls, (b) frame components

6.5 PERFORMANCE OBJECTIVES

The seismic performance of buildings is evaluated by examining their response with respect to performance objectives. Performance objectives define the extent of damage (defined via performance levels) which is considered to be acceptable for different intensities of earthquakes (usually defined by return periods). The relationship defined between the performance levels and intensity of earthquakes is dependent on the importance level and functional requirements of the building. In terms of building codes, the world trend is towards aiming for *Collapse Prevention* or better for an ordinary building under a 'very rare' earthquake, which is commonly quantified as a 2500 year return period (YRP) event (Buchanan et al., 2011). This applies to both the design of new buildings and assessment of existing buildings. The rehabilitation objectives of FEMA 356 (2000) which has formed the basis for the American Seismic Evaluation and Retrofit of Existing Buildings' standard, ASCE/SEI 41 (American Society of Civil Engineers, 2013), recommends the performance objective of *Life Safety* under a 500 year return period event (which is commonly considered as a 'rare' earthquake) and *Collapse Prevention* under a 2500 year return period event for the Basic Safety Objective (BSO) as shown in Table 6-3.

Table 6-3: Rehabilitation objectives recommended by FEMA 356 (2000)

Earthquake hazard level	Target building performance levels: Operational	Immediate Occupancy	Life Safety	Collapse Prevention
50%/50 year (75 YRP)	a	b	c	d
20%/50 year (225 YRP)	e	f	g	h
10%/50 year (500 YRP)	i	j	**k**	l
2%/50 year (2500 YRP)	m	n	o	**p**

k + p = Basic Safety Objective | k + p + any of a, e, i, b, f, or n = Enhanced Objectives | o, or m, or n alone = Enhanced Objectives | k or p alone = Limited Objectives | c, g, d, h, l = Limited Objectives

Currently the performance objective for the design of most Australian buildings is to "withstand severe earthquake shaking (ultimate) with a reasonable margin against structural collapse..." as well as failure of parts and components which can be life threatening to people inside or outside of the building. For the earthquake and gravity combination, “Ultimate” is taken to be a 500 year return period event for most buildings, that is, Type 2 buildings (Wilson & Lam, 2007). Since 2008 the Australian Building Code (Australian Building Codes Board, 2007) has slightly increased the return period for earthquake resistant design for higher importance level buildings, and these levels are currently adopted by the current National Construction Code (NCC) (Australian Building Code Board, 2016), shown in Table 6-4. However there is still no consideration given to the very rare events (usually taken as a 2500 year return period event in the international scene as mentioned above) which are the earthquakes that could have devastating consequences.

As stated previously in Section 2.2 consideration of higher return periods is more critical for low-to-moderate seismic regions than high seismic regions. This is because there is a significantly higher level of energy released in the low-to-moderate seismic regions for high return periods relative to that released for low return periods (Nordenson & Bell, 2000). Thus it is critical that a minimal performance objective of *Collapse Prevention* is set under very rare earthquake events for both design and assessment of buildings in Australia. Furthermore, higher performance objectives may be desired for Central Business Districts (CBD) of capital cities, as the economic loss due to structural damage and business interruptions may be substantial. For example, Goldsworthy et al. (2015)

suggest designing buildings with importance level of 2 and 3 as defined by the NCC (Australian Building Code Board, 2016) to achieve Damage Control and Collapse Prevention under a 2500 and 5000 YRP event, respectively. While these higher performance objectives may be feasible for design they are not considered to be viable for assessment of older existing buildings. For the purpose of assessment of buildings in Australia, Goldsworthy et al. (2015) recommends that serious consideration should be given to retrofitting buildings which do not achieve Collapse Prevention under a 2500 YRP event. In this study, the Basic Safety Objective described in FEMA 356 (2000) is adopted since it is suitable for the assessment of older buildings.

Table 6-4: Probability of exceedance for various importance level structures in accordance with BCA 2007 and NCC 2016

Importance level	Building type	Annual probability that the design event will be exceeded	
		BCA 2007	NCC 2016
1	Buildings or structures presenting a low degree of hazard to life and other property in the case of failure	1:500	1:250
2	Buildings and structures not included in importance levels 1, 3 or 4.	1:500	1:500
3	Building and structures that are designed to contain a large number of people.	1:500	1:1000
4	Buildings and structures that are essential to post-disaster recovery or associated with hazardous facilities.	1:800	1:1500

6.6 GROUND MOTION INTENSITY MEASURE

The development of fragility curves involves conditioning the structural response on the ground motion intensity measure (IM). It is critical that the IM selected shows a strong correlation between the seismic intensity and the structural response to reduce the uncertainty in the seismic assessment. In addition, the IM needs to effectively represent the level of seismic hazard, that is, it needs to be a parameter that can be correlated to various earthquake return periods (Giovenale et al., 2004).

Many different IMs exist and the choice of a suitable parameter is highly dependent on the type of analysis conducted and the type of structure which is being assessed. The IMs may be classified broadly in to two categories; structure-independent and structure-specific IM

(Celik, 2007). Structure-independent IMs include parameters which define the ground motion properties, such as: peak ground acceleration (PGA), peak ground velocity (PGV), peak ground displacement (PGD), and duration of the earthquake. Structure-specific IMs include spectral response parameters calculated at a specific period and therefore they account for the frequency content of the ground motion and the fundamental or effective building period of vibration. A third category may also be considered which includes the maximum spectral response parameters: maximum spectral acceleration response (RSA_{max}), maximum spectral velocity response (RSV_{max}), and maximum spectral displacement response (RSD_{max}). While the parameters are independent of the fundamental building period, their suitability may be dependent on the general fundamental period of the buildings assessed. For example, RSD_{max} is typically suitable for predicting the response of long-period structures whereas RSA_{max} is suitable for short-period structures.

Traditionally, the IM that has been commonly used for seismic assessment has been PGA. It is the parameter which is typically used to represent hazard on seismic hazard maps, including AS 1170.4:2007. However, the seismic hazard factor (Z) in AS 1170.4 is a nominal value and it is calculated by dividing the PGV values (in millimetres per second) by 750 (Wilson & Lam, 2007). This is because PGV is considered to provide a better indication of the level of structural damage since it is related to the energy in the ground motion (Glaister & Pinho, 2009; Wilson & Lam, 2007).

More recently, structure-specific IMs have been used for creating hazard maps and for conducting assessments. This category of IM has the ability to relate the seismic demand to the structural properties of the buildings which are being assessed. The most commonly used IM is the pseudo-spectral acceleration, typically calculated at the fundamental building period ($RSA(T_1)$) (Wilson & Lam, 2007). While it has been shown that $RSA(T_1)$ is a more efficient parameter than PGA to determine structural damage (Shome, 1999) it typically provides a poor indication of structural damage for buildings with higher fundamental periods or for buildings located on soil sites. Furthermore, the fundamental period may lengthen significantly at performance levels corresponding to high levels of damage and thus the increase in the fundamental period may need to be taken into consideration. Numerous studies have shown that the spectral displacement response provides a better indication of structural damage which has led to the development of displacement-based design and assessment procedures (Priestley, 1997; Priestley et al., 2007; Sullivan et al., 2012). Interestingly, while the spectral displacement response has been widely used to conduct nonlinear static assessment, it is typically not selected as an

IM for the development of fragility curves from dynamic time history analyses. This may be due to the fact that hazard studies and maps typically correlate PGA, PGV and RSA(T) to earthquake return period events.

In addition to the need to select the most suitable IM and the possible controversy this entails, there is also a lack of consistency between different researchers in the choice of the method adopted to calculate the IM when developing fragility curves. Baker and Cornell (2006) highlight that seismologists and earth scientists calculate the intensity measure of a particular earthquake event by computing the geometric mean of the two horizontal ground motion components. However, structural engineers often use a single component of the ground motion to define the IM for 2D analyses or for 3D analyses for which the building is only excited about one axis (i.e. no torsional effects). Therefore, there is an inconsistency when the structural responses are compared with hazard studies and ground motion prediction equations to define the level of damage for a particular earthquake return period. Baker and Cornell (2006) state that one method of overcoming this inconsistency is to compute the geometric mean of the two horizontal ground motion components even if during structural analysis the building is only excited using a single ground motion. Although the method is likely to increase the dispersion of the structural response obtained for a particular IM, Baker and Cornell (2006) reason that the method is more consistent with how hazard studies have been conducted. Another problem with their approach is that it increases the difficulty of conducting the time history analyses since suitable pair of records needs to be selected, which may be challenging when using generated or artificial records.

6.7 SUMMARY

In this chapter a detailed description has been provided of the framework that will be adopted to conduct the seismic fragility assessment of non-ductile RC buildings in Chapter 7. The cloud analysis method has been selected to develop the probabilistic seismic demand models due to the three key advantages that it provides: efficiency, the use of unscaled records, and the flexibility to select different IMs to develop the PSDM for the same set of analyses. A detailed review of the various definitions of performance levels and damage states has been provided and four performance levels have been defined which will be used to conduct the assessment of non-ductile RC buildings, including: *Serviceability*, *Damage Control*, *Life Safety*, and *Collapse Prevention*. In addition, the world trend in terms of the definition of performance objectives has been reviewed. The Basic Safety Objective as described in FEMA 356 (2000) is to be adopted to evaluate the seismic

performance of the archetypal buildings in Chapter 7 since it is considered to be suitable for assessing the performance of older buildings. Furthermore, the advantages and disadvantages of various intensity measures, as well as the different methods used to calculate the IMs for developing fragility curves, have been discussed. The selection of a suitable IM to develop the fragility curves for this study will be further evaluated in Chapter 7.

CHAPTER 7: SEISMIC FRAGILITY ASSESSMENT OF NON-DUCTILE RC BUILDINGS

7.1 INTRODUCTION

In this chapter the results obtained from the seismic fragility assessment of six archetypal buildings are presented. The buildings are representative of older buildings constructed in Australia before the requirement for seismic design was mandated on a national basis. Three building heights are investigated: 2-, 5-, and 9-storey. For each building height two plan configurations are analysed: one with plan symmetry and the other with plan asymmetry. Suitable ground motion records are selected to conduct nonlinear dynamic time history analyses. The probabilistic seismic demand models are developed using the cloud analysis method, from which fragility curves are computed for various performance levels. The importance of carefully selecting a suitable intensity measure is investigated since it can significantly affect the fragility curves and the conclusions derived about the seismic performance of the buildings. In addition, the difference in response for the various methods used to indirectly account for biaxial bending for the plan-asymmetric buildings is presented. Finally, the results are evaluated with respect to performance objectives in order to quantify the seismic vulnerability of the buildings.

7.2 ARCHETYPAL BUILDING CHARACTERISTICS AND NONLINEAR MODEL

In Section 3.2 it was identified that wind load and lateral stability were poorly considered in Australia until the late 1980s. In addition, seismic design was not considered nationally until 1995 when the requirement for earthquake loading and design was referred to in the Building Code of Australia. Therefore there are concerns that buildings constructed prior to 1995 are particularly vulnerable to earthquakes. Hence, in this chapter the design of the buildings being assessed is representative of buildings constructed prior to 1995 and they have been detailed in accordance with AS 3600:1988.

The following subsections describe the archetypal RC building characteristics, including building design and detailing, the material properties adopted for assessment, and the nonlinear model created for time history analyses.

7.2.1 Building designs

Six archetypal buildings are assessed which are 2-, 5-, and 9-storeys high. For each building height two building configurations are assessed: one with plan symmetry and one with plan asymmetry, where plan symmetry is defined as when the centre of mass of the building coincides with the initial centre of stiffness of the building. As mentioned earlier, the buildings are representative of older RC buildings constructed in Australia prior to the requirement for seismic load and design to be mandated on a national basis. The buildings have been designed in accordance with AS 3600:1988 Concrete Structures Standard, AS 1170.2:1983 Wind Actions Standard, and guidance from experienced practicing structural engineers. The frames are designed as ordinary moment resisting frames (OMRFs) and have detailing deficiencies as highlighted in Section 3.3. The core walls have low longitudinal reinforcement ratios (approximately 0.23 %) with no confinement and thus are likely to develop a single crack under lateral loading. The building plans are provided in Figure 7-1, Figure 7-2, and Figure 7-3 for the 2-, 5-, and 9-storey buildings, respectively. The gravity load resisting system of the buildings constructed in the 1980s typically included perimeter frames with deep beams (600-900 mm deep) to satisfy fire design requirements, and band-beams or flat-slab floor systems with column spacings of 7.0 to 8.4 m. Hence for the archetypal buildings a typical column spacing of 8.4 m is adopted with a perimeter beam depth of 650 mm. The design properties of the building components are provided in Table 7-1, and the detailing of the frame components and the core walls are provided in Figure 7-4 and Figure 7-5, respectively. Details of the interior system are not provided as the interior gravity system is not modelled since it is expected that the perimeter frames will fail prior to the interior gravity system. This is because the perimeter frames have significantly higher stiffness than the interior gravity frames and therefore they will be subjected to greater seismic forces. In addition, for the buildings with plan asymmetry, the largest displacement demand will be imposed on the perimeter frames.

Table 7-1: Summary of design properties for building components

	Slab	**Perimeter beams**	**Columns**	**Core walls**
f'_c (MPa)	25	25	40	40
f_y (MPa)	400	400	400	400
ρ_l (%)	0.67-1.33	1.30-2.70	2.0-4.0	0.23-0.24
ρ_t (%)	0.25	0.23	0.075-0.12	0.25

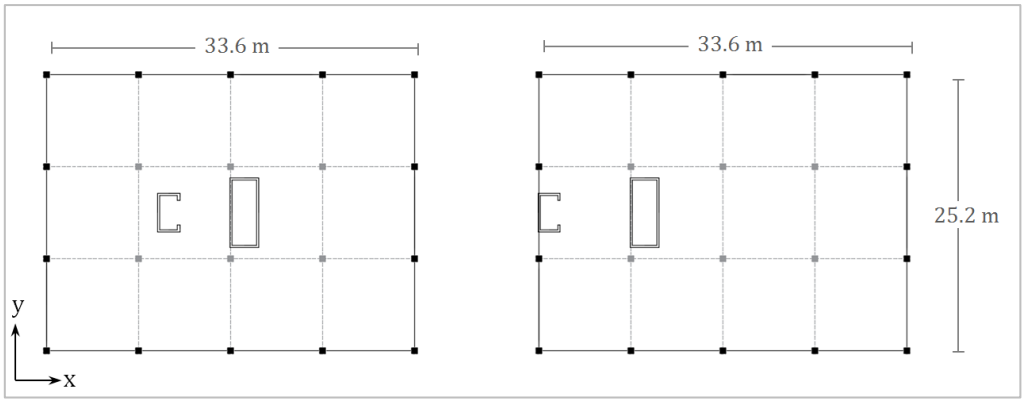

Figure 7-1: 2-storey building plans with plan symmetry and asymmetry

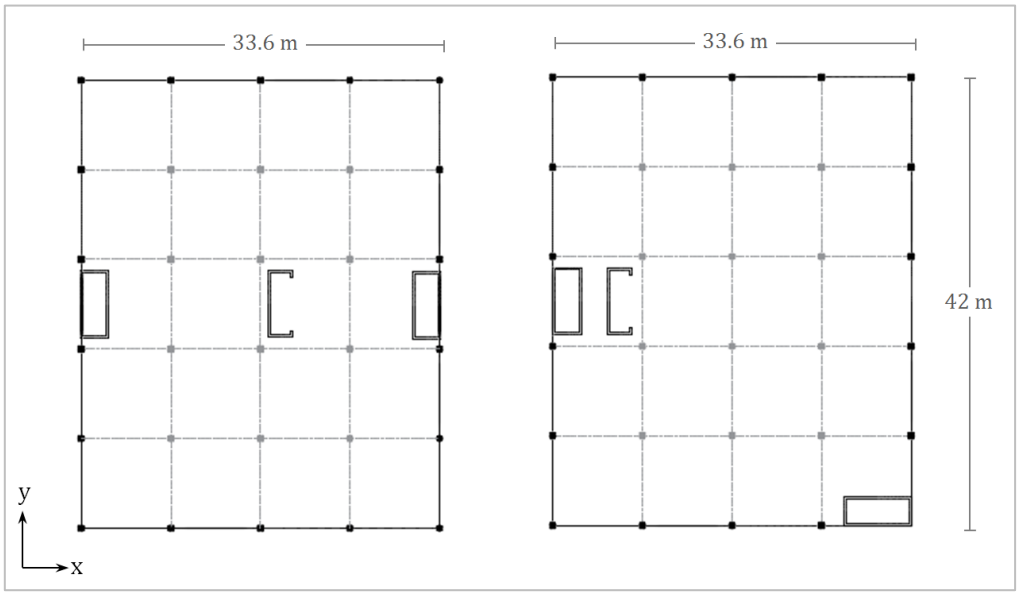

Figure 7-2: 5-storey building plans with plan symmetry and asymmetry

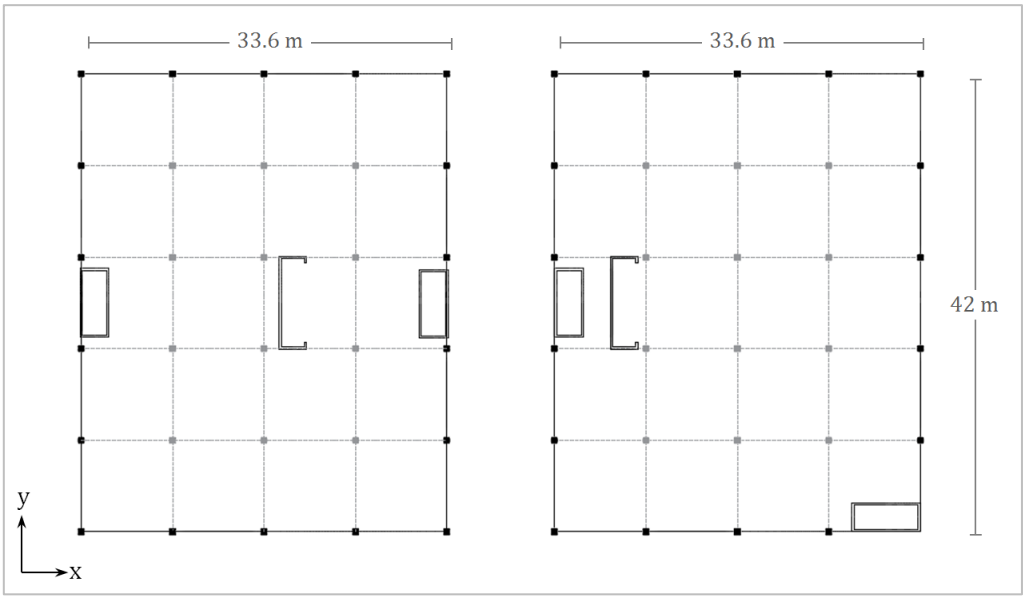

Figure 7-3: 9-storey building plans with plan symmetry and asymmetry

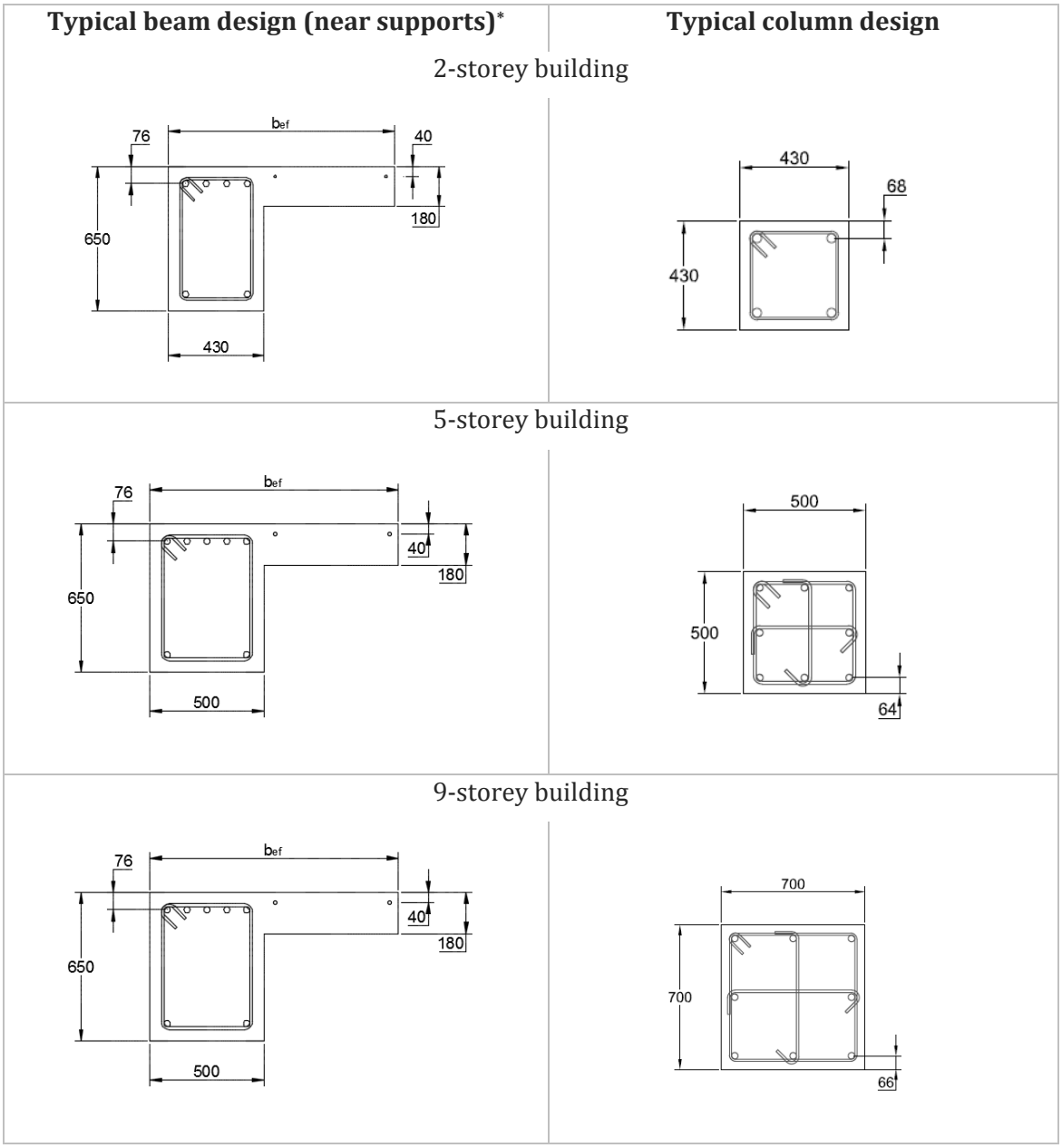

* Effective width of flange (b_{ef}) is also illustrated and it is calculated in accordance with AS 3600:2009

Figure 7-4: Perimeter beam and column designs for archetypal buildings

Typical stair core design (similar for all buildings)

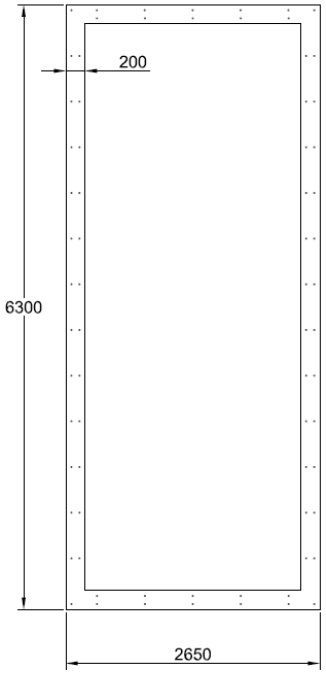

2-storey building lift core design

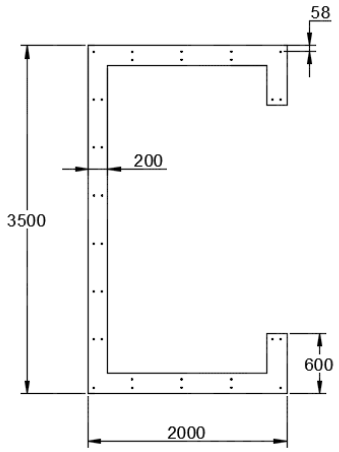

5-storey building lift core design

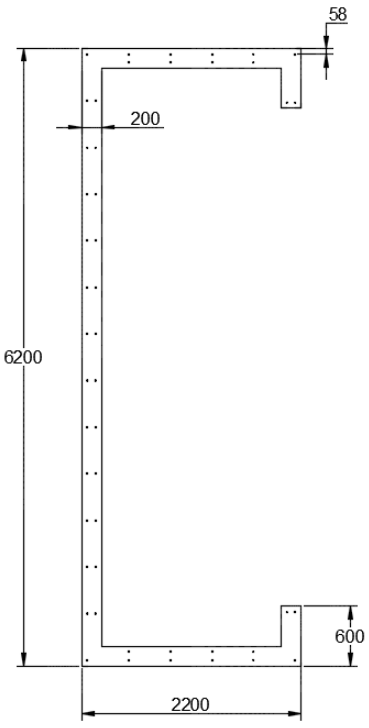

9-storey building lift core design

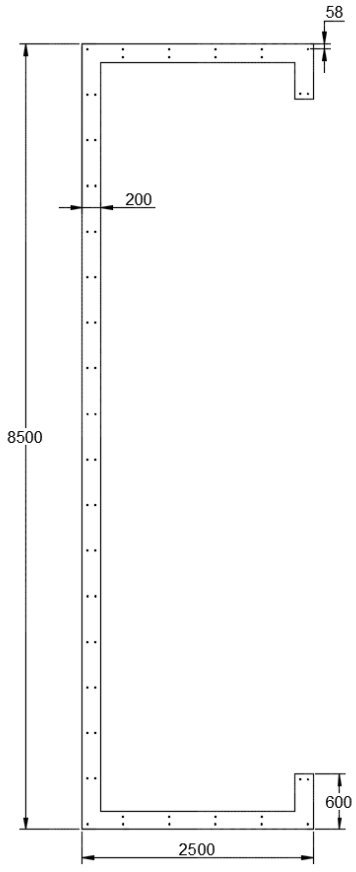

Figure 7-5: Stair and lift core designs for archetypal buildings

7.2.2 Material properties for assessment

As discussed in Section 3.6 when assessing the performance of buildings it is necessary to use the expected material properties. A summary of the material properties adopted in this study are provided in Table 7-2 which are based on the findings presented in Section 3.6.

Table 7-2: Adopted material properties for assessment

Material property	Adopted value for assessment
Expected (mean) compressive strength of concrete	$1.2f_c'$
Expected flexural tensile strength of concrete for walls	$0.6\sqrt{f_c'}$
Mean yield strength of reinforcement	460 MPa
Mean ultimate to yield strength ratio of reinforcement	1.21
Ultimate tensile strain of reinforcement	0.12

Note: f_c' is the design characteristic compressive strength of concrete

7.2.3 Nonlinear models of buildings

The nonlinear models for the six archetypal buildings described in Section 7.2.1 are created in the finite element analysis package, OpenSEES (McKenna et al., 2000). The columns, beams, and walls are modelled using lumped plasticity elements and the beam-column joint response is modelled using the scissor's model with rigid links approach as discussed in Chapter 5. As an example, the schematic of the modeling method for the 5-storey building with plan symmetry is shown in Figure 7-6. It is assumed that the walls and the columns are fixed to the ground. Furthermore a rigid diaphragm assumption is also adopted.

A limitation of the lumped plasticity approach is that biaxial bending is not captured during the analysis. The consideration of biaxial bending is particularly important for the buildings with plan asymmetry as the effect of biaxial bending is more pronounced, especially on the corner columns. Based on the experimental and numerical findings presented in Section 3.4.2.6 for columns and Section 3.4.3.4 for walls, reduction factors are applied to the moment and drift capacities described in Section 5.4.3 and 5.5.2 for columns and walls, respectively; which were established to develop backbone curves for components under unidirectional loading. However, since there are insufficient results available from experiments for the type of components being assessed; especially for the non-ductile lightly reinforced core walls, and since flexure-axial behaviour is not directly

captured in the nonlinear model, a range of backbones are investigated. Three backbone definitions are adopted for the columns and walls for the archetypal buildings with plan asymmetry (illustrated in Figure 7-7 and Figure 7-8):

i. No reduction is applied; that is, the backbone is the same as that obtained for unidirectional loading
ii. Medium bound reduction factors are applied; a *medium* approximation of reduction factors is adopted based on very limited component experimental results
iii. Lower bound reduction factors are applied; a *low* approximation of reduction factors is adopted which is likely to give a conservative representation of the response of non-ductile RC components

Gravity analysis is conducted first under the load combination used in AS 1170.0 (Standards Australia and Standards New Zealand, 2002) for when gravity loads are applied simultaneously with earthquake actions; 1.0G+0.3Q, where G represents the permanent actions and Q is the imposed actions. Based on these gravity loads, moment-curvature analysis is conducted for the various building components to obtain the required moment and curvature parameters to develop the backbone and hysteretic response parameters. The definition of the critical points for assessment is provided in Table 7-3.

Damping is incorporated by using Rayleigh damping model with the tangent stiffness proportional damping constant calibrated to provide 5 % equivalent viscous damping ratio for the first fundamental elastic mode. The first two fundamental periods (T_1 and T_2) for the nonlinear models of the buildings are presented in Table 7-4.

Table 7-3: Definition of critical points for defining component backbones

Critical point	Criteria
Cracking Moment	For walls: the extreme tensile concrete fibre stress equals the flexural tensile strength of concrete; $f_{ct.f} = 0.6\sqrt{f_c'}$ based on Cook et al., (2014) recommendation. For frame elements: the extreme tensile concrete fibre stress equals to zero.
Yield Moment	The extreme tensile steel fibre stress equals to the yield strength (f_y), or when the extreme compressive concrete fibre strain is equal to 0.002, depending on whichever occurs first as suggested by Priestley et al. (2007).
Nominal Yield Moment	The extreme tensile steel fibre strain equals to 0.015, or when the extreme compressive concrete fibre strain equals to 0.003, depending on whichever occurs first. The curvature at nominal yield is then calculated as suggested by Priestley et al. (2007); $\phi_{ny} = \frac{M_N}{M_y}\phi_y$
Ultimate Moment	Is the point at which maximum moment is observed but it is limited to the following conditions, depending on whichever one occurs first; when the extreme tensile steel fibre strain equals to $0.6\varepsilon_{su}$, or when the extreme compressive concrete fibre strain equals to 0.004.

Table 7-4: First two fundamental building periods (in seconds)

Building	$\mathbf{T_1}$	$\mathbf{T_2}$
2-storey plan-symmetric	0.162	0.085
2-storey plan-asymmetric	0.162	0.066
5-storey plan-symmetric	0.729	0.382
5-storey plan-asymmetric	0.787	0.458
9-storey plan-symmetric	1.673	0.897
9-storey plan-asymmetric	1.525	0.952

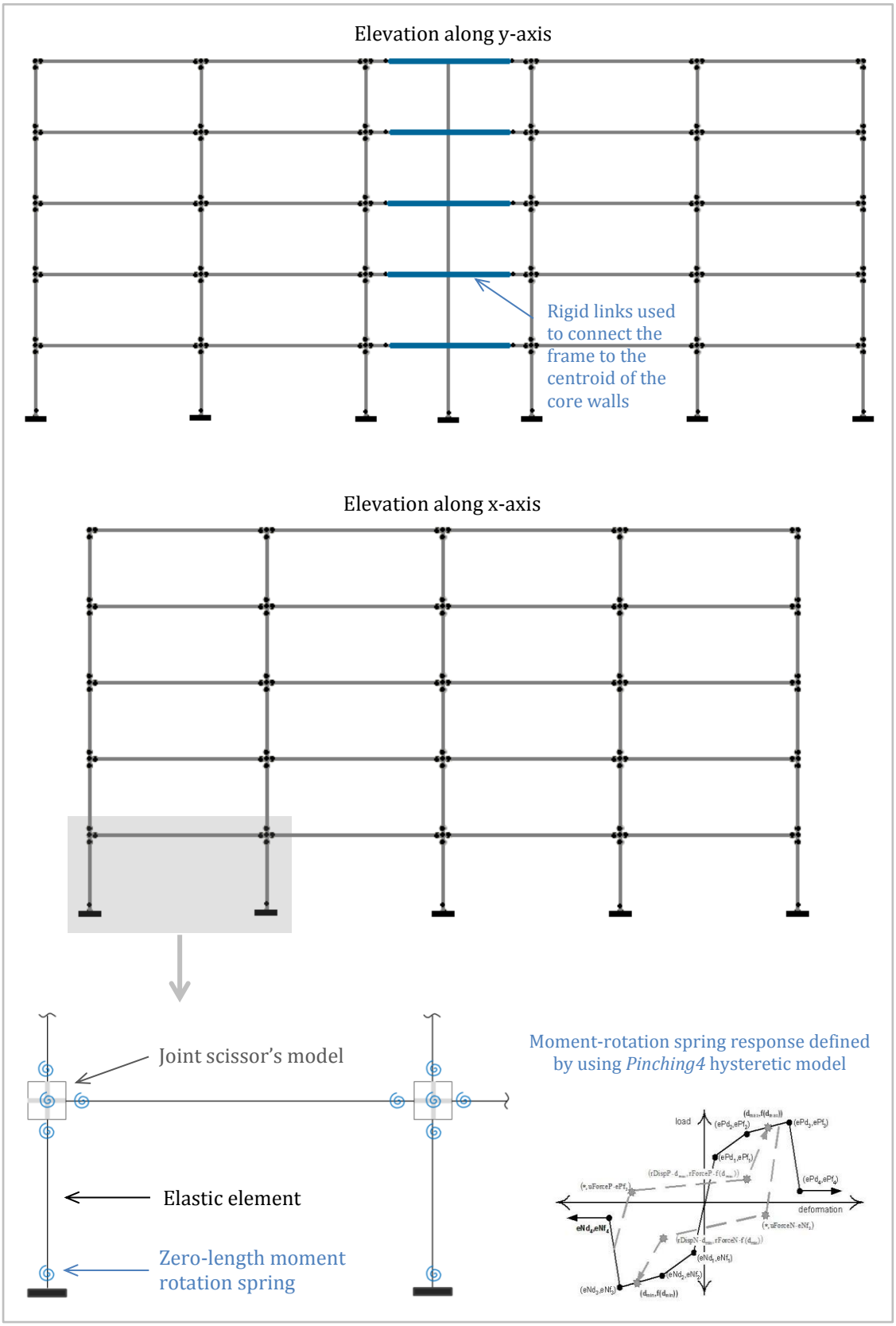

Figure 7-6: Schematic of nonlinear building model (example for 5-storey plan-symmetric building)

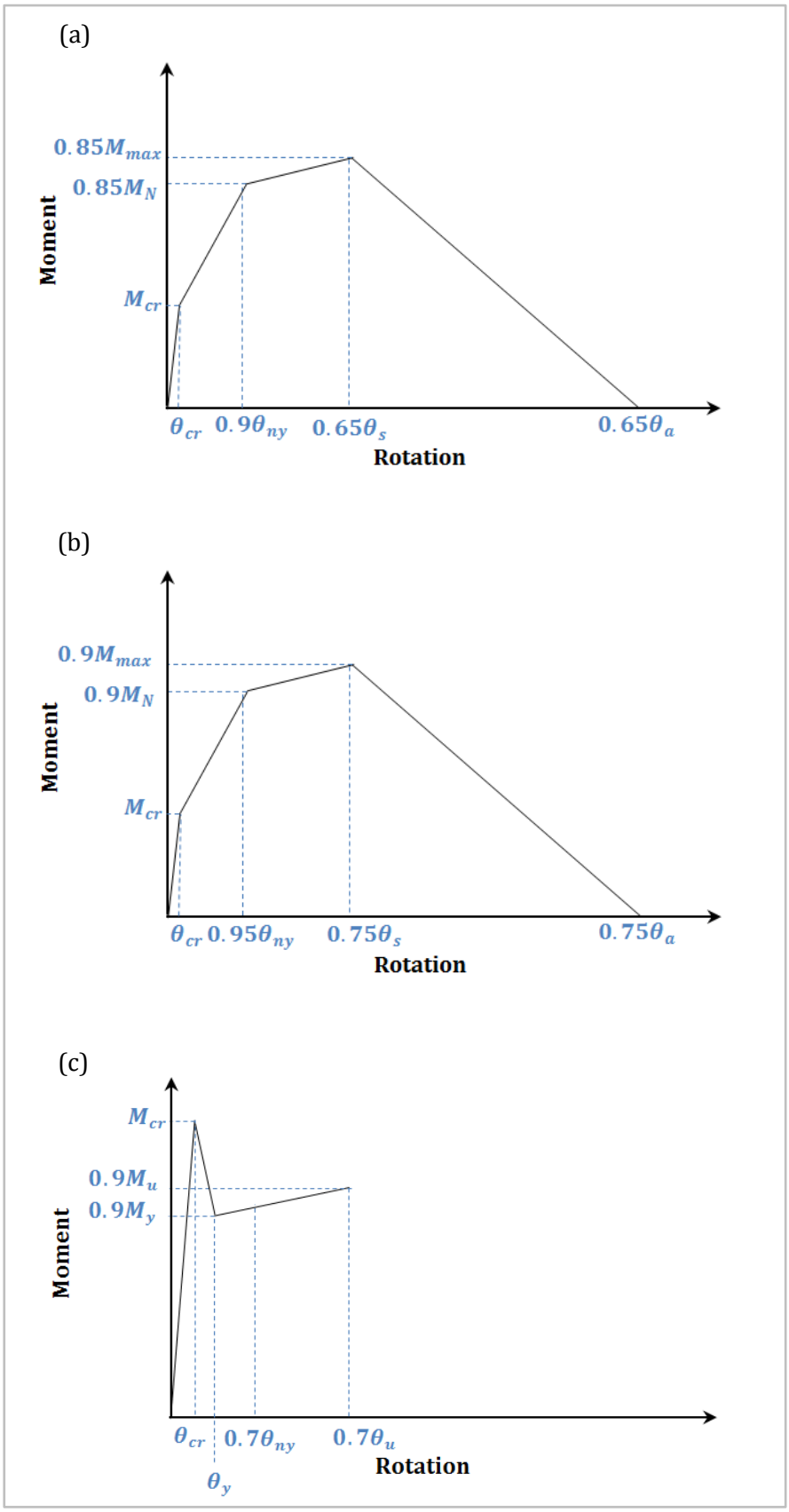

Figure 7-7: Medium bound reduction factors to account for biaxial bending for: (a) corner columns, (b) interior span perimeter columns, (c) walls

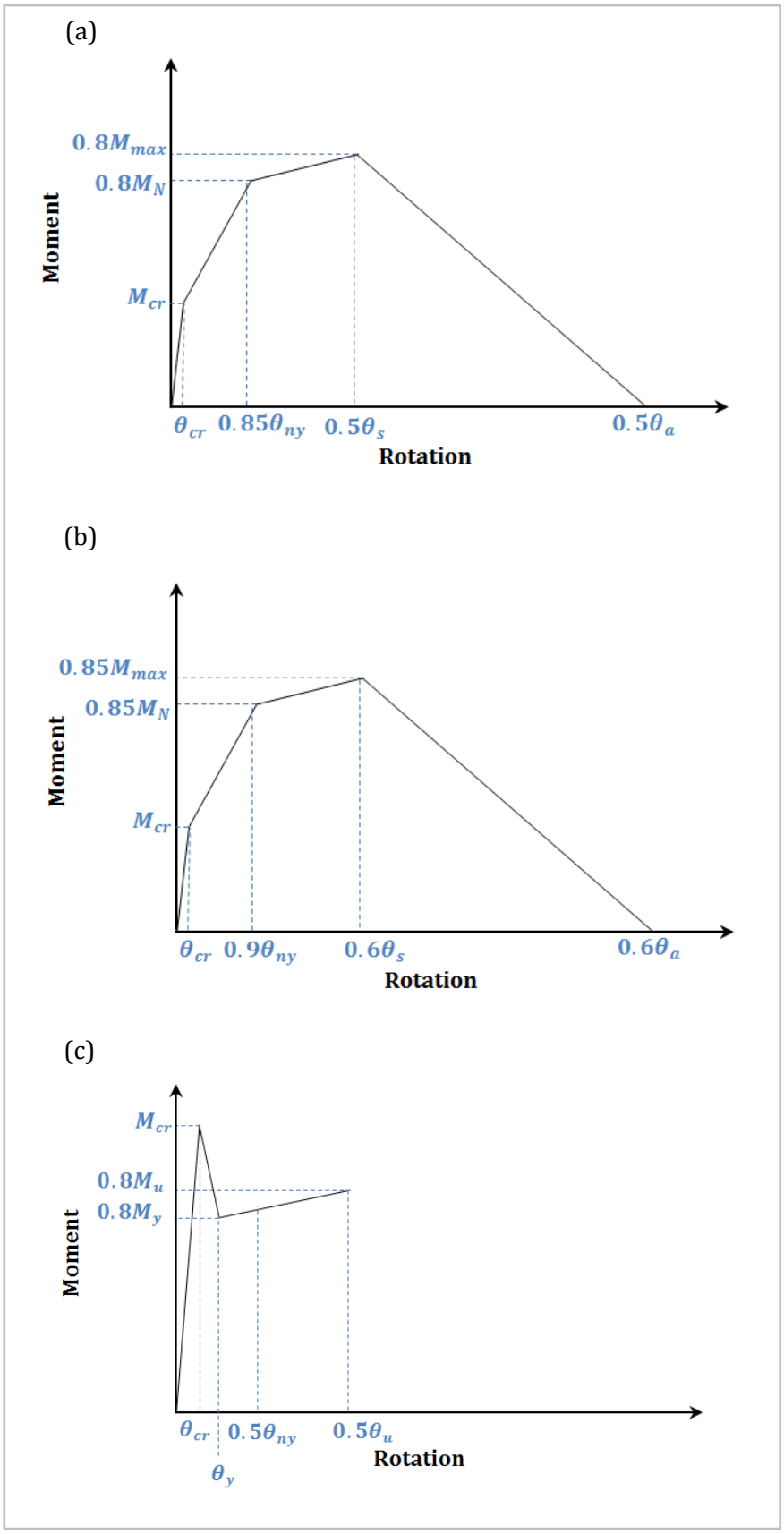

Figure 7-8: Lower bound reduction factors to account for biaxial bending for: (a) corner columns, (b) interior span perimeter columns, (c) walls

7.3 GROUND MOTIONS FOR TIME HISTORY ANALYSIS

One of the main challenges associated with conducting assessment of buildings in low-to-moderate seismic regions is the selection of ground motions. This is especially the case when bidirectional ground motions need to be applied. Most studies which have conducted bidirectional time history analyses have used historical records for which two horizontal components are available and thus are directly applied to the building model. The stronger component of the record, typically identified as the record with the higher PGA is applied along the primary direction of the building with the weaker component applied to the secondary direction (Humar & Kumar, 1999). However, as discussed previously, historical records are scarce for regions of low-to-moderate seismicity especially when conducting assessment of buildings which require strong motion records that cause collapse of buildings. Therefore previous studies which have not used historical records resort to using two generated records for a given intensity (Lumantarna, 2012; Ghersi and Rossi, 2001).

In this study 40 pairs of unscaled records have been selected to conduct dynamic time history analyses. The records have been selected such that they cover a wide range of IM values and are characteristic of Australian earthquakes. The pair of records selected are a combination of: (i) stochastically generated records obtained using the program GENQKE (Lam, 1999) which is capable of producing ground motions that are representative of Australian earthquakes (two records are generated for a given intensity), (ii) historical records with characteristics representative of Australian earthquakes, including that they are shallow earthquakes with reverse fault mechanisms (Brown & Gibson, 2004), (iii) simulated records on soil conditions by using the nonlinear site response program DEEPSOIL (Hashash et al., 2016) and using generated and historical rock records as input ground motions. It is noted that DEEPSOIL, which is capable of conducting nonlinear analysis, was used instead of SHAKE2000. SHAKE2000 is only capable of conducting equivalent linear analyses and some of the input records may have caused the soil strain to exceed the limits for which equivalent-linear analyses are valid. The soil profiles used are those presented in Section 2.4.4 which were utilised to develop the proposed model for incorporating the effects of local site conditions.

For the historical records, which comprise approximately 25 % of the 40 pairs of records, the median ratio of the PGA of the weaker-to-stronger components of the earthquake is 80 %, whereas the median ratio for the generated records is approximately 90 %. Therefore no reduction factor is required to be applied to the weaker component of the

generated records for the same magnitude and distance combination based on the conventional method of quantifying the intensity of earthquakes. In addition, it is noted that the median ratio of RSD_{max} of the weaker-to-stronger components of the historical earthquake records is 66 %, whereas the median ratio of the generated records is approximately 76 %. The median ratio of PGV of the weaker-to-stronger component of the historical earthquake records is 76 %, whereas the median ratio of the generated records is approximately 89 %. Hence, the ratios of the weaker to stronger IMs obtained for the two components of the historical records, and for the two components of the generated ground motion records, are reasonably similar when using the intensity measures: PGA, RSD_{max}, and PGV.

7.4 RESULTS FOR BUILDINGS WITH PLAN SYMMETRY

When investigating the performance of plan-symmetrical buildings, it is common practice to apply unidirectional seismic loading along the weaker principal axis of the building. This is because the simultaneous ground motion acting along the stronger axis of the building is likely to have a small effect on the response of the building in the weak direction. Hence for the archetypal buildings with plan symmetry, time history analyses are conducted by applying the stronger component of the two horizontal ground motions (defined by the larger PGA), referred to as the x-component, along the weaker axis of the buildings. For each analysis the maximum rotational or drift demand-to-capacity ratio, which defines the critical demand-to-capacity ratio (Y, also referred to as $\frac{\theta_D}{\theta_C}$), is obtained for each performance level as defined in Section 6.4. Then the cloud analysis method is used to develop the PSDMs. The following limits have been applied to consider *collapse* cases; that is, the data that is not included in the PSDM to compute $P(\mathrm{Y} > 1|IM, \bar{c})$, for the various performance levels:

- *Serviceability*, collapse cases are considered to be when $\mathrm{Y} > 500$
- *Damage Control*, collapse cases are considered to be when $\mathrm{Y} > 50$
- *Life Safety*, collapse cases are considered to be when $\mathrm{Y} > 10$
- *Collapse Prevention*, collapse cases are considered to be when $\mathrm{Y} > 5$

It is noted that the collapse case limits for *Serviceability* and *Damage Control* do not significantly affect the fragility curves since Y is much greater than 1.0 for most of the analyses, and hence similar results are obtained whether or not the limits are applied. The collapse case limits for *Life Safety* and *Collapse Prevention* have been selected to ensure that the outliers due to numerical instabilities are not included in the cloud data to obtain $\eta_{Y|IM,\bar{c}}$ and $\beta_{\mathrm{Y}|IM,\bar{c}}$.

Before the fragility curves are developed it is necessary to investigate which IM is the most suitable parameter for the particular study being conducted. Statistically, the IM that is most suitable for use in developing the fragility curves is the IM which provides the highest correlation with the buildings response and hence the lowest dispersion ($\beta_{Y|IM,\vec{c}}$). Therefore, regression analysis is conducted for the PSDMs using different IMs to obtain the dispersion for each performance limit. Firstly, the IMs investigated are obtained from the applied ground motion; that is, the x-component of the two horizontal ground motion records for each intensity. The IMs investigated are: peak ground acceleration (PGA), peak ground velocity (PGV), peak ground displacement (PGD), maximum spectral acceleration response (RSA_{max}), maximum spectral displacement response (RSD_{max}), the spectral acceleration and displacement response at the fundamental translational building period (T_1) and at multiples of the fundamental building period ($1.5T_1$ and $2.0T_1$). The dispersion obtained for the various IMs are displayed in Figure 7-9 for the 2-, 5- and 9-storey building. Secondly, the IMs are calculated by using the geometric mean of the x- and y-component of two horizontal ground motion records as suggested by Baker and Cornell (2006). It is noted that for IMs which are based on spectral response values that depend on the fundamental building period, the second fundamental translational period is used to obtain the spectral response for the y-component of the ground motions. The dispersion obtained using the geometric mean of the two components of the ground motions is provided in Figure 7-10 for the 2-, 5- and 9-storey building.

Interestingly, it is observed that in general the dispersion tends to decrease slightly when the geometric mean of the two components of the ground motions is computed rather than only the x-component. Since the results show an improved correlation when the geometric mean of the two horizontal components is used to compute the IM, it will be adopted in this study to represent the IM for symmetrical buildings which are only excited along the x-direction. This also allows a consistent comparison with asymmetrical buildings which are excited in both the x- and y-direction, and as discussed by Baker and Cornell (2006) it provides a more consistent method of relating the IM to hazard studies and return periods.

The results in both Figure 7-9 and Figure 7-10 show that a different IM provides the lowest dispersion for the different building heights and performance levels. However, the IMs that tend to provide the lowest dispersion for all of the buildings analysed and for the four performance levels investigated are PGV, PGD, and RSD_{max}. Interestingly, it is observed that the correlation with PGA, which has been the conventional IM for developing fragility curves, is quite poor in comparison to PGV, PGD, and RSD_{max}.

Furthermore, the results show that in general the correlation between any intensity measure and building response improves for performance levels corresponding to a higher level of damage. It is noted that this observation is primarily because the performance levels in this study have been defined based on multiple criteria, including the response of the building components and the maximum interstorey drift limits. Thus, a different criterion tends to govern the response of the building for a given performance level. Most of the previous studies which have examined the dispersion between the building response and intensity measure have only examined maximum interstorey or roof drift as the engineering demand parameter (Bojórquez et al., 2017; Jankovic & Stojadinovic, 2004; Lucchini et al., 2011). Hence, for these studies the dispersion is the same for all performance levels.

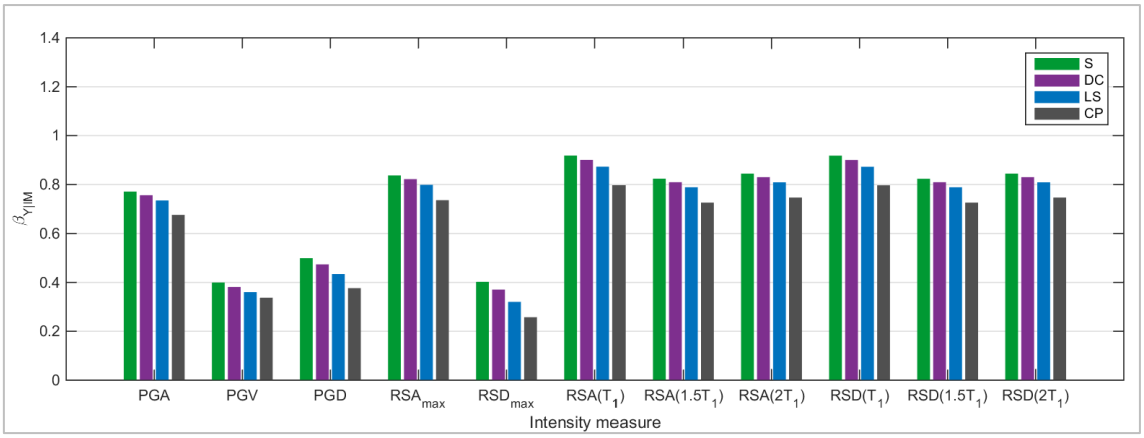

(a) 2-storey building

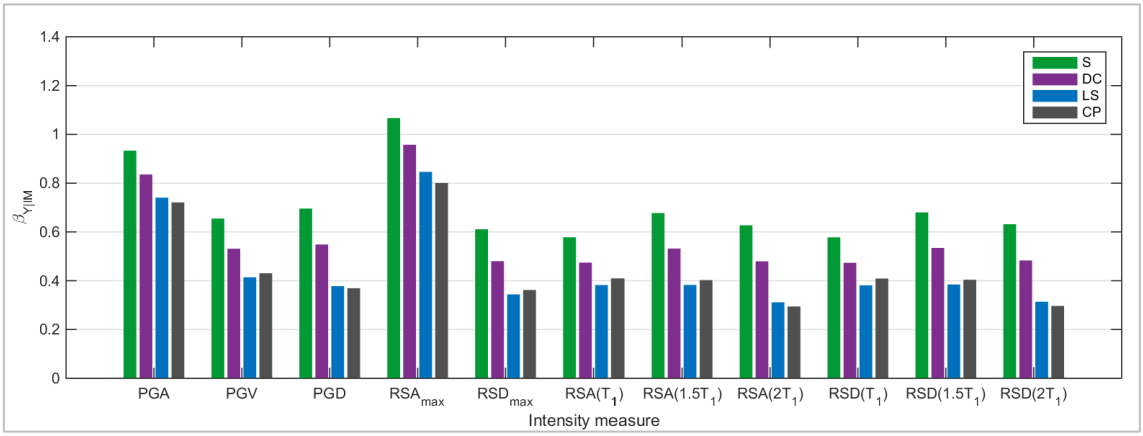

(b) 5-storey building

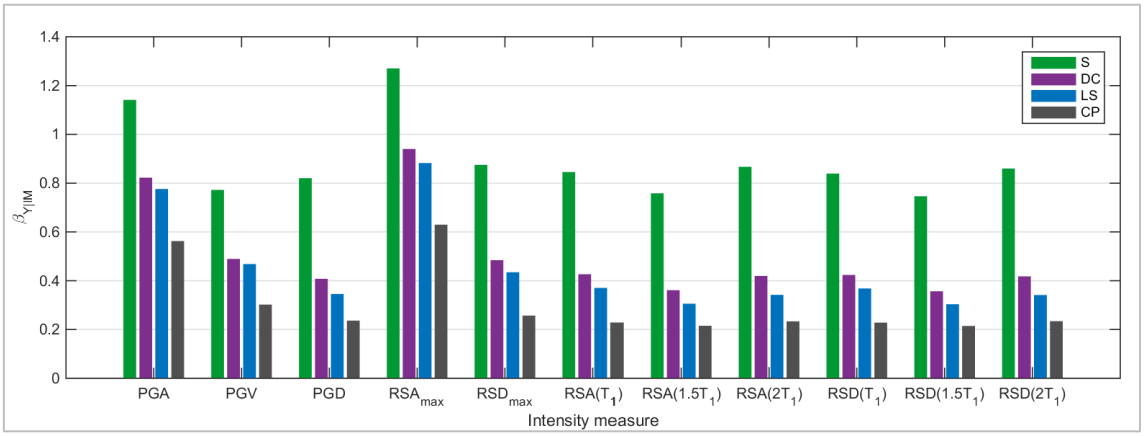

(c) 9-storey building

Figure 7-9: Dispersion factors for buildings with plan symmetry computed using only the x-component of the ground motion

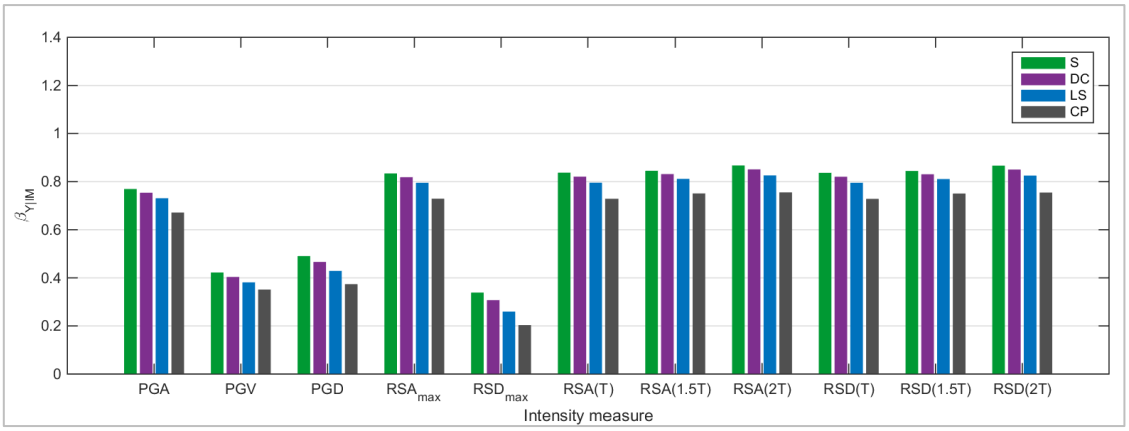

(a) 2-storey building

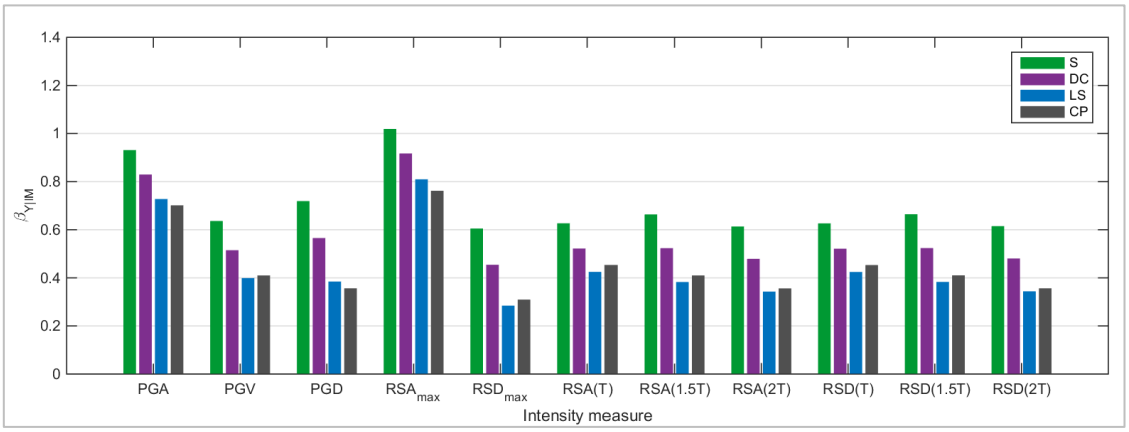

(b) 5-storey building

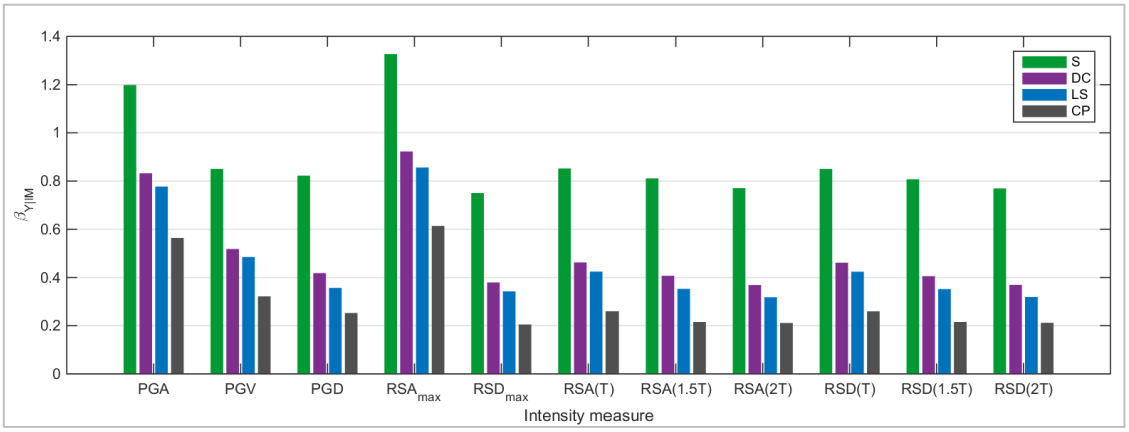

(c) 9-storey building

Figure 7-10: Dispersion factors for buildings with plan symmetry where the IM is computed using the geometric mean of x- and y-component of the ground motions

In addition to selecting an IM that provides a high correlation between the IM and the building response, it is also important to select an IM which is capable of accurately representing ground motion intensities that can be related to earthquake return periods. When conducting seismic hazard analyses and developing ground motion prediction equations it has not been common practice to define earthquake intensity with respect to

PGD. In Australia, the current hazard map in AS 1170.4:2007 has been developed based on PGV values on rock (PGV_{rock}) conditions (i.e. site Class B in accordance with AS 1170.4:2007) from which the notional PGA values are computed using Eq. 7-1. These notional PGA values represent the hazard factors (Z) in AS 1170.4:2007. The hazard values on the map correspond to a return period of 475 years (i.e. approximately 500 year return period event).

Building on the hazard values obtained from PGV_{rock}, various transformations have then been applied to develop the spectral shape factors ($C_h(T)$) in AS 1170.4:2007 for the different site classes. From the spectral shape factors the acceleration, velocity, and displacement response spectra may be obtained. The parameters which are of interest in this study are PGV and RSD_{max}, since they consistently provide the lowest dispersion between the IM and structural response of the buildings analysed. However, for the purpose of comparison, fragility curves will also be developed using the conventional IM, PGA.

The PGV values for various return periods may be obtained by multiplying the PGV on rock by the probability factor (k_p), in accordance with AS 1170.4:2007. Furthermore, the PGV values for various site conditions may be obtained by multiplying the PGV on rock by the site amplification factors in the velocity controlled region (F_v) which are computed from the spectral shape factors. The PGA values for various site conditions may be computed by multiplying the PGA on rock by the site amplification factors in the acceleration controlled region (F_a). The maximum spectral displacement response (RSD_{max}) may be obtained from the maximum spectral velocity response (RSV_{max}) by using the expression in Eq. 7-2. RSV_{max} in AS 1170.4:2007 has been computed by multiplying the PGV_{rock} and F_v by 1.8 as illustrated in Eq. 7-3. The 1.8 factor has been suggested by Wilson and Lam (2003) and similar methods of transforming PGV values to RSV_{max} are also suggested in more recent studies (Huang & Whittaker, 2015).

$$notional\ PGA_{rock}\ (g) = \frac{PGV_{rock}\ (mm/s)}{750} \quad \text{Eq. 7-1}$$

$$RSD_{max} = RSV_{max}\left(\frac{T_2}{2\pi}\right) = RSV_{max}\left(\frac{1.5}{2\pi}\right) \quad \text{Eq. 7-2}$$

$$RSV_{max} = 1.8PGV_{rock}.F_v \quad \text{Eq. 7-3}$$

To provide an indication of the performance of the buildings at various return periods, the PGA, PGV and RSD_{max} are computed for a 500 and 2500 YRP event in accordance with

AS 1170.4:2007 and are provided in Table 7-5, Table 7-6, and Table 7-7, respectively. The values have been computed for a site with a hazard factor (Z) of 0.1 g which corresponds to the hazard factor for Adelaide which is currently the capital city with the highest seismic hazard. Hence, the k_pZ values corresponding to a 500 and 2500 YRP event are 0.1 g and 0.18 g, respectively. Furthermore, in Table 7-7 the $\text{RSD}_{\max}$ values obtained from the site response study in Section 2.4.4, for a 500 and 2500 YRP event corresponding to k_pZ value of 0.1 g and 0.3 g, respectively is provided. It is noted that for the site response study, the k_pZ factor corresponding to a 2500 YRP event was taken as 0.3 g since it is believed to be a better representation of the increase in seismicity from a 500 YRP event to a 2500 YRP event for regions with low-to-moderate seismicity.

Table 7-5: PGA values for a 500 and 2500 YRP event corresponding to k_pZ factor of 0.1 g and 0.18 g on rock in accordance with AS 1170.4:2007

Site condition	**F_a**	**PGA (g)**	
		500 YRP	2500 YRP
Class A	0.80	0.08	0.15
Class B	1.0	0.1	0.18
Class C	1.25	0.13	0.23
Class D	1.25	0.13	0.23
Class E	1.25	0.13	0.23

Table 7-6: PGV values for a 500 and 2500 YRP event corresponding to k_pZ factor of 0.1 g and 0.18 g on rock in accordance with AS 1170.4:2007

Site condition	**F_v**	**PGV (mm/s)**	
		500 YRP	2500 YRP
Class A	0.80	61	110
Class B	1.0	76	137
Class C	1.42	108	195
Class D	2.25	172	309
Class E	3.50	267	481

Table 7-7: RSD_{max} values (in mm) for a 500 and 2500 YRP event in accordance with AS 1170.4:2007 and site response study

Site condition	**AS 1170.4:2007**		**Site response study**	
	500 YRP	2500 YRP	500 YRP	2500 YRP
Class A	26	47	26	79
Class B	33	59	37	115
Class C	47	84	55	173
Class D	74	133	74	225
Class E	115	207	NA	NA

The probabilistic seismic demand models using the cloud analysis method are provided for when the intensity measure is PGA, PGV, and RSD_{max}, for the 2-, 5- and 9-storey buildings in Figures 7-11 to 7-19. The corresponding fragility curves are provided in Figures 7-20 to 7-22. The fragility curves represented with a solid line are computed by only considering the dispersion due to the critical demand-to-capacity ratio as a function of IM for *non-collapse* data ($\beta_{Y|IM,\bar{c}}$), the fragility curves represented with a broken line are computed by considering $\beta_{Y|IM,\bar{c}}$ and dispersion due to uncertainty in defining the capacity of the building (β_C) and modelling uncertainties (β_M), which are set to 0.3 and 0.2, respectively as discussed in Section 6.2. The difference between not considering and considering β_C and β_M to compute the fragilities is greater for the performance levels corresponding to a higher level of damage, namely *Life Safety* and *Collapse Prevention*. This is because $\beta_{Y|IM,\bar{c}}$ is lower for these performance levels, thus adding β_C and β_M has more of an effect on the shape of the fragility curves. Furthermore, the fragilities computed for the performance levels corresponding to lower levels of damage, have a higher probability of exceedance at lower intensity measures, therefore the increase in uncertainty has a lower effect on the shape of the fragilities. Hence, it may be concluded that the consideration of uncertainties becomes particularly important for performance levels corresponding to higher levels of damage.

The results illustrate that there is a significant difference between the capacity of the buildings at *Life Safety* and *Collapse Prevention*, especially as the height of the buildings increases. The structural damage limits at these two performance levels were defined to correspond to the initiation of loss of lateral load carrying capacity and loss of axial load carrying capacity. The loss of lateral load carrying capacity is predominantly governed by the response of the core walls. The loss of axial load carrying capacity is predominantly governed by failure of the ground level columns since as the core walls start to lose their stiffness the lateral load is resisted by the gravity frames. Hence, the results show that collapse of the gravity system does not occur prior to the ultimate capacity of the core walls being reached.

Furthermore, to provide an indication of the performance of the buildings, the intensity measures corresponding to a 500 and 2500 YRP event in accordance with AS 1170.4:2007 for site classes ranging from A to E (defined in Table 7-6) are shaded on Figures 7-20 to 7-22. By looking at the extreme ends of the shaded regions (which represent the IM on Class A and Class E) it is apparent that the probability of exceedance for the various performance levels varies depending on the selected intensity measure. This is an interesting observation, as it illustrates that different conclusions could potentially be

derived for the same building depending on the IM selected to plot the fragility curves. The largest difference in the computed probability of exceedance is apparent when PGA instead of PGV or RSD_{max} is used as the IM. This is because PGA is not a good IM to represent the varying levels of ground shaking caused by earthquakes.

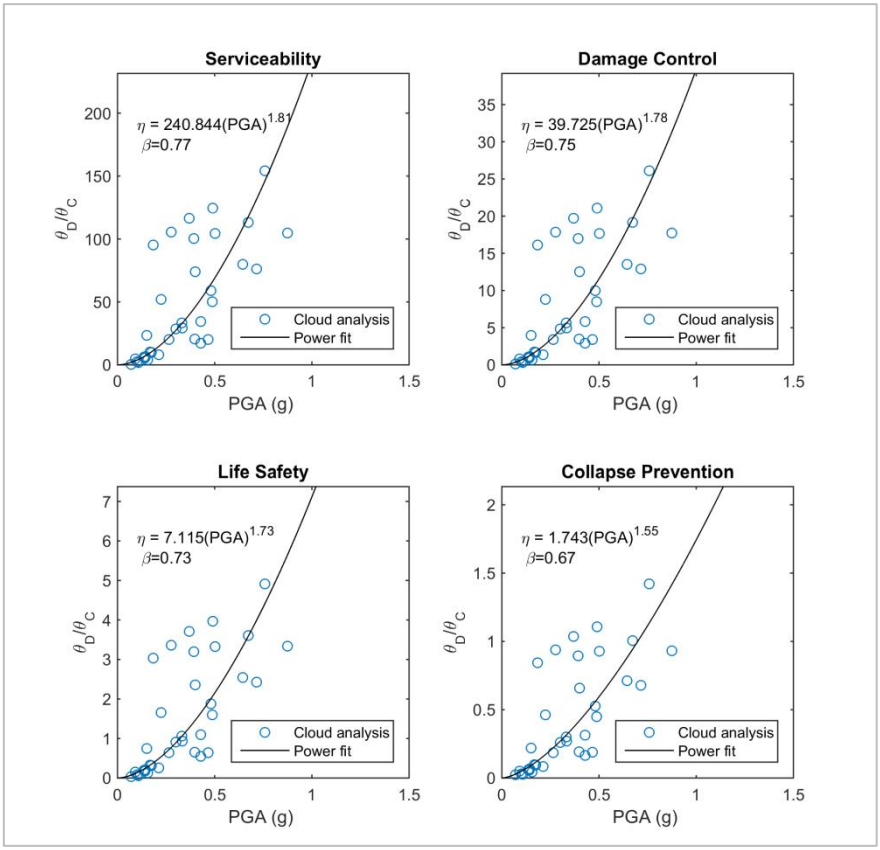

Figure 7-11: PSDM for 2-storey symmetric building with PGA as the IM

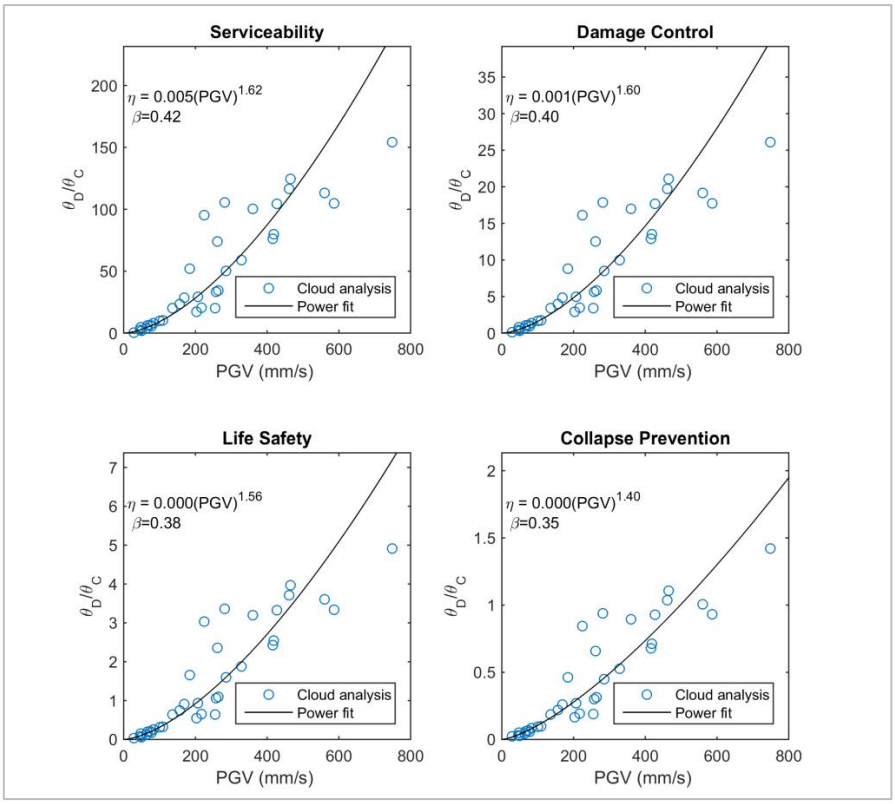

Figure 7-12: PSDM for 2-storey symmetric building with PGV as the IM

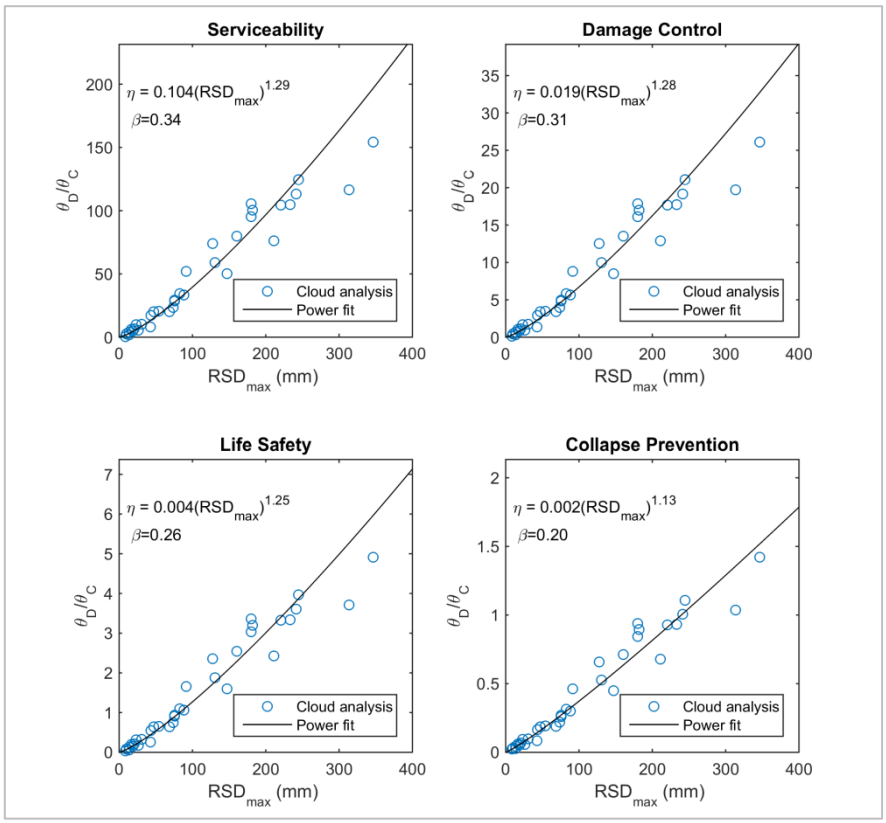

Figure 7-13: PSDM for 2-storey symmetric building with RSD_{max} as the IM

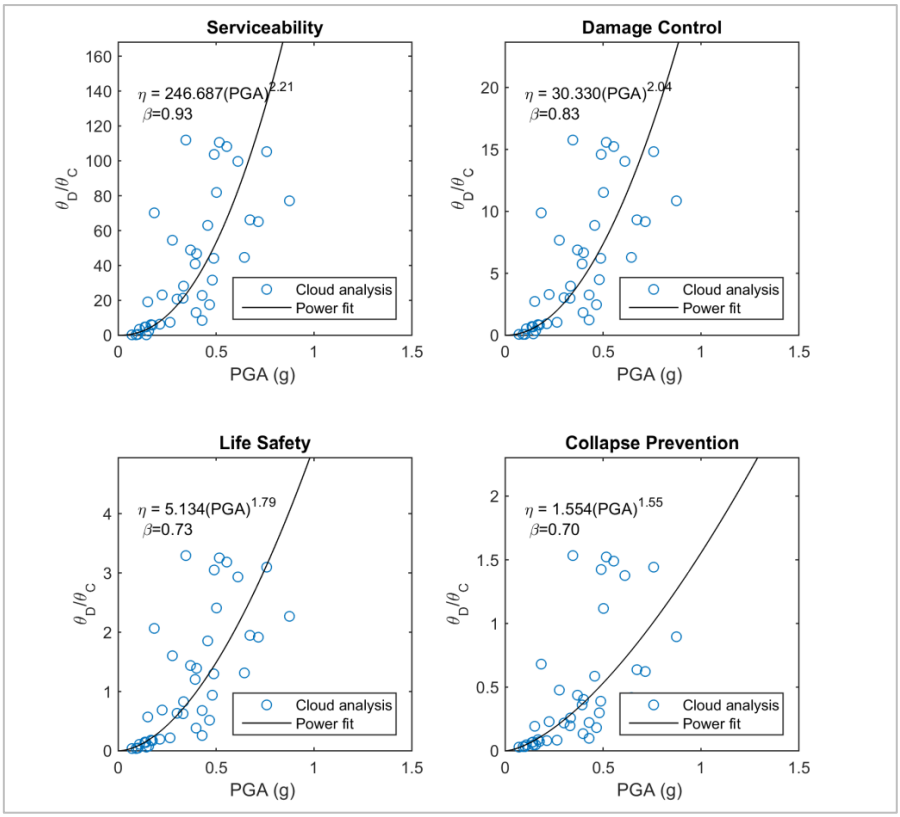

Figure 7-14: PSDM for 5-storey symmetric building with PGA as the IM

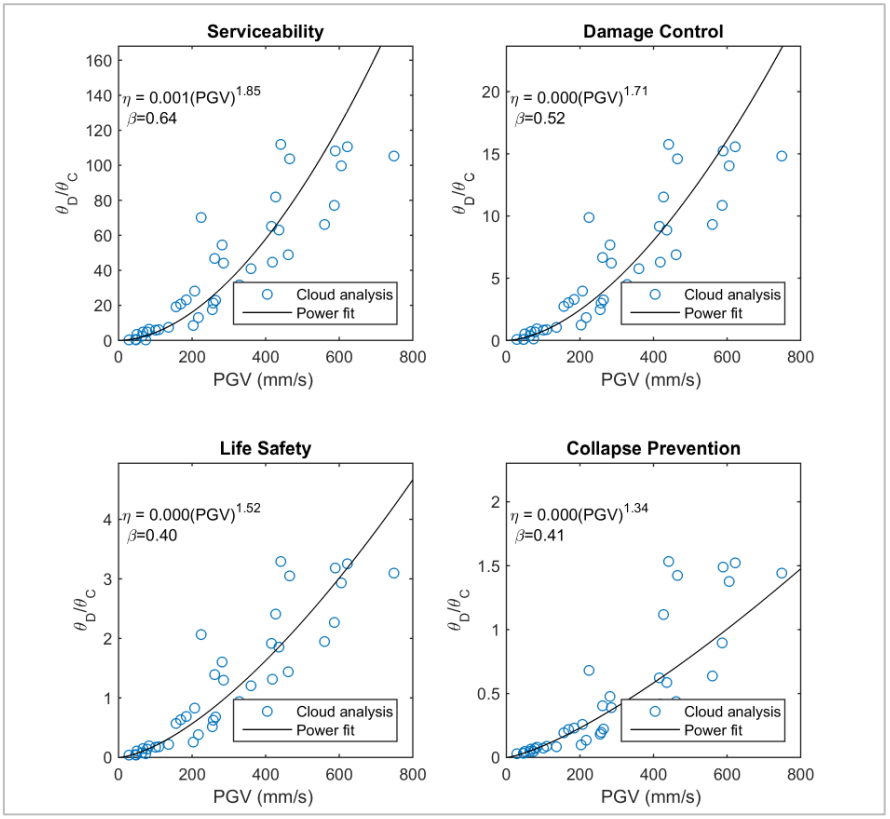

Figure 7-15: PSDM for 5-storey symmetric building with PGV as the IM

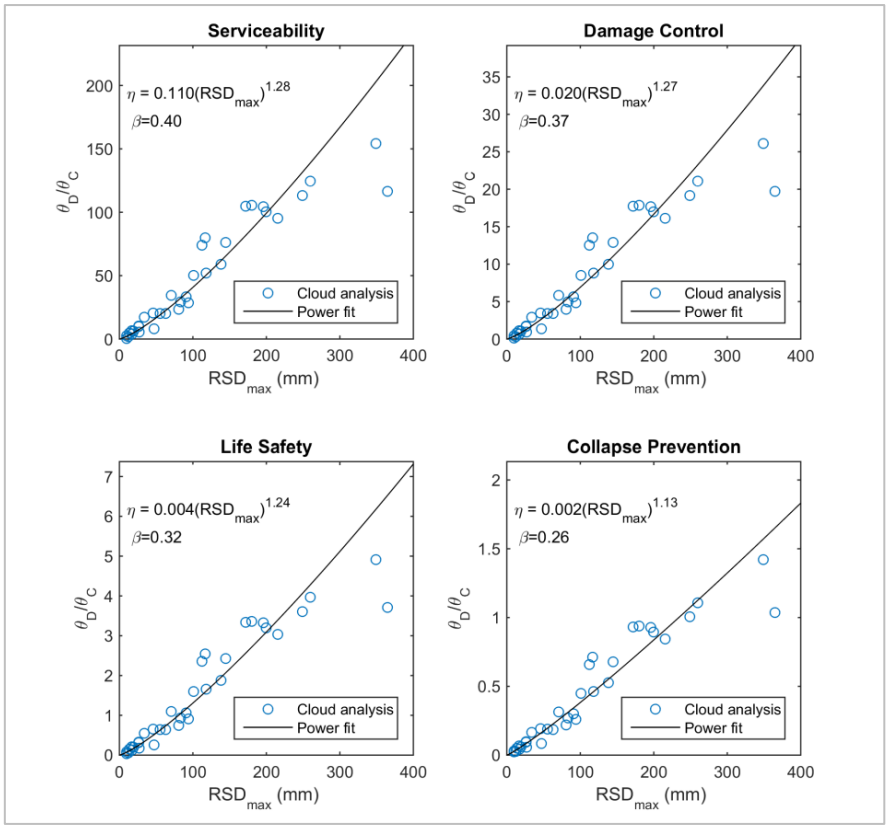

Figure 7-16: PSDM for 5-storey symmetric building with RSD_{max} as the IM

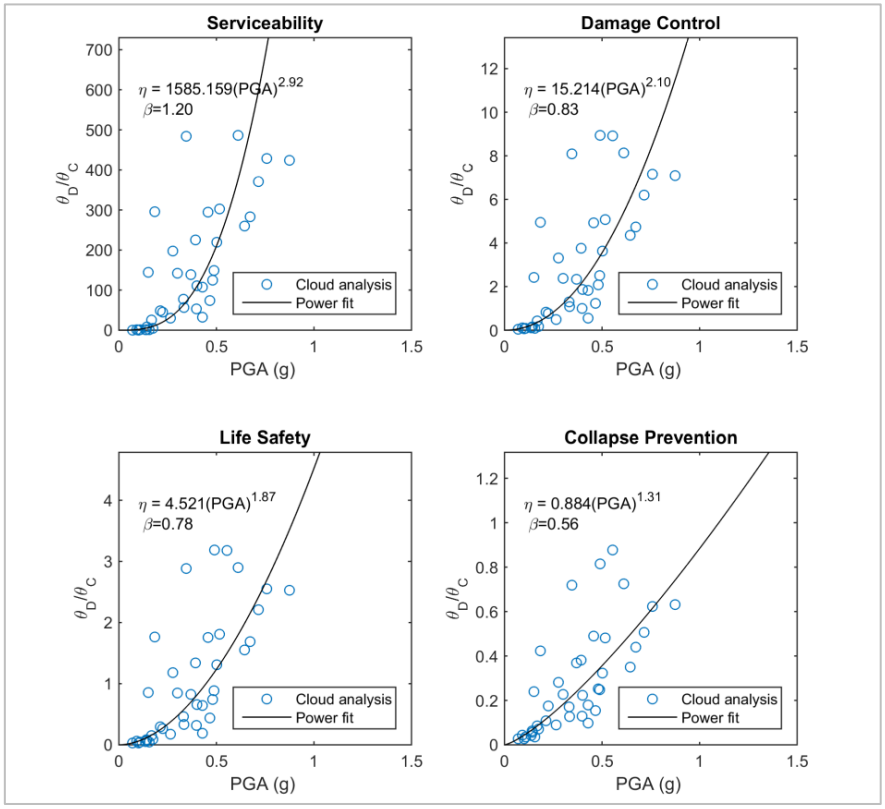

Figure 7-17: PSDM for 9-storey symmetric building with PGA as the IM

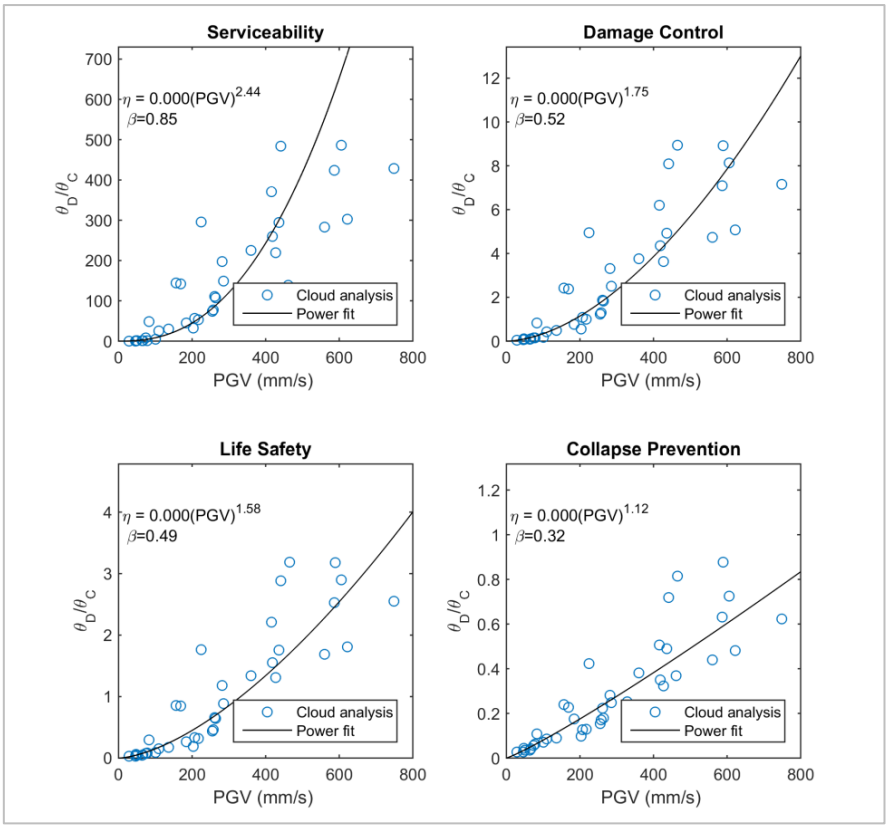

Figure 7-18: PSDM for 9-storey symmetric building with PGV as the IM

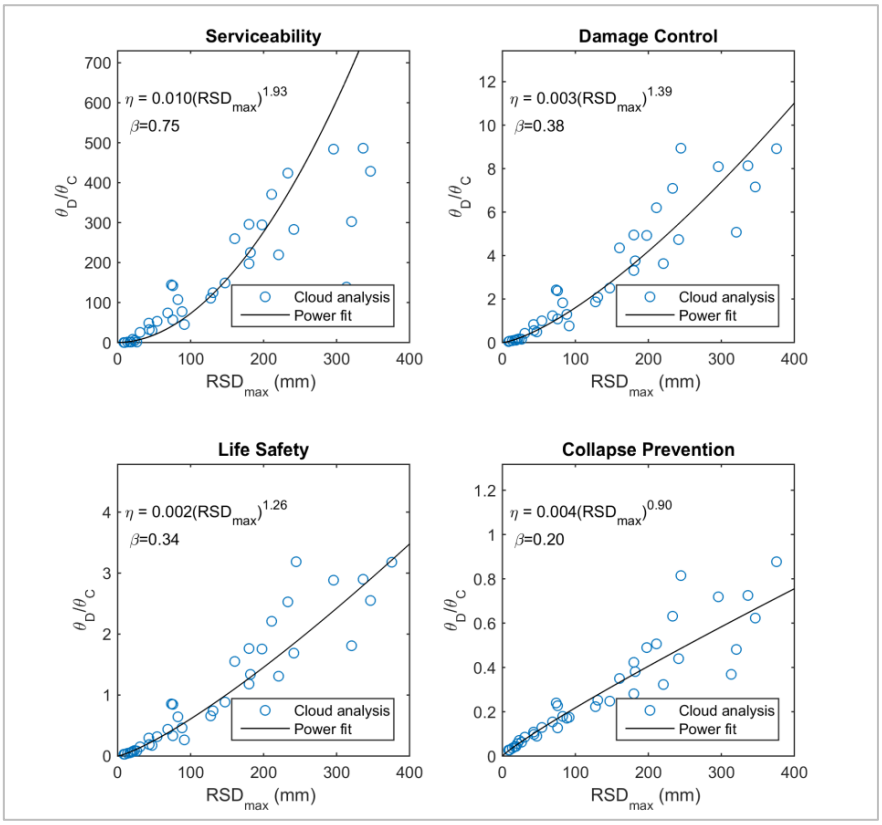

Figure 7-19: PSDM for 9-storey symmetric building with RSD_{max} as the IM

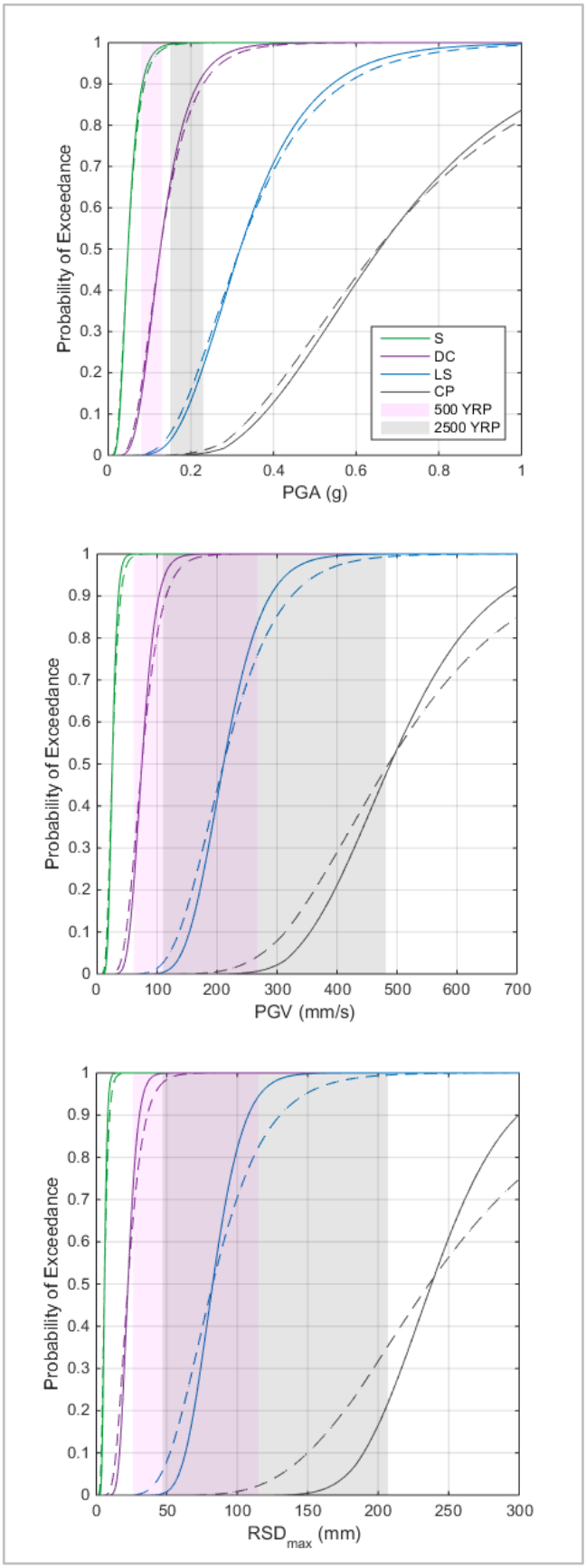

Figure 7-20: Fragility curves for 2-storey building, using PGA, PGV and RSD_{max} as IM, solid line: only $\beta_{Y|IM,\bar{c}}$ is considered, broken line: $\beta_{Y|IM,\bar{c}}$, β_C and β_M are considered

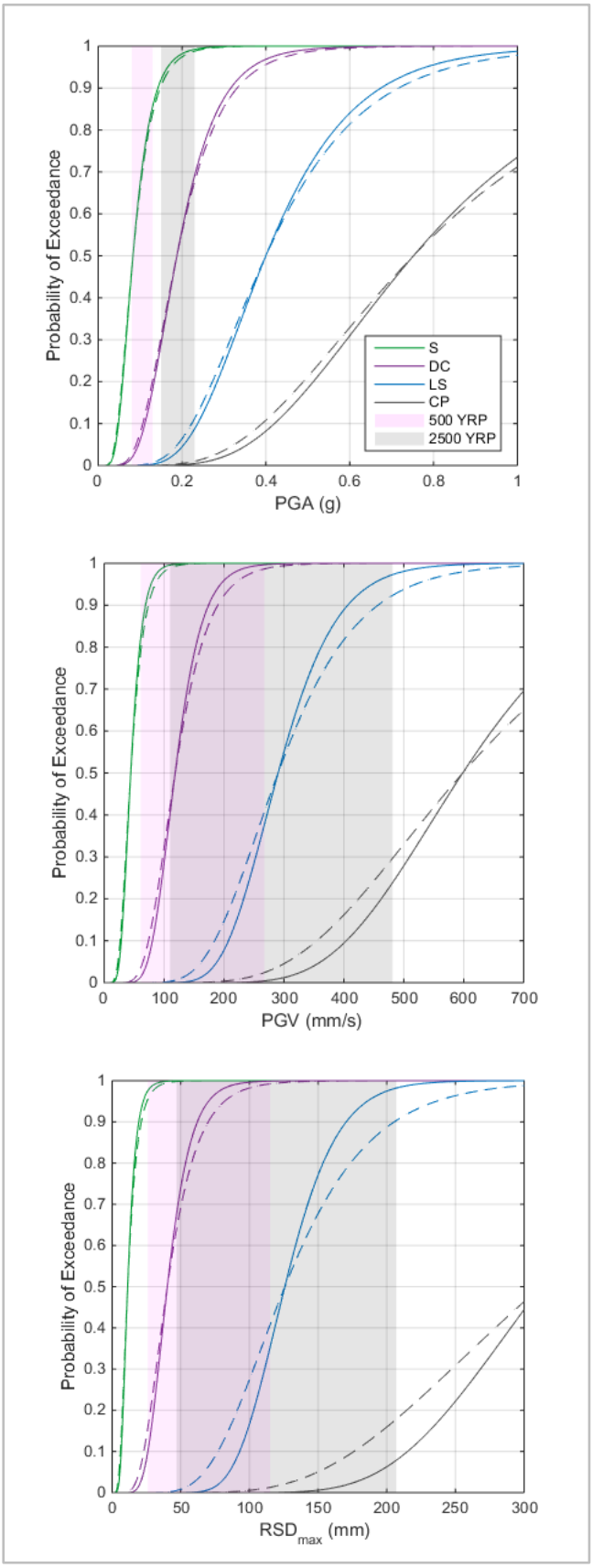

Figure 7-21: Fragility curves for 5-storey building, using PGA, PGV and RSD_{max} as IM, solid line: only $\beta_{Y|IM,\bar{c}}$ is considered, broken line: $\beta_{Y|IM,\bar{c}}$, β_C and β_M are considered

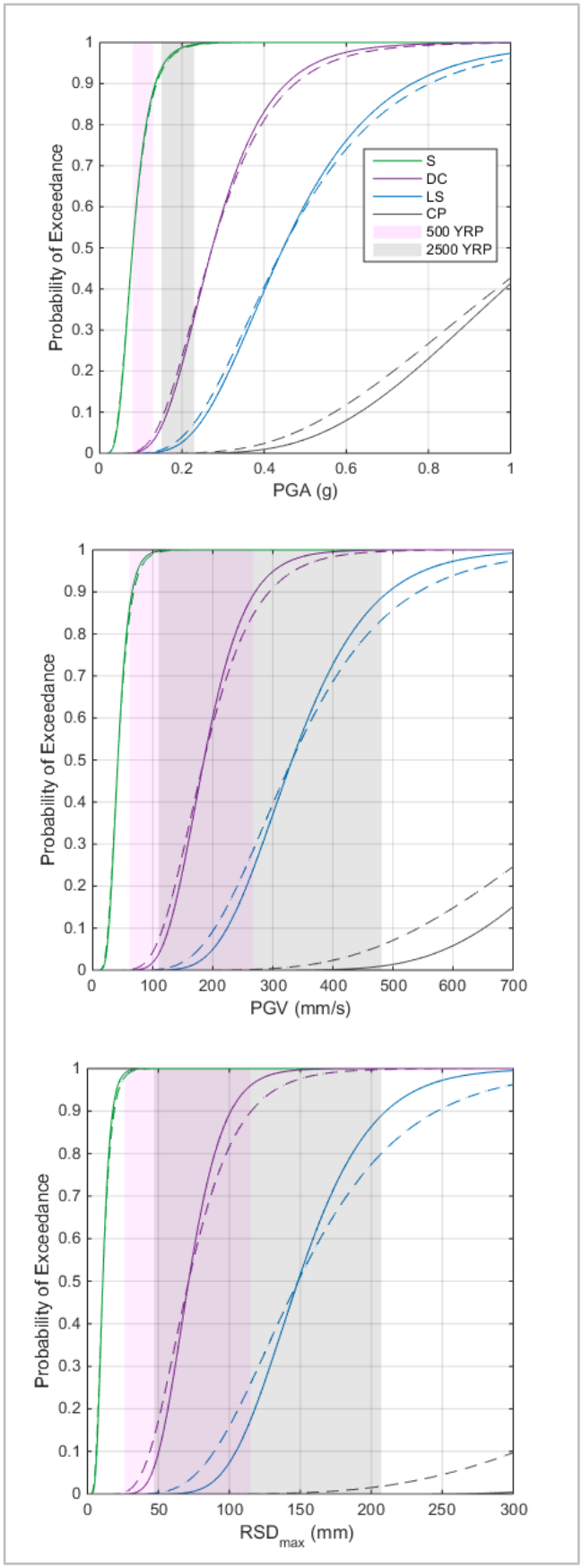

Figure 7-22: Fragility curves for 9-storey building, using PGA, PGV and RSD_{max} as IM, solid line: only $\beta_{Y|IM,\bar{c}}$ is considered, broken line: $\beta_{Y|IM,\bar{c}}$, β_C and β_M are considered

In order to select the IM to interpret the results obtained from the fragility curves with respect to performance objectives, direct comparison between the probability of exceedance computed when the IM is set to PGV or RSD_{max} is made for various site classes in Figure 7-23 and Figure 7-24 for a 500 YRP and 2500 YRP event, respectively as defined earlier in accordance with AS 1170.4:2007. It is noted that the probabilities of exceedance which are computed exclude β_C and β_M. Furthermore, PGA is not considered since it provides a poor correlation with the building response and it is not a suitable IM to represent the varying degrees of seismic excitation, particularly on soil sites.

The results in Figure 7-23 and Figure 7-24 illustrate that for the performance levels which correspond to lower levels of damage (*Serviceability* and *Damage Control*), higher probabilities of exceedance are predicted if RSD_{max} is adopted as the IM, for the cases for which the probability of exceedance is lower than 1.0. For the performance levels corresponding to higher levels of damage (*Life Safety* and *Collapse Prevention*), the probabilities of exceedance predicted using RSD_{max} and PGV as the IM are similar. However, it is noted that slightly higher probabilities of exceedance are predicted if PGV is adopted as the IM (the exceptions to this are the probabilities of exceedance predicted for the 2-storey building for the *Life Safety* limit state). When assessing the seismic performance of older buildings, the performance levels corresponding to higher levels of damage are often of greater interest. Therefore, for the case of plan-symmetric buildings, it is suitable to select PGV as the IM for conducting the assessment since it tends to provide conservative results for the performance levels corresponding to higher levels of damage. Furthermore, the relationships defined in AS 1170.4:2007 between the IM and return periods are more direct when the IM is PGV rather than RSD_{max}. The equation used to convert PGV_{rock} to RSD_{max} involves defining the second corner period. As discussed in Section 2.3.2, the second corner period for soil sites may be significantly different to rock sites; therefore the assumption of using a constant second corner period of 1.5 seconds introduces an additional source of inaccuracy.

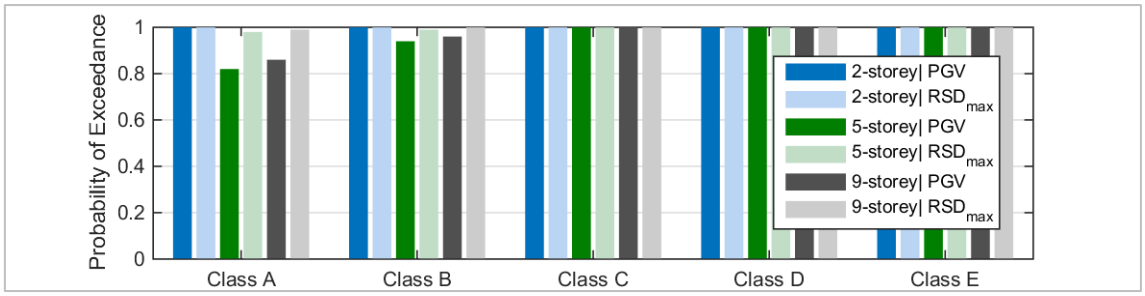

(a) Serviceability

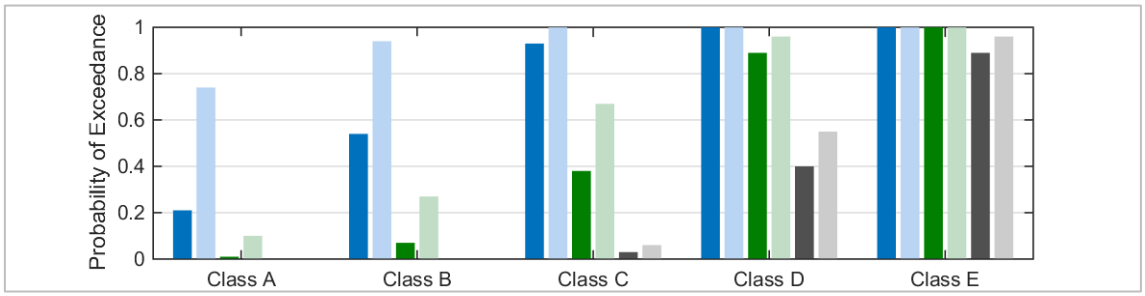

(b) Damage Control

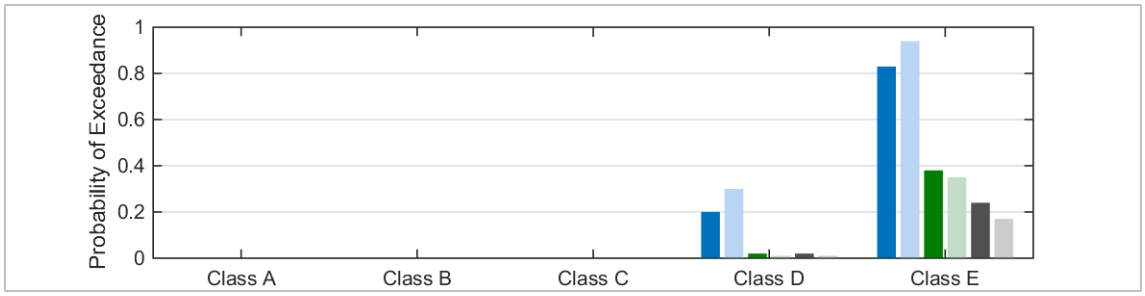

(c) Life Safety

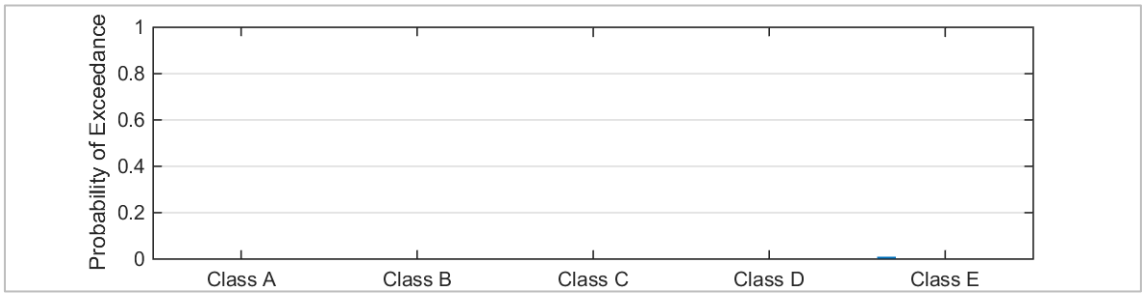

(d) Collapse Prevention

Figure 7-23: Comparison between the probability of exceedance computed using PGV and RSD_{max} as the IM under a 500 YRP event (k_pZ of 0.1 g) for four performance levels (β_C and β_M are not considered)

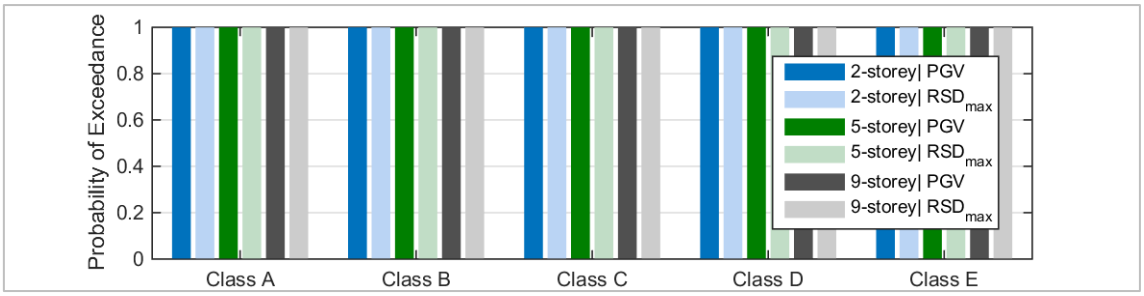

(a) Serviceability

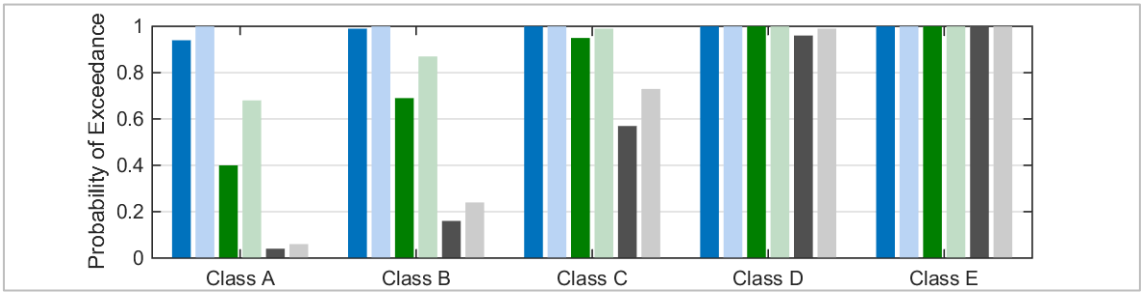

(b) Damage Control

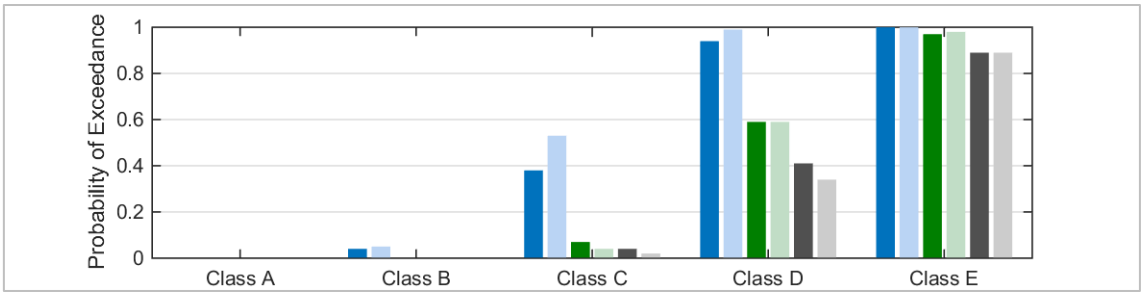

(c) Life Safety

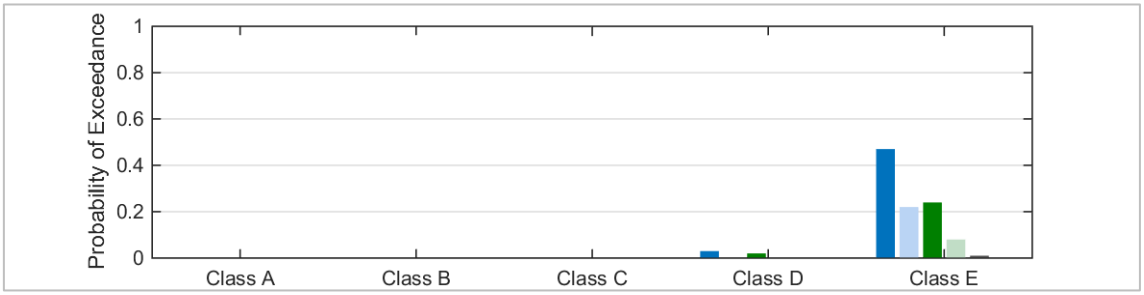

(d) Collapse Prevention

Figure 7-24: Comparison between the probability of exceedance computed using PGV and RSD_{max} as the IM under a 2500 YRP event (k_pZ of 0.18 g) for four performance levels (β_C and β_M are not considered)

7.5 RESULTS FOR BUILDINGS WITH PLAN ASYMMETRY

For buildings with plan asymmetry torsional resistance is provided by both the parallel and orthogonal elements. Therefore, the application of bidirectional ground motion becomes important to ensure that the contribution of the orthogonal elements is not over estimated during 3D time history analysis. Hence, for the archetypal buildings with plan asymmetry, time history analyses are conducted by applying the two horizontal components of the ground motion along the principal axes of the buildings. The stronger components of the two ground motions (i.e. the x-component) is applied along the weak direction of the building (i.e. along the x-axis), and the weaker component of the ground motions (y-component) is applied along the strong direction of the building (i.e. along the y-axis).

As discussed in Section 7.2.3, since the lumped plasticity approach is unable to capture the effects of biaxial bending, each plan-asymmetric archetypal building (2-, 5-, and 9-storey building) is analysed 3 times using different backbone definitions to investigate the effect of varying degrees of reduction of moment and drift capacities to account for biaxial bending. The three different wall and column backbone definitions which are modelled include when: (i) no reduction factors, (ii) medium bound reduction factors, and (iii) lower bound reduction factors, are applied to the backbones which have been originally defined for unidirectional loading.

For each time history analysis the critical demand-to-capacity ratio is obtained for each performance level in both the x- and y-direction. Due to the plan-asymmetric nature of the buildings, the performance levels may be reached first in either the x- or y-direction. To plot the fragility curves in one-dimension it is necessary to combine the building response in the x- and y-directions. One method to represent the building response for asymmetric buildings is to compute the square-root-of-the-sum-of-squares (SRSS) of the maximum response obtained in the x- and y-direction. This has mainly been adopted by studies which utilise storey level damage indicators (such as interstorey drift) to define performance levels and the effect of bidirectional loading is not directly captured on a local level (such as higher strain demands due to biaxial bending) (Jeong & Elnashai, 2004; Manie et al., 2015; Xu & Gardoni, 2016). Therefore this method of combination of the building response in the x- and y-direction is adopted to provide a better representation of the global response of the building due to bidirectional loading since a higher damage is predicted in comparison to considering the response of the building in one direction only. In this study this approach is most suitable to obtain the fragility curves for the plan-

asymmetric buildings which have been analysed without applying any reduction factors to the moment and drift capacity of the walls and columns to account for biaxial bending. Hence, the critical demand-to-capacity ratio for these building models may be computed using Eq. 7-4.

$$Y_{x,y.SRSS} = \sqrt{Y_x^2 + Y_y^2} \quad \text{Eq. 7-4}$$

The other method to combine the response obtained in the x- and y-direction is to simply take the maximum response obtained in either direction. This approach is a suitable method for this study for obtaining the fragility curves for the plan-asymmetric buildings for which the effects of biaxial bending have been considered. This is because the performance levels have been defined based on the first component which reaches a certain damage limit or when maximum interstorey drifts are reached at any location of the buildings. Therefore the SRSS method of computing the critical demand-to-capacity ratio would be too conservative since the effects of biaxial bending have already been accounted for at an element level. Hence, for these building models the critical demand-to-capacity ratio may be computed using Eq. 7-5.

$$Y_{x,y.max} = \text{maximum}(Y_x, Y_y) \quad \text{Eq. 7-5}$$

The intensity measure for the asymmetric buildings is obtained by calculating the geometric mean of the x- and y-component of the ground motion as discussed for the symmetric buildings. Furthermore, the same limits which were adopted for the various performance limits to define *collapse* cases have been applied to exclude data associated with numerical instabilities to compute $P(Y > 1|IM, \vec{c})$.

A comparison between the fragility curves obtained using the different methods to compute the critical demand-to-capacity ratio is provided in Figures 7-25 to 7-27. The fragility curves are computed for the plan-asymmetric buildings for which no reduction factors have been applied to account for biaxial bending. Four different methods are used to compute the critical demand-to-capacity ratio, including: (i) only the response in the x-direction is considered, Y_x, (ii) only the response y-direction is considered, Y_y, (iii) the response in the x- and y-direction are combined using the SRSS approach, $Y_{x,y.SRSS}$, and (iv) the maximum response in either the x- or y-direction is obtained, $Y_{x,y.max}$. Furthermore, the results are only presented for when PGV is selected as the IM, however, similar trends are expected for other IMs. The results indicate that the method used to compute the critical demand-to-capacity ratio has a larger effect for the performance

levels corresponding to higher levels of damage. The method of computing the critical demand-to-capacity ratio as $Y_{x,y.SRSS}$ always provides the most conservative response, that is; a higher probability of exceedance is predicted for the various performance levels in comparison to the other methods of computing Y. This is why this method is most suitable for obtaining the response of buildings for which the effects of bidirectional loading are not simulated in the nonlinear model. Furthermore, computing the critical demand-to-capacity ratio using $Y_{x,y.max}$, in general, provides higher probabilities of exceedance in comparison to computing the critical demand-to-capacity ratio in just one principal direction of the building. This implies that the method of computing the critical demand-to-capacity ratio as the maximum response in either of the principal directions of the building will generally result in conservative predictions for the fragility curves in comparison to computing the critical demand-to-capacity ratio by considering the response of the building in one direction only.

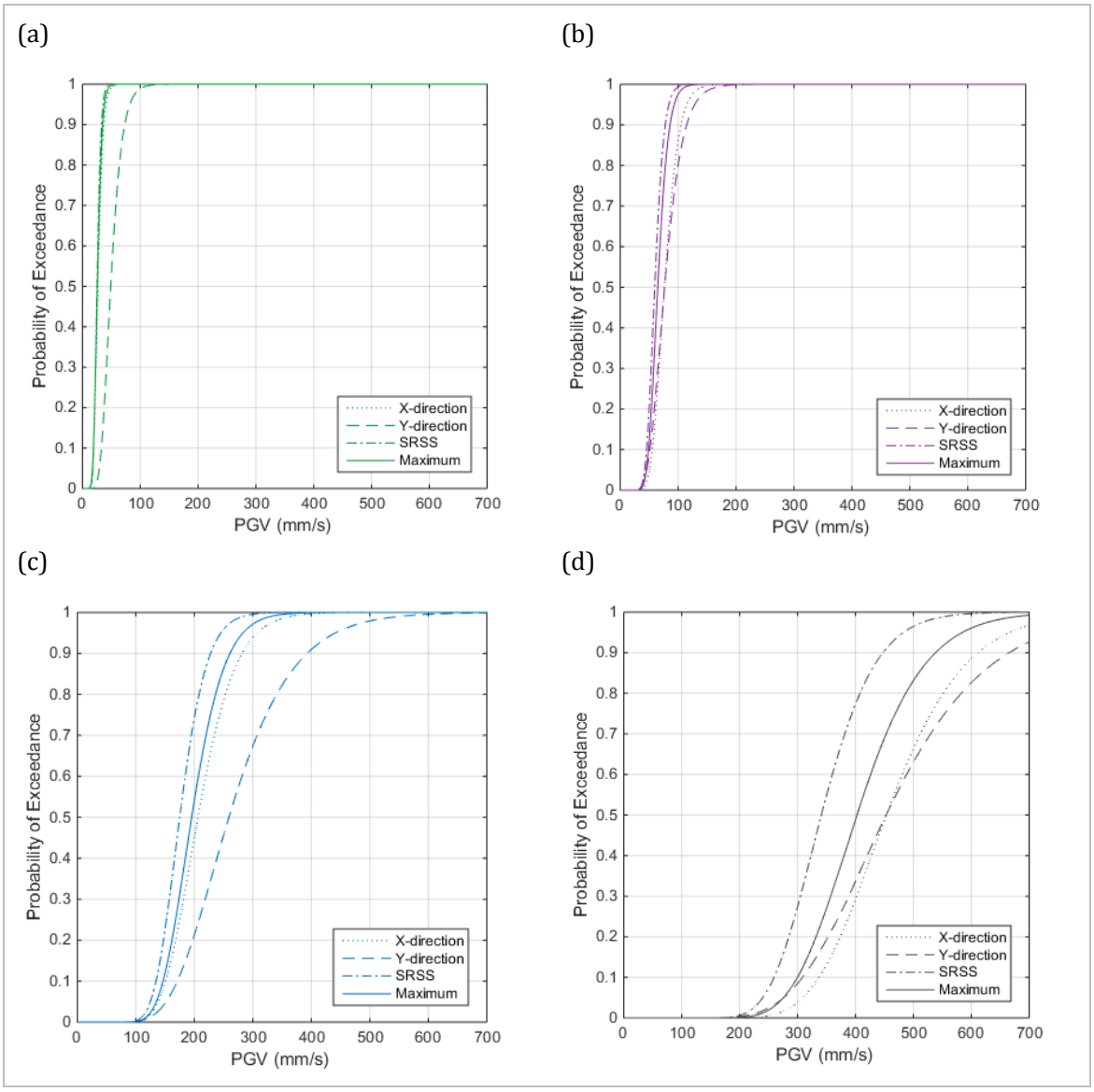

Figure 7-25: Comparison between different methods for calculating the critical demand-to-capacity ratio for the 2-storey plan-asymmetric building at different performance levels: (a) Serviceability, (b) Damage Control, (c) Life Safety, and (d) Collapse Prevention

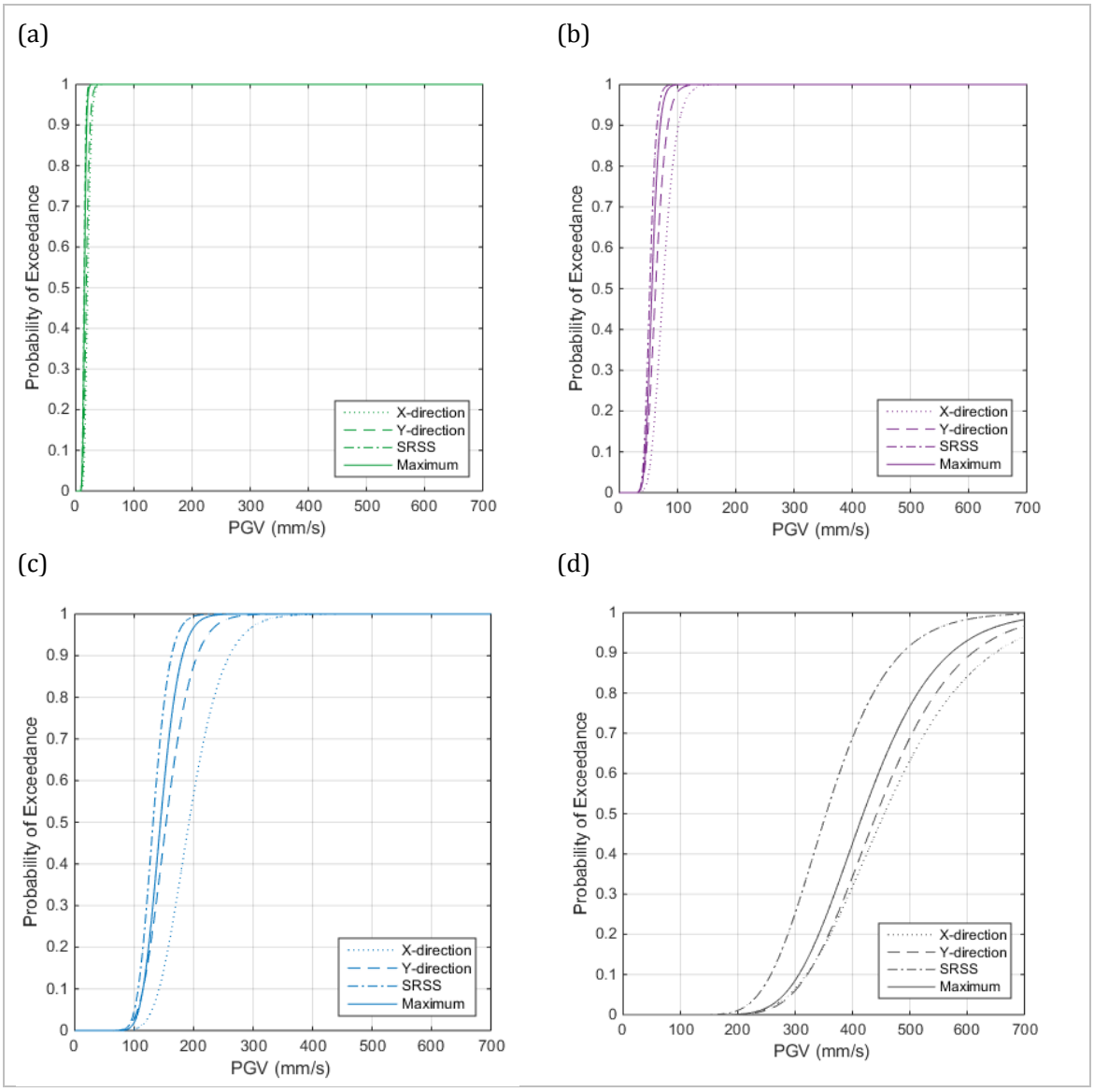

Figure 7-26: Comparison between different methods for calculating the critical demand-to-capacity ratio for the 5-storey plan-asymmetric building at different performance levels: (a) Serviceability, (b) Damage Control, (c) Life Safety, and (d) Collapse Prevention

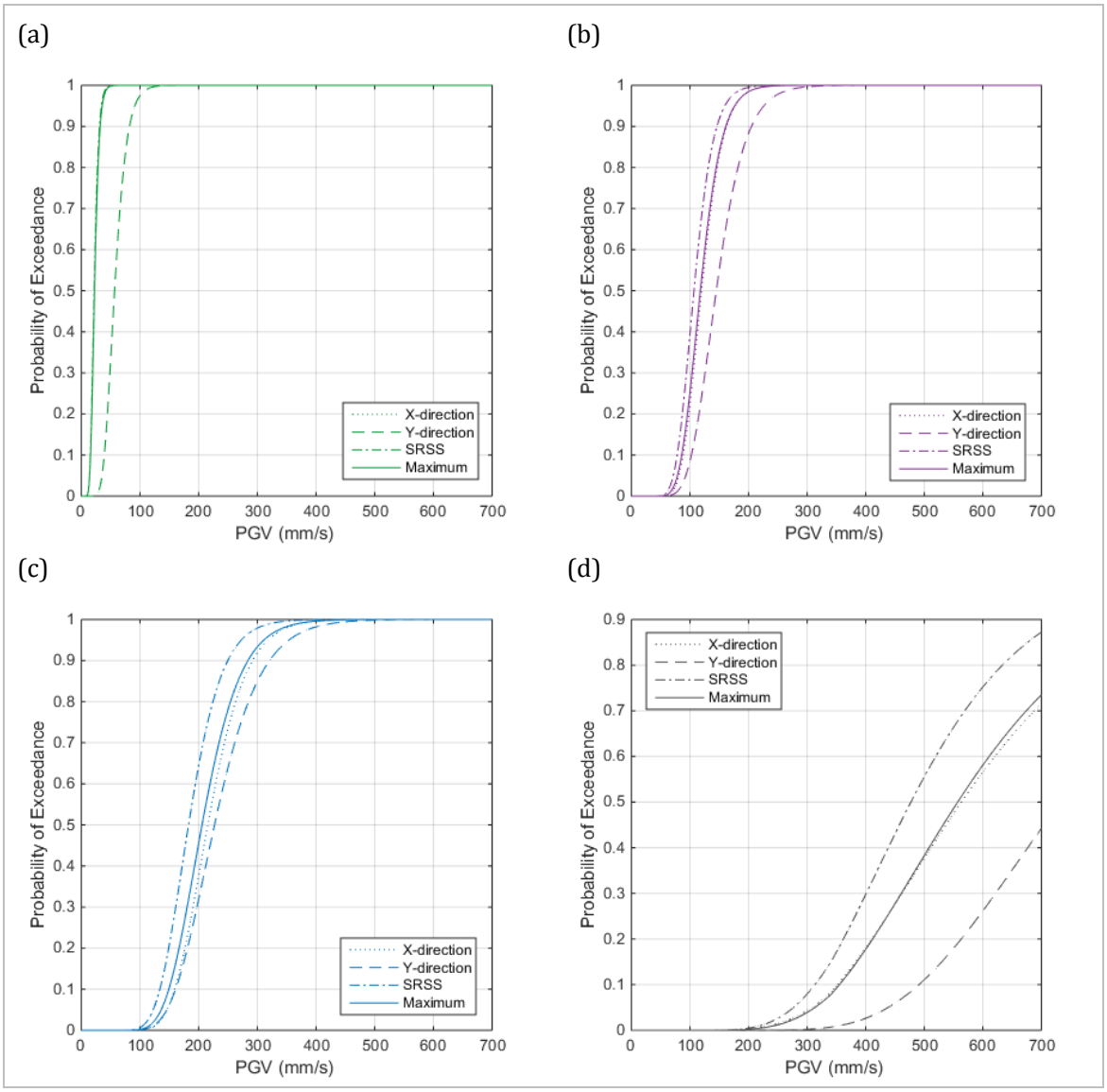

Figure 7-27: Comparison between different methods for calculating the critical demand-to-capacity ratio for the 9-storey plan-asymmetric building at different performance level: (a) Serviceability, (b) Damage Control, (c) Life Safety, and (d) Collapse Prevention

The results obtained from the plan-symmetric buildings indicated that PGV or RSD_{max} were the most suitable parameters for developing fragility curves for the buildings assessed. Furthermore, it was concluded that for the purpose of relating the fragility results to performance objectives PGV may be adopted. In order to examine the suitability of PGV and/or RSD_{max} for plan-asymmetric buildings, the dispersion related to the critical demand-to-capacity ratio as a function of IM ($\beta_{Y|IM,\bar{c}}$) is plotted in Figure 7-28 and Figure 7-29 where the critical demand-to-capacity ratio is calculated as $Y_{x,y.SRSS}$ and $Y_{x,y.max}$, respectively. The results presented are for the plan-asymmetric buildings for which no reduction factors have been applied to the wall and column backbones to account for biaxial bending. It is evident that there is no significant difference in correlation between

the building response and IM for whether the critical demand-to-capacity ratio is computed using $Y_{x,y.SRSS}$ or $Y_{x,y.max}$. Furthermore, similar to the buildings with plan symmetry, it is observed that in general the IMs which consistently demonstrate a good correlation with the building response for different performance levels and building heights are PGD, PGV, and RSD_{max}. Thus, PGV or RSD_{max} are both suitable IMs for plan-asymmetric buildings in terms of providing a good correlation with the building response.

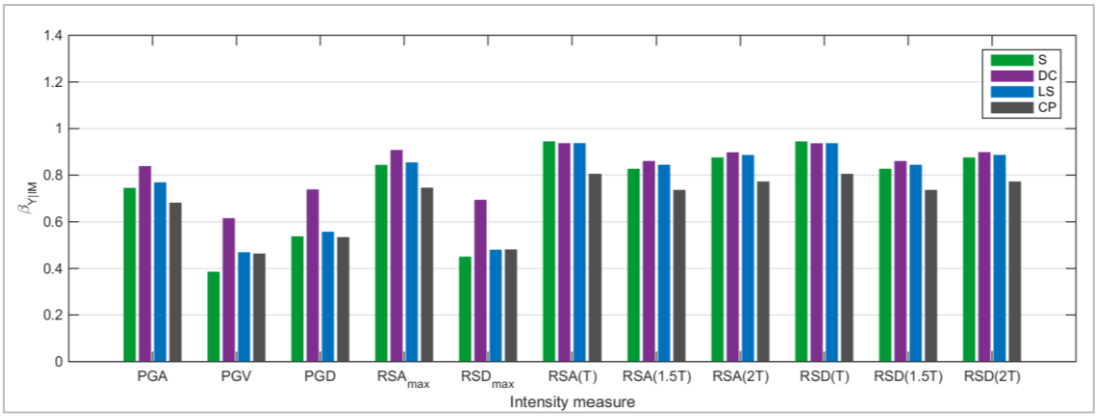

(a) 2-storey building

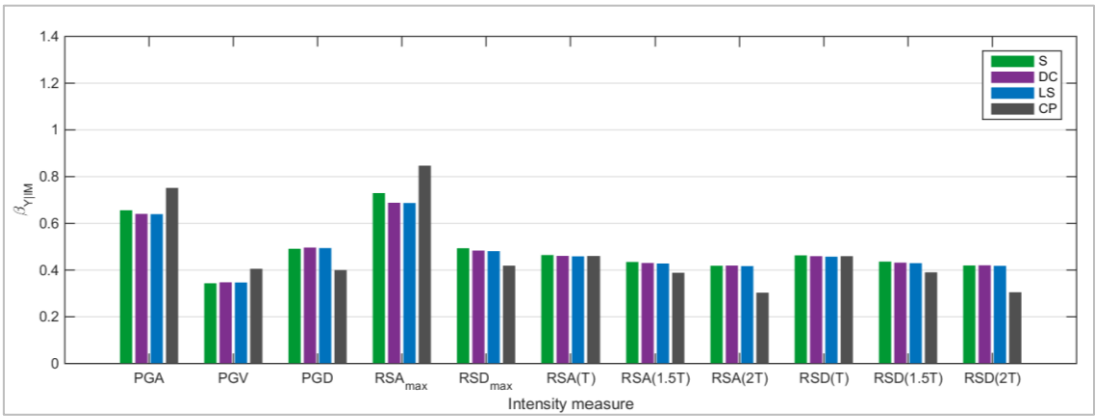

(b) 5-storey building

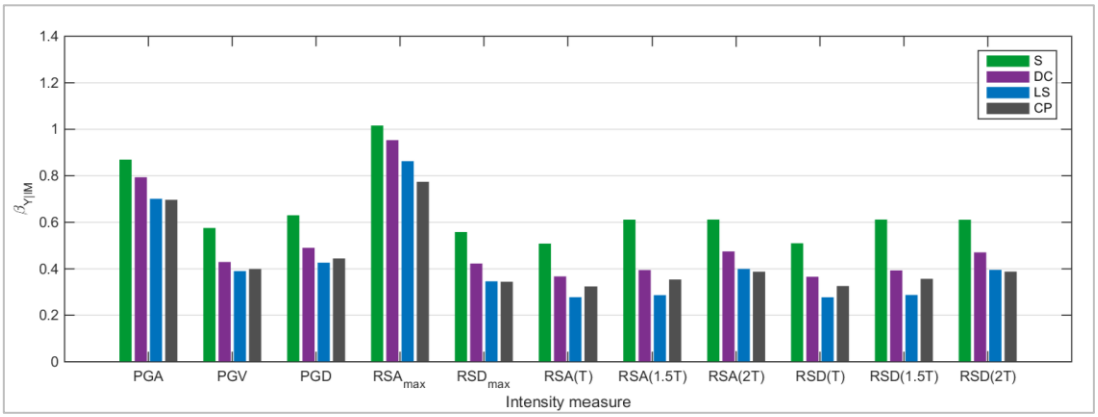

(c) 9-storey building

Figure 7-28: Dispersion factors for buildings with plan asymmetry where the critical demand-to-capacity ratio is calculated using $Y_{x,y.SRSS}$

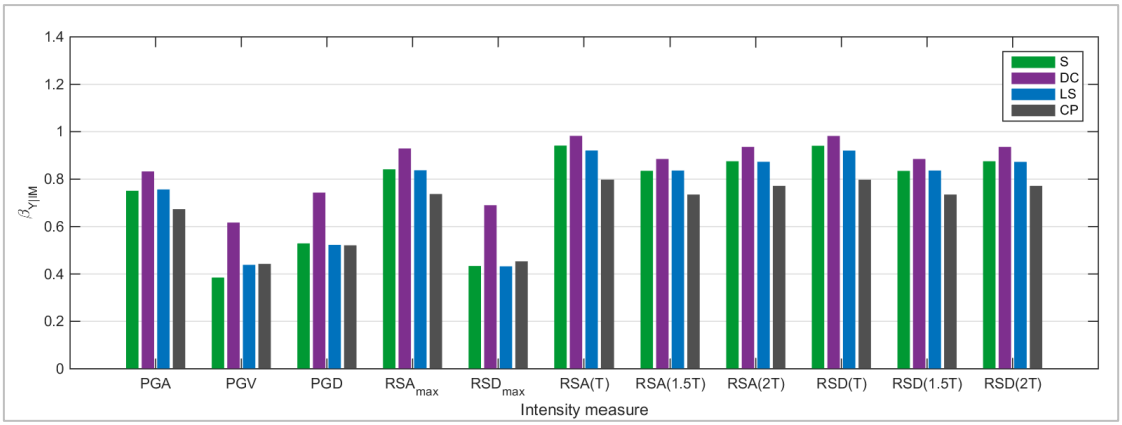

(a) 2-storey building

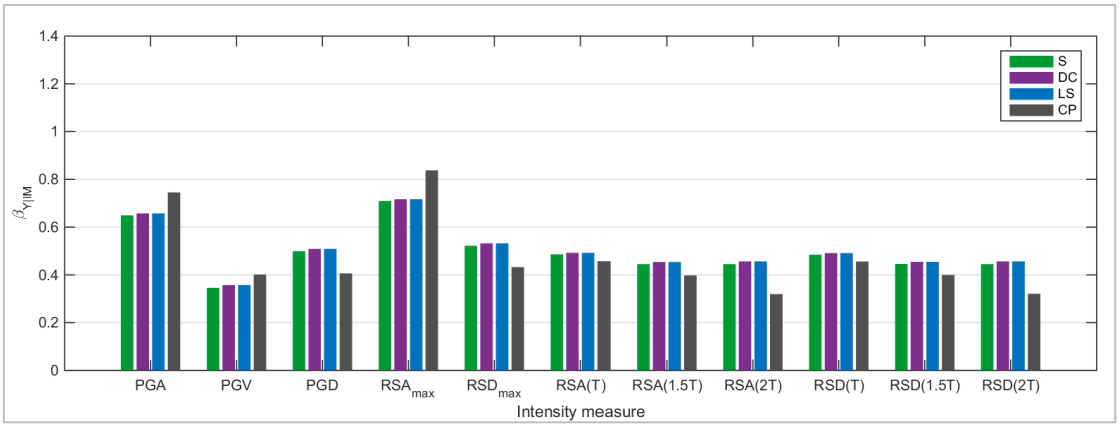

(b) 5-storey building

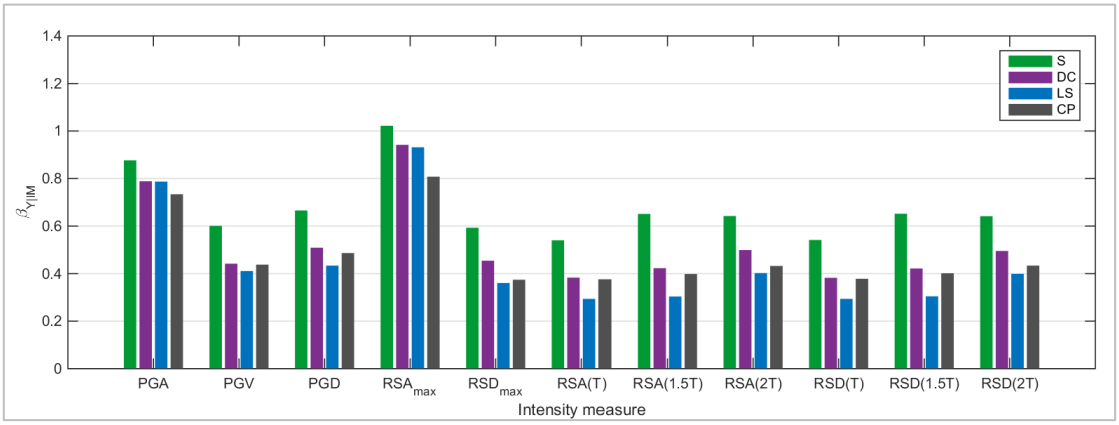

(c) 9-storey building

Figure 7-29: Dispersion factors for buildings with plan asymmetry where the critical demand-to-capacity-ratio is calculated using $Y_{x,y.max}$

Figures 7-30 to 7-32, compare the fragility curves computed for the 2-, 5-, and 9-storey building with plan symmetry and asymmetry for the four performance levels for which the intensity measure is set to PGV and RSD_{max}. Furthermore, for completion the results are also provided using the conventional IM, PGA. Different methods are used to compute the fragility curves for the plan-asymmetric buildings depending on how the buildings have

been modelled. For the building models which do not incorporate reductions for the walls and columns capacities to account for biaxial bending; the critical demand-to-capacity ratio are calculated using the SRSS of the response in the x- and y-direction (referred to as *Asym. no reduct. SRSS* model). For the purpose of comparison, for the same building model, the critical demand-to-capacity ratio is also calculated by taking the maximum response in the x- and y-direction (referred to as *Asym. no reduct. Maximum* model). For the building models for which either medium bound or lower bound reduction factors have been applied to compute the backbone for the walls and the columns, the critical demand-to-capacity ratio is calculated by taking the maximum response in the x- and y-direction (referred to as *Asym. med bound reduct.* model and *Asym. low bound reduct.* model). In addition, similar to the results presented for the plan-symmetric buildings, the intensity measures corresponding due to a 500 and 2500 YRP event in accordance with AS 1170.4:2007 for site classes ranging from A to E are shaded. It is also noted that the fragility curves presented are computed without considering the dispersion due to capacity and modelling uncertainties (β_C and β_M).

It can be seen that for all of the building heights investigated, the plan-asymmetric buildings perform worse than the plan-symmetric buildings. The difference in response between the fragility curves obtained for the plan-symmetric buildings and for the *Asym. no reduct. Maximum* plan-asymmetric building models, suggest that the poorer performance of the asymmetric buildings is predominantly based on the increase in seismic demand due to the plan configuration of the buildings.

It is also observed that the difference between the various methods used to model and compute the response of plan-asymmetric buildings becomes larger for performance levels corresponding to higher levels of damage. It is noteworthy that the difference in response for performance levels corresponding to lower levels of damage is almost negligible. This again highlights the variability in predicting the response of buildings at higher levels of damage especially close to collapse of RC buildings. The method suggested in the literature to obtain the building response by computing the SRSS of the maximum response in the x- and y-direction (i.e. *Asym. no reduct. SRSS* model) tends to provide similar predictions of probabilities of exceedance to the building models for which the effects of biaxial bending are incorporated by adopting medium bound reduction factors (i.e. *Asym. med bound reduct.* model). This indicates that the suitability of the SRSS method to account for bidirectional loading is highly dependent on the detailing of the RC buildings and the extent of damage that may occur under biaxial bending. In this study, the lower bound reduction factors were selected to be a conservative representation of the

response expected for non-ductile RC components and lightly reinforced walls since experimental data on these types of components is limited. The medium bound reduction factors provide a good representation of RC components with better detailing than those modelled in the archetypal buildings. Therefore the SRSS does not necessarily provide conservative results for poorly detailed RC buildings for which the effects of bidirectional loading are not considered. However, it is also noted that the approach of reducing the backbone prior to conducting the time history analyses, which is required for the lumped plasticity approach (adopted in this study), is not the most accurate method of simulating biaxial bending. Nevertheless, the adopted lumped plasticity approach is currently the most reliable method for simulating the response of 3D RC buildings up to the point of collapse.

In order to directly compare the difference in fragility curves computed using either PGV or RSD_{max}, the probability of exceedance for each performance level for the various site classes (without considering β_C and β_M) is presented using each IM under a 500 YRP and 2500 YRP event defined earlier in accordance with AS 1170.4:2007 in Figure 7-33 and Figure 7-34, respectively. For the purpose of comparison the results are only presented graphically for the plan-asymmetric buildings which have been modelled without any reduction in component capacities to account for biaxial bending and hence the critical demand-to-capacity ratio is computed as $Y_{x,y.SRSS}$. However, similar trends exist for the other modelling techniques adopted for the plan-asymmetric buildings.

It is observed that, in general, the probabilities of exceedance which are predicted using RSD_{max} are greater than those predicted using PGV as the IM, for *Serviceability, Damage Control*, and *Life Safety* for which the probability of exceedance is less than 1.0. However, similar to the plan-symmetric buildings, the probabilities of exceedance are higher for the *Collapse Prevention* limit state under a 2500 YRP event when PGV is used as the IM. Thus, depending on the performance objectives examined the use of PGV or RSD_{max} may provide more conservative results. However, as discussed in Section 7.4, the equation used to relate PGV to return periods and various site conditions is more direct than RSD_{max} when using the approach in AS 1170.4:2007. Therefore, PGV is considered to be a more reliable IM for evaluating the building response from fragility curves with relation to performance objectives.

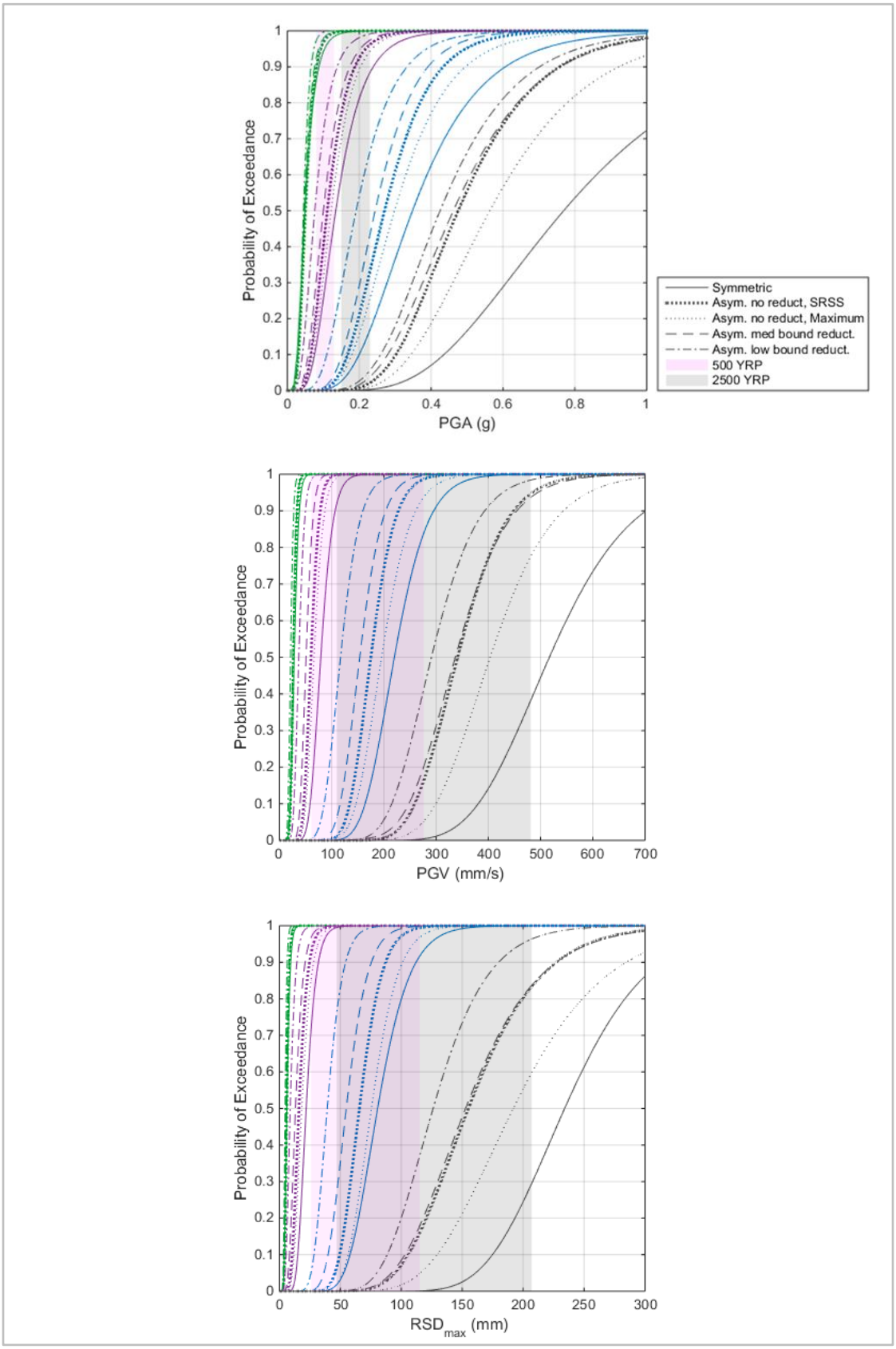

Figure 7-30: Comparison between fragility curves for 2-storey plan-symmetric and plan asymmetric buildings using PGA, PGV and RSD_{max} as IM (green curves: Serviceability, purple curves: Damage Control, blue curves: Life Safety, grey curves: Collapse Prevention)

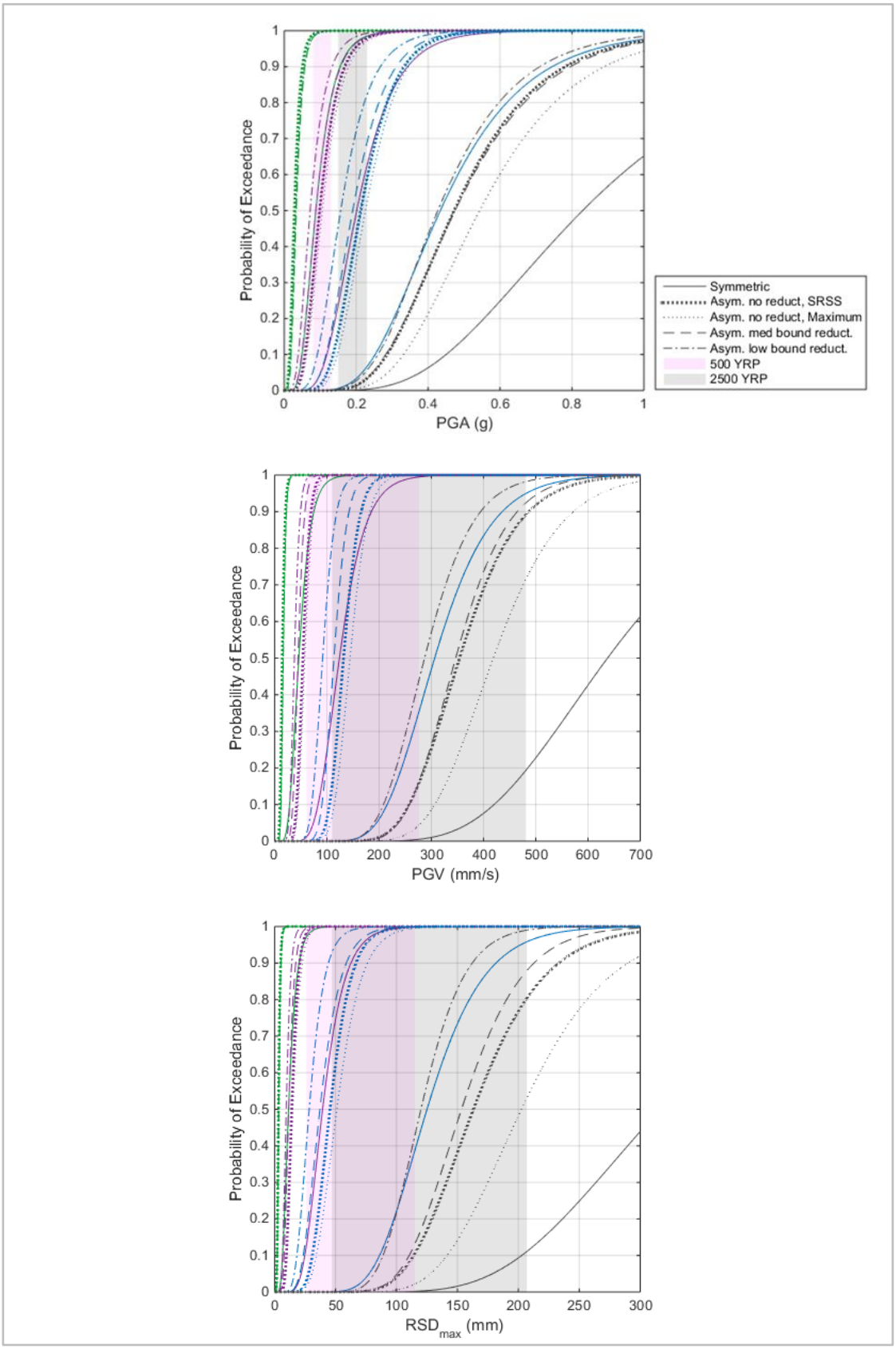

Figure 7-31: Comparison between fragility curves for 5-storey plan-symmetric and plan asymmetric buildings using PGA, PGV and RSD_{max} as IM (green curves: Serviceability, purple curves: Damage Control, blue curves: Life Safety, grey curves: Collapse Prevention)

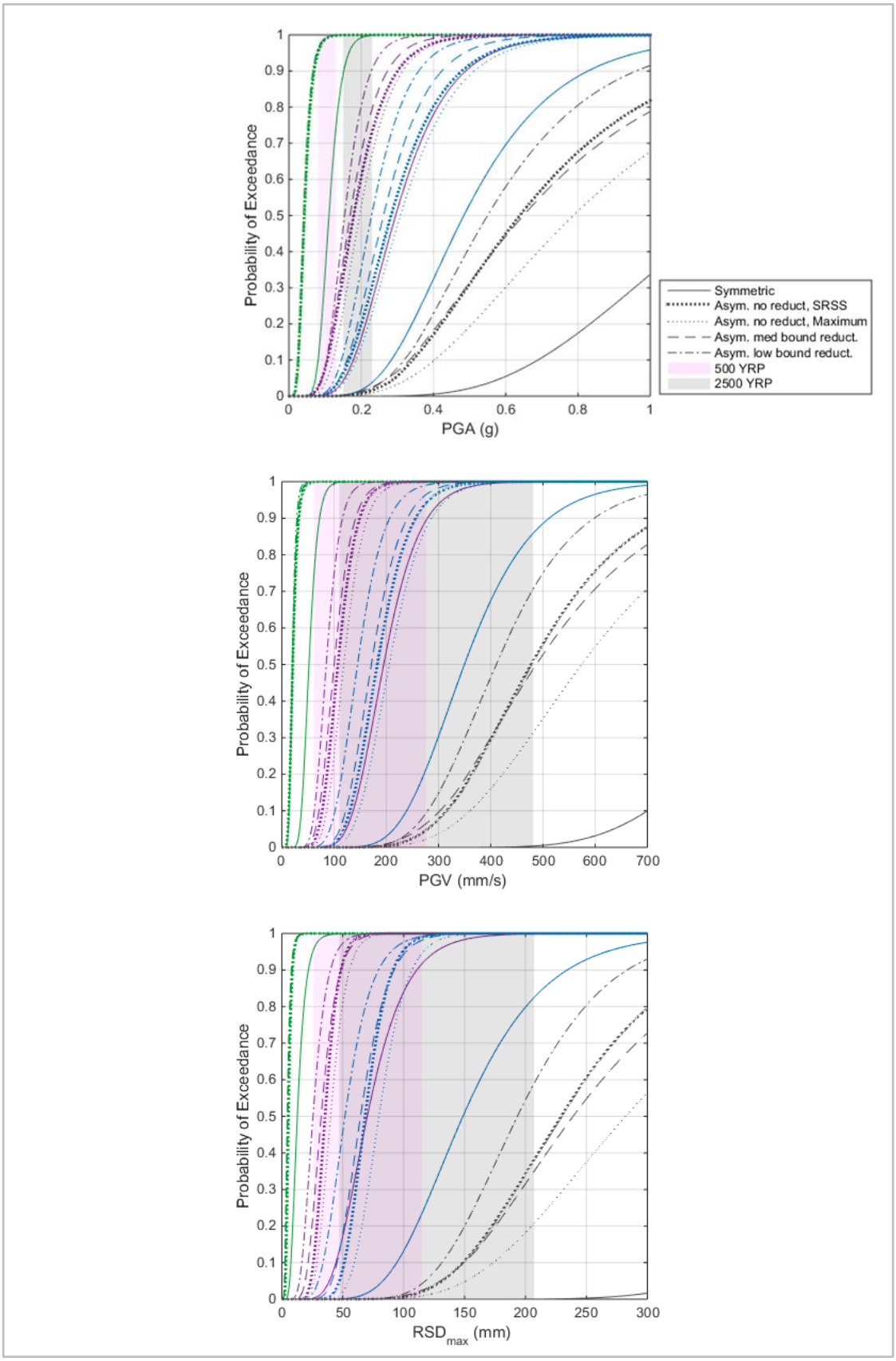

Figure 7-32: Comparison between fragility curves for 9-storey plan-symmetric and plan asymmetric buildings using PGA, PGV and RSD_{max} as IM (green curves: Serviceability, purple curves: Damage Control, blue curves: Life Safety, grey curves: Collapse Prevention)

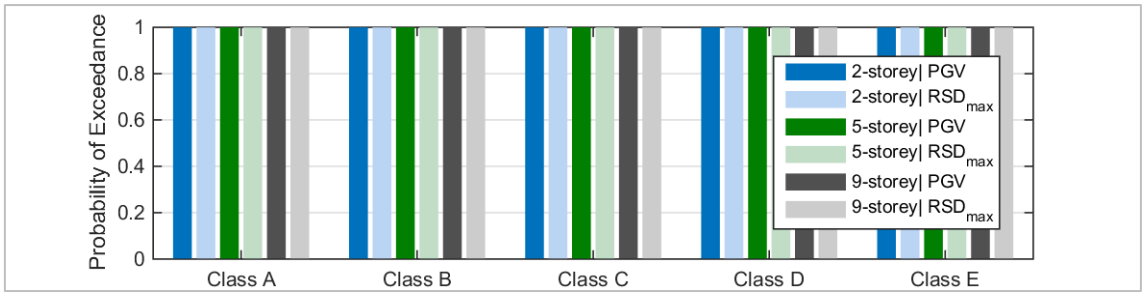

(a) Serviceability

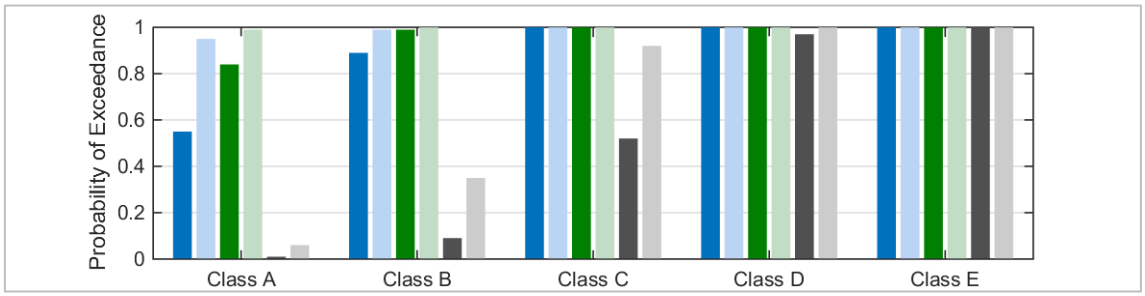

(b) Damage Control

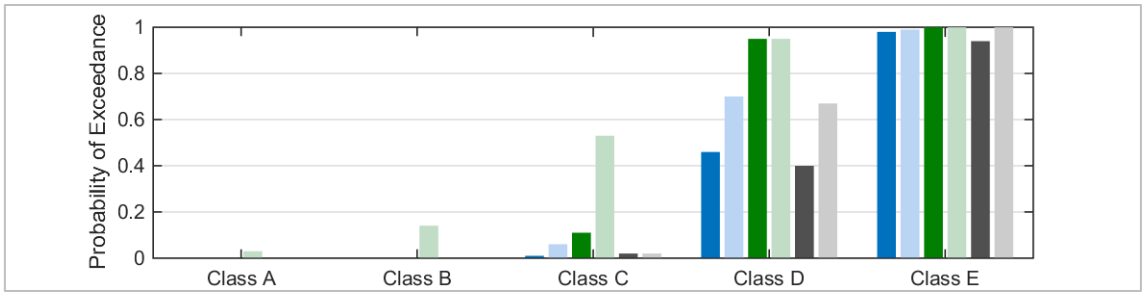

(c) Life Safety

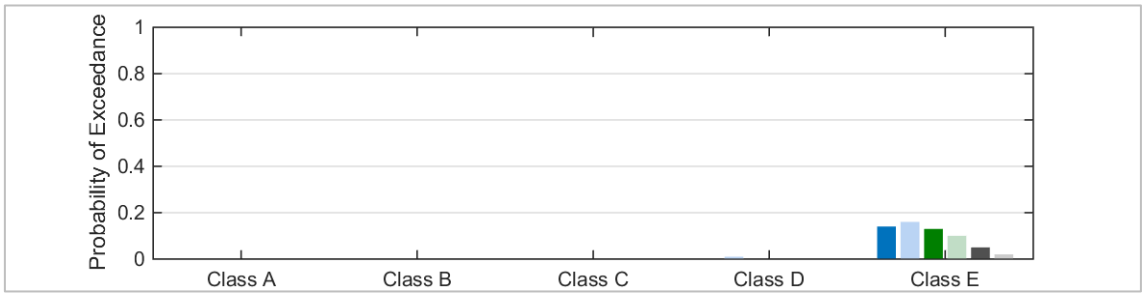

(d) Collapse Prevention

Figure 7-33: Comparison between the probability of exceedance computed using PGV and RSD_{max} as the IM under a 500 YRP event for four performance levels for asymmetric buildings without any reduction for biaxial bending

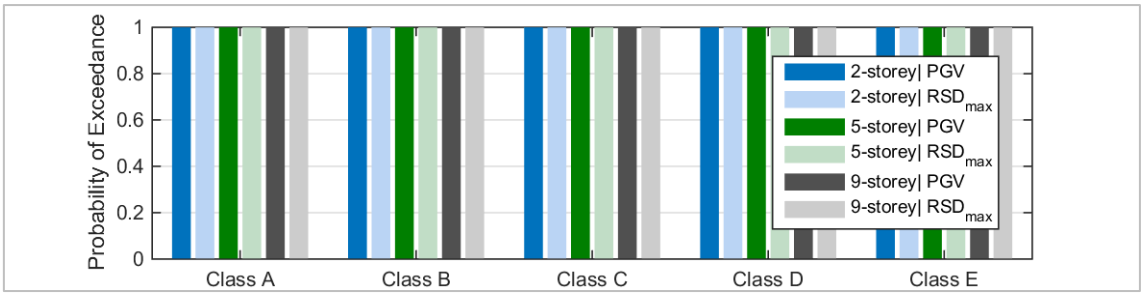

(a) Serviceability

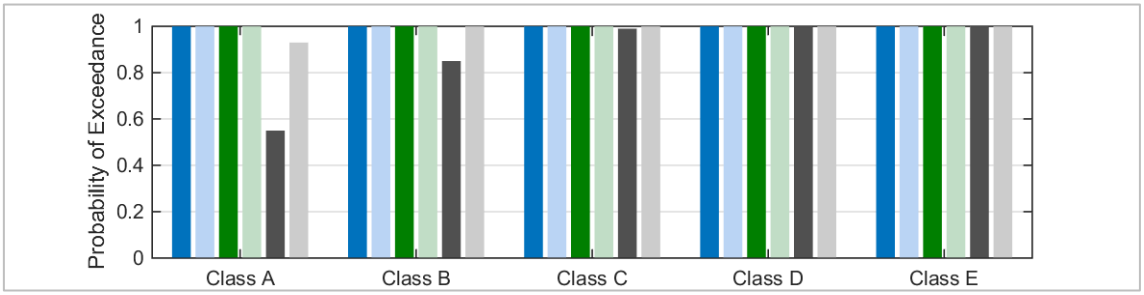

(b) Damage Control

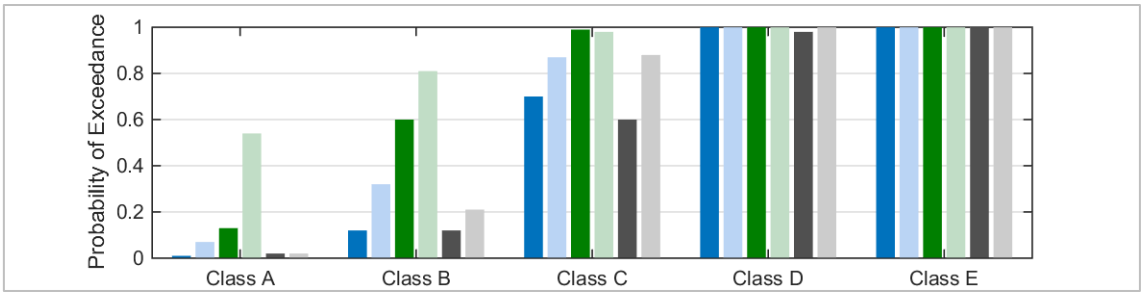

(c) Life Safety

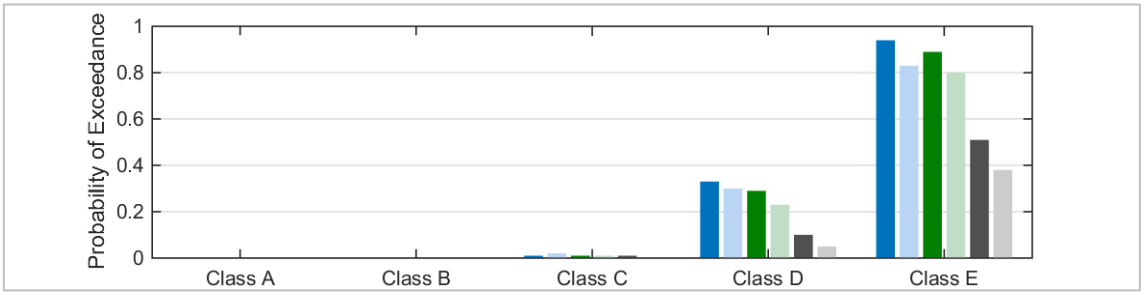

(d) Collapse Prevention

Figure 7-34: Comparison between the probability of exceedance computed using PGV and RSD_{max} as the IM under a 2500 YRP event for four performance levels for asymmetric buildings without any reduction for biaxial bending

7.6 EVALUATION OF THE SEISMIC PERFORMANCE OF THE ARCHETYPAL BUILDINGS

A summary of the median response of the fragility curves (i.e. the IM at the median probability of exceedance) for the various intensity measures; PGA, PGV, and RSD_{max} is provided in Tables 7-8 to 7-10, respectively. For the plan-asymmetric buildings, the median probability of exceedance is provided for the three different modelling approaches: (i) *Asym. no reduct. SRSS*, no reductions are applied to the unidirectional moment and drift capacities to account for biaxial bending and the critical demand-to-capacity ratio was computed using $Y_{x,y.SRSS}$, (ii) *Asym. med bound reduct.,* medium bound reduction factors are applied to account for biaxial bending for the wall and columns, and the critical demand-to-capacity ratio is computed using $Y_{x,y.max}$, and (iii) *Asym. low bound reduct.,* low bound reduction factors are applied to account for biaxial bending, and the critical demand-to-capacity ratio is computed using $Y_{x,y.max}$.

Table 7-8: Median PGA (g) response of the fragility curves for the various building models

Building model		Performance Level			
		S	DC	LS	CP
2-storey	Symmetric	0.054	0.135	0.349	0.769
	Asym. no reduct. SRSS	0.057	0.114	0.275	0.476
	Asym. med bound reduct.	0.049	0.106	0.251	0.468
	Asym. low bound reduct.	0.049	0.081	0.194	0.428
5-storey	Symmetric	0.090	0.206	0.439	0.832
	Asym. no reduct. SRSS	0.033	0.106	0.218	0.476
	Asym. med bound reduct.	0.041	0.089	0.194	0.476
	Asym. low bound reduct.	0.033	0.073	0.162	0.428
9-storey	Symmetric	0.117	0.296	0.492	1.207
	Asym. no reduct. SRSS	0.049	0.186	0.283	0.646
	Asym. med bound reduct.	0.049	0.170	0.267	0.654
	Asym. low bound reduct.	0.041	0.162	0.235	0.557

Table 7-9: Median PGV (mm/s) response of the fragility curves for the various building models

Building model		Performance Level			
		S	DC	LS	CP
2-storey	Symmetric	30	79	220	517
	Asym. no reduct. SRSS	28	61	176	342
	Asym. med bound reduct.	26	52	155	338
	Asym. low bound reduct.	22	38	117	292
5-storey	Symmetric	47	124	307	638
	Asym. no reduct. SRSS	15	55	133	355
	Asym. med bound reduct.	18	45	114	348
	Asym. low bound reduct.	18	38	93	287
9-storey	Symmetric	53	195	350	988
	Asym. no reduct. SRSS	22	108	183	478
	Asym. med bound reduct.	22	101	172	488
	Asym. low bound reduct.	20	85	146	411

Table 7-10: Median RSD_{max} (mm) response of the fragility curves for the various building models

Building model		Performance Level			
		S	DC	LS	CP
2-storey	Symmetric	7	22	81	235
	Asym. no reduct. SRSS	6	16	66	155
	Asym. med bound reduct.	6	13	55	153
	Asym. low bound reduct.	5	9	40	127
5-storey	Symmetric	12	40	125	317
	Asym. no reduct. SRSS	4	14	46	163
	Asym. med bound reduct.	4	12	38	154
	Asym. low bound reduct.	4	10	29	121
9-storey	Symmetric	13	70	149	559
	Asym. no reduct. SRSS	6	36	68	229
	Asym. med bound reduct.	5	33	65	240
	Asym. low bound reduct.	4	26	52	193

To evaluate the seismic performance of the archetypal buildings with respect to performance objectives the Basic Safety Objective as described in FEMA 356, discussed in Section 6.5, is adopted. A summary of the probability of exceedance for the plan-symmetric and plan-asymmetric buildings is presented in Figure 7-35 for *Life Safety* under a 500 YRP event, and *Collapse Prevention* under a 2500 YRP event (corresponding to k_pZ of 0.1 g and 0.18 g on rock) computed for the various site classes in accordance with AS 1170.4:2007, using PGV as the IM. The minimum (MIN) and maximum (MAX) probabilities of exceedance predicted by the various methods that are commonly used to obtain the fragility curves are plotted. For the plan-symmetric buildings this involves considering the predicted response using PGV as the IM and whether or not β_C and β_M are included in the fragility functions. In addition to these variables, for the plan-asymmetric buildings, the range of values also consider the various methods used to obtain the fragility curves, including: (i) the building model for which the effects of biaxial bending is not considered in the component capacities, however, the critical demand-to-capacity ratio is computed using $Y_{x,y.SRSS}$, (ii) the building model for which medium bound reduction factors are applied to account for biaxial bending for the wall and columns, and the critical demand-to-capacity ratio is computed using $Y_{x,y.max}$, and (iii) the building model for which lower bound reduction factors are applied to account for biaxial bending, and the critical demand-to-capacity ratio is computed using $Y_{x,y.max}$.

For most cases there is a range between the minimum and maximum probability of exceedance predicted for a particular building. The difference between the minimum and maximum values obtained is consistently greater for the buildings with plan asymmetry in comparison to the buildings with plan symmetry. This is because for the plan-asymmetric

buildings different modeling methods were considered to provide an approximation for the effects of biaxial bending. The maximum values are predominantly governed by the models for which lower bound reduction factors were applied to account for biaxial bending and, as discussed in Section 7.5, this is considered to be a better representation of the archetypal buildings being assessed here.

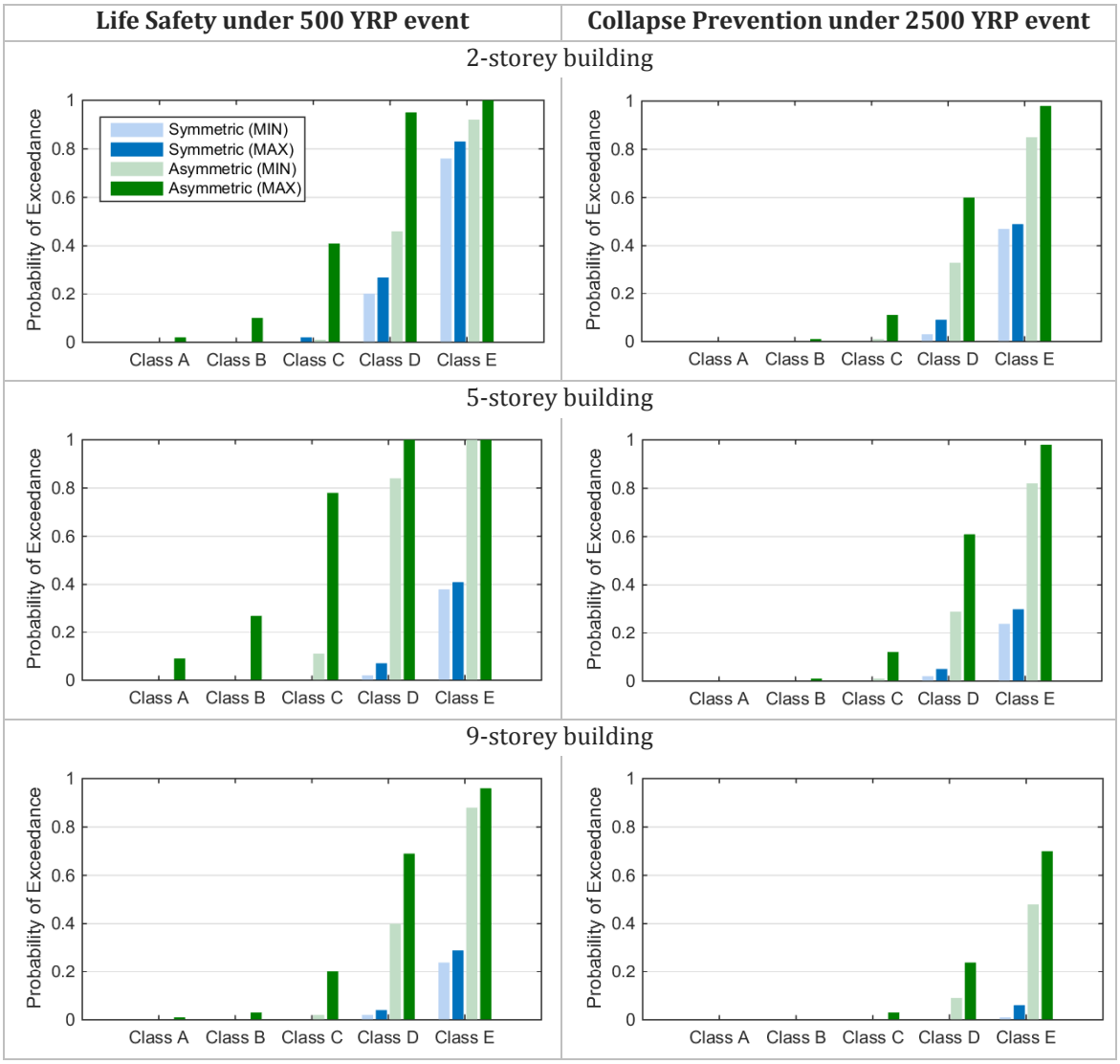

Figure 7-35: Maximum and minimum probability of exceedance computed for the archetypal buildings for basic safety performance objectives

The results clearly demonstrate the superior performance of the plan-symmetric buildings in comparison to the plan-asymmetric buildings. Furthermore, the results for the plan-symmetric buildings illustrate the poorer performance of the buildings with reduced height. This is generally expected since taller buildings perform better under earthquakes due to their inherent flexibility. However, the same observation is not made with the plan-asymmetric buildings, especially for the *Life Safety* limit state under a 500 YRP event. This

is due to the difference in plan configurations and different eccentricities and thus a direct comparison between the different buildings heights cannot be made. In summary, the results suggest that the most vulnerable buildings are plan-asymmetric buildings and plan-symmetric low-rise buildings. It is demonstrated that they may have a high probability of exceeding the *Life Safety* limit state under a 500 YRP event and the *Collapse Prevention* limit state under a 2500 YRP event if located on softer sites.

7.7 SUMMARY

The results for the seismic fragility assessment of six archetypal buildings which are 2-, 5- and 9-storeys high and have building configurations with plan symmetry and plan asymmetry have been presented in this chapter. The archetypal buildings are representative of older buildings constructed in Australia before the requirement for seismic design was mandated on a national basis. Therefore, the findings of the study may be used to determine the vulnerability of the older building stock in Australia.

The assessment is conducted by performing dynamic time history analyses of the 3D nonlinear models of the archetypal buildings. The cloud analysis method is used to develop probabilistic seismic demand models for four performance levels from which the fragility curves are computed. The importance of carefully selecting a suitable intensity measure has been discussed as it can significantly affect the level of vulnerability of the buildings that is predicted from the resulting fragility curves. In addition, other potential causes of variations in computing the fragility curves are presented, including the different ways used to account for the effects of biaxial bending when determining the response of plan-asymmetric buildings. Finally, the response of the buildings is evaluated by comparison with performance objectives suitable for existing buildings. This is achieved by looking at the maximum and minimum probabilities of exceedance predicted for the five site classes using the various methods that have been deemed suitable for computing the fragility curves for the archetypal buildings. PGV is used to represent the seismic demand in accordance with AS 1170.4:2007. The results illustrate that the plan-asymmetric buildings and the 2-storey plan-symmetric buildings are particularly vulnerable to exceeding the *Life Safety* limit state under a 500 year return period event and the *Collapse Prevention* limit state under a 2500 year return period event if located on softer sites.

CHAPTER 8: CONCLUSIONS AND RECOMMENDATIONS FOR FUTURE RESEARCH

8.1 CONCLUSIONS

It is generally accepted that many buildings in Australia will perform poorly in the event of a large earthquake. The predominant reason for this is that Australia is in an area of low-to-moderate seismicity, and hence the probability of a large earthquake occurring at a particular site within the lifetime of a building constructed on that site is small, and this has resulted in a lack of enforcement of appropriate practice for seismic design. However, over the years there has been an increasing interest in improving seismic design practice in Australia and in assessing the seismic resilience of existing buildings. This is due to a better understanding of the response of buildings to large seismic excitations and a greater global awareness of the catastrophic losses that can be caused by earthquakes. In particular, the Christchurch earthquake which occurred on 22nd February 2011 was a wake-up call for Australia since the characteristics of the earthquake were very similar to the type of earthquakes experienced in Australia. In addition, the buildings which performed very badly during the Christchurch earthquake were constructed in a manner which resembles the design practice in Australia, including poorly detailed RC buildings and unreinforced masonry buildings. Hence, there is a need to quantify the vulnerability of buildings to earthquakes in Australia in order to make informed seismic risk mitigation decisions. This has been recognised by the Australian Government through the establishment of the *Cost-Effective Mitigation Strategy Development for Building Related Earthquake Risk* project under the Bushfire and Natural Hazards Cooperative Research Centre (BNHCRC). This study forms part of the BNHCRC project.

The aim of this study was to assess the seismic performance of in-situ reinforced concrete buildings which are under 10-storeys high and were constructed prior to 1995; that is, prior to seismic design being mandated in all of the cities in Australia. This class of buildings has been identified to be particularly vulnerable to earthquakes due to the relatively low natural periods of buildings in this height range, and lack of consideration given to seismic design and detailing. In particular, this study investigated the performance of RC buildings detailed in accordance with AS 3600:1988. The assessment was conducted by developing six archetypal buildings with plan symmetry and plan asymmetry. Three building heights were investigated for each plan configuration, including: 2-storey, 5-storey, and 9-storey buildings. Fragility curves were developed for

the archetypal buildings by following the three stages of the performance-based earthquake engineering assessment procedure; this included conducting hazard analysis, structural analysis, and damage analysis. The seismic performance of the buildings was evaluated with respect to the Basic Safety Objective, which included ensuring *Life Safety* under a 500 year return period event and *Collapse Prevention* under a 2500 year return period event.

The main contribution of this study was to assess the seismic performance of the non-ductile RC buildings by considering the response of both the primary lateral load resisting system and the gravity load resisting system. The following are the major research findings and outcomes of this study which correspond to the research objectives stated in Chapter 1.

i. **Characterise the seismic demand and determine a suitable hazard model to be adopted for Australia.**

   A review of the hazard model adopted by the Australian earthquake loading standard, AS 1170.4:2007 was presented. This hazard model was predominantly based on probabilistic seismic hazard analysis that was completed in the early 1990s. Research is currently being undertaken by Geoscience Australia and in collaboration with other researchers to change the hazard model for the new revision of the Australian earthquake loading standard. However, some of the proposed hazard models have demonstrated a significant reduction in seismic hazard which has raised concerns within the Australian Earthquake Engineering Society. A potential engineering solution to the lack of agreement amongst the experts about the seismicity of Australia for the purpose of the design of new buildings is to provide a minimum threshold hazard level. Currently the proposed threshold is 0.08 g for a 500 year return period event which represents the current hazard for some of the capital cities of Australia, including Melbourne and Sydney. However, it is uncertain what form of changes will be applied to the probability factor, k_p, since the study conducted by GA demonstrated higher values than those incorporated in AS 1170.4:2007 for events with a return period higher than 500 years. Since, at the time this study was conducted there had been no consensus on a new hazard model for Australia, the hazard model in the current Australian earthquake loading standard, AS 1170.4:2007 has been used as a guide to evaluate the seismic performance of the archetypal buildings.

ii. Select suitable ground motions for site response analyses and nonlinear time history analyses of RC buildings.

Due to the paucity of historical records, one of the main challenges associated with conducting time history analyses for buildings located in low-to-moderate seismic regions is the selection of ground motions. The selection of suitable ground motion records was required in this study to conduct the site response study presented in Chapter 2 and the assessment of the RC buildings presented in Chapter 7. The selection of records for both cases have been selected following Kramer (1996) by using (i) historical records which are representative of earthquakes within the region of interest, supplemented by (ii) generated records since sufficient suitable historical records are not available.

Historical records were selected such that they had characteristics typical of Australian earthquakes, including: shallow earthquakes with reverse fault mechanisms (Brown & Gibson, 2004), and realistic magnitude and distance (M-R) combinations based on the attenuation models from Gaull et al. (1990) and Lam et al. (2000a). Stochastically generated earthquakes were obtained using the program GENQKE (Lam, 1999) which is capable of producing ground motions that are representative of Australian earthquakes. By using stochastically generated earthquakes to supplement the historical records, sufficient earthquake records were available so that it was not necessary to use scaled records within the site response study and the time history analyses of the buildings. Similar to the historical records, the generated records were selected with realistic M-R combinations as suggested by Australian attenuation models. However, for the stronger intensity motions (particularly those required to cause *Collapse Prevention* limit state of the buildings) some modifications had to be made to the suggested M-R combinations.

Furthermore, to conduct the site response analyses, ground motions on rock were selected such that their median response spectra approximately matched the acceleration and displacement response spectra computed for a 500 and 2500 year return period event. This is because some of the parameters obtained from the site response study were dependent on the shape of the acceleration response spectra. Therefore for the purpose of consistency between the proposed approach and the method in the standard it was necessary for the shape of the input rock motion to approximately match with the shape proposed in AS 1170.4:2007.

In order to conduct the 3D nonlinear dynamic time history analyses of the archetypal buildings ground motion records were required with two horizontal components. For the historical ground motions the recorded records in both the horizontal directions were used. For the stochastically generated records, two generated records for a given intensity were used, following the approach adopted in other studies which have used generated records to apply bidirectional excitation (Lumantarna, 2012; Ghersi and Rossi, 2001). Furthermore, simulated records on soil conditions were obtained by conducting nonlinear time history site response analyses of the soil profiles presented in the site response study in Chapter 2.

iii. Evaluate and improve the methods currently used to incorporate the influence of local site conditions on seismic site response.

A detailed study was conducted to investigate the effects of local site conditions, namely the weighted average shear wave velocity, depth to bedrock, and intensity of ground motions, on the seismic response of typical rock, clay and sand sites. The aim of the study was to examine the validity of the current method used to incorporate site effects in codes, in particular, the method that is used in AS 1170.4:2007. This is because recent studies have highlighted that the current codified approaches have signicant limitations, especially when used to determine the seismic demand on non-ductile buildings (Lam & Wilson, 2004; Tsang et al., 2013). In the study that was conducted, the effects of local site conditions were obtained based on correlations and observation of trends between site properties representative of individual rock/soil profiles and seismic site response parameters. This is in contrast to the method adopted by many studies which have formed the basis of codes and standards, which involve computing the effects of local site conditions by examining the average response spectra of numerous site conditions within a site class.

The results from the study illustrated the importance of considering the fundamental site period, which is a function of V_s and the depth to bedrock, rather than V_{s30} alone, in understanding the seismic site response. Based on the findings, re-classification of the site classes in AS 1170.4:2007 is recommended, with an emphasis on the site period as a key criteria in classifying soil/soft rock classes. Furthermore, a new systematic method is proposed for obtaining the displacement response spectra. This method helps to significantly improve the prediction of displacement response in the short period range up to the second corner period at

which maximum displacement response occurs. Furthermore, other interesting observations were obtained from the results which require further research. It was observed the acceleration response spectra resulting from this study were significantly higher than those in AS 1170.4:2007. The results also indicated that the response of the site is highly dependent on the soil type, namely the plasticity index of the soil, which is not currently directly accounted for by the standards and codes.

iv. Review the history of building design and construction in Australia and develop archetypal building designs representative of older existing buildings.

An investigation was conducted to obtain the history of the design of RC buildings in Australia and hence to provide an understanding of the existing building stock, including typical building configurations and design detailing. Since Australia does not have a publicly available comprehensive inventory about the structural information of existing buildings, this was achieved by speaking to and corresponding with experienced practicing structural engineers and by reviewing older editions of the Australian loading and concrete structures standards. The discussions with the structural engineers helped to establish typical building configurations and design details for buildings designed in the 1970s, 1980s, and 1990s, including: member spans, floor-to-floor heights, material properties, reinforcement detailing and typical axial load ratios of members. The review of the standards provided critical information about the detailing requirements, loading requirements, and design material properties.

Based on the investigation, it was identified that wind load and lateral stability were poorly considered in Australia until the late 1980s. In addition, nationally, seismic design was not considered until 1995 when the requirement for earthquake loading and design was referred to in the Building Code of Australia. Furthermore, it was identified that RC buildings constructed in Australia prior to 1990 typically have in-situ reinforced concrete core walls as the lateral load resisting system and perimeter moment resisting frames together with band-beam or flat-slab floor systems as the gravity load resisting system. The design of core walls to resist 100 % of the lateral loading has often resulted in the primary system and secondary system being designed separately. This has raised concerns about the displacement compatibility between the two systems and the potential for the gravity system to fail prior to or immediately after the loss of the lateral

load carrying capacity of the primary system. In addition, since consideration of lateral load was poorly considered until the 1990s, the layout of the core walls in buildings has often been governed by access and egress requirements (such as for fire); this applies to both lift cores and stair cores. As a result, most of the buildings constructed in this period have eccentrically placed cores since it was preferred from an architectural standpoint. These findings emphasised the need to adopt a holistic approach when assessing the buildings and to include the response of both the primary and the secondary structural systems. For the purpose of this study, the archetypal buildings were designed in accordance with AS 3600:1988. However, it is noted that the design practice used in this standard was similar to the preceding standards used in the mid-1970s and 1980s and the current concrete structures standard, AS 3600:2009.

v. **Identify the governing failure mechanisms of the building components belonging to the lateral load and gravity load resisting systems; that is, the core walls and the moment resisting frames.**

The RC buildings assessed in this study had components that have been designed with *ordinary* and *limited ductile* reinforcement detailing, namely; ordinary moment resisting frames and limited ductile shear walls. This level of detailing is generally categorised as non-ductile detailing (also referred to as non-conforming detailing) in the literature. It corresponds to the detailing requirements in high seismic regions prior to the 1970s; that is, prior to the introduction of seismic detailing and capacity design principles. Thus, the extensive research which has been conducted in regions of high seismicity, in addition to the research conducted in regions of low-to-moderate seismicity on non-ductile buildings, was reviewed to gain a better understanding of the local and global response of non-ductile buildings. Furthermore, reconnaissance from previous earthquakes has also provided very useful information in terms of understanding the deficiencies and failure mechanisms of non-ductile buildings.

Based on the review it was concluded that for frames, the columns and beam-column joints are the components most vulnerable to failure, and their failure can lead to the collapse of buildings (Ghannoum & Moehle, 2012; Park & Mosalam, 2013b). Column failure instead of beam failure is more likely in non-seismically designed gravity frames because the beams are designed to resist large bending moments due to large gravity loads, and since they do not follow capacity design principles, this has often resulted in the beams having larger moment capacities in

comparison to the columns. Therefore, under lateral loading the undesirable column-sway mechanism instead of the beam-sway mechanism is formed. Based on the detailing of non-ductile columns, predominantly due to insufficient shear reinforcement and confinement, it has been identified that they are particularly vulnerable to flexure-shear and sometimes shear failure modes. In particular, researchers have highlighted the importance of capturing flexure-shear behaviour since significant degradation of shear strength can occur with increasing deformations in the plastic hinge regions (Elwood & Moehle, 2003, 2005; Jeon et al., 2015; LeBorgne & Ghannoum, 2014a).

It was also identified that it was critical to consider the inelastic behaviour of the joints and that the rigid joint assumption adopted in design was not valid for assessment. The two key factors that had to be considered when assessing the performance of the joints included the shear panel response and the bar-slip of bottom longitudinal beam bars. Since the frames were not designed to follow capacity design principles, they were vulnerable to reaching the joint shear capacity before the beams and the columns reached their yield and ultimate moment capacities. Furthermore, for joints with poorly anchored bottom longitudinal beam bars, the positive yield and ultimate bending capacity of the beam had to be reduced to account for bar-slip.

The review of limited ductile walls, especially based on Australian studies, revealed that the walls assessed in this study are particularly vulnerable to a flexural failure mechanism. Many of the walls belonging to low- to mid-rise buildings in Australia typically have low longitudinal reinforcement ratios. This is because the Australian concrete structures standards have allowed for the design of lightly reinforced walls under certain criteria, including low axial load and low bending moment demands. Under lateral loading these walls are vulnerable to forming a single crack (or exhibiting minimal secondary cracking). High strains are developed in the longitudinal bars over a concentrated length of the wall, leading to fracture of the bars at low displacement demands. In addition, walls constructed in Australia, especially in buildings which are up to mid-rise in height, tend to have no confinement and are therefore vulnerable to brittle compression failures.

vi. **Determine appropriate material properties to be adopted for the assessment of the archetypal buildings.**

Once the archetypal buildings had been characterised based on their design properties, it was then necessary to determine the expected material properties of the buildings for assessment purposes. There are many different factors that can cause a difference in material properties (especially strength) from the specified design values. Since some of these factors are dependent on the manufacturer's specifications and on the local construction practice at the time, where possible (and suitable), the expected material properties were computed based on Australian based studies.

vii. **Evaluate various macro-finite element nonlinear modelling methods and determine a suitable approach to model the archetypal buildings. The models need to be capable of simulating damage progression up to the point of (near) collapse defined as loss of axial load carrying capacity of the building components.**

In order to determine the suitable modelling method for this study a critical review of the existing state-of-the-art approach for modelling RC building components in a macro-finite element modelling space was conducted. The modelling approaches investigated were focused on capturing the likely failure mechanisms of non-ductile RC frame components and walls with detailing deficiencies similar to those used in the building components of the archetypal buildings. The modelling methods investigated included the incorporation of the inelastic response of beam-column joints, flexural response of members, bar-slip of longitudinal reinforcement bars, flexure-shear behaviour of members, and the response of planar and non-planar walls.

The review revealed that there was a lack of consensus amongst researchers about the best method to model the various building components for the purpose of global analysis. In general, the non-ductile detailing of the building components significantly increases the difficulty of simulating their response under seismic loading since sudden lateral strength and stiffness degradation are likely to occur after the peak capacity of the components is reached. The sudden lateral strength and stiffness degradation typically cause numerical instabilities and convergence issues; especially when considering the system response of the building. Furthermore, some response mechanisms, namely shear and bar-slip, are not directly modelled using conventional macro-modelling approaches and must be

included indirectly, especially if the response is likely to govern the failure mechanism of the component. It was also evident that most of the approaches require the incorporation of semi-empirical or empirically based numerical models to capture the true response of the members and thus suitable equations need to be selected for the type of components being assessed.

The selection of the various semi-empirical or empirically based analytical models was validated by comparing the results with a database of experimental results. This eliminated any bias in selecting the analytical models and ensured that they provided a valid assessment of the seismic performance of the archetypal buildings. Furthermore, the various modelling approaches were evaluated in order to select the one most suitable for use in developing the macro-finite element nonlinear model of the archetypal buildings. This included examining the suitability of the modelling approach against three key criteria: accuracy, computational efficiency, and reliability and numerical stability. The accuracy of the various models was predominantly assessed at a component level. The computational efficiency and most importantly the reliability and numerical stability of the various modelling approaches were examined based on running simulations at a component level and then at a system level where the approach was utilised to develop 2D and 3D nonlinear models in OpenSEES.

In general, it was evident that the two competing modelling approaches suitable for global analysis could be broadly characterised as the distributed plasticity and the lumped (or concentrated) plasticity approaches. Distributed plasticity elements are only capable of simulating flexural response of members. Other mechanisms such as bar-slip and shear response need to be incorporated using other methods, such as including zero-length springs in series with the distributed plasticity elements. Distributed plasticity elements can simulate approximately correct distribution of plasticity and strain levels in the member if some form of calibration is applied. As demonstrated in this study (and similar methods have been proposed in other studies), one method to achieve this is to explicitly model the plastic hinge region based on the expected plastic hinge length which is also a key parameter in the concentrated plasticity approach. Lumped plasticity elements can simulate flexural behaviour of members and other phenomenological mechanisms since the response of the member is defined by the user at an element level. However, the accuracy of the simulated response is dependent on the accuracy of the definition of the hysteretic model used to define the response of

the zero-length springs. Therefore, there is a higher reliance on accurately defining the expected failure mechanism prior to conducting the analysis since the hysteresis definition cannot be changed during the analysis.

Based on detailed evaluation of the various modelling approaches the scissor's model with rigid links was used to model the beam-column joint response, and the lumped plasticity approach was selected to model the columns, beams, and walls. The lumped plasticity approach was primarily selected on the basis of it achieving reliability when conducting the structural analyses of the buildings; numerical instability issues were encountered when using the distributed plasticity approach. One potential reason for this observation could be due to the extreme non-ductile nature of the components. In addition, most of the state-of-the-art modelling approaches which are proposed in the literature have not been shown to be reliable (in terms of numerical stability) when considering the system response of buildings, in particular for non-ductile buildings modelled in 3D. Numerical stability was a critical criterion in this study when selecting the suitable modelling technique since the aim of the study was to assess the performance of the buildings up to the *Collapse Prevention* limit state (defined as loss of axial load carrying capacity of building components).

viii. **Determine an appropriate framework for conducting seismic fragility assessment of the buildings.**

Based on a detailed review of the literature a suitable seismic fragility assessment framework was adopted. The cloud analysis approach was selected to be the most appropriate approach to develop the probabilistic seismic demand models. To ensure that the correlations obtained between the intensity measure and the building response were not affected by outliers (predominantly due to numerical instabilities), the *collapse* and *non-collapse* results were separated. Furthermore, it was identified that the selection of a suitable intensity measure was dependent on the type of analysis conducted and therefore the intensity mesure was selected based on evaluating the results obtained from the nonlinear time history analyses. Existing performance levels in the literature and guidelines were also examined to help determine the performance levels suitable for use in the assessment of the archetypal buildings. Some of the suggestions in the literature are only appropriate for buildings with ductile detailing and therefore new damage limits were defined for the performance levels such that they are suitable for the assessment of non-ductile buildings. In total four performance levels were defined: *Serviceability,*

Damage Control, Life Safety, and *Collapse Prevention.* The performance criteria for structural damage were defined as when the first component in the building reaches a rotational limit. Separate limits were set for the primary and the secondary structural systems. Interstorey drift limits were also provided to limit the damage to non-structural components and to alleviate the danger of a side-sway collapse mechanism forming.

ix. Conduct the analyses and develop fragility curves for the archetypal buildings.

3D nonlinear models of the six archetypal buildings were developed in the macro-finite element modelling space using the approach determined in *Outcome vii*. Dynamic time history analyses were conducted to obtain the seismic building response. The buildings with plan symmetry were analysed by subjecting them to the stronger component of the 40 pairs of ground motions along the weaker axis of the buildings. For each analysis the critical demand-to-capacity ratio was obtained in accordance with the definition of the performance levels. The buildings with plan asymmetry were subjected to both components of the 40 pairs of ground motions along the principal axes of the buildings. Since, the effects of biaxial bending were not directly modelled, the analysis of the plan-asymmetric buildings were conducted three times using different backbone definitions. The wall and column backbone definitions which were investigated included applying: (i) no reduction factors, (ii) medium bound reduction factors, and (iii) lower bound reduction factors, to the backbones which had been originally defined for unidirectional loading. For the buildings which did not incorporate any reduction factors to account for the effects of biaxial bending, the critical demand-to-capacity ratio was computed by taking the SRSS of the maximum response obtained in the x- and y-direction. For the buildings which incorporated reduction factors to account for biaxial bending, the critical demand-to-capacity ratio was computed by taking the maximum response obtained in either the x- or y-direction. The fragility curves computed for the buildings for which no reduction was applied to the wall and column backbones were approximately the same as those obtained for the buildings for which medium bound reduction factors were applied to the wall and column backbones. This indicated that the suitability of the SRSS method to indirectly account for bidirectional loading is dependent on the detailing of the RC building components. The lower bound reduction factors were selected to be a

conservative representation of the response expected for non-ductile RC components.

Furthermore, it was demonstrated that the selection of the intensity measure to develop the fragility curves can significantly affect the conclusions derived about the performance of the buildings. Various intensity measures (IMs) were investigated in order to select the most suitable intensity measure for this study. The intensity measures which provided consistently the best correlations with the building response for the four performance levels and for the six archetypal buildings were the peak ground velocity (PGV), peak ground displacement (PGD), and maximum spectral displacement response (RSD_{max}). Interestingly, it was observed that PGA, which has been the conventional IM used to develop fragility curves, in general provided a poor correlation with the building response.

To evaluate the seismic performance of the buildings it was also necessary to select an IM which was capable of accurately representing ground motion intensity for various return periods and different site conditions in accordance with AS 1170.4:2007. Based on these additional criteria PGV was selected to be the most suitable IM to evaluate the seismic performance of the buildings. However, for the purpose of comparison, fragility curves were also developed for the archetypal buildings using RSD_{max} and PGA.

x. Evaluate the seismic performance of the archetypal buildings.

The seismic performance of the archetypal buildings was evaluated by examining their response under the Basic Safety Objective described in FEMA 356 (2000), which includes ensuring *Life Safety* under a 500 year return period event, and *Collapse Prevention* under a 2500 year return period event. The minimum and maximum probabilities of exceedance predicted by the various methods deemed suitable for obtaining the fragility curves were provided for the various site classes. The seismic demand was obtained in accordance with AS 1170.4:2007, corresponding to $k_p Z$ values of 0.1 g and 0.18 g on rock for 500 and 2500 year return period events, respectively.

The results demonstrated the superior performance of the plan-symmetric buildings in comparison to the plan-asymmetric buildings. Furthermore, the results for the plan-symmetric buildings illustrated the poorer performance of the buildings with reduced height. However, the same observation was not observed with the plan-asymmetric buildings. This was due to the difference in plan

configurations of the buildings and therefore a direct comparison between the different buildings heights could not be made. Furthermore, the results illustrated that there is a significant difference between the capacity of the buildings at *Life Safety* and *Collapse Prevention*. The structural damage limits at these two performance levels were defined to correspond to the initiation of loss of lateral load carrying capacity (governed by the wall response) and loss of axial load carrying capacity of the gravity system. Hence, the results show that collapse of the gravity system does not occur prior to the ultimate capacity of the core walls being reached.

In summary, the results indicated that the most vulnerable buildings are the plan-asymmetric buildings as well as the 2-storey plan-symmetric building. It was demonstrated that these buildings have a high probability of exceeding the *Life Safety* limit state under a 500 year return period event and the *Collapse Prevention* limit state under a 2500 year return period event if they are located on soft sites.

8.2 RECOMMENDATIONS FOR FUTURE RESEARCH

Recommendations for future research with respect to the various stages of the seismic fragility assessment procedure are provided here.

The results obtained from the seismic site response study conducted in Chapter 2 indicated that the response of softer sites is highly dependent on the soil type and the plasticity index of the soil. It is recommended that future studies investigate the effects of various plasticity index values on site response and the effect of selecting different shear modulus and damping curves. Currently none of the standards and codes account for soil type even though it has a significant effect on site response. Furthermore the acceleration response spectra obtained in the study were significantly higher than those in AS 1170.4:2007. Further research in this area is necessary since the change in acceleration response spectra would cause significant increases in the design actions for earthquake resistant design of structures if force-based methods are used.

In Chapter 3 a review of Australian building design and construction has been provided for buildings dating back to approximately the 1960s. However, the archetypal buildings assessed in this study are predominantly representative of buildings constructed in the 1970s, 1980s, and 1990s. Furthermore, the buildings were designed in accordance with AS 3600:1988 and the material properties were selected to be representative of buildings constructed in this era. It is recommended that future studies may use the information

presented in this chapter to assess the performance of buildings constructed in different periods and with different material properties.

As discussed throughout this study, when assessing the seismic performance of older existing buildings the performance levels corresponding to high levels of building damage are often of interest. In particular, the performance level corresponding to *Collapse Prevention* is critical and this is usually defined as when loss of axial load carrying capacity (typically for non-ductile buildings) and side-sway mechanisms (typically for ductile buildings) take place. However, there are currently very few experimental results available from tests conducted on non-ductile building components (especially for lightly reinforced core walls) which have been tested up to the point of axial load failure and under realistic lateral loading conditions, including bidirectional loading. A better understanding of component responses will significantly help to improve the seismic assessment of buildings and to reduce uncertainties about the building response. Thus, it is highly recommended that more experimental studies are conducted on non-ductile building components under bidirectional loading and up to the point of loss of axial load resistance.

The review and evaluation of the state-of-the-art macro-finite element modelling approaches conducted in Chapter 4 and Chapter 5 highlighted limitations of currently available modelling approaches for the purpose of conducting global analysis. Some of the more advanced approaches which have been developed, including distributed plasticity elements which capture flexure-axial interactions, and other modelling techniques which incorporate the effects of shear and bar-slip, have shown promising results in terms of accuracy when simulating the response of individual components. However, these approaches require further development in terms of numerical stability and reliability and computational efficiency. This is especially the case when the modelling approaches are incorporated in 2D or 3D nonlinear models to obtain the system response of non-ductile buildings. Therefore, it is recommended that further work needs to be conducted in improving the numerical stability and reliability of the more advanced modelling approaches for the purpose of conducting global analysis.

The structural analyses conducted in Chapter 7 have involved certain idealisation and assumptions about the response of the archetypal buildings. In was assumed that flexural response governs the core wall behaviour and that the walls will not lose their axial load carrying capacity prior to the gravity system. The shear failure of the walls and the columns due to exceedance of shear force capacity was not explicitly modelled since the

nonlinear component responses were modelled using zero-length moment rotation spring elements. Furthermore, a rigid diaphragm assumption has been adopted it this study and slab related failure mechanisms have not been incorporated. Punching shear failure and failure of the floor diaphragm (diaphragm detachment) may lead to slab collapse and column instability, thus contributing to the collapse mechanism of the building. In addition, soil-structure interactions have not been considered in this study which may also affect the global response of the buildings. The incorporation of the mechanisms that have not been directly modelled in this study to examine the effect they have on the seismic performance of non-ductile RC buildings could be investigated in future studies.

REFERENCES

ABCB (Australian Building Code Board). (2015). National Conctruction Code Series 2015 Guide to Volume One: Building Code of Australia Class 2 to Class 9 Buildings. Canberra, Australia.

ABCB (Australian Building Code Board). (2016). National Conctruction Code Series 2016 Guide to Volume One: Building Code of Australia Class 2 to Class 9 Buildings. Canberra, Australia.

Ahmed, S., & Gunasekaran, U. (2014). Testing and evaluation of reinforced concrete beam-column-slab joint. *Građevinar 66*(1), 21-36. doi: 10.14256/jce.971.2013

Alath, S., & Kunnath, S. K. (1995). *Modeling inelastic shear deformation in RC beam-column joints*. Paper presented at the Engineering Mechanics Proceedings of the 10 Conference, University of Colarado, Boulder, Colorado, ASCE, New York.

Almeida, J. P., Prodan, O., Rosso, A., & Beyer, K. (2017). Tests on thin reinforced concrete walls subjected to in-plane and out-of-plane cyclic loading. *Earthquake Spectra, 13*(1), 323-345. doi: doi.org/10.1193/101915EQS154DP

Almeida, J. P., Tarquini, D., & Beyer, K. (2016). Modelling Approaches for Inelastic Behaviour of RC Walls: Multi-level Assessment and Dependability of Results. *Archives of Computational Methods in Engineering, 23*(1), 69-100. doi: 10.1007/s11831-014-9131-y

Altheeb, A. H. (2016). *Seismic drift capacity of lightly reinforced concrete shear walls.* (PhD Thesis), Department of Infrastructure Engineering, The University of Melbourne.

Altoontash, A. (2004). *Simulation and damage models for performance assessment of reinforced concrete beam-column joints.* (PhD Dissertation), Department of Civil and Environmental Engineering, Stanford University, Stanford, California.

American Concrete Institute (ACI Committee 318). (2008). Building code requirements for structural concrete (ACI 318-08) and commentary. Farmington Hills, MI: American Concrete Institute.

American Concrete Institute (ACI Committee 318). (2011). Building code requirements for structural concrete (ACI 318-11) and commentary (318R-11). Farmington Hills, MI: American Concrete Institute.

American Society of Civil Engineers (ASCE/SEI). (2006). Seismic rehabilitation of existing buildings (ASCE/SEI 41-06). Reston, Virginia: Americal Society of Civil Engineers.

American Society of Civil Engineers (ASCE/SEI). (2013). Seismic evaluation and retrofit of existing buildings. Reston, Virginia: American Society of Civil Engineers.

Amirsardari, A., Goldsworthy, H. M., & Lumantarna, E. (2017). Seismic site response analysis leading to revised design response spectra for Australia. *Journal of Earthquake Engineering, 21*(6), 861-890. doi: 10.1080/13632469.2016.1210058

Anbazhagan, P., Sheikh, M. N., & Parihar, A. (2013). Influence of rock depth on seismic site classification for shallow bedrock regions. *Natural Hazards Review, 14*(2), 108-121. doi: 10.1061/(ASCE)NH.1527-6996.0000088

Applied Technology Council. (2009). FEMA P695: Quantification of building seismic performance factors. Washington, D.C.: Federal Emergency Management Agency.

Applied Technology Council. (2012). Seismic performance assessment of buildings (FEMA P-58) *Volume 1: Methodology*. Washington, D.C: Federal Emergency Management Agency.

Aslani, H., & Miranda, E. (2005). Probability-based seismic response analysis. *Engineering Structures, 27*(8), 1151-1163. doi: 10.1016/j.engstruct.2005.02.015

Australasian Wind Engineering Society. (2012). Wind loading hanbook for Australia and New Zealand: Background to AS/NZS 1170.2 Wind Actions. The University of Sydney.

Australian Building Codes Board. (2007). Final regulation impact statement for decision (RIS 2007-03) *Proposal to amend the earthquake provisions of the Building Code of Australia*.

Badri, R. K., Nekooei, M., & Moghadam, A. S. (2015). The Variance of Collapse Capacity of Symmetric and Asymmetric Low-Rise RC-SMF Buildings. *Journal of Earthquake Engineering, 19*(8), 1181-1196. doi: 10.1080/13632469.2015.1049387

Baker, J. W. (2015). Efficient analytical fragility function fitting using dynamic structural analysis. *Earthquake Spectra, 31*(1), 579-599. doi: 10.1193/

Baker, J. W., & Cornell, C. A. (2006). Vector-valued ground motion intensity measures for probabilistic seismic demand analysis *PEER Report 2006/08*: Pacific Earthquake Engineering Research Center (PEER), University of California, Berkeley.

Baradaran Shoraka, M., Yang, T. Y., & Elwood, K. J. (2013). Seismic loss estimation of non-ductile reinforced concrete buildings. *Earthquake Engineering & Structural Dynamics, 42*(2), 297-310. doi: 10.1002/eqe.2213

Behrouzi, A., Mock, A., Lowes, L., Lehman, D., & Kuchma, D. (2010). Summary of large-scale C-shaped reinforced concrete wall tests. United States.

Beres, A., White, R. N., Gergely, P., Pessiki, S. P., & El-Attar, A. (1992). *Behavior of existing non-seismically detailed reinforced concrete frames.* Paper presented at the Earthquake Engineering, Tenth World Conference, Balkema, Rotterdam.

Berry, M. P. (2006). *Performance modeling strategies for modern reinforced concrete bridge columns.* (PhD Dissertation), University of Washington, Seattle, WA.

Berry, M. P., & Eberhard, M. O. (2008). Performance modelling strategies for modern reinforced concrete bridge columns *PEER Report 2007/07*: Pacific Earthquake Engineering Research Center (PEER), University of California, Berkely.

Beyer, K. (2005). *Design and analysis of walls coupled by floor diaphragms.* (Masters Thesis), Rose School, Pavia, Italy.

Beyer, K., Dazio, A., & Priestley, M. J. N. (2008a). Inelastic Wide-Column Models for U-Shaped Reinforced Concrete Walls. *Journal of Earthquake Engineering, 12*(sup1), 1-33. doi: 10.1080/13632460801922571

Beyer, K., Dazio, A., & Priestley, M. J. N. (2008b). Quasi-Static Cyclic Tests of Two U-Shaped Reinforced Concrete Walls. *Journal of Earthquake Engineering, 12*(7), 1023-1053. doi: 10.1080/13632460802003272

Beyer, K., Dazio, A., & Priestley, M. J. N. (2011). Shear deformations of slender reinforced concrete walls under siesmic loading. *ACI Structural Journal, 108*(2), 167-177.

Beyer, K., Hube, M., Constantin, R., Niroomandi, A., Pampanin, S., Dhakal, R., . . . Wallce, J. W. (2017). *Reinforced concrete wall response under uni- and bi-directional loading.* Paper presented at the 16th World Conference on Earthquake Engineering (WCEE), Santiago, Chile.

Beyer, K., Simonini, S., Constantin, R., & Rutenberg, A. (2014). Seismic shear distribution among interconnected cantilever walls of different lengths. *Earthquake Engineering & Structural Dynamics, 43*(10), 1423-1441. doi: 10.1002/eqe.2403

Bohl, A., & Adebar, P. (2011). Plastic hinge lengths in high-rise concrete shear walls. *ACI Structural Journal, 108*(2), 148-157.

Bojórquez, E., Chávez, R., Reyes-Salazar, A., Ruiz, S. E., & Bojórquez, J. (2017). A new ground motion intensity measure I_B. *Soil Dynamics and Earthquake Engineering, 99*, 97-107. doi: 10.1016/j.soildyn.2017.05.011

Brown, A., & Gibson, G. (2004). A multi-tiered earthquake hazard model for Australia. *Tectonophysics, 390*(1-4), 25-43. doi: 10.1016/j.tecto.2004.03.019

Buchanan, A. H., Bull, D., Dhakal, R., MacRae, G., Palermo, A., & Pampanin, S. (2011). Base isolation damage-resistant technologies for improved seismic performance of buildings *A report written for the Royal Commission of inquiry into building failure caused by the Canterbury earthquakes*. Christchurch, New Zealand: University of Canterbury.

Burbidge, D. R. (2012). The 2012 Australian earthquake hazard map *Record 2012/71*. Canberra: Geoscience Australia.

Calvi, G. M., Magenes, G., & Pampanin, S. (2002). Relevance of Beam-Column Joint Damage and Collapse in RC Frame Assessment. *Journal of Earthquake Engineering, 6*(sup001), 75-100. doi: 10.1080/13632460209350433

Calvi, G. M., Sullivan, T. J., & Welch, D. P. (2014). A Seismic Performance Classification Framework to Provide Increased Seismic Resilience. *34*, 361-400. doi: 10.1007/978-3-319-07118-3_11

Canterbury Earthquakes Royal Commission (CERC). (2012a). Canterbury Televsion Building (CTV) *Canterbury Earthquakes Royal Commission final report* (Vol. 6).

Canterbury Earthquakes Royal Commission (CERC). (2012b). The performance of Christchurch CBD buildings *Final Report (Volume 2)*. Wellington, New Zealand.

Celik, O. C. (2007). *Probabilistic assessment of non-ductile reinforced concrete frames susceptible to mid-America ground motions.* (PhD Thesis), Georgia Institute of Technology.

Celik, O. C., & Ellingwood, B. R. (2008). Modeling Beam-Column Joints in Fragility Assessment of Gravity Load Designed Reinforced Concrete Frames. *Journal of Earthquake Engineering, 12*(3), 357-381. doi: 10.1080/13632460701457215

Celik, O. C., & Ellingwood, B. R. (2010). Seismic fragilities for non-ductile reinforced concrete frames – Role of aleatoric and epistemic uncertainties. *Structural Safety, 32*(1), 1-12. doi: 10.1016/j.strusafe.2009.04.003

Chandler, A., Lam, N., Wilson, J., & Hutchinson, G. (2001). Review of modern concepts in the engineering interpretation of earthquake response spectra. *Proceedings of the Institution of Civil Engineers: Structures and Buildings, 146*(1), 75-84.

Coleman, J., & Spacone, E. (2001). Localization issues in force-based frame elements. *Journal of Structural Engineering, 127*(11), 1257-1265.

Concrete Institute of Australia. (2007). Recommended practice: Reinforcement detailing handbook for reinforced and prestressed concrete *Based upon the Australian concrete structures standard - AS 3600:2007*.

Constantin, R., & Beyer, K. (2016). Behaviour of U-shaped RC walls under quasi-static cyclic diagonal loading,". *Engineering Structures, 106*(1), 36-52.

Cook, D., Fenwick, R., & Russell, A. (2014). *Amendment 3 to NZS3101.* Paper presented at the The New Zealand Concrete Industry Conference, Taupo, New Zealad.

Cornell, C. A., Jalayer, F., Hamburger, R. O., & Foutch, D. A. (2002). Probabilistic basis for 2000 SAC Federal Emergency Management Agency steel moment frame guidelines. *Journal of Structural Engineering, 128*(8), 526-533. doi: 10.1061//ASCE/0733-9445/2002/128:4/526

Crouse, C. B., & McGuire, J. W. (1996). Site response studies for purpose of revising NEHRP seismic provisions. *Earthquake Spectra, 12*(3), 407-439.

Dazio, A., Beyer, K., & Bachmann, H. (2009). Quasi-static cyclic tests and plastic hinge analysis of RC structural walls. *Engineering Structures, 31*(7), 1556-1571. doi: 10.1016/j.engstruct.2009.02.018

Deierlein, G. C., Krawinkler, H., & Cornell, C. A. (2003). *A framework for performance-based earthquake engineering*. Paper presented at the 2003 Pacific Conference on Earthquake Engineering.

Dhakal, P., & Maekawa, K. (2002). Reinforcement stability and fracture of cover concrete in reinforced concrete members. *Journal of Structural Engineering, ASCE, 128*(10), 1253-1262.

Dhakal, R. P., Lin, S.-L., Loye, A. K., & Evans, S. J. (2013). Seismic design spectra for different soil classes. *Bulletin of the New Zealand Society of Earthquake Engineering, 46*(2), 79-87.

Dhakal, R. P., Pan, T.-C., Irawan, P., Tsai, K.-C., Lin, K.-C., & Chen, C.-H. (2005). Experimental study on the dynamic response of gravity-designed reinforced concrete

connections. *Engineering Structures, 27*(1), 75-87. doi: 10.1016/j.engstruct.2004.09.004

Dobry, R., Borcherdt, R. D., Crouse, C. B., Idriss, I. M., Joyner, W. B., Martin, G. R., . . . Seed, R. B. (2000). New site coefficients and site classfication system used in recent building seismic code provisions. *Earthquake Spectra, 16*(1), 41-67.

Ehsani, M. R., & Wight, J. K. (1985). Effect of transverse beams and slab on behaviour of reinforced concrete beam-to-column connection. *ACI Journal*, 188-195.

Elwood, K. J. (2004). Modelling failures in existing reinforced concrete columns. *Canadian Journal of Civil Engineering, 31*(5), 846-859. doi: 10.1139/l04-040

Elwood, K. J., & Moehle, J. P. (2003). Shake table tests and analytical studies on the gravity load collapse of reinforced concrete frames *Pacific Earthquake Engineering Research Center, PEER Report 2003/01*. University of California, Berkeley.

Elwood, K. J., & Moehle, J. P. (2005). Drift capacity of reinforced concrete columns with light transverse reinforcement. *Earthquake Spectra, 21*(1), 71-89. doi: 10.1193/1.1849774

European Standard. (2004a). Eurocode 2: Design of concrete structures - Part 1-2: General Rules - structural fire design *EN 1992-1-2:2004*. Brussels: European Committee for Standardization.

European Standard. (2004b). Eurocode 8: Design of structures for earthquake resistance, EN 1998-1 Part1: General rules, seismic actions and rules for buildings. Brussels: European Committee for Standardization.

Fardipour, M. (2012). *Seismic performace of limited-ductile RC columns in moderate seismicity regions.* (PhD thesis), Department of Infrastructure Engineering, The University of Melbourne.

Federal Emergency Management Agency. (1997). NEHRP Guidelines for the seismic rehabilitation of buildings, FEMA-273. Washington, DC: Federal Emergency Management Agency.

Federal Emergency Management Agency. (2003). NEHRP Recommended provisions for seismic regulations for new buildings and other structures (FEMA 450) *Part 1: Provisions, 2003 Edition*. Washington, D.C: Federal Emergency Management Agency.

Federal Emergency Management Agency. (2009). Effects of strength and stiffness degradation on seismic response, FEMA-P440A. Washington, DC: Federal Emergency Management Agency.

Federal Emergency Management Agency (FEMA). (2000). Prestandard and commentary for the seismic rahbilitation of buildings, FEMA-356. Washington, D.C: Federal Emergency Management Agency.

Federal Emergency Management Agency (FEMA). (2010). HAZUS-MH MR5 Technical Manual - Earthquake Model. Washington, D.C.: U.S. Department of Homeland Security.

fib: féderation internationale du béton (International Federation for Structural Concrete). (2008). *Practitioners' guide to finite element modelling of reinforced concrete structures: State-of-art report prepared by Task Group 4.4*. Lausanne, Switzerland.

fib: féderation internationale du béton (International Federation for Structural Concrete). (2010). Model Code 2010, First complete draft *Volume 1*. Lausanne, Switzerland.

Foster, S. J., Stewart, M. G., Loo, M., Ahammed, M., & Sirivivatnanon, V. (2016). Calibration of Australian Standard AS3600 Concrete Structures: part I statistical analysis of material properties and model error. *Australian Journal of Structural Engineering, 17*(4), 242-253. doi: 10.1080/13287982.2016.1246793

Fox, M. J., Sullivan, T. J., & Beyer, K. (2015). Evaluation of seismic assessment procedures for determining deformation demands in RC wall buildings. *Earthquakes and Structures, 9*(4), 911-936. doi: 10.12989/eas.2015.9.4.911

Gaull, B. A., Michael-Leiba, M. O., & Rynn, J. M. W. (1990). Probabilistic earthquake risk maps of Australia. *Australian Journal of Earth Sciences, 37*(2), 169-187. doi: 10.1080/08120099008727918

Geoscience Australia. (2017). Working together to improve understanding of Australia's earthquake hazard. Retrieved 19-07-2017, 2017, from http://www.ga.gov.au/news-events/news/latest-news/working-together-to-improve-understanding-of-australias-earthquake-hazard

Ghannoum, W. M., & Moehle, J. P. (2012). Dynamic collapse analaysis of a concrete frame sustaining column axial failures. *ACI Structural Journal, 109*(3), 403-412.

Giovenale, P., Cornell, C. A., & Esteva, L. (2004). Comparing the adequacy of alternative ground motion intensity measures for the estimation of structural responses. *Earthquake Engineering & Structural Dynamics, 33*(8), 951-979. doi: 10.1002/eqe.386

Glaister, S., & Pinho, R. (2009). Development of a Simplified Deformation-Based Method for Seismic Vulnerability Assessment. *Journal of Earthquake Engineering, 7*(sup001), 107-140. doi: 10.1080/13632460309350475

Goldsworthy, H. M. (2012). Lessons from the 22 February 2011 Christchurch earthquake. *Australian Journal of Structural Engineering, 13*(2). doi: 10.7158/s11-136.2012.13.2

Goldsworthy, H. M. (2013). *Moving towards displacement-based assessment in Australia.* Paper presented at the New Zealand Society for Earthquake Engineering 2013 Conference, Wellington, New Zealand.

Goldsworthy, H. M., & Gibson, G. (2012). *Changes in seismic design philosophy for RC structures in areas of low to moderate seismicity following the Christchurch earthquake.* Paper presented at the 15th World Coference on Earthquake Engineering, Lisbon, Portugal.

Goldsworthy, H. M., McBean, P., & Somerville, P. (2015). *Mitigation of seismic hazard in Australia by improving the robustness of buildings.* Paper presented at the Proceedings of the Tenth Pacific Conference on Earthquake Engineering, Sydney, Australia.

Gomes, A., & Appleton, J. (1997). Nonlinear cyclic stress-strain relationship of reinforcing bars including buckling. *Engineering Structures, 19*(10), 822-826.

Hakuto, S., Park, R., & Tanaka, H. (2000). Seismic load tests on interior and exterior beam-column joints with substandard reinforcing details. *ACI Structural Journal, 97*(1), 11-25.

Haselton, C. B., Liel, A. B., Deierlein, G. G., Dean, B. S., & Chou, J. H. (2011). Seismic collapse safety of reinforced concrete buildings. I: Assessment of ductile moment frames. *Journal of Structural Engineering, ASCE, 137*(4), 481-491. doi: 10.1061/(ASCE)ST.1943-541X.0000318

Haselton, C. B., Liel, A. B., Lange, S. T., & Deierlein, G. G. (2008). Beam-column element model calibrated for predicting flexural response leading to global collapse of RC frame buildings, PEER Report 2007/03: Pacific Earthquake Engineering Research Center, University of California, Berkeley.

Haselton, C. B., Liel, A. B., Taylor-Lange, S. C., & Deierlein, G. G. (2016). Calibration of Model to Simulate Response of Reinforced Concrete Beam-Columns to Collapse. *ACI Structural Journal, 113*(6). doi: 10.14359/51689245

Hashash, Y. M. A., Musgrove, M. I., Harmon, J. A., Groholski, D. R., Phillips, C. A., & Park, D. (2016). DEEPSOIL 6.1. Retrieved from http://deepsoil.cee.illinois.edu/

Hassan, W. M. (2011). *Analytical and experimental assessment of seismic vulnerability of beam-column joints without transverse reinforcement in concrete buildings.* (PhD thesis), University of California, Berkeley, Department of Civil and Environmental Engineering.

Hassan, W. M., & Moehle, J. P. (2012). *A cyclic nonlinear macro model for numerical simulation of beam-column joints in existing concrete buildings.* Paper presented at the 15th World Conference on Earthquake Engineering, Lisbon, Portugal.

Henry, R. S. (2013). *Assessment of the minimum vertical reinforcement limits for RC walls.* Paper presented at the New Zealand Society Earthquake Engineering (NZSEE) Conference, Auckland, New Zealand.

Hoult, R., Goldsworthy, H., & Lumantarna, E. (2017). Plastic hinge length for lightly reinforced rectangular concrete walls. *Journal of Earthquake Engineering*. doi: 10.1080/13632469.2017.1286619

Hoult, R., Goldsworthy, H., & Lumantarna, E. (2018). Plastic hinge length for lightly reinforced C-shaped concrete walls. *Journal of Earthquake Engineering*. doi: 10.1080/13632469.2018.1453419

Hoult, R. D. (2017). *Seismic assessment of reinforced concrete walls in Australia.* (PhD Thesis), Department of Infrastructure Engineering, The University of Melbourne, Melbourne, Australia.

Hoult, R. D., Goldsworthy, H. M., & Lumantarna, E. (2014). *Seismic performance of typical C-shaped reinforced concrete shear cores in Australia.* Paper presented at the Australian Earthquake Engineering Society 2014 Conference, Lorne, Victoria.

Huang, Y.-N., & Whittaker, A. S. (2015). On the calculation of peak ground velocity for seismic performance assessment. *Earthquake Spectra, 31*(2), 785-794. doi: 10.1193/081112EQS261T

Humar, J. L., & Kumar, P. (1999). Effect of orthogonal inplane structural elements on inelastic torsional response. *Earthquake Engineering & Structural Dynamics, 28*, 1071-1097.

Ibarra, L. F., Medina, R. A., & Krawinkler, H. (2005). Hysteretic models that incorporate strength and stiffness deterioration. *Earthquake Engineering & Structural Dynamics, 34*(12), 1489-1511. doi: 10.1002/eqe.495

Ile, N., & Reynouard, J. M. (2005). Behaviour of U-Shaped Walls Subjected to Uniaxial and Biaxial Cyclic Lateral Loading. *Journal of Earthquake Engineering, 9*(1), 67-94. doi: 10.1080/13632460509350534

International Code Council. (2012). International Building Code. Whittier, Calfornia.

ISESD. (2014). Internet Site for European Strong-motion Database. http://www.isesd.hi.is/esd_local/Database/Database.htm

Jalayer, F., & Cornell, C. A. (2009). Alternative non-linear demand estimation methods for probability-based seismic assessments. *Earthquake Engineering & Structural Dynamics, 38*(8), 951-972. doi: 10.1002/eqe.876

Jalayer, F., De Risi, R., & Manfredi, G. (2014). Bayesian Cloud Analysis: efficient structural fragility assessment using linear regression. *Bulletin of Earthquake Engineering, 13*(4), 1183-1203. doi: 10.1007/s10518-014-9692-z

Jalayer, F., Ebrahimian, H., Miano, A., Manfredi, G., & Sezen, H. (2017). Analytical fragility assessment using unscaled ground motion records. *Earthquake Engineering & Structural Dynamics*. doi: 10.1002/eqe.2922

Jalayer, F., Franchin, P., & Pinto, P. E. (2007). A scalar damage measure for seismic reliability analysis of RC frames. *Earthquake Engineering & Structural Dynamics, 36*(13), 2059-2079. doi: 10.1002/eqe.704

Jankovic, S., & Stojadinovic, B. (2004). *Probabilistic performance-based seismic demand model for R/C frame buildings.* Paper presented at the 13th World Conference on Earthquake Engineering (WCEE) Vancouver, B.C., Canada.

Jeon, J.-S. (2013). *Aftershock vulnerability assessment of damage reinforced concrete buildings in California.* (PhD Thesis), School of Civil and Environemental Engineering, Georgia Institute of Technology.

Jeon, J.-S., Lowes, L. N., DesRoches, R., & Brilakis, I. (2015). Fragility curves for non-ductile reinforced concrete frames that exhibit different component response

mechanisms. *Engineering Structures, 85*, 127-143. doi: 10.1016/j.engstruct.2014.12.009

Jeong, S.-H., & Elnashai, A. S. (2004). *Analytical and experimental seismic assessment of irregular RC buildings.* Paper presented at the 13th World Conference on Earthquake Engineering (WCEE), Vancouver, Canada.

Kabeyasawa, T., Kato, S., Sato, M., Kabeyasawa, T., Fakuyama, H., Tani, M., . . . Hosokawa, Y. (2014). *Effects of bidirectional lateral loading on the strength and deformability of reinforced concrete walls with/without boundary columns.* Paper presented at the 10th U.S. National Congress on Earthquake Engineering (NCEE), Anchorage, ALaska.

Kam, W. Y., & Jury, R. (2017). *Performance-based seismic assessment: simplified methods and collapse indicatiors.* Paper presented at the 16th World Conference on Earthquake Engineerinf (WCEE), Santiago, Chile.

Kam, W. Y., Pampanin, S., & Elwood, K. (2011). Seismic performance of reinforced concrete buildings in the 22 February Christchurch (Lyttelton) earthquake. *Bulletin of the New Zealand National Society for Earthquake Engineering, 44*(4), 239-278.

Karimiyan, S., Kashan, A. H., & Karimiyan, M. (2014). Progressive collapse vulnerability in 6-Story RC symmetric and asymmetric buildings under earthquake loads. *Earthquakes and Structures, 6*(5), 473-494. doi: 10.12989/eas.2014.6.5.473

Kayen, R. E., Carkin, B. A., Allen, T., Collins, C., McPherson, A., & Minasian, D. (2015). Shear-wave velocity and site-amplification factors for 50 Australian sites determined by the spectral analysis of surface waves methods: U.S. Geological Survey Open-FIle Report 2014-1264, 118 p. doi: http:/dx.doi.org/10.3133/ofr20141264

Kazaz, İ. (2013). Analytical Study on Plastic Hinge Length of Structural Walls. *Journal of Structural Engineering, 139*(11), 1938-1950. doi: 10.1061/(asce)st.1943-541x.0000770

Kim, J., & LaFave, J. M. (2009). Joint shear behavior of reinforced concrete beam-column connections subjected to seismic lateral loading *Report No. NSEL-020*: Newmark Structural Engineering Laboratory (NSEL), Department of Civil and Environemntal Engineering, University of Illinios at Urbana-Champaign.

Kim, T.-W., Foutch, D. A., LaFave, J. M., & Wilcoski, J. (2004). Performance assessment of reinforced concrete structural walls for seismic loads. Urbana, Illinois: Deaprtment of Civil and Environmental Engineering, University of Illinois

Köroglu, M. A., Arslan, M. H., & Körez, M. K. (2014). Use of regression analysis in determining the length of plastic hinge in reinforced concrete columns. *International Journal of Civil and Environmental Engineering, 8*(4), 401-406.

Kramer, S. L. (1996). *Geotechnical earthquake engineering*: Upper Saddle River, N.J: Prentice Hall.

Kuang, J. S., & Ho, Y. B. (2007). Inherent ductility of non-seismically designed and detailed reinforced concrete shear walls. *HKIE Transactions, 14*(1), 7-12. doi: 10.1080/1023697X.2007.10668063

Kunnath, S. K., Hoffmann, G., Reinform, A. M., & Mander, J. B. (1995). Gravity-load-designed reinforced concrete buildings - Part II: seismic evaluation of existing construction. *ACI Structural Journal, 92*(4), 470-478.

Kurose, Y., Guimaraes, G. N., Liu, Z., Kreger, M. E., & Jirsa, J. O. (1988). Study or reinforced concrete beam-column joints under uniaxial and biaxial loading *PMFSEL Report No. 88-2* (pp. 146): Department of Civil Engineering, University of Texas at Austin.

Kwon, O.-S., & Elnashai, A. (2006). The effect of material and ground motion uncertainty on the seismic vulnerability curves of RC structure. *Engineering Structures, 28*(2), 289-303. doi: 10.1016/j.engstruct.2005.07.010

Lam, N., & Wilson, J. (2004). Displacement modelling of intraplate earthquakes. *ISET Journal of Earthquake Technology, 41*(1), 15-52.

Lam, N., Wilson, J., Chandler, A., & Hutchinson, G. (2000a). Response spectral relationships for rock sites derived from component attenuation model. *Earthquake Engineering & Structural Dynamics, 29*, 1457-1489.

Lam, N., Wilson, J., Chandler, A., & Hutchinson, G. (2000b). Response spectrum modelling for rock sites in low and moderate seismicity regions combining velocity, displacement and acceleration predictions. *Earthquake Engineering & Structural Dynamics, 29*, 1491-1525.

Lam, N. T. K. (1999). "GENQKE" User's Guide: Program for generating synthetic earthquake accelerograms based on stochastic simulations of seismological models. Department of Civil and Environmental Engineering, The University of Melbourne, Australia.

Lam, N. T. K., Wilson, J. L., & Chandler, A. M. (2001). Seismic displacement response spectrum estimated from frame analogy soil amplification model. *Engineering Structures, 23*, 1437-1452.

LeBorgne, M. R. (2012). *Modeling the post shear failure behaviour of reinforced concrete columns.* (PhD Dissertation), The University of Texas at Austin.

LeBorgne, M. R., & Ghannoum, W. M. (2014a). Analytical Element for Simulating Lateral-Strength Degradation in Reinforced Concrete Columns and Other Frame Members. *Journal of Structural Engineering, 140*(7), 04014038. doi: 10.1061/(asce)st.1943-541x.0000925

LeBorgne, M. R., & Ghannoum, W. M. (2014b). Calibrated analytical element for lateral-strength degradation of reinforced concrete columns. *Engineering Structures, 81*, 35-48. doi: 10.1016/j.engstruct.2014.09.030

Lee, S.-H., Sun, C.-G., Yoon, J.-K., & Kim, D.-S. (2012). Development and verification of a new site classification system and site coefficients for regions of shallow bedrock in Korea. *Journal of Earthquake Engineering, 16*(6), 795-819. doi: 10.1080/13632469.2012.658491

Lehman, D. E., & Moehle, J. P. (2000). Seismic performance of well-confined concrete bridge columns, PEER Report 1998/01: Pacific Eathquake Engineering Research Center (PEER), University of California, Berkeley.

Leonard, M., Burbidge, D., & Edwards, M. (2013). Atlas of seismic hazard maps of Australia: seismic hazard maps, hazard curves and hazard spectra *Record 2013/41*. Canberra: Geoscience Australia.

Liberty OneSteel. (n.d.). History of Australian reinforcing bar standards. 2017, from https://www.libertyonesteel.com/resources/content/rebar-standards-history/

Liel, A. B., Haselton, C. B., & Deierlein, G. G. (2011). Seismic collapse safety of reinfroced concrete buildings. II: Comparitive assessment of nonductile and ductile moment frames. *Journal of Structural Engineering, ASCE, 137*(4), 492-502. doi: 10.1061/(ASCE)ST.1943-541X.0000275.

Lowes, L. N., & Altoontash, A. (2003). Modelling reinforced-concrete beam-column joints subjected to cyclic loading. *ASCE Journal of Structural Engineering, 129*(12), 1686-1697. doi: 10.1061//ASCE/0733-9445/2003/129:12/1686

Lowes, L. N., Mitra, N., & Altoontash, A. (2004). A beam-column joint model for simulating the earthquake response of reinforced concrete frames, PEER Report 2003/10: Pacific Earthquake Engineering Center, University of California, Berkeley.

Lu, Y., Henry, R. S., Gultom, R., & Ma, Q. T. (2016). Cyclic testing of reinforced concrete walls with distributed minimum vertical reinforcement. *Journal of Structural Engineering*, 1-17. doi: 10.1061/(ASCE)ST.1943-541X.0001723

Lucchini, A., Mollaioli, F., & Monti, G. (2011). Intensity measures for response prediction of a torsional building subjected to bi-directional earthquake ground motion. *Bulletin of Earthquake Engineering, 9*(5), 1499-1518. doi: 10.1007/s10518-011-9258-2

Lumantarna, E., Wilson, J. L., & Lam, N. T. K. (2012). Bi-linear displacement response spectrum model for engineering applications in low and moderate seismicity

regions. *Soil Dynamics and Earthquake Engineering, 43*, 85-96. doi: 10.1016/j.soildyn.2012.07.006

Lynn, A. C., Moehle, J. P., Mahin, S. A., & Holmes, W. T. (1996). Seismic evaluation of existing reinforced concrete building columns. *Earthquake Spectra, 12*(4), 715-739.

Mander, J. B., Priestley, M. J. N., & Park, R. (1988). Theoretical stress-strain model for confined concrete. *ASCE Journal of Structural Engineering, 114*(8), 1804-1825.

Manie, S., Moghadam, A. S., & Ghafory-Ashtiany, M. (2015). Collapse behavior evaluation of asymmetric buildings subjected to bi-directional ground motion. *The Structural Design of Tall and Special Buildings, 24*(8), 607-628. doi: 10.1002/tal.1202

Maqsood, T., Wehner, M., Ryu, H., Edwards, M., Dale, K., & Miller, V. (2014). GAR15 Regional Vunerability Functions: Reporting on the UNISDR/GA SE Asian Regional Workshop on Structural Vulnerability Models for the GAR Global Risk Assessment, 11–14 November, 2013, Geoscience Australia, Canberra, Australia. *Record 2014/38*. Canberra, ACT: Geoscience Australia.

McBean, P. C. (2008). Drift intolerant facade systems and flexible shear walls: Do we have a problem. *Australian Journal of Structural Engineering, 8*(1), 77-84.

McCue, K. (2013). *Some historical earthquakes in Tasmania with implications for seismic hazard assessment.* Paper presented at the Australian Earthquake Engineering Society 2013 Conference, Hobart, Tasmania.

McKenna, F., Fenves, G. L., Scott, M. N., & Jeremic, B. (2000). Open System for Earthquake Engineering Simulation (OpenSEES) (Version 2.4.5, 2013): Pacific Earthquake Engineering Research Center, University of California, Berkeley, CA. Retrieved from http://opensees.berkeley.edu/

McPherson, A., & Hall, L. (2013). Site classification for earthquake hazard and risk assessment in Australia. *Bulletin of the Seismological Society of America, 103*(2A), 1085-1102. doi: 10.1785/0120120142

Megget, L. M. (2003). The Seismic Design and Performance of Reinforced Concrete Beam-Column Knee Joints in Buildings. *Earthquake Spectra, 19*(4), 863-895. doi: 10.1193/1.1623782

Menegotto, M., & Pinto, P. E. (1973). *Method of analysis for cyclically loaded reinforced concrete plane frames including changes in geometry and non-elastic behavior of elements under combined normal force and bending.* Paper presented at the IABSE Sympoium on Resistance and Ultimate Deformability of Structures Acted on by Well-Defined Repeated Loads, International Association for Bridge and Structural Engineering, Zurich, Switzerland.

Moehle, J., & Deierlein, G. G. (2004). *A framework methodology for performance-based earthquake engineering.* Paper presented at the 13th World Conference on Earthquake Engineering (WCEE), Vancouver, Canada.

Morris, G. J., Bull, D. K., & Bradley, B. A. (2015). In situ conditions affecting the ductility capacity of lightly reinforced concrete wall structures in the Canterbury earthquake sequence. *Bulletin of the New Zealand National Society for Earthquake Engineering, 48*(3), 191-204.

Moyer, M. J., & Kowalsky, M. J. (2003). Influence of tension strain on buckling of re-bar in concrete columns. *ACI Structural Journal, 100*(1), 75-85.

Nazari, Y. R. (2017). *Seismic fragility analysis of reinforced concrete shear wall buildings in Canada.* (PhD thesis), University of Ottawa, Canada.

Ning, C.-L., Yu, B., & Li, B. (2016). Beam-Column Joint Model for Nonlinear Analysis of Non-Seismically Detailed Reinforced Concrete Frame. *Journal of Earthquake Engineering, 20*(3), 476-502. doi: 10.1080/13632469.2015.1104759

Nordenson, G. J. P., & Bell, G. R. (2000). Seismic design requirements for regions of moderate seismicity. *Earthquake Spectra, 16*(1), 205-225.

Norton, J. A., King, A. B., Bull, D. K., Chapman, H. E., McVerry, G. H., Larkin, T. J., & Spring, K. C. (1994). Northridge earthquake reconnaissance report. *Bulletin of the New Zealand National Society for Earthquake Engineering, 27*(4), 235-342.

NZSEE. (2006). Assessment and improvement of the structural performance of buildings in earthquakes *Recommendations of a NZEE study group on earthquake risk buildings June 2006: including corrigendum Nos 1, 2 & 3*: New Zealand Society for Earthquake Engineering.

NZSEE. (2016). The seismic assessment of existing buildings: technical guidelines for engineering assessments *Revised draft 1- October 2016*: Ministry of Business, Innovation and Employment, the Earthquake Commission, the New Zealand Society for Earthquake Engineering, the Structural Engineering Society and the New Zealand Geotechnical Society.

Oesterle, R. G., Fiorato, A. E., Johal, L. S., Carpenter, J. E., Russell, H. G., & Corley, W. G. (1976). Earthquake resistant structural walls - tests of isolated walls (pp. 318). Skokie, Illinios: Research and Development Construction Technology Laboratories, Portland Cement Association.

Ordonez, G. A. (2014). SHAKE2000 (Version 9.99.6 - May 2014). Retrieved from http://www.geomotions.com/

Pampanin, S., Kam, W. K., Tasligedik, A. S., Gallo, P. Q., & Akguzel, U. (2011). *Considerations of the seismic performance of pre-1970s RC buildings in the Christchurch CBD during the 4th Sept 2010 Canterbury earthquake: was that really a big one? .* Paper presented at the Ninth Papcific Conference on Earthquake Engineering (PCEE): Building an Earthquake-Resilient Society, Auckland, New Zealand.

Pantelides, C. P., Hansen, J., Nadauld, H., & Reaveley, L. D. (2002). Assessment of reinforce concrete building exterior joints with substandard details *PEER 2002/18*: Pacific Earthquake Engineering Center, University of California, Berkeley.

Papaspiliou, M., Kontoe, S., & Bommer, J. J. (2012). An exploration of incorporating site response into PSHA-part II: Sensitivity of hazard estimates to site response approaches. *Soil Dynamics and Earthquake Engineering, 42*, 316-330. doi: 10.1016/j.soildyn.2012.05.001

Park, R. (2002). A Summary of Results of Simulated Seismic Load Tests on Reinforced Concrete Beam-Column Joints, Beams and Columns with Substandard Reinforcing Details. *Journal of Earthquake Engineering, 6*(2), 147-174. doi: 10.1080/13632460209350413

Park, S., & Mosalam, K. M. (2012). Analytical model for predicting shear strength of unreinforced exterior beam-column joints. *ACI Structural Journal, 109*(2), 149-159.

Park, S., & Mosalam, K. M. (2013a). Experimental investigation of nonductile RC corner beam-column joints with floor slabs. *Journal of Structural Engineering, 139*(1), 1-14. doi: 10.1061/(ASCE)ST.1943-541X.0000591

Park, S., & Mosalam, K. M. (2013b). Simulation of reinforced concrete frames with nonductile beam-column joints. *Earthquake Spectra, 29*(1), 233-257. doi: 10.1193/1.4000100

Paulay, T., Park, R., & Priestley, M. J. N. (1978). Reinforced concrete beam-column joints under seismic actions *ACI Structural Journal, 75*(11), 585-593. doi: 10.14359/10971

Paulay, T., & Priestley, M. J. N. (1992). *Seismic design of reinforced concrete and masonry buildings*. New York: John Wiley & Sons, Inc.

PEER. (2014). Pacific Earthquake Engineering Research (PEER) Ground Motion Database. http://peer.berkeley.edu/peer_ground_motion_database

Pessiki, S. P., Conley, C. H., Gergely, P., & White, R. N. (1990). Seismic behavior of lightly-reinforced concrete column and beam-column joint details *Technical Report NCEER-90-0014*: National Center for Earthquake Engineering Research, State University of New York at Buffalo, New York.

Pitilakis, K., Riga, E., & Anastasiadis, A. (2013). New code site classification, amplification factors and normalized response spectra based on a worldwide ground-motion database. *Bulletin of Earthquake Engineering, 11*(4), 925-966. doi: 10.1007/s10518-013-9429-4

Popovics, S. (1973). A numerical approach to the complete stress strain curve for concrete. *Cement and concrete research, 3*(5), 583-599.

Porter, K. (2016). A beginner's guide to fragility, vulnerability, and risk (pp. 92). Denver CO, USA: University of Colorado Boulder.

Porter, K., Kennedy, R., & Bachman, R. (2007). Creating Fragility Functions for Performance-Based Earthquake Engineering. *Earthquake Spectra, 23*(2), 471-489. doi: 10.1193/1.2720892

Priestley, M. J. N. (1995). *Displacement-based seismic assessment of exisiting reinforced concrete buildings.* Paper presented at the Pacific Conference on Earthquake Engineering, PCEE 95, Melbourne, Victoria.

Priestley, M. J. N. (1997). Displacement-Based Seismic Assessment of Reinforced Concrete Buildings. *Journal of Earthquake Engineering, 1*(1), 157-192. doi: 10.1080/13632469708962365

Priestley, M. J. N., Calvi, G. M., & Kowalsky, M. J. (2007). *Displacement-based seismic design of structures*. Pavia, Italy: IUSS Press.

Pugh, J. S., Lowes, L. N., & Lehman, D. E. (2015). Nonlinear line-element modeling of flexural reinforced concrete walls. *Engineering Structures, 104*, 174-192. doi: 10.1016/j.engstruct.2015.08.037

Rajeev, P., Franchin, P., & Pinto, P. E. (2008). Increased accuracy of vector-IM-based seismic risk assessment? *Journal of Earthquake Engineering, 12*(sup1), 111-124. doi: 10.1080/13632460801925798

Rajeev, P., Franchin, P., & Tesfamariam, S. (2014). *Probabilistic seismic demand model for RC frame buildings using cloud analysis and incremental dynamic analysis.* Paper presented at the Tenth U.S. National Conference on Earthquake Engineering (NCEE), Anchorage, Alaska.

Reddiar, M. K. M. (2009). *Stress-strain model of unconfined and confined concrete and stress-block parameters.* (Thesis), Office of gRaduate Studies of Texas A&M University.

Robinson, D., Fulford, G., & Dbu, T. (2005). EQRM: Geoscience Australia's Earthquake Risk Model, Technical Manual Version 3.0 *Record 2005/01*. Canberra, ACT: Geoscience Australia.

Rodrigues, H., Arêde, A., Varum, H., & Costa, A. (2013). Damage evolution in reinforced concrete columns subjected to biaxial loading. *Bulletin of Earthquake Engineering, 11*(5), 1517-1540. doi: 10.1007/s10518-013-9439-2

Rodríguez-Marek, A., Bray, J. D., & Abrahamson, N. (1999). Task 3: Characterization of site response general site categories *PEER 1999/03*: Pacific Earthquake Engineering Research Center, Pacific Gas and Electric Company, David and Lucile Packard Foundation.

Rodríguez-Marek, A., Bray, J. D., & Abrahamson, N. A. (2001). An empirical geotechnical seismic site response procedure. *Earthquake Spectra, 17*(1), 65-87.

Rodsin, K. (2007). *Seismic performance of soft-storey buildings in low to moderate seismicity regions.* (Phd Thesis), Department of Civil and Environmental Engineering,The University of Melbourne, Australia.

Ruitong, D., & Park, R. (1987). A comparison of the behaviour of reinforced concrete beam-column joints designed for ductility and limited ductility. Department of Civil Engineering, University of Canterbury, Christchurch, New Zealand.

Rutenberg, A. (2004). The seismic shear of ductile cantilever wall systems in multistorey structures. *Earthquake Engineering & Structural Dynamics, 33*(7), 881-896. doi: 10.1002/eqe.384

Saatcioglu, M., & Ozcebe, G. (1989). Response of reinforced concrete columns to simulated seismic loading. *ACI Structural Journal*, 3-12.

Scott, M. H., & Fenves, G. L. (2006). Plastic hinge integration methods for force-based beam-column elements. *Journal of Structural Engineering, 132*(2), 244-252. doi: 10.1061//ASCE/0733-9445/2006/132:2/244

Seed, H. B., Ugas, C., & Lysmer, J. (1976). Site-dependent spectra for earthquake-resistant design. *Bulletin of the Seismological Society of America, 66*(1), 221-2243.

Seo, J., Hu, J., & Davaajamts, B. (2015). Seismic Performance Evaluation of Multistory Reinforced Concrete Moment Resisting Frame Structure with Shear Walls. *Sustainability, 7*(10), 14287-14308. doi: 10.3390/su71014287

Sezen, H. (2002). *Seismic behavior and modeling of reinforced concrete columns.* (PhD Dissertation), University of California, Berkeley.

Sezen, H., Elwood, K. J., Whittaker, A. S., Mosalam, K. M., Wallace, J. W., & Stanton, J. F. (2000). Structural engineering reconnaissance of the August 17, 1999 Earthquake: Kocaeli (Izmit), Turkey University of Calfornia, Berkeley: Pacific Earthquake Engineering Research Center, College of Engineering.

Sezen, H., & Moehle, J. P. (2004). Shear strength model for lightly reinforced concrete columns. *Journal of Structural Engineering, 130*(11), 1692-1703. doi: 10.1061/(ASCE)0733-9445(2004)130:11(1692)

Shafaei, J., Zareian, M. S., Hosseini, A., & Marefat, M. S. (2014). Effects of joint flexibility on lateral response of reinforced concrete frames. *Engineering Structures, 81*, 412-431. doi: 10.1016/j.engstruct.2014.09.046

Shome, N. (1999). *Probabilistic seismic demand analysis of nonlinear structures.* (PhD Thesis), Department of Civil and Environmental Engineering, Standford University.

Shome, N., & Cornell, C. A. (2000). *Structural seismic demand analysis: consideration of collapse.* Paper presented at the 8th ASCE Speciality Conference on Probabilistic Mechanics and Structural Reliability, University of Notre Dame, South Bend, Indiana.

Simonini, S., Constantin, R., Rutenberg, A., & Beyer, K. (2012). *Pushover analysis of multi-storey cantilevel wall systems.* Paper presented at the 15th World Conference of Earthquake Engineering (WCEE), Lisbin, Portugal.

Sritharan, S., Beyer, K., Henry, R. S., Chai, Y. H., Kiwalsky, M., & Bull, D. (2014). Understanding poor seismic performance of concrete walls and design implications. *Earthquake Spectra, 30*(1), 307-334.

Standards Australia. (1988). AS 3600-1988: Concrete structures. Sydney, NSW: Standards Association of Australia.

Standards Australia. (1991). AS 1302:1991 Steel reinforcing bars for concrete. Sydney, NSW: Standards Association of Australia.

Standards Australia. (1993). AS 1170.4 Supplement 1-1993 *Minimum design loads on structures, Part 4: Earthquake loads - Commentary*. Sydney, NSW.

Standards Australia. (2007). AS 1170.4-2007: Structural design actions, Part 4: Earthquake actions in Australia. Sydney, NSW: SAI Global.

Standards Australia. (2009). AS 3600-2009: Concrete structures. Sydney, NSW: SAI Global.

Standards Australia. (2014). AS 3600-2009 Supp 1: 2014: Concrete structures - Commentary (Supplement to AS 3600-2009).

Standards Australia and Standards New Zealand. (2002). AS/NZS 1170.0-2002: Structural design actions, Part 0: General principles. Syndey, NSW, and Wellington: SAI Global and Standards New Zealand.

Standards Australia and Standards New Zealand. (2011). AS/NZS 1170.2-2011 (R2016): Structural design actions, Part 2: Wind actions. Sydney, NSW, and Wellington.

Standards New Zealand. (2004). NZS 1170.5:2004 Structural design actions - Part 5: earthquake actions - New Zealand. Wellington.

Standards New Zealand. (2006). NZS 3101: Part 1 The design of concrete structures. Wellington, NZ.

Stathopoulos, K. G., & Anagnostopoulos, S. A. (2005). Inelastic torsion of multistorey buildings under earthquake excitations. *Earthquake Engineering & Structural Dynamics, 34*(12), 1449-1465. doi: 10.1002/eqe.486

Sullivan, T. J., Priestley, M. J. N., & Calvi, G. M. (2012). *A model code for the displacement-based seismic design of structures*. Instituto Universitario di Studi Superiori di Pavia: IUSS Press.

Sullivan, T. J., Welch, D. P., & Calvi, G. M. (2014). Simplified seismic performance assessment and implications for seismic design. *Earthquake Engineering and Engineering Vibration, 13*(S1), 95-122. doi: 10.1007/s11803-014-0242-0

Takeda, T., Sozen, M. A., & Nielsen, N. N. (1970). Reinforced concrete response to simulated earthquakes. *Journal of STructural Division, 96*(12), 2557-2573.

Tatsuya, I. (1996). *Post-yield behaviours of multi-story reinforced concrete shear walls subjected to bilateral deformations under axial loading.* Paper presented at the 11th World Conference on Earthquake ENgineering (WCEE)

The Atlantic Monthly Group. (2014). The Northridge Earthquake: 20 Years Ago Today. 2017, from https://www.theatlantic.com/photo/2014/01/the-northridge-earthquake-20-years-ago-today/100664/

Thomsen, J., & Wallace, J. (2004). Displacement-Based Design of Slender Reinforced Concrete

Structural Walls-Experimental Verification. *Journal of Structural Engineering, ASCE, 130*(4), 618-630. doi: doi:doi:10.1061/(ASCE)0733-9445(2004)130:4(618)

Tsang, H. H., Chandler, A. M., & Lam, N. T. K. (2006a). Estimating non-linear site response by single period approximation. *Earthquake Engineering & Structural Dynamics, 35*(9), 1053-1076. doi: 10.1002/eqe.567

Tsang, H. H., Chandler, A. M., & Lam, N. T. K. (2006b). Simple models for estimating period-shift and damping in soil. *Earthquake Engineering & Structural Dynamics, 35*(15), 1925-1947. doi: 10.1002/eqe.614

Tsang, H. H., Lam, N. T. K., & Wilson, J. L. (2013). *A design spectrum model featuring resonant-like soil-amplification.* Paper presented at the Australian Earthquake Engineering Society 2013 Conference, Hobart, Tasmania.

Vamvatsikos, D., & Cornell, C. A. (2002). Incremental dynamic analysis. *Earthquake Engineering & Structural Dynamics, 31*(3), 491-514. doi: 10.1002/eqe.141

Venkatesan, S., Lam, N., & Wilson, J. (2006). *Simple model accounting for the soil resonance phenomenon.* Paper presented at the Australian Earthquake Engineering Society 2006 Conference, Canberra, Australian Capital Territory.

Walker, G. (2011). Comparison of the impacts of Cyclone Tracy and the Newcastle earthquake on the Australian building and insurance industries. *Australian Journal of Structural Engineering, 11*(3), 283-293.

Wen, Y. K., Ellingwood, B. R., & Bracci, J. (2004). Vulnerability function framework for consequence-based engineering *MAE Center Project DS-4 Report*.

Wibowo, A., Wilson, J. L., Lam, N., & Gad, E. (2013). Seismic performance of lightly reinforced structural walls for design purposes. *Magazine of Concrete Research, 65*(13), 809-828. doi: 10.1680/macr.13.00021

Wibowo, A., Wilson, J. L., Lam, N. T. K., & Gad, E. F. (2014). Drift performance of lightly reinforced concrete columns. *Engineering Structures, 59*, 522-535. doi: 10.1016/j.engstruct.2013.11.016

Wilson, J., & Lam, N. (2003). A recommended earthquake response spectrum model for Australia. *Australian Journal of Structural Engineering, 5*(1), 17-27. doi: 10.1080/13287982.2003.11464924

Wilson, J., & Lam, N. (2007). AS 1170.4-2007 commentary: Structural design actions. Part 4, Earthquake actions in Australia. Victoria: Australian Earthquake Engineering Society: McKinnon.

Wilson, J. L., Lam, N. T. K., & Gad, E. F. (2015). *Hazard identification and behaviour of reinforced concrete framed buildings in regions of lower seismicity.* Paper presented at the Tenth Pacific Conference on Earthquake Engineering (PCEE), Building an Earthquake-Resilient Pacific, Sydney, Australia.

Wilson, J. L., Wibowo, A., Lam, N. T. K., & Gad, E. F. (2015). Drift behaviour of lightly reinforced concrete columns and structural walls for seismic design applications. *Australian Journal of Structural Engineering, 16*(1). doi: 10.7158/s14-002.2015.16.1

Wood, S. L., Stark, R., & Greer, S. A. (1991). Collapse of eight-storey RC building during 1985 Chile earthquake. *Journal of Structural Engineering, 117*(2), 600-619.

Xu, H., & Gardoni, P. (2016). Probabilistic capacity and seismic demand models and fragility estimates for reinforced concrete buildings based on three-dimensional analyses. *Engineering Structures, 112*, 200-214. doi: 10.1016/j.engstruct.2016.01.005

Zhao, J., & Sritharan, S. (2007). Modeling of strain penetration effects in fiber-based analysis of reinforced concrete structures. *ACI Structural Journal, 104*(2), 133-141.

Zhao, X., Wu, Y.-F., Leung, A. Y., & Lam, H. F. (2011). Plastic Hinge Length in Reinforced Concrete Flexural Members. *Procedia Engineering, 14*, 1266-1274. doi: 10.1016/j.proeng.2011.07.159

APPENDIX A

Details of the historical and stochastically generated records are provided in Table A1 and Table A2.

Table A1: Details of input motion for k_pZ 0.1 g

Source	Earthquake ID	Earthquake Name/Country	Faulting Mechanism	Magnitude	Hypocentral distance (km)	Epicentral distance (km)	PGA (g)
ISESD	63 (Station 36)	Friuli, Italy (1976)	Reverse	6.0	-	28	0.1017
	65 (Station 26)	Friuli, Italy (1976)	Reverse	6.0	-	12	0.1365
	93 (Station 69)	Serbia & Montenegro (1979)	Reverse	6.9	-	105	0.0749
	108 (Station 68)	Serbia & Montenegro (1979)	Reverse	6.2	-	30	0.0769
PEER	NGA 23	San Francisco (1957)	Reverse	5.28	13.7	-	0.1073
	NGA 72	San Fernando (1971)	Reverse	6.61	27.46	-	0.1631
	NGA 946	Northridge (1994)	Reverse	6.69	66.31	-	0.0559
	NGA 957	Northridge (1994)	Reverse	6.69	29.05	-	0.1403
	NGA 1021	Northridge (1994)	Reverse	6.69	52.91	-	0.0793
	NGA 1033	Northridge (1994)	Reverse	6.69	63.71	-	0.0683
	NGA 1074	Northridge (1994)	Reverse	6.69	64.22	-	0.0941
GENQKE	Generated earthquake	Australian characteristics	Reverse	6.0	27	-	-
	Generated earthquake	Australian characteristics	Reverse	7.0	45	-	-
	Generated earthquake	Australian characteristics	Reverse	7.0	50	-	-
	Generated earthquake	Australian characteristics	Reverse	7.0	70	-	-

Table A2: Details of input motion for k_pZ 0.3 g

Source	Earthquake ID	Earthquake Name/Country	Faulting Mechanism	Magnitude	Hypocentral distance (km)	Epicentral distance (km)	PGA (g)
ISESD	34 (Station 20)	Friuli, Italy (1976)	Reverse	6.5	-	23	0.3567
	93 (Station 64)	Serbia & Montenegro (1979)	Reverse	6.9	-	21	0.2231
	93 (Station 68)	Serbia & Montenegro (1979)	Reverse	6.9	-	65	0.2558
	2322 (Station 3311)	Avej, Iran (2002)	Reverse	6.5	-	28	0.4459
PEER	NGA 1645	Sierra Mandre (1991)	Reverse	5.61	13.63	-	0.2350
	NGA 994	Northridge (1994)	Reverse	6.69	30.86	-	0.2458
	NGA 1050	Northridge (1994)	Reverse	6.69	26.85	-	0.4085
	NGA 1091	Northridge (1994)	Reverse	6.69	41.9	-	0.1449
GENQKE	Generated earthquake	Australian characteristics	Reverse	7.0	20	-	-
	Generated earthquake	Australian characteristics	Reverse	7.5	35	-	-
	Generated earthquake	Australian characteristics	Reverse	7.5	30	-	-

APPENDIX B

Shear wave velocity profiles of soil sites considered in Section 2.4.4.4 The legend also shows the corresponding site ID as presented in Kayen et al. (2015).

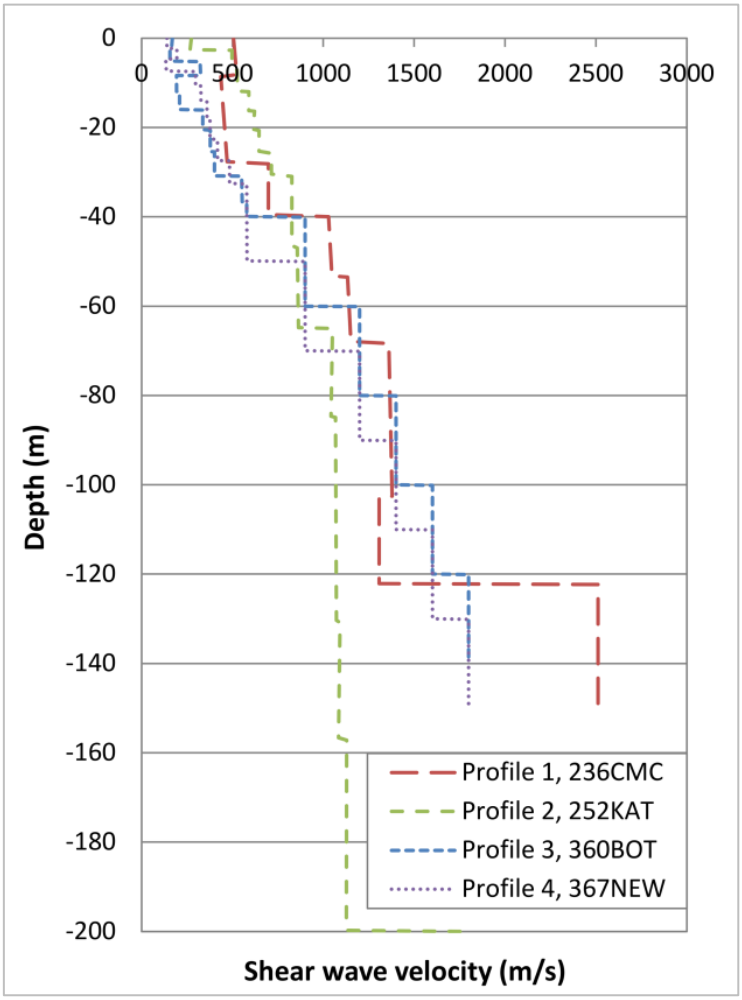

Figure B1: Shear wave velocity profiles classified as Class C

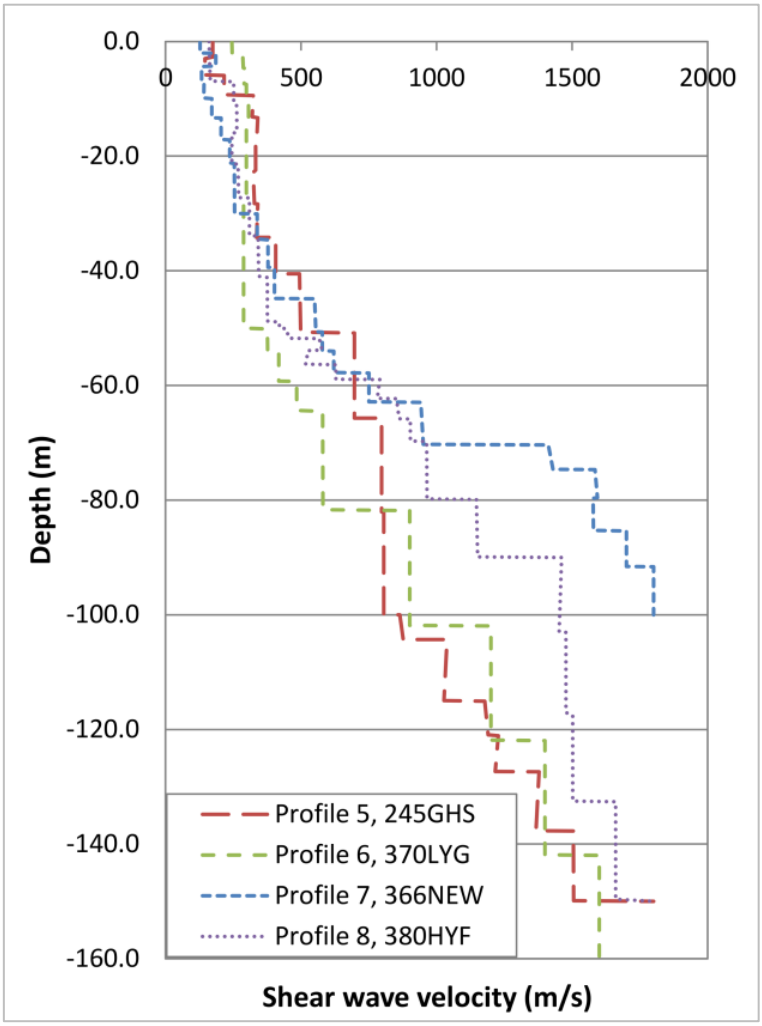

Figure B2: Shear wave velocity profiles classified as Class D

APPENDIX C

The comparison of simulated and experimental response of the ten non-ductile columns presented in Table 5-9 for which detailed response was not presented in Section 5.4.3.2.

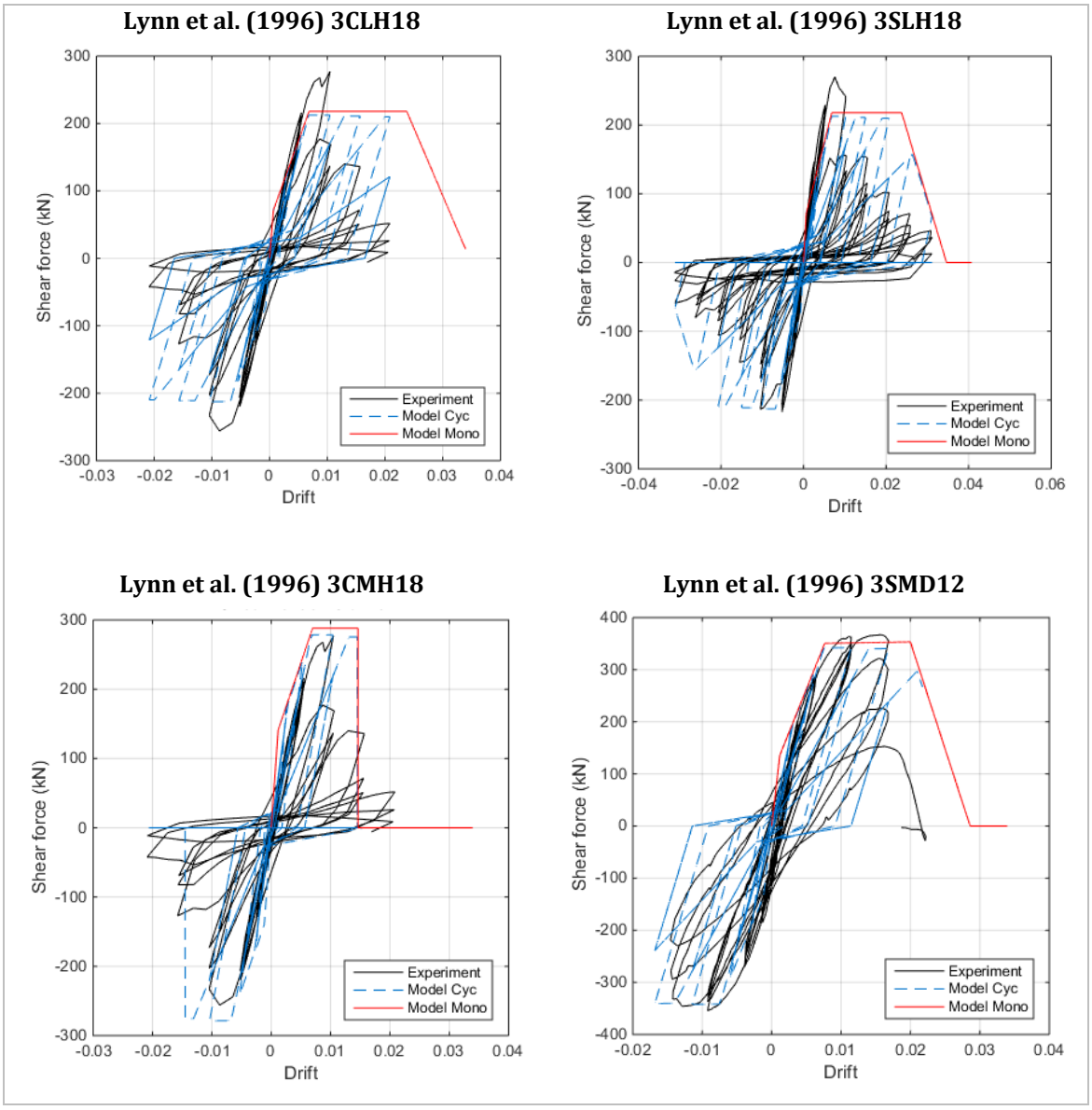

Figure C1 continued on next page

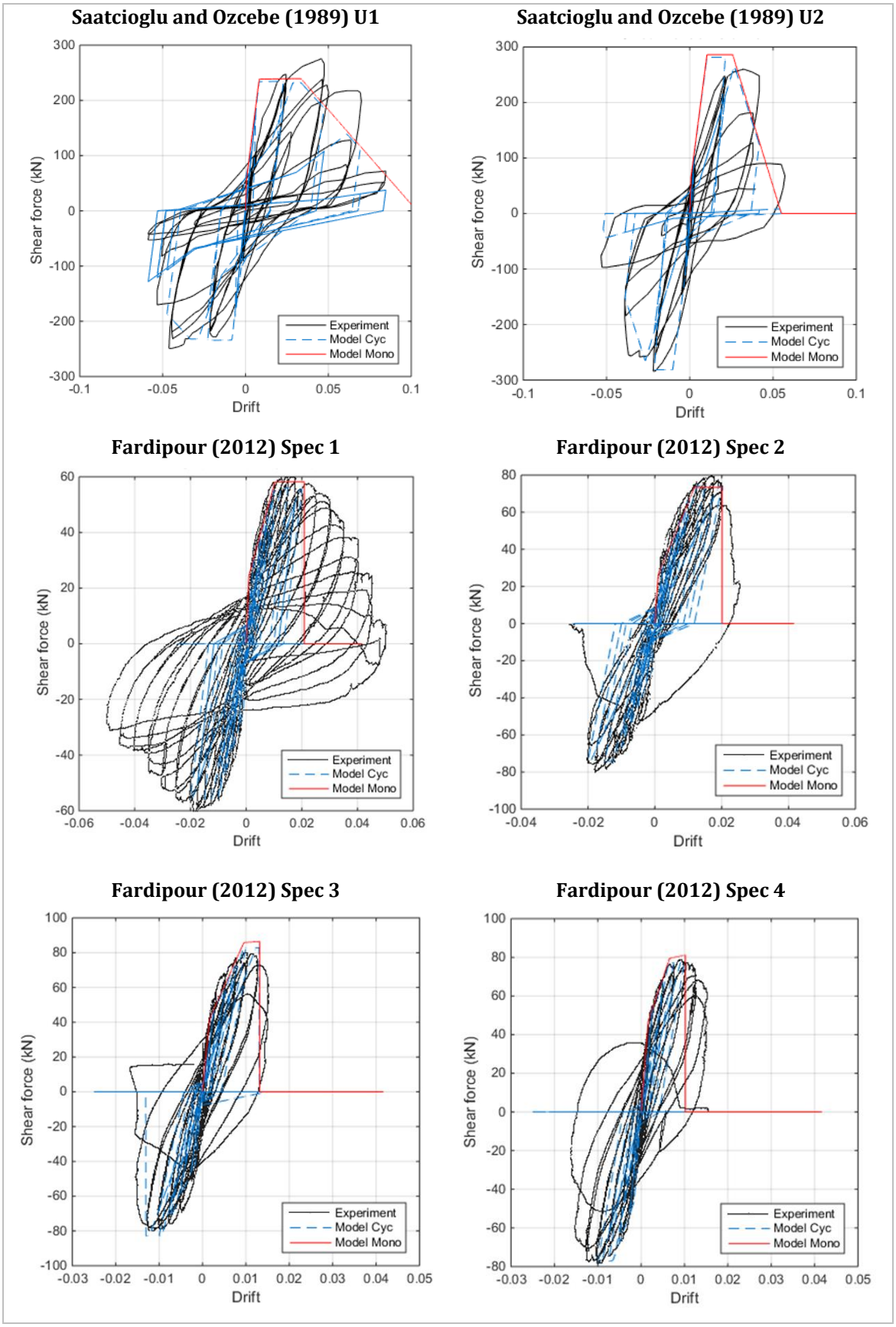

Figure C1: Comparison of simulated and experimental response of ten of the twenty non-ductile columns presented in Table 5-9